SPECIAL REPORT 98-12

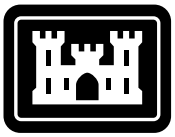

US Army Corps of Engineers®
Cold Regions Research & Engineering Laboratory

Technical Assessment of Maglev System Concepts

Final Report by the Government Maglev System Assessment Team

James H. Lever, Editor

October 1998

Abstract: The Government Maglev System Assessment Team operated from 1991 to 1993 as part of the National Maglev Initiative. They assessed the technical viability of four U.S. maglev system concepts, using the French TGV high-speed train and the German TR07 maglev system as assessment baselines. Maglev in general offers advantages that include high speed potential, excellent system control, high capacity, low energy consumption, low maintenance, modest land requirements, low operating costs, and ability to meet a variety of transportation missions. Further, the U.S. maglev concepts could provide superior performance to TR07 for similar cost or similar performance for less cost. They also could achieve both lower trip times and lower energy consumption along typical U.S. routes. These advantages result generally from the use of large-gap magnetic suspensions, more powerful linear synchronous motors, and tilting vehicles. Innovative concepts for motors, guideways, suspension, and superconducting magnets all contribute to a potential for superior long-term performance of U.S. maglev systems compared with TGV and TR07.

How to get copies of CRREL technical publications:

Department of Defense personnel and contractors may order reports through the Defense Technical Information Center:

DTIC-BR SUITE 0944
8725 JOHN J KINGMAN RD
FT BELVOIR VA 22060-6218
Telephone 1 800 225 3842
E-mail help@dtic.mil
msorders@dtic.mil
WWW http://www.dtic.mil/

All others may order reports through the National Technical Information Service:

NTIS
5285 PORT ROYAL RD
SPRINGFIELD VA 22161
Telephone 1 703 487 4650
1 703 487 4639 (TDD for the hearing-impaired)
E-mail orders@ntis.fedworld.gov
WWW http://www.fedworld.gov/ntis/ntishome.html

A complete list of all CRREL technical publications is available from

USACRREL (CECRL-IB)
72 LYME RD
HANOVER NH 03755-1290
Telephone 1 603 646 4338
E-mail techpubs@crrel.usace.army.mil

For information on all aspects of the Cold Regions Research and Engineering Laboratory, visit our World Wide Web site:
http://www.crrel.usace.army.mil

Special Report 98-12

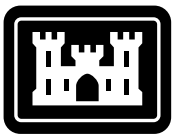

US Army Corps
of Engineers®
Cold Regions Research &
Engineering Laboratory

Technical Assessment of Maglev System Concepts

Final Report by the Government Maglev System Assessment Team

James H. Lever, Editor

October 1998

Prepared for
NATIONAL MAGLEV INITIATIVE

PREFACE

This report was edited by Dr. James H. Lever, Mechanical Engineer, Ice Engineering Research Division, U.S. Army Cold Regions Research and Engineering Laboratory. Funding for this work was provided by the U.S. Army Corps of Engineers and the U.S. Department of Transportation Federal Railroad Administration as part of the National Maglev Initiative.

The contents of this report are not to be used for advertising or promotional purposes. Citation of Brand names does not constitute an official endorsement or approval of the use of such commerical products.

FOREWORD

This report describes the findings of the Government Maglev System Assessment (GMSA) team, which operated from 1991 to 1993 as part of the National Maglev Initiative (NMI). Our task was to assess the technical viability of five maglev system concepts for use in the U.S., using high-speed rail as a baseline. After struggling with what this meant, we adopted a series of cross-system comparisons supported by detailed analyses. The result, I believe, served the NMI's need to assess these systems, and also improved the Government's ability to understand and guide the contracted System Concept Definitions (SCD).

We have not identified specific authors for much of this report, because it reflects consensus of the team as a whole. However, sections describing the detailed subsystem and system analyses were the responsibility of individuals or small groups. Acknowledgment to the identified authors should be given when referencing these sections.

One of the most satisfying moments during the GMSA occurred at the Maglev '93 conference at Argonne National Laboratory, after we presented our preliminary results. Conference attendees were pleased, and surprised, that we had kept up with the flood of technical data generated by the NMI contractors. Moreover, several SCD contractors were grateful to see independent verification of the key features of each concept.

Most of the analyses in this report were completed by September 1993, to provide input to the Final Report on the National Maglev Initiative (USDOTFRA 1993). However, verification issues arose with the system simulations, then being conducted at the Volpe National Transportation Systems Center, just as the NMI ended. We decided to postpone publication until we could simulate the performance of all five maglev systems with confidence. Unfortunately, with team members moving on to other projects, this took much longer than we expected and eventually required a new simulation software. The bottom line is that this report reflects the state of maglev development as we understood it at the end of 1993. We have made no attempt to account for subsequent research. Nevertheless, we hope it will find a place as a thorough, independent technical assessment of different ways to configure this promising technology.

Jim Lever
CRREL

GMSA TEAM MEMBERS

Primary contributors

George Anagnostopoulos
Volpe National Transportation
Systems Center
U.S. Department of Transportation
55 Broadway, Kendall Square
Cambridge, MA 02142

Richard Armstrong
CEHND-ED-SY
U.S. Army Engineer Division, Huntsville
P. O. Box 1600
Huntsville, AL 35807

James T. Ballard
CEWES-SVA
U.S. Army Engineer Waterways
Experiment Station
3909 Halls Ferry Road
Vicksburg, MS 39180-6199

Christopher J. Boon
Canadian Institute of Guided Ground
Transport
St. Lawrence Building
Queen's University
Kingston, Ontario
Canada K7L 3N6

Dr. Howard T. Coffey
Center for Transportation Research
Energy Systems Division
Argonne National Laboratory
9700 South Cass Avenue, ES/362 2B
Argonne, IL 60439-4815

Michael Coltman
Volpe National Transportation
Systems Center
U.S. Department of Transportation
55 Broadway, Kendall Square
Cambridge, MA 02142

Robert Hasse
CEHND-ED-CS
U.S. Army Engineer Division, Huntsville
P. O. Box 1600
Huntsville, AL 35807

Dr. Jianliang He
Center for Transportation Research
Energy Systems Division
Argonne National Laboratory
9700 South Cass Avenue, ES/362 2B
Argonne, IL 60439-4815

Dr. James H. Lever, Team Leader
CECRL-EI
USACRREL
72 Lyme Road
Hanover, NH 03755-1290

Dr. John Potter
CEHND-ED
U.S. Army Engineer Division, Huntsville
P. O. Box 1600
Huntsville, AL 35807

James Milner
National MAGLEV Initiative
C/O RDV 7 DOT/FRA
400 7th Street SW
Washington, DC 20590

Dr. James Ray
CEWES-SSR
U.S. Army Engineer Waterways
Experiment Station
3909 Halls Ferry Road
Vicksburg, MS 39180-6199

Frank L. Raposa, P.E.
Consulting Engineer
24 Brewster Lane
Acton, MA 01720

Richard Suever
CEHND-PM-MD
U.S. Army Engineer Division, Huntsville
P. O. Box 1600
Huntsville, AL 35807

Kenneth Shaver
CEHND-ED-ME
U.S. Army Engineer Division, Huntsville
P.O. Box 1600
Huntsville, AL 35807

Zian Wang
Center for Transportation Research
Energy Systems Division
Argonne National Laboratory
9700 South Cass Avenue, ES/362 2B
Argonne, IL 60439-4815

David Tyrell
Structures & Dynamics Division
Volpe National Transportation
Systems Center
U.S. Department of Transportation
Kendall Square
Cambridge, MA 02142

Other contributors

Dr. Dennis M. Bushnell
Fluid Mechanics Division
Langley Research Center
National Aeronautics and
Space Administration
Mail Stop 197
Hampton, VA 23681-0001

Candido P. Damian
CEHND-ED-ME
U.S. Army Engineer Division, Huntsville
P. O. Box 1600
Huntsville, AL 35807-4301

Rodney Darby
CEHND-ED-CS
U.S. Army Engineer Division, Huntsville
P. O. Box 1600
Huntsville, AL 35807

Dr. John Harding
Federal RR Administration, RDV-7
400 Seventh Street, S.W.
Washington, DC 20590

Stuart Kissinger
Corps of Engineers/NMI
RDV-8
400 Seventh Street, SW
Washington, DC 20590

James Lacombe
CECRL-RG
USACRREL
72 Lyme Road
Hanover, NH 03755-1290

Dr. John Loyd
CEHND-ED-SY
U.S. Army Engineer Division, Huntsville
P. O. Box 1600
Huntsville, AL 35807

James Mitchell
National Maglev Initiative
C/O RDV 7 DOT/FRA
400 7th Street SW
Washington, DC 20590

Dr. Mark E. Pitstick
Center for Transportation Research
Energy Systems Division
Argonne National Laboratory
9700 South Cass Avenue, ES/362-2B
Argonne, IL 60439-4815

Dr. Herbert Weinstock
Structures & Dynamics Division
Volpe National Transportation
Systems Center
U. S. Department of Transportation
Kendall Square
Cambridge, MA 02142

Raymond Wlodyka
U.S. Department of Transportation
Transportation Systems Center
Kendall Square
Cambridge, MA 0214

Dr. Stanley Woodson
CEWES-SSR
U.S. Army Engineer Waterways
Experiment Station
3909 Halls Ferry Road
Vicksburg, MS 39180-6199

CONTENTS

ILLUSTRATIONS

TABLES

EXECUTIVE SUMMARY

The Federal Government organized the National Maglev Initiative (NMI) to determine whether it should actively encourage investment in maglev (magnetically levitated ground transportation). The NMI's principal tasks were to assess the technical and economic viability of maglev in the U.S. and to recommend the most appropriate Federal role for its development.

The NMI sought industry's perspective on the best ways to implement maglev technology. It awarded four System Concept Definition (SCD) contracts to teams led by Bechtel Corp., Foster-Miller, Inc., Grumman Aerospace Corp., and Magneplane International, Inc. These 11-month contracts totaled $8.7 million and resulted in very thorough descriptions and analyses of four different maglev concepts.

The NMI also formed an independent Government Maglev System Assessment (GMSA) team. This team consisted of scientists and engineers from the U.S. Army Corps of Engineers (USACE), the U.S. Department of Transportation (USDOT) and Argonne National Laboratory (ANL), plus contracted transportation specialists. The GMSA team assessed the technical viability of the four SCD concepts, the German TR07 maglev design, and the French TGV high-speed train. This report describes the GMSA's assessment methods, evaluation results, and supporting analyses.

Essentially, we viewed technical viability as encompassing three main issues:

- *Technical feasibility*—Will a concept work as intended?
- *Mission suitability*—How well will a concept fulfill its transportation mission?
- *Relative advantage*—Do U.S. concepts possess superior performance potential relative to foreign ones?

To address these, we developed an assessment process consisting of four main steps.

Verification of subsystem performance

Team members developed numerical models to verify the performance of key high-risk or high-cost subsystems—guideway structures, magnetic suspensions and stray fields, motor and power systems, and vehicle–guideway interaction. These models employed standard engineering approaches and yielded good agreement with published data for TGV and TR07. When applied to the SCD concepts, they produced performance data and identified areas of concern generally comparable to the contractors' results.

Verification of system performance

To compare concept performance at the system level, team members developed two additional models: 1) a system simulator to investigate the performance of each concept along the SCD Severe Segment Test (SST) route, and 2) a standard methodology to estimate guideway technology costs. The system simulator helped us resolve broad technical issues, such as the suitability of each concept along Interstate Highway System rights-of-way. It also yielded estimates of trip times and energy consumption for each concept along a common route. Standardized cost estimates allowed us to reduce cost variability ascribable to different physical assumptions (e.g., column height) and different definitions of subcomponents. It also allowed independent verification of contractors' cost estimates.

Application of SCD system criteria

The NMI targeted intercity transportation as maglev's primary mission. Its SCD request for proposals included a set of system criteria to guide concept development towards that mission. We thus adopted these criteria to assess mission suitability. For each criterion, we developed qualitative and quantitative cross checks on the performance of each concept. These cross checks included checking data sources, analyses used, and the consistency of related characteristics. In many cases, these criteria also dictated the specific data products sought in our modeling effort. We then rated each concept's performance against the criterion.

Application of other criteria

In addition to the SCD system criteria, other characteristics may affect maglev's technical viability in the U.S. We therefore developed additional assessment criteria and applied them to each concept in a similar way to how we applied the SCD system criteria. Several of these other criteria (particularly mission flexibility, aerodynamics, and energy efficiency) became focal points of analysis and debate. We again rated each concept against these other criteria and added the results to those obtained for the SCD system criteria to complete our assessment of mission suitability.

OVERVIEW OF SYSTEM CONCEPTS

Train à Grande Vitesse (TGV)

The TGV is a steel-wheel-on-steel-rail technology, made optimal for high-speed operation (83 m/s [185 mph]). It uses fixed-consist, nontilting trainsets (with articulated coaches and a power car at each end of the consist). Power cars use AC synchronous rotary traction motors for propulsion. Roof-mounted pantographs collect power from an overhead catenary; several voltage options exist. Braking is by a combination of rheostatic brakes, tread brakes on powered axles, and disc brakes mounted on trailer axles; all axles possess anti-lock braking and the powered axles have anti-slip control. Although an operator controls train speed, interlocks exist, including automatic overspeed protection and enforced braking.

The TGV track structure is that of a conventional standard-gauge railroad with a specially engineered base (compacted granular materials). The track consists of continuous-welded rail on concrete and steel ties with elastic fasteners. Its high-speed switch is a conventional-style, precision-built swing-nose turnout.

Transrapid 07 (TR07)

The Transrapid 07 (TR07) is a commercially ready electromagnetic suspension (EMS) system using separate sets of conventional iron-core magnets to generate vehicle lift and guidance. The vehicle wraps around a T-shaped guideway. Attraction between vehicle magnets and edge-mounted guideway rails provides guidance; attraction between a second set of vehicle magnets and the propulsion stator packs on the underside of the guideway generates lift. Control systems regulate levitation and guidance forces to maintain a small (8-mm) air gap. TR07 has demonstrated safe operation at 120 m/s (268 mph) at a test facility in Germany, and its design is capable of achieving cruising speeds of 134 m/s (300 mph).

TR07 uses two or more nontilting vehicles in a consist. Propulsion is by a long-stator linear synchronous motor (LSM). Guideway stator windings generate a traveling wave that interacts with the vehicle levitation magnets for synchronous

propulsion. Centrally controlled wayside stations provide the required variable-frequency, variable-voltage power to the LSM. Primary braking is regenerative through the LSM, with eddy-current braking and high-friction skids for emergencies. The TR07 guideway uses steel or concrete beams constructed and erected to very tight tolerances. Its switch is a bendable steel guideway beam.

Bechtel SCD

The Bechtel concept is an innovative, flux-canceling electrodynamic suspension (EDS) system. The vehicle contains six sets of eight superconducting magnets per side. It straddles a concrete box-beam guideway. Interaction between the vehicle magnets and a laminated aluminum ladder on each guideway sidewall generates lift. Similar interaction with guideway-mounted null-flux coils provides guidance. LSM propulsion windings, also attached to the guideway sidewalls, interact with these same vehicle magnets to produce thrust. Centrally controlled wayside stations provide the required variable-frequency, variable-voltage power to the LSM.

The vehicle consists of a single car with an inner tilting shell. It uses aerodynamic control surfaces to augment magnetic guidance forces. In an emergency, it drops onto air-bearing pads. The guideway consists of a post-tensioned concrete box girder. Because of high magnetic fields, the concept calls for nonmagnetic, fiber-reinforced plastic (FRP) reinforcing rods and stirrups in the upper portion of the box beam. The concept's switch is a bendable beam constructed entirely of FRP.

Foster-Miller SCD

The Foster-Miller concept is an EDS generally similar to the Japanese MLU002. Superconducting magnets in the vehicle generate lift by interacting with null-flux levitation coils located in the sidewalls of a U-shaped guideway; similar interaction with series-coupled propulsion coils provides null-flux guidance. Its innovative propulsion scheme is called a locally commutated linear synchronous motor (LCLSM). Individual H-bridge inverters sequentially energize propulsion coils as they become lined up with the vehicle magnets. The inverters synthesize a waveform that moves down the guideway, synchronously with the vehicle.

The vehicle consists of passenger modules and attachable nose sections that create multiple-car consists. These modules have magnet bogies at each end that they share with adjacent cars; each bogie contains four magnets per side. The U-shaped guideway consists of two parallel, post-tensioned concrete beams joined transversely by precast concrete diaphragms. Because of high magnetic fields, the upper post-tensioning rods are FRP. The high-speed switch uses switched null-flux coils to guide the vehicle through a vertical turn-out; it requires no moving structural members.

Grumman SCD

The Grumman concept is an EMS with similarities to Transrapid 07. However, Grumman's vehicles wrap around a Y-shaped guideway and use just one set of vehicle magnets and guideway rails for levitation, guidance, and propulsion. The vehicle magnets are superconducting coils around horseshoe-shaped iron cores. The legs are attracted to iron rails on the underside of the guideway. Normal coils on each iron-core leg modulate levitation and guidance forces to maintain a large (40-mm) air gap. It requires no secondary suspension to maintain adequate ride quality. Propulsion is by conventional LSM embedded in the guideway rail.

Vehicles have tilt capability and may be single- or multi-car consists. Magnets are located along the full vehicle length. The innovative guideway superstructure

consists of slender Y-shaped guideway sections (one for each direction) mounted by outriggers every 4.5 m to a single 27-m-span spine girder. Switching is accomplished with a TR07-style bending guideway beam, shortened by use of a sliding or rotating section.

Magneplane SCD

The Magneplane concept is a single-vehicle EDS using a trough-shaped, 0.2-m-thick aluminum guideway for sheet levitation and guidance. Centrifugal forces cause the "Magplanes" to bank in curves. Earlier laboratory work on this concept validated the levitation, guidance, and propulsion schemes.

Superconducting levitation and propulsion magnets are grouped at the front and rear of the vehicle. The centerline magnets interact with conventional LSM windings for propulsion and also generate some electromagnetic guidance force (called the keel effect). The magnets on the sides of each group react against the aluminum guideway sheets to provide levitation.

The vehicle uses aerodynamic control surfaces and LSM-phase control to provide active damping of vehicle motions. The aluminum levitation sheets in the guideway trough form the tops of two structural aluminum box beams. These box beams are supported directly on piers. The high-speed switch uses switched null-flux coils to guide the vehicle through a fork in the guideway trough; it requires no moving structural members.

SPECIFIC CONCLUSIONS

The GMSA revealed that maglev offers significant opportunities to develop a transportation system exceptionally well suited to U.S. transportation needs. Summarized here are those opportunities offered by maglev generally and U.S. maglev particularly. Also summarized are the main innovations resulting from the SCD efforts.

Opportunities for maglev generally

Maglev offers transportation characteristics that we easily recognize as desirable against the backdrop of current modes. Because maglev will be a new mode, such characteristics will complement the existing transportation infrastructure.

High speed

High-speed potential is essentially an inherent characteristic of maglev. Lift, guidance, and propulsion occur without physical contact, and speeds in excess of 220 m/s (500 mph) are well within the technology. Furthermore, magnetic drag is small at high speeds so that only aerodynamic drag consumes appreciable energy. The top speed of maglev is a trade-off decision, not a physical or engineering limit. All maglev technologies investigated here will achieve cruising speeds of 134 m/s (300 mph) and several SCD concepts can substantially exceed this in their present form. By comparison, typical HSR (high-speed rail) commercial speeds of 83 m/s (185 mph) will rise only gradually and with significant development effort and capital investment. Maglev will achieve 300-mph service more easily than HSR, and a desire for future speed increases favors maglev.

From the consumer's view, trip time is the key measure of speed. Here, 134-m/s maglev has a significant advantage over air travel for trips under about 500 km. This advantage is partly attributable to better access to maglev's smaller stations and partly attributable to taxiing and idling overhead for air travel. Maglev

remains competitive with nonstop air to about 800 km and with one-stop air to about 2000 km. Compared with HSR, maglev offers higher acceleration and top speed, and better performance on curves, all of which lower trip times.

Excellent system control

Use of dedicated, powered guideways provides maglev with decisive control advantages over air and automobile. A maglev system can be fully automated, with exceptional sensing and control of vehicle locations. Such control capability, coupled with redundant braking modes, allows use of very short vehicle headways (less than 1 minute). Maglev also offers a potential for fully automated freight transport, with goods arriving within seconds of their scheduled time.

High capacity

Short headways allow a dual maglev guideway to achieve very high capacity. The five maglev concepts studied can all deliver 12,000 passengers per hour in each direction. An equivalent air capacity would be 60 Boeing 767's per hour *in each direction* departing and arriving at 1-minute intervals. This would tax even the most efficient airports. Comparable highway traffic would require about 10 full lanes (5 lanes per direction).

Low energy consumption

Maglev can offer trip times competitive with air travel for a small fraction of the energy consumed by an aircraft. The basic physics of magnetic lift and electrical propulsion underlie maglev's energy efficiency.

Based on energy consumed at the system connection (i.e., airport or electrical supply), maglev's energy intensity (energy / seat-meter) ranges from one-eighth to one-quarter that of the efficient Boeing 737-300 for 200- to 1000-km trips. Applying electrical conversions efficiencies typical of modern power plants narrows the gap, yet maglev still consumes only one-quarter to half the energy of a 737-300.

Electric power derives from many sources; aircraft rely exclusively on petroleum. Thus, in addition to being more efficient, maglev can decouple intercity transportation from exclusive dependence on petroleum.

Low wear and maintenance

By its nature, maglev requires no physical contact between vehicles and guideways. Lift and guidance forces are distributed over large areas, producing low contact stresses. Linear synchronous motors (LSMs) offer noncontact propulsion and braking, and avoid the need to transfer propulsion power to the vehicle. These features contrast strongly with HSR, where high stresses from wheel–rail contact and power transfer dictate rigorous maintenance programs. Overall, maglev offers the potential for significantly lower maintenance costs.

Safety, availability, and cost

High-speed rail in Europe and Japan, and air travel generally, have outstanding safety records. However, both technologies require sophisticated preventative maintenance (inspections and adjustments) to achieve such safety. Maglev possesses characteristics than should allow it to operate safely under more extreme conditions and with less maintenance.

Maglev's dedicated guideways, excellent control features, redundant braking, and lower susceptibility to weather should allow it to maintain operations in con-

ditions that would slow or halt air travel. Fog, rain, heavy snow, and high winds should pose fewer safety issues with maglev than with air. Also, maglev has far fewer moving parts, better fault tolerance, and fewer catastrophic failure modes; it should thus have better equipment-related availability, and should require less maintenance than air to ensure adequate safety.

Compared with HSR, maglev concepts offer exceptional "derailment" protection by using either wrap-around vehicles or wrap-around guideways. Large-gap maglev systems will be much more tolerant of earth displacements (e.g., from earthquakes) than HSR. Maglev's noncontact propulsion and braking render it less susceptible to snow, ice, and rain, and elevated guideways are less prone to snow drifting than at-grade railroads. And, as noted, maglev requires less maintenance than HSR to achieve its normal high-speed capability. Maglev should be capable of achieving HSR's outstanding safety record. Its greater tolerance of earthquakes and adverse weather may well be decisive advantages in availability and cost in the demanding U.S. environment.

Modest land requirements

As with HSR, maglev's narrow vehicles permit very modest station sizes. This contrasts strongly with air travel, where land requirement has become a major limit to airport expansion. Between stations, dual maglev guideways require only about 15 m of right-of-way width. Furthermore, elevated guideways can be located along existing rail and highway rights-of-way to bring maglev vehicles directly into inner-city terminals. These features will help maglev offer much lower access times and better intermodal connections compared with air. They also ease concerns over land acquisition issues.

Maglev guideways offer the flexibility of being at-grade or elevated. In areas where land-use issues are important, this flexibility is a significant advantage. For example, elevated guideways may be essential in constricted urban areas, and elevated guideways would minimally disrupt agricultural and other current land uses along rural routes. By comparison, HSR loses its principal advantage, lower capital cost, if elevated viaducts are necessary.

Low operating costs

Maglev's low energy consumption, low-maintenance potential, and fully automated operation combine to offer a potential for extremely low operating costs. Operators should have little difficulty covering such low costs and a portion of capital costs.

Also, while maglev's guideways require substantial initial investment, they offer enormous capacity. Operators can set low incremental ticket prices that will nevertheless exceed incremental costs. This can lead to very large passenger volumes, helping to justify the original capital investment, and making the system attractive in the long term.

Low magnetic fields

All four U.S. maglev concepts and TR07 achieve static magnetic fields in passenger seating areas less than 1 G (about twice the Earth's field). They do this through various combinations of magnet grouping and passive–active shielding. Indeed, the U.S. concepts demonstrate the benefit of dealing with such issues early in conceptual design: all four concepts incurred very little cost or weight penalty to achieve a 1-G limit. Through good design, maglev can achieve fields much lower than those measured on some existing transit vehicles.

Lower noise

Unlike aircraft, maglev and HSR can control their noise emissions near terminals by departing slowly. This is an important advantage that helps permit use of urban terminals. Furthermore, maglev is quieter than HSR by eliminating wheel–rail contact and pantograph–catenary contact. These noise sources predominate at low speeds, and their absence gives maglev a significant performance advantage in urban areas. For example, to meet a noise restriction of 80 dBA, a maglev vehicle should be able to travel at 50 m/s (112 mph) compared with 40 m/s (89 mph) for a quiet HSR train. This speed advantage will yield reduced trip times along noise-limited routes (i.e., most urban areas).

Even at high speeds, maglev is significantly quieter than HSR. For example, at 83 m/s (185 mph), maglev is 5–7 dBA quieter than HSR. This is a significant reduction in noise emissions that will be beneficial along quiet, rural routes.

Mission flexibility

HSR is best suited to short and intermediate intercity trunk service. TGV's fixed-consist, nontilting trains, lower cruise speed, and lower overall acceleration–deceleration render it less well suited to meet other missions or transportation needs. This lack of flexibility ultimately limits the market penetration and profitability of HSR.

Besides offering superior intercity trunk service, maglev concepts (particularly U.S. concepts) show considerable potential for additional uses. This potential derives from the great performance capability of the technology, although flexibility to serve other missions should be considered at the design stage.

Mission flexibility helps to reduce the risk that intercity trunk service is not where the greatest high-speed ground transportation (HSGT) market lies. Also, by offering other services (regional airport connector, commuter trunk, point-point, long-haul trunk), maglev increases its overall ridership potential as a major transportation network. This provides some confidence that an investment in maglev will fulfill a broad spectrum of U.S. transportation needs.

Opportunities for U.S. maglev

The SCD concepts offer numerous performance improvements over TR07. Some of these are concept-specific, while others result from generic improvements that target needs of the U.S. market and environment.

Performance efficiency

Comparison of TR07 with U.S. maglev concepts revealed two important findings: U.S. maglev can offer slightly better performance than TR07 at much lower cost (especially for at-grade sections), and U.S. maglev can offer much better performance than TR07 at similar cost.

For example, the Grumman system offers 9% lower SST trip time and 9% lower energy intensity for about 12% lower elevated-guideway cost (or 37% lower at-grade guideway cost) compared with TR07. Similarly, the Bechtel concept offers a 14% SST trip-time savings for about 2% higher elevated-guideway cost (or 20% lower at-grade guideway cost).

While these are specific SCD concepts, they illustrate the potential performance and cost advantages likely to result from a U.S. maglev development effort. They also suggest some flexibility in the selection of system characteristics to optimize performance and cost for U.S. market conditions.

Suitability to existing rights-of-way

Based on the SCD concepts, a generic U.S. maglev system will be much better suited than TR07 to deployment along existing rights-of-way (ROW). A U.S. system will require about half the curve radius of TR07 at 134 m/s (300 mph); it will climb five-times steeper grades at full speed; and, from a stop, it will reach 134 m/s in about half the time. These characteristics mean that a U.S. maglev system will achieve much shorter trip times along existing, lower-speed rights-of-way. For example, 18 minutes of Bechtel's 21-minute SST trip-time advantage over TR07 occurs in the first, twisty segment that represents an Interstate Highway ROW.

In principle, Transrapid could upgrade TR07 with a tilting vehicle body and a larger LSM. However, the former would require a major redesign of the vehicle, an increase in roll stiffness of the magnetic suspension, and use of stronger curved guideway beams. Upgrading the LSM may prove more difficult because stator slot width limits the diameter (and hence the current capacity) of the stator windings. While these improvements are possible, they would not be possible without significant R&D (research and development) time, costs, and risks.

Energy efficiency

Compared with TR07, the average energy intensity of the two most efficient U.S. concepts is 18% lower at steady cruise and 12% lower for the SST. Interestingly, these same two concepts complete the SST in about 11% less time than TR07. It appears that U.S. maglev may offer superior performance for less energy, an impressive combination.

Several factors account for U.S. maglev's superior trip times and energy efficiency. The most important is the provision of vehicle tilting. Tilting allows a vehicle to maintain good ride comfort at higher speeds through turns. This reduces trip time directly and reduces the energy needed to accelerate the vehicle to cruise speed following the turn. The effect is most pronounced along twisty routes (e.g., typical Interstate ROW). U.S. maglev concepts are also lighter than TR07, which further helps to reduce both trip times and energy consumption.

Another important factor affecting trip time and energy consumption is the aerodynamic drag acting on the vehicle. TR07's aerodynamic drag coefficients are well established and are comparable to those of high-speed trains. Some SCD contractors, however, selected lower drag coefficients that anticipate drag-reduction efforts expected in a U.S. maglev development program. Nevertheless, one of the two most energy-efficient concepts (Foster-Miller's) has drag coefficients similar to TR07's. Its aerodynamic drag is a bit lower because of its lower frontal area. Foster-Miller's higher energy efficiency is also attributable in part to its more efficient motor. Improvements in aerodynamic drag and motor efficiency are reasonable to expect under a comprehensive U.S. maglev development program. Such improvements, combined with lighter, tilting vehicles, would indeed provide U.S. maglev with superior energy efficiency and lower trip times compared with TR07.

High vehicle efficiency

All SCD vehicles use modern aerospace construction techniques, and two of the four use advanced composite construction. Superconducting magnets also have greater lift:magnet-weight ratios than TR07's normal electromagnets and do not require heavy back-up batteries to ensure safe hover. Thus, despite their tilting capability, U.S. maglev vehicles are lighter than TR07. On average, the SCD vehicles are 18% lighter per passenger than TR07, and the composite vehicles average

24% less mass per passenger (values calculated using 0.80 m^2 of cabin area as a standard passenger). Composites also offer superior fatigue and corrosion resistance relative to aluminum construction.

Lower vehicle mass improves energy efficiency and lowers guideway costs by reducing vehicle loads. Although composite construction currently carries a capital-cost premium, system life-cycle costs may favor its use. Also, further developments in the aerospace industry should reduce the cost of composite vehicles. The U.S. aerospace industry leads the world in composite aircraft construction; it is thus reasonable to expect that U.S. maglev vehicles will benefit from this expertise.

Large-gap, active vehicle suspensions

Three of the four SCDs possess active vehicle suspensions. Coupled with a large gap, an active suspension can maintain a safe, smooth ride over very flexible and rough guideways. This allows use of, respectively, less structural material and less stringent construction tolerances, reducing guideway costs.

Maglev's large magnetic forces make active control of the primary suspension an attractive option; Grumman selected this approach. Bechtel and Magneplane chose to use active control of aerodynamic surfaces. All three concepts have sufficiently large gaps to realize guideway cost reductions resulting from active suspensions. While TR07 also has an active suspension, it must use a small gap and thus requires a very stiff, well aligned, and expensive guideway.

Electromagnetic switches

Foster-Miller and Magneplane proposed electromagnetic (EM) switches as their high-speed switches, and Betchel investigated an EM switch as an alternate concept. Relative to TR07's bending-beam switch, EM switches offer much shorter cycle times, no moving structural members, less maintenance, and lower susceptibility to snow, ice, and dust. Additionally, Foster-Miller's and Magneplane's vehicles both retain their tilt capability in the turnout direction. This permits higher exit speeds than is possible with TR07 for a given switch length.

Higher speed potential

GMSA motor and suspension analyses showed that TR07 is near its speed limit at 134 m/s (300 mph). To meet levitation requirements, TR07's LSM has a shorter pole pitch than the SCD concepts. It thus operates at a higher frequency (255 Hz compared with less than 100 Hz for the SCD concepts). This increases performance demands on converter-station power electronics. As noted, stator slot width also limits the LSM current and hence peak thrust. Altering these parameters would entail a major redesign of TR07's motor and levitation systems.

Despite very tight guideway tolerances, TR07's suspension appears to be near its ride-comfort and safety limits at 134 m/s. Power transfer to the vehicle, saturation of the levitation magnets, and the use of a passive secondary suspension provide a second set of limits to the speed potential of TR07.

The U.S. concepts, by comparison, are much farther from their ultimate speed limits at 134 m/s than is TR07. They use lower frequency LSMs and have greater freedom in stator conductor sizing. They also require much less onboard power. Furthermore, several concepts have adopted active suspensions to maintain adequate safety and ride comfort over rougher, more flexible guideways than TR07's; if these concepts used guideways built to TR07's tolerances, their suspensions could handle much higher speeds.

Innovations

Large-gap EMS

A major concern about TR07's suitability for the U.S. environment is its small, 8-mm suspension gap. To achieve adequate ride comfort and safety margin, TR07's guideway must be very stiff and well aligned. These requirements increase the guideway's cost and its susceptibility to foundation settlement, earthquake movement, thermal expansion, and ice accretion.

Grumman uses iron core, superconducting magnets to increase the suspension gap of its EDS concept to 40 mm. It actively controls this gap with normal electromagnets (for high-frequency disturbances) and by slowly varying currents in the superconducting magnets. The vehicle requires no secondary suspension, and it maintains adequate ride comfort and safety over irregularities many times larger than TR07's limits. This suspension also simplifies hardware requirements by using the same magnets and reaction rails to provide all lift and guidance forces. Overall, these improvements should simplify guideway design and construction, lower guideway costs, and reduce susceptibility to environmental disturbances.

Locally commutated linear synchronous motor (LCLSM)

Foster-Miller's LCLSM energizes discrete guideway coils through individual inverters to propel a maglev vehicle. A computer controls the current and synthesizes a three-phase wave form through each set of coils using pulse-width modulation of a DC supply voltage.

The LCLSM could become a very significant innovation in vehicle propulsion. Its advantages include very high overall efficiency (91% as seen at electrical supply), significant capability to operate in a degraded mode, very flexible vehicle control, and use of the same coils for power transfer.

Its principal risk is that the IGBT-based inverters are at present too expensive for the LCLSM to be economical. Foster-Miller has argued that the large number of inverters needed (about 2400 per kilometer of dual guideway) will enable mass production to reduce their cost by a factor of 10. Experience with other semiconductor products suggests that this cost reduction may be possible.

Spine-girder dual guideway

Grumman has proposed an innovative dual guideway concept called a spine girder. A central structural "spine" girder carries, on outriggers, a narrow EMS guideway along each side. Government cost estimates confirm that this is a very efficient structure in terms of performance and cost. Indeed, it is responsible for Grumman's 10% cost advantage over TR07's guideway (also an EMS concept).

Power transfer

Both Magneplane and Grumman developed concepts that use the LSM stator winding as an inductive linear generator to transfer auxiliary power from the wayside to the vehicle. Foster-Miller's concept for power transfer uses its LCLSM. These innovations offer potential for noncontact power transfer to high-speed maglev vehicles sufficient for all onboard needs.

Cable-in-conduit superconducting magnets

To date EDS maglev vehicles have used niobium-titanium (NbTi) superconductors immersed in liquid helium near its boiling point of 4.2 K. This cooling scheme places tremendous demands on its refrigerator and can also result in "flashing" or evaporation of the sloshing liquid as the vehicle moves.

Two of the SCD concepts use cable-in-conduit magnets. This approach offers a higher operating temperature by using niobium-tin (Nb_3Sn) superconductors with supercritical helium as the coolant. Each cable consists of many wires of Nb_3Sn conductor contained in a tube that is then wound to form the magnet. Supercritical helium is circulated through the tube to cool the superconductor. A coolant temperature about 8 K is adequate, resulting in much less refrigeration power. Also, the coolant is a single phase, so there is no danger of flashing. Such magnets appear well suited for use in maglev vehicles compared with existing NbTi magnets.

Fiber-reinforced plastic (FRP)

Bechtel and Foster-Miller have sufficiently high magnetic fields in portions of their concrete guideway beams that they may not be able to use conventional steel reinforcing rods. Thus, they have both proposed using FRP rods. Bechtel has also proposed a bending-beam switch constructed entirely of FRP.

Although well established as an aerospace structural material, FRPs have not significantly penetrated civil construction. However, they possess many potential advantages over steel reinforcing, including high strength vs. weight, good corrosion resistance, and high failure stress. Many researchers expect that FRPs will eventually be commonplace in civil structures. Maglev may well prove to be the first broad construction use of these materials.

Despite their higher cost, FRPs do not pose a significant overall capital cost penalty on guideways employing them. Because they are new, however, FRPs have unknown durability for long-life civil structures (typically 50 years). The effects of long-term, cyclic loading on the attachments for post-tensioning rods are particularly difficult to predict. This durability risk is critical for concepts that must employ FRP, and research is currently underway to address it.

High efficiency EDS

At cruise speed, Bechtel's ladder EDS concept achieves a magnetic lift:drag ratio greater than 100, and Foster-Miller's coil EDS approach has a magnetic lift:drag over 170. These are very efficient EDS suspensions. Their benefits include low energy consumption, high payload:weight ratio, and low liftoff and landing speeds. Indeed, Bechtel's 10-m/s liftoff speed could allow it to use vertical motor thrust to support its vehicle into and out of stations (it would use air bearings only for emergencies). Essentially, high-efficiency EDS suspensions offer similar low-speed support and low energy consumption to EMS concepts.

Cryosystems

To date, EDS maglev vehicles have used niobium-titanium (NbTi) superconductors immersed in liquid helium, with cryogenic refrigerators reliquefying the helium vapor. Such refrigerators consume significant power and are considered the least reliable component in the maglev suspension. All four SCD concepts have avoided using this approach.

The two concepts using liquid-helium baths (Foster-Miller and Grumman) recompress the helium vapor and store it, rather than reliquefying it. They replenish the required liquid helium as a daily maintenance operation. This avoids need for an energy-intensive, unreliable onboard refrigerator; stationary reliquefaction is more efficient and reliable.

The other two SCD concepts, Bechtel and Magneplane, use cable-in-conduit superconductors. These Nb_3Sn superconductors operate at 6–8 K with supercritical helium as the coolant. Bechtel proposes to use an isochoric (constant volume) sys-

tem. It accepts daily charges of liquid helium into a sealed reservoir and magnet loop; as the coolant warms up, it pressurizes the loop but retains sufficient heat capacity for the day's cooling needs. Magneplane uses a cryorefrigerator to keep its supercritical helium in the working temperature range. However, the energy required to do so is much less than that needed to reliquefy the helium, and the refrigerator needed is much more reliable.

Air bearings

Bechtel and Magneplane proposed using air bearings for low-speed support rather than wheels. Such bearing have been used for very low speed (less than 5 m/s) support of freight pallets. The vehicles are supported by a thin air film trapped between the vehicle and the guideway. Relatively low flow rates are needed, so equipment and power requirements are very modest. Air bearings offer a potential for lower weight, cost, and stresses vs. conventional wheels. However, they will require some development for application at the higher speeds (10–50 m/s [22–112 mph]) needed to support these maglev vehicles.

OVERALL CONCLUSIONS

The GMSA's main goal was to assess the technical viability of maglev in the U.S. We examined in detail the NMI's four contracted SCD concepts and compared their performance potential with that of TGV and TR07.

We found that all maglev concepts studied are potentially technically feasible. As expected, verification of the feasibility and practicality of some features clearly requires further work.

All five maglev concepts studied offer much greater performance potential than TGV. Maglev offers higher speed, better acceleration and performance in curves, and potentially lower maintenance and higher availability for comparable safety.

The four U.S. concepts also offer a performance advantage over TR07, and they could do so for similar or lower cost.

Further development will likely improve the performance of both TGV and TR07. However, such development work will necessarily entail additional time and cost.

Technical Assessment of Maglev System Concepts
Final Report by the Government Maglev System Assessment Team

JAMES H. LEVER, EDITOR

CHAPTER 1. INTRODUCTION

1.1 MAGLEV DEVELOPMENT HISTORY

Magnetic levitation (or maglev) uses magnetic forces to lift, guide, and propel vehicles. Both attractive and repulsive magnetic forces may be used, and many maglev concepts have been developed using various lift, guidance, and propulsion schemes.

In the early part of the 20th century, Emile Bachelet conceived of a magnetic suspension utilizing repulsive forces generated by alternating currents. Bachelet's concept required impractical amounts of power for conventional conductors, however. It remained dormant until the 1960s, when superconducting magnets became available. At that point, practical development of repulsive-mode magnetically levitated transportation systems began.

In the early 1920s, work by Hermann Kemper in Germany pioneered attractive-mode maglev. Kemper pursued this concept through the 1930s and 40s and established the basic design for practical, attractive-mode maglev in a 1953 paper. During the 1970s, German interest in developing a maglev transportation system eventually focused on an attractive-mode magnetic suspension.

Maglev development in the U.S. began in earnest as a result of the High-Speed Ground Transportation (HSGT) Act. This act authorized Federal funding for HSGT research projects, including those involving magnetic levitation. This government stimulus enabled U.S. investigators to jump to an early lead over their foreign counterparts in maglev research; for example, Americans pioneered the concept of superconducting magnetic levitation and dominated the early experimental work in this area.

As early as 1963, James Powell (1963) and Gordon Danby of Brookhaven National Laboratory recognized that superconductivity could overcome the power limitations in Bachelet's concept. In 1966 the two researchers (Powell and Danby 1966) presented their maglev concept of using superconducting magnets in a vehicle and discrete coils on a guideway. Rapid passage of the magnets over the conducting coils generates currents in the coils; these currents in turn establish magnetic fields of the same polarity as the imposed fields. The resulting repulsive forces are sufficient to lift and guide passenger-carrying vehicles, provided powerful (i.e., superconducting) magnets are used. This technique became known as an electrodynamic suspension (EDS) system. Their subsequent design improvement, known as the "null-flux" system (Powell and Danby 1967), was eventually adopted by the Japanese for use in the only high-speed superconducting maglev system in operation today. The presence of powerful magnets aboard the vehicles also makes practical the use of an air-core linear synchronous motor (LSM) for propulsion.

Subsequently, researchers from Stanford Research Institute (SRI) (Barbee et al. 1969), Atomics International (Guderjahn et al. 1969), and

Sandia Corporation (Guderjahn et al. 1969) developed a continuous-sheet guideway (CSG) concept. This EDS concept also used superconducting magnets aboard a vehicle. Here, the moving magnetic fields of the vehicle magnets induce currents in a continuous sheet of conducting material such as aluminum. CSG tests involving "rotating drum" simulations and test guideways up to 150 m long continued through the early 1970s at SRI, at Ford Motor Company (Reitz 1970), General Motors Corporation (Dukowicz et al. 1973), and MIT (Kolm and Thornton 1972). During this period, a locally commutated linear motor was invented at GM, and the original "Magneplane" was invented at MIT. The latter CGS concept underwent model testing at $1/25^{th}$ scale, eventually operating at speeds as high as 27 m/s.

Other significant U.S. maglev work during the early 1970s included development by Rohr Corporation of its ROMAG people-mover demonstration vehicle. In this system, normally conducting electromagnets generated attractive forces between the vehicle and ferromagnetic material in the guideway. This is termed an electromagnetic suspension (EMS) system. Unlike EDS, an EMS is statically unstable; a control system must vary the currents in the electromagnets to maintain proper clearance between the vehicle and the guideway. This technology was later transferred to the Boeing Company and ultimately licensed by Carnegie-Mellon University.

Maglev research in the U.S. came to a standstill in 1975 owing to an abrupt halt in government funding of HSGT research and a slowdown in the growth of U.S. transportation demands.

Maglev transportation research outside of the U.S. has been dominated by the Japanese and Germans. The Japanese began on a relatively modest level in the early 1960s. By 1970, Japanese efforts, under the sponsorship of the Japanese National Railway (JNR), had significantly expanded. At the same time, research in West Germany began and quickly grew. The Japanese were successfully levitating a demonstration vehicle in 1972 and constructing a large-scale test track in 1974. In West Germany, proof-of-concept test vehicles were operating as early as 1970 under two government sponsored maglev research programs. When U.S. Government funding of HSGT ended in 1975, high-speed rail and maglev research in Japan and West Germany continued to expand. Considerable progress toward commercial maglev transportation was made by both countries during the late 1970s and 1980s (Wyczalek 1990).

The Japanese have pursued two distinct maglev concepts: one (MLU series) employs an EDS while the other (HSST series [high-speed surface transportation]) employs an EMS. The MLU series full-scale prototypes have achieved speeds of 139 m/s, while HSST series prototypes have traveled as fast as 83 m/s. German research, in the meantime, has culminated in the development of a single EMS concept known as the Transrapid system (TR series). The latest full-scale version of the Transrapid vehicle and guideway (TR07) has been in operation for several years at a test track in Emsland, Germany. The TR07, with a projected maximum speed of 139 m/s, is the only maglev system in the world that is immediately available for commercial service. It is currently competing against high-speed rail systems for ground transportation projects in the U.S.

In 1988, owing to a renewed desire for a national HSGT capability, the U.S. Congress investigated the possibility of reviving maglev research and development. Studies revealed that maglev was attractive as a means of relieving the congestion and delays in our ground- and air-transport systems (Johnson et al. 1989, Grumman Corp. 1989a,b). The transportation "niche" envisioned for maglev was generally 160- to 960-km (100- to 600-mile) trips, where the personal car is too slow and uncomfortable, and the commercial airplane is too inefficient. A maglev technical advisory committee, made up of representatives from a wide range of government and private transportation organizations, reviewed the situation and reported to Congress in June of 1989. It recommended that the U.S. develop and demonstrate a second-generation maglev concept utilizing superconducting technology that will be usable along the Interstate Highway network, and well suited to U.S. weather conditions (Grumman Corp. 1989a, b). Congress responded by authorizing the formation in 1990 of the National Maglev Initiative (NMI) (USACE 1990).

1.2 ROLE OF THE NATIONAL MAGLEV INITIATIVE

Maglev makes possible high-speed, high-capacity travel with potentially low operating costs and convenient access. Yet, despite these attributes, U.S. firms have been reluctant to invest in the technology. Maglev's development risks, large capital cost, and uncertain market response are likely reasons for this reluctance.

To determine whether it should actively

encourage maglev investment, the Federal Government organized the National Maglev Initiative (NMI). The NMI's principal tasks were to assess the technical and economic viability of maglev in the U.S. and to recommend the most appropriate Federal role for its development and implementation.

The NMI executed these tasks within a three-phase strategic plan:

- Phase I—Planning and coordination.
- Phase II—Assessment of technology and economics.
- Decision.
- Phase III—Development and implementation.

Phase II culminated with a report summarizing the NMI's findings (USDOTFRA 1993) and outlining possible implementation strategies. The work described here, technical assessment of maglev system concepts, was the primary assessment of maglev technology conducted in Phase II. Economic assessments performed in Phase II are described in the NMI's final report.

The NMI obtained maglev technical data through two sets of procurements. The first was a set of contracts exploring specific technological issues, so-called *Broad Agency Announcements* (BAA). The second consisted of four relatively larger contracts seeking conceptual definitions of maglev systems suitable for the U.S., so-called *System Concept Definitions* (SCDs). The resulting SCD reports contain quite thorough descriptions and analyses of the major subsystems, their interconnections, and the resulting performance of potential maglev systems (Bechtel 1992a,b; Foster-Miller, Inc. 1992a,b; Grumman Aerospace Corp. 1992a,b; Magneplane International, Inc. 1992a,b).

1.3 ROLE OF THE GOVERNMENT MAGLEV SYSTEM ASSESSMENT

The Government Maglev System Assessment (GMSA) team consisted of scientists and engineers from the U.S. Army Corps of Engineers (USACE), the U.S. Department of Transportation (USDOT) and the Department of Energy's Argonne National Laboratory (ANL), plus contracted transportation specialists. Its overall role was to assist the NMI with its assessment of maglev technology. The GMSA's specific tasks were as follows:

- Develop a process to evaluate the technical viability of maglev system concepts.
- Apply this evaluation process to Transrapid 07 (TR07) maglev and to TGV high-speed rail to establish comparative baselines.
- Apply this process to alternative U.S. maglev concepts.
- Assess the overall technical viability of maglev generally, and TR07 and alternative U.S. concepts specifically. Where appropriate, use TGV as a baseline to describe the performance potential of maglev in the U.S.

Insofar as possible, we sought to integrate our process for assessing maglev's technical viability with that of the NMI's process for assessing economic viability. Note also that our assessment pertained to maglev system concepts, not contractor performance. This report describes the results of our assessment of maglev's technical viability for the U.S.

1.4 DEFINITIONS OF TECHNICAL VIABILITY

As noted, the NMI was tasked to assess the technical and economic viability of maglev systems for use in the U.S. In effect, this assessment must determine whether maglev can fulfill a significant transportation role in a commercially acceptable way. Also, the NMI must consider whether a U.S. maglev system would fulfill this role better than existing foreign HSGT systems. To this end, we may group issues of maglev's technical viability into three broad categories:

- *Technical feasibility*—Will a particular system concept work as intended? This involves assessing the soundness of the physical principles and engineering sciences upon which the concept is based.
- *Mission suitability*—Given its performance characteristics, how well will such a system concept fulfill its required mission? This involves examining the concept's performance characteristics and simulating its behavior along realistic routes.
- *Relative advantage*—Do U.S.-developed concepts possess superior performance potential compared with foreign HSGT alternatives? This requires comparing U.S. concepts to foreign ones, and assessing their potential for superior performance and the attendant development risks.

We structured our evaluation process to address issues in all three categories of technical viability.

1.5 MAGLEV'S TRANSPORTATION MISSION

Several studies have identified an urgent need to improve U.S. intercity transportation. High-Speed Ground Transportation (HSGT) technologies, including maglev, appear well suited to address this need. Thus, the NMI targeted this intercity role for maglev in its SCD request for proposals (SCD-RFP, USDOTFRA [1991], sections C - 2.2 and 2.3):

> In soliciting the system concepts, the National Maglev Initiative views Maglev as an intercity transportation system which will supplement and interconnect with existing modes... Maglev systems should be safe and reliable. In the 160-km to 1000-km (100- to 600-mi-) trip range, Maglev should be competitive in terms of travel times, cost, reliability and comfort.
>
> It should be clean and energy efficient. It should provide good connections with airports and major centers. Insofar as possible, it should utilize existing highway, railroad, and utility rights-of-way. Its design should anticipate upgrade. It should be economically and financially attractive. It should be robust in terms of its susceptibility to adverse weather and its requirements for maintenance. It should efficiently handle passengers and consideration should be given to its mail and freight handling capability.

We used these statements for our basic evaluation of the "mission suitability" aspects of technical viability. However, we also recognized that maglev may address other national transportation needs, and that adaptability of concepts to those missions is also an important viability issue. Thus, we developed four additional mission statements (see section 3.4.1) and examined how well each HSGT technology fitted those missions.

1.6 EVALUATION BASELINES AND MAGLEV SYSTEM CONCEPTS

HSGT is not yet widely available in the U.S. It basically provides service in a speed range intermediate to automobiles and jet aircraft (say, 50–200 m/s). Maglev is one possible HSGT technology; high-speed rail (HSR) is another.

Several recently developed HSR systems have impressive performance characteristics and could meet many of the requirements for broad market appeal in the U.S. Indeed, the French-built TGV (train à grande vitesse) offers a proven, commercially successful 83-m/s service, and this service is available for the U.S. with essentially no development risk. In addition, its performance limits appear to be governed more by cost/benefit calculation rather than by physical constraints. Further development will undoubtedly raise these limits, albeit with some attendant costs and risks.

We adopted the view that the lack of development costs and risks is critical in the debate over the merits of HSR and maglev. Thus, we chose a commercially available HSR technology, TGV-Atlantique (TGV-A), as one of our evaluation baselines. We did not try to anticipate further performance improvements. Such improvements will undoubtedly occur, but their associated costs and risks offset TGV-A's critical advantage. On this basis, we feel that TGV-A serves as a fair baseline for comparison with maglev.

For similar reasons, we selected the German Transrapid 07 (TR07) electromagnetic maglev system as a second evaluation baseline. Transrapid has extensively tested this technology at its Emsland test facility. Although it has not yet been integrated into a commercial system, it has been proposed for use along several corridors in the U.S. Again, its critical advantage over possible U.S.-designed systems is the perceived lack of development costs and risks. However, because of its lack of system-level integration and commercial history, TR07 represents a greater risk than TGV; it also offers potentially greater performance.

The NMI's four contracted SCD's were by far the most well defined U.S. maglev concepts available to us. Each contractor produced a detailed report describing the concept's major components, the interconnection between them, analyses of component and system performance, and capital and operating cost estimates. We thus chose to examine in detail these four concepts as representative U.S. maglev systems. In over-simplified terms, they represent an updated EMS comparable to TR07 (Grumman), an updated discrete-coil EDS comparable to the Japanese MLU002 (Foster-Miller), a well known sheet-guideway EDS (Magneplane), and a new ladder-coil EDS (Bechtel).

1.7 OVERVIEW OF EVALUATION PROCESS

To assess the technical viability of maglev concepts, the GMSA developed an evaluation process consisting of four main steps:

- *Applying the SCD-RFP system criteria as assessment criteria*. We developed qualitative and quantitative cross-checks to determine whether a maglev concept met each of the criteria defined in the SCD-RFP (USDOTFRA 1991).
- *Verifying subsystem performance.* We developed numerical models to verify the performance characteristics of critical subsystems for each concept.
- *Verifying system performance.* We developed a numerical model to simulate the overall performance of each system concept. We also estimated the main technology-dependent capital costs for the maglev concepts using a standardized procedure.
- *Applying other criteria.* We developed qualitative and quantitative cross-checks to determine whether a maglev concept met performance criteria that reflect technical viability but that were not included in the SCD-RFP (USDOTFRA 1991).

These four evaluation steps generated much of the input for our overall assessment of the technical viability of maglev for the U.S. As noted, we evaluated both TGV-A and TR07 as baseline concepts and the four SCD concepts as representative U.S. maglev systems. Insofar as possible, we referenced our conclusions regarding the viability of these concepts to specific evaluation data products.

Chapter 2 of this report describes the relevant characteristics of the HSGT technologies examined. Chapter 3 describes in detail each of the four evaluation steps discussed above, and presents for each concept the resulting evaluation data products. Chapter 4 presents our specific conclusions regarding the technical viability of maglev in the U.S. It is structured to reflect the key issues in the debate over maglev's technical viability.

CHAPTER 2. CHARACTERISTICS OF SPECIFIC HSGT CONCEPTS

Sections 2.1–2.6 briefly describe each of the HSGT concepts examined. Section 2.7 summarizes their general characteristics and lists performance parameters useful for evaluations.

2.1 HIGH-SPEED RAIL—TGV*

2.1.1 Concept

The TGV (train à grande vitesse) uses steel wheels on steel rails. It is based on essentially conventional railroad vehicles, tracks, and propulsion, power distribution, and signaling and control subsystems, albeit very highly developed and made optimal for high-speed operation (83-m/s service speed). Figure 1 shows a typical trainset, its track, and overhead catenary power lines. The rolling stock is operated in fixed-consist trainsets (1-8-1 for the first-generation PSE [Paris–Sud–Est], 1-10-1 for the second-generation TGV-A [Atlantique], 1-8-1 for the third generation TGV-R [Reseau] and TGV-Bilevel); the trainsets can be operated as coupled pairs.

Figure 1. TGV–Atlantique.

2.1.2 Vehicles

All TGV trainsets have a power car on each end, followed by a transition car with one regular and one articulated truck; all other cars are articulated, sharing trucks at either end. The unpowered trucks are equipped with coil-spring primary and airbag secondary suspensions. The powered trucks have coil-spring primary and secondary suspensions. TGV-A and later trainsets are propelled by eight body-suspended 1100-kW AC synchronous rotary traction motors. The maximum axle load is limited to 17 tonnes, and the maximum unsprung mass to 2.2 tonnes/axle. Trainset seating capacity ranges between 376 (TGV-R) and 547 (TGV-Bilevel). The trainsets do not incorporate active or passive tilting.

Propulsion power and hotel power are collected from an overhead catenary through roof-mounted pantographs. The TGV fleet in SNCF (French National Railways) service carries at least two pantographs per power car, for 25 kV, 50 Hz, and 1.5 kV DC. Some trainsets are equipped for operation under three or even four different voltages. A 25-kV roof-mounted trainline is used to permit operation with only one pantograph raised. Braking on the TGV-A is by means of a combination of rheostatic, axle-mounted disc brakes (four per unpowered axle) and tread brakes (on powered axles). The TGV-R and later versions will eliminate the tread brakes in favor of disc brakes, even on the powered axles. All axles are equipped with anti-lock braking and the powered axles have anti-slip control. Top commercial speed is 83 m/s, though a modified 1-3-1 version of the TGV-A set the world wheel-on-rail speed record of 143 m/s. Sustained operation at 134 m/s on a 3.5% gradient is not possible.

2.1.3 Guideway

The basic TGV track structure is that of a conventional standard-gauge railroad, but built on an engineered support structure of granular materials selected to ensure free drainage and compacted to achieve a uniformly high track modulus. Minimum ballast depth is 30 cm. The track consists of continuously welded rail on twin-block concrete–steel ties with elastic fasteners and a 9-mm stiff rubber pad. All viaducts and bridge structures are ballast-decked and are built to span-length deflection tolerances. Alignment geometry for 83 m/s calls for 6000-m radius horizontal curves, although 4000-m radius curves are used exceptionally. Vertical curve radius at crests and troughs is 25,000 m, with 16,000 m used exceptionally at crests and 14,000 m exceptionally in troughs. Gradients of up to 3.5% are acceptable. Tunnel cross-sections range between 46 m^2 (single-track, 56 m/s) and 71 m^2 (double-track, 75 m/s).

The high-speed lines are built with full double track having bidirectional signals. Crossovers at 25-km intervals are 1:46 units, permitting 44 m/s in the diverted direction and full line speed in the

* Written by Christopher J. Boon, Canadian Institute of Guided Ground Transport.

through direction. High-speed (1:65) swing-nose turnouts permit 61 m/s in the diverted direction currently; SNCF expects to increase this to 64 m/s when concrete switch ties replace the wooden ties used in the original switch installations.

Propulsion and hotel power is supplied through a 2- × 25-kV overhead catenary system (OCS) in phase opposition. The OCS contact wire is 150 mm^2 at 5.1 m height. Substations have 220-kV single-phase supply feed with 60- to 120-MVA installed capacity.

Signaling and control is by means of full CTC (computerized train control), employing coded track circuits, track-to train voice and data links, and in-cab signals, with an automatic train protection system having speed adherence override and enforced braking.

2.1.4 Status

TGV-A has been in regular commercial service between Paris and west–southwest France since 1989. Its predecessor, TGV-Paris-Sud-Est, has been in commercial service since 1981. Both lines have been extremely popular and have experienced steady ridership increases. The French federal government and SNCF plan additional lines in France, and the technology has been deployed or proposed for commercial operation in corridors in Spain, Australia, Korea, Taiwan, Canada, and the U.S.

2.2 TRANSRAPID 07 (TR07)*

2.2.1 Concept

The TR07 has an electromagnetic suspension (EMS) system that uses separate sets of conventional iron-core magnets to generate vehicle lift and guidance by means of magnetic attraction (Fig. 2). It is capable of achieving cruising speeds of 134 m/s. Both the levitation and guidance systems have their own dedicated control systems for regulating the air gap between magnet and guideway rail. The control systems maintain the air gap at 8 mm nominally. The levitation system operates at all speeds. Propulsion is provided by a synchronous long-stator linear motor using the levitation magnets to interact with propulsion windings mounted in the stator packs on the guideway. The vehicle wraps around a T-shaped guideway, with the guidance rails mounted on the outside edges and the levitation and propulsion stator packs mounted underneath the guideway.

2.2.2 Vehicle

Transrapid 07 uses two or more vehicles in a consist, with each designed to carry 100 passengers (72 in first-class). Each vehicle is 25.5 m long, 3.92 m high, and 3.7 m wide. It is constructed of aluminum frames with sandwich shells of glass-fiber reinforced plastic panels. The reported weight is 106,000 kg per two-vehicle consist. Each TR07 vehicle in a consist is capable of independent operation and each has 32 levitation and 30 guidance magnets. The stator pack, which is

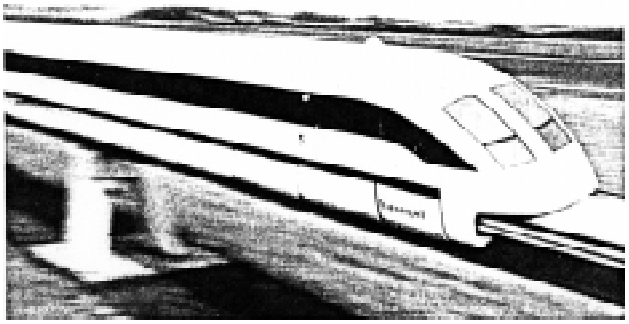

a. Exterior view.

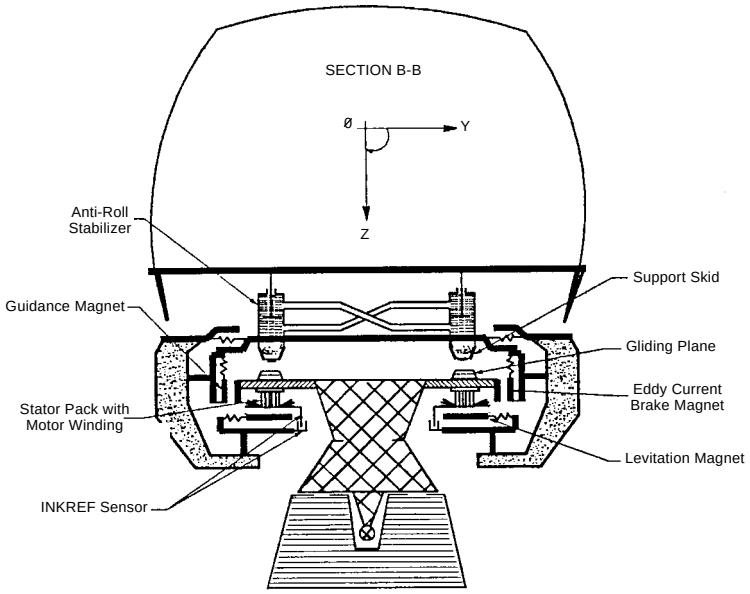

b. Cross section showing principal lift, guidance, and propulsion elements (INKREF is a displacement sensor).

Figure 2. TR07 vehicle.

* Written by Richard Armstrong and Robert Hasse, U.S. Army Engineer Division, Huntsville.

mounted on the guideway, is composed of a laminated iron core, stator winding, and attachment hardware. The stator windings are 300 mm^2, soft aluminum, with double shields and an external conductive sheath, in a three-phase configuration. The propulsion force is generated by the interaction of the vehicle magnet exciter windings and the guideway stator windings. The primary braking is regenerative, through linear motor current reversal in response to phase angle modulation. An eddy-current braking system is used only if the regenerative braking fails. On board hotel and levitation power is provided by Ni-Cd batteries at low speeds (below 28 m/s) and by linear generators at increased speeds. The power is transferred using harmonic frequencies of the LSM fields. The proposed maximum speed for the TR07 in a commercial service is 138 m/s (311 mph), with a maximum operational speed of 118 m/s (265 mph). The top speed that has been recorded at Emsland is 120 m/s (270 mph).

2.2.3 Guideway

The TR07 guideway uses beams supported by A-shaped, steel-reinforced concrete piers. The piers are supported on either spread or pile foundations, depending on the soil conditions. The Emsland test track has both steel and concrete beams, while Transrapid has proposed only the steel beams for commercial service. The concrete beam is post-tensioned over a single span and steel reinforced, having a single cell, hollow box cross-section, with slanted webs. The steel beam also has a single cell, hollow box cross-section, with slanted webs, but it is continuous over two spans and is welded out of steel plates. Both beams are constructed and erected to very tight tolerances. The stator packs are bolted to the beams. Maximum guideway superelevation (tilt or banking) is 12°. Switching is accomplished by bending a special guideway beam section, in which the continuous steel beam is fixed at one end and laterally bent to the proper alignment by eight actuators.

Electrical power is distributed along the guideway at 110 kV, 50 Hz to wayside power conditioning stations. There are two 5–6 MW, variable-frequency–variable-voltage power conditioning units operating in parallel to power the guideway.

2.2.4 Status

TR07 is a proven technology that is currently undergoing performance testing at Transrapid's Emsland test facility. It has yet to be deployed commercially, although it has been proposed for commercial operation along several European and U.S. corridors. The GSMA's (1992) *Transrapid TR07 Baseline Report* contains a more thorough description of this technology.

2.3 BECHTEL*

2.3.1 Concept

The Bechtel concept is a novel, flux-canceling electrodynamic suspension (EDS) system. The vehicle contains six sets of eight superconducting magnets per side. It straddles a concrete box-beam guideway. Interaction between the vehicle magnets and a laminated aluminum ladder on each guideway sidewall generates lift. Similar interaction with null-flux coils mounted on the guideway provides guidance. LSM propulsion windings, also attached to the guideway sidewalls, interact with these same vehicle magnets to produce thrust. Figure 3 shows the overall layout of Bechtel's concept.

2.3.2 Vehicle

The baseline vehicle consists of a single 106- to 120-passenger car. The 106-passenger vehicle provides 90 coach seats with six abreast seating and 16 first-class seats with four abreast seating. The 120-passenger vehicle has only coach seats. The Bechtel vehicle uses aerodynamic control surfaces to augment magnetic guidance and damping forces. When it is not levitating (at low speeds or in emergencies), the vehicle operates on air-bearing pads. By incorporating special lift coils in the guideway, the vehicle may liftoff at zero speed. Two methanol-powered fuel cells provide a total of 186 kW of onboard power.

The vehicle is constructed with an outer aluminum shell and an inner shell made of composite material. The intent of this construction is to enable tilting of the inner shell while maintaining a smooth aerodynamic outer surface. The vehicle can tilt to 15°.

2.3.3 Guideway

The baseline guideway consists of single-span, post-tensioned concrete box beams supported on concrete piers with 25-m spacing. The laminated aluminum suspension ladder, null-flux guidance coils, and six-phase LSM windings are all compactly mounted on the upper portion of each

* Written by Dr. John Potter, U.S. Army Engineer Division, Huntsville.

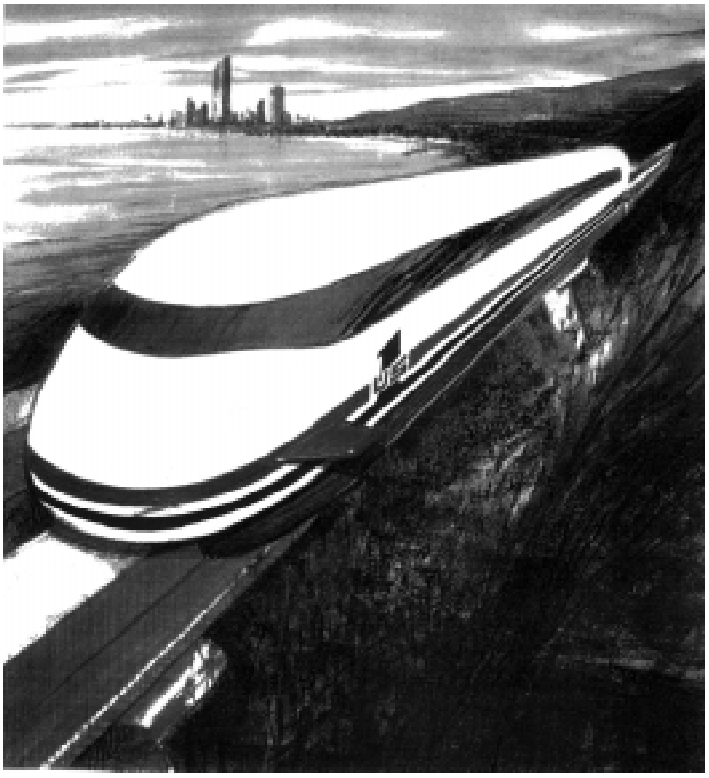

a. Exterior view.

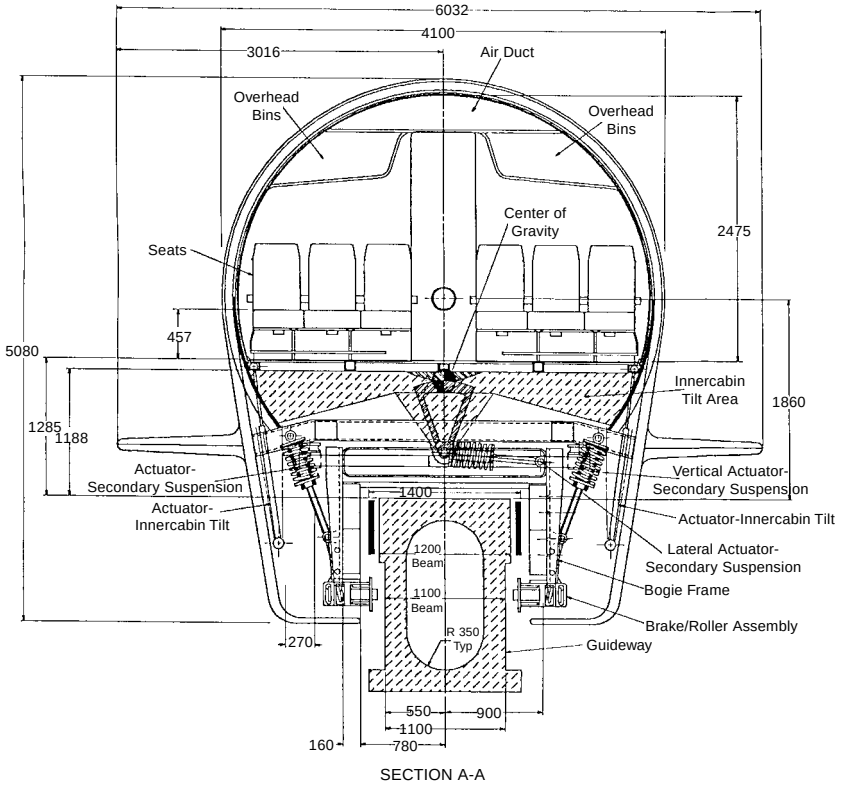

b. Cross section.

Figure 3. Bechtel vehicle on box-shaped guideway (dimensions in mm).

guideway sidewall; this assembly is then enclosed with a cover plate. The critical gap for this concept is the 50-mm horizontal gap between the superconducting coils and the cover plate. Because of high magnetic fields, the concept calls for nonmagnetic, FRP reinforcing rods in the upper portion of the box beam. Guideway superelevation of up to 15° is planned. The concept's baseline switch is a bendable beam constructed of FRP.

The guideway mounted propulsion coils are conventionally constructed and configured as a six-phase system. DC power is distributed along the guideway at 24 kV to frequency converters located near the guideway. The typical zone length for a frequency converter is 4000 m and an LSM blocklength is 2000 m.

2.3.4 Status

This concept is one of the four NMI-contracted SCDs. These contracts did not call for proof-of-concept or subsystem tests and none had been conducted prior to this work.

2.4 FOSTER-MILLER*

2.4.1 Concept

The Foster-Miller concept is an EDS generally similar to the Japanese MLU002. Superconducting magnets in the vehicle generate lift by interacting with null-flux levitation coils located in the sidewalls of a U-shaped guideway; similar interaction with series-coupled propulsion coils provides null-flux guidance. Its innovative propulsion scheme is called a locally commutated linear synchronous motor (LCLSM). Individual H-bridge inverters sequentially energize propulsion coils as they line up with the vehicle magnets.

* Written by Frank L. Raposa, Consulting Engineer.

a. Exterior view.

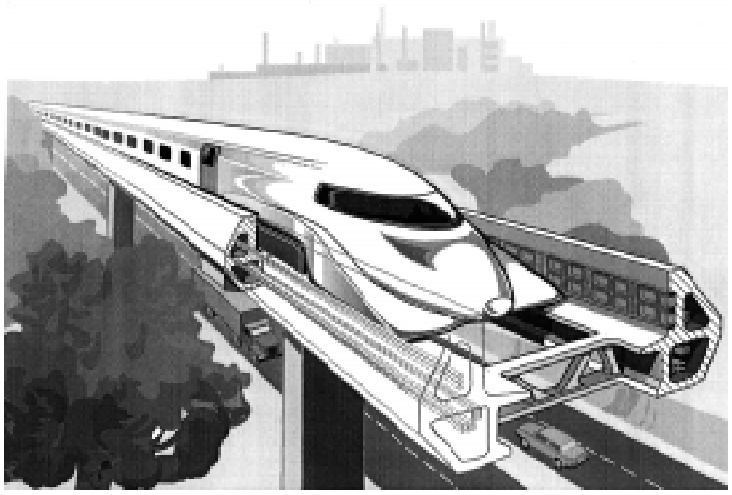

b. Cross section.

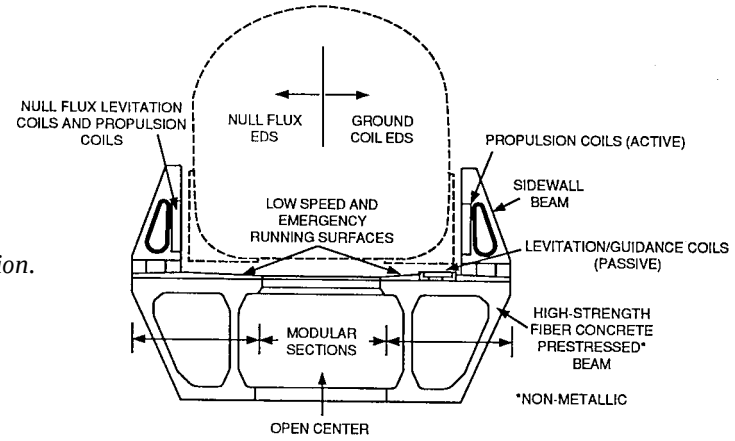

Figure 4. Foster-Miller vehicle in U-shaped guideway.

These inverters synthesize a waveform that moves down the guideway, synchronously with the vehicle. Figure 4 shows the overall layout of Foster-Miller's concept.

2.4.2 Vehicle

The baseline vehicle consists of two 75-passenger modules with attached nose and tail sections. Smaller or larger vehicles can be made up by incorporating fewer or additional passenger modules. These modules have magnet bogies at each end, containing four magnets per side, that they share with adjacent cars. The port and starboard superconducting magnets are series-connected electrically to provide balanced guidance in the event of a magnet quench (catastrophic loss of superconductivity). To reduce exposure to magnetic fields, there are no passenger seats over the bogies.

The vehicles are made of lightweight composite materials with five across seating. The vehicles have 12° tilting capability.

2.4.3 Guideway

The U-shaped guideway consists of two parallel, post-tensioned concrete beams joined transversely by precast concrete diaphragms. The baseline guideway uses two-span assemblies of such beams supported at 27-m intervals. Each beam has an integral sidewall that carries the null-flux levitation coils and the propulsion coils. Because of high magnetic fields, the upper post-tensioning rods are FRP. The space between the beams is open to allow direct runoff of rain, snow, and debris. Guideway superelevation may be up to 16°. The baseline high-speed switch uses switched null-flux coils to guide the vehicle through a vertical turnout. It requires no moving structural members.

The propulsion coils are located in the sidewall behind the levitation coils. Each sidewall coil is electrically connected in series to a corresponding coil on the opposite sidewall. The superconducting coils on each side of the bogie interact with the connected sidewall propulsion coils to provide guidance. The design air gap for guidance is 100 mm and the system is designed to be very stiff.

The sidewall propulsion coils do not overlap and are individually switched from H-bridge inverters. Each is controlled by its own H-bridge that is adjacent to its coil. As mentioned the system is called the LCLSM. The LCLSM will energize the propulsion coils as they become lined up with the superconducting magnets mounted on the bogies. The H-bridge inverters synthesize a three-phase waveform that moves down the guideway in synchrony with the vehicle.

The LCLSM coils that are located between the bogies also operate as the high-frequency primary of an air-core transformer. This method of operation is also produced by the H-bridge inverters. The LCLSM coils interact with adjacent coils on the vehicle to transfer power to the vehicle inductively for onboard electrical loads.

2.4.4 Status

This concept is one of the four NMI-contracted SCDs. Although the contractor conducted no proof-of-concept tests, the Japanese MLU002 is similar (superconducting EDS with U-shaped guideway and vertical null-flux levitation). Because the Japanese have conducted extensive tests and development work on the MLU002, it must be viewed as a proven concept (although not yet a commercial product). However, a significant departure of the Foster-Miller concept from the MLU002 is the LCLSM; this propulsion scheme is as yet unproven.

2.5 GRUMMAN*

2.5.1 Concept

The Grumman concept is an EMS with similarities to Transrapid 07. However, Grumman's vehicles wrap around a Y-shaped guideway (as opposed to the TR07's T-shaped guideway) and use just one set of vehicle magnets and guideway rails for levitation, guidance, and propulsion (Fig. 5). The vehicle magnets are superconducting coils around Vanadium-Permendur iron cores that are horseshoe shaped. The horseshoe legs are attracted to iron rails on the underside of the guideway. Normal coils on each iron-core leg modulate levitation and guidance forces to maintain a large (40-mm) air gap. Propulsion is by conventional LSM embedded in the guideway rail.

2.5.2 Vehicle

The baseline consist is a two-vehicle configuration for 100 passengers; it can be shortened to a single 50-passenger vehicle or lengthened to a 150-passenger, three-vehicle consist. Passengers are seated in two groups of ten rows of two-by-

* Written by Dr. John Potter, U.S. Army Engineer Division, Huntsville.

a. Exterior view.

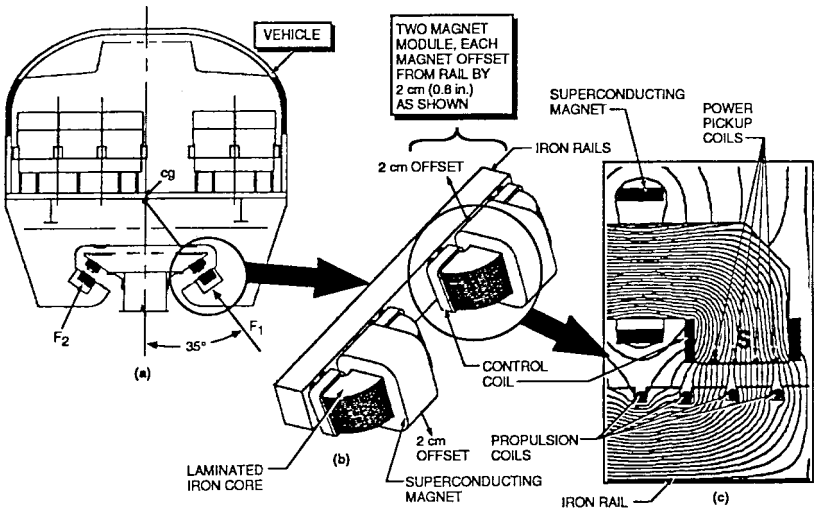

b. Levitation, propulsion, and guidance system.

Figure 5. Grumman vehicle.

three. The vehicles are made of lightweight composite materials.

The vehicle body is attached to the chassis by tilting mechanisms that provide for up to 9° of body tilt. Each chassis provides the secondary suspension and mounting for two pairs of magnets on each side and actuators for lateral magnet movement for guideway clearance in curves. The magnets are alternately offset 1.5 cm to the left and right of the guideway rail to provide roll control. Normal coils on each of the iron-core legs modulate levitation and guidance forces while keeping the superconducting magnets operating at nearly constant current.

Each magnet consists of 1020 turns of NbTi conductor carrying 53 A (for 54 kAT) at 4.5 K. The cryostats are mostly aluminum, with reservoirs for both liquid helium and liquid nitrogen. N_2 vapor is vented, while He vapor is compressed and stored for later reliquefaction at a fixed plant.

Onboard power is provided by conventional inductive coils mounted on the ends (or faces) of the magnet cores. This system provides up to 170 kW per car using a combination of slot harmonics and high-frequency current injected into the LSM.

2.5.3 Guideway

The innovative guideway superstructure consists of slender Y-shaped guideway sections (one for each direction) mounted by outriggers every 4.5 m to a 27-m main beam or "spine girder." The structural spine girder serves both directions and is in turn supported by conventional piers on piled or spread footings (as foundation conditions dictate). Maximum guideway superelevation is 15°.

Switching is accomplished with a TR07-style bending guideway beam, except that the Grumman bending section is complemented by a slid-

ing or rotating, elongated frog section that allows for a shorter length of bending guideway. Propulsion is by conventional, three-phase LSM embedded in the guideway rail in 500-m blocks.

2.5.4. Status

This concept is one of the four NMI-contracted SCDs. Although the contractor conducted no proof-of-concept tests, the concept is similar to the well-tested Transrapid 07 (EDS levitation and guidance, conventional LSM, bending-beam switch). However, Grumman's use of a single set of magnets and reaction rails for levitation and guidance, and its use of superconducting magnets to achieve a larger suspension gap, are essentially unproven innovations.

2.6 MAGNEPLANE*

2.6.1 Concept

The Magneplane concept is a single-vehicle EDS system using a trough-shaped, 0.2-m-thick aluminum guideway for sheet levitation and guidance (Fig. 6). Centrifugal force rotates the vehicle (or "Magplane") in the trough for coordinated banking in curves. No additional tilting suspension is required even for 45° bank angles. Superconducting levitation and propulsion magnets are grouped at the front and rear of the vehicle The centerline magnets interact with conventional LSM windings and also generate some electromagnetic guidance force (called the keel effect). The magnets on the sides of each group react against the aluminum guideway sheets to provide levitation (at a 0.15-m gap).

2.6.2 Vehicle

The baseline vehicle is a 140-passenger "Magplane," which can be complemented by a 45-seat version. The seats are configured in 28 rows of two-by-three in a lightweight composite body.

The magnets are grouped at each end of the vehicle for cryogenic and magnetic field considerations; there is no secondary suspension or body tilting system. Vertical and horizontal control surfaces are mounted on the nose and tail of the vehicle to provide damping (especially in roll) and increased directional stability. Air bearings support the vehicle at speeds below about 40 m/s.

Each magnet group consists of six superconducting propulsion coils along the centerline and two superconducting levitation coils on each side. Each end propulsion coil is designed for 390 kAT, while the mid coils are designed for 780 kAT. Each levitation coil is sized for 252 kAT. All of the coils are Nb_3Sn cable-in-conduit-conductors, which use steel conduit to carry supercritical He for cool-

a. Exterior view.

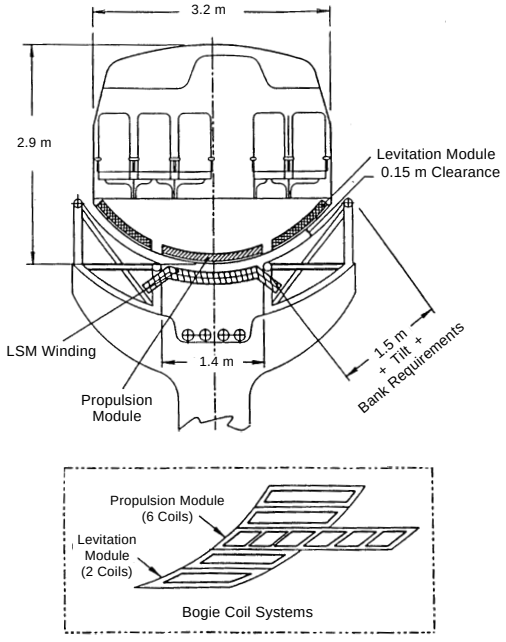

b. Vehicle cross-section and bogie coils.

Figure 6. Magneplane vehicle in aluminum guideway trough.

* Written by Dr. John Potter, U.S. Army Engineer Division, Huntsville.

ing to between 6 and 8 K. A closed-cycle onboard refrigeration system provides the recycled supercritical He at 6 K.

Onboard power (185 kW) is generated by inductive coupling to high-frequency currents injected into the LSM.

2.6.3 Guideway

The aluminum levitation sheets in the guideway trough form the tops of two aluminum box beams that support the LSM winding located in the center of the trough. These box beams are supported every 9.14 m by columns on piles or spread footings, as foundation conditions dictate.

The baseline switch uses switched null-flux coils to guide the vehicle through a fork in the guideway trough. It requires no moving structural members.

The centrally mounted LSM is a conventional, single-phase winding with 2000-m blocklengths. Through phase-angle control, the LSM also provides additional vertical damping forces to the vehicle.

2.6.4 Status

This concept is one of the four NMI-contracted SCDs. Although the contractor conducted no tests, earlier laboratory work on this concept has essentially proven the levitation, guidance, and propulsion schemes. No full-scale system or subsystem tests have yet been conducted. A Magneplane consortium has proposed the concept for a commercial route in Florida.

2.7 PHYSICAL CHARACTERISTICS AND PERFORMANCE PARAMETERS*

It is frequently helpful to compare general physical characteristics of each HSGT system, such as consist mass, number of passengers per consist, etc. Table 1 presents a summary of such physical parameters for the concepts studied here. Because of rounding, these numbers may differ

* Written by Dr. James Lever, CRREL, and Dr. John Potter, U.S. Army Engineer Division, Huntsville.

Table 1. General physical characteristics of concepts studied.

Parameter / *Basic concept*	*TGV-Atlantique steel wheel-on-rail*	*TR07 EMS, separate lift and guidance*	*Bechtel EDS, ladder levitation*	*Foster-Miller EDS, sidewall null-flux*	*Grumman EMS, common lift and guidance*	*Magneplane EDS, sheet levitation*
Vehicles / consist	1-10-1	2	1	2	2	1
Seats / consist	485	156	106	150	100	140
Gross mass (10^3 kg)	490	106	63	73	61	48
Cabin area / seat (m^2)	1.2	0.83	0.80	0.74	0.93	0.61
Cabin volume / seat (m^3)	—	2.2	1.7	1.5	1.8	1.1
Cruise speed (m / s)	83	134	134	134	134	134
Minimum headway (s)	240	57	36	55	30	45
Total bank angle (°)	7	12	30	28	24	35
Primary suspension	passive	active	passive	passive	active	semi-active
Secondary suspension	passive	passive	active	passive	none	none
Critical air gap (mm)	N / A	8	50	75	40	150
Low-speed support	N / A	maglev	air bearings	wheels	maglev	air bearings
Liftoff speed (m / s)	N / A	0	10	50	0	50
Primary braking	rheostatic	regen.	regen.	regen.	regen.	regen.
Secondary braking	friction	eddy	aero.	wheel, aero.	eddy	skids
Emergency braking	—	skids	drouge	skids	friction	aero.
Normal braking (g)	0.045	0.12	0.20	0.16	0.16	0.16
Emergency braking (g)	0.10	0.30	0.25	0.25	0.20	0.50
Cryogenic system	N / A	none	isochoric	recompress.	recompress.	refrigerator
Onboard power (kW)	9000	460	190	220	170	190
Guideway type	ballasted rail	T-shaped	box beam	sidewall	Y-shaped	trough
Span length, *L* (m)	N / A	25	25	27	27	9.1
Static *L* / deflection	—	5600	3500	5000	3000	2400
Dynamic *L* / deflection	4000	4000	2500	2300	2500	2000
Switch concept	swing-nose rails	bendable steel beam	bendable FRP beam	vertical elect.-mag.	bendable steel beam	horizontal elect.-mag.

slightly from those in the SCD reports or elsewhere in this report.

We also computed several performance parameters suitable for comparative evaluation of each concept, such as energy efficiency, guideway unit cost, etc. Table 2 shows these. For these parameters, we attempted to compare concepts equally, insofar as possible. For example, we computed energy efficiency as energy consumption per passenger-meter to allow for differing numbers of passengers per consist. However, each concept also allotted a different amount of cabin space per passenger. We corrected for this by defining a standard passenger (SP) as one occupying 0.80 m^2 of cabin floor area (including galleys and lavatories). This value is roughly the average floor area per passenger for the five maglev concepts studied, and it approximates business-class airline seating. This correction prevents indirect penalization of concepts with more spacious passenger cabins. We used cabin floor area rather than, say, cabin volume to define our standard passenger because we felt it reflected the spatial measure of greatest relevance to paying passengers. Other normalization approaches may be equally valid, but we feel this one is fair and relevant.

Table 2. Evaluation parameters for each concept. All performance values reflect GMSA analyses unless noted.

Parameter	*TGV-A*	*TR07*	*Bechtel*	*Foster-Miller*	*Grumman*	*Magneplane*
Standard passengers per consist (SP)	700	160	110	140	120	110
Gross mass / SP (kg)	700	650	600	520	530	440
Max. low-speed accel. (g)	0.044	0.10	0.23	0.16	0.093	0.23
Reserve accel. at 134 m / s (g)	N / A	0.006	0.12	0.044	0.048	0.039
3.5% Grade speed (m / s)	30	110	140	140	140	140
10% Grade speed (m / s)	N / A	14	140	100	5	90
0–134 m / s time (s)	N / A	320	77	120	180	123
Minimum radius* (m)	*6000*	5800	2600	2800	3300	2200
Prop. efficiency† at 134 m / s	*[0.82]*	0.83	0.85	0.91	0.78	0.84
Power factor† at 134 m / s	*[0.91]*	0.74	0.98	0.97	0.98	0.99
Aero. drag / SP at 134 m / s (N)	220	360	430	280	240	160
Total drag / SP at 134 m / s (N)	240	380	480	350	270	350
Energy intensity at 134 m / s (J / SP-m)	310	460	560	390	340	400
SST energy intensity (J / SP-m)	N / A	540	720	450	490	580
SST trip time (min.)	N / A	140	120	130	130	130
Guideway tolerance limits						
Ride comfort (mm)	1–3	2	3	12	5	20
Safety (mm)		5	6	25	30	50
Consist cost** / SP ($K)	41	58	39	93	71	190
Dual elevated cost						
SCD** ($M / km)		9.7	15	8.1	9.4	14
GMSA ($M / km)	14	12	13	17	11	16

*TGV 83 m / s, 0.05 g unbalanced acceleration, maglev 134 m / s, 0.10 g unbalanced acceleration.
†Propulsion efficiency and power factor measured at utility connection for steady cruise *[TGV 83 m/s]*.
**Cost directly from SCD, TGV or TR07 reports; variations compared with GMSA costs are primarily ascribable to differences in unit costs, subcomponent groupings and guideway heights used (see section 3.3.2).

CHAPTER 3. APPLICATION OF EVALUATION PROCESS

As noted, the GMSA's main role was to assess the technical viability of maglev for use in the U.S. This assessment addressed issues concerning the feasibility of the technical approach, the suitability of the concept to a desired transportation mission, and the possible advantages of U.S. maglev vs. foreign alternatives. To this end, we developed an evaluation process consisting of four main steps:

1. Application of the maglev *System Concept Definition-Request for Proposals* (USDOTFRA 1991, hereafter SCD-RFP) system criteria as assessment criteria (section 3.1).
2. Verification of subsystem performance (section 3.2).
3. Verification of system performance (section 3.3).
4. Application of other criteria (section 3.4).

These four steps gave us a common way to assess all aspects of the technical viability of each concept. They also generated the data necessary to support our conclusions. We evaluated both TGV-A and TR07 as baseline concepts and the four SCD concepts as representative U.S. maglev systems. This chapter describes the methodology used for each evaluation step and presents the results for each system studied. Chapter 4 presents our conclusions based on this work.

3.1 SYSTEM CRITERIA*

3.1.1 Source and rationale

The NMI's SCD-RFP sought a "system level conceptual definition and analysis effort resulting in a description of all the major subsystems and components of a maglev transportation system ..." It provided a mission statement (USDOTFRA 1991, sections C-2.2 and 2.3) defining how the NMI viewed the role for maglev in the national transportation network. It also contained a more specific set of system criteria (USDOTFRA 1991, section C-3.1) that described required or desirable performance characteristics of a maglev system, its vehicles, and guideways.

Participants in a July 1990 workshop at Argonne National Laboratory developed these maglev system criteria by consensus. They were intended to guide the SCDs towards performance characteristics thought to be important for maglev to fulfill its transportation mission. We adopted these criteria as assessment criteria for this very reason; measuring a concept against these criteria gives one indication of how well it fulfills its mission. Furthermore, by checking SCD characteristics against the TGV and TR07 baselines, we may assess each U.S. concept's potential for superior relative performance. This process thus provided us with data on both the mission suitability and the relative advantages of each concept's technical attributes.

3.1.2 Application

For each SCD-RFP system criterion, we developed both qualitative and quantitative cross-checks on the stated performance of TR07 and the four SCD concepts. Because of its proven commercial record, we accepted TGV data as fact. We examined technical data used to derive these performance characteristics and cross-checked such data against those of closely related characteristics. For SCD concepts, we also examined the contractors' modeling methods and trade-off analyses used to justify each performance characteristic.

As done in the SCD-RFP, those criteria followed by MR (minimum requirements) are performance specifications that a system must meet to be acceptable. Those that are preceded by DG (design goals) are target performance levels and are considered important but not essential conditions of acceptability. We recognized this distinction for evaluation by prioritizing the system criteria (high, medium, low). We also assigned a numerical weighting to these priorities: high = 3, medium = 2, low = 1.

The following three subsections show our use of the SCD-RFP system criteria list as a technical-viability evaluation step. Listed first for each criterion is its description from section C-3.1 of USDOTFRA (1991). Next are the cross-checks that we developed to assess concept performance against the criterion. Lastly, for each criterion, we prepared a table containing the actual assessments for TGV, TR07, and the four SCDs. Each assessment consists of a descriptive component and a numerical rating as derived in Table 3. The product of the rating and the priority values forms the net result for the assessment.

* Written by Dr. James Lever, CRREL.

Table 3. Numerical rating scheme.

Rating	*Score*
1. Can't evaluate concept against criterion	0
2. Concept doesn't meet criterion	–1
3. Concept meets criterion	1
4. Concept exceeds criterion	1.2

Table 4. Actual assessments for speed.

System	*Evaluation comments*	*Rating*
TGV-A	83 m / s service speed Tested at 133 m / s sustained speed, 143 m / s downhill Operates at full speed through switches (demonstrated 143 m / s), operates at 64 m / s along turnouts Speed through curves limited by nontilting body and 7.15° superelevation of track Insufficient residual acceleration to achieve 134 m / s in reasonable time Brakes not designed for 134 m / s Significant power transfer and maintenance issues must be resolved to achieve 134-m / s cruising speed in commercial service Significant additional investment needed to meet criterion	–1
TR07	TR07 demonstrated 121 m / s on test track Motor analyses indicate that concept can achieve 134 m / s Thrust capability motor limits operation on 10% grade to very low speeds (about 14 m / s) Structural analyses indicate guideway is capable of supporting 134-m / s loads Vehicle-dynamics model confirms that vehicle can meet ride-comfort criteria and can safely maintain gap at 134 m / s Switch through-speed demonstrated at 112 m / s (probably can do 134 m / s), demonstrated turnout speed of 56 m / s Speed through curve limited by nontilting body and 12° guideway tilt (min. radius of 5800 m at 134 m / s with 0.10-g unbalanced lateral acceleration)	1
Bechtel	Motor analysis indicates sufficient power and reserve acceleration to exceed 134 m / s Thrust capability enables 134-m / s sustained speed on 10% grade Structural analyses show guideway to be strong enough, but FRP reinforcing is unproven Vehicle dynamics not verified owing to insufficient detail on active suspension in final report Primary suspension has required lift and guidance forces	1.2
Foster-Miller	Motor analysis indicates sufficient power and reserve acceleration to exceed 134 m / s Thrust capability enables 100-m / s sustained speed on 10% grade LCLSM is unproven and must work as intended Structural analyses show guideway to be strong enough, but FRP post-tensioning tendons are unproven and must work Vehicle-dynamics model shows need for tuning of passive secondary suspension, but should not pose problems Primary suspension has required lift and guidance forces	1.2
Grumman	Motor analysis indicates sufficient power and reserve acceleration to exceed 134 m / s Thrust capability of 60-kN baseline motor limits operation on 10% grade to very low speeds (about 5 m / s) Structural analyses show guideway to be strong enough, steel reinforcing adequate Control of primary suspension may not capitalize on large gap, but vehicle should meet ride-comfort and safety requirements at 134 m / s Lift, lateral-guidance, and roll forces are adequate	1
Magneplane	Motor analysis indicates sufficient power and reserve acceleration to exceed 134 m / s Thrust capability enables 90-m / s sustained speed on 10% grade Need to correct power factor, conduct cost vs. performance trade-offs Structural analyses show guideway to be strong enough Vehicle suspension relies on active aerodynamic control surfaces—this system requires significant engineering research for implementation (actuators, control software, etc.) Lift and guidance forces are probably adequate (unable to verify magnetic keel effect, but it seems reasonable)	1.2

System Requirements

*Speed (DG)**. A cruising speed of 134 m/s (300 mph) or more is desirable. The cruising speed for a particular system is the result of trade-offs of route alignment, power supply capacity, and passenger throughput, along with other parameters. The maglev system speed should be sufficient to allow total trip times equal to or better than those achieved by current commercial air systems.

This is a high priority item. We checked the following:

- Aerodynamic drag, magnetic drag, motor drag.
- Motor thrust, power consumption.
- Vehicle structural capability (load transmission).
- Guideway structural capability, including bending and torsion.
- Acceleration achievable, including residual at 134 m/s.
- Reserve thrust in headwinds.
- Guidance force available in crosswinds.
- Increased drag in crosswinds.
- Aerodynamic consequences of tilting vehicles.
- Considerations given to tunnel design.
- Induced drag from vertical lift, lift in curves.
- Control implications from aerodynamic loads (damping, vortex).
- Dynamics related to vehicle–guideway geometry.
- Speed though switches.
- Time and distance to achieve 0 to 134 m/s.

Table 4 gives the evaluation comments and ratings for speed.

Capacity (DG). Capacity should be in the range of 4,000 to 12,000 passenger seats per hour in each direction. The lower figure would be appropriate with a guideway of low cost. The higher figure would appear to be required to serve the very highest volume markets, possibly with some increase in capital cost.

This is a high priority item. We checked the following:

- Vehicle headway and braking requirements.
- Vehicle capacity.
- Power system capacity.
- Cyclic loading capability of motor. (Data or past experience?)
- Cyclic loading capability of power supply.
- System control.
- Cycle time on switches, including mechanical movement, acknowledgment of safe closure, response time to problems, transit speed through switch.
- Passenger and baggage handling time implications, dwell time.
- Operational strategy, control system characteristics.
- Effect of power consumption on electric utility.

Table 5 gives the evaluation comments and ratings for capacity.

Ride comfort. The NMI forwarded new ride-comfort guidelines to the SCD contractors following awarding of the contracts. These set design goals and minimum requirements for ride vibration and motion sickness, and added a seated–belted category for curving performance and jerk. See Appendix A for these requirements.

This is a high priority item. We checked the following:

- Suspension system analysis.
- Guideway tolerances and flexibility.
- Banking, tilt control.

Table 6 gives the evaluation comments and ratings for ride comfort.

Noise and vibration (DG). The noise and vibration produced by total system operation should be designed to meet existing Federal standards and industry practices, as appropriate, for stationary facilities such as maintenance areas and stations. Noise and vibration produced by the vehicle traversing the guideway should be minimized. Potential noise and vibration effects and possible mitigation methods in urban areas should be given special attention. The Code of Federal Regulations, Title 40, Chapter I, part 201, *Noise Emission Standards for Transportation Equipment; Interstate Rail Carriers*, should be used for guidance but caution must be used in extrapolating such information to high-speed operations at or near grade.

This has been given a medium priority. We checked Transrapid data for comparison and the BAA on this topic. However, this criterion was not usable for our evaluation. The Federal Code permits speed reduction or abatement measures. More useful evaluation would be to compute noise emissions at 134 m/s, but this is beyond our scope. So, Table 7 contains comments only.

* DG means that this item is a design goal, and MR means that it is a minimum requirement.

Table 5. Actual assessments of capacity.

System	*Evaluation comments*	*Rating*
TGV-A	4-minute headway, large train capacities including bilevel cars Can now do 14,550 seats / hr at 83 m / s, will do 22,000 seats / hr with bilevel cars	1.2
TR07	Can meet 12,000 seats / hr with current concept (no guideway upgrade needed); e.g., six vehicle-consist every 3 minutes 57-second minimum headway Power supply and motor can meet demand, but current densities would be 50–100 times higher than standard practice—reduces life of conductor (potentially significant cost issue) Cannot easily increase conductor diameter because of limited slot width	1.2
Bechtel	36-second minimum headway Uses 120-passenger (all coach-class) vehicles to meet capacity using 36-second headways Guideway strength O.K. with larger vehicle Unable to analyze vehicle dynamics	1
Foster-Miller	55-second minimum headway Six-car consists at 2-minute headways will meet 12,000 seats / hr (headway well within capability of switch) Could run vehicles very close together (nose-to-tail) if locally commutated motor could take cycling Cost analysis accounts for frequent replacement of LCLSM coils due to high current densities Structural analyses show guideway can handle four-car consists, should also handle six-car consists Vehicle dynamics should be O.K. with six-car consists, provided secondary suspension is correctly tuned	1.2
Grumman	30-second minimum headway Three-vehicle consists at 45-second headways will meet 12,000 seats / hr, can add more vehicle modules Guideway structure O.K.	1.2
Magneplane	45-second minimum headway using power leap-frog strategy, 20-second minimum headway with each block fully powered 42-second headways needed to reach 12,000 seats / hr with single (140-passenger) vehicles	1.2

Magnetic fields (DG). Human exposure to steady and fluctuating magnetic fields must be minimized. So, current research findings must be examined. This is a high priority item. We checked the following:

- Approach to field control.
- Modeling methods used.
- Results with independent calculations (Government models).
- Approaches and cost to achieve the following levels at floor level where passengers and crew are seated (USDOTFRA 1991, section C-3.2.1): 1) maximum 50-G static and 1-G alternating fields, 2) maximum 5-G static and 1-G alternating fields, and 3) maximum 1-G static and 0.1-G alternating fields.

We reviewed all available models and the BAA on this topic. We can analyze static fields, but alternating fields are beyond our scope. We calculated static stray fields for stationary vehicles for all EDS concepts examined. These are worst-case fields—currents induced by vehicle motion generate canceling magnetic fields. At cruise speeds, stray fields in EDS concepts will be much smaller than values cited here. Table 8 gives the evaluation comments and ratings for magnetic fields.

Weather (DG). Operation should be compatible with all common U.S. weather conditions (e.g., wind, snow, rain, fog, icing, heat, lightning, etc.) with minimal degradation in system performance. In the region of operation, maglev should be the transportation mode least affected by adverse weather conditions.

In addition to the foregoing, some contractors requested and received guidance on wind conditions suitable as input to guideway structural analyses and vehicle dynamics calculations. This guidance is reproduced in Appendix B.

This item has been given a medium priority. We checked the following:

- Guideway configuration for susceptibility to weather.
- Concept of operations (mitigation, control system response).
- Sensors used for hazard detection, integrity monitoring.
- Susceptibility to blown abrasive or magnetic material.

Table 6. Actual assessments of ride comfort.

System	*Evaluation Comments*	*Rating*
TGV	A good ride experienced by team member at 83 m/s Ride comfort at 83 m/s is clearly commercially acceptable and it meets or exceeds design goal of ISO 1-hr reduced-comfort limits Good ride requires very tight tolerances (i.e., rigorous rail and wheel maintenance) and stiff rail bed	1
TR07	Uses a linear, passive secondary suspension between magnet bogies and vehicle body, so can't relax guideway flexibility (as analyses show) Ride comfort (not magnet clashing) governs guideway flexibility Meets most criteria (Appendix A) Good ride requires very tight tolerances and stiff guideway	1
Bechtel	Requires active aerodynamic control surfaces Also uses an active secondary suspension—details not available in final report (although contractor claims ride comfort is acceptable) Without secondary suspension details, we cannot confirm that vehicle meets ride-comfort criteria	0
Foster-Miller	Discrete coils cause ripple in lift, guidance, and low-speed thrust forces, but these are probably smoothed out by suspension Very stiff guideway required for use with passive secondary suspension (and to lesser extent discrete-bogie vehicles) Passive secondary suspension needs tuning, but not likely to be a problem	1
Grumman	Single active suspension, large gap Has potential to achieve acceptable ride over rough and flexible guideways, but control algorithm does not appear to capitalize on this potential Can be made to meet ride comfort with simple control algorithm, but requires guideway comparable to TR07	1
Magneplane	Sheet guideway (smoother forces) Single, semi-active suspension (active damping using aerodynamic control surfaces and LSM phase angle) Hardware to achieve active aerodynamic damping is critical and may push state-of-the-art Must use coordinated turns (reduced speed through turn puts vehicle in wrong place) Nevertheless, expect vehicle to meet ride-comfort criteria	1

Table 7. Comments on noise and vibration.

System	*Evaluation comments*
TGV	Maintenance needed to meet ride quality; also keeps wheel rumble low Nevertheless, wheel–rail contact produces additional noise that can predominate at low speeds
TR07	Noise appears to be acceptable (lower than HSR at low speeds, comparable at high speeds)
Bechtel	Wings for aerodynamic control are noise sources
Foster-Miller	Diaphragms are potential noise sources
Grumman	Outriggers are potential noise sources Control of suspension at 70–80 Hz may transfer guideway irregularities to vehicle
Magneplane	Wings for roll control are noise sources

Table 8. Actual assessments of magnetic fields.

System	*Evaluation comments*	*Rating*
TGV	DC fields not an issue	1
	Dietrich and Feero (1992) and Dietrich et al. (1993) did not measure TGV fields	
	Check fields for Amtrak, which uses 12 kV, 60 Hz (versus 25 kV, 50 Hz for TGV)	
	Catenary fields important, as could be fields from 25-kV trainline in roof of cars used to transfer power from single catenary to second powered car	
TR07	Iron-core magnets inherently confine fields	1
	Dietrich and Feero (1992) and analyses agree	
	Measured static field maximum of 1.5 G at floor level	
	Mean static field at floor below 1 G	
	Not sure how Earth's field of 0.5 G influenced these measurements	
	Measured alternating field maximum of 0.25 G	
	Mean alternating field below 0.1 G	1
Bechtel	Distributed magnets well below passengers	
	Analysis shows about a 31-G static field at floor without shielding (meets 50-G limit unshielded)	
	5-G level met with active shielding coils (1 kW extra power, 500 kg or 0.8% extra weight, $55,000 or 1% extra cost for vehicle)	
	1-G level met with active shielding coils (2 kW extra power, 1500 kg or 2% extra weight, $165,000 or 4% extra cost for vehicle)	
	Baseline vehicle weight does not include shielding coils	
Foster-Miller	Very high fields over bogies (walkway–baggage compartment)	1
	Power transfer coils along center of vehicle also of concern	
	Passengers seated away from bogies	
	Analysis shows about a 20-G static field at floor without shielding (meets 50-G limit unshielded)	
	5-G limit met with ferromagnetic box (800 kg or 1% extra weight for baseline vehicle)	
	1-G limit met with ferromagnetic box (2000 kg or 3% extra weight for baseline vehicle)	
	Baseline vehicle weight includes 2000 kg shield for 1-G limit	
Grumman	Iron-core magnets inherently confine fields	1
	Static fields about 1 G at a distance of 1 m above magnets and 1.5 m to side	
	Minimal or no shielding required to meet 1-G level	
Magneplane	Fields in cabin above bogies very high, passengers seated away from bogies	1
	50-G limit met with no shielding (maximum 50 G at floor of first row of seats)	
	5-G level met with active shielding coils (22 kW extra power, 2300 kg or 5% extra weight for vehicle)	
	1-G level met with active shielding coils (33 kW extra power, 3400 kg or 7% extra weight for vehicle)	
	Baseline vehicle weight includes 2400 kg shield for 5-G limit	

We also reviewed existing DOT guidelines, as well as the BAA, on sensors. Table 9 presents the evaluation comments and the ratings for weather effects.

Controls (MR). All controls must be fully automated and fail-safe (DG). A central facility will operate the system, receiving and integrating data regarding the status and integrity of all vehicles and guideways, the locations of all vehicles, guideway power requirements, vehicle routing requests, etc. (MR). The system control software must also be fail-safe, equivalent to the level of reliability defined by the Federal Aviation Administration (FAA) for flight control software for military and civilian aircraft.*

This is a high priority item. We checked the following:

- Methodology—fault tolerance.
- Response to faults.
- Results with available tools.
- Operating strategy.
- Redundancy management, containment of faults.
- Availability and reliability estimates.

In addition, software design for fault tolerance requires very specific approaches but we were not able to assess quantitative level of reliability. We considered the methodology used for fault tolerance (with guidance). Table 10 provides the evaluation comments and ratings for controls.

Safety (MR). A system safety plan must be included that discusses possible failure modes,

* See *Federal Aviation Regulation* 25.1309, *Amendment* 25-23 and *Advisory Circular* 25.1309-1.

Table 9. Actual assessments of weather effects.

System	*Evaluation comments*	*Rating*
TGV	TGV has experienced some wind-related damage; modified catenary and pantograph as a result Train slows down when winds exceed 19 m/s because of catenary dynamics Icing also affects catenary dynamics Train may be slowed at operator's request because of low visibility in fog, heavy rain, or snow Reduced adhesion likely in heavy rain, snow, and ice; may reduce braking performance (although thresholds for reduced performance not known) Dust increases maintenance Must manage thermal expansion for continuous rails Very well grounded—good lightning protection	1
TR07	40-GHz communication link examined—may have some attenuation problems in wet snow, sleet, and rain Redundancy in control system—communication link with vehicle not required Icing on guideway a potentially serious problem (small gap) Emergency braking skids may not be as effective when wet or icy Good lightning protection, small LSM gap is preferred path to ground	1
Bechtel	Recesses in guideway may accumulate snow and ice Smallest gap, 50 mm, still quite large but will be reduced by icing Tallest vehicle (5.3 vs. 4.1 m for TGV) Active aerodynamic control will be affected by windshear and icing Wind-induced yaw moment is design limit for primary suspension (full-speed operation for lateral winds less than 18 m/s, reduced speed operation for lateral winds to 27 m/s) Vehicle safe on guideway for 54 m/s, bare guideway designed for 89-m/s lateral wind	1
Foster-Miller	Partial trough may collect snow and ice, but relatively large gap (75 mm) Guideway provides partial wind protection, but increases turbulence incident to vehicle No aerodynamic control surfaces needed Vehicle operational wind limit not known Guideway designed for basic wind speed of 38 m/s with stationary vehicle present	1
Grumman	40-mm gap under vehicle, largely protected from freezing rain Bare guideway designed for steady lateral wind of 45 m/s Vehicle can operate at full speed with steady cross-wind of 22 m/s and peak gusts of 33 m/s, significantly higher winds than guidelines above (guideway designed for these added loads) Contractor's specifications call for unaffected vehicle operation with snow accumulations of up to 50 mm, rain rates up to 50 mm/hr and up to 63 mm of ice on the guideway However, friction-brake performance would likely worsen in rainy or icy conditions	1.2
Magneplane	Curved guideway may collect snow and ice, although magnetic-drag losses will significantly heat guideway (for frequent vehicle passings) and reduce or eliminate this concern Bare guideway designed for 38-m/s basic wind speed Vehicle can operate at full speed with steady cross-wind of 13 m/s and peak gusts of 21 m/s (guideway also designed for these loads) Guideway provides partial wind protection, but may increase turbulence incident to vehicle Active aerodynamic control will be affected by wind shear (design calls for de-icing and anti-icing provisions)	1.2
All HSGT	Visibility affects obstacle detection—may need to reduce speeds in low visibility	NA
All maglev concepts	No traction problems for acceleration or normal braking Noncontact power transfer Emergency braking performance using skids will deteriorate in snow, ice, and rain	NA

human operation considerations, evacuation procedures, system restart, equipment and software availability, safety inspections, consequences of vandalism and trespassing, etc. The central control facility will log all operations and communications for subsequent analysis in the event of a failure. Consideration must be given to safe use of materials and construction methods, and to the safety of other users of the ROW. This has a high priority. We checked the following:

- Hazard analysis for reasonableness.
- Control system response to hazards.
- Access to failed components.

Table 10. Actual assessments of controls.

System	*Evaluation comments*	*Rating*
TGV	Little reliance on micro-processor based controls Fail-safe design with more traditional electromechanical equipment Consistent with modern European practice Automatic supervision, not automatic control In-cab signals generated by coded track signals Voice communication with operators Control system can stop train if needed Newest versions use solid-state devices, can provide near automatic control	1
TR07	FRA safety analysis indicates that control system is adequate for U.S. use Control software does not meet guidelines developed under Broad Agency Announcement Don't know and can't evaluate whether TR07 software meets Federal Aviation Administration regulation reliability level Does meet DG (central control), has LSM Designed to German standards	1
Bechtel	Central control, LSM Good control-system expertise, good approach	1
Foster-Miller	Central control, LSM Good control-system expertise, good approach	1
Grumman	Central control, LSM Good control-system expertise, good approach	1
Magneplane	Central control, LSM Good description of hardware, good expertise More demanding, flexible vehicle scheduling at very high system capacities, but they have considered how to do this	1

Table 11. Actual assessments of safety.

System	*Evaluation comments*	*Rating*
TGV	Examined by FRA safety team Fundamentally safe as built and used in France Some incompatibility with FRA specifications FRA issuing Rules of Special Applicability Sharing of track with freight and other trains could be a problem	1
TR07	TSC published three safety reports—no serious problems encountered	1
Bechtel	Have recognized hazards and developed safety strategy	1
Foster-Miller	Have recognized hazards and developed safety strategy	1
Grumman	Have recognized hazards and developed safety strategy	1
Magneplane	Have recognized hazards and developed safety strategy	1

In addition, we reviewed BAA work, and the Transrapid hazard analysis. This criterion was not very helpful for evaluation (it calls for a safety plan only—estimates of actual levels of safety beyond SCD scope). Table 11 gives the evaluation comments and ratings for safety.

Station operation (DG). Provision should be made for convenient and efficient intermodal and intramodal transfer and transport of passengers, baggage, and freight. This has a low priority and we omitted it as an evaluation parameter.

Availability and reliability (DG). The design should have high system availability and subsystem reliability, maintainability, and ease of inspection. This is a high priority item. We checked the following:

- Reliability plan.
- Failure mode analysis.
- Failure response plans, e.g., removing failed vehicles.
- Safety assurance plan.
- Redundancy, modularity.
- Diagnostics, maintenance on condition.
- Maintenance plan.
- Costs reflecting maintenance, availability.

We also reviewed the BAA on diagnostic sensors. Table 12 gives the evaluation comments and ratings for system availability and reliability.

Table 12. Actual assessments of system availability and reliability.

System	*Evaluation comments*	*Rating*
TGV	Good operating experience 93% probability of meeting its schedule within 5 minutes, average delay 40 seconds Fleet size dominated by peak demand, small (5%) surplus to ensure high availability Surplus may need to change with service pattern Must schedule routine maintenance for wheel reprofiling, bearing service, and other operations associated with wheel–rail systems Nontilting vehicle (less complex) Proven, conventional switch quite reliable	1
TR07	Potentially significant guideway maintenance owing to tight tolerances (small gap, passive secondary) Needs either adjustments for beams on piers or very conservative foundation design (geotechnical investigation for every pier) Earthquake sensitivity may seriously affect availability in certain corridors Three-phase, dual LSM windings and controls can tolerate a winding failure and still operate (degraded mode) Bending beam switch, reliability unproven	1
Bechtel	Complete fault-tolerant system design Relatively low takeoff speed (10 m/s) Contactless air cushion for low-speed support (unproven, 10 times higher speed than current applications of this technology), although they may use active coils instead Cable-in-conduit superconductor cooling (no sloshing or flashing) Has liquid helium reservoir, no refrigerator Nb_3Sn wire has higher transition temperature than NbTi but is more brittle Fluctuating loads from ladder will cause eddy current losses in dewars and magnets that will require cooling beyond that identified in final report Six-phase, dual LSM windings and controls can tolerate a winding failure and still provide operational capability (degraded mode) Bending beam switch, reliability unproven	1.2
Foster-Miller	Landing speed of 20–50 m/s moderately high, requires wheels Helium bath provides thermal reservoir, no refrigerator but sloshing and flashing possible NbTi wire has lower transition temperature than Nb_3Sn but is less brittle Fluctuating loads from discrete coils will cause eddy current losses in dewars and magnets that will require cooling beyond that identified in final report LCLSM requires an H-bridge for each coil, so many opportunities for failure of electronic components However, LCLSM coils are independently controlled, so motor can operate in degrade mode with individual coils disabled (also, repair or replacement need not shut system down) Electromagnetic switch potentially very reliable	1.2
Grumman	Zero-speed hover possible, no landing gear needed Helium bath provides thermal reservoir, no refrigerator but sloshing and flashing possible (daily recharge—recompress and store helium gas) Control coils interacting with SC magnets are key to reliable design (unproven concept) Three-phase, dual LSM windings and controls can tolerate a winding failure and still provide operational capability (degraded mode) Bending beam switch, reliability unproven	1.2
Magneplane	Concern over reliability of air-bag supports and low-friction landing skids High takeoff speed (50 m/s) places demands on low-friction skids Cable-in-conduit with 30-minute reserve of liquid helium, no sloshing or flashing Cryogenic refrigerator least reliable component Nb_3Sn wire has higher transition temperature than NbTi but is more brittle Significant guideway heating owing to sheet levitation scheme (about 95°C temperature rise for 20-second headways) and ambient air temperature and sun (additional 83°C rise) Continuous-sheet guideway avoids fluctuating forces produced by discrete coils, good for magnets Aluminum and concrete react so attachments may corrode or fatigue (more maintenance) Single three-phase LSM not as reliable as dual LSM concepts (no degraded mode for LSM failure) Nontilting vehicle is more reliable Electromagnetic switch potentially very reliable	1
All maglev	Noncontact for lift, guidance, propulsion, braking, and power transfer. Should allow “on-condition” maintenance, which is preferred to scheduled maintenance (inspections still done during down time) Repeated transient loads will accelerate settlement If suspension can smooth out ride (e.g., active control of primary or secondary) then magnet contact limits allowable guideway irregularities—large gap systems yield big advantage in this case	

Table 13. Actual assessments of vehicle capacity.

System	*Evaluation comments*	*Rating*
TGV	1.2 m^2 cabin-floor area / passenger Plenty of headroom Overhead luggage racks Car size variable (standard gauge) Freight car possible	1
TR07	0.83 m^2 cabin-floor area / passenger Multiple-vehicle consists possible, width variable	1
Bechtel	0.80 m^2 cabin-floor area / passenger Single vehicles, width variable Meets ADA requirements	1
Foster-Miller	0.74 m^2 cabin-floor area / passenger Multiple-vehicle consists possible, width fixed Meets ADA requirements	1
Grumman	0.93 m^2 cabin-floor area / passenger Multiple-vehicle consists possible, width variable Meets ADA requirements	1
Magneplane	0.61 m^2 cabin-floor area / passenger Limited headroom Single vehicles, length variable Meets ADA requirements	1

Aesthetics (DG). Attention to aesthetics should be evidenced in the design to increase public acceptance and ensure consideration of economic aspects. This is a low priority item (omitted.)

Communications (DG). The system will include provisions for nonvital voice, data, and video communication capability. This is a low priority item (omitted.)

Human factors (DG). Human factors should be considered in the design, including the operator, passengers, and maintenance personnel. This is a low priority item (omitted.)

Vehicle requirements

Capacity (DG). Vehicles of different sizes, configured to carry passengers or freight, or both, should be feasible with the same basic design. This item has a medium priority. We checked the following:

- Ergonomics (seat size, headroom, luggage space, etc.).
- Dimensions vs. aircraft cabins.
- Egress times.
- ADA (Americans with Disabilities Act) requirements.

Table 13 gives the evaluation comments and ratings for capacity.

Braking system (MR). Vehicles must have redundant braking systems that are fail-safe (DG). Normal braking of up to 0.2 g should be considered. This has a high priority. We checked the following:

- Controls.
- Levels of redundancy.
- For one system independent of wayside power (minimum).
- Cabin equipment and procedures (warnings, seat belts, airbags).
- Load distribution—vehicle and guideway (especially emergency).
- Impacts to power system.
- Use of frictional braking in rain, snow, ice.
- Skid design, heat buildup.
- Wheel–guideway traction.
- Asymmetrical magnetic braking.

Table 14 gives the evaluation comments and ratings for the breaking system.

Structural integrity (MR). Vehicles must safely withstand high-speed collisions with small objects such as birds, debris, snow, and ice. Vehicles must also have adequate fatigue life and low-speed crash worthiness and should sustain only minimum damage in a 2.2-m / s (5-mph) impact.

This has a low priority and has been omitted as an evaluation parameter.

Onboard power (DG). All power for normal hotel functions, controls, levitation, etc., should be transferred from the guideway (MR). The vehicle must be equipped with emergency power for

Table 14. Actual assessments of braking system.

System	*Evaluation comments*	*Rating*
TGV	All braking (except aerodynamic drag) traction limited Primary service braking via rheostats on powered axles Secondary braking via disc brakes on unpowered axles and tread brakes on powered axles Anti-skid control of each wheel set to prevent wheel lock Normal service braking at 0.03–0.06 g, emergency braking at 0.10 g Traction will limit emergency braking	1
TR07	Aerodynamic braking, eddy current braking and emergency skids are all independent of wayside power Aerodynamic and eddy current braking are independent of onboard power Normal braking as linear generator—power dissipated in resistors (rather than regenerative) Can also apply reverse thrust by reversing motor direction Control system deflates air bag in secondary suspension for asymmetric magnet loss to control braking direction Normal braking at 0.12 g Emergency braking at 0.30 g	1.2
Bechtel	Primary: regenerative Secondary: aerodynamic–electrodynamic Emergency: drogue Normal braking at 0.20 g Emergency braking at 0.25 g	1.2
Foster-Miller	Primary: regenerative Secondary: aerodynamic–wheels Emergency: skids Normal braking at 0.16 g Emergency braking at 0.25 g	1.2
Grumman	Primary: regenerative Secondary: electrodynamic–eddy Emergency: friction / skids Normal braking at 0.16 g Emergency braking at 0.20 g	1.2
Magneplane	Primary: regenerative Secondary: aerodynamic–sheet drag Emergency: skids Normal braking at 0.16 g Emergency braking at 0.50 g	1.2

operation, as appropriate within the system safety plan. This is a high priority item. We checked the following:

- System safety plan for failure contingencies.
- Emergency braking power requirements.
- Power to move failed vehicle to off-load locations.

Table 15 provides the evaluation comments and ratings for onboard power.

Emergency systems (MR). Vehicles must include emergency systems for fire fighting, lighting, HVAC, evacuation, communication, etc., as appropriate within the system safety plan. This was given a low priority and was omitted as an evaluation parameter.

Instrumentation and controls (MR). The system should include instruments that monitor the integrity of the guideway (presence of debris, snow, and ice, misalignment or deterioration of guideway, etc.) and the status of onboard systems (propulsion, levitation, guidance, power, safety, etc.). Data acquired should be recorded and fully integrated into vehicle and overall-system controls to allow appropriate response in emergency and normal operations. In normal operation, vehicles will be monitored or controlled from a central facility. However, vehicles will include manual controls for emergencies and maintenance.

Priority is high for this (debris being defined as extraneous matter that poses a hazard to the vehicle). We checked the following:

- Completeness of sensor system.
- Previous experience of contractor.
- Response of sensors to adverse weather.

Table 15. Actual assessments of onboard power.

System	*Evaluation comments*	*Rating*
TGV	No levitation power needed Onboard power (batteries) for commutation to use traction motors for braking Backup power for anti-lock braking and skid control	1
TR07	Dual battery systems for emergency hover Has rescue strategy to relevitate and move stranded vehicle	1
Bechtel	Onboard methanol-powered fuel cell requires fuel aboard vehicle	–1
Foster-Miller	LCLSM coils, when not in propulsion mode, function as the primary of an air-core transformer for inductive power transfer to vehicle Power transfer works provided LCLSM works Not speed dependent Emergency batteries for wheel deployment and braking	1
Grumman	High-frequency, single-phase excitation of LSM windings in conjunction with linear generator provides inductive power transfer Speed independent	1
Magneplane	Inductive power transfer by injection of high-frequency, three-phase current into LSM windings in direction opposite to LSM propulsion current Speed dependent	1

Table 16. Actual assessments of instruments and controls.

System	*Evaluation comments*	*Rating*
TGV	Normal daily operation begins with scout train at lower speed Have fragile-wire sensors to detect rock slides Extensive onboard controls and diagnostics (interlocked with central control)	1
TR07	Gap sensing permits monitoring of guideway degradation Good lightning protection	1
Bechtel		1
Foster-Miller		1
Grumman		1
Magneplane		1
All systems	Concern over reliability of forward obstacle detection in bad weather	
All maglev	Concepts include integrated sensors and control systems (details vary) LSM controls vehicle position well inherently	

- Block and central control hierarchy.
- Integration of instrumentation into maintenance plans.
- Interface between instrumentation and control facility.
- State-of-the-art of the sensors being proposed.

We also reviewed BAA information (Martin-Marietta 1992). Table 16 gives the evaluation comments and ratings for instrumentation and controls.

Sanitary facilities (MR). Space must be provided for sanitary facilities, including a retention system. This has been given a low priority (omitted).

Guideway requirements

Structural integrity (MR). A civil structure (foundation and structure supporting the guideway) should have a minimum 50-year life. Consideration should be given to structural integrity during earthquakes and in high winds.

The seismic criterion was later updated to require that the guideway structure be designed to the specifications for seismic zone 2 of the *Uniform Building Code* (International Conference of Building Officials 1992). Zone 2 covers most of the continental U.S. except for California, Nevada, and isolated regions near St. Louis and in the Rocky Mountains.

A common set of wind specifications was also later provided to the contractors (see Appendix B). Not all contractors were instructed to use these specifications, so we cannot apply them as minimum requirements. However, Table 17 reports design wind speeds for comparison. Note that the specification for guideway structural integrity called for use of a 38-m/s basic wind speed. Structural integrity has a high priority. We checked the following:

Table 17. Actual assessments of structural integrity.

System	*Evaluation comments*	*Rating*
TGV	Viaducts built to $L/4000$ Ballast is relatively easy to realign and maintain	1
TR07	Designed for $L/4000$ dynamic deflection ratio Although not considered in original design, California–Nevada proposal indicated that guideway would meet California codes for seismic design (more severe than zone 2 requirement) Low stress levels (all compressive) in concrete owing to deflection-limited design—very good for fatigue and durability behavior of concrete Attachments would have shorter lives Florida proposal indicates wind loads not a problem—should easily meet wind-load requirements Steel beam life comparable to steel bridges in Germany (about 80 years) California–Nevada proposal indicates that they have considered thermal stresses	1
Bechtel	Simple, conventional superstructure design Requires controversial FRP transverse reinforcing in upper half of girder to prevent magnetic effects. However, FRP is not used for prestressing (which is more controversial) Numerous attachments Girders designed for $L/2500$ dynamic deflection ratio Structural analyses indicate low deflections and stresses in guideway, promoting good ride quality, fatigue life and durability. Should meet 50-year life requirement. Thermal stresses not a problem owing to support conditions. Differential thermal deflections not a problem given large magnet–guideway gap Designed for seismic zone 2 Guideway designed for 38-m/s crosswinds. Vehicle operation allowed at full speed with lateral gusts to 18 m/s; will reduce speed for 18- to 27-m/s range. These vehicular loadings controlled portions of guideway design	1
Foster-Miller	Innovative modular superstructure, possibly complex to construct Design dependent on viability of FRP post-tensioning Girders designed for $L/4500$ dynamic deflection ratio Structural analyses indicate low deflections and stresses in the guideway, promoting good ride quality, fatigue life and durability. Should meet 50-year life requirement Thermal stresses not a problem owing to support conditions. Differential thermal deflections not a problem because of the large magnet–guideway gap Designed for seismic zone 2 Guideway designed for 38-m/s winds. Partial enclosure of vehicle by guideway provides some crosswind protection	1
Grumman	Innovative modular superstructure that has a single (spine girder) substructure EMS design does not require FRP reinforcing Structural analyses indicate total dynamic deflection ratio is $L/2400$ as input to vehicle Structural analyses indicate low stresses in the guideway, promoting good fatigue life and durability. Should meet 50-year life requirement Thermal stresses not a problem owing to support conditions. Differential thermal deflections not a problem owing to large magnet–guideway gap. SPC-B seismic design comparable to zone 2 requirement Guideway designed for steady side wind of 44.7 m/s with no vehicles operating, and a steady 22.3-m/s wind with gusts up to 33 m/s while vehicles are traveling at 134 m/s	1
Magneplane	Superstructure requires nationally significant quantities of aluminum Structural analyses indicate very low deflections, well below $L/2000$ design limit Stresses well below allowable fatigue limits for infinite number of cycles. Should meet 50-year life requirement Temperature differentials of 83°C considered in thermal analysis Designed for seismic zone 2 Guideway designed for 38-m/s crosswind. Vehicle designed to operate at 134 m/s in steady crosswinds of 13.4 m/s with 22.3-m/s gusts	1

- Earthquake analysis—should meet seismic zone 2 requirements.
- Design wind loads and structural response.
- Use of sensors to forecast winds, earthquakes.
- Discussion of fatigue, degradation.
- Measures to meet 50-year minimum life (e.g., cathodic protection).
- Effects of thermal stresses.
- Long-term serviceability.
- Magnetic effects.
- Methods for calculating vehicle loads.
- Possible aeroelastic loads.

Configuration (DG). Guideways will normally be elevated and have bi-directional capability, but must also accommodate near grade and underground situations. Single guideways must include provision for passing vehicles and future expansion. Dual guideways must include crossovers to sustain partial service during routine maintenance and repair of local failures. The central facility will control crossovers and bi-directional traffic.

This item has a medium priority. We checked the connection to the operation plan and control systems. Table 18 gives the evaluation comments and ratings for guideway configuration.

Structure (DG). To facilitate maintenance, repair of local failures, and eventual system upgrade, guideways should be of modular construction with an independent support structure. This support structure (foundations, piers, beams, and connectors) should be designed to accommodate growth in traffic (see *System Capacity*). The design should also include means for vertical and lateral adjustment of guiding elements to maintain required tolerances.

This is a high priority item. We checked the following:

Table 18. Actual assesments of guideway configuration.

System	*Evaluation comments*	*Rating*
TGV	Not normally elevated (heavy) Fully grade separated on high-speed sections No switching problems	–1
TR07	Normally elevated, can be at near-grade Switch proven	1
Bechtel	Normally elevated, can be at near-grade	1
Foster-Miller	Normally elevated, can be at near-grade	1
Grumman	Normally elevated, can be at near-grade	1
Magneplane	Normally elevated, can be at near-grade	1

Table 19. Actual assessments of guideway structure.

System	*Evaluation comments*	*Rating*
TGV	Ballast provides modularity, means for alignment	1
TR07	Can replace motor sections Guidance elements cannot be adjusted Single-span beams can be adjusted (with difficulty) on piers Foundation settlement would require lengthy repair	1
Bechtel	Single-span beams can be adjusted (with difficulty) on piers Levitation, guidance and propulsion package adjustable on beam using shims	1
Foster-Miller	Levitation, and guidance–propulsion coils separately adjustable on beam Two-span beams can be adjusted on piers, but with more difficulty than single-span beams	1
Grumman	Multiple adjustment points (rails, slab beams, spine girder seats) Innovative adjustable post-tensioning can compensate for concrete creep Short-span slab beams easily adjusted	1
Magneplane	Very simple girder layout, easily adjusted Two-span beams are short so shouldn't pose extra adjustment problems	1

- Realignment features.
- Modularity.
- Constructiblity.
- Integration with maintenance plan (50-year life).
- Features for capacity upgrade.

Table 19 provides the evaluation comments and ratings for guideway structure.

Vehicle entry and exit (DG). Entry and exit to off-line stations, feeder lines, and other main lines should require minimal vehicle headway and overall trip time. This item has high priority. We checked the following:

- Reasonableness of technique.
- Safety implications.
- References to controls, operation plan.
- Headway restrictions, implications for capacity.
- Hypothetical route costs for entry–exit.

Note that turnout speeds for all switches depend upon radius of curve and hence length of switch. Because switch radius is a design trade-off with cost, turnout speeds do not generally indicate the relative merits of each switch type. Turnout speeds in Table 20 are minimum achievable values for baseline switches.

Instrumentation and controls (MR). The system shall include instruments that monitor guideway integrity (presence of debris, snow, and ice, misalignment or deterioration of guideway, etc.), the status of its subsystems (propulsion, levitation, guidance, power, entries–exits, etc.), and the locations and velocities of all vehicles. Data acquired should be fully integrated into guideway and overall system controls to allow response in both emergency and normal operations.

This is a high priority item. We checked integration with central control and operation plan, and vehicle control issues (vehicle position and

Table 20. Actual assessments of vehicle entry and exit from the guideway.

System	*Evaluation comments*	*Rating*
TGV	No jerk at 61 m/s Full speed possible straight through switch Turnout possible at 95 m/s Standard rail switch, reasonably fast and reliable Minimum headway 81 seconds with emergency braking of 0.10 g (actually uses 4 minutes of headway)	1
TR07	Bendable steel beam is baseline switch (proven at Emsland) Has physical interlock to confirm switch status No superelevation possible, and vehicle does not tilt so turnout speed limited Large jerk (0.5 g/s) also limits turnout speed Turnout possible at 56 m/s Mechanical movement and interlock results in relatively slow switch cycle time	1
Bechtel	Baseline bending beam switch is all composite material (FRP) No superelevation of bending beam, but vehicle tilts Turnout possible at 32 m/s Mechanical movement and interlock results in relatively slow switch cycle time Electromagnetic switch studied as an alternative	1
Foster-Miller	Baseline high-speed switch is electromagnetic (vertical, switched null-flux coils with moving safety floor as interlock) Turnout possible at 50 m/s Vertical orientation for turnout should permit higher speeds Relatively fast cycle time should be possible (except for need to move safety floor) Two lower-speed switches developed: full 20 m/s segmented switch, 20–12 m/s switch for vehicle on wheels	1.2
Grumman	Baseline switch consists of a bending-beam section (similar to TR07) and a rotated section to allow superelevation Turnout possible at 65 m/s Mechanical movement and interlock results in relatively slow switch cycle time	1
Magneplane	Electromagnetic horizontal switch using null-flux coils Angling of coils permits banked turnouts for higher turnout speeds Turnout possible at 100 m/s Relatively fast cycle time should be possible Vehicle maintains self-banking capability, so switch on curve possible	1.2

Table 21. Actual assessments of guideway instrumentation and controls.

System	*Evaluation comments*	*Rating*
TGV	Misalignment a less severe issue—regular track and catenary diagnostics Can detect rail breakage	1
TR07	Guideway senses vehicle position and control system uses this information	1
Bechtel	Well-developed control system	1
Foster-Miller	Well-developed control system	1
Grumman	Well-developed control system	1
Magneplane	Well-developed control system Intelligent vehicle, so no sensors on guideway	1
All systems	Expect that all will probably use Japanese-style earthquake detection and response Sensors needed for forward obstacle detection, reliability in bad weather a concern	

Table 22. Actual assessments of guideway power systems.

System	*Evaluation comments*	*Rating*
TGV	Can't maintain full speed (83 m/s) up sustained 3.5:100 grade 82% overall efficiency from electrical source, 0.91 power factor	–1
TR07	83% overall efficiency from electrical source, 0.74 power factor A lot of redundancy, some fault tolerance Large land requirement for power system Larger capacity needed to meet grade and wind requirements Current design has residual acceleration of only 0.006 g at 134 m/s (0.6:100) so cannot maintain full speed up sustained 3.5:100 grade 10% grade climbing capability only at very low speeds (14 m/s) Increased thrust capability limited by stator current density–conductor life trade-off Stator slot width limits conductor size so upgrade not easy	–1
Bechtel	85% overall efficiency from electrical source, 0.98 power factor High-voltage DC distribution with inverters along wayside provides a continuous guideway distribution system Inverters adjacent to guideway avoids feeder cables but requires real estate for inverters High-voltage DC circuit breakers may be difficult and costly Can climb 10% grade at 134 m/s with some reserve acceleration (0.02 g)—excellent grade climbing capability Reserve acceleration at level 134 m/s is 0.12 g	1.2
Foster-Miller	91% overall efficiency from electrical source, 0.97 power factor DC distribution to individual H-bridges Locally commutated LSM—high risk, high benefit item Blocklengths are a consist length, so LCLSM has potential for very high efficiency (91%) Can climb 10% grade at 100 m/s Reserve acceleration at level 134 m/s is 0.044 g (can maintain full speed up 3.5% grade)	1
Grumman	78% overall efficiency from electrical source, 0.98 power factor Conventional LSM and inverters (as per TR07) Inverters at substations with feeder cables Typical LSM blocklengths of 500 m, in conjunction with feeder cables for 4-km inverter spacing 10% grade climbing capability only at very low speeds (5 m/s) for 60-kN baseline design Reserve acceleration at level 134 m/s is 0.048 g (can maintain full speed up 3.5% grade) Replacing aluminum LSM windings with copper enables 100-kN motor thrust (at extra cost)	1
Magneplane	83% overall efficiency from electrical source, 0.31 power factor if uncorrected Conventional LSM and inverters (as per TR07) Inverters at substations with feeder cables Typical LSM blocklengths of 2 km, longer blocks require power-factor correction 84% overall efficiency from electrical source, 0.99 power factor if corrected Can climb 10% grade at 90 m/s Reserve acceleration at level 134 m/s is 0.039 g (can maintain full speed up 3.5% grade)	1

velocity may be sensed by the vehicle, not the guideway). Table 21 gives the evaluation comments and ratings for instrumentation and controls.

Tunnels (MR). The design of tunnels should address issues of comfort, noise, and safety, with special attention to vehicle entry and passing vehicles. This has a low priority (omitted).

Power systems (DG). Power systems should be sized so that the vehicle can accelerate and brake at all operating conditions, and they should be capable of meeting requirements for system capacity. Guideway power systems should be capable of sustaining vehicles at full cruising speed up sustained grades of 3.5:100, and provide vehicle propulsion at reduced speeds up a maximum grade of 10:100. This item has a high priority. We checked the following:

- Parametric study.
- Redundancy, spacing of equipment.
- Interface with controls.
- Cyclic loading response.
- Nonlinear currents.
- Power factor, demand, upgrade potential.
- Diagnostics, maintenance plans.
- Design against existing IEEE (Institute of Electrical and Electronics Engineers) standards.
- Relationship to single and multiple vehicle configurations.
- Nature of transients to grid.
- Dynamic vs. regenerative braking.
- Total energy analysis.

Table 22 provides the evaluation comments and ratings for power systems.

Superelevation (MR). Superelevated (banked) guideways must allow safe operation of vehicles at all speeds from zero to the maximum design speed of the curve. Emergency evacuation must be possible from vehicles stopped in a curve. This has a medium priority. We checked the following:

- Stopping and restarting in curves.
- Guideway sidewall strength.
- Evacuation procedures in curves.
- Loads from coordinated* vs. non-coordinated turns.
- Transition designs (shape, cost, length, effect on modularity).

Table 23 presents evaluation comments and ratings for superelevation.

3.1.3 Results of system-criteria assessment

Table 24 shows a numerical summary of our use of the SCD system criteria to assess technical viability. Essentially, the concepts fall into three groups. The top one consists of the Foster-Miller, Grumman, and Magneplane concepts. They each exceed the requirements for five or six criteria and meet all other requirements.

The middle group consists of TR07 and the Bechtel concept. Despite exceeding the requirements for a few criteria, these systems each fail to meet a high-priority criterion: TR07 cannot climb a 3.5% grade at 134 m/s, and Bechtel's vehicle includes a methane fuel cell to meet onboard power needs. The Bechtel concept suffers further

* Means that all loads are normal to the guideway top.

Table 23. Actual assessments of guideway superelevation.

System	*Evaluation comments*	*Rating*
TGV	Can evacuate at-grade easily	1
TR07	Beams designed for maximum lateral loads Guideway can support vehicle stopped in curve Can evacuate vehicle stopped in curves (chutes, walkways) Can coast to safe-stopping location	1
Bechtel	Have considered loads in structural analysis Tilting vehicle cabin returns to horizontal if stopped	1
Foster-Miller	Has considered loads in structural analysis Tilting vehicle body returns to horizontal if stopped	1
Grumman	Has central box girder for evacuation Tilting vehicle body returns to horizontal if stopped	1
Magneplane	Vehicle rolls to horizontal position if stopped in curve Walk on LSM to evacuate Guideway may be hot Has considered loads in structural analysis	1

Table 24. Summary of system criteria assessment.

Parameter	*Weight*	*TGV-A*	*TR07*	*Bechtel*	*Foster-Miller*	*Grumman*	*Magneplane*
System							
Speed	3	–1	1	1.2	1.2	1.2	1.2
Capacity	3	1.2	1.2	1	1.2	1.2	1.2
Ride comfort	3	1	1	0	1	1	1
Noise / vibration	0	—	—	—	—	—	—
Magnetic fields	3	1	1	1	1	1	1
Weather	2	1	1	1	1.2	1.2	1.2
Controls	3	1	1	1	1	1	1
Safety	3	1	1	1	1	1	1
Station operation	0	—	—	—	—	—	—
Availability / reliability	3	1	1	1.2	1.2	1.2	1
Aesthetics	0	—	—	—	—	—	—
Communications	0	—	—	—	—	—	—
Human factors	0	—	—	—	—	—	—
Subtotal	23	18	24	21	25	25	25
Vehicle							
Capacity	2	1	1	1	1	1	1
Braking	3	1	1.2	1.2	1.2	1.2	1.2
Structural integrity	0	—	—	—	—	—	—
Onboard power	3	1	1	-1	1	1	1
Emergency syst.	0	—	—	—	—	—	—
Instr. / controls	3	1	1	1	1	1	1
Sanitary facilities	0	—	—	—	—	—	—
Subtotal	11	11	12	6	12	12	12
Guideway							
Structural integrity	3	1	1	1	1	1	1
Configuration	2	–1	1	1	1	1	1
Structure	3	1	1	1	1	1	1
Entry / exit	3	1	1	1	1.2	1	1.2
Instr. / controls	3	1	1	1	1	1	1
Tunnels	0	—	—	—	—	—	—
Power systems	3	–1	–1	1.2	1	1	1
Superelevation	2	1	1	1	1	1	1
Subtotal	19	9	13	20	20	19	20
Total	53	38	48	46	56	56	56

because the final report did not provide sufficient information for us to determine whether the vehicle would satisfy ride-comfort requirements. The importance of these shortcomings differ for the two systems, however.

As discussed in the text, stator slot width limits the LSM thrust capability of TR07. While some additional thrust is possible with further work, the system will not easily provide the thrust needed to climb a 3.5% grade at 134 m / s. Conversely, Bechtel's choice of a fuel cell vs. batteries to provide onboard power reflected a cost–weight tradeoff. Substitution of batteries for the fuel cell would not be difficult or involve major changes in the concept. Also, further work would likely yield details of a suspension that could be shown to meet ride-comfort requirements. These improvements are straightforward and would move the Bechtel concept into the upper grouping.

TGV received the lowest assessment results here. This is not surprising, given that the SCD system criteria were established to guide U.S. maglev concepts towards performance superior to current high-speed rail systems. In particular, TGV-A cannot achieve a level cruise speed 134 m / s and cannot climb a 10% grade. It is also not normally an elevated system. Failing to meet these three criteria produced its low assessment result.

Use of the SCD system criteria for assessment served as a key step in our evaluation of technical viability. Essentially, it summarized the performance of each concept against requirements thought to be important to maglev's viability in the U.S. market. It also provided a focus for our

analytical efforts by identifying specific performance questions that required data from our models to answer. Indeed, we found that we could not complete this evaluation step until our models had yielded the required data. Overall, this step tells us that U.S. maglev concepts should perform slightly better than TR07 and substantially better than TGV-A.

It is worth emphasizing that neither TGV nor TR07 were designed to meet the SCD system criteria, and both systems will undoubtedly improve with further development. However, it is beyond our scope to assess the likely outcome of such development in terms of the time, costs, and risks associated with specific performance improvements. We chose TGV-A and TR07 as baselines for evaluation because their perceived lack of development costs and risks are critical in the debate of whether these systems represent preferred alternatives to developing a U.S.-designed maglev system. Thus, we believe this is a fair assessment.

3.2 SUBSYSTEM VERIFICATION

As noted, one aspect of maglev's technical viability is technical feasibility: the soundness of the physical principles and engineering sciences upon which the concept is based. To assess this, the GMSA identified several critical subsystems that warranted direct verification. In general, these subsystems represented high-risk or high-cost items: guideway structure, linear synchronous motor, magnetic suspension (including stray fields), and vehicle suspension (including guideway interactions). We developed our own numerical models to assess the technical feasibility of these subsystems for TR07 and the SCD concepts. Because of the enormous scope of this undertaking, we focused most analysis effort on those items deemed critical to each concept.

The following four sections present the results our subsystem verification work. Each section describes specific objectives for the study, methodology used, critical issues examined for each concept, results obtained, and brief conclusions regarding each concept's technical feasibility.

3.2.1 Guideway structure*

Objectives

The supporting guideway of a Maglev system is generally the most expensive subsystem. As such, it represents the greatest potential for cost savings through good design. The objectives of this section were to identify key issues affecting the viability and economy of the TR07 and SCD guideway designs and to analyze their structures to address the key issues.

Methodology

To evaluate each guideway design, we did the following: reviewed all structural details; identified key issues that were deemed to have a direct effect on the viability and economy of the guideway design; and applied structural analysis "tools" to address the key issues for each design.

The following steps were taken to study the guideway structural designs:

- Identify the most appropriate and efficient analytical tools for the desired structural calculations.
- Test the analytical tools in a baseline evaluation of the German TR07 guideway.
- Use these tools to evaluate the four SCD guideway designs.

All analytical work was concentrated on the superstructure (girder) elements since the substructure elements (piers and footings) were all conventional designs with little or no innovations that required special consideration.

A vast array of "tools" exists for structural analysis and design, ranging from conventional hand calculations to complex, three-dimensional finite-element computer programs. For our analyses here, we used a combination of hand calculations (as discussed in Nilson 1978) and two different finite-element programs, ADINA (ADINA R&D, Inc. 1987) and ABAQUS (HKS, Inc. 1988). Hand calculations were used for the design and verification of reinforcing requirements within the concrete cross sections and for a cross-check of the finite-element analytical results. The finite-element analyses were used for the more complex studies involving static and dynamic response and resulting stress distributions from vehicular loadings.

German TR07 guideway

Key Issues. Since the TR07 guideway is currently in prototype operation and has performed successfully, the key issues for this design are mainly economic. The only structural question regards their use of pseudo-static loadings for their designs in place of actual dynamic vehicle–guideway interaction analyses. The economics of the guideway may be addressed by a study of the

*Written by Dr. James Ray, U.S. Army Waterways Experiment Station.

design to verify that it is as structurally efficient as possible.

In addition to structural efficiency, the construction requirements will also directly affect the cost of the guideway. The construction tolerance requirements for this guideway are far greater than current construction practice in the U.S. These tolerances will have a significant effect on the construction time and, thus, cost requirements. The sloping sides and rounded bottom of the TR07 superstructure girder are very aesthetically pleasing and possibly serve a minimal purpose in reducing wind loadings on the structure. However, these features also add to the complexity and cost of the structure.

Approach. During the initial stages of the GMSA work, sufficient details for a structural analysis of the TR07 guideway were sparse. To fill in the information gaps, the team members conducted an extensive literature search. Most of the useful design information obtained on the TR07 guideway came initially from five sources (see *Bauingenieur* 1983; City of Las Vegas 1987; *L'Industrial Italiana del Cemento* 1989; Maglev Transit, Inc. 1989; *The Indian Concrete Journal* 1991). The initial guideway analyses (using the pseudo-static loads) were based on this information. Missing details were filled in as necessary by assuming that the German designs corresponded closely to the U.S. specifications outlined in the design code published by the American Concrete Institute (1989).

The design details used in the analyses are as follows. All girders are single span and simply supported. Three different span lengths and, thus, three different girder cross-sections are used in the TR07 guideway (see Fig. 7). The 24.82-m span is the most common and is used in all straight portions of the guideway. The other two span lengths, 31.05 and 37.24 m, are used in curved sections of the guideway. A combination of straight and parabolically draped Dywidag post-tensioning bars reinforce each girder as shown in Figure 8. A German class B45 concrete is used in the girders, which corresponds to a concrete test cube strength of 45 N / mm^2 (approx. 5530-lb / in.^{2} test cylinder strength by U.S. standards). The girders have been constructed and post-tensioned in such a way as to practically eliminate long-term deflection changes attributable to concrete creep.

Maglev Transit, Inc. (1989) provides a complete set of pseudo-static load cases that reportedly were used for the design of the guideway in place of rigorous dynamic analyses. Seismic loadings were not considered in the design of these girders, although it has been reported to the GMSA team that the design is sufficient to resist seismic loadings. The girders were designed for a live load deflection ratio of 1:4000, which for the 24.82-m span corresponds to a mid-span downward deflection of approximately 6.2 mm. A permanent upward camber (under dead load only) of approximately 3.6 mm is induced in the beams by the post-tensioning to improve the total deflection characteristics under live loading.

All of the information discussed above was used for the initial analytical effort, with the pseudo-static loads provided in Maglev Transit, Inc. (1989). These analyses checked the longitudinal post-tensioning steel and the transverse reinforcing steel used in the three different TR07 guideway cross sections shown in Figure 7.

To verify the German pseudo-static loads and to validate the finite-element tools, we conducted a series of dynamic analyses of the TR07 girder. A comparative set of analyses, using both a beam-element and a solid-element model, confirmed the use of the simpler beam element model for most of the vehicle–guideway interaction studies. Vehicle speeds ranging from 100 to 500 km / hr (28 to 139 m / s) were considered. Dynamic vehicle

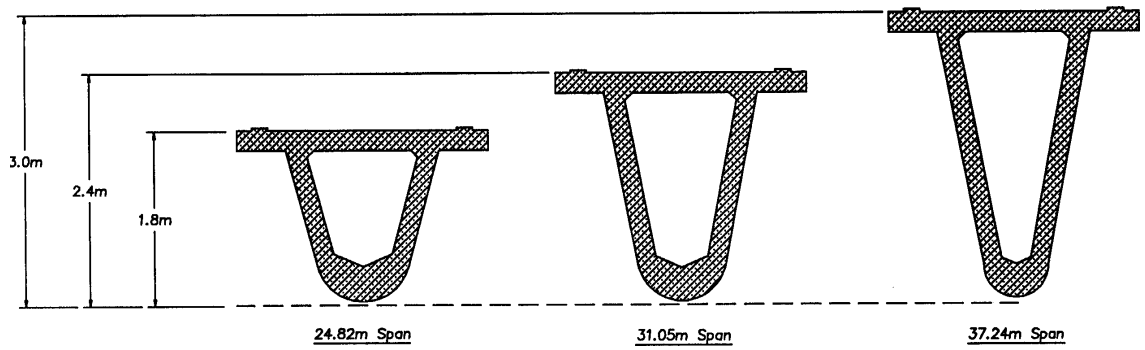

Figure 7. Cross sections of TR07 guideway girders.

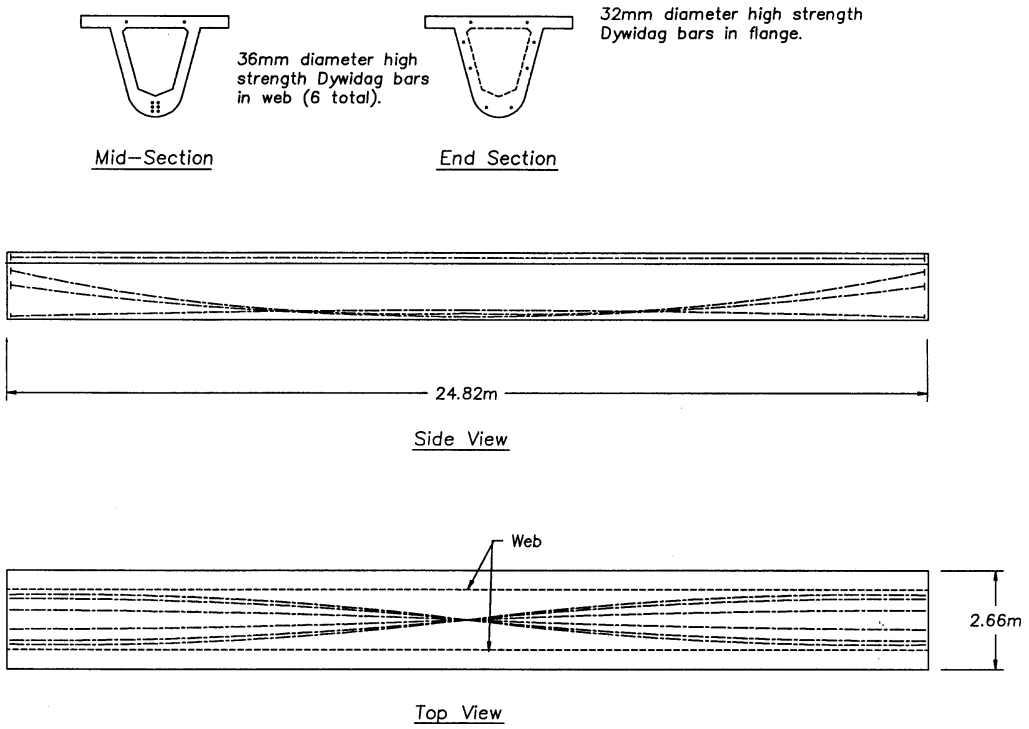

Figure 8. Post-tensioned steel arrangements in the TR07 girder.

loads were supplied by the Transportation Systems Center (TSC) of the Department of Transportation. Their vehicle model, discussed in section 3.2.4, provides load-time functions that represent the dynamic guideway loadings from the vehicle, attributable to both its "sweeping" passage across the guideway and its mass response (a function of vehicle mass and bogie suspension characteristics) to guideway roughness and deflection.

Before analyzing the solid-element finite-element model, and after completing the work with the beam-element finite-element model, we obtained an actual set of design drawings for the TR07 guideway from the Canadian Institute of Guided Ground Transport. These drawings provided more complete and accurate details of the 24.82-m girder. A comparison of the details in these drawings with those previously deduced from earlier documents revealed that the cross-sectional dimensions were slightly different. The new details gave the section a slightly lower moment of inertia than had previously been calculated. Since the new drawings were considered more accurate, the analyses using the solid-element model were made with these drawings.

Results. Longitudinal post-tensioning requirements were determined for the three different guideway span lengths and their corresponding cross sections using conventional prestress design procedures (discussed in Nilson 1978). These requirements were determined using the pseudo-static loads provided in Maglev Transit, Inc. (1989). For the design of longitudinal post-tensioning, the worst-case loading was for the case of the vehicle in a "trough," which produced a maximum downward load of 32.62 kN / m. The post-tensioning requirements were the same for the both the 1.8- and 2.4-m-deep sections, consisting of a combination of 32- and 36-mm-diameter high-strength Dywidag bars, as shown for the 1.8-m-deep section in Figure 8. The post-tensioning for the 3.0-m-deep section was approximately the same, except that two additional 36-mm-diameter draped bars were required.

As seen in Table 25, the resulting maximum stresses in the sections were well within the allowable limits defined by the American Concrete Institute (1989). In fact, the bottom portion of the section only had 1.10 MPa of tensile stress under its maximum downward loading, which is well below the allowable stress of 3.10 MPa. These low tensile stresses are very desirable for a concrete beam, since they will improve its long-term durability (weather resistance) and fatigue life. Because of the low stresses, the post-tensioning designs discussed above were apparently completely

Table 25. Analysis and design results for TR07 girder with 24.82-m span.

Deflections (mm)

*Load case**	*Hand calcs.*	*ABAQUS*	*Criteria**
IPS + DL†	–3.6	–3.55	NA
EPS + DL	–2.5**	—	–3.6
PS+DL+LL (trough)	6.1	—	6.2
PS*+DL+LL (curve)	—	5.25	NA

Stresses (MPa)

Load case	*Location*	*Hand calcs.*	*ABAQUS*	*Criteria*
IPS + DL†	Top	—	–3.20	–22.88
	Bottom	—	–5.20	+1.54
EPS + DL	Top	–2.90	—	–17.17
	Bottom	–3.31	—	+3.10
PS+DL+LL (trough)	Top	–5.52	—	–17.17
	Bottom	+1.10	—	+3.10
PS*+DL+LL (curve)	Top	—	–4.5	–17.17
	Bottom	—	–0.80	+3.10

* IPS = initial prestress, DL = dead load, EPS = effective prestress, LL = live load, NA = not applicable.

† Dead load of beam only

** Concrete creep neglected; creep increases camber

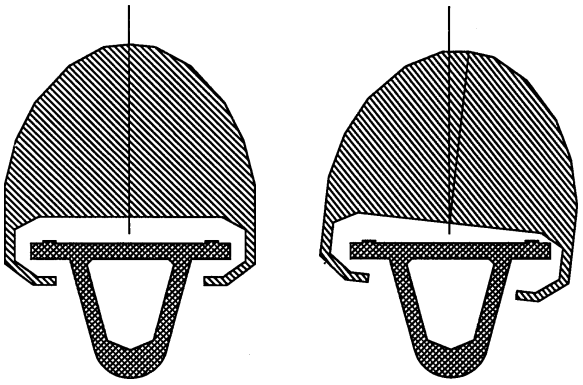

Figure 9. Roll motion of TR07 vehicle.

driven by the strict deflection limitations at the midspan (previously discussed).

Transverse reinforcing requirements were determined for the 24.82-m span subjected to the Maglev Transit, Inc. (1989) pseudo-static loadings. The worst-case shear and torsion loadings were for the vehicle in a circular curve, which induced a downward shear force of 31.2 kN/m and a torsional moment of 7.1 kN-m/m. The worst case loading for transverse bending within the box section was not discussed in Maglev Transit, Inc. (1989) and was thus assumed to be caused by a vehicle rolling completely to one side of the guideway, as demonstrated in an exaggerated form in Figure 9. This would cause the total vehicle loading to be transferred through the magnets on one side of the guideway only, thus inducing a large transverse bending moment into the section.

The design of reinforcing for the combined effects of transverse bending, shear, and torsion is very complex. The hand calculation procedure (Nilson 1978) is only an approximation and should be used with considerable conservatism. For an important design such as a maglev guideway, a three-dimensional finite-element analysis should be used to accurately define the maximum design stresses and thus reduce the required design conservatism.

The hand calculations showed that the shear and torsional stresses in the girder were quite low and could actually be carried by the concrete alone, without transverse reinforcing steel. The transverse bending stresses from the vehicle roll to one side were found to govern the design, which resulted in a maximum transverse steel requirement of 13-mm-diameter bars at 20 cm on center. This is fairly close to the more conservative TR07 design of 14-mm-diameter bars at 17 cm on center (considering the approximate nature of our calculations and the understandable conservatism of the TR07 design).

The midspan deflection–time histories resulting from the beam-element model are compared in Figure 10. From these plots, we can see that the girder has a natural frequency of approximately 6.0 Hz, which is the same as the hand-calculated value. The maximum deflections increase with vehicle passage speed because of the dynamic effect, with the largest deflection increase between 400 and 500 km/hr. The maximum dynamic deflection at 500 km/hr was approximately 3.6 mm. Note that this value was much less than the maximum allowable deflection for the TR07 girder (governed by ride quality and magnetic gap) of 6.2 mm. This should be the case since the loadings used for this model were not the worst case loadings, which result from the vehicle passing through a trough.

The ratio of the maximum dynamic deflection and the deflection of the span under the same statically applied loading is called the dynamic load factor (DLF). This value is used as a static load amplification factor in the conventional static design of structures. Based upon the 3.6-mm dynamic deflection of the girder at a vehicle speed of 500 km/hr and the hand-calculated static deflection of 2.3 mm, the DLF for the TR07 girder was calculated to be 1.56. This corresponds very closely to the DLF value of 1.40 reported in

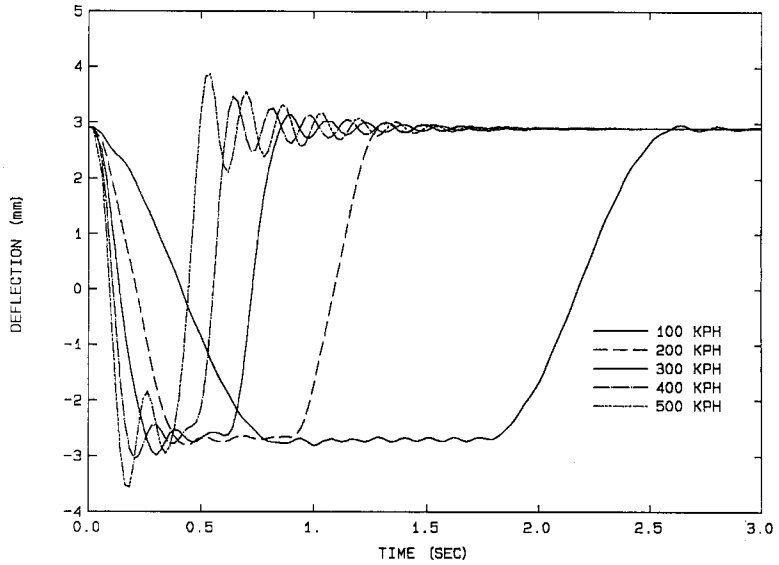

Figure 10. Midspan deflection–time histories for beam-element model of TR07 girder (KPH = kilometers per hour).

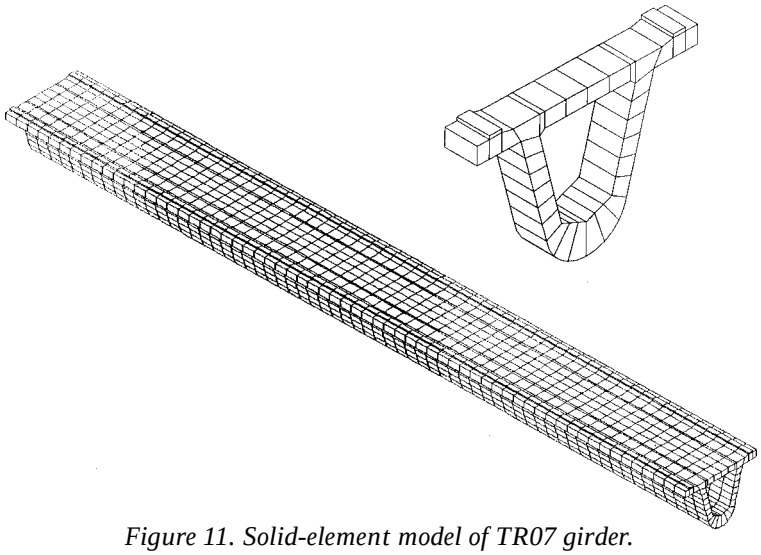

Figure 11. Solid-element model of TR07 girder.

Maglev Transit, Inc. (1989), which was used to determine the pseudo-static loadings reported therein.

The solid-element model is shown in Figure 11. The midspan dynamic deflections from this model are compared to those for the beam-element model in Figure 12. We attribute the small differences in stiffnesses and deflections between the plots to the soild-element model using the more accurate, less stiff cross section from the Canadian Institute of Guided Ground Transport drawings and the beam-element model using the section extracted from literature prior to receipt of those drawings, as previously discussed. The stress distributions and magnitudes obtained from this model also agreed well with the hand-calculated values.

Conclusions. Our analyses showed that the superstructure of the TR07 guideway is an efficient design and meets all of the stated requirements relating to allowable deflections and stresses. The Germans appear to have designed both an aesthetically pleasing and economical structure, a combination that is sometimes difficult to achieve. However, it should again be emphasized that the aesthetics add to the construction cost and the benefit to cost ratio of this combination must be carefully weighed. It should also be reemphasized that the required construction tolerances for this guideway will have a significant effect on its construction cost. In addition, continued maintenance of these tolerances on a structure in the U.S. could be very difficult and costly because of the highly varied soil conditions and seismic activity throughout the country.

The analytical tools provided an effective means of assessing the TR07 guideway and provided good agreement with the published data on the TR07. These tools should also prove sufficient for evaluating the SCD designs.

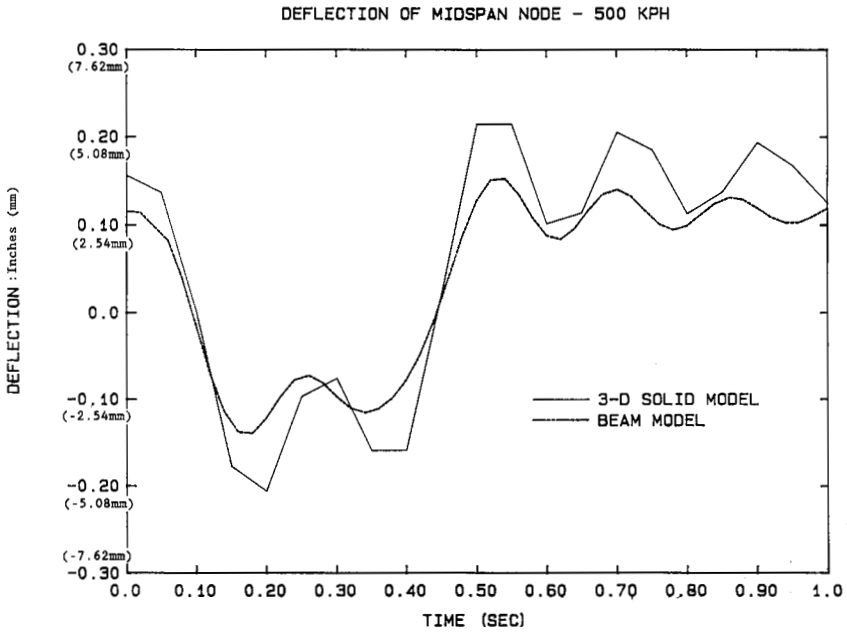

Figure 12. Comparison of results from beam- and solid-element models of TR07 girder.

Bechtel guideway

General. Bechtel's final SCD guideway concept is shown in Figure 13. It is a single-cell box girder made of prestressed concrete with both straight and parabolically draped post-tensioned reinforcement in the longitudinal direction. The post-tensioning details shown in Figure 13 are for curved sections of guideway. Slightly less post-tensioning is used in straight guideway sections. A combination of conventional steel reinforcing and FRP reinforcing is used in the transverse direction to resist shear and torsional stresses. The FRP reinforcing is used in the upper half of the girder to prevent magnetic interaction with the levitation–guidance system.

The baseline design calls for simply supported spans over the entire guideway. It also shows that multiple continuous spans (up to eight-span continuous) can be built in a future design if desired. In fact, Bechtel's earlier baseline design called for an eight-span continuous guideway with simple spans in the curves when necessary. Because a portion of the analytical work reported here was done prior to the completion of the final baseline design, some of it was based on an eight-span continuous guideway and the final portion was based on a simply supported guideway. This is differentiated throughout the discussion.

Key issues.

- As with all guideway designs, the dynamic interaction between the passing consist and the guideway (vehicle–guideway interaction) must be carefully studied to ensure desired ride quality and to give us a complete understanding of the loads applied to the guideway.
- The width of the guideway girder is relatively small. As a result, its torsional stability could be insufficient, especially for the guideway sections in curves and the vehicle consist in crosswinds.
- FRP reinforcing is a very new technology. Many important factors, such as long-term durability and end anchorage, have yet to be studied in sufficient detail. This technology is very promising as an alternative to steel reinforcing, but is currently a technological risk that must be considered.
- As discussed in Bechtel's final report, the cost benefits of using a large number of continuous spans must be carefully weighed. The use of continuous spans will allow more efficient piers and girders, but the construction complexity, and thus cost, will be greater. Maintenance of continuous span girders may also be more difficult.

Approach. The dynamic response of the girder to vehicle passage was studied using a beam-type finite-element model and the ADINA code. Speeds ranging from 100 to 500 km / hr (28 to 139 m / s) were considered. The required properties for the beam model (mass, stiffness, and moments

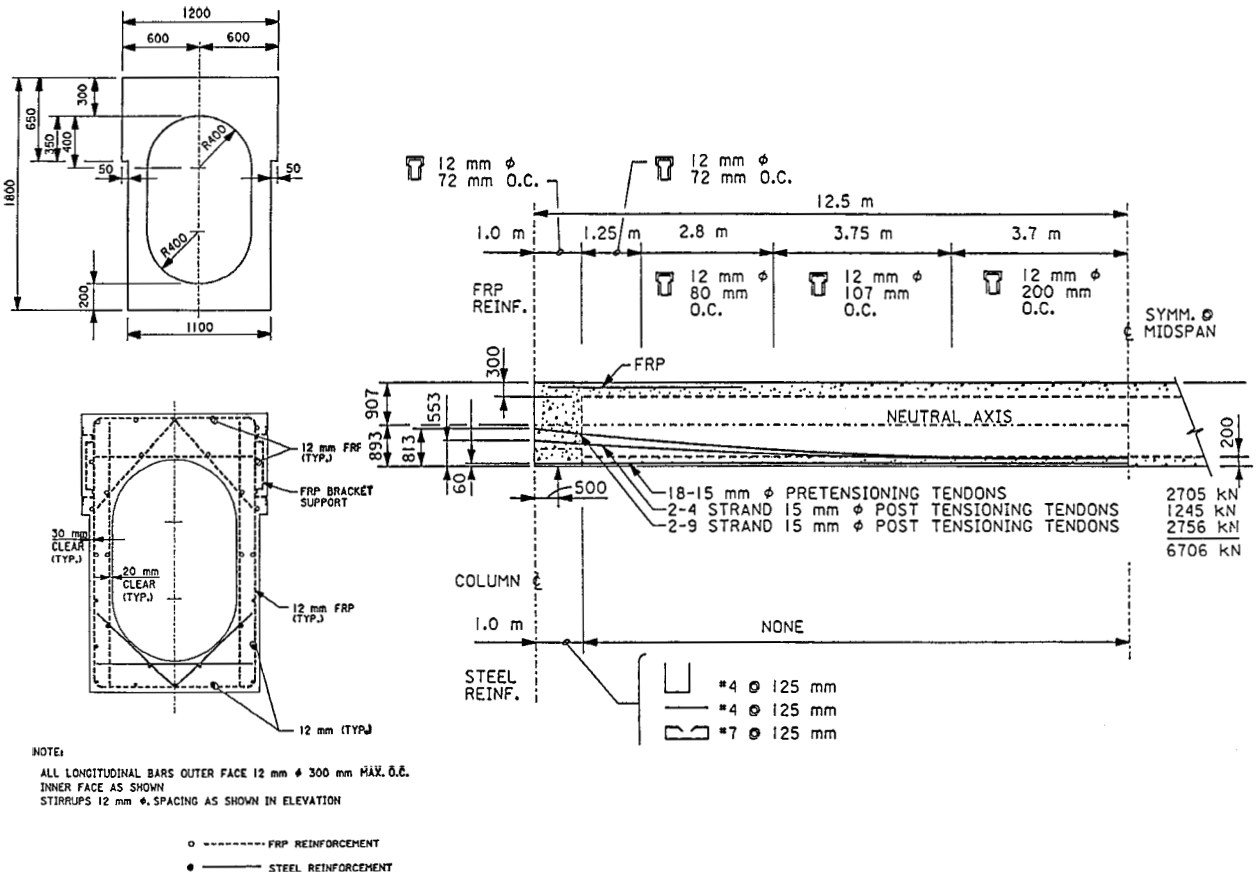

Figure 13. Bechtel girder design.

of inertia about the principal axes) were determined by conventional hand calculations. These calculations were made prior to the final baseline design and were thus based on an eight-span continuous structure over a flat surface.

The dynamic loadings were produced by distributing the vehicle weight out to each of the vehicle bogies and over the length of each bogie. Through use of a computer program, these loadings were then "swept" across an assumed straight and flat guideway and a load–time history was calculated for each loaded node. These loadings were simplified and are by no means a "worst-case" loading scenario. These calculations were only done to study the DLF associated with the specific combination of girder stiffness and bogie passage frequency. A more in-depth dynamic analysis would include more accurate vehicle loadings, accounting for vehicle suspension characteristics, guideway irregularity and curvature, and pre-camber and flexure of the guideway. If time had allowed on this project, these loadings would have been obtained from the vehicle–guideway interaction model produced by the Transportation Services Center (TSC), as described in section 3.2.4 of this report.

A three-dimensional finite-element model using 20-node solid elements is shown in Figure 14. It was employed along with the ABAQUS

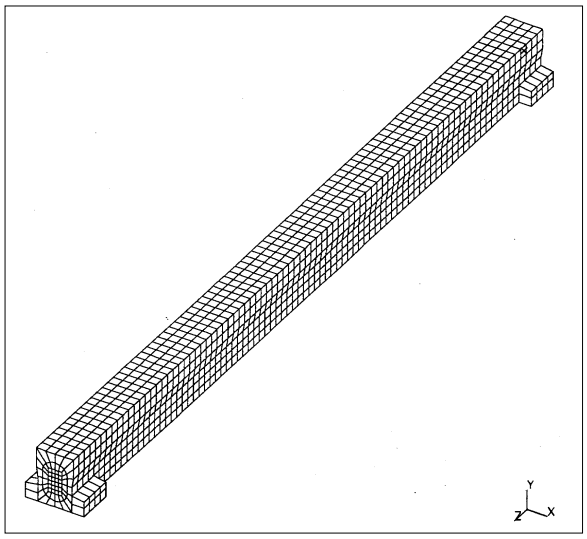

Figure 14. Solid-element model of Bechtel girder.

finite-element program to study the complex shear and torsional stresses within the girder and to determine its dynamic flexural characteristics. While reinforcing designs were provided by Bechtel for both straight and curved guideway sections, only the reinforcing for curved sections was modeled. The effect of the parabolically draped post-tensioning was modeled by applying an equivalent upward uniform load along the length of the girder and centered axial loads at the girder ends (as discussed in Nilson 1978). The straight post-tensioning was modeled by applying axial loads at the appropriate eccentricities at the ends of the girder. For expediency, the transverse reinforcing was not modeled and the concrete was assumed to be a linearly elastic isotropic material. These assumptions were reasonable since the deflections were known to be small and thus stresses would likely be low. More in-depth modeling would need a nonlinear concrete model that, upon cracking, would transfer all stresses to the reinforcing.

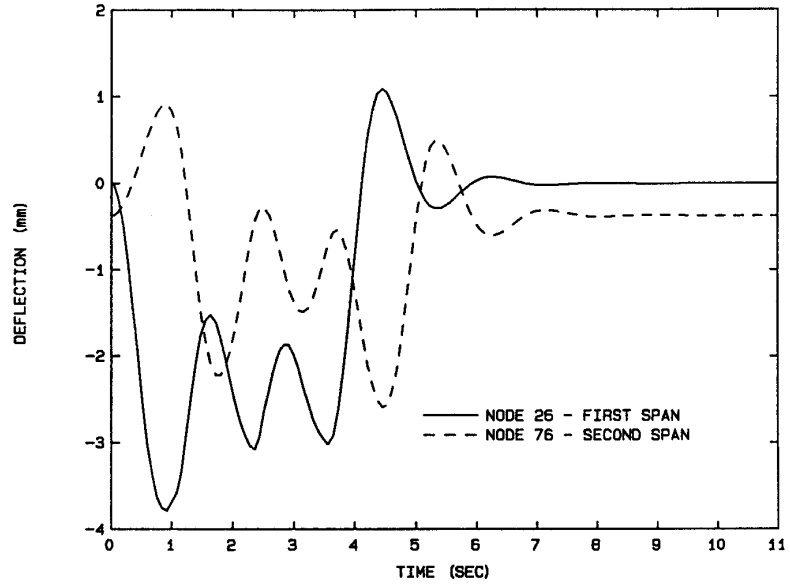

a. 100-km/hr vehicle passage.

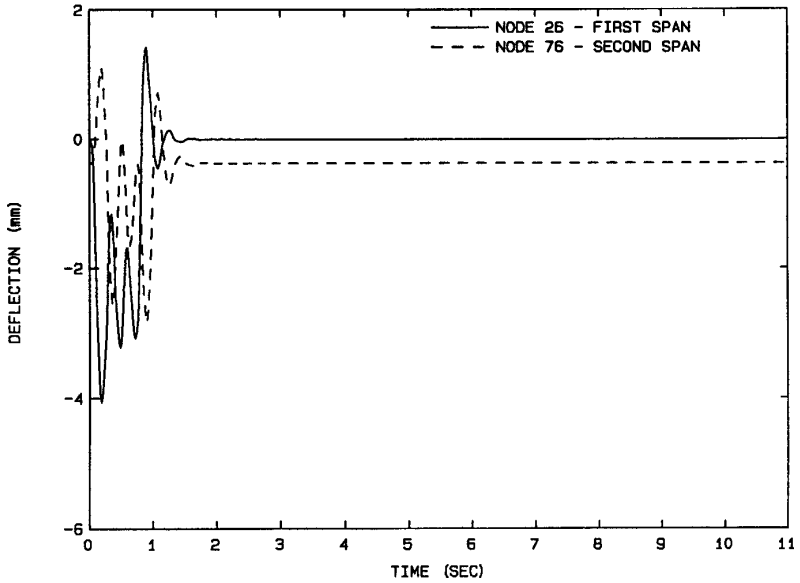

b. 500-km/hr vehicle passage.

Figure 15. Dynamic analysis results from Bechtel beam-element model.

The design loadings for the propulsion–levitation–guidance system defined in section C2 of the Bechtel (1992a) SCD report were applied to the soild-element model. These loadings result from the vehicle in a curve at full speed and tilt with a 40-mph (18 m / s) crosswind, and with the larger fraction of wind force concentrated near the nose of the vehicle. These forces were assumed transferred to the guideway girder in the form of vertical and horizontal forces (levitation and guidance) at the attachment points for the levitation and guidance hardware.

An eigenvalue analysis was also performed on the solid-element model using the ABAQUS program. This type of analysis is used to study the varied mode shapes and natural frequencies that make up the total dynamic response of the girder. It is very useful for understanding the manner in which a structure will respond to actual dynamic loadings.

Results. The results of the dynamic analyses with the beam element model are summarized in Figure 15 for the 100- and 500-km / hr vehicle passes. Both plots show deflection–time histories for the maximum response nodes of both spans 1 and 2 of an eight-span continuous structural system. We can see that, since span 1 was pinned at one end, its response to loading was greater than that of span 2, which was continuous across both of its supports. This demonstrates the effectiveness of continuous spans in reducing deflections. The response of span 1 is most similar to that which would be expected from a simply supported span, as called for in the final baseline design.

The maximum dynamic deflections varied from approximately 3.8 mm for the 100-km / hr vehicle passage to 4.2 mm for the 500-km / hr passage. If we assume that the 100-km / hr passage is equivalent to a static loading, this corresponds to a very low DLF of 1.10. The Bechtel report indicates that they conservatively used a DLF of 1.4 to design the girder. The low DLF shows the value of closely spaced bogies on the vehicle.

Please note that the loadings applied to the beam model were not the worst case and thus the deflections calculated were less than can be expected under more severe loadings. In addition, the post-tensioning for the beam element model was based on approximate values, since the Bechtel design was not complete at the time of these analyses. The results of these calculations should only be used to study the dynamic amplification effects of the bogie spacing and beam stiffness combination.

The displaced shape of the solid-element model resulting from the applied static loads discussed above is shown in Figure 16. Note that the girder bent about both the *x*- and *y*-axes as well as twisted about the *z*-axis. This was expected because of the way that the loads were applied. The deflected

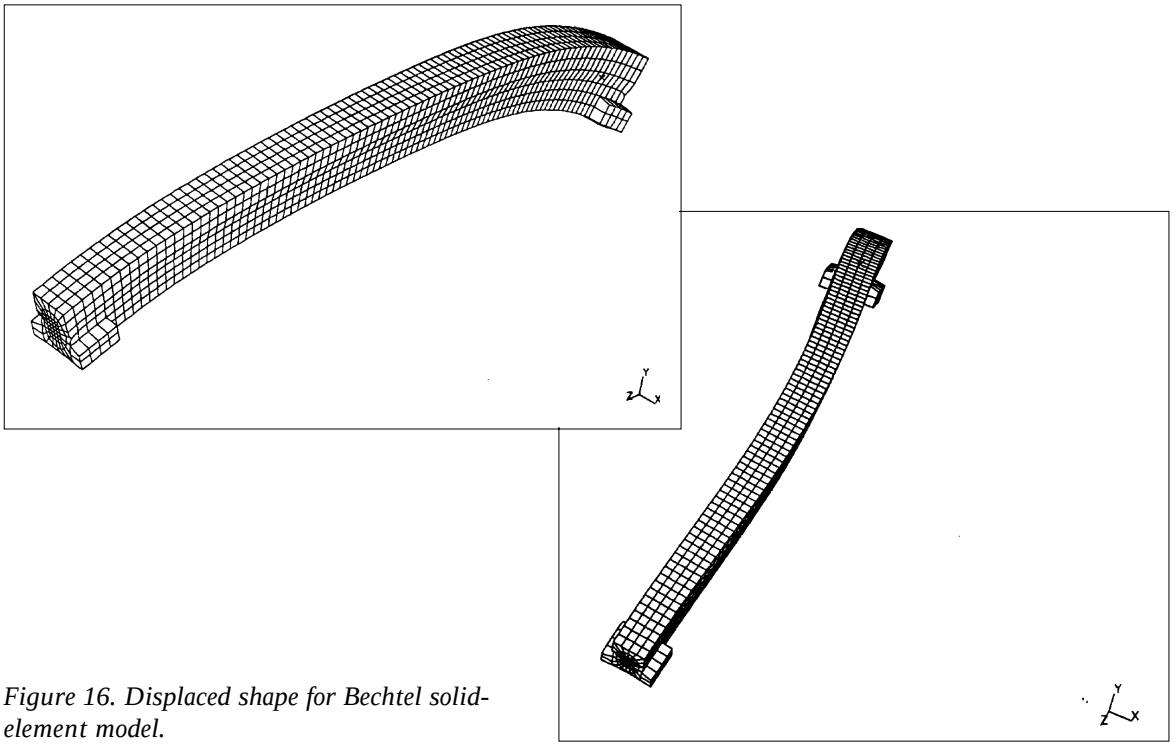

Figure 16. Displaced shape for Bechtel solid-element model.

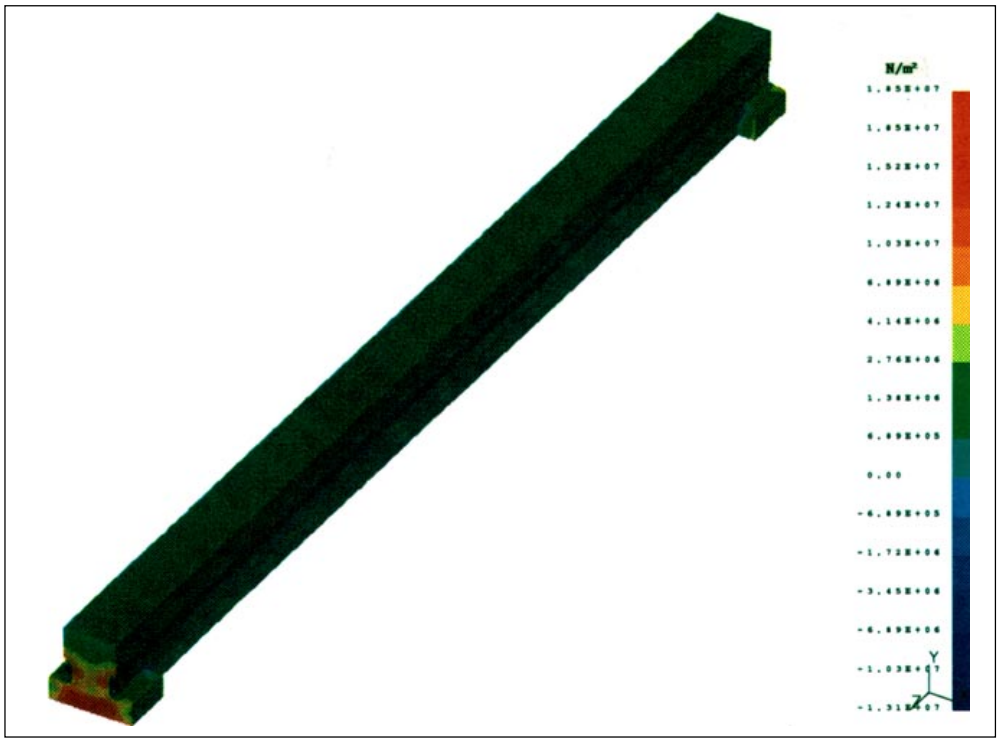

Figure 17. Maximum principal stress contours for Bechtel girder.

shapes are magnified several hundred times to show more detail. The actual deflections were quite small. The maximum (*y*-axis) deflection was only approximately 1 mm downward from its original 7.8-mm upward cambered position. The 7.8-mm upward camber may appear extreme at first. However, Bechtel designed their girder for a dynamic span:deflection ratio of 2500, which means they allowed for a 10-mm deflection response to a worst-case dynamic loading. Under this loading, the guideway would only deflect approximately 2 mm past its flat position if it had an initial 7.8-mm upward camber. A similar philosophy was used by the TR07 designers.

The maximum horizontal displacement (*x*-axis) was 3 mm. We expect that the load case used for this analysis was close to the worst case for horizontal guideway deflections. Therefore, little problem should result from a 3-mm horizontal displacement, since the physical lateral gap between the magnets in this direction is 50 mm. The maximum difference between *x*-displacements at the top and bottom of the girder, representing the degree of twist, was a negligible 0.4 mm. Therefore, even though the girder originally appeared torsionally weak, we may conclude that it is torsionally sufficient. This statement is also supported by the low stresses discussed in the following paragraph.

As seen in Figure 17, the principal stresses ascribable to the applied loads were low. The maximum principal tensile stresses were about 18.5 MPa, but these were at the ends where the prestressing forces were applied. In reality, these stresses would be more spread out owing to the normal methods of post-tensioning. The other principal stresses were quite uniform along the length and depth of the girder and were in the ±0.689-MPa range. Nilson (1978) says that principal tensile stresses in the concrete in the range of 2.5% of compressive strength are acceptable. This limit for a 69-MPa compressive strength concrete (Bechtel's design) is 1.73 MPa. The applied stresses (excluding those at the prestress anchor points) are below this value, without even allowing for the transverse reinforcing. However, the loading combination used to produce these stresses was not necessarily a worst-case combination for stress.

The first three dynamic bending modes are shown in Figure 18. These were as expected, showing the girder being weakest in bending about the *y*-axis, and then about the *x*-axis. The frequencies for the first through third bending modes were 6.3, 6.7, and 20.0 Hz, respectively.

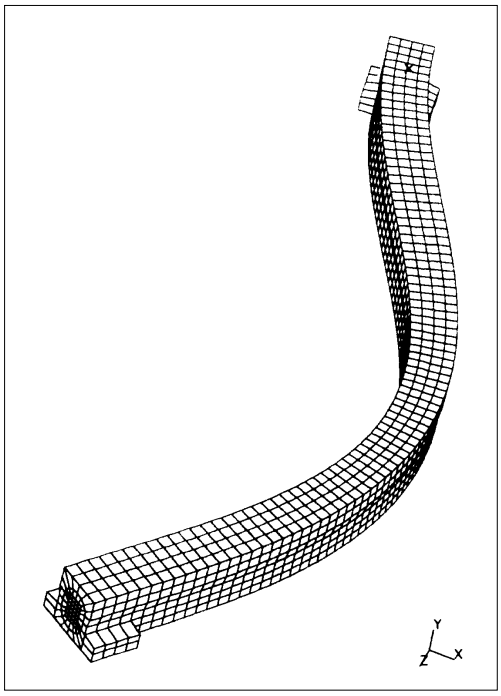

a. First.

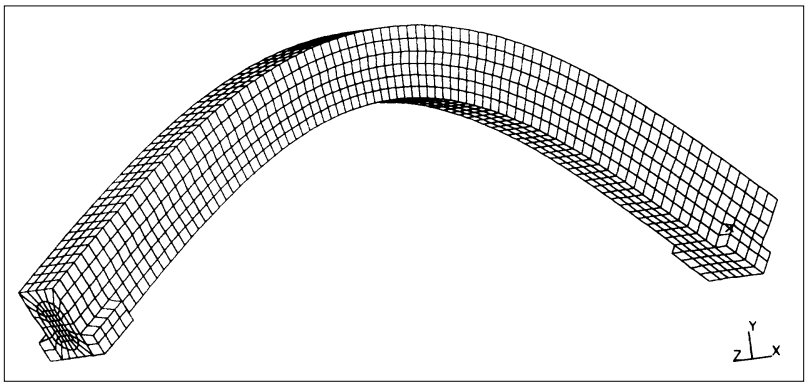

b. Second.

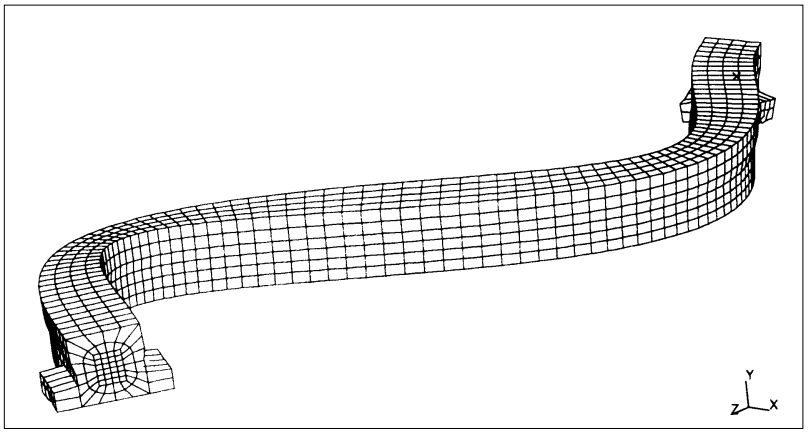

c. Third.

Figure 18. Dynamic flexural modes for Bechtel girder.

Since the vehicle bogies are closely spaced, these beam frequencies should not cause problems by resonance in any direction. This was also shown in the beam element analyses for bending about the *x*-axis only.

To address the viability of FRP reinforcing, we conducted a literature search to determine the state-of-the-art in FRP reinforcing. Little information was found on its use in major structures, especially pertaining to long-term durability and overall structural performance. However, this type of reinforcing has captured the interest of many researchers and much more information can be expected in the future. The advent of maglev promises to spur further interest and development in this area. Some basic information on different types of FRP reinforcing was assembled and is summarized in Table 26.

Conclusions. Although a complete range of static and dynamic loadings was not considered, the analyses told us that the girder should perform within its required limits. The variations of stresses (stress cycles) were not studied since a dynamic analysis was not made with the solid-element model. However, the low stresses and small deflections observed for the static load case show that the fatigue life of the structure should not be a problem.

Further study of this girder should include dynamic analyses with the solid-element model using more realistic and worst-case vehicular loadings, as provided from a dynamic vehicle model. These analyses would allow a study of stress cycles within the girder, which would give a better look at of its durability and the amount of transverse reinforcement actually required. Reducing the amount of transverse reinforcing would be beneficial since much of it is FRP reinforcing, the viability of which is yet to be proven.

Insufficient information exists at this time to allow strong conclusions about the viability of FRP reinforcing. The technology does appear to be evolving rapidly and holds promise. In the Bechtel girder, FRP is only used

Table 26. Characteristics of fiber-reinforced plastic (FRP) composite reinforcing.

Type	Longitudinal tensile strength (MPa)[a]	Transverse tensile strength	Young's Modulus	Anchorage			Fatigue resistance	Chemical resistance	Durability
				Expense	Problems[d]	Creep			
Prestressing steel	1600–1800	Same as longitude	200 GPa	Least	No	—	Susceptable to salt	Good	Good
Carbon fiber	Up to 2800[c]	Low	129 GPa[c]	Most[c]	Yes	—[e]	O.K.	Good[g]	—[h]
Aramid fiber	1200–1400	Low	41–65 MPa	Medium	Yes	—[e]	O.K.	Good[g]	—[h]
Glass fiber[b]	700–1500	Low	41–65 MPa	Least of FRP	Yes	—[e]	Least[f]	Good[g]	—[h]

[a] Strength increases with smaller diameter fibers because of less surface area for defects. FRP has no yield point prior to failure (straight line to failure).
[b] Most research data thus far. Most susceptible to surface flaws that affect strength.
[c] Depends upon purity of carbon fibers.
[d] Some successful methods exist but are expensive and difficult to use effectively. Post-tensioning presents most problems because of localized end anchorage. More research needed.
[e] No data on creep of FRP, except for small amount of conflicting data on GFRP. However, low modulus of FRP means concrete creep will cause less prestress loss.
[f] Alkali sensitive. Concrete is a strong alkali, so careful protection necessary.
[g] FRP not susceptible to fatigue-producing longitudinal magnetic forces from train passage. Fatigue from beam flexure dependent upon applied stresses, same as steel.
[h] No data on FRP. Research needed to study effects of water, oxygen, heat, light, etc., on creep, strength, polymer solubility, alkali resistance, etc.

for the top portion of the transverse reinforcing and it is not prestressed. This is considerably less risky than when it is used as main longitudinal reinforcing, especially when prestressed.

Foster-Miller guideway

General. The concept for the Foster-Miller guideway is shown in Figure 19. The guideway girder is a unique structure with an open-cell, integral sidewall constructed from modular units. Two symmetrical halves are coupled together by a series of intermittently spaced truss-type diaphragms. The modular system is designed to be lightweight enough that each half can be built at a central off-line facility and easily transported to the construction site.

The system is held together by post-tensioning tendons that run horizontally through the section. It is reinforced in the longitudinal direction by a combination of pre- and post-tensioned steel tendons in the lower half and FRP tendons in the upper half. While there is no bonded shear reinforcing, a combination of FRP post-tensioning and polypropylene-fiber-reinforced concrete is used to keep tensile stresses in the concrete within allowable limits. The girders will be placed on the pier supports as simple-span units. Then every other support will be made continuous through the application of external FRP post-tensioning, making a two-span continuous system.

Key issues.

- The Foster-Miller vehicle has bogies only at its ends, at spacings of 24.7 m. At these large spacings, the passage frequency of the bogies is very close to the primary flexural mode frequencies of the guideway, meaning that there are potential resonance problems. This interaction can greatly increase the dynamic flexural response and resulting stresses within the guideway.
- Since the cross section is quite complex and is loaded horizontally, vertically, and longitudinally through its sidewalls, conventional analytical methods for the prediction of local shear and bending stresses will not apply.
- The unique guideway design heavily depends upon the viability of FRP reinforcing as a nonmagnetic substitute for conventional steel reinforcing.
- Bending stresses within the cross section must be kept low enough through use of FRP prestressing and wall thickness adjustments to alleviate the need for bonded transverse shear reinforcing.
- The size and construction complexity of this guideway are a concern. The modular girders will be easy to transport, but this approach could have a significant effect on the complexity of construction.

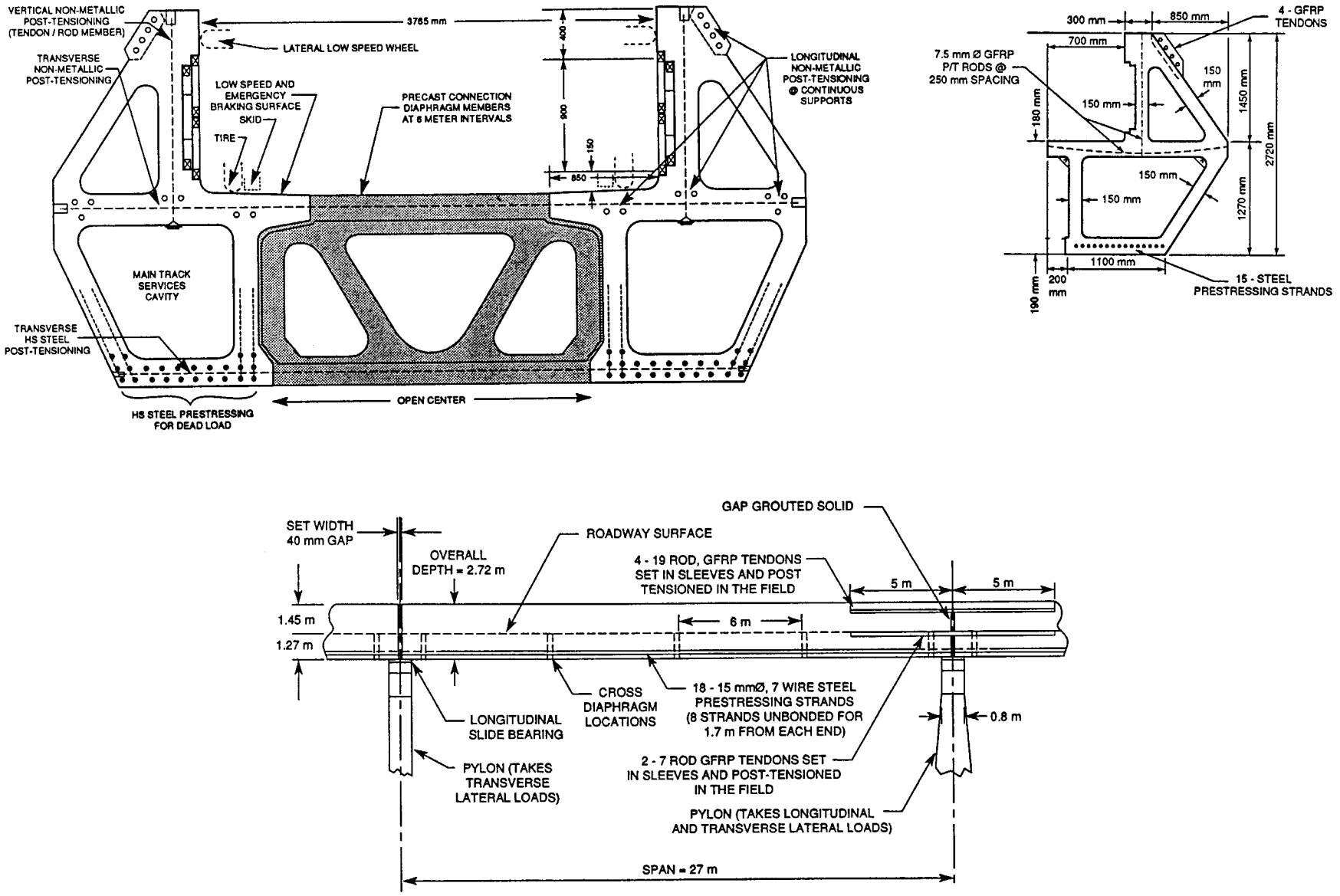

Figure 19. Foster-Miller guideway superstructure.

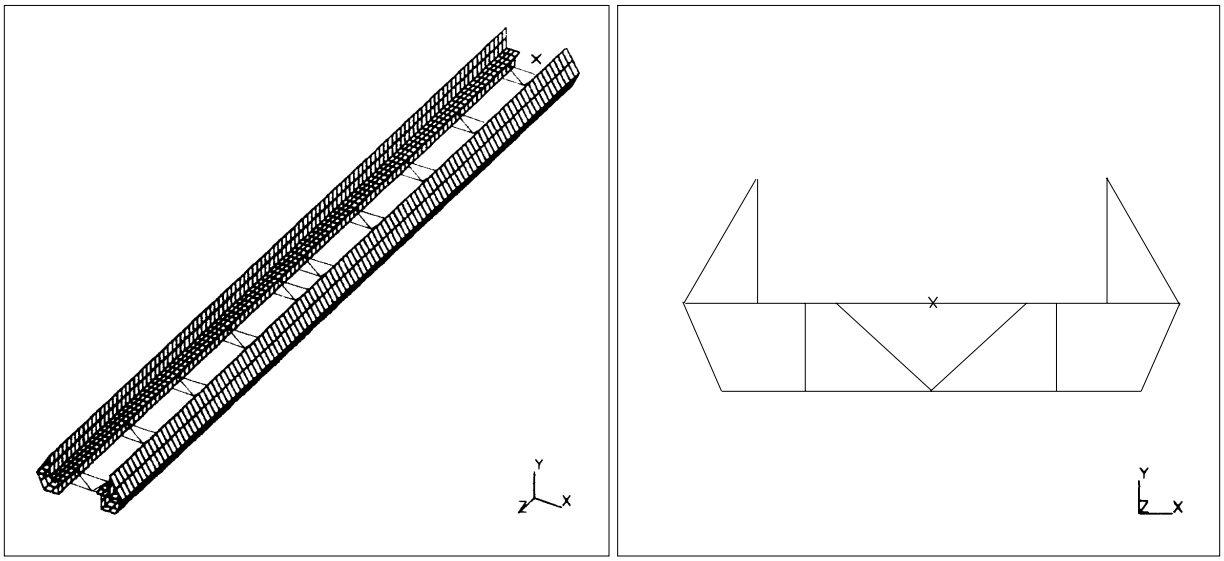

Figure 20. Shell-element model for Foster-Miller superstructure.

Approach. We studied the dynamic response of the girder to vehicle passage in the same way that we used for the Bechtel guideway. These calculations were made prior to the final baseline design and were thus based on a slightly different cross section than the final recommended design shown in Figure 19. However, the differences were small and should have little effect on the analytical results.

A three-dimensional finite-element model of the Foster-Miller guideway, using eight-node thin-shell elements, is shown in Figure 20. A two-span continuous structure was modeled. The ABAQUS code was used with this model to study the complex stress combinations within the girder and to study its dynamic flexural characteristics. All pre- and post-tensioning bars were modeled within the shell elements as rebar elements with initial stress conditions. The concrete was assumed to be a linearly elastic isotropic material.

The vertical and horizontal vehicular loadings discussed in section 3.4.4 of the Foster-Miller (1992a) final report were statically applied to the model. The vertical loadings were 51 kN / m and the horizontal loadings were 31 kN / m, both distributed over the 5-m bogie lengths. The horizontal loads were only applied to one side of the guideway at each bogie location. Since the structure is continuous over a support, two different load cases were considered. Load case 1 had only one bogie set in the middle of the first span, representing a vehicle halfway across. Load case 2 represented a vehicle with its midpoint at the middle (continuous) support and thus had a bogie set near the middle of each span. For load case 2, the horizontal portion of the loadings were applied in opposite directions from each other.

Results. The results of the dynamic analyses with the beam element model are summarized in Figure 21 for the 100- and 500-km / hr (28- and 139-m / s) vehicle passes. Both plots are for the maximum response nodes of span 1 only. The response of the second span was always identical to that of the first, indicating no dynamic coupling between the two spans. The maximum dynamic deflections varied from approximately 0.8 mm for the 100-km / hr vehicle passage to 1.7 mm for the 500-km / hr passage. If we assume that the 100-km / hr passage is equivalent to a static loading, this corresponds to a significant DLF of 2.10. The high DLF compared to that of the Bechtel design shows the trade-off associated with larger bogie spacings. Again, please note that the loadings applied to the beam element model were not a worst case and, thus, the deflections calculated were less than can be expected under more severe loadings.

The displaced shape of the shell element model resulting from load case 2 is shown in Figure 22. Of the two load cases, this one caused the greatest deflections and stresses. Bending occurred about both the *x*- and *y*-axes. The maximum downward (*y*-axis) deflection was 2.6 mm from its original 0.3-mm upward cambered position, ending up at 2.3 mm down from a flat position.

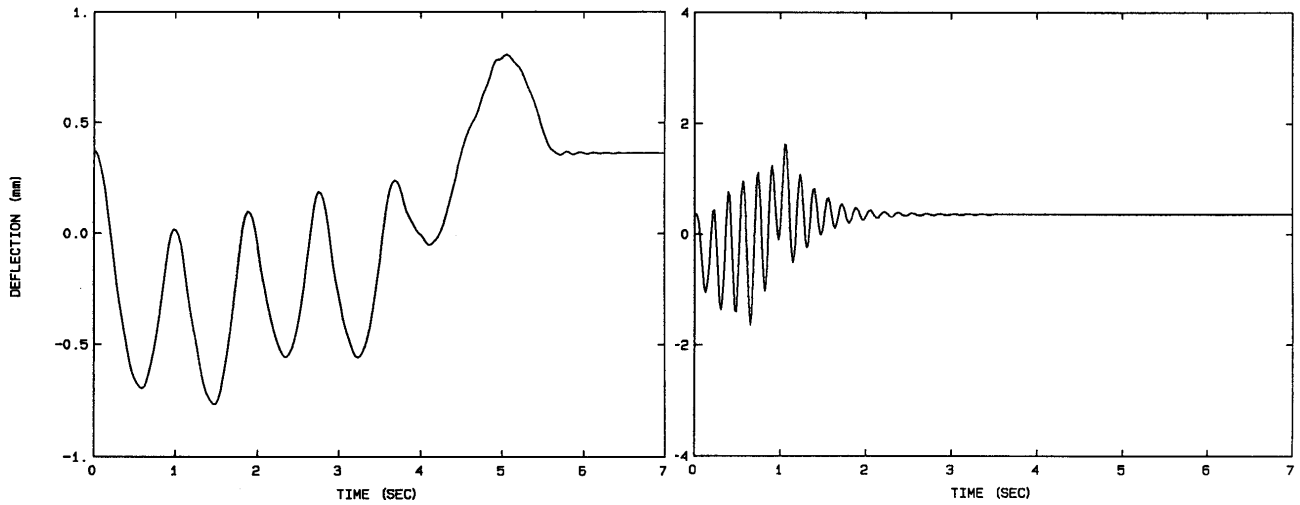

a. 100-km/hr vehicle passage. *b. 500-km/hr vehicle passage.*

Figure 21. Dynamic analysis results from beam-element model of Foster-Miller guideway.

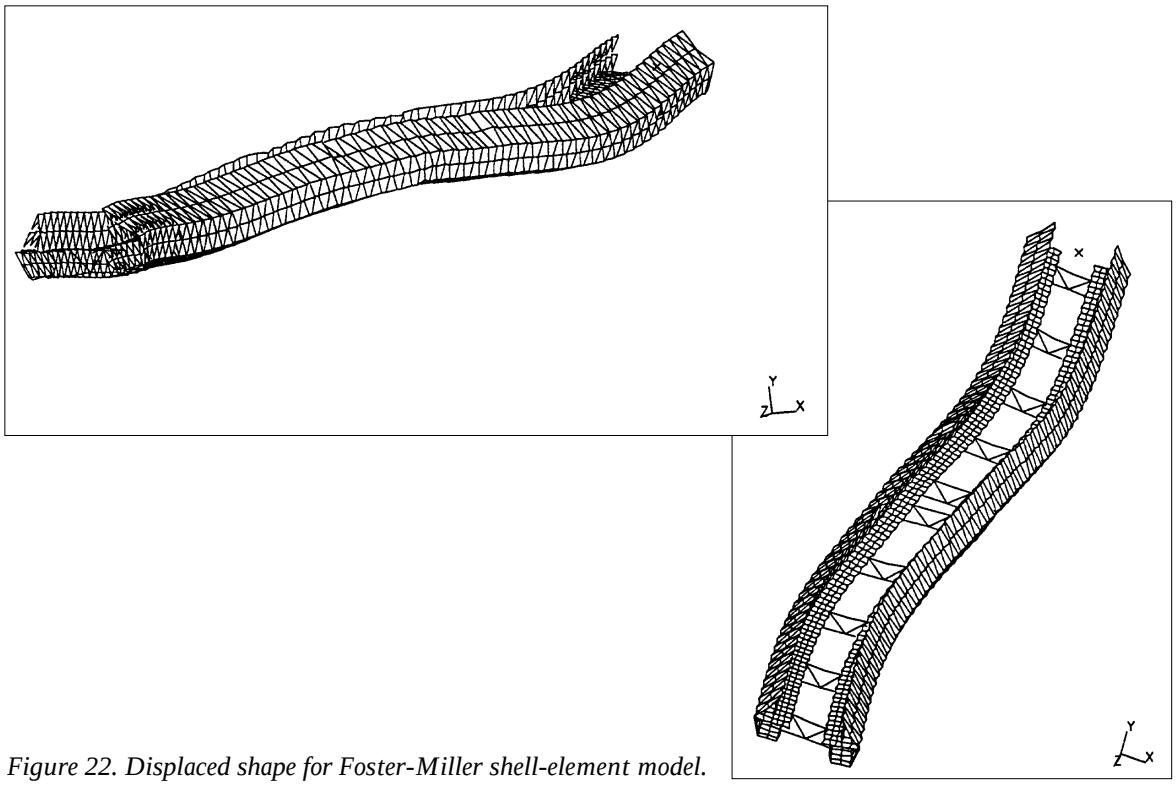

Figure 22. Displaced shape for Foster-Miller shell-element model.

The maximum horizontal (*x*-axis) displacement was 6.7 mm. The design horizontal gap between the magnets is 75 mm. Obviously, the lateral displacements would have been smaller if the lateral loadings had not been acting in opposite directions from each other. These were all static deflections and, according to the previously discussed dynamic analyses, would have been approximately twice as much if applied as sweeping dynamic vehicular loadings. The same applies to the stresses discussed below.

Although they resulted from the greatest of the two load cases considered, the principal stresses for load case 2 (Fig. 23) were low. The majority of the girder experienced compressive stresses below 0.96 MPa. If we neglect stress concentrations

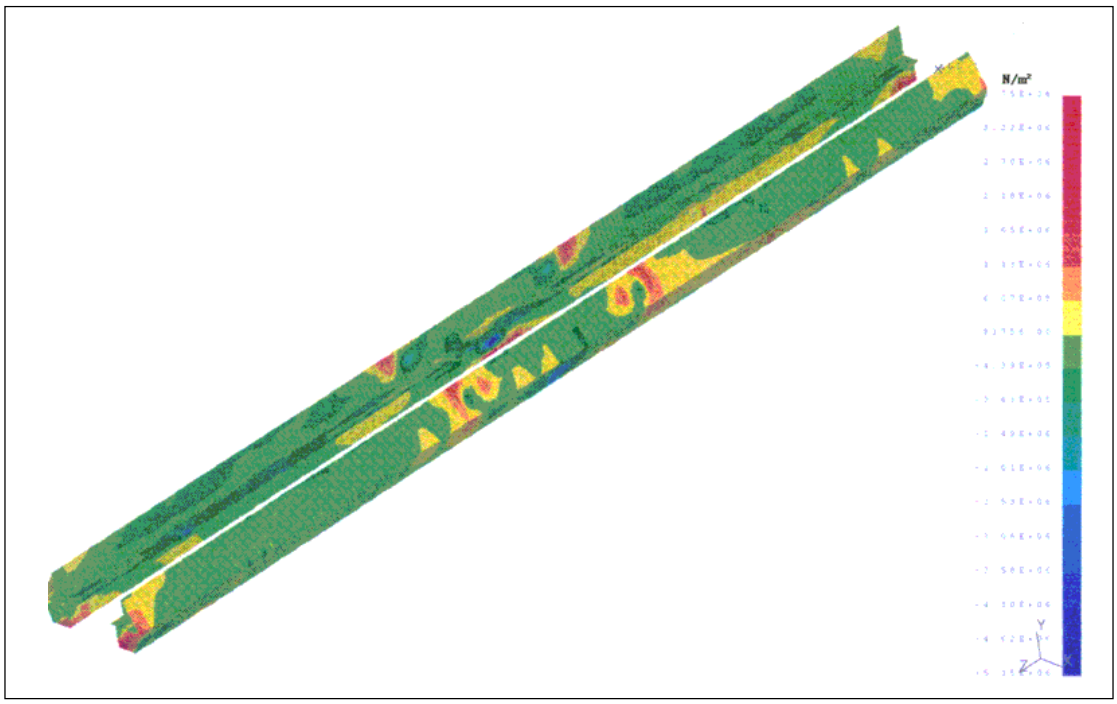

a. Top view.

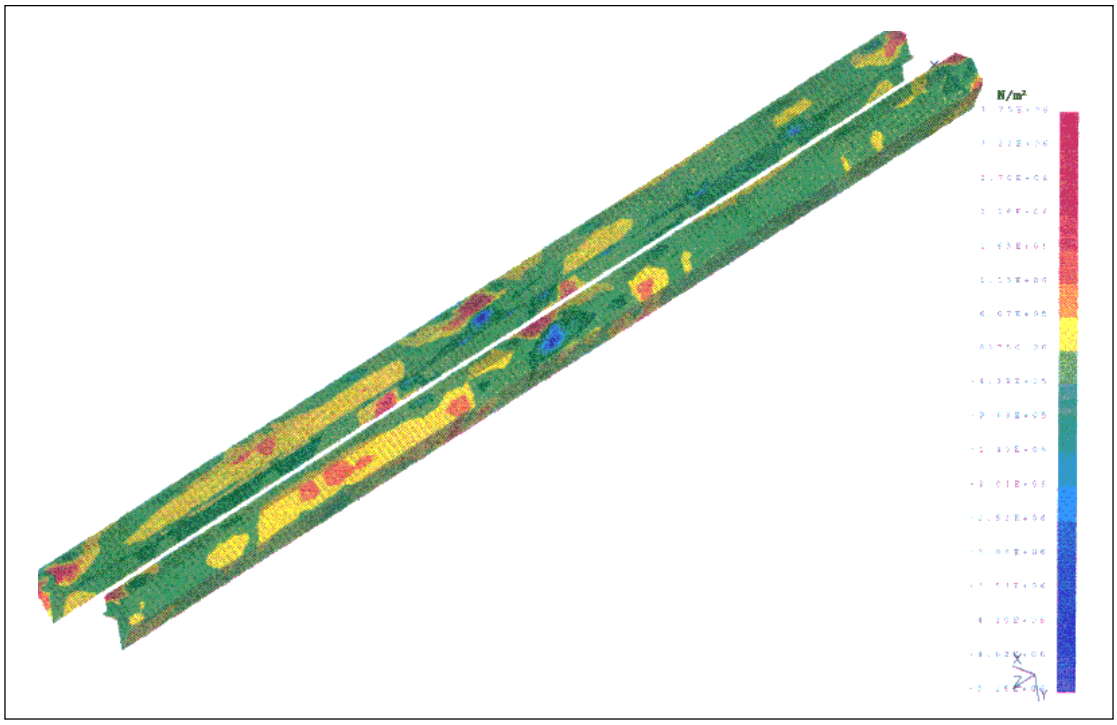

b. Bottom view.

Figure 23. Maximum principal stresses for load case 2, Foster-Miller.

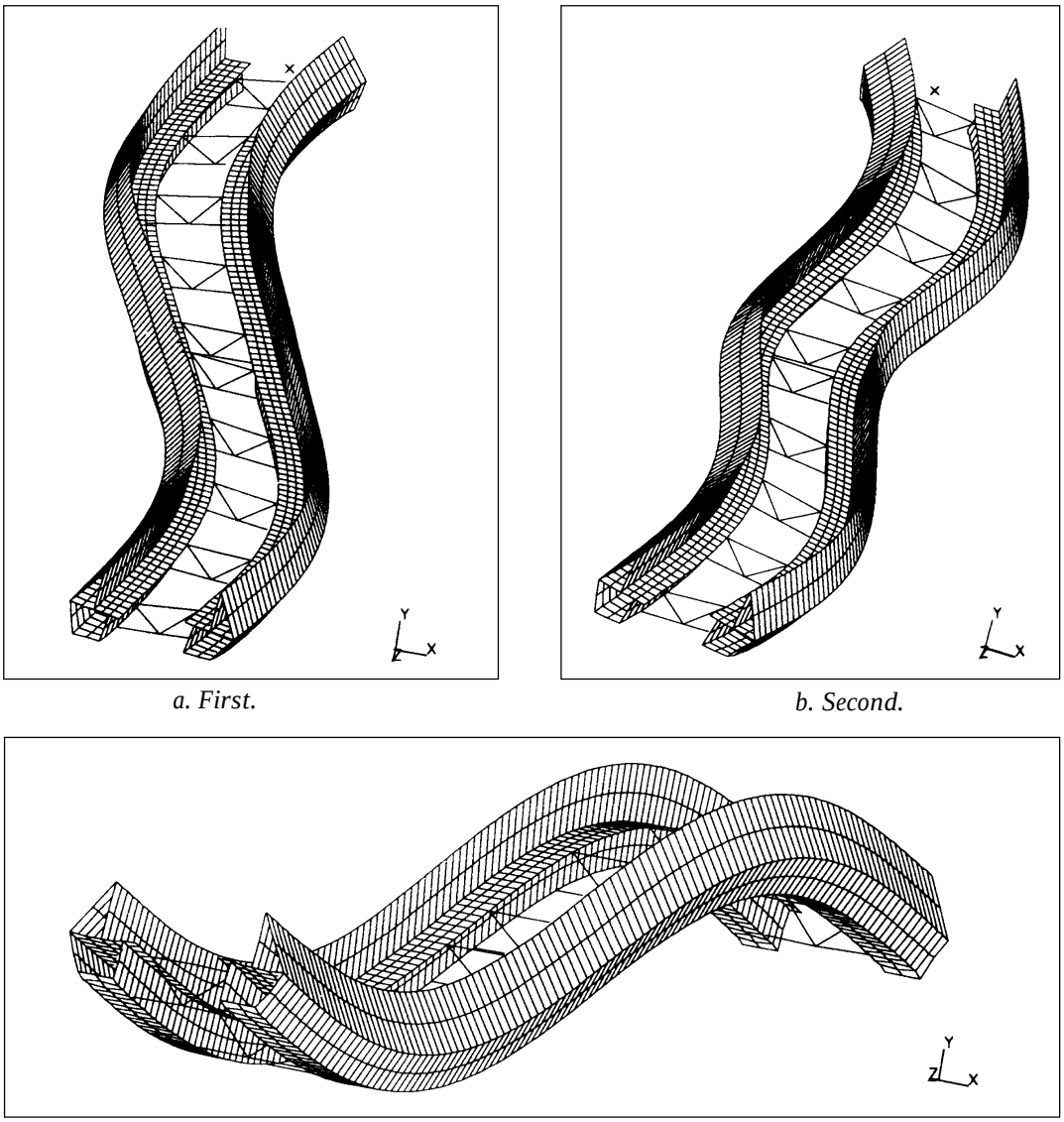

a. First.

b. Second.

c. Third.

Figure 24. Dynamic flexural mode for Foster-Miller superstructure.

ascribable to prestress anchoring and support conditions, the majority of maximum principal tensile stresses were below 0.61 MPa. These tensile stresses were well below commonly accepted allowable limits for pre-stressed concrete, which are in the 1.4-MPa range (Nilson 1978). Low stresses are desirable for the static case since the dynamic case could cause as much as a factor of 2 increase.

The first three dynamic bending modes are shown in Figure 24. These were somewhat surprising, since the first two modes were for bending about the vertical *y*-axis, indicating the structure to be weakest in this direction. However, upon closer study, it is understandable. The connecting diaphragms (between the beam units) are parallel to each other and perpendicular to the beam units, and thus add no stiffness in the horizontal bending direction. The frequencies for the first through third bending modes were 4.4, 5.2, and 5.7 Hz, respectively. These frequencies are of concern since the bogie passage frequency for the vehicle (with 24.7-m bogie spacings and traveling at 500 km / hr) is very close at 5.4 Hz. A complete set of dynamic analyses considering simultaneous vertical and horizontal loadings should be conducted.

Conclusions. The Foster-Miller guideway is a

very innovative design that apparently meets all of their stated objectives. However, because of the complexity of the structure and the limited scope of this and the SCD analytical work, much more in-depth analyses should be conducted before its actual construction. Specifically, a more thorough study, possibly with a more refined finite-element grid, should be made of localized shear and bending stresses resulting from worst-case dynamic vehicle passages inducing three-dimensional loadings. Note that these dynamic vehicle loads may well result from resonance conditions. This study is particularly important since the current design employs no bonded shear reinforcing in the precompressed zones, mandating that tensile stresses be kept very low for safety and durability.

The analyses showed that the principal stresses within the structure were low for the load cases considered. Principal stresses are useful in visualizing the flow of stresses in uncracked beams. They also provide useful information on the location and orientation of diagonal tension cracking and the load at which these cracks might occur. However, because small increases in load beyond this point can cause disproportionate increases in diagonal tensile stresses, principal stresses do not give us a good indication of the inherent safety of the structure. A strength analysis, based on direct tensile and shear stresses, is necessary for this. The shell element model used here can provide this information.

The heavy dependence of this guideway on nonmagnetic FRP reinforcing is a concern because the longevity of this material is not currently well known. In particular, the durability of the attachments of post-tensioning rods is an issue requiring further study. Also, the consequences of using conventional steel reinforcing in this guideway warrant investigation to determine whether FRP is enabling technology or enhancing technology. Despite these issues, FRP appears headed for use in high-performance civil structures, so that practical experience with it will soon begin to accumulate. This experience will undoubtedly address its durability and hence its desirability for use in maglev guideways.

Grumman guideway

General. The concept for the Grumman superstructure is shown in Figures 25. The superstructure design is very innovative in that it allows for two guideways to use the same substructure system. The relatively small hat-type slab elements that are actually traversed by the vehicles are each supported on closely spaced (4.6-m centers) outrigger elements, which are connected to a central simply supported "spine" box girder.

The slab elements are precast reinforced concrete units, continuous over the outriggers and simply supported only at 27-m centers to match the spine girder. To reduce deflections further, part of each levitation rail is designed to act compositely with the slab elements.

The spine girder is constructed from 4.5-m-long precast segments that are post-tensioned together. The post-tensioning has been equally divided between adjustable and nonadjustable profiles. The adjustable tendons allow periodic changes in the span deflections to cancel the effects of concrete creep.

Key issues.

- Since two vehicles may pass simultaneously on opposite sides of the spine girder, complex deflections and stresses may be induced, both of which will affect the total movement and thus ride quality experienced by the passing vehicles.
- The combined bending and torsional stresses within the central spine girder cannot be accurately predicted with conventional analytical methods.

Approach. The three-dimensional finite-element model used for the analyses of the Grumman guideway is shown in Figure 26. The spine girder and outriggers were modeled with combinations of four- and eight-node thin shell elements, and the guideway slab elements were modeled with beam elements. The composite-acting levitation hardware on the slab elements was not modeled. The ABAQUS code calculated both static and dynamic responses. We modeled the post-tensioning effect in the spine girder by applying an equivalent upward uniform load along the length of the girder and central axial loads at the girder ends (Nilson 1978). We modeled the post-tensioning effect in the outriggers by applying axial loads at the anchor points for the tendons. This method did not accurately account for the draping of the outrigger tendons through the cross section; future modeling should account for this. The transverse reinforcing in the spine girder was not modeled and the concrete was assumed to be a linearly elastic isotropic material. These assumptions were reasonable since the deflections were known to be small, likely keeping stresses low. More in-depth modeling would employ a nonlinear concrete model that, upon cracking,

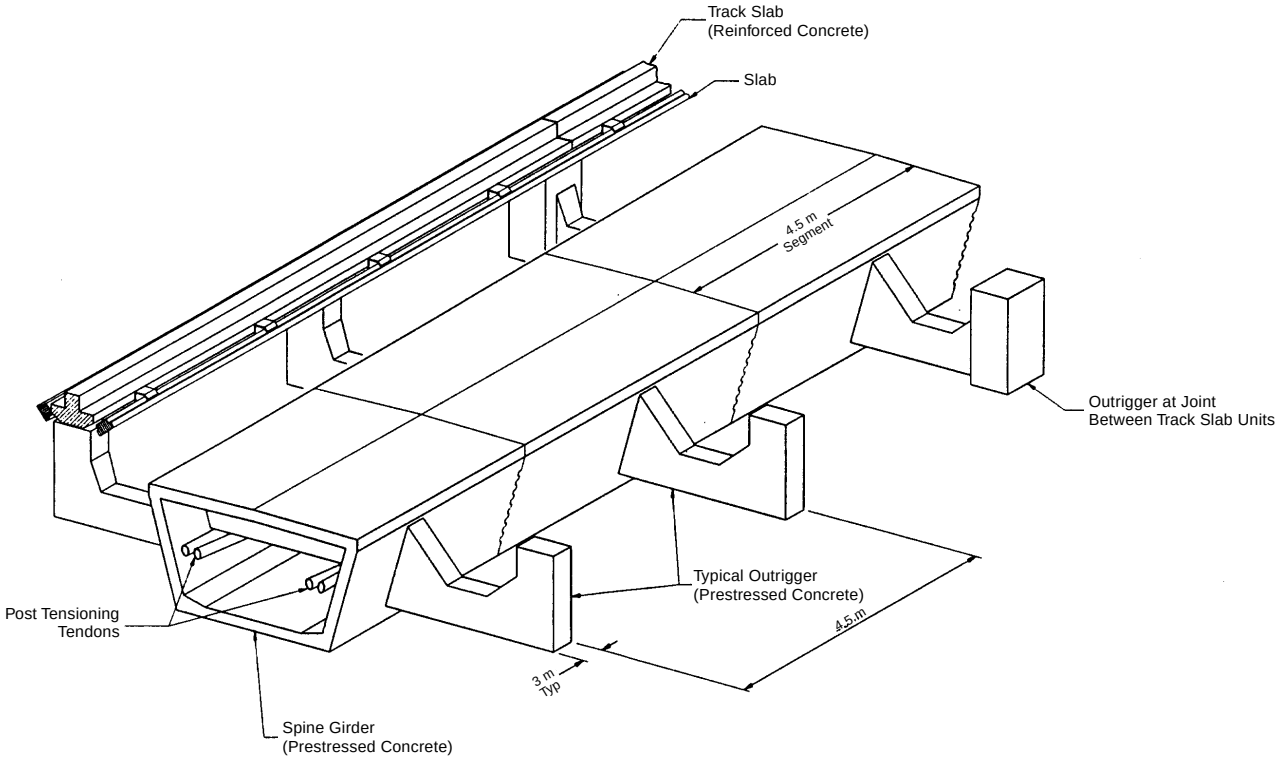

a. Detail view.

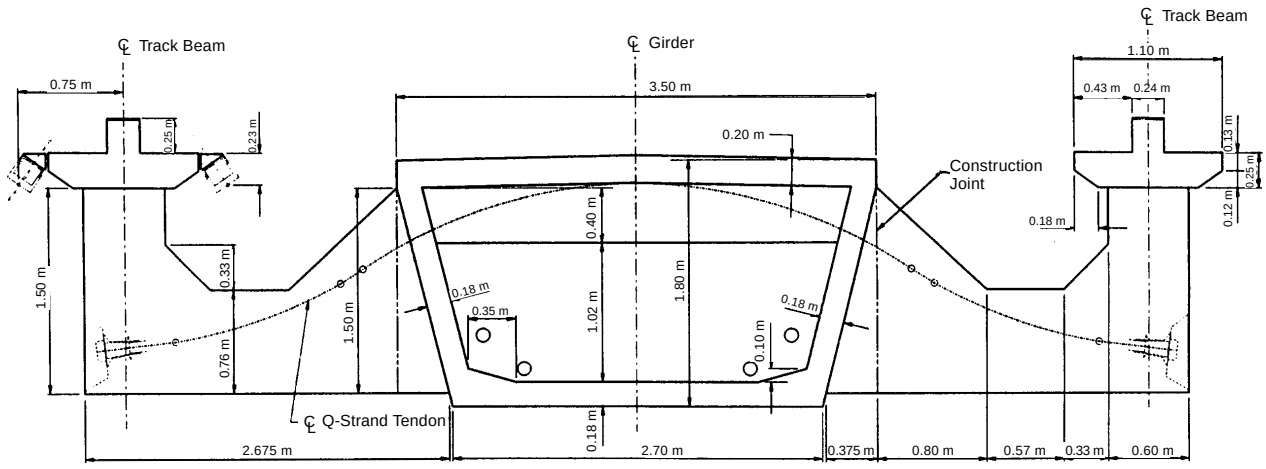

b. Cross-sectional detail.

Figure 25. Grumman's spine-girder superstructure.

would transfer all stresses to the reinforcing. This will be especially important for ultimate strength and earthquake response calculations.

Because of time limitations, only two load cases were considered. The first was the static application of vehicle loads on one side of the guideway only, and the second was the dynamic application of the same vehicle loads moving across the span at 500 km/hr (139 m/s). The dynamic loadings were produced by distributing the vehicle weight out to and over the length of each of the vehicle bogies. Through use of a computer program, these loadings were then swept across an assumed straight and flat guideway and a load–time history was calculated for each loaded node. Note that these loadings were simplified and by no means were a worst-case loading scenario.

Results. The magnified displaced shape of the finite-element model resulting from the dynamic load case is shown in Figure 27. The deflected

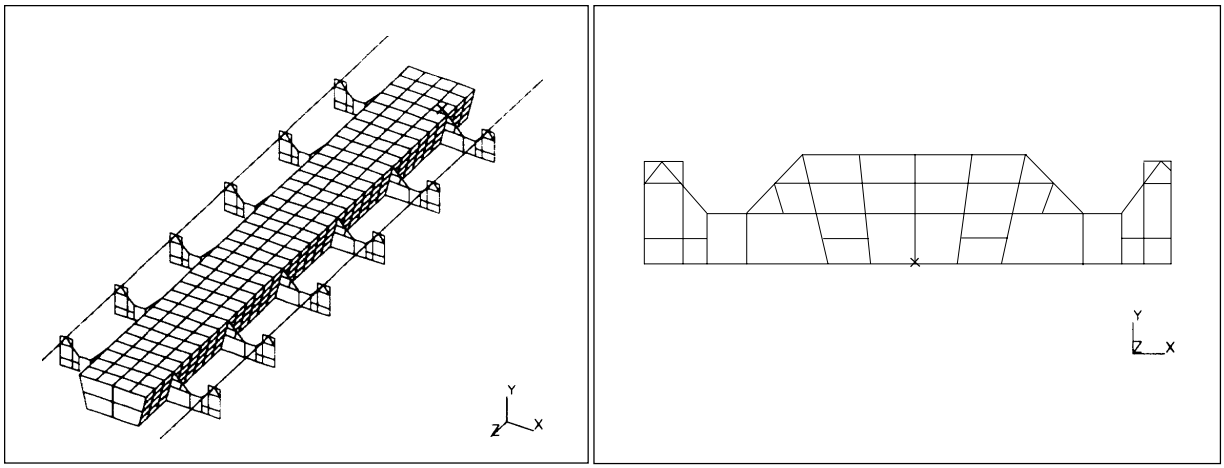

Figure 26. Finite-element model for Grumman superstructure.

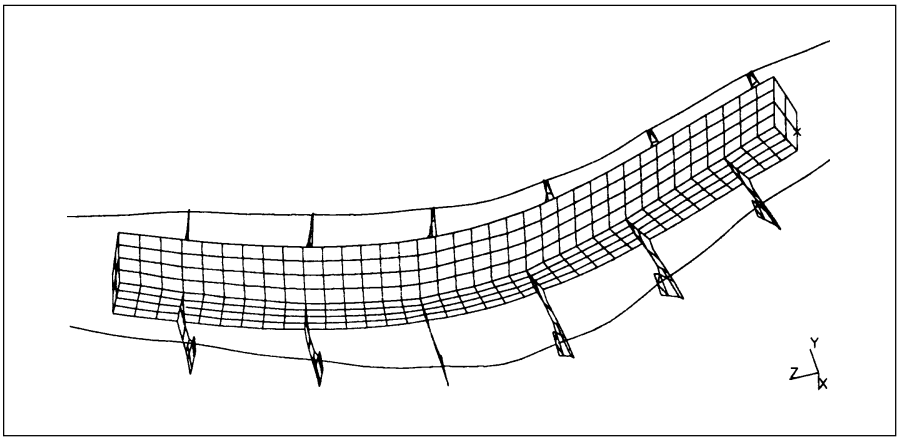

Figure 27. Displaced shape of Grumman finite-element model at t *= 0.22 s.*

shape for the static load case was the same, except that no deflection was seen in the unloaded slab elements on the opposite side of the guideway. These elements experienced deflections for the dynamic case because of their inertial response to motion.

Figure 28 compares nodal deflections along the length of the structure for both the static and dynamic cases. The deflections of both the loaded and unloaded beam elements (track slab) are shown, together with both the loaded and unloaded side of the spine girder. Comparing these deflections shows the amount of torsional twist experienced by the spine girder and the local and total deflections experienced by the beam elements.

For the dynamic case (Fig. 28b), the maximum local deflection of the loaded beam elements between outrigger supports was only about 1 mm. However, the total deflection, accounting for spine girder twist and vertical deflection and outrigger flexure, was 11 mm. The vehicle bogies should respond mainly to the local deflection of 1 mm and thus minimum gap requirements should easily be met. However, the vehicle as a whole will be affected by the total 11-mm movement of the guideway and ride quality may be affected. Note that the outrigger flexure accounted for much of the total movement. The outriggers could be stiffened by a redesign of their shape or of the post-tensioning. It is also possible that the way in which the outrigger post-tensioning was modeled was too simplified and showed more deflection than would actually be the case. Future analytical work should address this possibility.

Comparing the static and dynamic deflections in Figure 28 gives a DLF of approximately 1.6 for the slab elements and 1.4 for the spine girder. These values are a bit higher than the 1.2 value that Grumman used in their design calculations.

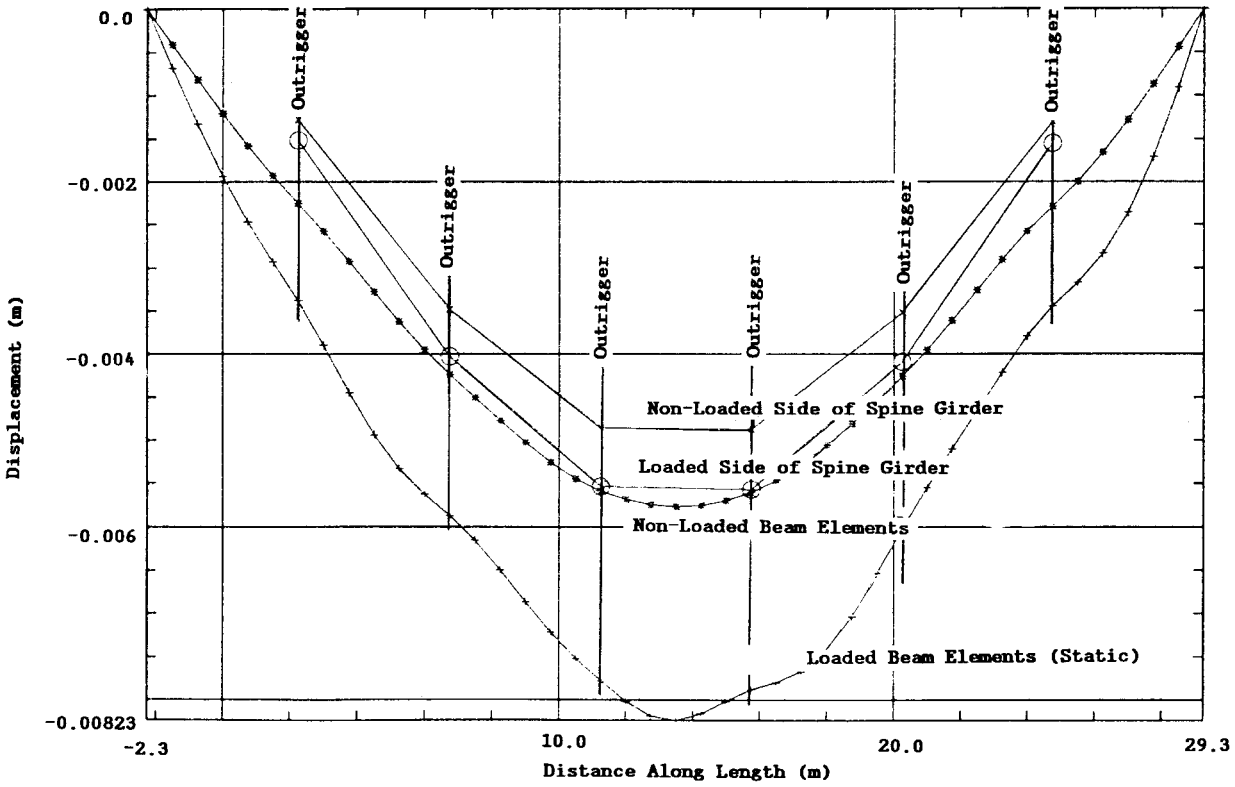

a. Static vehicular loading.

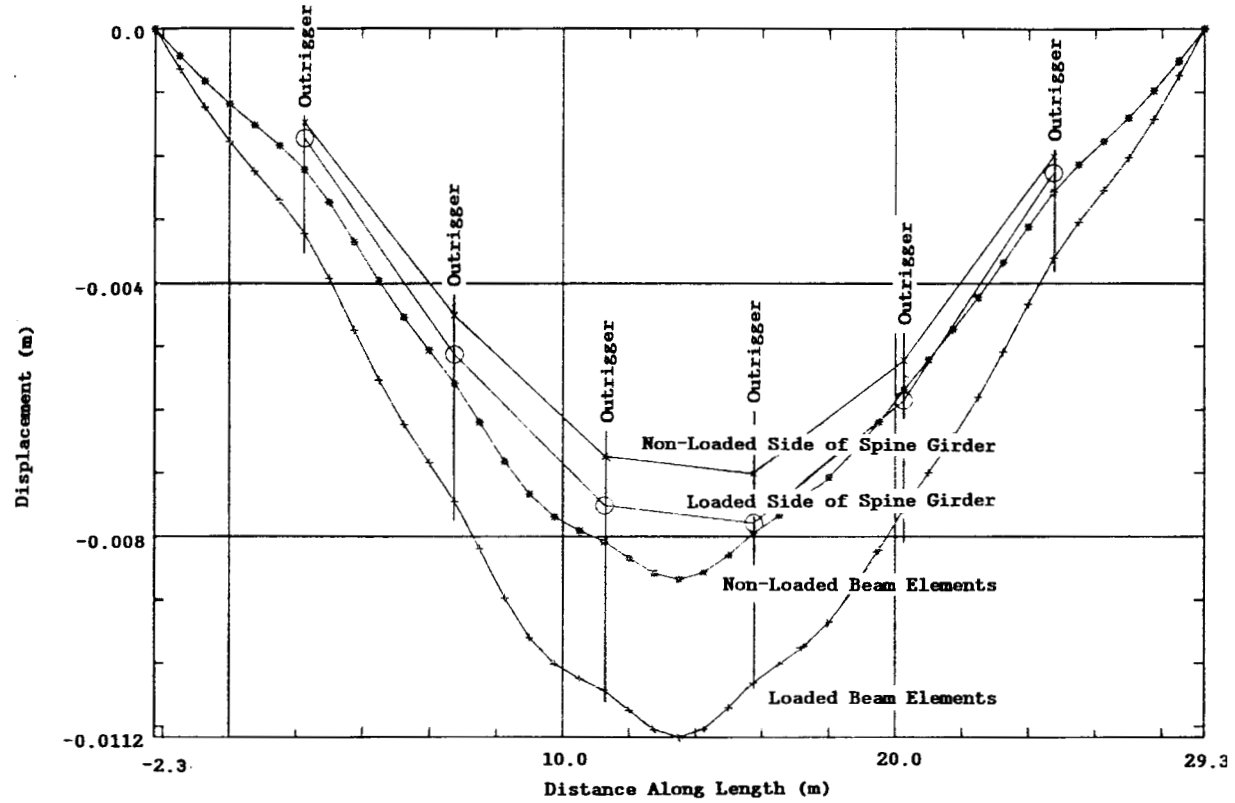

b. Dynamic vehicular passage.

Figure 28. Displacement along length of Grumman superstructure.

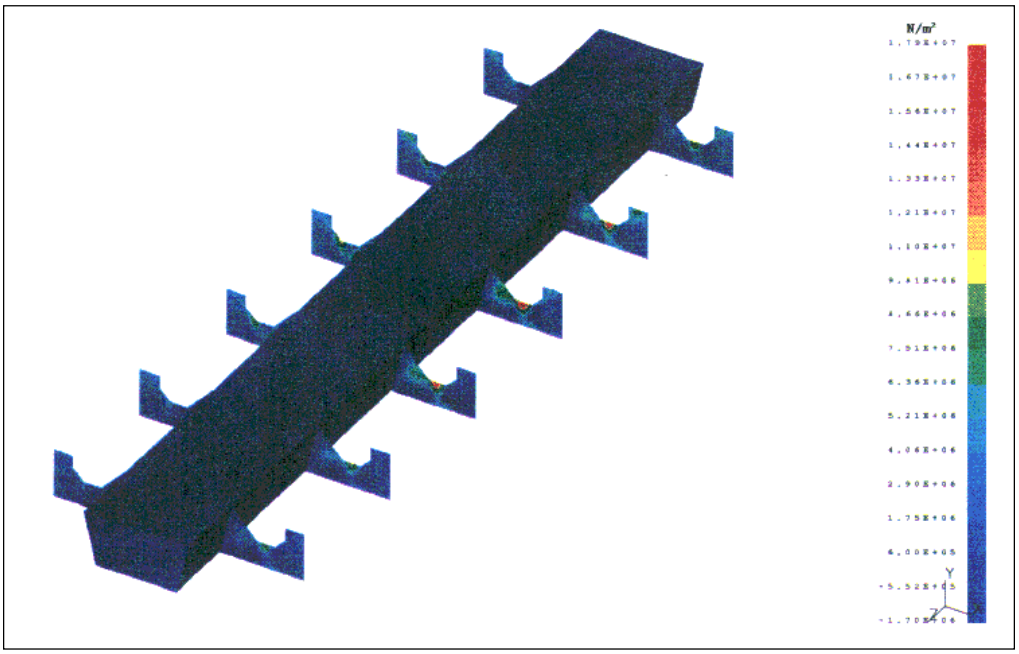

Figure 29. Maximum principal stresses from Grumman analysis at t *= 0.22 s.*

The reason for the relatively high DLF for the slab elements is not readily clear because the Grumman vehicle has closely spaced bogies that would normally load the guideway at a high enough frequency to avoid large dynamic increase effects. However, the slab elements may be of short enough span and stiff enough that their natural frequencies are close to the loading frequency. Also, the loading frequency that the spine girder actually experiences may be considerably lower than the bogie passage frequency since it is transmitted to the spine girder through the 4.6-m center to center outriggers. Further study should be made of the dynamic response of the guideway, especially with simultaneous vehicle passages on both sides.

The maximum principal stresses for the dynamic load case at the time of maximum deflection are shown in Figure 29. Most of the guideway experienced compressive stresses around 1.7 MPa. We saw very little principal tensile stresses throughout most of the structure. The exception is at the tops of the outriggers, where the principal tensile stresses were approximately 17.9 MPa. Such stresses would likely cause cracking of the concrete and hence could affect its durability. Nevertheless, the problem is easily rectified by adjusting the drape or the degree of post-tensioning in these areas or by changing the overall dimensions of the outriggers. We do not see this as a critical issue.

The first three dynamic bending modes are shown in Figure 30. The first mode had a frequency of 4.4 Hz and represented overall bending of the entire structure. The next two modes had basically identical frequencies of around 4.9 Hz and represented flexure of the outrigger elements.

Conclusions. The Grumman guideway appears to be very efficient—it allows two guideways to use the same substructure. The analyses tell us that it will perform this function within allowable limits. However, a much more dynamic analysis would be required before it is actually built. These analyses should include more accurate vehicle loadings accounting for vehicle suspension characteristics, guideway irregularity and curvature, pre-camber and flexure of the guideway, and unbalanced loadings on the vehicle. In addition, various combinations of simultaneous vehicle loadings (i.e., one on each side of the guideway) must be considered.

Magneplane guideway

General. The Magneplane guideway, called a "Magway," consists of a trough and its supporting substructure (Fig. 31). The trough is composed of two aluminum levitation plate box beams connected by an LSM winding. The design varies, depending upon the required span length and guideway curvature–superelevation requirements. The design discussed here had a 9.14-m

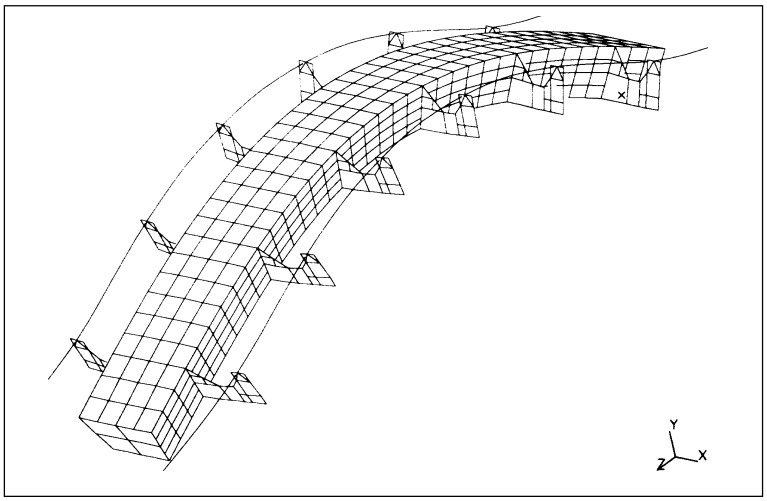

a. First.

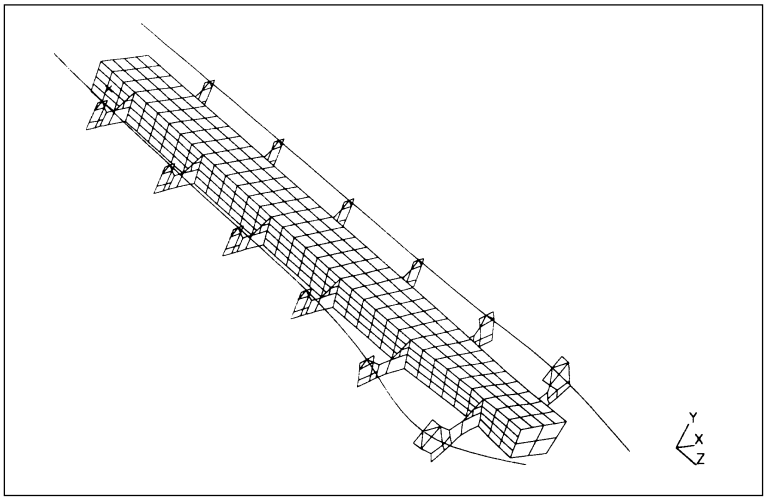

b. Second.

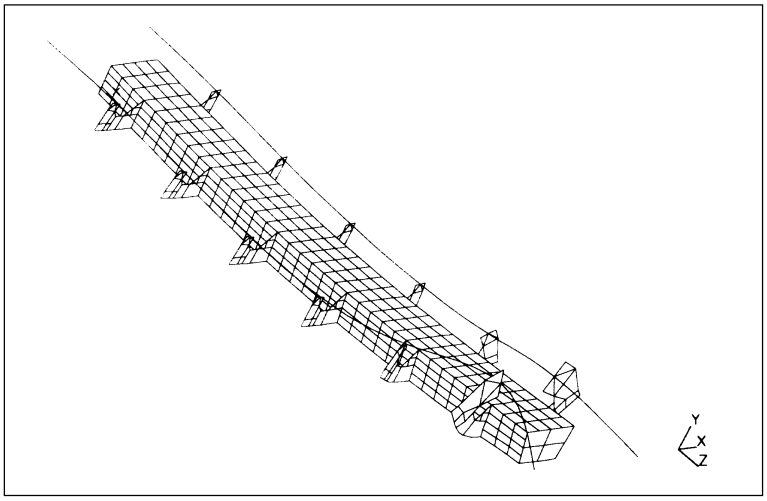

c. Third.

Figure 30. Dynamic flexural modes for Grumman superstructure.

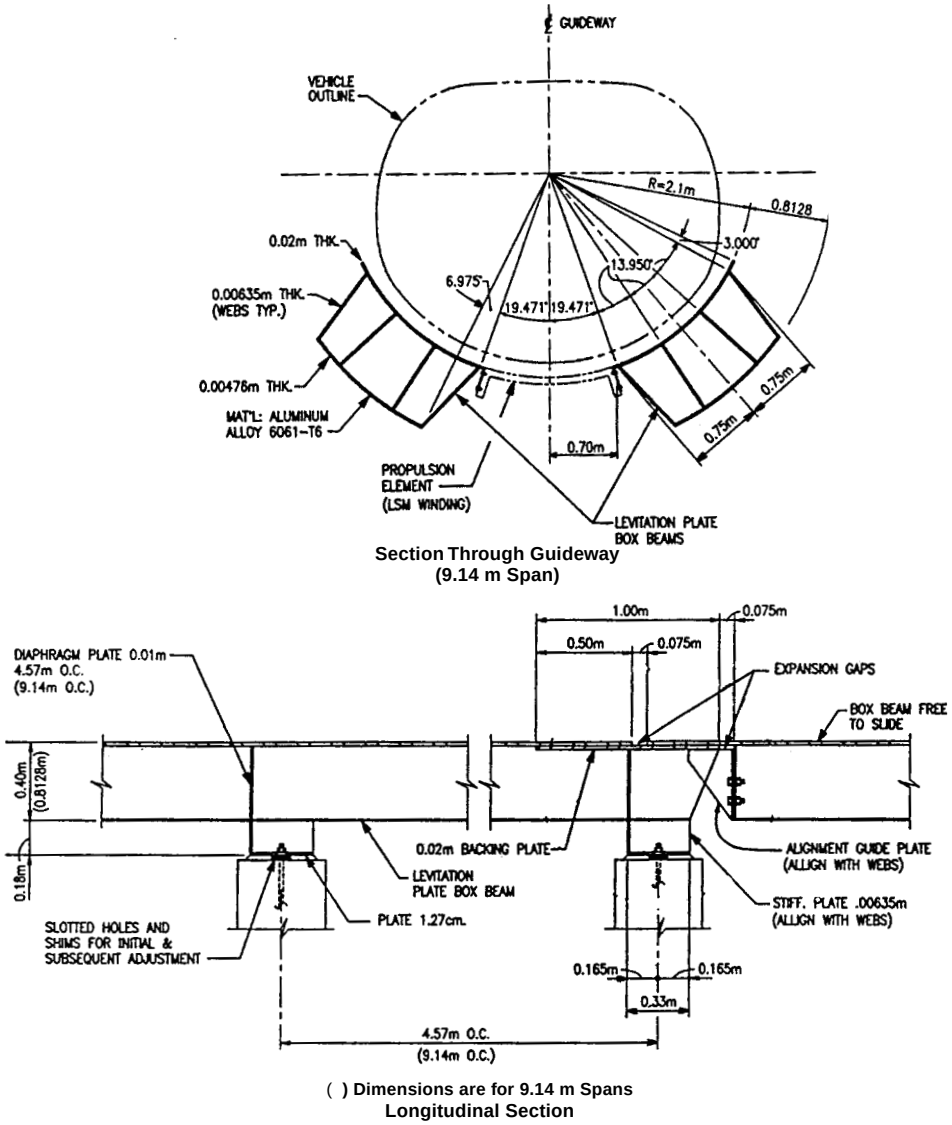

Figure 31. Magneplane guideway superstructure.

span and the levitation box beams were 0.81 m deep. These beams are two-span continuous and connected to adjacent beams, as shown in Figure 31.

Key Issues.

- Aluminum structures are very susceptible to fatigue failure, and as a result have a short life expectancy unless the applied cyclic stresses are within durability limits. Because of the structure's complexity, conventional analytical methods may not reliably predict the actual stress states experienced by the structure.
- Aluminum also experiences a high degree of movement with temperature variations. This property will require careful and innovative designs for expansion joints within the trough and the connections of the aluminum trough to its supporting structure and LSM winding.
- Because of the vehicle's high banking angles in curves, large tangential and torsional loadings will be applied to both the superstructure and substructure and must be carefully considered in the design.

Approach. The three-dimensional finite-element model used for the analyses of the guideway is shown in Figure 32. The ABAQUS code was used to calculate static response and to study dynamic flexural characteristics. All parts of the guideway, including the diaphragms, were modeled with eight-node thin shell elements. The aluminum 6061-T6 material was modeled as an isotropic

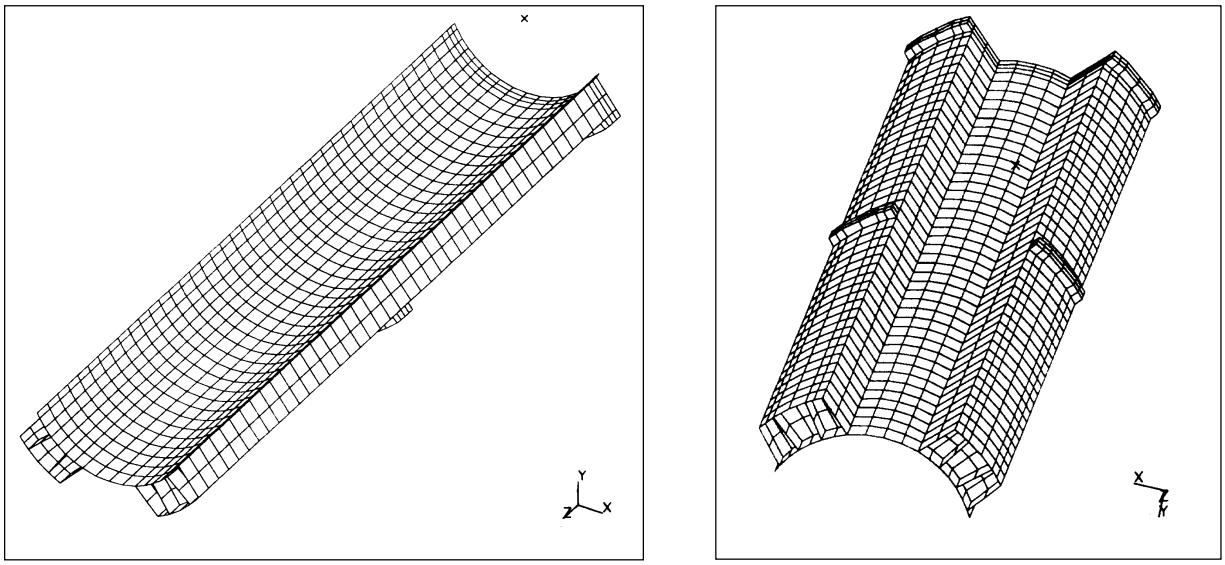

a. Top view. *b. Bottom view.*

Figure 32. Shell-element finite-element model for Magway.

linear–elastic material with an elastic modulus of 68,950 MPa. The LSM winding between the box beams was modeled as the same material and was assumed to be continuously connected to each of the adjacent box beams. It is actually constructed from a composite FRP material and is bolted to the box beams, the details of which could not be found. The assumption of a continuous connection to the box beams may not have been conservative and, therefore, the analytical results should be considered with this in mind.

Since the Magway is two-span continuous, two different static load cases were considered. Load case 1 had only one bogie set in the middle of one span, representing a vehicle at the halfway point across the span. Load case 2 represented a vehicle with its midpoint at the middle Magway support and, thus, had a bogie set near the middle of each span.

Results. The magnified displaced shape from load case 1 is shown in Figure 33a. It had a maximum downward deflection of 2.9 mm in a direc-

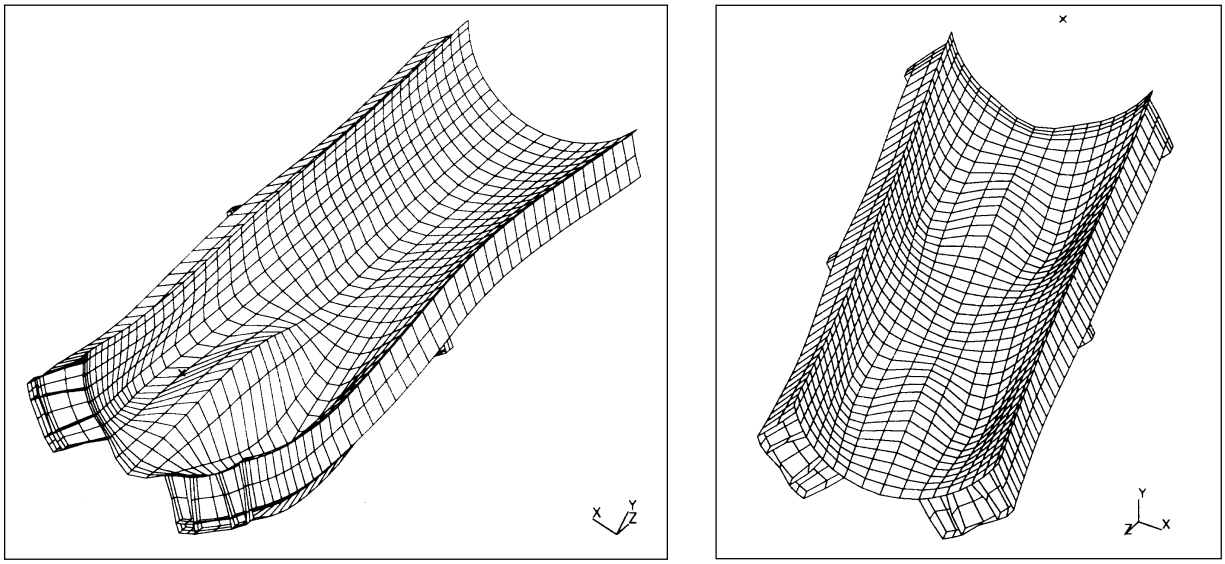

a. Load case 1. *b. Load case 2.*

Figure 33. Displaced Magway shape.

tion normal to the vertical axes of the box beams. Figure 33b shows the deflected shaped for load case 2, which produced a maximum displacement of 2.6 mm normal to the box beams. Figure 33a shows that the deflections were somewhat localized and transferred to the bottom plate, mainly through the longitudinal stiffeners directly beneath the bogies. Although not required on the basis of these analyses, further stiffness could be added to the Magway through additional transverse diaphragms along its length, which would allow more load sharing between the longitudinal

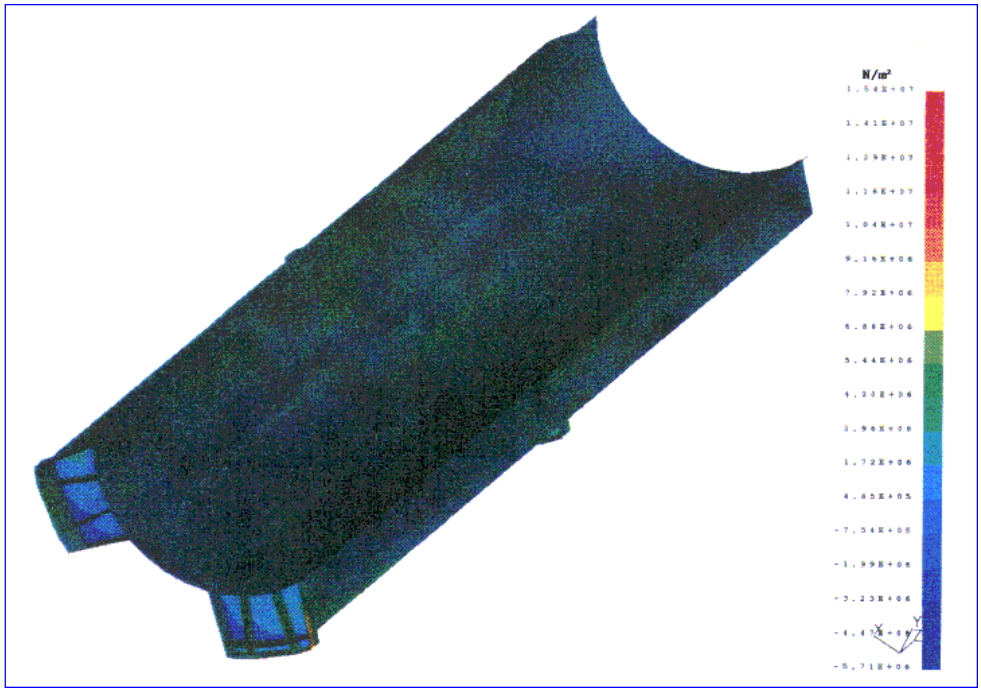

a. Top view.

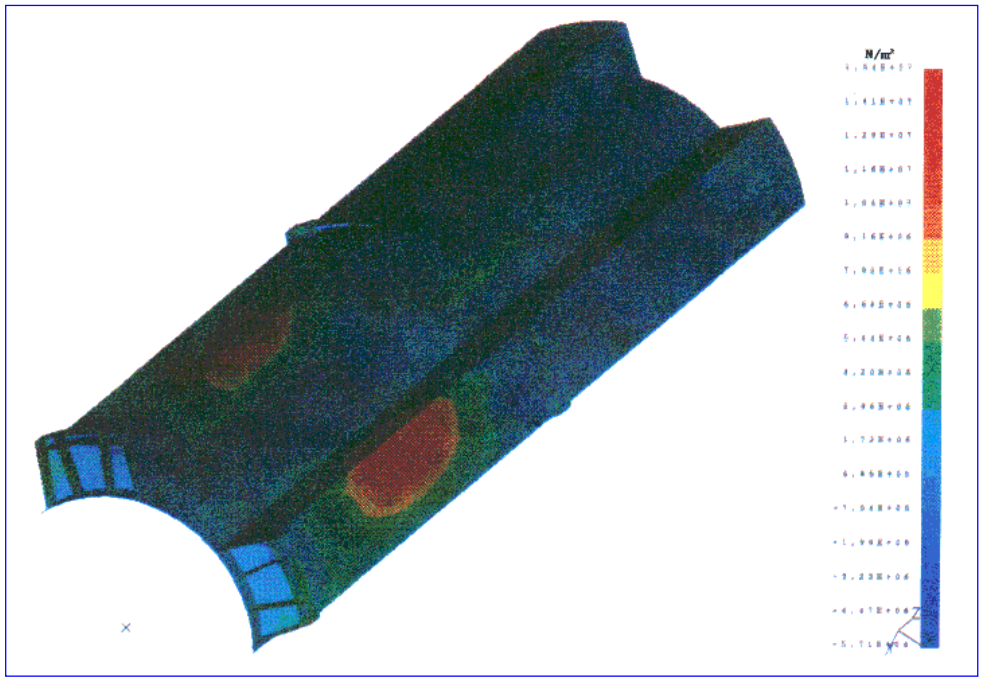

b. Bottom view.

Figure 34. Maximum principal stresses from Magway dynamic analysis, load case 1.

stiffeners. This addition could possibly reduce the required thicknesses for the top and bottom plates (although Magneplane's top-plate thickness is based on magnetic considerations).

Maximum principal stress contours are shown for load case 1 (worst of the two cases) in Figure 34. These stresses were all below 15.4 MPa tension and 5.7 MPa compression. Although no dynamic calculations were performed to determine the cyclic stresses, these low static stresses are well below the 41.40-MPa fatigue limit for Aluminum 6061-T6.

Figure 34 shows that the LSM winding (as modeled) fully shares in the compressive bending stresses at the top of the Magway. Depending upon how it is attached to the box beams, this may not actually be the case. If it is attached in a way that allows for its unrestrained longitudinal movement, it will not share in any of the longitudinal bending stress of the box beams and the stresses in these beams will be slightly higher than calculated here. However, they will likely still be well within the allowable fatigue limits.

The first four dynamic bending modes are shown in Figure 35. The frequencies of these modes were 30.7, 34.6, 37.7, and 39.3 Hz, respectively. The Magway is much stiffer than the other SCD guideways because of its shorter span and relatively deeper (in relation to span length) section. Because of the Magway's high-frequency response, there will likely be no large dynamic effects from the vehicle passage. This is true even

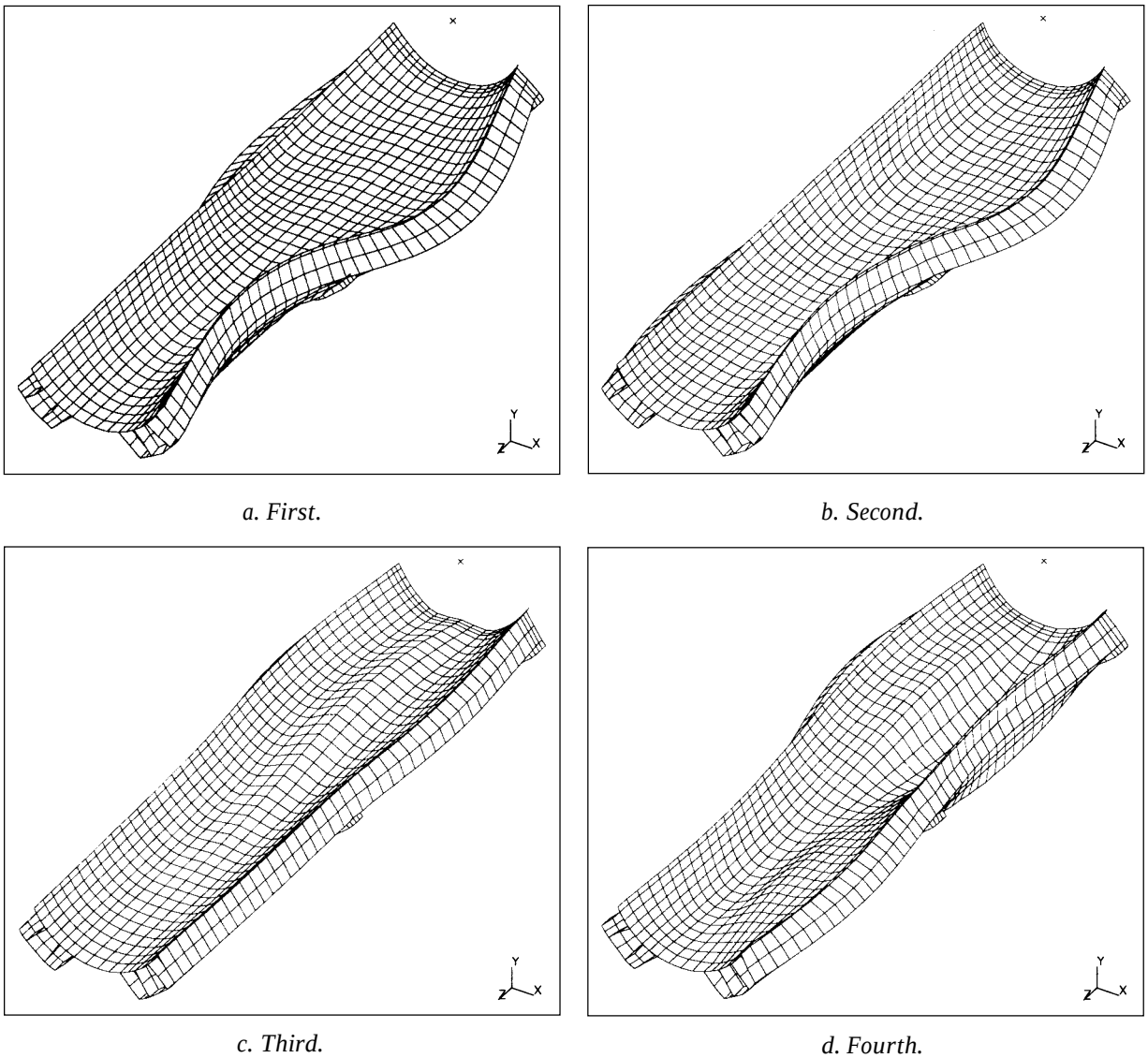

a. First. *b. Second.*

c. Third. *d. Fourth.*

Figure 35. Dynamic flexural mode for Magway.

though the bogies are spaced far apart, like those on the Foster-Miller vehicle, which had a significant dynamic effect.

Conclusions. The limited analyses tell us that the Magway is a very stiff and well-designed structure. The stresses appear to be low throughout, which is a primary requirement for an aluminum structure under cyclic loading.

Further study of this structure should include a series of dynamic analyses with worst-case vehicular loadings, including guideway curvature. While the stiff Magway will likely prevent much of an increase in the dynamic deflections over the static case, a thorough study of the dynamic stress variations within the structure is necessary to ensure its fatigue durability.

3.2.2 Linear synchronous motor*

Objectives

All of the maglev concepts investigated use guideway-mounted linear synchronous motors (LSMs) to propel the vehicles. These motors present high capital costs, and their power consumption creates the system's highest operating cost. For these reasons, the GMSA team required an LSM model as a performance-evaluation tool. Also, LSM performance data were needed to simulate the operational performance of each concept along specific corridors (see section 3.3.1). The resulting model (LSMPOWER) is able to evaluate both iron-core and air-core LSMs and fulfills both needs.

The specific objectives of this work are:

- To determine the equivalent circuit parameters from the basic size and layout of the guideway-mounted stator winding and vehicle-mounted field windings.
- To determine the required electrical characteristics at the terminals of the LSM to meet the specified thrust conditions.
- To compute the thrust margins required in each concept (i.e., the thrusts required for acceleration and for operation on a grade).
- To compute performance data (power, efficiency, power factor, etc.) at the input to the LSM and at the output of the variable frequency converters located along the guideway.
- To evaluate, from the performance data, the LSM's thrust capability for vehicle acceleration and grade climbing.

Introduction

LSMs consist of two electromagnetic members: the armature and the field. In long-stator systems, the LSM armature, commonly called the stator, is located on the guideway and the field is located on the vehicle. Short-stator systems have these structures reversed.

Electromagnetic suspension (EMS) systems make use of iron structures for both the field and the stator. The saturation of flux density in the iron limits the magnitude of the flux density that can be obtained in the air gap. This limits an EMS to small air gaps, typically of the order of 10 mm. The Grumman SCD's innovative use of superconducting coils in conjunction with the iron-core stator has the potential for increasing the stator-to-field air gap to 40 mm.

Electrodynamic suspension (EDS) systems use air-core structures for both the field and stator. Superconducting field windings on the vehicle are required to achieve the large flux densities required for operating EDS at large air gaps. These air gaps typically operate with a 100- to 200-mm spacing between the stator and the field.

LSMs can be controlled to produce orthogonal forces, for example, forces that act in the longitudinal direction and in the direction perpendicular to the longitudinal. Almost all maglev systems make use of LSMs to achieve either lift and propulsion, or guidance and propulsion. The LSM used in the TR07, for example, provides both lift and propulsive forces. The LSM is similar to its rotary counterpart in that a machine of fixed dimensions and materials produces a finite total force. Trade studies then determine how to apportion the split of the orthogonal forces. Iron-core structures typically produce large vertical forces because of the presence of the iron. On the other hand, the operation of air-core structures can be tailored through their control system to split the force capability from being all longitudinal to all vertical or a combination of both.

The power factor, that is the ratio of power consumed (P) to power applied (S), for LSMs can be significantly less than unity because of the inductance of the motor. The inductance causes LSMs to operate with a lagging power factor. The principal component of inductance in iron-core machines is a result of the magnetic circuit of the iron. For air-core machines, the relatively large size

* Written by Frank L. Raposa, Consulting Engineer.

of the stator winding, which is required to maximize the mutual coupling between stator and field windings, also results in a large inductance. Air-core machines typically have lower power factors than iron-core machines. Further, the field winding of an iron-core machine can be overexcited and controlled to provide power factor compensation, with the result that unity or even leading power factors can be achieved.

Methodology

Table 27 summarizes the pertinent assumptions and considerations for the model. The key to analyzing electromechanical devices is to set the electrical power equal to the mechanical power at the air gap. Figure 36 identifies the basic modeling equations used to determine the values of electrical and magnetic parameters required to meet specific thrust-speed conditions. The phasor diagram shown in Figure 37 defines the terminal conditions for determining the components of electrical power for specific thrust-speed conditions of the LSM.

Figure 38 illustrates the joining of the LSM model to a model of the wayside power distribution system to form the model LSMPOWER. The vehicle is shown as a moving wedge of magnetic length l_v. The magnetic length of the vehicle is the aggregate length of the LSM field windings for each LSM stator on the guideway. For example, in a distributed magnet system, such as the TR07, l_v is the sum of all field magnets on one side of the vehicle. For a bogie system such as Magneplane, l_v is the sum of all of the vehicle-mounted propulsion superconducting coils. The remaining terms of the model are defined on the figure.

LSMPOWER models from the LSMs to the converter stations used to supply conditioned power. That is, it does not model the connection of each system's converter stations to a utility grid (energy

Table 27. LSM model description.

Based on classical synchronous motor models
- Two-axis theory model for iron-core LSMs
- Magnetic coupling model for air-core LSMs

Basic assumptions
- Linear behavior of the magnetic field
- Effects of harmonics not critical to performance

Basic modeling equation at the air gap sets the electrical power equal to the mechanical power

$$P_{\text{electrical}} = P_{\text{mechanical}}$$

$$N_p \cdot E_1 \cdot I_1 \cdot \cos(\gamma_0) = F_a \cdot u_s$$

Single LSM model can be used for both iron-core and air-core LSM modeling equations for maglev performance model.

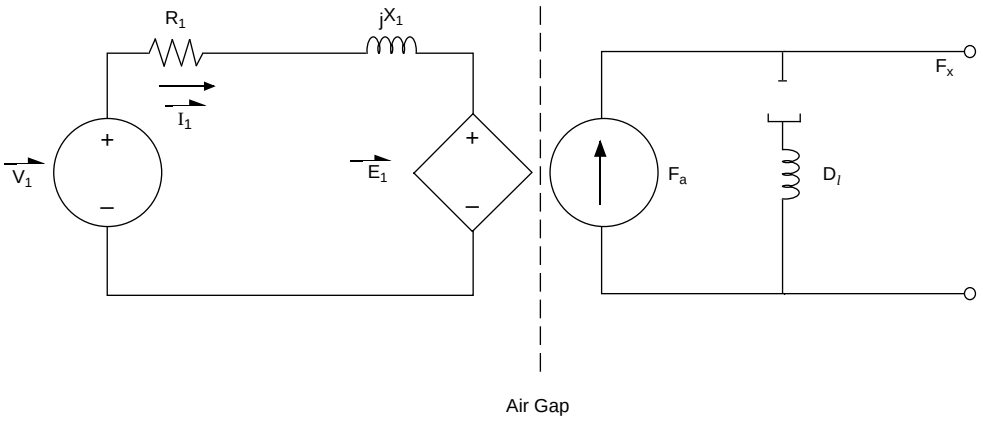

$P_{\text{electrical}} = P_{\text{mechanical}}$

$N_p \cdot E_1 \cdot I_1 \cdot \cos(\gamma_0) = F_a \cdot u_s$

$E_1 = \sqrt{2} \cdot l \cdot p \cdot N \cdot B_1 \cdot u_s$

$B_1 = (\pi/2) \cdot [\Phi/(\tau_p \cdot l)]$

$\Phi = M_f \cdot I_f / p$

$f_1 = u_s/(2 \cdot \tau_p)$

P: Power
V_1: Stator voltage
N_p: Number of phases
F_a: Air gap thrust
F_x: Output thrust
u_s: Vehicle velocity
B_1: Air gap flux density
Φ: Air gap flux
l: Stator width
p: Field pole pairs
N: Turns / pole / phase (or no. of slots / pole / phase)
γ_0: Angle between E_1 and I_1
τ_p: Field winding pole pitch
D_1: Mechanical losses
I_1: Stator current
R_1: Stator resistance
X_1: Stator reactance
E_1: Back EMF
f_1: Frequency
M_f: Mutual inductance
I_f: Field current

Figure 36. LSM equivalent circuit.

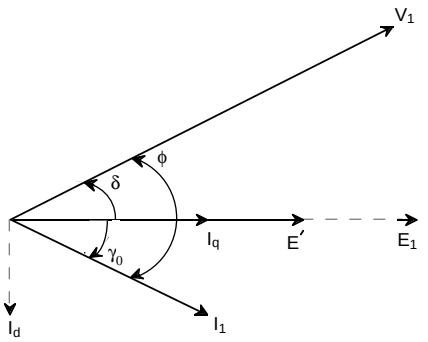

At the terminals of the LSM: $\vec{V}_1 = \vec{I}_1 \cdot (R_1 + jX_1) + \vec{E'}$

The output power is given by:

Real power $P = N_p \cdot V_1 \cdot I_1 \cdot \cos(\phi)$

Reactive power $Q = N_p \cdot V_1 \cdot I_1 \cdot \sin(\phi)$

Complex power $S = N_p \cdot V_1 \cdot I_1$

In terms of the power angle (δ):

Real power $P = N_p \cdot [V_1 \cdot I_d \cdot \sin(\delta) + V_1 \cdot I_q \cdot \cos(\delta)]$

Where I_d and I_q are the component phasors of I_1

Figure 37. LSM power output relationships.

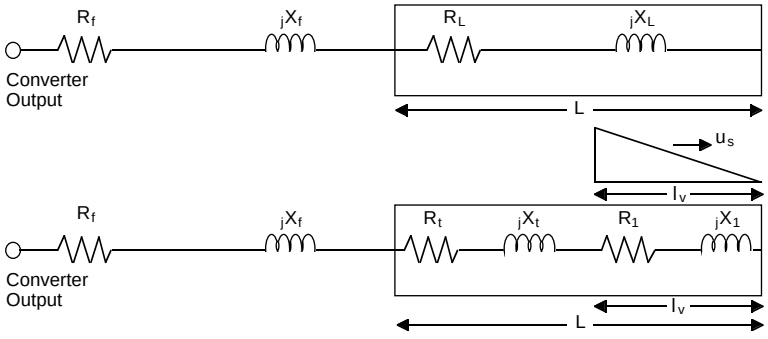

L: LSM block length
l_v: Magnetic length of vehicle

R_f: Feeder cable resistance
L_f: Feeder cable inductance ($X_f = 2\pi f_1 L_f$)

R_L: LSM block length resistance
L_L: LSM block length inductance ($X_L = 2\pi f_1 L_L$)

R_t: $R_t = R_L \cdot [(L - l_v)/L]$
L_t: $L_t = L_L \cdot [(L - l_v)/L]$ ($X_t = 2\pi f_1 L_t$)

X: Reactance
f: Frequency

Figure 38. LSM and power system model.

source). We did this to highlight differences attributable to the LSMs. Thus, most of the results here for energy consumption and power factor are at the output of the converter stations. Nevertheless, we separately computed efficiencies and power factors for these converter stations, and we present resulting overall values for each system in the last subsection here.

Model verification

We used information from Terman (1943), Fitzgerald et al. (1971), Brown and Hamilton (1984), Friedrich et al. (1986), Nasar and Boldea (1987), Miller (1987), and Heinrich and Kretzschmar (1989) to develop and verify the model. In particular, Miller (1987) provided speed-thrust and power data for TR06-II. This earlier vehicle has a similar shape to TR07 and should closely approximate its performance. We, therefore, used the TR06-II data to verify LSMPOWER. We also compared the model's results to those generated by the SCD contractors. In general, agreement was excellent, giving us high confidence in our results.

Application of LSMPOWER to the TR07

Published references could not be obtained that define the thrust-speed requirement for the TR07. However, because of the pending application of TR07 in Florida, private data on several TR07 systems were given to the Government to aid in evaluation. TR07 LSM propulsion-performance data have been released to the GMSA team for their inclusion in this report.

We used the configuration of the Emsland test track power system and frequency converter capacity to estimate the thrust-speed capability of the TR07. The motor current limit of 1200 A per LSM establishes the maximum thrust capability and the frequency converter output transformer ratings of 7.2 MVA per LSM limit the maximum power capability (Heinrich and Kretzschmar 1989). The Transrapid system intended for Florida is expected to have the same 1200-A limit per LSM, but the power capacity of the converter stations is unknown at this time.

Using the LSMPOWER model, we produced performance data for the TR07 operating under the above conditions. The baseline vehicle assumed was a two-car consist. The following parametric data were developed for the analysis:

Blocklength resistance R_L:	0.1209 Ω
Blocklength inductance L_L:	0.0005236 H
Direct axis inductance L_{dm}:	0.0002274 H
Quadrature axis inductance L_{qm}:	0.0000944 H
Vehicle magnetic length l_v:	45 m
Longitudinal length of stator L:	300 m
Field winding pole pitch t_p:	0.258 m
Width of LSM stator l:	0.16 m
Pole pairs per LSM p:	75
Slots per pole per phase N:	1
Number of phases N_p:	3
Number of LSMs per consist N_m:	2
Resistance of feeder cable R_f:	0.3 Ω
Inductance of feeder cable L_f:	0.0006 H
Air gap flux density B_1:	0.959 T
Maximum stator current per LSM:	1200 A
Maximum power per LSM:	7.2 MVA

The above data were obtained from available references (Heinrich and Kretzschmar 1989, Friedrich et al. 1986, p. 243–249) and, where possible, were independently verified through calculation.

Figure 39 summarizes the performance capability of the TR07 LSM. The maximum thrust capability of TR07 was determined as 55.1 kN per LSM or 110.2 kN for the consist. Because of the power limit, the LSM switches from constant thrust to constant power at some speed condition. For the data analyzed, constant thrust changed to constant power at approximately 60 m/s. From this speed to the maximum speed of 133.3 m/s, the power was held constant at the 7.2 MVA per LSM. Thrust and related power, voltages, and current data are shown in Figure 39 for three locations, namely, the input to the active LSM at the vehicle, the input to the LSM stator blocklength, and the output of the frequency converter stations.

The efficiency of the LSM at maximum thrust capability varies considerably, depending on the measurement location. For example, the efficiency peaks at 99% at the input to the active LSM and is fairly constant over a wide speed range. At the frequency converter output, the efficiency peaks at 87% at a speed of 133.3 m/s. The efficiency at this point is also quite sensitive to speed because of the power losses in the feeder cable and LSM blocklength. The power factor shows similar trends, with it being approximately 90% lagging at the active input to the LSM and approximately

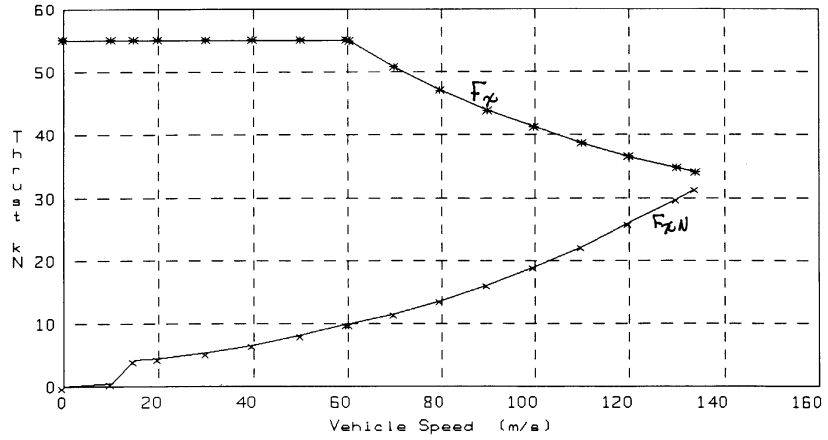

U_s (m/s)	F_x (kN)	F_{xN} (kN)	E_1 (V)	V_1 (V)	I_1 (A)	P (MW)	S (MVA)	PF (PU)	E_{ff} (PU)
0.0	55.1	0.0	0	22	1201	.08	.08	1.00	0.00
10.0	55.1	0.5	163	193	1201	.63	.69	.91	.88
15.0	55.1	4.1	244	279	1201	.90	1.01	.90	.91
20.0	55.1	4.5	326	366	1201	1.18	1.32	.90	.93
30.0	55.1	5.4	488	539	1201	1.73	1.94	.89	.95
40.0	55.1	6.6	651	712	1201	2.28	2.56	.89	.97
50.0	55.1	8.1	814	885	1201	2.83	3.19	.89	.97
60.0	55.1	9.9	977	1058	1201	3.38	3.81	.89	.98
60.5	54.9	10.0	985	1066	1196	3.40	3.82	.89	.98
70.0	50.7	11.6	1140	1223	1105	3.62	4.05	.89	.98
80.0	47.0	13.7	1302	1388	1024	3.82	4.26	.90	.99
90.0	43.8	16.2	1465	1552	955	3.99	4.45	.90	.99
100.0	41.1	19.1	1628	1716	895	4.15	4.61	.90	.99
110.0	38.7	22.3	1791	1880	843	4.29	4.76	.90	.99
120.0	36.6	25.9	1954	2044	797	4.42	4.89	.91	.99
130.0	34.7	29.8	2116	2208	756	4.54	5.01	.91	.99
134.0	34.0	31.5	2182	2274	741	4.59	5.05	.91	.99

a. LSM thrust vs. speed, maximum thrust.

Figure 39. Performance capability of the TR07 LSM.

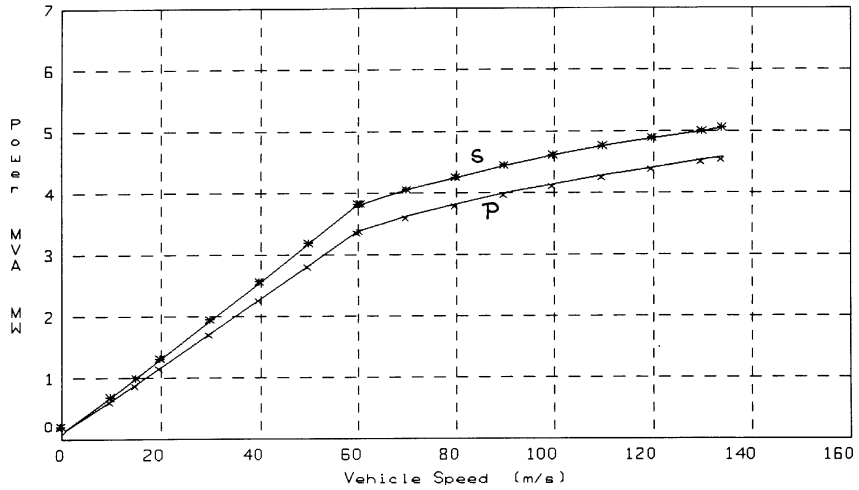

b. LSM power vs. speed, maximum thrust.

U_s(m/s)	F_x(kN)	F_xN(kN)	E_1(V)	V_1(V)	I_1(A)	P(MW)	S(MVA)	PF(PU)	E_{ff}(PU)
0.0	55.1	0.0	0	22	1201	.08	.08	1.00	0.00
10.0	55.1	0.5	163	193	1201	.63	.69	.91	.88
15.0	55.1	4.1	244	279	1201	.90	1.01	.90	.91
20.0	55.1	4.5	326	366	1201	1.18	1.32	.90	.93
30.0	55.1	5.4	488	539	1201	1.73	1.94	.89	.95
40.0	55.1	6.6	651	712	1201	2.28	2.56	.89	.97
50.0	55.1	8.1	814	885	1201	2.83	3.19	.89	.97
60.0	55.1	9.9	977	1058	1201	3.38	3.81	.89	.98
60.5	54.9	10.0	985	1066	1196	3.40	3.82	.89	.98
70.0	50.7	11.6	1140	1223	1105	3.62	4.05	.89	.98
80.0	47.0	13.7	1302	1388	1024	3.82	4.26	.90	.99
90.0	43.8	16.2	1465	1552	955	3.99	4.45	.90	.99
100.0	41.1	19.1	1628	1716	895	4.15	4.61	.90	.99
110.0	38.7	22.3	1791	1880	843	4.29	4.76	.90	.99
120.0	36.6	25.9	1954	2044	797	4.42	4.89	.91	.99
130.0	34.7	29.8	2116	2208	756	4.54	5.01	.91	.99
134.0	34.0	31.5	2182	2274	741	4.59	5.05	.91	.99

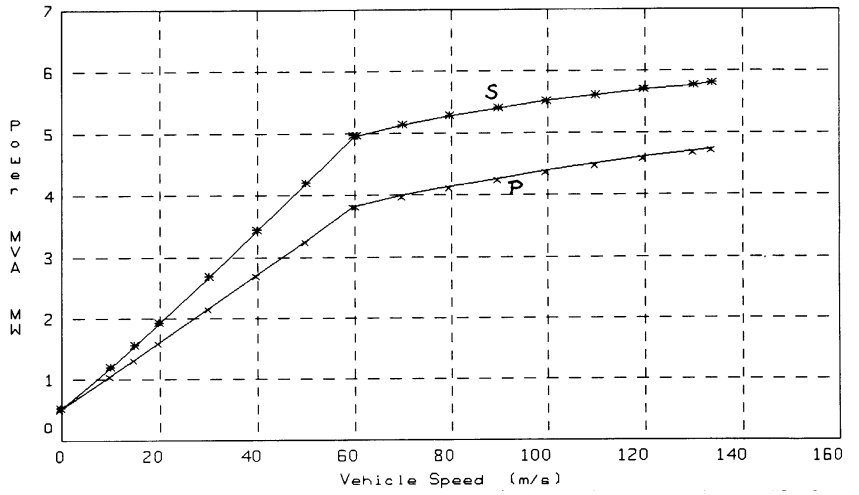

c. Blocklength input power, maximum thrust.

U_s(m/s)	F_x(kN)	F_xN(kN)	E_1(V)	VL(V)	I_1(A)	PL(MW)	SL(MVA)	PF(PU)	E_{ff}(PU)
0.0	55.1	0.0	0	145	1201	.52	.52	1.00	0.00
10.0	55.1	0.5	163	332	1201	1.07	1.20	.90	.51
15.0	55.1	4.1	244	434	1201	1.35	1.56	.86	.61
20.0	55.1	4.5	326	537	1201	1.62	1.94	.84	.68
30.0	55.1	5.4	488	746	1201	2.18	2.69	.81	.76
40.0	55.1	6.6	651	956	1201	2.73	3.44	.79	.81
50.0	55.1	8.1	814	1167	1201	3.28	4.20	.78	.84
60.0	55.1	9.9	977	1378	1201	3.83	4.96	.77	.86
60.5	54.9	10.0	985	1386	1196	3.84	4.97	.77	.86
70.0	50.7	11.6	1140	1548	1105	3.99	5.13	.78	.89
80.0	47.0	13.7	1302	1716	1024	4.14	5.27	.79	.91
90.0	43.8	16.2	1465	1883	955	4.27	5.39	.79	.92
100.0	41.1	19.1	1628	2049	895	4.40	5.50	.80	.93
110.0	38.7	22.3	1791	2214	843	4.51	5.60	.81	.94
120.0	36.6	25.9	1954	2379	797	4.62	5.69	.81	.95
130.0	34.7	29.8	2116	2543	756	4.72	5.77	.82	.96
134.0	34.0	31.5	2182	2609	741	4.75	5.80	.82	.96

Figure 39 (cont'd). Performance capability of the TR07 LSM.

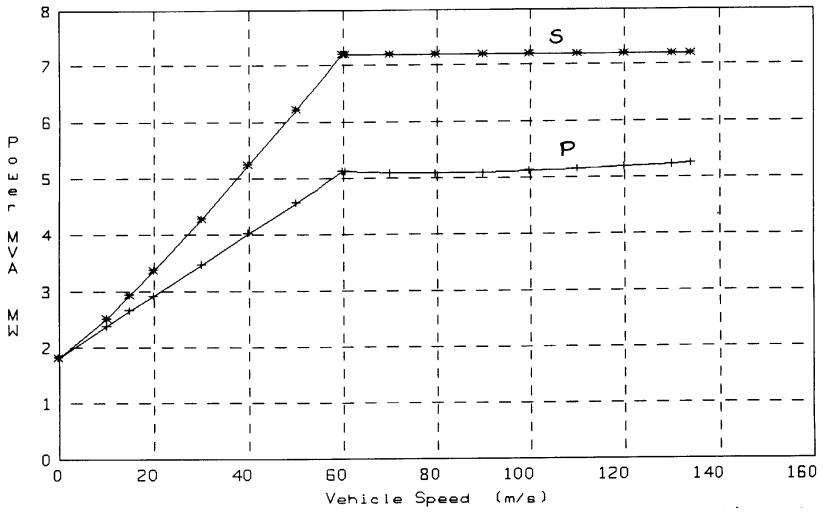

d. Converter station output power, maximum thrust.

U_s(m/s)	F_x(kN)	F_xN(kN)	V_s(V)	I_s(V)	P_s(MW)	S_s(MVA)	PF(PU)	E_{ff}(PU)
0.0	55.1	0.0	505	1201	1.82	1.82	1.00	0.00
10.0	55.1	0.5	699	1201	2.37	2.52	.94	.23
15.0	55.1	4.1	814	1201	2.65	2.93	.90	.31
20.0	55.1	4.5	936	1201	2.92	3.37	.87	.38
30.0	55.1	5.4	1192	1201	3.47	4.29	.81	.48
40.0	55.1	6.6	1457	1201	4.02	5.25	.77	.55
50.0	55.1	8.1	1726	1201	4.58	6.22	.74	.60
60.0	55.1	9.9	1998	1201	5.13	7.20	.71	.64
60.5	54.9	10.0	2007	1196	5.13	7.20	.71	.65
70.0	50.7	11.6	2173	1105	5.09	7.20	.71	.70
80.0	47.0	13.7	2344	1024	5.08	7.20	.71	.74
90.0	43.8	16.2	2513	955	5.09	7.20	.71	.77
100.0	41.1	19.1	2681	895	5.12	7.20	.71	.80
110.0	38.7	22.3	2847	843	5.15	7.20	.72	.83
120.0	36.6	25.9	3011	797	5.19	7.20	.72	.85
130.0	34.7	29.8	3175	756	5.23	7.20	.73	.86
134.0	34.0	31.5	3240	741	5.25	7.20	.73	.87

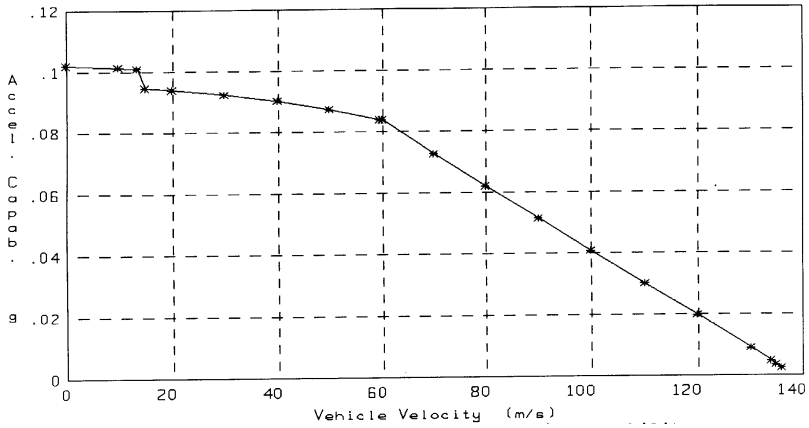

e. Acceleration capability, maximum thrust.

U_s(m/s)	F_x(kN)	F_xN(kN)	Accel(g)	Accel(m/s^2)
0.0	55.1	0.0	0.102	1.001
10.0	55.1	0.4	0.101	0.994
13.4	55.1	0.6	0.101	0.990
15.0	55.1	4.1	0.095	0.927
20.0	55.1	4.4	0.094	0.920
30.0	55.1	5.4	0.092	0.904
40.0	55.1	6.6	0.090	0.882
50.0	55.1	8.1	0.087	0.854
59.7	55.1	9.9	0.084	0.822
60.1	55.1	9.9	0.084	0.821
70.0	50.7	11.6	0.073	0.712
80.0	47.0	13.7	0.062	0.606
90.0	43.8	16.2	0.051	0.502
100.0	41.1	19.1	0.041	0.400
110.0	38.7	22.3	0.030	0.298
120.0	36.6	25.9	0.020	0.194
130.0	34.7	29.8	0.009	0.088
134.0	34.0	31.5	0.005	0.045
135.0	33.8	31.9	0.003	0.034

Figure 39 (cont'd).

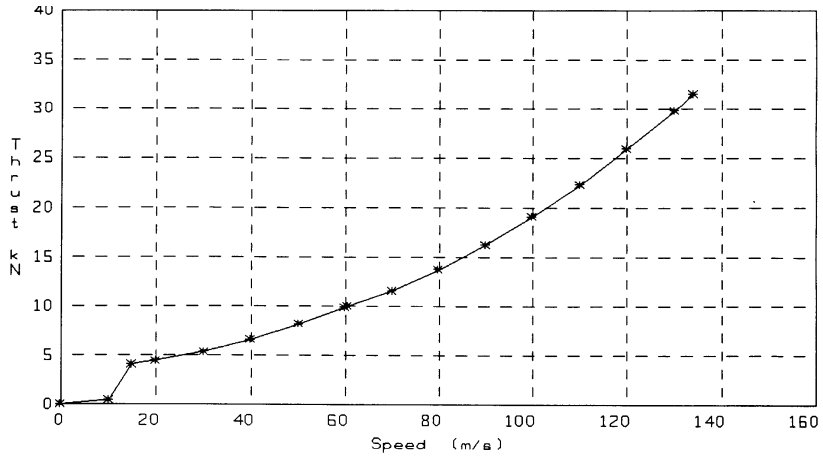

f. LSM thrust vs. speed, normal thrust.

U_s(m/s)	F_x(kN)	E_1(V)	V_1(V)	I_1(A)	P(MW)	S(MVA)	PF(PU)	E_{ff}(PU)
0.0	0.0	0.0	0.0	0.0	0.00	0.00	.94	1.00
10.0	0.5	162.8	163.1	10.9	.01	.01	.94	1.00
15.0	4.1	244.2	246.7	89.4	.06	.07	.94	.99
20.0	4.5	325.6	328.7	97.0	.09	.10	.94	.99
30.0	5.4	488.4	492.9	116.8	.16	.17	.94	1.00
40.0	6.6	651.2	657.9	143.4	.26	.28	.93	1.00
50.0	8.1	814.0	823.5	176.7	.41	.44	.93	1.00
60.0	9.9	976.8	990.1	215.4	.60	.64	.93	1.00
60.5	10.0	984.9	998.4	216.9	.60	.65	.93	1.00
70.0	11.6	1139.6	1157.1	252.0	.81	.87	.93	1.00
80.0	13.7	1302.4	1325.4	298.1	1.10	1.19	.93	1.00
90.0	16.2	1465.2	1495.3	352.9	1.46	1.58	.93	1.00
100.0	19.1	1628.0	1666.9	415.7	1.92	2.08	.92	1.00
110.0	22.3	1790.8	1840.5	486.3	2.47	2.69	.92	.99
120.0	25.9	1953.6	2016.2	564.7	3.13	3.42	.92	.99
130.0	29.8	2116.4	2194.4	650.3	3.90	4.28	.91	.99
134.0	31.5	2181.5	2266.5	686.7	4.25	4.67	.91	.99

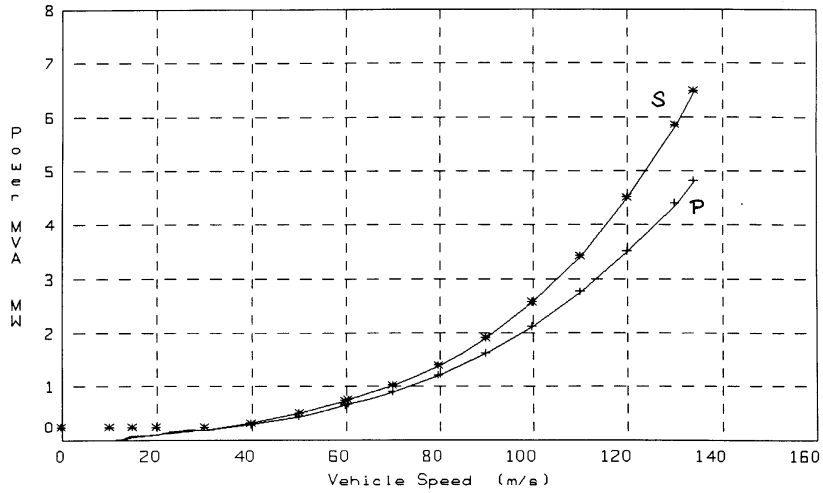

g. Converter station output power, normal thrust.

U_s(m/s)	F_x(kN)	V_s(V)	I_s(A)	P_s(MW)	S_s(MVA)	PF(PU)	E_{ff}(PU)
0.0	0.0	0.0	0.0	0.00	0.00	.94	1.00
10.0	0.5	167.7	10.9	.01	.01	.94	.97
15.0	4.1	286.4	89.4	.07	.08	.93	.86
20.0	4.5	374.0	97.0	.10	.11	.93	.88
30.0	5.4	553.3	116.8	.18	.19	.92	.90
40.0	6.6	739.4	143.4	.29	.32	.91	.91
50.0	8.1	933.8	176.7	.44	.50	.90	.91
60.0	9.9	1137.4	215.4	.65	.73	.89	.91
60.5	10.0	1147.4	216.9	.66	.75	.89	.91
70.0	11.6	1345.2	252.0	.89	1.02	.87	.91
80.0	13.7	1568.2	298.1	1.21	1.40	.86	.91
90.0	16.2	1808.8	352.9	1.61	1.91	.84	.90
100.0	19.1	2069.6	415.7	2.13	2.58	.82	.90
110.0	22.3	2353.6	486.3	2.75	3.43	.80	.89
120.0	25.9	2664.3	564.7	3.51	4.51	.78	.89
130.0	29.8	3005.0	650.3	4.41	5.86	.75	.88
134.0	31.5	3150.6	686.7	4.82	6.49	.74	.88

Figure 39 (cont'd). Performance capability of the TR07 LSM.

72% lagging at the frequency converter output. The low power factor at the converter output location is heavily influenced by the reactance of the feeder cable.

The results of the LSMPOWER analysis for the TR07 compare well with the limited published data and the private data available to the Government.

Application of LSMPOWER to the SCD linear synchronous motors

Grumman. The Grumman LSM concept provides integrated levitation, guidance, and propulsion with a single machine. It has an iron-core LSM with a conventional stator. Like the TR07, there are two LSMs per vehicle. The levitation magnets are distributed over the length of the vehicle, and these magnets use superconducting coils in conjunction with iron cores. Conventional control coils on the magnets are used for levitation, and the combination of superconducting coils with conventional control coils achieves an air gap of 40 mm.

The LSM blocklengths are typically 1000 m and are center-fed in 500-m segments. Converter station blocklengths are 4000 m with cables feeding each 1000-m block. The LSM field current is set for operation at a leading power factor, with the intent of achieving a power factor that is close to unity at the input to the LSM block.

Linear generator coils are set into the field winding pole faces in a way similar to the TR07 to transfer power to the vehicle. In addition to these coils, high-frequency power is injected into the LSM stator coils and transferred to the vehicle via a transformer. These two techniques, when taken together, provide all-speed power transfer capability to the Grumman SCD vehicle; this concept does not require the auxiliary batteries of the TR07.

We produced performance data using the LSMPOWER model for the Grumman SCD operating as described above. The baseline vehicle was assumed to be a two-car consist. Grumman's baseline concept also makes use of an aluminum LSM winding, which produces a maximum thrust of 30 kN per LSM. This results in a low-speed acceleration capability of only 0.09 g. For better acceleration and grade-climbing capability, the Grumman LSM would have to be modified by replacing the aluminum LSM stator winding with a copper winding.

We used the following parametric data, determined from the baseline case of aluminum stator windings, in our analysis:

Blocklength resistance R_L:	0.1772 Ω
Blocklength inductance L_L:	0.0012 H
Direct axis inductance L_{dm}:	0.00005 H
Quadrature axis inductance L_{qm}:	0.00003 H
Vehicle magnetic length l_v:	18 m
Longitudinal length of stator L:	500 m
Field winding pole pitch t_p:	0.75 m
Width of LSM stator l:	0.20 m
Pole pairs per LSM p:	12
Slots per pole per phase N:	3
Number of phases N_p:	3
Number of LSMs per consist N_m:	2
Resistance of feeder cable R_f:	0.139 Ω
Inductance of feeder cable L_f:	0.0012 H
Air gap flux density B_1:	0.896 T
Maximum stator current per LSM:	1343 A
Maximum power per LSM:	7.5 MVA

The above data were obtained from information provided by Grumman during the in-progress reviews (IPRs) and from the SCD final report (Grumman 1992a), and, where possible, were independently verified through calculation.

Figure 40 summarizes the performance capability of the Grumman SCD LSM. The maximum thrust capability of Grumman's two-car consist is 30 kN per LSM or 60 kN for the consist. The design provides a constant thrust up to the design speed of 134 m/s. The charts in these figures show thrust and related power, voltages, and current data for two locations, namely, the input to the active LSM at the vehicle and the output of the frequency converter stations. Data are shown for both maximum- and nominal-thrust conditions. The power-limited condition of 7.5 MVA per LSM is just reached at 134 m/s.

Figure 40e shows the acceleration capability for the baseline 61,224-kg vehicle. With a total thrust of 60 kN, the LSM may maintain a maximum vehicle acceleration of about 0.09 g from zero speed to 60 m/s; this diminishes to 0.05 g at 134 m/s.

Grumman also developed the parameters for an LSM with a copper stator winding. This motor has a maximum thrust of 100 kN. It has a low-speed acceleration capability of about 0.16 g and has reserve acceleration of about 0.09 g at 134 m/s. Figure 40f shows the acceleration vs. speed capability of this 100-kN LSM.

The efficiency of the LSM at maximum thrust varies considerably, depending on the measurement location. For example, the efficiency peaks at 99% at the input to the active LSM and is fairly constant over a wide speed range. At the frequency converter output, the efficiency peaks at 70% at a speed of 134 m/s. The efficiency at this location is also quite sensitive to speed because

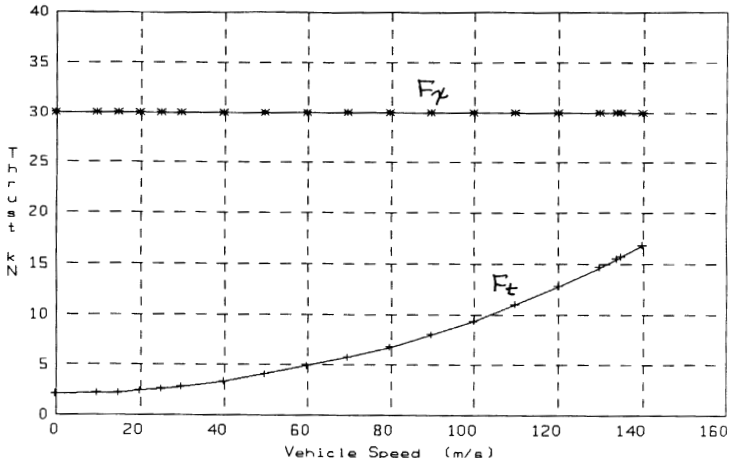

U_s(m/s)	F_x(kN)	F_t(kN)	E_1(V)	V_1(V)	I_1(A)	P(MW)	S(MVA)	Q(MVAR)	PF(PU)	E_{ff}(PU)
0.0	30.0	2.05	0.0	8.6	1343.0	0.03	0.03	0.00	1.000	0.000
10.0	30.0	2.13	91.2	96.3	1343.0	0.33	0.39	-0.20	0.863	0.897
15.0	30.0	2.23	136.9	140.7	1343.0	0.48	0.57	-0.29	0.855	0.929
20.0	30.0	2.37	182.5	185.2	1343.0	0.63	0.75	-0.39	0.850	0.946
25.0	30.0	2.55	228.1	229.7	1343.0	0.78	0.93	-0.49	0.848	0.956
30.0	30.0	2.77	273.7	274.1	1343.0	0.93	1.10	-0.59	0.846	0.963
40.0	30.0	3.33	364.9	363.1	1343.0	1.23	1.46	-0.79	0.844	0.972
50.0	30.0	4.05	456.2	452.1	1343.0	1.53	1.82	-0.98	0.842	0.978
60.0	30.0	4.93	547.4	541.1	1343.0	1.83	2.18	-1.18	0.842	0.981
70.0	30.0	5.75	638.6	630.0	1343.0	2.13	2.54	-1.37	0.841	0.984
80.0	30.0	6.77	729.9	719.0	1343.0	2.43	2.90	-1.57	0.840	0.986
90.0	30.0	7.99	821.1	808.0	1343.0	2.73	3.26	-1.77	0.840	0.987
100.0	30.0	9.40	912.3	897.0	1343.0	3.03	3.61	-1.96	0.840	0.989
110.0	30.0	10.99	1003.6	985.9	1343.0	3.33	3.97	-2.16	0.839	0.990
120.0	30.0	12.76	1094.8	1074.9	1343.0	3.63	4.33	-2.36	0.839	0.991
130.0	30.0	14.69	1186.0	1163.9	1343.0	3.93	4.69	-2.55	0.839	0.991
134.0	30.0	15.52	1222.5	1199.5	1343.0	4.05	4.83	-2.63	0.839	0.991
135.0	30.0	15.72	1231.7	1208.4	1343.0	4.08	4.87	-2.65	0.839	0.992

a. LSM thrust vs. speed, maximum thrust.

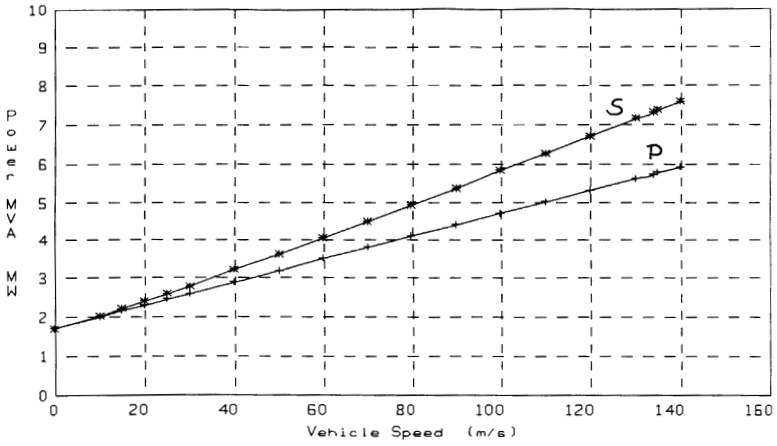

U_s(m/s)	F_x(kN)	F_t(kN)	V_s(V)	I_s(A)	P(MW)	S(MVA)	Q(MVAR)	PF(PU)	E_{ff}(PU)
0.0	30.0	2.05	424.7	1343.0	1.711	1.711	0.000	1.000	0.000
10.0	30.0	2.13	506.2	1343.0	2.011	2.040	0.341	0.986	0.149
15.0	30.0	2.23	551.1	1343.0	2.161	2.221	0.511	0.973	0.208
20.0	30.0	2.37	598.0	1343.0	2.311	2.409	0.682	0.959	0.260
25.0	30.0	2.55	646.4	1343.0	2.461	2.604	0.852	0.945	0.305
30.0	30.0	2.77	695.9	1343.0	2.611	2.804	1.022	0.931	0.345
40.0	30.0	3.33	797.8	1343.0	2.911	3.214	1.363	0.906	0.412
50.0	30.0	4.05	902.2	1343.0	3.211	3.635	1.704	0.883	0.467
60.0	30.0	4.93	1008.4	1343.0	3.511	4.063	2.045	0.864	0.513
70.0	30.0	5.75	1115.9	1343.0	3.811	4.496	2.385	0.848	0.551
80.0	30.0	6.77	1224.3	1343.0	4.111	4.933	2.726	0.833	0.584
90.0	30.0	7.99	1333.4	1343.0	4.411	5.372	3.067	0.821	0.612
100.0	30.0	9.40	1443.1	1343.0	4.711	5.814	3.408	0.810	0.637
110.0	30.0	10.99	1553.2	1343.0	5.011	6.258	3.748	0.801	0.659
120.0	30.0	12.76	1663.6	1343.0	5.311	6.703	4.089	0.792	0.678
130.0	30.0	14.69	1774.3	1343.0	5.611	7.149	4.430	0.785	0.695
134.0	30.0	15.52	1818.7	1343.0	5.731	7.328	4.566	0.782	0.701
135.0	30.0	15.72	1829.8	1343.0	5.761	7.372	4.600	0.781	0.703

b. Converter station output power, maximum thrust.

Figure 40. Performance capability of the Grumman SCD LSM.

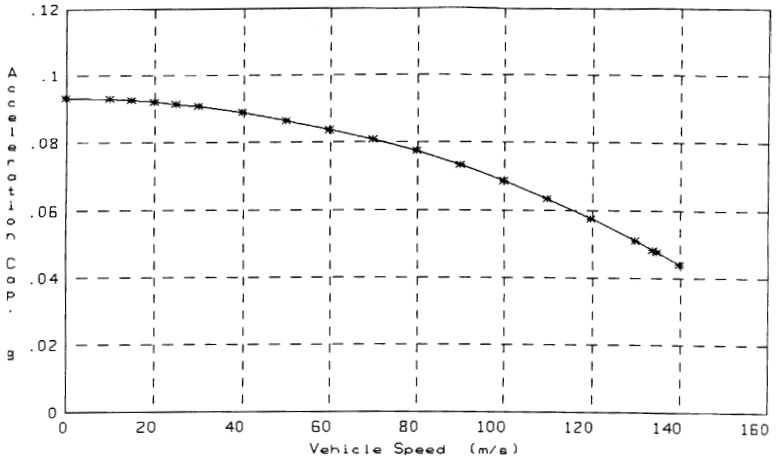

U_s (m/s)	F_x (kN)	F_t (kN)	Accel (g)	Accel (m/s^2)
0.0	30.0	2.05	0.093	0.913
10.0	30.0	2.13	0.093	0.910
15.0	30.0	2.23	0.093	0.907
20.0	30.0	2.37	0.092	0.903
25.0	30.0	2.55	0.091	0.897
30.0	30.0	2.77	0.091	0.890
40.0	30.0	3.33	0.089	0.871
50.0	30.0	4.05	0.086	0.848
60.0	30.0	4.93	0.084	0.819
70.0	30.0	5.75	0.081	0.792
80.0	30.0	6.77	0.077	0.759
90.0	30.0	7.99	0.073	0.719
100.0	30.0	9.40	0.069	0.673
110.0	30.0	10.99	0.063	0.621
120.0	30.0	12.76	0.057	0.563
130.0	30.0	14.69	0.051	0.500
134.0	30.0	15.52	0.048	0.473
135.0	30.0	15.72	0.048	0.466

c. Acceleration capability, maximum thrust.

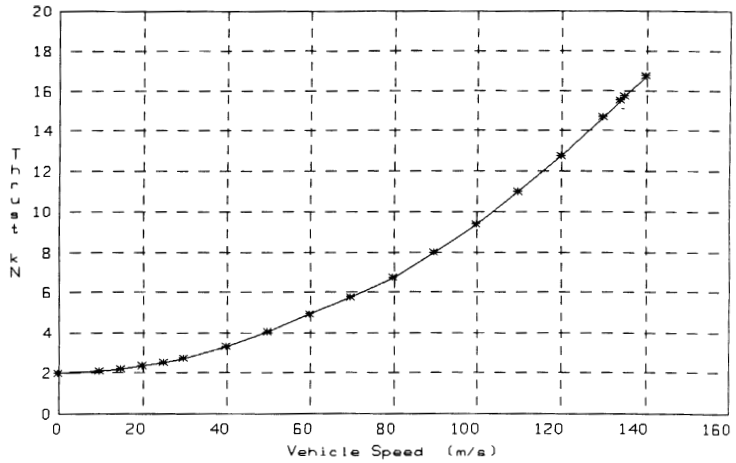

U_s (m/s)	F_x (kN)	E_1 (kN)	V_1 (V)	I_1 (A)	P (MW)	S (MVA)	Q (MVAR)	PF (PU)	E_{ff} (PU)
0.0	2.05	0.0	0.6	91.8	0.00	0.00	0.00	1.000	0.000
10.0	2.13	91.2	91.6	95.4	0.02	0.03	-0.02	0.820	0.992
15.0	2.23	136.9	137.1	99.8	0.03	0.04	-0.02	0.819	0.994
20.0	2.37	182.5	182.7	106.1	0.05	0.06	-0.03	0.819	0.995
25.0	2.55	228.1	228.2	114.2	0.06	0.08	-0.04	0.819	0.996
30.0	2.77	273.7	273.7	124.0	0.08	0.10	-0.06	0.819	0.996
40.0	3.33	364.9	364.7	149.1	0.13	0.16	-0.09	0.819	0.997
50.0	4.05	456.2	455.6	181.3	0.20	0.25	-0.14	0.820	0.997
60.0	4.93	547.4	546.3	220.7	0.30	0.36	-0.21	0.820	0.997
70.0	5.75	638.6	636.9	257.4	0.40	0.49	-0.28	0.821	0.997
80.0	6.77	729.9	727.3	303.1	0.54	0.66	-0.38	0.822	0.997
90.0	7.99	821.1	817.5	357.8	0.72	0.88	-0.50	0.823	0.997
100.0	9.40	912.3	907.3	420.9	0.94	1.15	-0.65	0.824	0.996
110.0	10.99	1003.6	996.9	492.1	1.21	1.47	-0.83	0.825	0.996
120.0	12.76	1094.8	1086.1	571.1	1.54	1.86	-1.05	0.826	0.996
130.0	14.69	1186.0	1175.0	657.8	1.92	2.32	-1.30	0.827	0.996
134.0	15.52	1222.5	1210.4	694.6	2.09	2.52	-1.41	0.828	0.996
135.0	15.72	1231.7	1219.2	704.0	2.13	2.57	-1.44	0.828	0.996

d. LSM thrust vs. speed, normal thrust.

Figure 40 (cont'd).

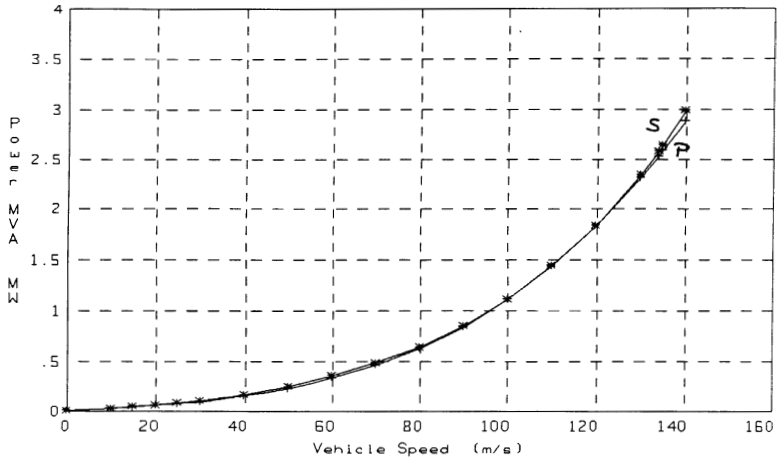

U_s (m/s)	F_x (kN)	V_s (V)	I_s (A)	P (MW)	S (MVA)	Q (MVAR)	PF (PU)	E_{ff} (PU)
0.0	2.05	29.0	91.8	0.008	0.008	0.000	1.000	0.000
10.0	2.13	113.1	95.4	0.030	0.032	-0.012	0.925	0.712
15.0	2.23	156.8	99.8	0.043	0.047	-0.019	0.914	0.780
20.0	2.37	200.8	106.1	0.058	0.064	-0.027	0.909	0.816
25.0	2.55	244.8	114.2	0.076	0.084	-0.035	0.908	0.838
30.0	2.77	288.8	124.0	0.098	0.107	-0.045	0.909	0.851
40.0	3.33	376.1	149.1	0.154	0.168	-0.067	0.917	0.863
50.0	4.05	462.4	181.3	0.234	0.252	-0.093	0.929	0.867
60.0	4.93	547.3	220.7	0.342	0.362	-0.120	0.944	0.865
70.0	5.75	630.3	257.4	0.465	0.487	-0.143	0.956	0.865
80.0	6.77	713.0	303.1	0.629	0.648	-0.158	0.970	0.861
90.0	7.99	796.6	357.8	0.841	0.855	-0.156	0.983	0.856
100.0	9.40	883.0	420.9	1.108	1.115	-0.122	0.994	0.848
110.0	10.99	975.0	492.1	1.439	1.439	-0.039	1.000	0.840
120.0	12.76	1076.2	571.1	1.840	1.844	0.116	0.998	0.832
130.0	14.69	1191.0	657.8	2.321	2.350	0.373	0.987	0.823
134.0	15.52	1241.8	694.6	2.537	2.588	0.511	0.980	0.820
135.0	15.72	1255.0	704.0	2.593	2.650	0.549	0.978	0.819

e. Converter station output power, normal thrust.

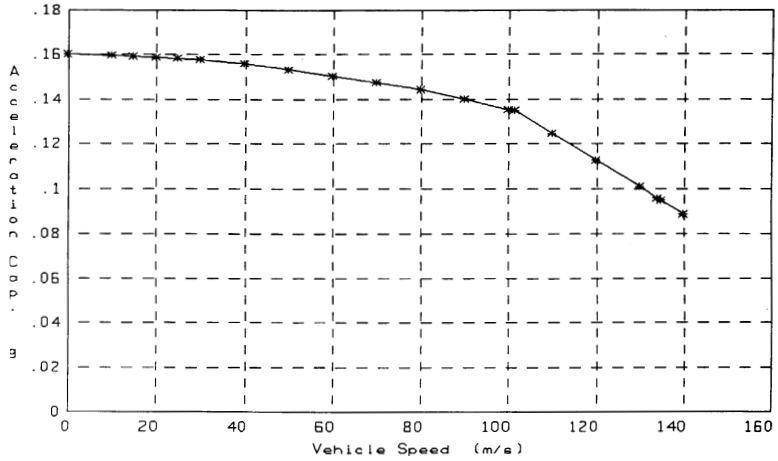

U_s (m/s)	F_x (kN)	F_t (kN)	Accel (g)	Accel (m/s^2)
0.0	50.0	2.05	0.160	1.566
10.0	50.0	2.13	0.159	1.564
15.0	50.0	2.23	0.159	1.560
20.0	50.0	2.37	0.159	1.556
25.0	50.0	2.55	0.158	1.550
30.0	50.0	2.77	0.157	1.543
40.0	50.0	3.33	0.155	1.525
50.0	50.0	4.05	0.153	1.501
60.0	50.0	4.93	0.150	1.472
70.0	50.0	5.75	0.147	1.446
80.0	50.0	6.77	0.144	1.412
90.0	50.0	7.99	0.140	1.372
100.0	50.0	9.40	0.135	1.326
101.6	50.0	9.65	0.134	1.318
110.0	48.3	10.99	0.124	1.220
120.0	46.5	12.76	0.113	1.104
130.0	44.9	14.69	0.101	0.988
134.0	44.4	15.52	0.096	0.942

f. Acceleration capability for 100-kN design, maximum thrust.

Figure 40 (cont'd). Performance capability of the Grumman SCD LSM.

of the power losses in the feeder cable and LSM blocklength.

The power factor shows similar trends: it is approximately 87% leading at the active input to the LSM, is unity as intended at the input the LSM blocklength, and is approximately 80% lagging at the frequency converter output location. The relatively high power factor at this location is the result of the leading power factor, which partly compensates for the reactive power requirements of the feeder cable.

The LSM parameters used by LSMPOWER for the Grumman concept differ somewhat from those specified by Grumman, particularly with respect to the internal phase angle of the machine. LSMPOWER derives these parameters, where in the Grumman model they are apparently specified. However, the LSMPOWER performance results agree fairly closely with those predicted by Grumman. The difference in model parameters appears to be caused by the different modeling approaches taken.

Magneplane. The Magneplane LSM is an air-core machine with a conventional meander winding. The concept uses one LSM per vehicle, with a propulsion winding air gap of approximately 250 mm. Superconducting propulsion coils are located on bogies at each end of the vehicle. The propulsion coil design is intended to minimize the stray fields in the passenger compartment. This is accomplished by operating the inboard superconducting coils at lower field strengths compared to the outboard coils. The LSM thrust control angle is set for zero lift capability for normal operation. This angle is controlled to provide lift from the LSM for heave damping.

The LSM blocklengths are 2000 m for the baseline concept and are end-fed from the converter stations. Converter stations are located at every other blocklength and are assumed to be located close enough to the guideway as to not require feeder cables of any significant length. Here, we include feeder cables in the analysis for comparison with the other concepts.

The LSM stator winding is a high inductance winding, and a power factor correction for each LSM winding is planned. Magneplane did not fully develop the details of the power factor correction; the analysis here considers one preliminary case of power factor correction to estimate its effect.

For obtaining vehicle power, the LSM windings will be used as the primary of an air-core transformer. The LSM interacts with an 18-m coil that is located under the vehicle and between the two bogies. High-frequency power is injected into the LSM stator winding and transferred to the vehicle via the air-core transformer.

We produced the following performance data using the LSMPOWER model for the Magneplane SCD operating as described above. The baseline vehicle was a one-car consist.

Blocklength resistance R_L:	0.20 Ω
Blocklength inductance L_L:	0.0142 H
Vehicle magnetic length l_v:	2000 m
Longitudinal length of stator L:	2000 m
Field winding pole pitch t_p:	0.75 m
Width of LSM stator l:	1.2 m
Pole pairs per LSM p:	2
Slots per pole per phase N:	4
Number of phases N_p:	3
Number of LSMs per consist N_m:	1
Resistance of feeder cable R_f:	0.139 Ω
Inductance of feeder cable L_f:	0.0012 H
Back EMF characteristic at a specified speed E_1:	2326 V at 150 m/s
Maximum stator current per LSM:	3224 A
Maximum mechanical power output:	7.5 MW for vehicle

The above data were obtained from information provided by Magneplane during the IPRs and from their SCD final report (Magneplane 1992a), and where possible were independently verified through calculation. These data show the magnetic length of the vehicle being the same as the LSM blocklength to account for the equivalent circuit parameters as specified by Magneplane.

Figure 41 summarizes the performance capability of the Magneplane SCD LSM. The Magneplane design requires nearly constant thrust at all speeds, primarily because of the high magnetic drag at low speeds and the high aerodynamic drag at high speeds. The magnetic drag peaks in the vicinity of 20–40 m/s. The maximum thrust capability of the one-car consist was 150 kN. Thrust and related power, voltages, and current data are shown in the following charts for two locations, namely, the input to the LSM blocklength and the output of the frequency converter station.

The thrust-speed breakpoint from constant thrust to constant power occurs at 50 m/s. The very high megavolt-ampere requirement at this point, 94 MVA compared to 14 MW of active power, was a result of the very high inductance of the stator winding without any capacitive compensation. The power factor correction planned by Magneplane should take care of this problem.

Figures 41e and f show preliminary estimates of the reduced megavolt-ampere requirement

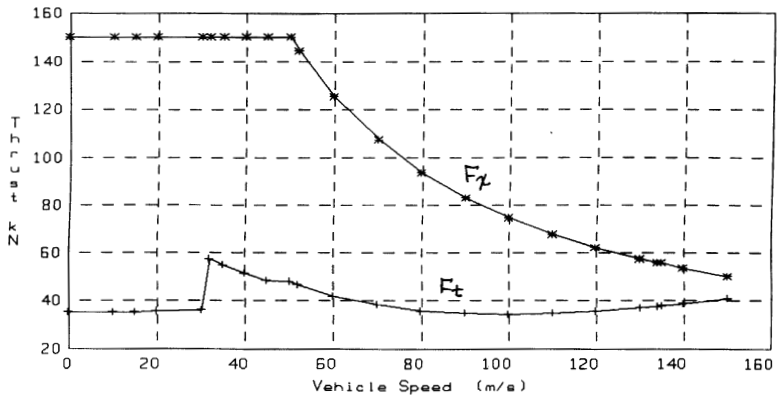

U_s(m/s)	F_x(kN)	P_x(MW)	F_t(kN)	E_1(V)	V_1(V)	I_1(A)	P(MW)	S(MVA)	PF(PU)	E_{ff}(PU)
0.0	150.0	0.00	35.08	0.0	644.9	3224.	6.24	6.24	1.000	0.000
10.0	150.0	1.50	35.18	155.1	2078.1	3224.	7.74	20.10	0.385	0.194
15.0	150.0	2.25	35.32	232.6	3007.7	3224.	8.49	29.09	0.292	0.265
20.0	150.0	3.00	35.50	310.1	3952.9	3224.	9.24	38.24	0.242	0.325
30.0	150.0	4.50	36.04	465.2	5859.8	3224.	10.74	56.68	0.189	0.419
32.0	150.0	4.80	57.34	496.2	6242.5	3224.	11.04	60.39	0.183	0.435
35.0	150.0	5.25	54.92	542.7	6816.9	3224.	11.49	65.94	0.174	0.457
40.0	150.0	6.00	51.37	620.3	7775.3	3224.	12.24	75.21	0.163	0.490
45.0	150.0	6.75	48.34	697.8	8734.4	3224.	12.99	84.49	0.154	0.520
50.0	150.0	7.50	47.90	775.3	9694.2	3224.	13.74	93.77	0.147	0.546
52.0	144.2	7.50	46.46	806.3	9695.1	3100.	13.27	90.18	0.147	0.565
60.0	125.0	7.50	41.87	930.4	9701.2	2687.	11.83	78.20	0.151	0.634
70.0	107.1	7.50	38.14	1085.5	9713.4	2303.	10.68	67.11	0.159	0.702
80.0	93.8	7.50	35.91	1240.5	9729.4	2015.	9.94	58.82	0.169	0.755
90.0	83.3	7.50	34.76	1395.6	9748.6	1791.	9.43	52.39	0.180	0.796
100.0	75.0	7.50	34.42	1550.7	9770.8	1612.	9.06	47.26	0.192	0.828
110.0	68.2	7.50	34.74	1705.7	9795.7	1466.	8.79	43.07	0.204	0.853
120.0	62.5	7.50	35.61	1860.8	9823.2	1344.	8.58	39.59	0.217	0.874
130.0	57.7	7.50	36.93	2015.9	9853.2	1240.	8.42	36.66	0.230	0.890
134.0	56.0	7.50	37.58	2077.9	9865.9	1203.	8.37	35.61	0.235	0.896
135.0	55.6	7.50	37.76	2093.4	9869.1	1194.	8.36	35.36	0.236	0.898
140.0	53.6	7.50	38.68	2170.9	9885.6	1152.	8.30	34.15	0.243	0.904

a. LSM thrust vs. speed, maximum thrust.

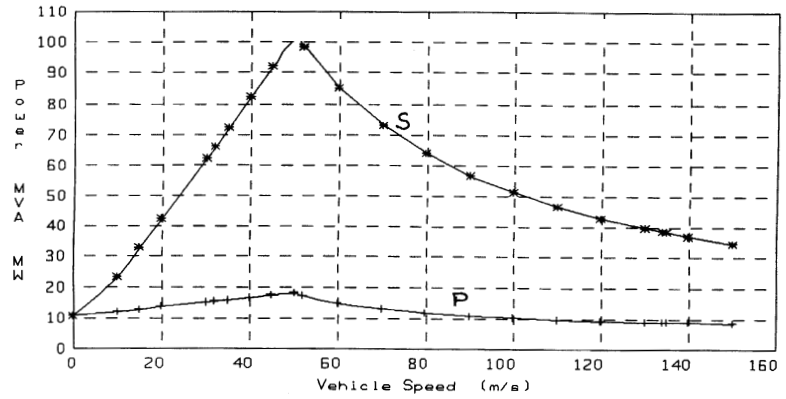

U_s(m/s)	F_x(kN)	F_t(kN)	V_s(V)	I_s(A)	P_s(MW)	S_s(MVA)	PF(PU)	E_{ff}(PU)
10.0	150.00	35.18	2425.7	3224.4	12.074	23.465	0.515	0.124
15.0	150.00	35.32	3389.9	3224.4	12.824	32.792	0.391	0.175
20.0	150.00	35.50	4390.3	3224.4	13.574	42.468	0.320	0.221
30.0	150.00	36.04	6431.6	3224.4	15.074	62.214	0.242	0.299
32.0	150.00	57.34	6843.1	3224.4	15.374	66.195	0.232	0.312
35.0	150.00	54.92	7461.5	3224.4	15.824	72.177	0.219	0.332
40.0	150.00	51.37	8494.5	3224.4	16.574	82.170	0.202	0.362
45.0	150.00	48.34	9529.7	3224.4	17.324	92.184	0.188	0.390
50.0	150.00	47.90	10566.4	3224.4	18.074	102.212	0.177	0.415
52.0	144.23	46.46	10564.5	3100.4	17.276	98.263	0.176	0.434
60.0	125.00	41.87	10561.7	2687.0	14.843	85.138	0.174	0.505
70.0	107.14	38.14	10566.1	2303.2	12.895	73.006	0.177	0.582
80.0	93.75	35.91	10576.4	2015.3	11.630	63.942	0.182	0.645
90.0	83.33	34.76	10591.0	1791.3	10.763	56.917	0.189	0.697
100.0	75.00	34.42	10609.3	1612.2	10.143	51.313	0.198	0.739
110.0	68.18	34.74	10630.6	1465.6	9.685	46.742	0.207	0.774
120.0	62.50	35.61	10654.8	1343.5	9.336	42.944	0.217	0.803
130.0	57.69	36.93	10681.5	1240.2	9.064	39.740	0.228	0.827
134.0	55.97	37.58	10692.9	1203.1	8.972	38.595	0.232	0.836
135.0	55.56	37.76	10695.8	1194.2	8.950	38.320	0.234	0.838
140.0	53.57	38.68	10710.7	1151.6	8.849	37.003	0.239	0.848

b. Converter station output power, maximum thrust.

Figure 41. Performance capability of the Magneplane SCD LSM.

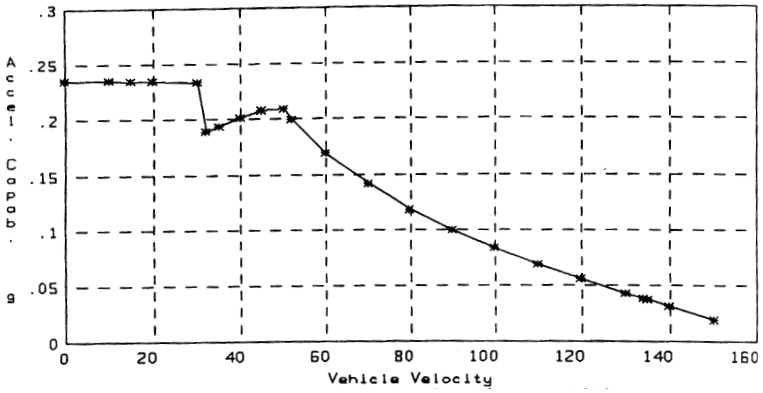

U_s (m/s)	F_x (kN)	F_t (kN)	Accel (g)	Accel (m/s^2)
0.0	150.00	35.08	0.234	2.298
10.0	150.00	35.18	0.234	2.296
15.0	150.00	35.32	0.234	2.294
20.0	150.00	35.50	0.234	2.290
30.0	150.00	36.04	0.232	2.279
32.0	150.00	57.34	0.189	1.853
35.0	150.00	54.92	0.194	1.902
40.0	150.00	51.37	0.201	1.973
45.0	150.00	48.34	0.207	2.033
50.0	150.00	47.90	0.208	2.042
52.0	144.23	46.46	0.199	1.955
60.0	125.00	41.87	0.170	1.663
70.0	107.14	38.14	0.141	1.380
80.0	93.75	35.91	0.118	1.157
90.0	83.33	34.76	0.099	0.972
100.0	75.00	34.42	0.083	0.812
110.0	68.18	34.74	0.068	0.669
120.0	62.50	35.61	0.055	0.538
130.0	57.69	36.93	0.042	0.415
134.0	55.97	37.58	0.038	0.368
135.0	55.56	37.76	0.036	0.356
140.0	53.57	38.68	0.030	0.298

c. Acceleration capability, maximum thrust.

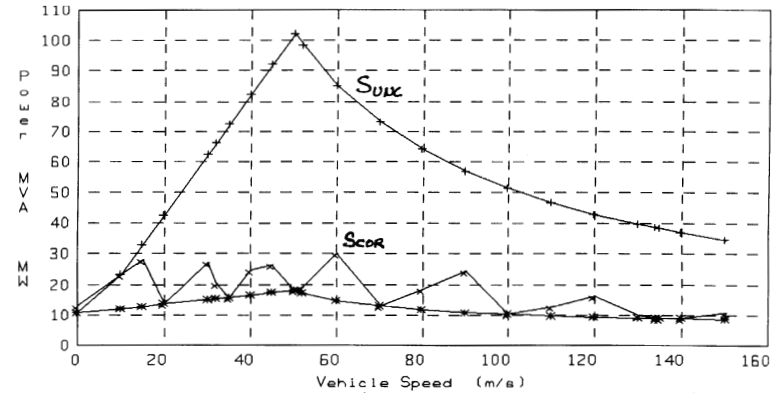

U_s (m/s)	F_x (kN)	F_t (kN)	V_s (V)	I_s (A)	P_s (MW)	S_s (MVA)	PF (PU)	E_{ff} (PU)	C_{pf} (uF)
0.0	150.00	35.08	1336.9	3224.4	10.574	12.932	0.818	0.000	1E12
10.0	150.00	35.18	2425.7	3224.4	12.074	23.465	0.515	0.124	1E12
15.0	150.00	35.32	2902.5	3224.4	12.824	28.076	0.457	0.175	9000
20.0	150.00	35.50	1408.0	3224.4	13.574	13.620	0.997	0.221	9000
30.0	150.00	36.04	2789.0	3224.4	15.074	26.979	0.559	0.299	3000
32.0	150.00	57.34	2093.4	3224.4	15.374	20.250	0.759	0.312	3000
35.0	150.00	54.92	1636.6	3224.4	15.824	15.831	1.000	0.332	3000
40.0	150.00	51.37	2562.3	3224.4	16.574	24.786	0.669	0.362	3000
45.0	150.00	48.34	2717.6	3224.4	17.324	26.289	0.659	0.390	1500
50.0	150.00	47.90	1873.4	3224.4	18.074	18.122	0.997	0.415	1500
52.0	144.23	46.46	2068.6	3100.4	17.276	19.240	0.898	0.434	1500
60.0	125.00	41.87	3754.9	2687.0	14.843	30.268	0.490	0.505	1500
70.0	107.14	38.14	1867.7	2303.2	12.895	12.905	0.999	0.582	750
80.0	93.75	35.91	3061.4	2015.3	11.630	18.508	0.628	0.645	750
90.0	83.33	34.76	4531.1	1791.3	10.763	24.350	0.442	0.697	750
100.0	75.00	34.42	2101.6	1612.2	10.143	10.165	0.998	0.739	375
110.0	68.18	34.74	2920.4	1465.6	9.685	12.841	0.754	0.774	375
120.0	62.50	35.61	4009.2	1343.5	9.336	16.159	0.578	0.803	375
130.0	57.69	36.93	2628.7	1240.2	9.064	9.780	0.927	0.827	200
134.0	55.97	37.58	2506.0	1203.1	8.972	9.045	0.992	0.836	200
135.0	55.56	37.76	2503.3	1194.2	8.950	8.969	0.998	0.838	200
140.0	53.57	38.68	2626.5	1151.6	8.849	9.074	0.975	0.848	200

d. Converter station output power with power factor correction, maximum thrust.

Figure 41 (cont'd).

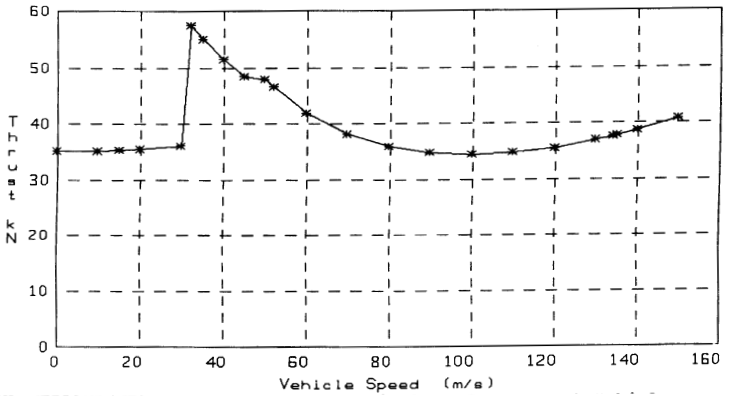

U_s (m/s)	F_x (kN)	P_x (MW)	E_1 (V)	V_1 (V)	I_1 (A)	P (MW)	S (MVA)	PF (PU)	E_{ff} (PU)
0.0	35.08	0.00	0.0	150.8	754.0	0.34	0.34	1.000	0.000
10.0	35.18	0.35	155.1	544.2	756.3	0.70	1.23	0.563	0.506
15.0	35.32	0.53	232.6	778.8	759.2	0.88	1.77	0.494	0.605
20.0	35.50	0.71	310.1	1019.1	763.2	1.06	2.33	0.454	0.670
30.0	36.04	1.08	465.2	1515.2	774.7	1.44	3.52	0.409	0.750
32.0	57.34	1.83	496.2	2460.7	1232.5	2.75	9.10	0.302	0.668
35.0	54.92	1.92	542.7	2578.4	1180.6	2.76	9.13	0.302	0.697
40.0	51.37	2.05	620.3	2758.4	1104.2	2.79	9.14	0.305	0.737
45.0	48.34	2.18	697.8	2925.1	1039.1	2.82	9.12	0.310	0.771
50.0	47.90	2.40	775.3	3215.9	1029.8	3.03	9.93	0.305	0.790
52.0	46.46	2.42	806.3	3248.6	998.7	3.01	9.73	0.310	0.801
60.0	41.87	2.51	930.4	3399.0	900.1	3.00	9.18	0.327	0.838
70.0	38.14	2.67	1085.5	3634.8	819.8	3.07	8.94	0.344	0.869
80.0	35.91	2.87	1240.5	3929.1	771.9	3.23	9.10	0.355	0.889
90.0	34.76	3.13	1395.6	4287.8	747.2	3.46	9.61	0.360	0.903
100.0	34.42	3.44	1550.7	4717.9	740.0	3.77	10.47	0.360	0.913
110.0	34.74	3.82	1705.7	5226.8	746.8	4.16	11.71	0.355	0.919
120.0	35.61	4.27	1860.8	5822.4	765.4	4.62	13.37	0.346	0.924
130.0	36.93	4.80	2015.9	6512.9	793.9	5.18	15.51	0.334	0.927
134.0	37.58	5.04	2077.9	6817.6	807.9	5.43	16.52	0.328	0.928
135.0	37.76	5.10	2093.4	6896.5	811.6	5.49	16.79	0.327	0.928
140.0	38.68	5.41	2170.9	7307.0	831.4	5.83	18.22	0.320	0.929

e. LSM thrust vs. speed, normal thrust.

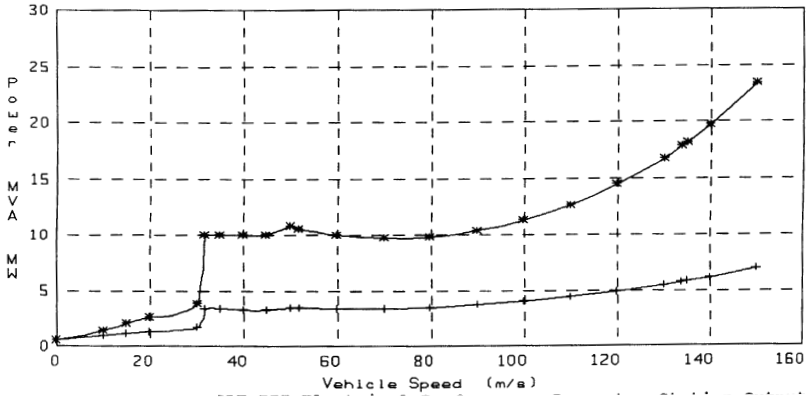

U_s (m/s)	F_x (kN)	V_s (V)	I_s (A)	P_s (MW)	S_s (MVA)	PF (PU)	E_{ff} (PU)
0.0	35.08	255.6	754.0	0.578	0.578	1.000	0.000
10.0	35.18	638.2	756.3	0.934	1.448	0.645	0.377
15.0	35.32	883.0	759.2	1.116	2.011	0.555	0.475
20.0	35.50	1137.2	763.2	1.302	2.604	0.500	0.545
30.0	36.04	1666.6	774.7	1.692	3.874	0.437	0.639
32.0	57.34	2703.4	1232.5	3.380	9.996	0.338	0.543
35.0	54.92	2827.5	1180.6	3.340	10.015	0.334	0.576
40.0	51.37	3017.7	1104.2	3.295	9.996	0.330	0.624
45.0	48.34	3194.0	1039.1	3.273	9.957	0.329	0.665
50.0	47.90	3506.5	1029.8	3.474	10.833	0.321	0.690
52.0	46.46	3540.1	998.7	3.430	10.606	0.323	0.704
60.0	41.87	3696.6	900.1	3.337	9.982	0.334	0.753
70.0	38.14	3944.9	819.8	3.353	9.702	0.346	0.796
80.0	35.91	4257.4	771.9	3.479	9.859	0.353	0.826
90.0	34.76	4640.6	747.2	3.696	10.402	0.355	0.846
100.0	34.42	5102.1	740.0	3.999	11.327	0.353	0.861
110.0	34.74	5649.9	746.8	4.389	12.659	0.347	0.871
120.0	35.61	6292.6	765.4	4.868	14.449	0.337	0.878
130.0	36.93	7039.1	793.9	5.442	16.766	0.325	0.882
134.0	37.58	7368.9	807.9	5.700	17.860	0.319	0.884
135.0	37.76	7454.2	811.6	5.767	18.150	0.318	0.884
140.0	38.68	7898.7	831.4	6.118	19.700	0.311	0.885

f. Converter station output power, normal thrust.

Figure 41 (contd). Performance capability of the Magneplane SCD LSM.

resulting from power-factor correction. Through the speed range below 60 m/s, this correction reduces megavolt-ampere requirements by nearly a factor of 3; above 60 m/s, the reduction is about a factor of 2. The maximum megavolt-amperes for an uncorrected power factor was in excess of 100 at 50 m/s. The partial power-factor correction applied here reduced this maximum to 30 MVA at the same speed.

The efficiency of the LSM varies considerably over the vehicle's speed and is a direct result of the high LSM stator current required to meet the high thrust being produced. The efficiency peaks at 92% at the design point speed of 150 m/s.

The acceleration capability of the Magneplane LSM with a 50,000-kg vehicle exceeds 0.16 g for speeds up to 65 m/s. The maximum acceleration then falls rapidly with speed to 0.08 g at 100 m/s and 0.038 g at 134 m/s.

The uncorrected power factor is quite low across all speeds, being approximately 26% lagging at the design point speed. Power factor correction is expected to significantly improve the situation, and its effects on both efficiency and power factor can be considered by the LSMPOWER model once the implementation details are specified.

The LSM parameters used by LSMPOWER for the Magneplane concept closely match the corresponding parameters reported by Magneplane. The LSMPOWER performance results agree quite closely with those reported by Magneplane. A preliminary analysis of power-factor correction tells us that a significant improvement in the power factor is possible; this should result in significant energy savings. The incremental capital cost to make such a correction must be weighed against the potential energy cost savings.

Bechtel. The Bechtel LSM is an air-core machine with conventional stator windings mounted on the box beam sidewalls. There are two LSMs per vehicle, each with a sidewall air gap of approximately 0.10 m. Superconducting propulsion coils are located on distributed bogies along each side of the vehicle. The stator coils are configured as a six-phase system, with one set of stator windings located on the upper portion of the box-beam sidewall and a second set on the lower portion. The baseline vehicle is a one-car consist.

The LSM blocklengths are 2000 m for the baseline concept and are end-fed from the converter stations. Converter stations are located at every other blocklength and are assumed to be located under the guideway so as to not require feeder cables of any significant length. High-voltage DC (30,000-V) is obtained from rectifier stations located at each utility interface and this voltage is transmitted along the guideway to the frequency converter stations.

We produced the following performance data using the LSMPOWER model for the Bechtel LSM concept operating as described above.

Blocklength resistance R_L:	0.16 Ω
Blocklength inductance L_L:	0.0016 H
Vehicle magnetic length l_v:	2000 m
Longitudinal length of stator L:	2000 m
Field winding pole pitch t_p:	1.0 m
Width of LSM stator l:	0.30 m
Pole pairs per LSM p:	12
Slots per pole per phase N:	2
Number of phases N_p:	6
Number of LSMs per consist N_m:	2
Resistance of feeder cable R_f:	0 Ω
Inductance of feeder cable L_f:	0 H
Air gap flux density:	0.90 T
Maximum stator current per LSM:	1300 A
Maximum power per LSM:	11 MVA

The above data were obtained from information provided by Bechtel and MIT at the IPR and from the SCD final report; where possible, they were independently verified through calculation. The above data show the magnetic length of the vehicle to be equal to the LSM blocklength to account for circuit parameters specified by MIT.

Figure 42 summarizes the performance capability of the Bechtel LSM. The maximum thrust capability for a one-car consist is 143 kN. This concept provides constant thrust from 0 to 112 m/s and then operates at a constant power of 22 MVA for higher speeds. The acceleration capability for a 63,300-kg vehicle exceeds 0.16 g for speeds up to 118 m/s, and it exceeds 0.11 g at 135 m/s.

The efficiency of the LSM at maximum thrust varies considerably with speed and reaches 87% at 135 m/s. Under normal thrust conditions, the efficiency is relatively constant at about 90–92% for speeds above 50 m/s. The power factor is about 90% for maximum thrust conditions at most speeds and about 95% or more at nearly all speeds for nominal thrust conditions.

LSMPOWER predicted approximately the same results as those reported by Bechtel. Bechtel's plan to use power-factor correction resulted in the low inductance values input to LSMPOWER and apparently their own model. However, they didn't describe the specifics of this correction, and its relative improvements vs. its costs would need to be examined.

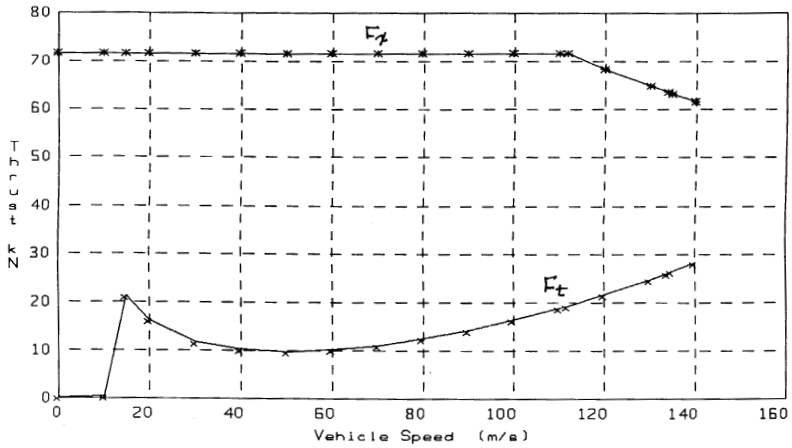

U_s (m/s)	F_x (kN)	F_t (kN)	E_1 (V)	V_1 (V)	I_1 (A)	P (MW)	S (MVA)	PF (PU)
0.0	71.5	0.3	0.0	208.0	1300	1.62	1.62	1.000
10.0	71.5	0.4	91.6	305.8	1300	2.34	2.39	0.980
15.0	71.5	21.4	137.5	357.5	1300	2.69	2.79	0.966
20.0	71.5	16.3	183.3	410.0	1300	3.05	3.20	0.954
30.0	71.5	11.8	274.9	516.7	1300	3.77	4.03	0.935
40.0	71.5	10.1	366.6	624.6	1300	4.48	4.87	0.920
50.0	71.5	9.7	458.2	733.2	1300	5.20	5.72	0.909
60.0	71.5	10.1	549.8	842.3	1300	5.91	6.57	0.900
70.0	71.5	11.1	641.5	951.6	1300	6.63	7.42	0.893
80.0	71.5	12.5	733.1	1061.1	1300	7.34	8.28	0.887
90.0	71.5	14.3	824.8	1170.7	1300	8.06	9.13	0.882
100.0	71.5	16.5	916.4	1280.5	1300	8.77	9.99	0.878
110.0	71.5	18.9	1008.1	1390.3	1300	9.49	10.84	0.875
111.8	71.5	19.4	1024.7	1410.2	1300	9.62	11.00	0.874
120.0	68.3	21.7	1099.7	1476.2	1242	9.68	11.00	0.880
130.0	64.7	24.8	1191.3	1556.9	1178	9.75	11.00	0.886
134.0	63.4	26.1	1228.0	1589.3	1154	9.78	11.00	0.889
135.0	63.1	26.4	1237.2	1597.4	1148	9.78	11.00	0.889
140.0	61.5	28.1	1283.0	1638.0	1119	9.82	11.00	0.893

a. LSM thrust vs. speed, maximum thrust.

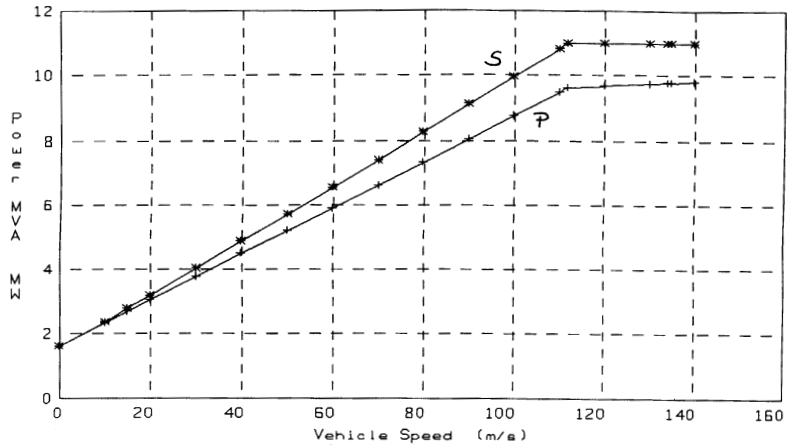

U_s (m/s)	F_x (kN)	F_t (kN)	V_s (V)	I_s (A)	P_s (MW)	S_s (MVA)	PF (PU)	E_{ff} (PU)
0.0	71.5	0.3	208	1300	1.622	1.622	1.000	0.000
10.0	71.5	0.4	306	1300	2.337	2.386	0.980	0.306
15.0	71.5	21.4	357	1300	2.695	2.788	0.966	0.398
20.0	71.5	16.3	410	1300	3.052	3.198	0.954	0.468
30.0	71.5	11.8	517	1300	3.767	4.030	0.935	0.569
40.0	71.5	10.1	625	1300	4.482	4.872	0.920	0.638
50.0	71.5	9.7	733	1300	5.196	5.719	0.909	0.688
60.0	71.5	10.1	842	1300	5.911	6.570	0.900	0.726
70.0	71.5	11.1	952	1300	6.626	7.422	0.893	0.755
80.0	71.5	12.5	1061	1300	7.341	8.276	0.887	0.779
90.0	71.5	14.3	1171	1300	8.056	9.132	0.882	0.799
100.0	71.5	16.5	1280	1300	8.770	9.988	0.878	0.815
110.0	71.5	18.9	1390	1300	9.485	10.844	0.875	0.829
111.8	71.5	19.4	1410	1300	9.615	11.000	0.874	0.831
120.0	68.3	21.7	1476	1242	9.675	11.000	0.880	0.847
130.0	64.7	24.8	1557	1178	9.748	11.000	0.886	0.863
134.0	63.4	26.1	1589	1154	9.777	11.000	0.889	0.869
135.0	63.1	26.4	1597	1148	9.784	11.000	0.889	0.871
140.0	61.5	28.1	1638	1119	9.819	11.000	0.893	0.878

b. Converter station output power, maximum thrust.

Figure 42. Performance capability of Bechtel SCD LSM.

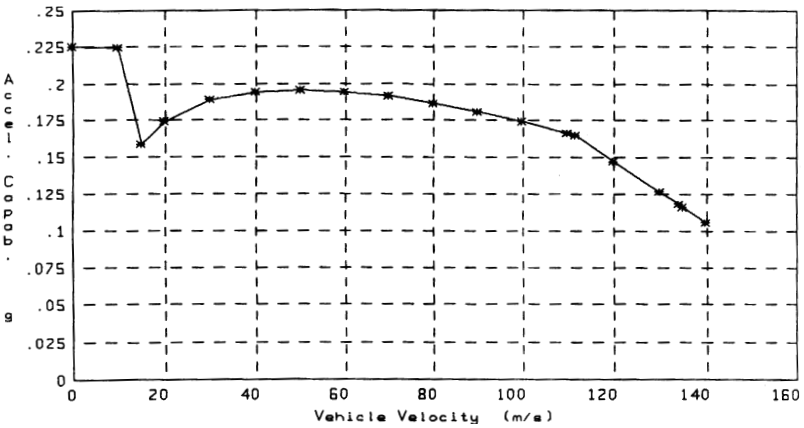

U_s (m/s)	F_x (kN)	F_t (kN)	Accel (g)	Accel (m/s^2)
0.0	71.5	0.3	0.225	2.207
10.0	71.5	0.4	0.225	2.203
15.0	71.5	21.4	0.159	1.554
20.0	71.5	16.3	0.174	1.709
30.0	71.5	11.8	0.189	1.851
40.0	71.5	10.1	0.194	1.903
50.0	71.5	9.7	0.195	1.915
60.0	71.5	10.1	0.194	1.902
70.0	71.5	11.1	0.191	1.872
80.0	71.5	12.5	0.186	1.828
90.0	71.5	14.3	0.181	1.772
100.0	71.5	16.5	0.174	1.706
110.0	71.5	18.9	0.166	1.630
111.8	71.5	19.4	0.165	1.615
120.0	68.3	21.7	0.147	1.445
130.0	64.7	24.8	0.126	1.240
134.0	63.4	26.1	0.118	1.159
135.0	63.1	26.4	0.116	1.138
140.0	61.5	28.1	0.106	1.037

c. Acceleration capability, maximum thrust.

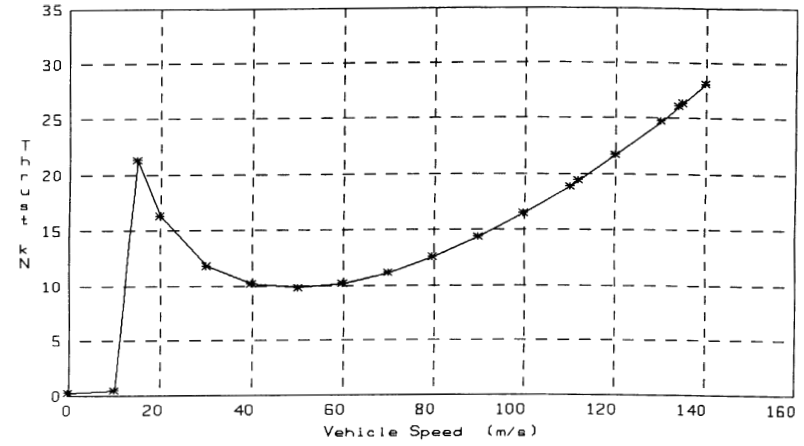

U_s (m/s)	F_x (kN)	E_1 (V)	V_1 (V)	I_1 (A)	P (MW)	S (MVA)	PF (PU)
0.0	0.32	0.0	0.9	6	0.000	0.000	1.000
10.0	0.45	91.6	92.9	8	0.005	0.005	1.000
15.0	21.35	137.5	201.5	388	0.465	0.469	0.991
20.0	16.35	183.3	232.6	297	0.412	0.415	0.993
30.0	11.79	274.9	310.7	214	0.398	0.400	0.995
40.0	10.10	366.6	397.5	184	0.437	0.438	0.996
50.0	9.73	458.2	488.3	177	0.517	0.519	0.996
60.0	10.14	549.8	581.7	184	0.641	0.644	0.996
70.0	11.11	641.5	677.1	202	0.817	0.821	0.995
80.0	12.52	733.1	774.3	228	1.052	1.058	0.994
90.0	14.32	824.8	873.4	260	1.354	1.365	0.992
100.0	16.46	916.4	974.6	299	1.732	1.750	0.989
110.0	18.92	1008.1	1078.0	344	2.195	2.226	0.986
111.8	19.40	1024.7	1097.0	353	2.289	2.323	0.986
120.0	21.69	1099.7	1184.0	394	2.752	2.803	0.982
130.0	24.75	1191.3	1293.1	450	3.413	3.493	0.977
134.0	26.06	1228.0	1337.7	474	3.708	3.804	0.975
135.0	26.39	1237.2	1349.0	480	3.784	3.885	0.974
140.0	28.10	1283.0	1405.8	511	4.185	4.311	0.971

d. LSM thrust vs. speed, normal thrust.

Figure 42 (cont'd)

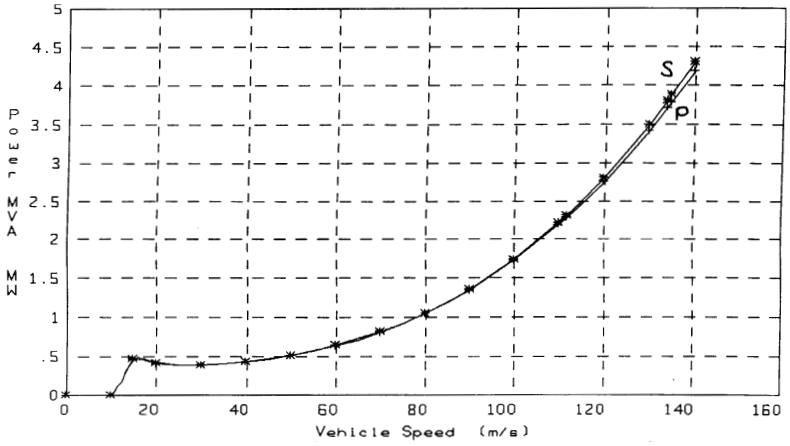

U_s (m/s)	F_t (kN)	V_s (V)	I_s (A)	P_s (MW)	S_s (MVA)	PF (PU)	E_{ff} (PU)
0.0	0.32	1	6	0.000	0.000	1.000	0.000
10.0	0.45	93	8	0.005	0.005	1.000	0.986
15.0	21.35	201	388	0.465	0.469	0.991	0.689
20.0	16.35	233	297	0.412	0.415	0.993	0.794
30.0	11.79	311	214	0.398	0.400	0.995	0.889
40.0	10.10	397	184	0.437	0.438	0.996	0.926
50.0	9.73	488	177	0.517	0.519	0.996	0.942
60.0	10.14	582	184	0.641	0.644	0.996	0.949
70.0	11.11	677	202	0.817	0.821	0.995	0.952
80.0	12.52	774	228	1.052	1.058	0.994	0.953
90.0	14.32	873	260	1.354	1.365	0.992	0.952
100.0	16.46	975	299	1.732	1.750	0.989	0.950
110.0	18.92	1078	344	2.195	2.226	0.986	0.948
111.8	19.40	1097	353	2.289	2.323	0.986	0.948
120.0	21.69	1184	394	2.752	2.803	0.982	0.946
130.0	24.75	1293	450	3.413	3.493	0.977	0.943
134.0	26.06	1338	474	3.708	3.804	0.975	0.942
135.0	26.39	1349	480	3.784	3.885	0.974	0.942
140.0	28.10	1406	511	4.185	4.311	0.971	0.940

e. Converter station output power, normal thrust.

Figure 42 (cont'd). Performance capability of Bechtel SCD LSM.

Foster-Miller. The Foster-Miller LSM is an air-core machine where the LSM coils are located on both channel-guideway sidewalls. The sidewall air gap is approximately 100 mm. Superconducting propulsion coils are located on bogies at each end of the vehicle and with a shared bogie for each car section. The pole pitch of the propulsion coils mounted on the vehicle is different from the coils mounted on the sidewall, the ratio being approximately 1.5:1 vehicle coil to guideway coil.

The propulsion coils are individually controlled by adjacent solid-state bridges (H-bridges) installed in the guideway, and the concept is called a Locally Commutated Linear Synchronous Motor (LCLSM). These LSM coils do not overlap and three-phase operation is obtained electronically by control of the H-bridges. The sequence of control of the propulsion coils is to energize a set of LSM coils at the instant a bogie is opposite them. The idea is to synthesize a traveling wave down the guideway to propel the vehicle, but only those coils adjacent to vehicle magnets are energized at any time.

High-voltage DC (2100 V) is obtained from rectifier stations located at approximately every 8000 m. This DC power is distributed along the guideway to each of the LCLSMs. Each of the opposite LSM coils in the guideway sidewalls is connected electrically in parallel to the H-bridge. For the baseline two-car consist, this is equivalent to 18 individual LSMs powering it. For an eight-car consist, this is equivalent to 54 individual LSMs.

A key function of the LCLSM control system is to alternately switch the propulsion coils from a thrust mode to a power transfer mode as the vehicle moves down the guideway. The LCLSM coils that are located between the bogies are operated as an air-core transformer interacting with a vehicle-mounted coil to transfer power from the guideway to the vehicle.

We produced performance data using the LSMPOWER model for the Foster-Miller LSM concept operating as described above.

Blocklength resistance R_L:	0.0049 Ω
Blocklength inductance L_L:	0.000123 H
Vehicle magnetic length L_v:	4000 m

Longitudinal length of stator L:	4000 m
Field winding pole pitch t_p:	1.3 m
Width of LSM stator l:	0.7 m
Pole pairs per LSM p:	1
Number of conductors per winding:	11
Number of phases N_p:	1
Number of LSMs per consist N_m:	18
Resistance of feeder cable R_f:	0.38 Ω
Inductance of feeder cable L_f:	0 H
Back EMF characteristics at a specified speed E_1:	1370 V at 135 m/s
Maximum stator current per LSM pair:	857 A
Maximum power per LSM pair:	0.74 MW

The above data were obtained from information provided by Foster-Miller during the IPRs, from the SCD final report, and from supplemental material provided by Foster-Miller. Where possible the data were independently verified through calculation.

Figure 43 summarizes the performance capability of the Foster-Miller SCD LSM. The maximum thrust capability of the LCLSM for the two-car consist was 7 kN per LSM, or a total of 126 kN for the consist. The thrust-speed breakpoint from constant thrust to constant power occurs at 83.5 m/s, where the consist power limit is set to 10.6 MW. Similar performance exists for an eight-car consist, with the maximum power scaling to 31.9 MW.

The acceleration capability for a two-car consist of 72,700 kg exceeds 0.14 g for speeds up to 83.5 m/s. Above this speed, acceleration capability decreases nearly linearly to 0.05 g at 135 m/s. The eight-car consist shows similar performance, except that the maximum acceleration is about 0.13 g. This results from a slight reduction in the allowable maximum current for each LSM.

The efficiency of the LCLSM is essentially constant over a wide speed range. It exceeds 99% at the output of the H-bridge and is approximately 95% at the output of the rectifier station. The power factor at the output of the H-bridge is approximately 80% lagging and is essentially constant over the entire speed range.

The current requirement for the H-bridge devices is approximately 860 A per device for maximum thrust. The high switching speeds intended for the H-bridge devices will probably require them to be

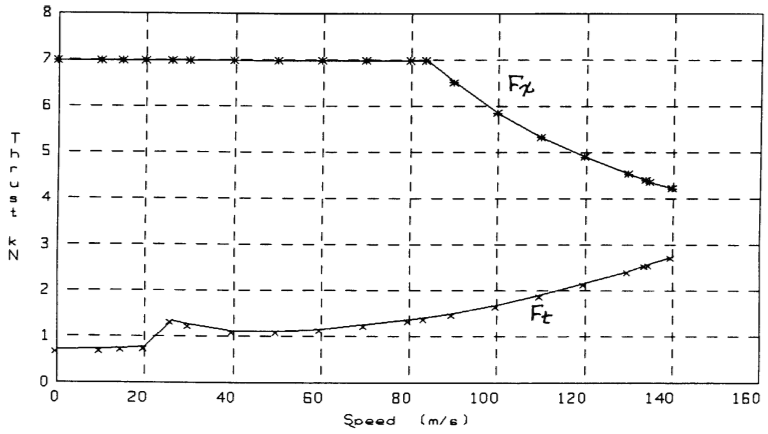

U_s (m/s)	F_x (kN)	F_t (kN)	E_1 (V)	V_1 (V)	I_1 (A)	P (MW)	S (MVA)	PF (PU)	E_{ff} (PU)
0.0	6.99	0.71	0.1	4.2	857.0	0.004	0.004	1.000	0.010
10.0	6.99	0.73	101.5	106.4	857.0	0.074	0.091	0.806	0.951
15.0	6.99	0.74	152.2	157.9	857.0	0.108	0.135	0.802	0.967
20.0	6.99	0.76	203.0	209.4	857.0	0.143	0.179	0.799	0.975
26.0	6.99	1.33	263.9	271.2	857.0	0.185	0.232	0.798	0.981
30.0	6.99	1.24	304.4	312.4	857.0	0.213	0.268	0.797	0.983
40.0	6.99	1.12	405.9	415.4	857.0	0.283	0.356	0.796	0.987
50.0	6.99	1.11	507.4	518.4	857.0	0.353	0.444	0.795	0.990
60.0	6.99	1.16	608.9	621.4	857.0	0.423	0.533	0.794	0.991
70.0	6.99	1.25	710.4	724.4	857.0	0.493	0.621	0.794	0.993
80.0	6.99	1.35	811.9	827.5	857.0	0.563	0.709	0.794	0.994
83.5	6.99	1.40	847.3	863.5	857.0	0.587	0.740	0.794	0.994
90.0	6.50	1.50	913.3	929.3	796.3	0.588	0.740	0.794	0.995
100.0	5.86	1.68	1014.8	1030.5	718.1	0.588	0.740	0.795	0.996
110.0	5.33	1.90	1116.3	1131.7	653.9	0.589	0.740	0.796	0.996
120.0	4.90	2.15	1217.8	1233.0	600.2	0.589	0.740	0.796	0.997
130.0	4.52	2.43	1319.3	1334.3	554.6	0.590	0.740	0.797	0.997
134.0	4.39	2.55	1359.9	1374.8	538.3	0.590	0.740	0.797	0.998
135.0	4.36	2.58	1370.0	1384.9	534.3	0.590	0.740	0.797	0.998

a. LSM thrust vs. speed, maximum thrust.

Figure 43. Performance capability of Foster-Miller SCD LSM.

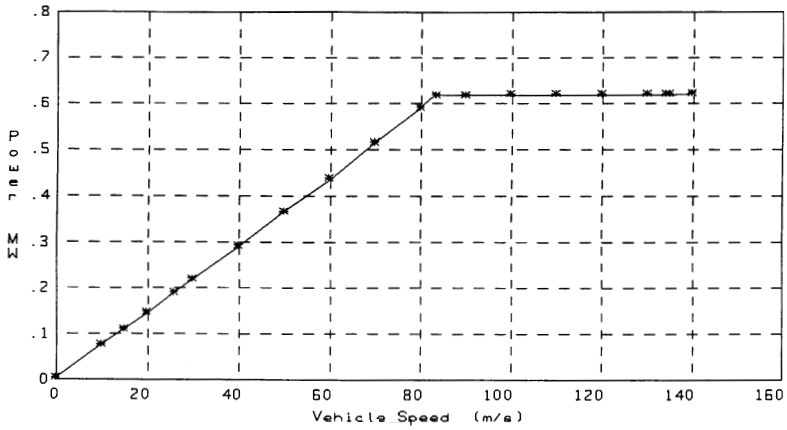

U_s (m/s)	F_x (kN)	F_t (kN)	V_s (V)	VL (V)	V_sL (V)	IL (A)	P_s (MW)	E_{ff} (PU)
0.0	6.99	0.71	2101.0	2100.0	1.02	2.7	0.006	0.006
10.0	6.99	0.73	2113.7	2100.0	13.66	36.0	0.076	0.920
15.0	6.99	0.74	2120.0	2100.0	19.99	52.6	0.112	0.940
20.0	6.99	0.76	2126.3	2100.0	26.31	69.2	0.147	0.950
26.0	6.99	1.33	2133.9	2100.0	33.90	89.2	0.190	0.955
30.0	6.99	1.24	2139.0	2100.0	38.96	102.5	0.219	0.956
40.0	6.99	1.12	2151.6	2100.0	51.62	135.8	0.292	0.957
50.0	6.99	1.11	2164.3	2100.0	64.27	169.1	0.366	0.955
60.0	6.99	1.16	2176.9	2100.0	76.92	202.4	0.441	0.952
70.0	6.99	1.25	2189.6	2100.0	89.57	235.7	0.516	0.948
80.0	6.99	1.35	2202.2	2100.0	102.22	269.0	0.592	0.944
83.5	6.99	1.40	2206.6	2100.0	106.64	280.6	0.619	0.943
90.0	6.50	1.50	2206.7	2100.0	106.72	280.8	0.620	0.943
100.0	5.86	1.68	2206.8	2100.0	106.83	281.1	0.620	0.944
110.0	5.33	1.90	2206.9	2100.0	106.92	281.4	0.621	0.945
120.0	4.90	2.15	2207.0	2100.0	107.00	281.6	0.621	0.945
130.0	4.52	2.43	2207.1	2100.0	107.06	281.7	0.622	0.946
134.0	4.39	2.55	2207.1	2100.0	107.09	281.8	0.622	0.946
135.0	4.36	2.58	2207.1	2100.0	107.09	281.8	0.622	0.946

b. Converter station output power, maximum thrust.

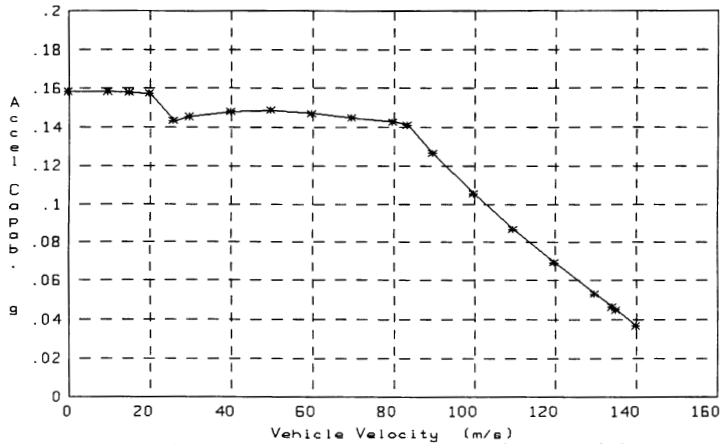

U_s (m/s)	F_x (kN)	F_t (kN)	Accel (g)	Accel (m/s^2)
0.0	6.99	0.71	0.158	1.554
10.0	6.99	0.73	0.158	1.551
15.0	6.99	0.74	0.158	1.547
20.0	6.99	0.76	0.157	1.542
26.0	6.99	1.33	0.143	1.401
30.0	6.99	1.24	0.145	1.425
40.0	6.99	1.12	0.148	1.454
50.0	6.99	1.11	0.148	1.456
60.0	6.99	1.16	0.147	1.443
70.0	6.99	1.25	0.145	1.421
80.0	6.99	1.35	0.142	1.395
83.5	6.99	1.40	0.141	1.384
90.0	6.50	1.50	0.126	1.237
100.0	5.86	1.68	0.105	1.033
110.0	5.33	1.90	0.087	0.850
120.0	4.90	2.15	0.069	0.679
130.0	4.52	2.43	0.053	0.518
134.0	4.39	2.55	0.046	0.456
135.0	4.36	2.58	0.045	0.440

c. Acceleration capability, maximum thrust.

Figure 43 (cont'd). Performance capability of Foster-Miller SCD LSM.

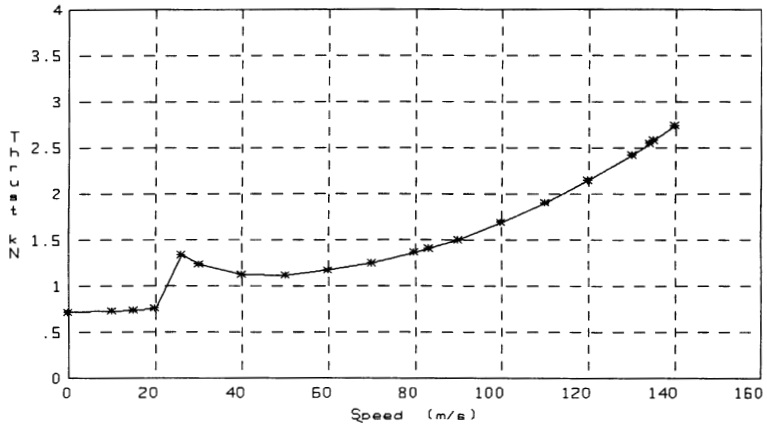

U_s(m/s)	F_t(kN)	E_1(V)	V_1(V)	I_1(A)	P(MW)	S(MVA)	PF(PU)	E_{ff}(PU)
0.0	0.71	0.1	0.5	87.4	0.000	0.000	0.998	0.087
10.0	0.73	101.5	102.0	88.9	0.007	0.009	0.804	0.995
15.0	0.74	152.2	152.8	90.8	0.011	0.014	0.804	0.996
20.0	0.76	203.0	203.7	93.4	0.015	0.019	0.803	0.997
26.0	1.33	263.9	265.2	163.3	0.035	0.043	0.803	0.996
30.0	1.24	304.4	305.8	151.4	0.037	0.046	0.803	0.997
40.0	1.12	405.9	407.4	137.2	0.045	0.056	0.803	0.998
50.0	1.11	507.4	509.1	136.0	0.056	0.069	0.802	0.998
60.0	1.16	608.9	611.0	142.7	0.070	0.087	0.802	0.999
70.0	1.25	710.4	712.9	153.4	0.088	0.109	0.802	0.999
80.0	1.35	811.9	814.9	166.1	0.109	0.135	0.802	0.999
83.5	1.40	847.4	850.6	171.8	0.117	0.146	0.802	0.999
90.0	1.50	913.3	917.0	184.0	0.135	0.169	0.802	0.999
100.0	1.68	1014.8	1019.3	206.5	0.169	0.211	0.801	0.999
110.0	1.90	1116.3	1121.8	233.2	0.210	0.262	0.801	0.999
120.0	2.15	1217.8	1224.4	263.7	0.258	0.323	0.801	0.999
130.0	2.43	1319.3	1327.3	297.9	0.316	0.395	0.800	0.999
134.0	2.55	1359.9	1368.5	312.5	0.342	0.428	0.800	0.999
135.0	2.58	1370.0	1378.8	316.3	0.349	0.436	0.800	0.999

d. LSM thrust vs. speed, normal thrust.

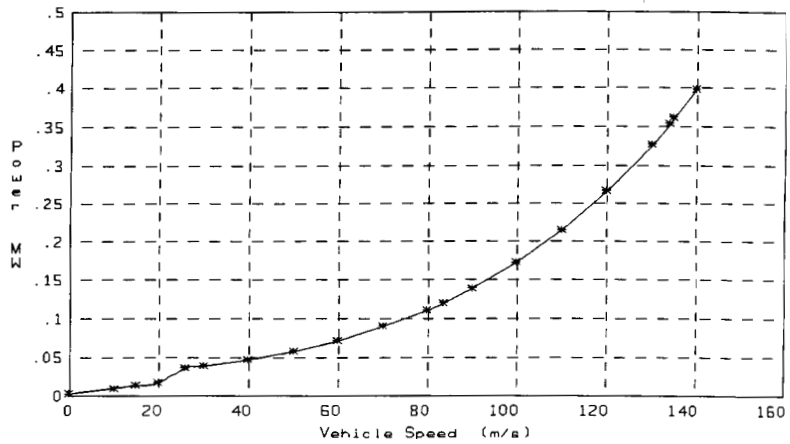

U_s(m/s)	F_t(kN)	V_s(V)	VL(V)	V_sL(V)	IL(A)	P_s(MW)	E_{ff}(PU)
0.0	0.71	2100.4	2100.0	0.37	1.0	0.002	0.002
10.0	0.73	2101.7	2100.0	1.68	4.4	0.009	0.780
15.0	0.74	2102.4	2100.0	2.38	6.3	0.013	0.844
20.0	0.76	2103.1	2100.0	3.13	8.2	0.017	0.880
26.0	1.33	2106.7	2100.0	6.65	17.5	0.037	0.939
30.0	1.24	2107.1	2100.0	7.09	18.7	0.039	0.943
40.0	1.12	2108.5	2100.0	8.48	22.3	0.047	0.952
50.0	1.11	2110.4	2100.0	10.41	27.4	0.058	0.959
60.0	1.16	2113.0	2100.0	13.02	34.3	0.072	0.965
70.0	1.25	2116.2	2100.0	16.23	42.7	0.090	0.969
80.0	1.35	2120.0	2100.0	20.00	52.6	0.112	0.971
83.5	1.40	2121.6	2100.0	21.57	56.8	0.120	0.972
90.0	1.50	2124.8	2100.0	24.84	65.4	0.139	0.973
100.0	1.68	2130.9	2100.0	30.89	81.3	0.173	0.973
110.0	1.90	2138.3	2100.0	38.28	100.7	0.215	0.972
120.0	2.15	2147.1	2100.0	47.14	124.0	0.266	0.969
130.0	2.43	2157.6	2100.0	57.60	151.6	0.327	0.966
134.0	2.55	2162.3	2100.0	62.27	163.9	0.354	0.964
135.0	2.58	2163.5	2100.0	63.48	167.1	0.361	0.964

e. Converter station output power, normal thrust.

Figure 43 (cont'd).

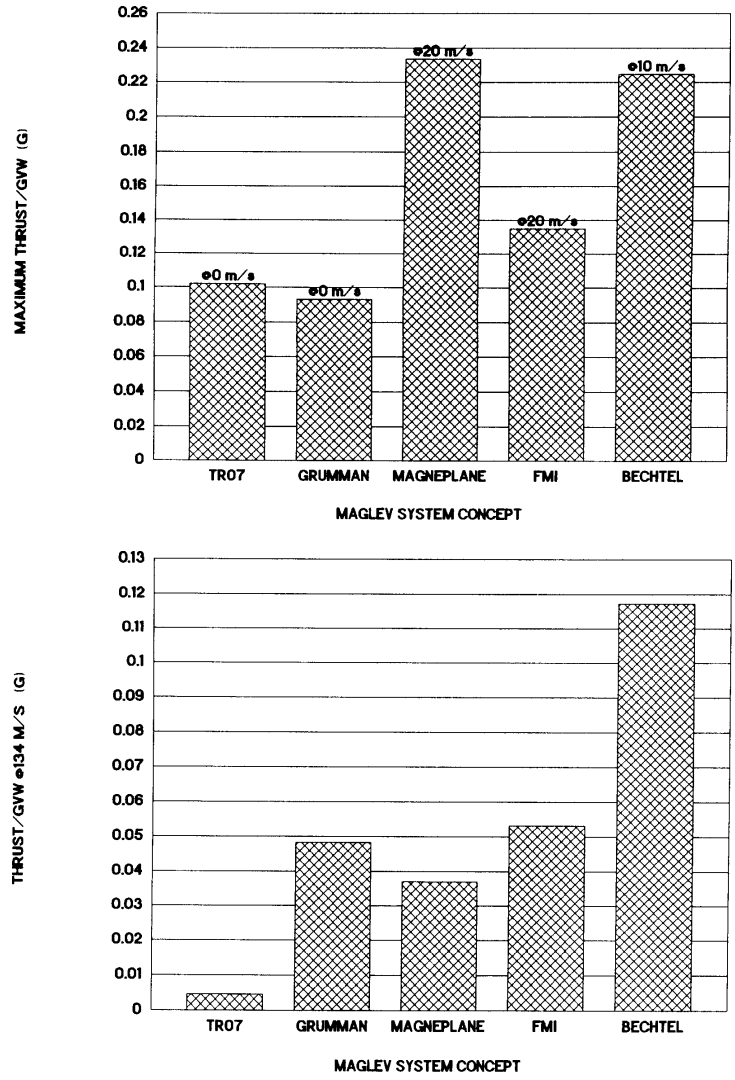

a. Low speed.

b. 134 m/s.

Figure 44. Comparison of acceleration capabilities.

IGBTs (insulated gate bipolar transistors), since the switching speeds required are beyond those recommended for GTOs (gate turnoff thyristors). Current commercially available IGBTs are limited to 600-A ratings with voltage ratings of 1400 V, such as the soon to be introduced Fuji device. Using devices of this type in the LCLSM would require at least two in series and two in parallel per H-bridge leg, or a total of at least 12 devices per H-bridge. The continuing evolution of IGBTs will probably reduce this to six devices per H-bridge within the foreseeable future.

The performance results from LSMPOWER compare well to those reported by Foster-Miller. However, the controllability of the LCLSM is an important technical issue that was not addressed in this analysis. It would require additional effort that would perhaps be best handled with an experimental scale model of the LCLSM. Section 4.4 and Appendix C of this report give more detail about the risks and benefits of this innovative propulsion concept.

Comparative performance of the LSM concepts

The results of the LSMPOWER runs for each of the SCD concepts and the TR07 were compared for their relative performance in acceleration and grade climbing capability. The SCD RFP (USDOTFRA 1991) required that the system concepts be able to maintain the maximum cruising speed on a +3.5% grade, and that, further, they be capable of operating at some speed on a +10% grade.

Acceleration capability. Figure 44a gives the low-speed acceleration capability for the five systems

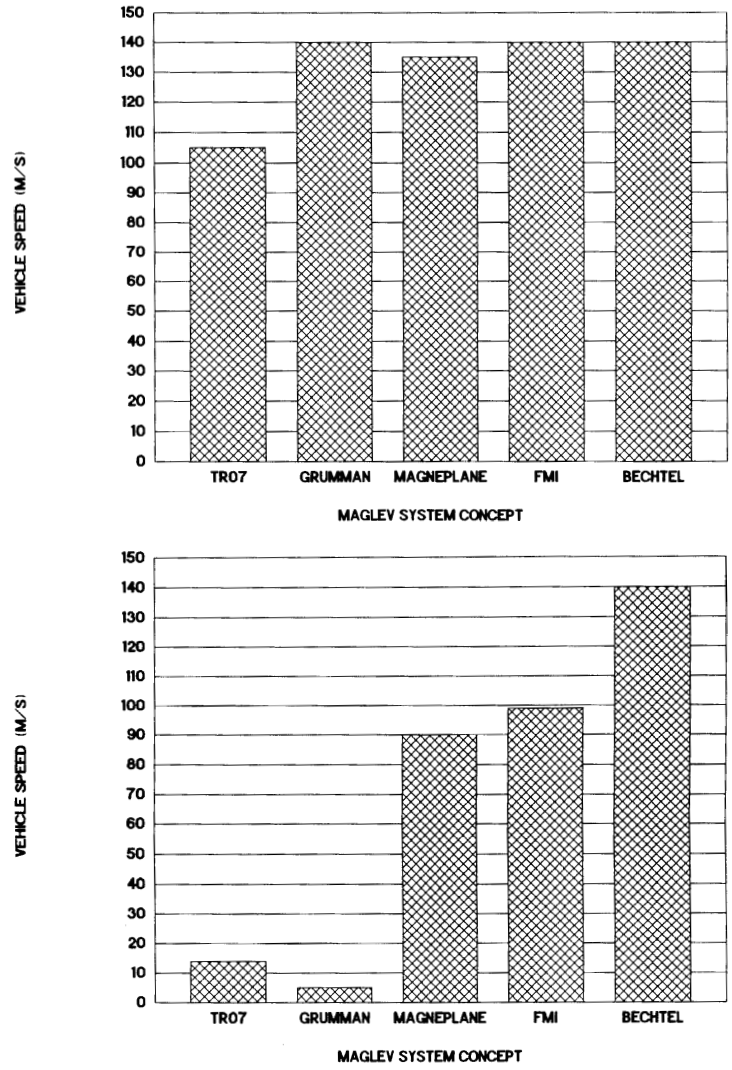

a. 3.5% grade.

b. 10% grade.

Figure 45. Comparison of speeds sustained on grades.

analyzed. The maximum acceleration capabilities at the zero liftoff speed for the TR07 and Grumman baseline SCD are 0.102 and 0.093 g, respectively. Grumman's optional 100-kN LSM increases its maximum acceleration to 0.16 g. For the EDS concepts, the acceleration capabilities at a 20-m/s liftoff speed for the Magneplane and Foster-Miller vehicles are 0.234 and 0.157 g, respectively. The Bechtel concept can achieve 0.226 g at its liftoff speed of 10 m/s.

Figure 44b shows that the acceleration capability remaining at the maximum cruise speed of 134 m/s is 0.006 g for TR07, 0.05 g for Grumman, 0.04 g for Magneplane, 0.05 g for Foster-Miller, and 0.12 g for Bechtel. Grumman's optional 100-kN LSM raises its value to 0.10 g.

Grade climbing capability. Figure 45a shows the maximum speeds that the SCDs and TR07 may maintain up a 3.5% grade. These are the steady-state balance speeds and do not consider grade length and inertia to pass over the grade at some changing speed. Also, these calculations were based on the baseline configurations discussed earlier and do not account for any LSM configuration changes at the grade condition. Note that all SCD concepts are able to maintain maximum cruise speed up a 3.5% grade, as required. The 7.2-MVA power limit for the TR07 limits its 3.5%-grade-climbing speed to 105 m/s. The LSMPOWER model determined that this power limit would have to be increased to slightly more than 10 MVA (i.e., by about 40%) for the TR07 to maintain 134 m/s up a 3.5% grade.

Figure 45b shows the maximum speeds that the SCDs and TR07 may maintain up a 10% grade. The values vary considerably: about 5 m/s for

Grumman's baseline design, 90 m/s for Magneplane, 100 m/s for Foster-Miller, and 140 m/s for Bechtel. As with the 3.5% grade results, these are the steady-state balance speeds based on the baseline LSM configurations. For example, the Grumman concept has aluminum conductors for the LSM stator coil. Changing these conductors to copper on the grade portion of the guideway would enable Grumman's optional 100-kN LSM to maintain 125 m/s up a 10% grade.

The TR07 is in a similar situation as the Grumman concept; it cannot maintain much speed (about 14 m/s) up a 10% grade. As with Grumman, however, replacing TR07's aluminum stator windings with copper for the grade section would substantially increase this speed.

LSM stator winding lifetime. The lifetime of the LSM stator winding depends heavily on the thermal stresses to which it is exposed. The motors typically fail when the winding insulation deteriorates, which is accelerated by thermal stresses. A well known practice in electrical machine design is to assume that insulation lifetime halves for each 10°C rise in temperature above its design operating temperature. Industry practice for the design of rotating machinery and bus bars in power installations translates to a current density of about 1.7 MA/m^2 of conductor cross section.

Figure 46 shows the current density in millions of amperes per square meter for each of the five concepts compared with industry practice. The Grumman, Bechtel, and TR07 current densities are all about 4 MA/m^2. Magneplane's current density is lowest at about 2 MA/m^2, and Foster-Miller's is highest at about 6 MA/m^2.

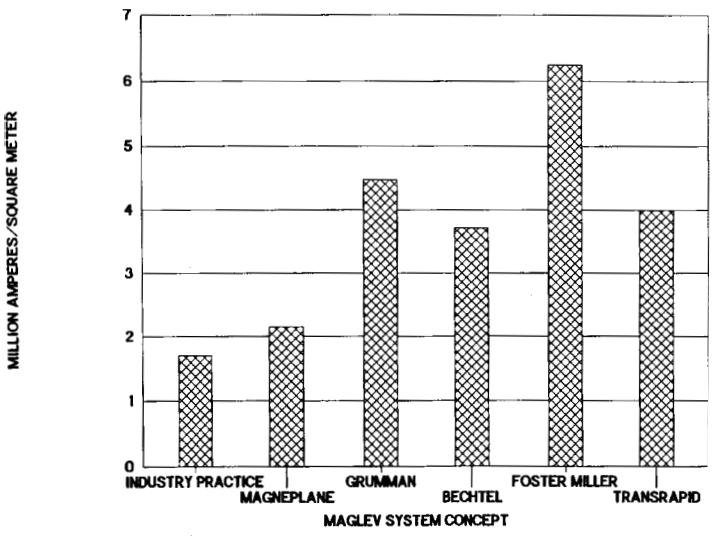

Figure 46. Comparison of the current densities of LSM stator windings.

Not enough is known about the absolute expected lifetime of the LSM stator windings for the duty cycles possible for these systems. However, the above comparisons can be used to estimate the relative stator lifetimes for each of the five concepts. From a thermal stress consideration, the Magneplane LSM should have the longest lifetime, while the Foster-Miller LSM should have the shortest.

LSM stator winding construction. All SCD blocklength LSMs use a stator winding that has overlapping coils, with the coil entrance and exit at the same location on the guideway. This technique is in contrast with the Transrapid Emsland test facility, where the stator coils enter the guideway at the beginning of a block and exit at the end of the block. The advantages of the SCDs' overlapping approach are that it may simplify electrification construction, and it enables a larger pole pitch by having multiple slots (i.e., conductors) per pole. The larger pole pitch in turn lowers the operating frequency of the LSM and the control inverters. This construction technique should improve both performance and cost over the technique used at Emsland.

Efficiency and power factor at electrical source. The converter stations connecting each system to an electrical source differ somewhat. TGV uses AC power directly so that it connects to a source using only a transformer. All other systems connect to a source through solid state AC–DC converters; however, they use the resulting DC power differently.

TR07, Grumman, and Magneplane distribute DC power to widely spaced inverter stations (several kilometers apart). They then use feeder cables to power LSM blocks. Bechtel distributes its high-voltage DC to more closely spaced inverter stations along the guideway. They then power each LSM block using the stator windings as the feeder cables. Foster-Miller distributes lower-voltage DC directly to its LCLSM inverters adjacent to each coil.

We estimated the efficiency and power factor for each system's converter stations and applied these to the output of LSMPOWER to obtain overall values as seen at the electrical source. Table 28 shows a summary of these results for each system. Note that the results for Magneplane include the power-factor correction discussed in their final report.

Table 28. Overall efficiency and power factor for each system at 134 m/s (except TGV-A, which is at 83 m/s).

Parameter	*TGV-A (1-10-1)*	*TR07*	*Bechtel*	*Foster-Miller*	*Grumman*	*Magneplane*
Overall efficiency	0.82	0.83	0.85	0.91	0.78	0.84
Power factor	0.91	0.74	0.98	0.97	0.98	0.99

As expected, Foster-Miller's LCLSM yields the highest overall efficiency of the concepts studied.

Summary and conclusions

The linear synchronous motor model, LSMPOWER, was developed for two main purposes. First, we used it for an assessment tool to address issues of thrust-speed performance, power and energy consumption requirements, and, to a lesser extent, LSM and related power distribution, power conversion, and control costs. Second, we used it to provide propulsion data to simulate each concept's operational performance on corridors (section 3.3.1). The model fulfilled both purposes.

An important general finding of this work is that, in virtually all cases, LSMPOWER predicted performance similar to that reported by the SCD studies. More specifically, the GMSA team reached the following conclusions regarding the LSM concepts studied:

- The LSMs considered in all SCD studies, perhaps with the exception of the locally commutated LSM (LCLSM), appear to be technically feasible and are incremental improvements over contemporary designs. However, three of the LSM concepts (Foster-Miller, Grumman, and Magneplane) use the stator as a power transfer component, and the effect of power transfer on LSM performance was not assessed here or in the SCD studies.
- The LCLSM is potentially a major innovation, but it is unproven and requires additional effort to establish its technical feasibility and cost. There are many control issues involved with the LCLSM, and evaluating those issues is beyond the scope of the existing LSMPOWER model. The LCLSM also may require state-of-the art switching devices as part of the power electronics control; the cost of such devices is extremely difficult to predict.
- For both iron-core and air-core LSMs, high efficiencies are attainable. The LCLSM is capable of the highest efficiency because its blocklength is always equal to a consist length.
- The need for feeder cables to energize alternate LSM blocklengths does have some adverse effect on efficiency. It also can significantly reduce the power factor. Both of these increase the cost for electrical energy. Feeder cable requirements can be traded off with more closely spaced converter stations; such trade-off analyses must be part of any route-specific studies.
- The air-core LSMs had the lowest power factors because of the large coil geometries required for the air-core stator coils. Most of the SCD studies recognized the potential need for power factor correction to improve performance. Power factor correction requires more detailed study to assess performance improvement and cost trade-offs. The LSMPOWER model as it currently exists can assess the effects of power correction on performance.
- Acceleration and grade climbing, as expected, require significantly more LSM thrust capability than the steady-state thrust-speed requirements. Meeting these two requirements could significantly and adversely affect both efficiency and power factor. Tailoring the LSM design to meet acceleration and grade climbing performance for route-specific conditions would result in more optimum LSM designs.
- The current density of the LSM is one measure of expected stator-winding lifetime. The SCDs and TR07 all have stator-winding current densities that exceed industry practice (by factors of 1.3 to 4) for what is considered to be conservative, long-lifetime designs. While it is true that, initially, these LSMs will have duty cycle loadings lower than industry practice designs, this advan-

tage may disappear under the close headway operation expected for a mature maglev system. Upgrading the stator windings may be appropriate should this take place.

Recommendations

- The LCLSM requires additional study to establish its technical feasibility. This concept, as envisioned, will make use of computer control to become energized in the propulsion mode at the instant that the superconducting field magnets mounted on the vehicles' bogies are sensed to be present, to synthesize the desired waveforms for driving the LSM coils, and effectively to operate all LSM coils in parallel with equal current sharing. These are control issues that must be addressed. The LCLSM will also function as the power transfer mechanism whenever it is not operating in the propulsion mode; control implications for this power-transfer function should also be examined. These issues are amenable to scale-model evaluation, and such tests should be started immediately to maintain the LCLSM as a viable option. In addition, trade-off studies should determine optimum DC supply voltage and inverter switching speed; both of these have effects on efficiency and cost.
- The power transfer methods that make use of the LSM stator as an inductive coupler are new ideas at the power levels being considered. The feasibility of these concepts to transfer the needed power levels effectively and efficiently, without adversely affecting LSM performance, needs to be established. While many of the questions of feasibility can be addressed analytically, experimental validation of the power transfer techniques is necessary and could be done at the reduced scale.
- The current SCD studies did not quantify the benefits of power regeneration. Regeneration was not assessable at this time in LSMPOWER. We recommend that the analytical and modeling work needed to implement regeneration be done initially through an expansion of the LSMPOWER model and subsequently incorporated into the system simulator.
- Analysis of power-factor correction requires additional effort. All concepts need correction. The specific concepts providing power-factor correction should be investigated and assessed for both their technical merits as well as their total costs. The current LSMPOWER can model the technical performance effects of various power-factor correction strategies. Existing cost models can be adapted to analyze the total cost.
- The scope and schedule of the recently completed SCD studies limited the choice with linear motors to making incremental improvements over conventional LSM machines. Several experimental linear motors exist that make use of passive field structures. These are attractive because of their potential simplicity over conventional iron-core and air-core LSMs. This could significantly simplify vehicle-carried equipment. Each of these concepts has been shown experimentally to produce thrust, levitation, and guidance forces within a single integrated structure. These machines warrant additional R&D work to determine their performance and costs compared to the more conventional linear motors.

3.2.3 Magnetic fields*

Objectives

Forces resulting from magnetic fields generated both aboard the vehicle and in the guideway are essential for the suspension and propulsion of maglev vehicles. Magnetic fields incidental to these essential functions will exist in the passenger compartment and in regions surrounding the vehicle and guideway. The effects of these fields on passengers and the environment are not well established at this time and so are a matter of concern. Ways of shielding these fields are available, but including them will inevitably increase the weight and cost of the vehicle. In this section, the magnetic forces and stray fields of the TR06/07 maglev system and the four SCDs are analyzed and compared with known and proposed values. These calculations were made to assure that the values presented to the Government are "reasonable." They should not be interpreted as designs or improvements of the concepts analyzed. For expediency, approximate methods have been used in some cases where they serve to verify that the values being checked are credible.

* Written by Dr. Howard Coffey, Center for Transportation Research, Argonne National Laboratory.

Methodology

Methods for calculating electromagnetic fields and forces are well known. However, no single model is adequate for the analysis of all the systems proposed by the SCD contractors. Systems composed of current-carrying coils can be analyzed using straightforward, but sometimes tedious, methods, with the accuracy of the results being limited only by the accuracy with which the input currents and geometries are known. Prudence demanded that simplifications be made in some cases. This method of analysis is appropriate to some electrodynamic maglev systems using simple or "null-flux" coils in the guideway and superconducting magnets on the vehicle. For iron-cored magnets, electrodynamic systems in which the guideway current is induced in continuous sheets, or inter-connected coils such as ladder tracks, however, these methods are insufficient.

A straightforward but complex Dynamic Circuit Theory model computer code, developed by He et al. (1991) of Argonne National Laboratory and verified in part by experiments at ANL (Mulcahy et al. 1993), uses numerical techniques to calculate the time-dependent forces of coil-type suspension systems. This model was used in the analysis of the Foster-Miller concept. A similar model was combined with a harmonic analysis technique to obtain closed-form formulas to analyze the Bechtel concept. Finally, for computing the stray fields from the magnets, He formulated a computer code to calculate the magnetic fields from finite-element conducting filaments in any spatial orientation. The code has been compared to results from the three-dimensional computer code TOSCA with good agreement. These codes are discussed below where they were used.

The analysis of electromagnetic systems containing ferromagnetic materials is complicated by the nonlinear permeability of ferromagnetic materials. For systems in which the magnetic induction is well below the saturation values of the materials used, and for geometries in which the magnetic flux is well confined, the fields and forces can be approximated by analytic formulas. Where this approach is inadequate, which for maglev is generally the case, computer calculations must be made. In making such calculations, a spatial mesh is designed upon which the fields and permeabilities are first approximated and then iterated until a sufficient degree of accuracy is obtained. We used two-dimensional meshes for geometries in which one dimension is extensive or in which a field geometry is encountered that permits a symmetrical boundary condition to be imposed. More complicated geometries require a three-dimensional mesh and time-consuming computer calculations to obtain reasonable accuracy. Several commercial computer codes are available for this purpose.

Generally, these codes do not provide for cases involving relative motion between the elements of the system. Relative motions result in induced eddy currents in elements of the system that are exposed to time-varying magnetic fields. Since these eddy currents can be substantially reduced by using laminated structures, and since all the ferromagnetic systems analyzed use such structures, this restriction is not believed to be a substantial limitation to the accuracy of the results presented here.

Solutions for the forces in EDS systems that induce the reactive current in a continuous conducting sheet in the guideway have only been obtained for simple geometries in which the sheet forms a closed cylinder or is planar and infinite. Although approximate solutions have been found for some simple geometries, solutions for sheets forming surfaces of finite dimensions must be analyzed using finite-element computer codes similar to those used for ferromagnetic materials but including the motion of the conductor.

Two-dimensional finite-element calculations for simple ferromagnetic structures were made using PE2D, and three-dimensional calculations were made for more complex ferromagnetic structures using TOSCA. All of these are in commercial use and are regarded as reliable. ELEKTRA*, which includes moving media, is relatively new. It is the only commercially available finite-element code of which we are aware that is capable of these computations. It has been used at ANL to calculate the forces on small magnets mounted close to finite, moving, conducting surfaces of various shapes and dimensions (Mulcahy et al. 1993). The results are credible for these small systems. For larger systems, however, a limitation is encountered in the relationship between the velocity and the required distance between nodes in the mesh. For realistic sizes and velocities of maglev magnets, the mesh size becomes extremely small and the number of nodes required becomes prohibitively large for the com-

* The computer codes PE2D, TOSCA, and ELEKTRA are commercial computer codes of Vector Fields, Inc., Aurora, IL.

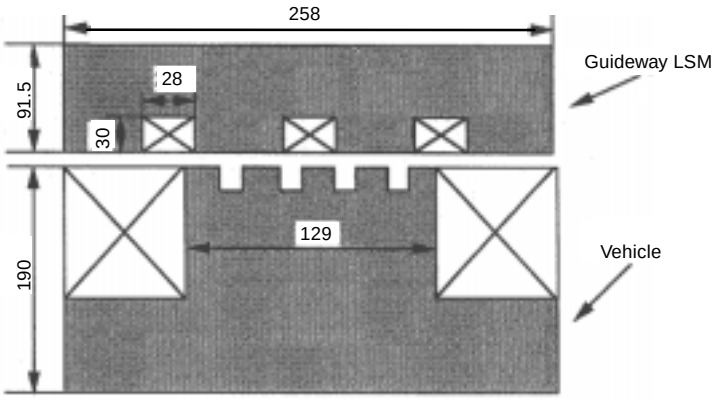

Figure 47. TR06 levitation and propulsion configuration (dimensions in mm).

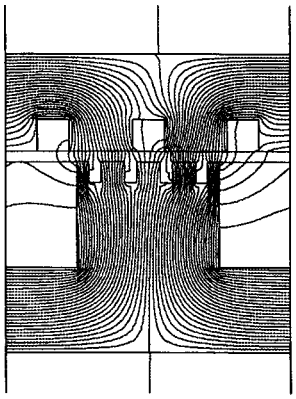

a. Levitation and propulsion system.

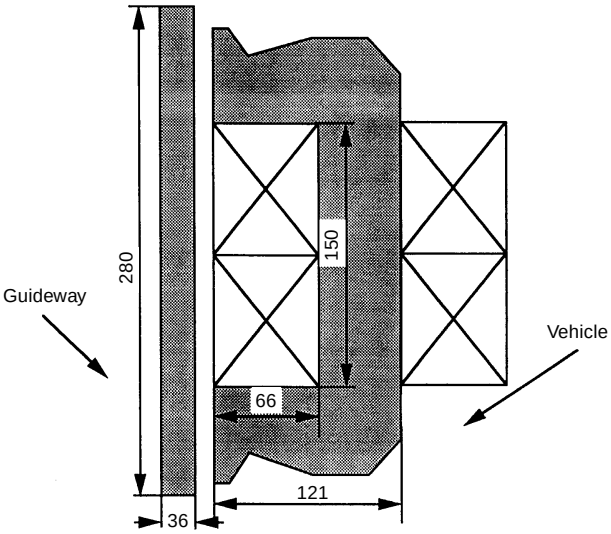

Figure 48. TR07 guidance configuration (dimensions in mm).

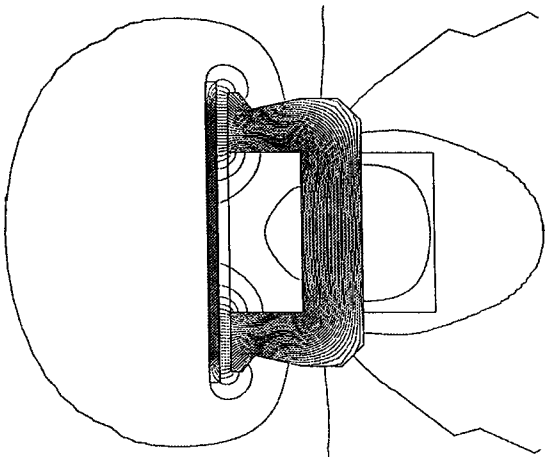

b. Guidance system.

Figure 49. TR06 flux patterns.

puters available in this effort. Consequently, only partial results have been obtained for this case.

Application of computational techniques to TR06/07

Data are available for both the TR06 and TR07 systems, which were developed by Transrapid International in Germany (Freidrich et al. 1985, Bohn and Steinmets 1985, Meins et al. 1988, Heinrich and Kretzschmar 1989). These data were used as test cases for the procedures used in the other analyses.

Magnetic forces, TR06. The TR06 two-car vehicle is levitated and propelled using 64 magnets, each 1.3 m long, and having five poles with the approximate dimensions shown in Figure 47. Motion of the vehicle is from the left to the right of the figure. The upper structure is the stator of the linear synchronous motor and is contained in the guideway. The lower structure or "rotor" is mounted on the vehicle and interacts with the stator to generate both levitation and propulsion forces. The windings in the stator, shown by the large Xs, are the three-phase excitation windings of the LSM. The Xs in the rotor are the excitation windings of the onboard magnets. The slots in the rotor contain additional windings that pick up power from the LSM for onboard use, as discussed in the previous section, and are not considered further. Each magnet comprises five poles, each pole having an excitation current of 6480 AT.

Associated with each levitation magnet is a guidance magnet of equal length and having the approximate dimensions shown in Figure 48. In this figure, the motion is into the page; the flat plate is the vertical reaction rail in the guideway.

The forces in these magnets were modeled using the two-dimensional PE2D computer code. Since the levitation and propulsion forces are interrelated, and depend on the phase currents in the stator winding, the calculations were done with 50% of the maximum phase current in phases A and C and 100% in phase B. The resulting flux patterns are shown in Figure 49, and the data used and the results of the calculations are given in Tables 29 and 30 and Figure 50. They are in reasonable agreement with reported values. The results suggest that the 36,000 AT current reported for TR06 is the maximum rather than the nominal operating excitation current for the system.

Magnetic forces, TR07. The levitation and guidance magnets were changed in TR07, reducing the weight and changing the dimensions. As shown in Figure 51, a notch was placed in the levitation magnets as part of this effort. Our calculated weight exceeds the reported weight by 22%, suggesting that additional, unknown weight reductions were implemented. The levitation magnets were increased in length to 3.022 m and the number of poles per magnet was increased to 10. The pole pitch of 0.258 m was retained to maintain compatibility with the LSM stator. The number of levitation magnets was changed to 30. The configuration of the guidance magnets was revised to incorporate the double windings shown in Figure 52 rather than the single windings of Figure 48. In addition, the length of these magnets was doubled from approximately 1.5 to 3.0 m. This change reduced the stray fields from the guidance magnets which, as discussed later, are the major source of external fields from the vehicle in this system. The excitation currents are not well known for either type of magnet; we assumed 4500 AT per pole for the levitation magnets and 8450 AT for the guidance magnets. The resulting flux patterns are shown in Figure 53, and the forces are shown in Tables 31 and 32. These forces for other currents and gaps are shown in Figures 54 and 55.

To good approximations, the lift force F_L and guidance force F_G of TR07 can be fitted by the following equations:

Table 29. TR06 levitation forces.

Specification	*PE2D*	*TR06*
Excitation magnet height	0.190 m	0.190 m
Number of magnets	64	64
Excitation / magnet	32,400 AT	36,000 AT
Air gap	0.010 m	0.010 m
Pole pitch	0.258 m	0.258 m
Stator pack		
width	0.185 m	0.185 m
height	0.0915 m	0.0915 m
Current	1200 A	1200 A
Lift force	1284 kN	1196 kN

Table 30. TR06 guidance forces.

Specification	*PE2D*	*TR06*
Excitation current	15 A	15 A
Turns	840	unknown
Air gap	0.010 m	0.010 m
Force / magnet	11 kN	9 kN

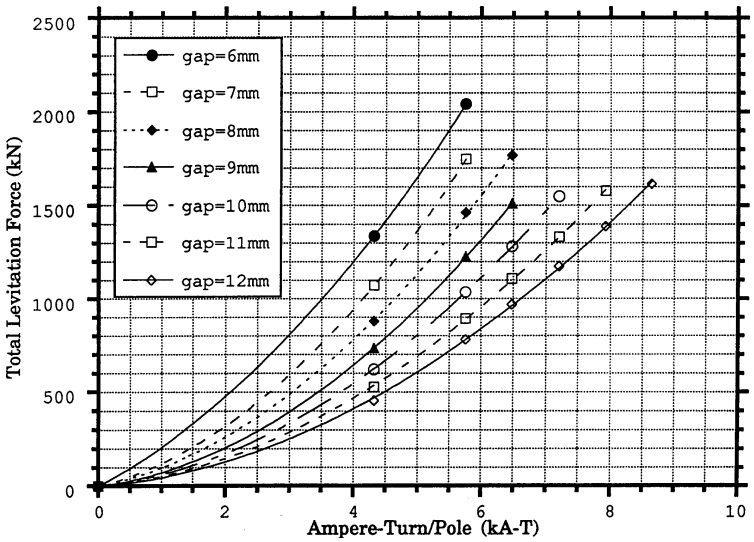

Figure 50. TR06 levitation forces.

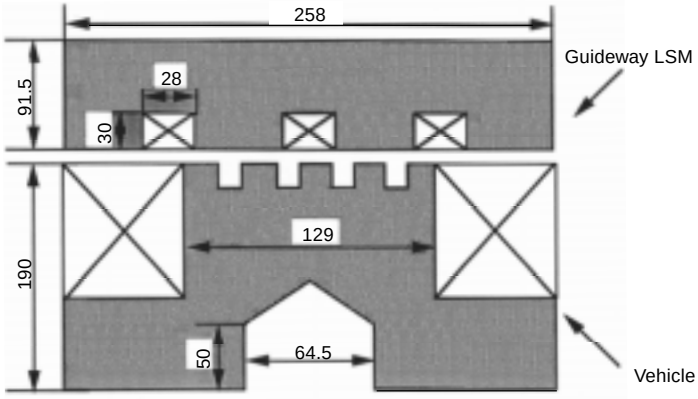

Figure 51. TR07 levitation and propulsion configuration (dimensions in mm).

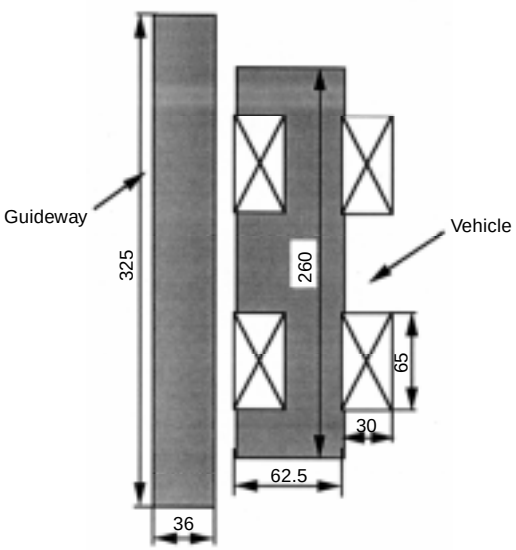

Figure 52. TR07 guidance configuration (dimensions in mm).

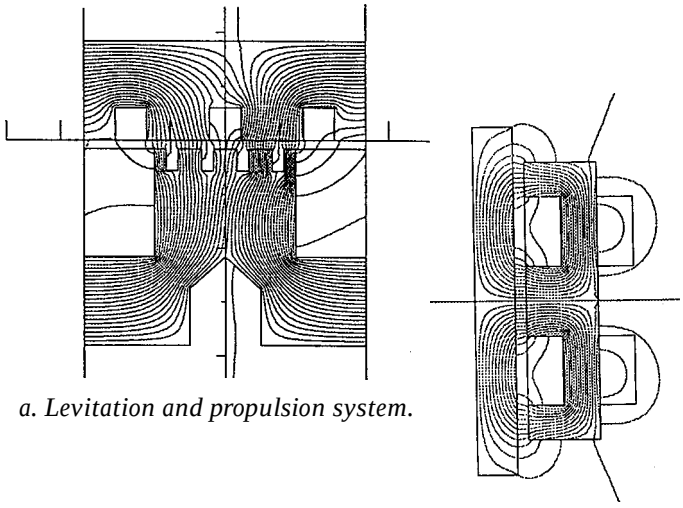

a. Levitation and propulsion system.

b. Guidance system.

Figure 53. TR07 flux patterns.

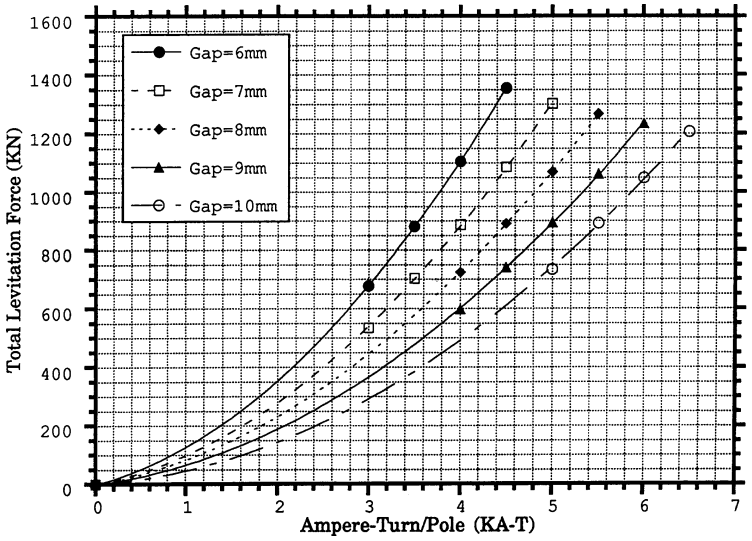

Figure 54. TR07 levitation forces.

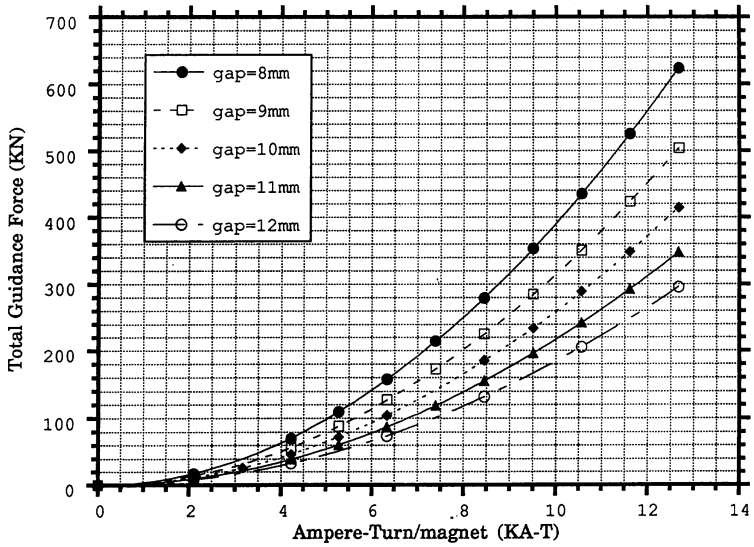

Figure 55. TR07 guidance forces.

Table 31. TR07 levitation force.

Specification	*PE2D*	*TR07*
Weight of magnets	14,500 kg	11,800 kg
Number of magnets	30	30
Excitation / magnet	45,000 AT	Unknown
Air gap	0.008 m	0.008 m
Stator current	1200 A	1200 A
Pole pitch	0.258 m	0.258 m
Stator pack		
width	0.180 m	0.180 m
height	0.0915 m	0.0915 m
Lift force	917 kN	882 kN

Table 32. TR07 guidance force.

Specification	*PE2D*	*TR07*
Number of magnets	30	30
Weight of magnets	11,600 kg	9,400 kg
Excitation current	8,450 AT	Unknown
Air gap	0.010 m	0.010 m
Force / magnet	12.39 kN	Unknown

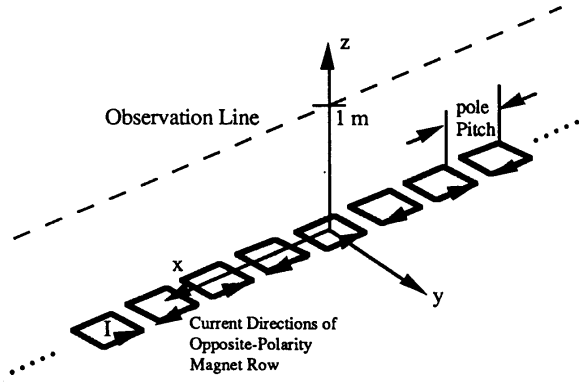

Figure 56. Row of magnets with alternating polarities. (Magnet length = 19.5 cm; magnet width = 24.4 cm; coil current = 45 kAT; pole pitch = 25.8 cm; 20 magnets.)

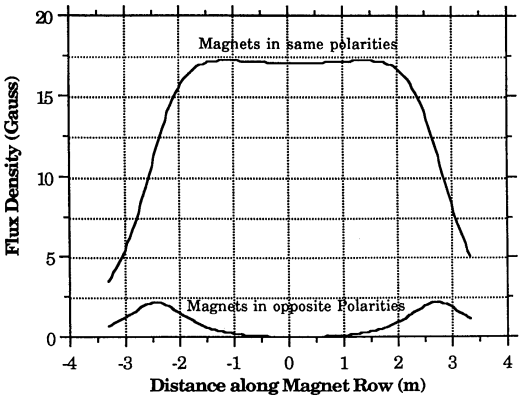

Figure 57. Comparison of magnetic fields from a row of magnets having the same and alternating polarities (magnetic field 1 m above magnet row).

$$F_L = 2337 \cdot (kAT)^{1.876} - 5500 \cdot (kAT)^4 / g^5$$

$$F_G = 180 \cdot (kAT)^2 / g^{1.843}$$

where *kAT* is the number of kilo-ampere-turns in the windings and *g* is the gap dimension in meters.

Since no guidance force is generated when the vehicle is in the equilibrium position, the guidance force indicated is that resulting from having the guidance magnets energized on one side and de-energized on the other.

Stray magnetic fields, TR06/07, from levitation–propulsion magnets. The levitation–propulsion magnets of TR06 / 07 are arranged along the sides of the vehicle and alternate in polarity as required to move the vehicle. The magnetic field at a distance from such an array of magnets is the difference of the fields from the individual magnets. The magnitude of the field depends on the distance from the magnets relative to their lengths, the field being lower if the magnets are short relative to the distance at which the measurement is made. This is illustrated in Figures 56 and 57, where the fields of 20 magnets are calculated at a distance of 1 m above them. From this illustration, the stray fields around the vehicle from this source are expected to be small.

The assumption is better than the figures indicate owing to the presence of iron in the system. Although this analysis would be best if done with a detailed, three-dimensional magnetic model including iron, it does not appear to be necessary in light of this approximate analysis and reported magnetic field measurements made on TR07 (Electric Research and Management, Inc., no date). At the ends of the array, the fields increase. It should be noted that the field from the stator moves with the same velocity as the vehicle and appears to the vehicle as a constant magnetic field. A detailed calculation of the fields in the cabin directly above the levitation magnets is shown in Figure 58.

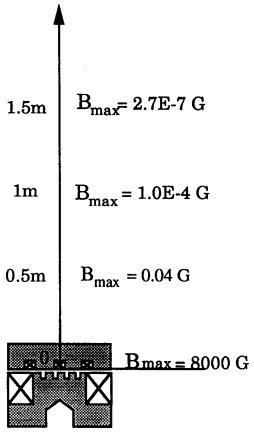

Figure 58. Magnetic fields above TR07 levitation–propulsion magnets.

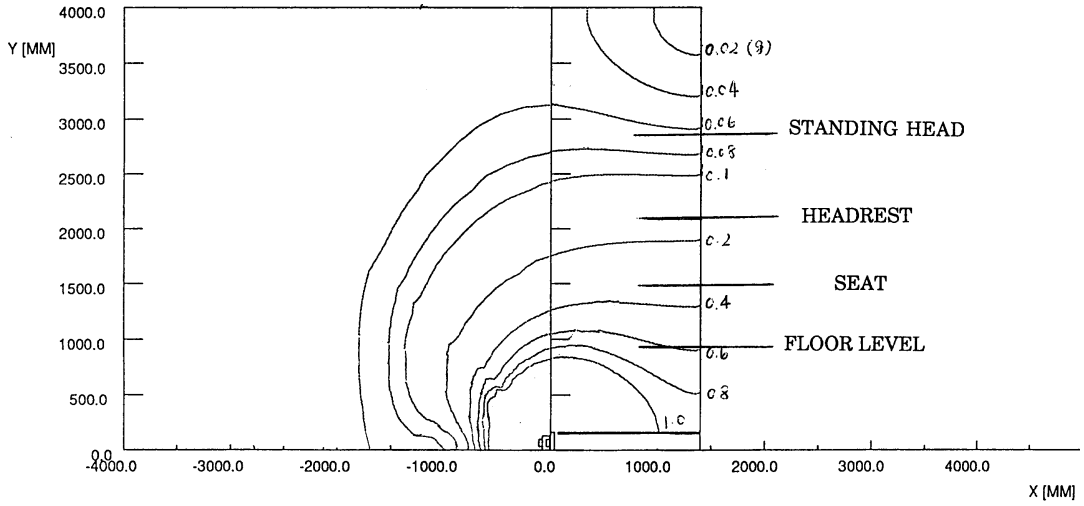

Figure 59. Flux density (G) around TR07 guidance magnet.

Stray magnetic fields, TR06/07, from the guidance magnets. The major source of stray fields in the TR07 system appears to be the guidance magnets. These magnets are 3 m long and therefore do not benefit as greatly, at close distances, from alternation of the poles. As noted above, the configuration of these magnets was changed in TR07, resulting in better confinement and cancellation of fields at large distances. The calculated magnetic fields (in Gauss) at various positions in and around the vehicle are shown in Figure 59. A steel guideway was included in this analysis; an iron-reinforced concrete guideway would alter these stray fields somewhat. The static field of the Earth is about 500 mG and must be added or subtracted from these values to obtain the total static field. The presence, if any, of ferromagnetic materials in the cabin will alter these values. The fields in Table 33 were calculated and are compared with the static fields in the passenger compartment as measured by Electric Research and Management, Inc. (no date).

These fields are shown as static, but will rarely be constant since the vehicle is in motion and the currents in the guidance magnets vary to correct the guidance forces. These variations reflect minor perturbations in the guideway, cornering of the vehicle, and wind gusts, and perhaps aerodynamic turbulence on the body of the vehicle, and cannot be calculated. The currents in the magnets can be expected to vary by perhaps ±10–20% in routine operation, leading to AC fields that are this percentage of the static fields. The frequencies of these AC fields will increase as the speed of the vehicle increases, as reflected in the AC measurements made at head level by Electric Research and Management, Inc. (no date) during the operation of TR07. Below about 200 km/hr (55 m/s), the major components of the field were below 100 Hz, while at 400 km/hr (111 m/s) they increased to more than 200 Hz. A prominent, and unexplained, spike of about 15 mG is seen in the 400-km/hr data at about 10 Hz.

In the data presented in Table 34, the values again peak at floor level, suggesting that most of the fields are generated by the magnets and wiring at or below floor level.

Wiring to the control system, as well as other electrical equipment in the vehicle, can contribute fields of the same magnitude in the cabin if they are not adequately shielded. These include wiring for hotel power, electronic converters, etc. A single straight wire carrying 1 A will generate a field of 2 mG at a radius of 1 m, decreasing

Table 33. Magnetic fields (mG) in the TR07.

		Measured		
	Calculated	*Minimum*	*Mean*	*Maximum*
Floor	700	150	820	1500
Seat	300	50	610	1100
Headrest	150	210	620	1020
Standing head	75	150	500	950

Table 34. ERM magnetic field data (mG) for all frequencies from 5–2560 Hz.

	Minimum	*Mean*	*Maximum*
Floor	30	100	255
Seat	20	50	140
Headrest	10	30	75
Standing head	≈ 7	20	55

inversely with the radius. Since the guidance magnets operate at a nominal 15 A, the cables to these magnets could contribute 30 mG DC at 1 m and 15 mG DC at 2 m if not shielded, and some fraction of these fields will appear as AC fields in the same manner as the fields generated by the guidance magnets. The same is true of currents to the levitation magnets (of unknown magnitude) and of the AC currents to onboard equipment. These cables have apparently been shielded, or used in pairs for cancellation, since fields of this magnitude do not appear in the data. If they have not been shielded, doing so is a minor matter.

Application to SCD concepts

As noted earlier, there are considerable differences in the designs presented by the four SCD contractors, and no single model suffices to analyze all of them. The methods of calculation used and the results are presented in this section.

The Bechtel concept uses no ferromagnetic materials but does have a ladder guideway that is not amenable to direct analysis by the dynamic circuit theory model, PE2D, or TOSCA. The dynamic circuit theory model was modified to include the LSM waveform as a continuous sine wave extending the length of the vehicle. This is analogous to the approach used in conventional motor theory. It is an approximation in that higher order harmonics, eddy currents in the coils, and the end effects resulting from the finite lengths of the magnets are not included. Nevertheless, the model approximates the results of the contractor and indicates the "reasonableness" of their computations. A separate computer program was written to analyze the null-flux guidance forces in this system.

The Foster-Miller concept uses no ferromagnetic materials or continuous conducting sheets and can be analyzed with reasonable confidence using the dynamic circuit theory model. This model was used to calculate the lift, propulsion, and guidance forces resulting from the interaction of the superconducting magnets aboard the vehicle with null-flux and propulsion coils in the guideway. Stray fields were calculated using the discrete current-carrying element model.

The Grumman concept uses ferromagnetic materials for suspension, guidance, and propulsion and was analyzed as described above for the TR06/07 system. Unlike the Transrapid systems, however, the gap in the ferromagnetic circuit is 40 mm rather than 8–10 mm, resulting in more flux leakage in the gap and requiring three-dimensional analyses using the TOSCA program.

The Magneplane concept uses continuous sheet guideways that cannot be analyzed with significant accuracy by simple means, requiring that the previously mentioned ELEKTRA computer code be used. Also, as mentioned earlier, the number of mesh elements that could be used was restricted and limited results were obtained. The contractor did not present the methods by which their forces were calculated. Stray fields have been calculated for the vehicle at rest, which represents the worst case.

Bechtel

Unique features. The Bechtel concept (see Fig. 3) is unique in that it uses a ladder type of guideway and an array of onboard magnets with alternating polarities to effectively achieve a "null-flux" configuration. When the onboard magnets are symmetrically located with respect to the centerline of the ladder track, no net flux is experienced by the ladder track, and no currents or forces result. The equilibrium operating position of the magnets is a few centimeters below this centerline.

The 96 magnets aboard the vehicle in this system are contained in six modules on each side of the vehicle, the 1-m-long and 0.3-m-wide magnets being positioned with their planes in the vertical direction. The modules are spaced 1 m apart along the length of the vehicle, each module containing eight magnets arranged so that each magnet is adjacent to other magnets with different polarities. The modules are 4 m long and 0.6 m wide.

Adaptations of model for analysis. The dynamic circuit model was used in combination with a harmonic analysis to evaluate the lift and drag forces of the Bechtel design. A steady-state circuit approach was used in the model and provides closed-form analytical solutions that are well suited for the analysis of coil type EDS systems. Guidance in this system is derived from interactions of the onboard magnets with the null-flux guidance coils, with the levitation ladder, and with the propulsion motor. The interaction with the null-flux coils provides the dominant guidance force. The octapole magnets on the vehicle interact with figure-eight-shaped null-flux coils in the guideway that are connected in series with corresponding coils on opposite sides of the guideway.

Modeling results for levitation and guidance. The results of the model lift force calculations are shown in Figure 60a, in which the forces are nor-

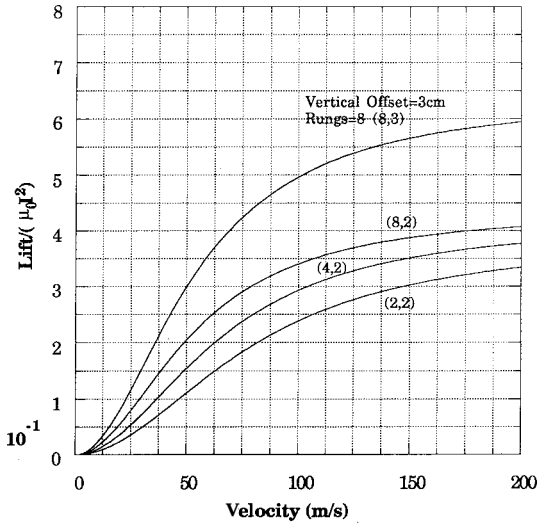

a. Model lift force calculations.

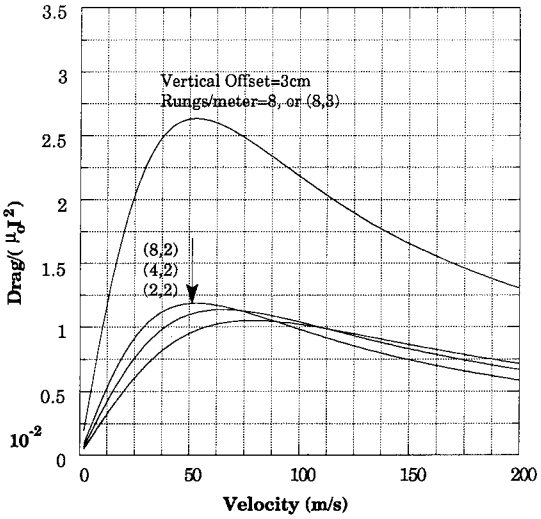

a. Model lift force calculations

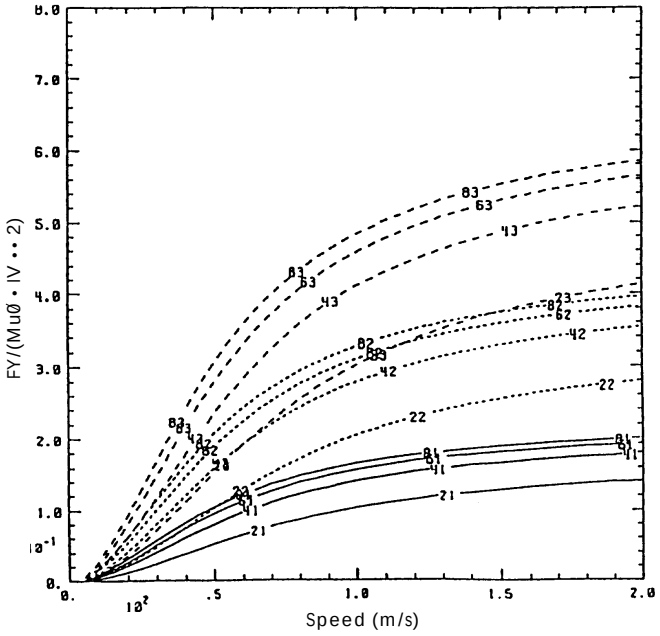

b. Bechtel's results.

Figure 60. Normalized lift vs. speed for Bechtel concept, with rung number and vertical offset as parameters. The notation 8,3 etc., refers first to the number of rungs per meter in the ladder guideway and second to the displacement in centimeters of the vehicle-mounted magnets below the centerline of the ladder.

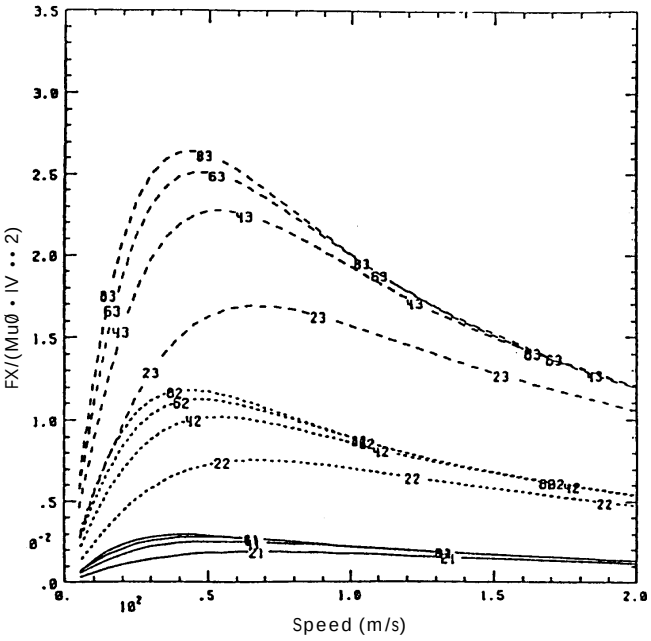

b. Bechtel's results.

Figure 61. Normalized drag vs. speed for Bechtel concept, with rung number and vertical offset as parameters.

malized in the same manner as those presented by Bechtel in Figure 60b as part of their parametric studies. These calculations are for an array of four coils for comparison with the corresponding calculations by Bechtel. The upper and lower horizontal rails of the ladder used in these calculations are 0.030 m high and 0.020 m thick, while the rungs, or vertical members of the ladder, are 0.01 m wide and 0.020 m thick. Bechtel does not give details of their calculation or the model used. In our calculations, the skin effect is ignored, which is appropriate if the lamination technique proposed by Bechtel is successful. Furthermore, our calculations consider only the first harmonic

of the waveform. Consequently, we adjusted the effective resistivity in our model to obtain the agreement shown. The resistivity remains within a factor of two of its expected value, and the adjustment is in the direction that makes the Bechtel calculation more conservative than ours. Figure 61 shows the resulting drag forces.

The lift and drag forces, lift-to-drag ratio, and the ladder-interaction guidance force resulting from one of the six bogies composed of two magnet modules, one on each side of the vehicle (16 magnets per bogie), are shown in Figure 62 as functions of the vertical offset of the magnets from the centerline of the ladder track. The same parameters are plotted in Figure 63 as functions of the vehicle speed.

At 134 m/s, the vertical offset will be about 0.030 m to support the 61,000-kg vehicle. The offset will be greater at lower speeds. The model calculates a lift-to-drag ratio of 140 at 134 m/s.

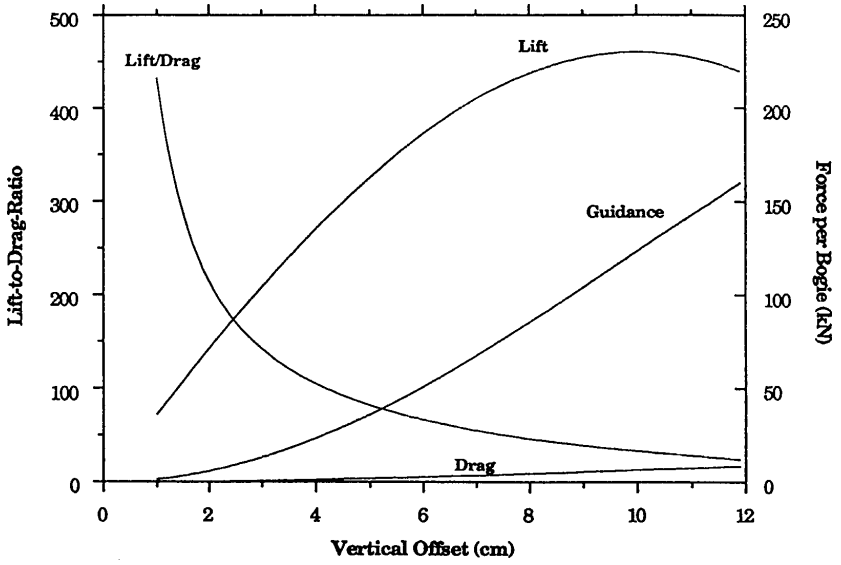

Figure 62. Magnetic force vs. vertical displacement for Bechtel concept (8 rungs/m; 0.20-m gap; 400-kAT magnetic current; 16 magnets/bogie).

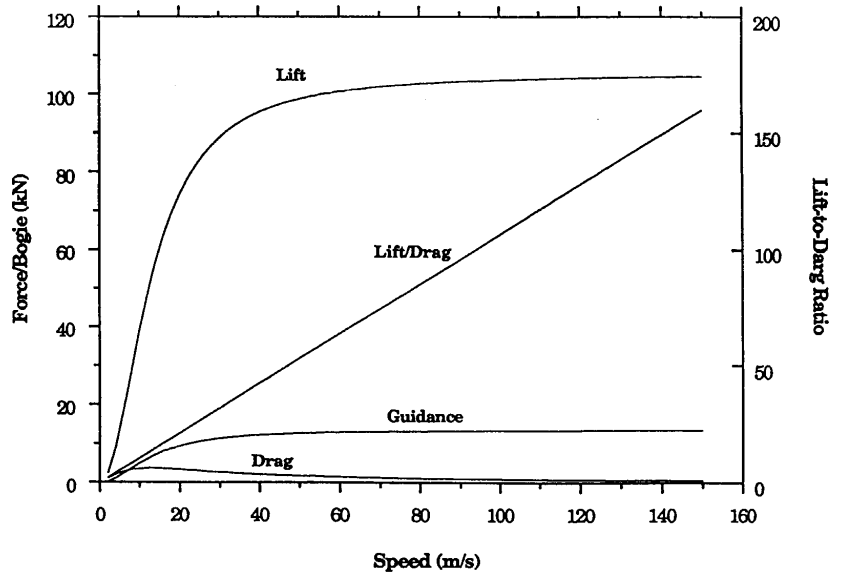

Figure 63. Magnetic forces vs. speed for Bechtel concept (8 rungs/m; 0.20-m gap; 400-kAT magnetic current; 16 magnets/bogie).

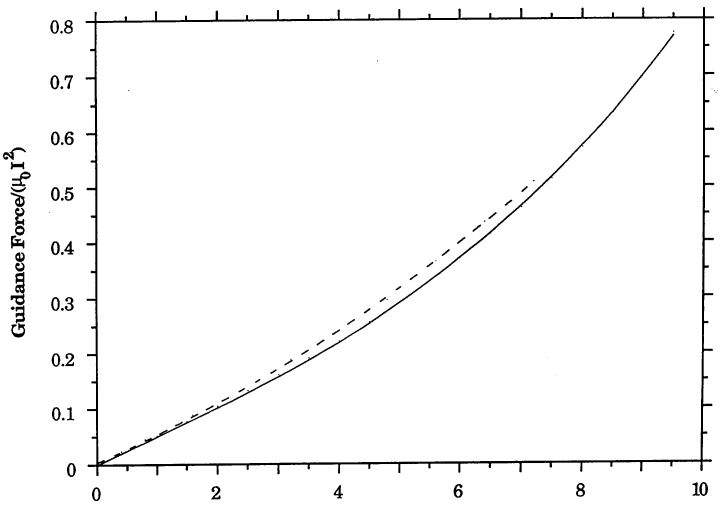

Figure 64. Guidance force vs. lateral displacement for Bechtel concept. Normalized guidance force is acting on eight SCMs, with four on the left and four on the right (solid line shows Argonne results; dashed line shows Bechtel results).

Bechtel calculated power losses in the coils to be 630 kW at this speed, leading to a lift-to-drag ratio of 130 in the absence of eddy current losses or 110 including such losses.

The primary guidance force from the null-flux coil interaction is shown in Figure 64 as a function of the lateral displacement (based on the dimensions given on page B-35 of the Bechtel [1992a] report) and compared with the forces reported by Bechtel (1992a) in their Figure D1-6c. The forces shown for their calculation are the result of summing the separate forces on the two sides of the bogie. The cross-sectional area and conductivity of the conductor were not reported and have been adjusted within physically permissible limits to achieve the agreement shown. A value of 0.1 on the scale shown corresponds to 20 kN for an eight-magnet bogie, resulting in 240 kN of restoring force for the entire vehicle when it slips to the side by 0.02 m.

Modeling results for stray fields. Stray fields for the Bechtel system were computed using the computer code, mentioned earlier, that sums the magnetic fields from each of the finite length current elements of the array of magnets. For simplicity, we considered the magnets to be arranged in a continuous line along each side of the vehicle, whereas each 4-m-long magnet module is actually separated from the next by a distance of 1 m. The effect of considering the magnet modules as continuous rather than spaced apart is to ignore the ballooning of the magnetic field between adjacent modules. This effect will be less than the "end effect" shown in Figure 57 since in that figure the magnet array was not continued beyond the end, while in this case the "end" is followed by another magnet array. The actual "end effect" around the vehicle is shown in Figure 65a, where the fields are calculated along the centerline of the vehicle. The fields in the transverse plane of the vehicle

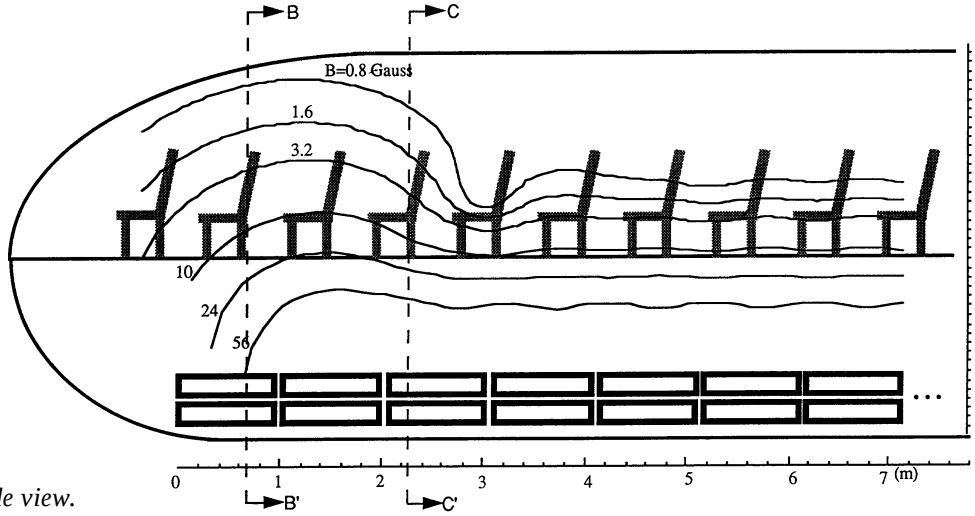

a. Side view.

Figure 65. Stray fields along centerline of Bechtel vehicle.

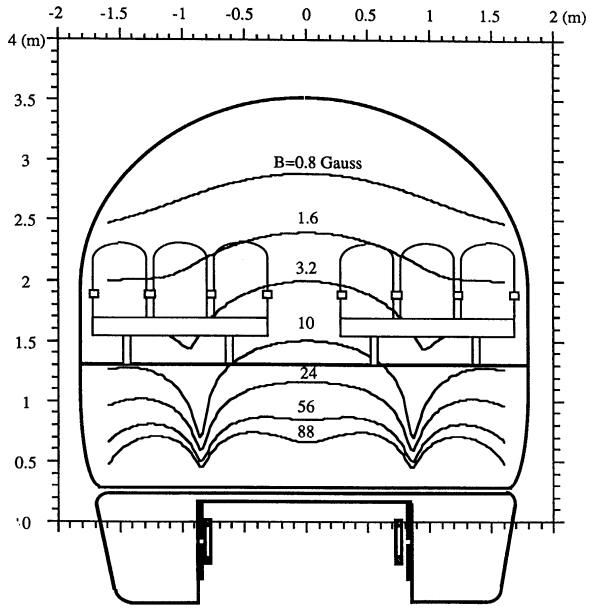

b. Cross-sectional view along B–B′ plane. SCM current is 400 kA/coil.

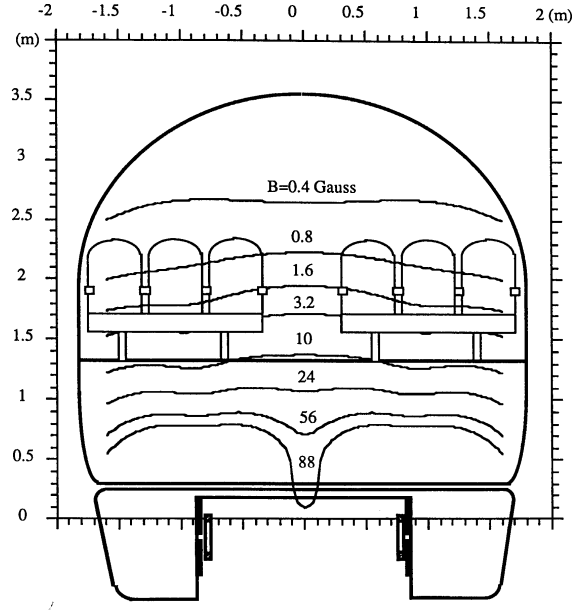

c. Cross-sectional view along C–C′ plane. SCM current is 400 kA/coil.

Figure 65 (cont'd).

at cuts B–B′ and C–C′ are shown in Figures 65b and c. In making these calculations, we assumed the currents to be the same as those used in calculating the magnetic forces. Corresponding calculations from Bechtel are shown in Figure 66. The contours depend on the exact location in the vehicle at which the calculation is made, and on the polarities of the magnets on opposite sides of the vehicle. The exact arrangement calculated by Bechtel is not known but the magnitudes of the two calculations are in good agreement.

Foster-Miller

Unique features. The Foster-Miller concept (see Fig. 4) uses racetrack-shaped superconducting magnets on the vehicle that interact with sidewall-mounted coils for levitation, guidance, and propulsion. Levitation, and a portion of the guidance force, is achieved using figure-eight-shaped null-flux levitation coils that are vertically positioned. The vehicle is propelled and guided by a single set of coils that are cross-connected across the guideway and powered in parallel from the wayside. The propulsion system uses a unique locally commutated linear synchronous motor, as discussed in section 3.2.2. The baseline 150-passenger, 73-tonne, 2-car train is levitated and propelled on three bogies. Each bogie contains eight "racetrack" shaped superconducting magnets and must generate a vertical force of 238 kN to levitate 24.3 tonnes. Each magnet has a mean winding width of 0.5 m, a mean length of 1.0 m, and 1800 kAT of current. The magnets interact with null-flux coils in the guideway that are 0.74 m long, 0.90 m high, and 0.04×0.04 m in cross section.

Model used for analysis. We used the dynamic circuit theory model, originally developed to analyze null-flux type systems, to directly analyze this system.

Modeling results for levitation and guidance. The magnets aboard the vehicle and the null-flux coils in the guideway must be displaced from their symmetrical positions to generate levitation or guidance forces. The computed levitation forces generated at 134 m/s (300 mph) are shown in Figure 67a as functions of the vertical displacement (offset) and in Figure 67b as functions of the velocity with a 0.035-m offset. This offset achieves the required lift force of 240 kN/bogie at 134 m/s and results in a lift-to-drag ratio of about 180. At 134 m/s, the maximum lift capability of the bogie is about 640 kN, and it occurs at an offset of 0.14 m. The lift-to-drag ratio is significantly lower at this large offset. Foster-Miller's computation of lift vs. deflection (Fig. 68) gives a maximum supportable load of 2.6 times the vehicle weight (essentially the same result as ours). It should be noted that the displacements at takeoff (50 m/s) and landing (20 m/s) will be greater than the 0.035 m discussed here, and the

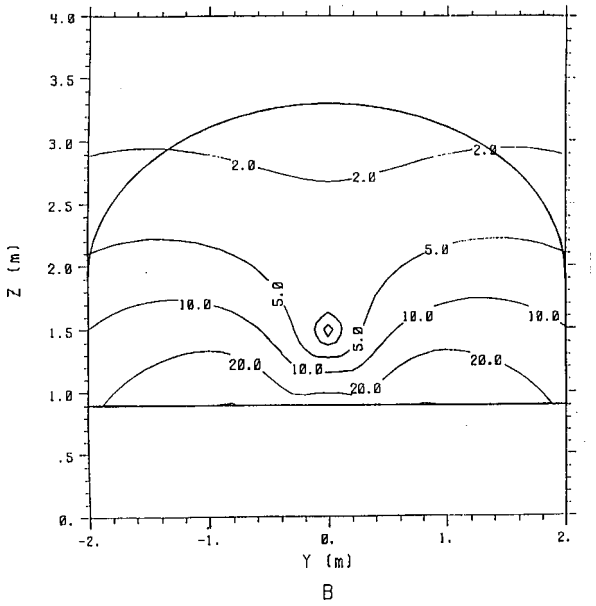

a. Contours of constant magnetic field magnitude (G) along centerline plane.

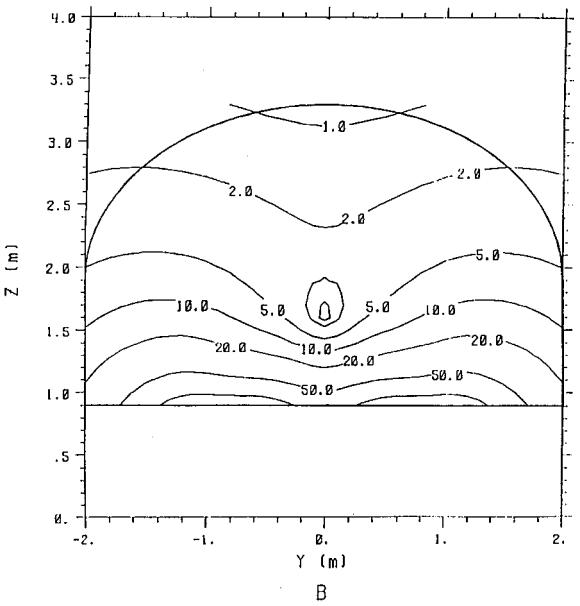

b. Contours of constant magnetic field magnitude (G) along a plane through the center of the mid-vehicle magnets.

Figure 66. Cross-sectional view of stray fields of Bechtel vehicle (as calculated by the contractor).

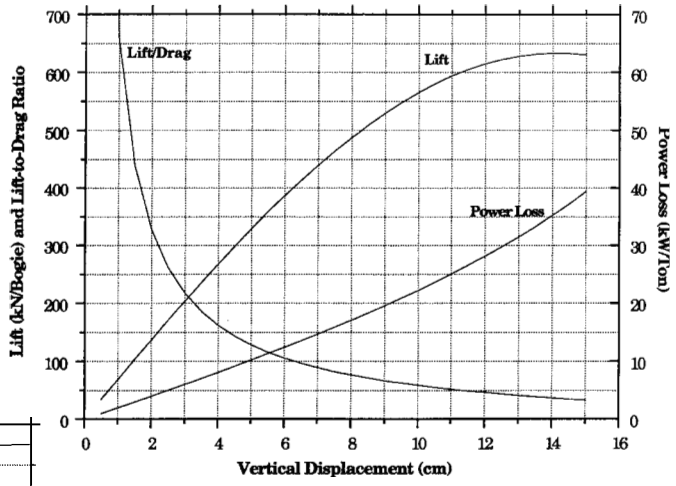

a. Versus vertical offset.

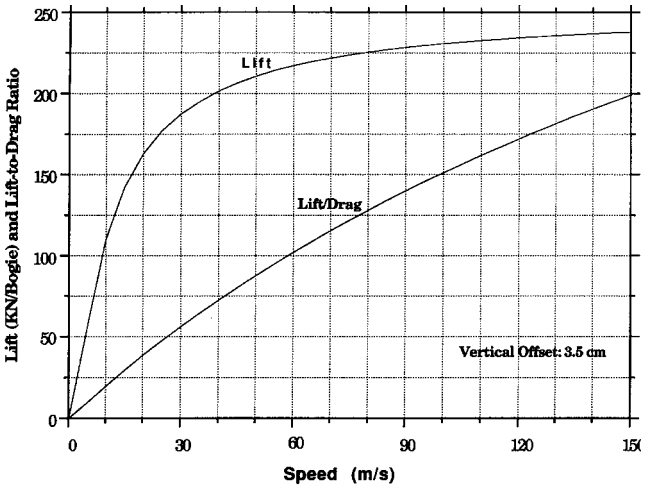

b. Versus speed.

Figure 67. Magnetic suspension force for Foster-Miller concept (27.5-cm gap; 134-m/s speed; 1800-kAT SCM current; 16-cm^2 conductor cross-sectional area; eight SCMs/bogie).

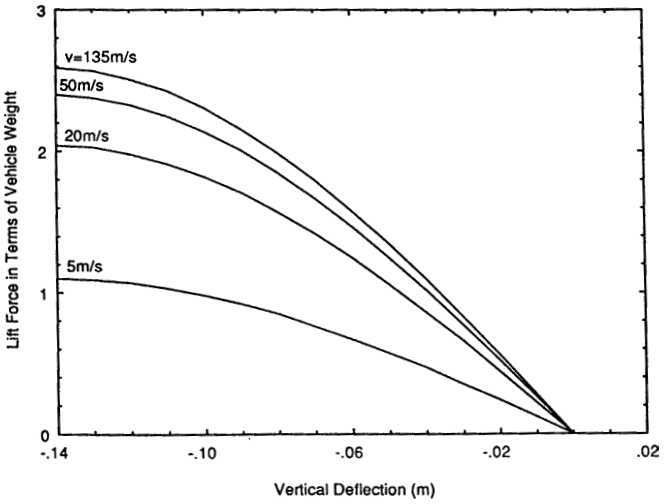

Figure 68. Lift force vs. vertical deflection (Foster-Miller).

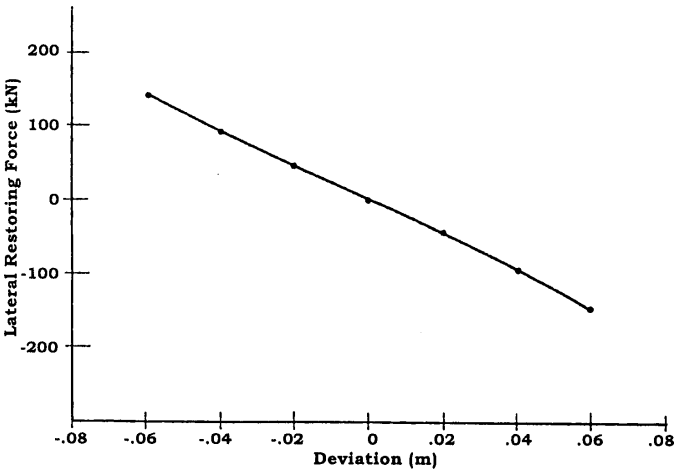

a. Foster-Miller's calculations.

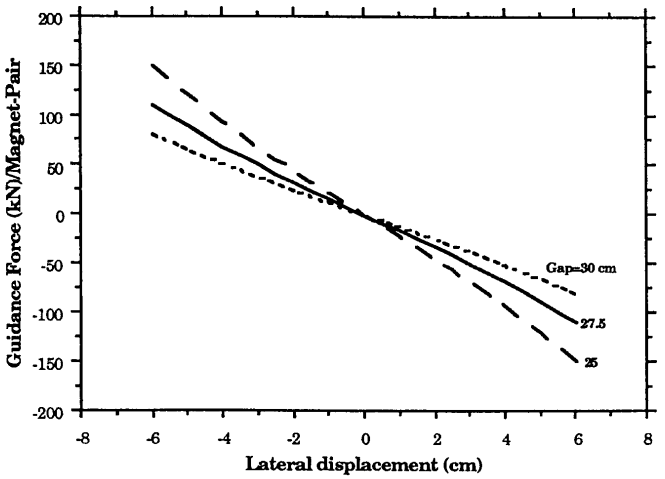

b. Our calculations for various air gaps.

Figure 69. Guidance force vs. lateral deflection.

marginal lift will be reduced. Normal takeoff and landing will presumably occur in tangent sections of the track and should not require the full safety margins provided for high-speed operation.

Since the coils in this system can be wound with multiple turns, the conductors can be thinner than the skin depth. Thus, increases in resistivity induced by skin effects are not a concern. The calculations assume copper conductors in the guideway with the cross-sectional area indicated.

The primary guidance forces in this system result from interaction of the vehicle magnets with the cross-connected propulsion coils. Foster-Miller's calculated guidance forces for one pair of magnets as functions of lateral displacements of the vehicle are shown in Figure 69a. Our calculation of the corresponding force is shown in Figure 69b and is lower by about 15%. The total restoring force for a 0.030-m lateral displacement is calculated to be about 400 kN. Smaller, additional guidance forces result from the propulsion current in the coils and from interactions with the null-flux coils that provide levitation.

Modeling results for stray fields. Magnets on opposite sides of the vehicle have been arranged to have the same polarity in this design, resulting in lower magnetic fields at the center of the cabin than would occur if the magnets had opposite polarities. Foster-Miller's calculation of the field at floor level is shown in Figure 70a and confirmed by our calculation shown in Figure 70b. Although this polarization scheme reduces the field in the center of the cabin, the field at the side of the cabin is little affected by the polarization, as can be seen by comparing Figure 70b and Figure 71.

The fields in a vertical plane near the windows and extending along the length of the vehicle were calculated for the latter case and are shown in Figure 72. In this figure, the passengers closest to the magnets would be located at the 10.5-m position. The fields in the cross section centered over the bogie array (the 6-m point of Fig. 72) are shown in Figure 73. (The view is from the front of the vehicle; no seats are located in this plane.) Referring to Figure 72, we can see that the field at this symmetrical position between the magnets is actually lower than in other planes along the axis of the vehicle. A five-sided ferromagnetic

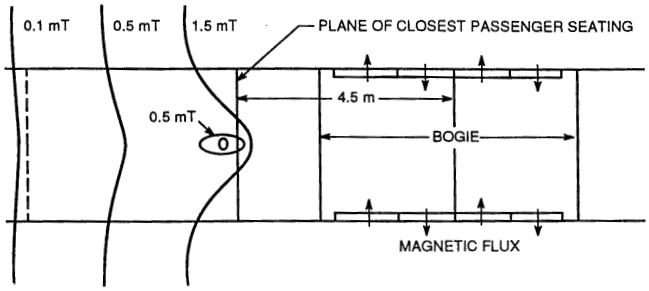

a. Foster-Miller's calculations.

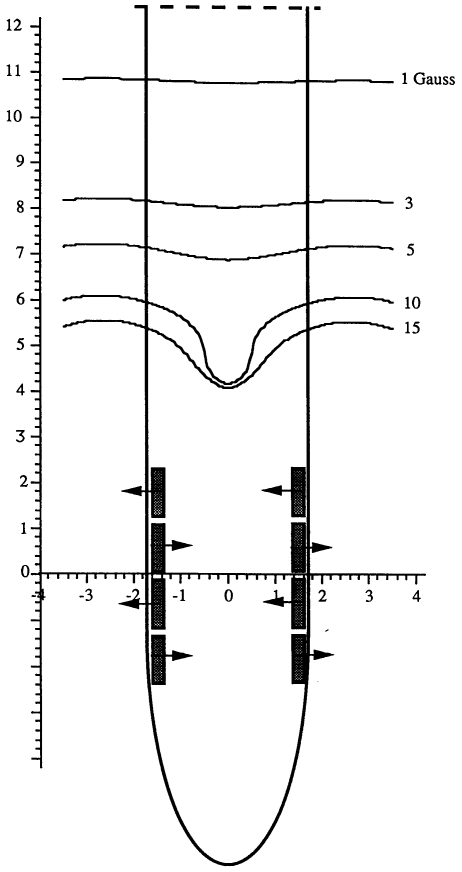

b. Our calculations (floor level, no bucking coils).

Figure 70. Top view of stray fields for Foster-Miller aiding-flux arrangement.

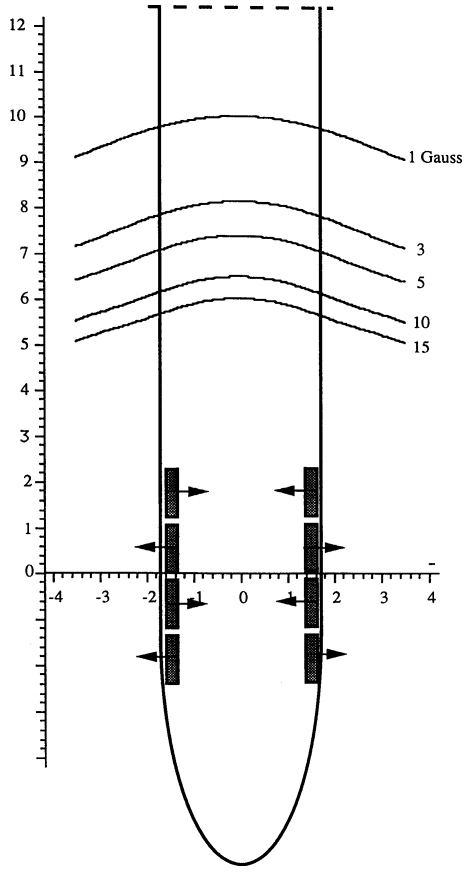

Figure 71. Top view of stray fields for Foster-Miller canceling-flux arrangement (floor level, no bucking coils).

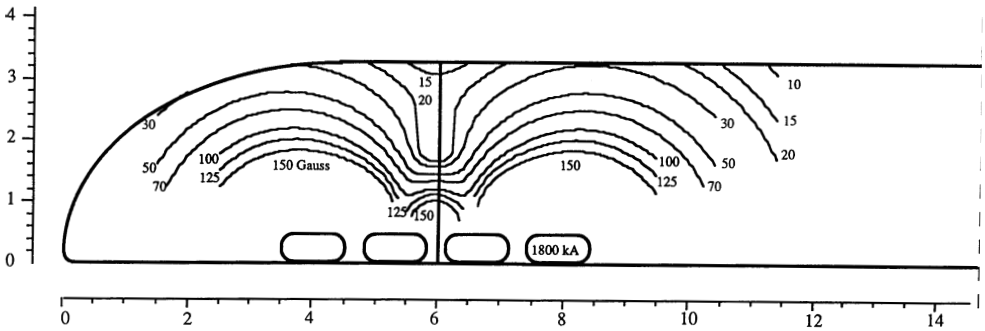

Figure 72. Side view of stray fields for Foster-Miller vehicle near a window.

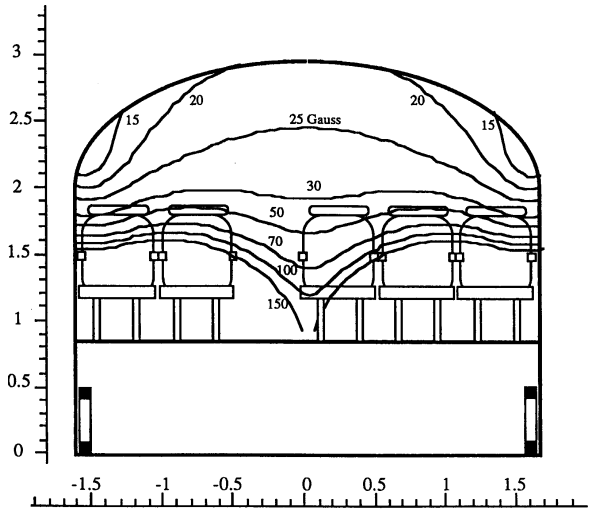

Figure 73. Cross-sectional view of stray fields for Foster-Miller's vehicle at center of magnet array (6-m point of Fig. 72).

shield around the passenger compartment is proposed to lower the fields in this compartment further. Although the fields of Figures 72 and 73 have not been extended outside the vehicle, the external fields near the magnets will clearly be rather intense and will not be significantly reduced by the use of the ferromagnetic shield.

Grumman

Unique features. The Grumman conceptual design (see Fig. 5) is an EMS system using constant-current superconducting magnets to generate the magnetomotive force for the iron poles of the onboard magnets. The magnetic field is dynamically controlled by separate trim coils near the pole faces of the magnet. In addition, the gap between the iron poles and the LSM stator is increased from the 8–10 mm used in TR07 to 40 mm. Unlike the TR07 system, which uses separate magnets for suspension and guidance, this system uses one set of magnets acting against a single reaction plate (the stator of the LSM) that is mounted at a 35° angle from horizontal in the guideway. This concept, unlike TR07, requires that a restoring force be generated when the magnets are displaced sideways on the rail. The baseline vehicle carries 100 passengers and weighs 61.4 tonnes.

Model used for analysis. We used the three-dimensional finite-element code TOSCA to analyze this system because of our concerns about the effects of fringing of the field in the long gap of this system.

Modeling results. The baseline magnetic structure is shown in Figure 74. The pole faces are square with sides of 0.200 m and react against a square cross-section rail also having sides of 0.200 m. Inside the superconducting magnet, the iron core is 0.280 m in diameter (Fig. 74a). The corresponding motor pole pitch is 0.75 m. The superconducting magnet has an inside diameter of 0.330 m and an outside diameter of 0.380 m

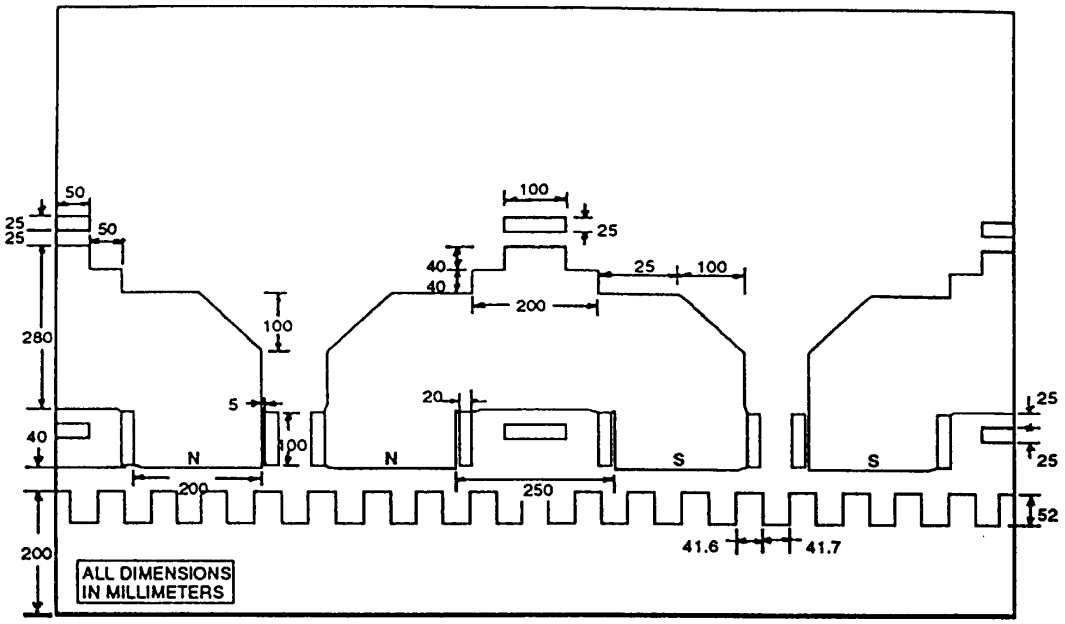

a. Pole and rail geometry.

Figure 74. Baseline magnetic structure of the Grumman concept.

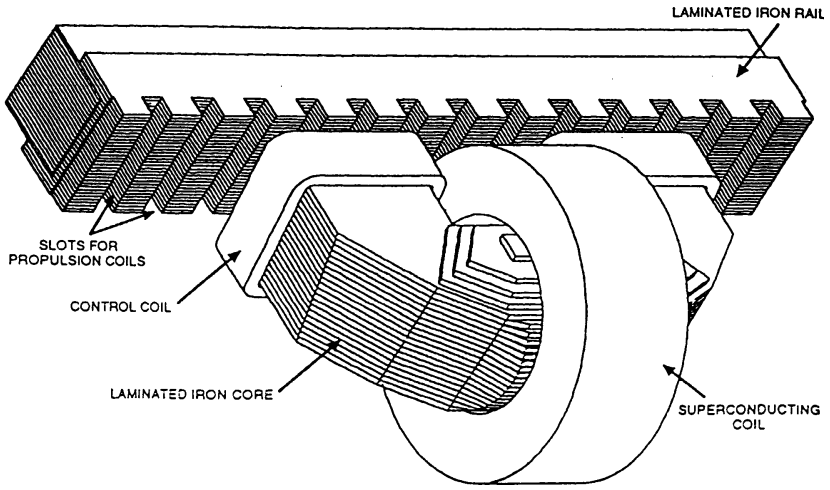

b. Electromagnetic suspension system.

Figure 74 (cont'd). Baseline magnetic structure of the Grumman concept.

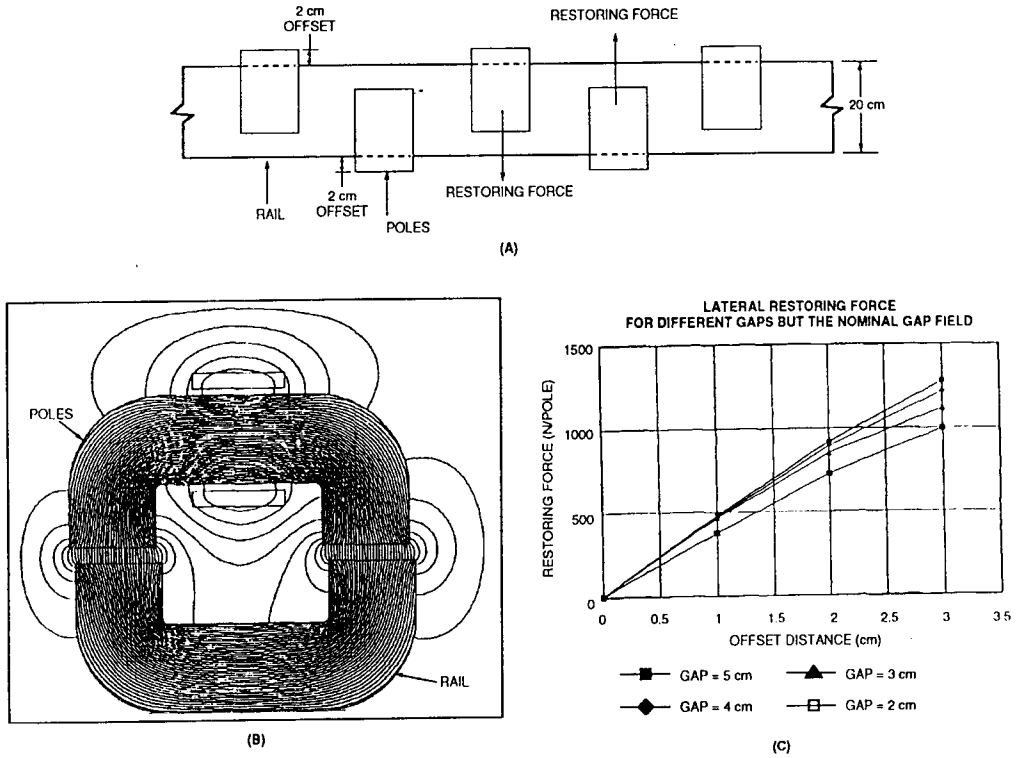

Figure 75. Pole arrangement and resulting lateral forces (Grumman).

(Fig. 74a). These dimensions are inconsistent with the "coil diameter" of 0.288 m given in the final report and the dimensions of the iron pole. This inconsistency has more effect on the mechanical structure than the magnetics. It is possible that the legs of the "C" magnet might have to be lengthened to accommodate the cryostat, which has an extremely limited capacity of helium above the magnet. Grumman has chosen to use 48 magnets of this type, 24 on each side of the vehicle. The arrangement of the magnets on the rail provides stability as the magnet moves to the side of the rail (Fig. 75). Each pole extends to the side of the rail by 0.020 m. A typical matrix of points on which the fields were calculated is shown in Figure 76.

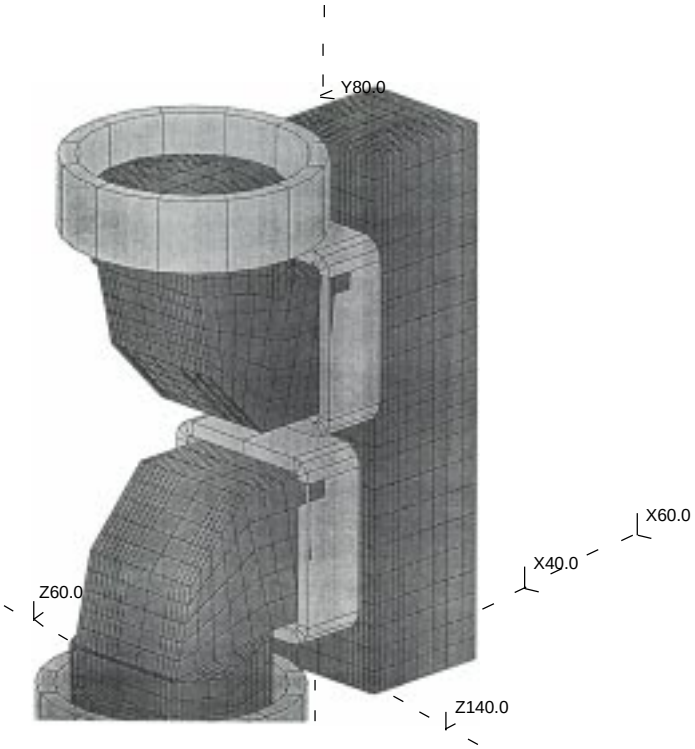

Figure 76. Typical matrix array for finite-element analysis of Grumman suspension.

The baseline configurations used in the calculations are given in Table 35.

Model results for levitation and guidance. The Grumman vehicle magnets interact with a single reaction rail (i.e., stator pack) on each side of the vehicle to generate levitation, guidance, and propulsion forces. This approach inherently couples levitation and guidance forces. We calculated the magnetic forces in the directions perpendicular to and parallel to the reaction-rail face for comparison with Grumman's computed results. These are the fundamental suspension forces. The actual vertical and horizontal guidance forces are combinations of these values, and their control is the major issue addressed in section 3.2.4.

Table 35. Baseline configuration used in Grumman's analysis and our TOSCA analysis.

Parameter	*Units*	*Grumman*	*Tosca*
Pole pitch	m	0.75	0.75
Number of poles	—	48	48
Pole–rail gap	m	0.040	0.040
Iron-core diameter	m	0.28	0.28
Pole dimensions	m	0.20×0.20	0.20×0.20
Pole material	—	Vanadium-Permendur	M43
Rail width	m	0.20	0.20
Rail thickness	m	0.20	0.20
Rail material	—	M43	M43
Current per pole	kA	50	50

The calculated forces normal to the faces of the poles (referred to as both the normal force and the total lift force) are shown in Figure 77 as functions of the current in the trim coils with the baseline current of 50 kAT in the superconducting magnet. The trim coil current in the Grumman figure (Fig. 77b) is shown as that in a single trim coil, while ours is the sum of the currents in both trim coils, accounting for the factor of two difference in these currents. A more detailed comparison of the agreement between the two computations is shown in Figure 78. The vertical lift force on the vehicle is the sum of these normal forces on each magnet, multiplied by cos35°. At the nominal operating point shown, the vertical force is about 940 kN, while the vehicle weighs about 630 kN, so a provision of 50% in lift has been made for cornering, wind, and safety factors.

The suspension controller can feed different control currents to magnets on opposite sides of the vehicle. This generates a lateral guidance force equal to the difference between forces on opposing sides, multiplied by sin35°. This requires no verification because the forces derive from the total lift force verified above (see Fig. 78).

The suspension also generates restoring forces for motion parallel to the face of each rail. The configuration of the magnets that provides this stabilization force was shown in Figure 75. In this configuration, alternate magnets are located 0.020 m beyond their respective sides of the rail. There is no net restoring force in this position. As the magnets are displaced, one moves onto and the other off of the rail, resulting in a force that tends to restore the magnets to their equilibrium positions. Grumman calculated the restoring force shown in Figure 75 for the case where the magnetic field in the gap is constant. The capability of specifying a constant gap field is not contained in TOSCA, so we varied the current to approximate this condition, and then scaled the forces to the appropriate fields using a field-strength squared (B^2) scaling to obtain the results shown in Figure 79. This approach approximates a condition in which the normal force is constant.

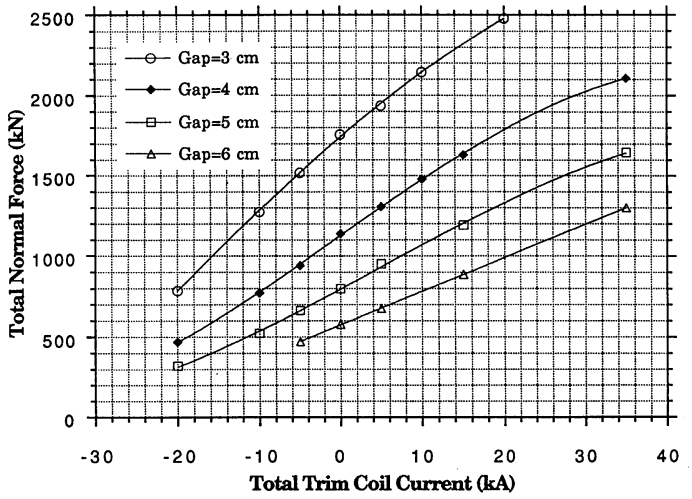

a. Our calculations with total current in the trim coils as variable, assuming a constant 50-kAT current in the superconducting magnets.

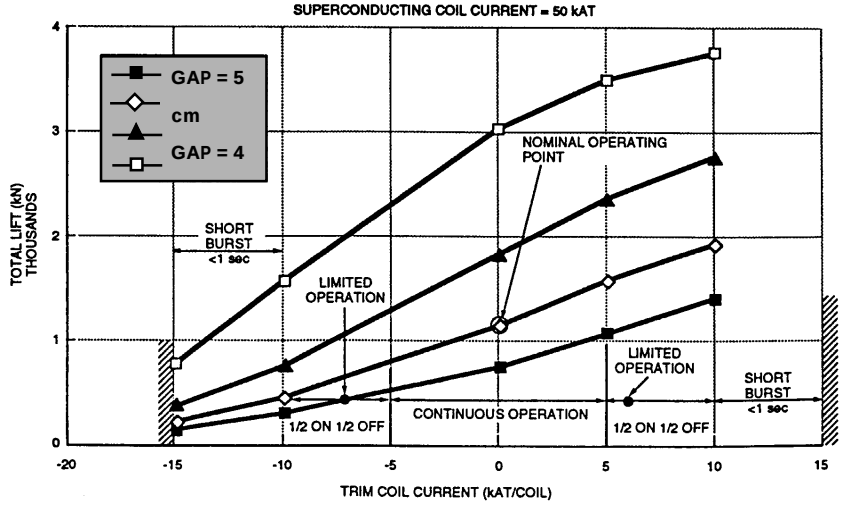

b. Grumman's calculations with current in a single trim coil as variable, assuming a constant 50-kAT current in the superconducting magnets.

Figure 77. Total normal force vs. trim current for Grumman suspension.

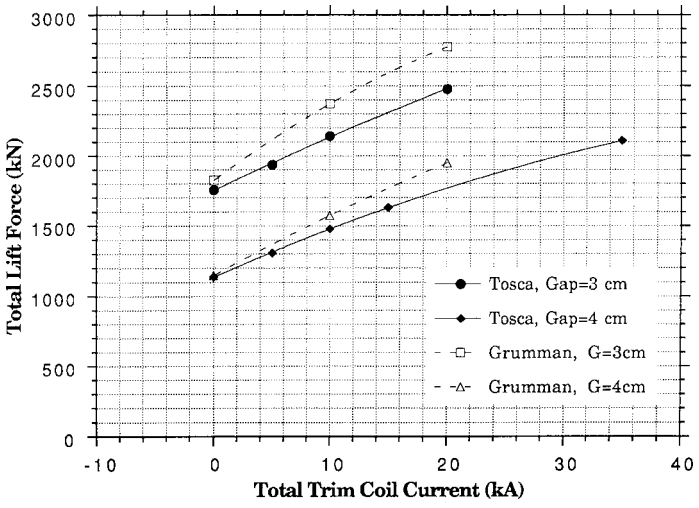

Figure 78. Comparison between ANL and Grumman computations of lift forces (with trim coil as variable; Isc *= 50 kA).*

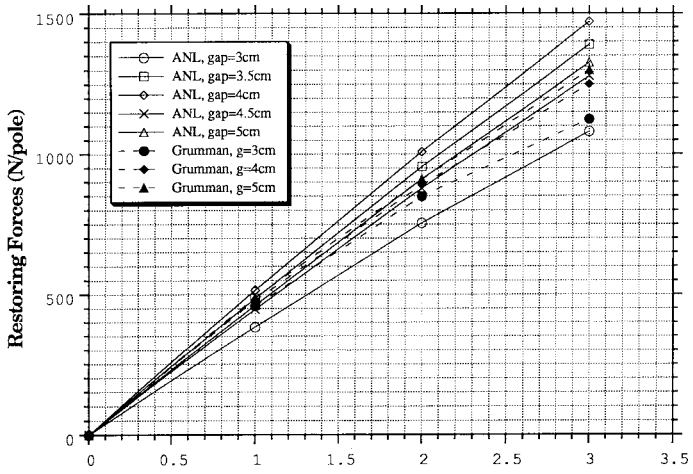

Figure 79. Comparison between ANL and Grumman computations of restoring forces for one magnet moved parallel to rail face (gap field = 0.75 T*).*

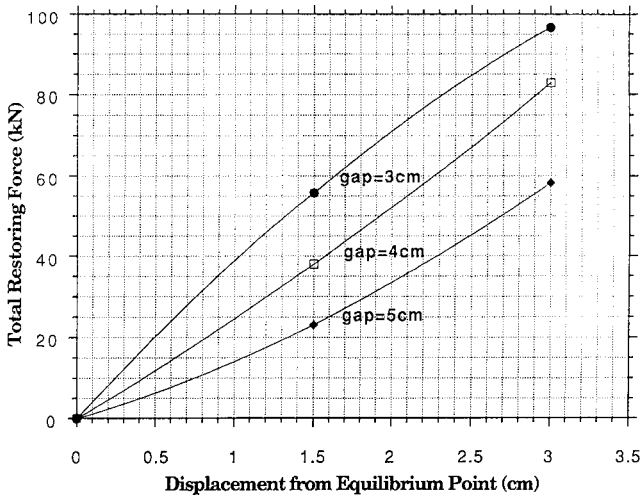

*Figure 80. Grumman restoring force for constant current for one magnet moved parallel to rail face (*I *= 50 kA).*

The restoring force is stabilizing with all the gap spacings evaluated, with our results indicating a somewhat greater variation with the gap dimension than do the Grumman data.

If the current rather than the field is maintained constant, the results of Figure 80 are obtained, telling us that the restoring force increases as the gap decreases.

Modeling results for stray fields. The magnetic fields in both the TR06 / TR07 and the Grumman system are better confined than in any of the EDS systems using superconducting magnets. The field in the cabin is more uniformly distributed along the length of the vehicle since the magnets are in a row beneath it. The magnetic fields around the magnets are shown in Figure 81. The fields external to the vehicle will be of the same magnitude.

Magneplane

Unique features. The Magneplane system (see Fig. 6) is the only continuous sheet levitation system proposed by the SCD contractors. In this setup, eight magnets aboard the vehicle induce currents in aluminum sheets in the guideway as the vehicle passes over. These currents in turn interact with the magnets to produce repulsive forces between the vehicle and the guideway. The guideway, shaped as a trough, permits the vehicle to roll in a turn, avoiding the use of a separate tilt mechanism. Continuous-sheet guideways, unlike those using discrete coils, provide a smoother interaction with the supercon-

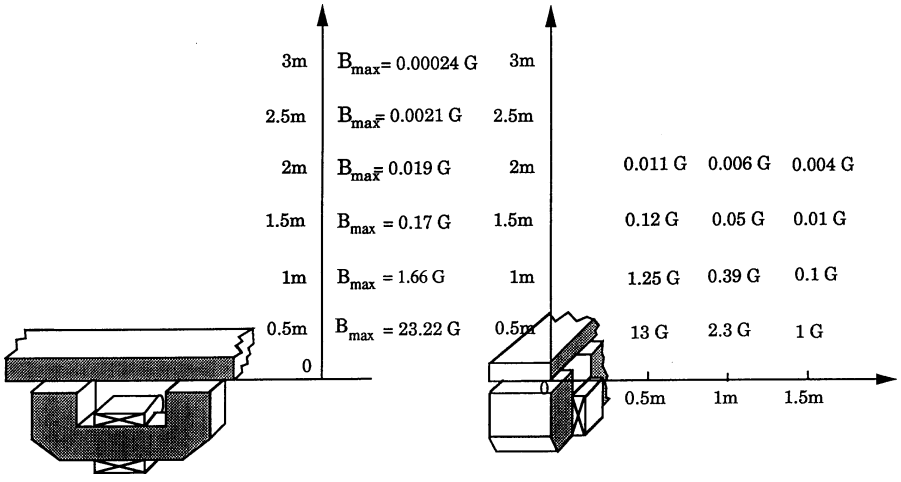

*Figure 81. Stray fields around the center of Grumman magnet (*I *= 50 kA;* g *= 4 cm).*

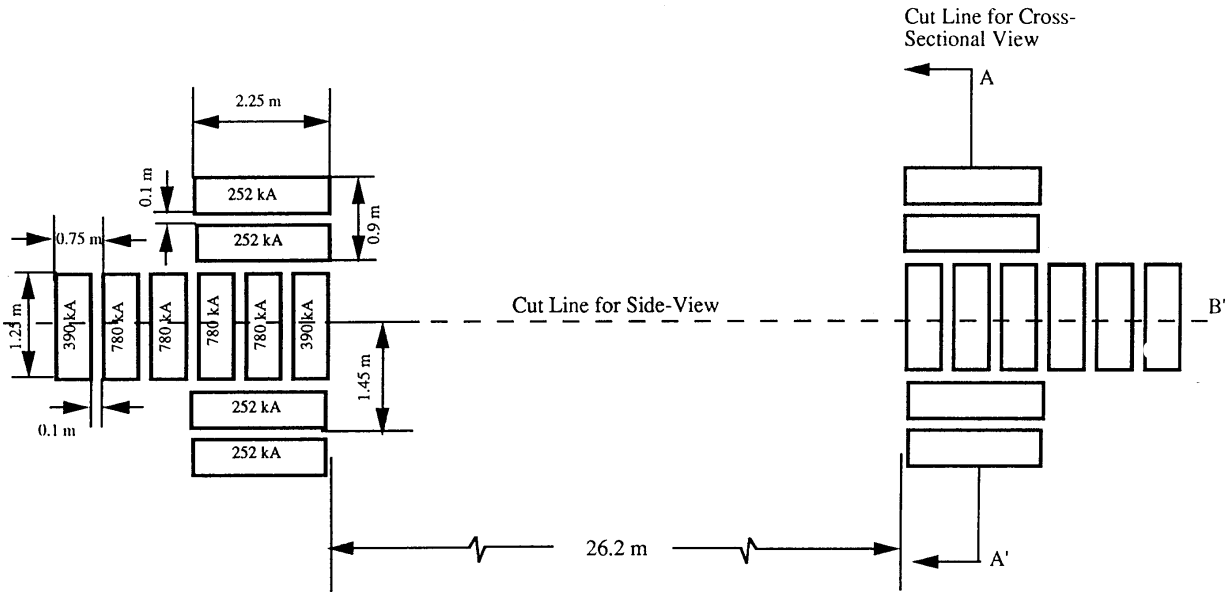

Figure 82. Layout of Magneplane's superconducting coils (A–A' in Fig. 89a).

ducting magnets, simplifying the achievement of ride comfort, and reducing the AC losses in the cryostat and magnet. The system is stabilized in the roll direction by the interaction of the propulsion coils with the edge of the guideway and by airfoils. Propulsion of the system is analogous to the other EDS systems, except that the 12 magnets used are separate from those used for levitation, and the LSM windings are under the vehicle. The dimensions, currents, and layout of the magnets are shown in Figure 82.

Model used for analysis. The stray fields for the Magneplane system were analyzed in the same manner as those in the other systems.

Analytical models are available for calculating the magnetic lift and drag forces on magnets moving above an infinitely wide conducting ground plane. Analyses for single magnets have been given by Chilton and Coffey (1971), Coffey et al. (1972), Coffee et al. (1973), Reitz (1970), and Davis and Reitz (1972). A similar analysis has been made by Lee and Menendez (1974) for multiple magnets. The latter formulation was programmed and used in the analysis of this system. Values for a single magnet obtained using this formulation compare well with a previous program based on the above-mentioned references, which has been validated at ANL by numerous experiments. The guideway is sufficiently wide that the results are expected to be affected only marginally by its finite width.

Electrodynamic interactions of magnets with the edges of finite conductors as encountered in the keel stabilization of the magplane have not been solved in analytical form and require computer computation using finite-element analyses. The ELEKTRA computer code discussed earlier is capable, in principle, of performing this task. In practice, however, the problem could only be addressed in reduced sizes at very low velocities that are insufficient for evaluating the details of this interaction.

Modeling results for levitation and guidance. The lift and drag forces were calculated for two levitation magnets shown in the previous figure and configured for the baseline 45-passenger vehicle. The lift and drag forces for a bogie composed of two sets of two magnets are shown in Figure 83. The variation of the levitation force with the suspension height, with the velocity as a parameter, is shown in Figure 84. This figure shows the effective spring constant of the vehicle. Since the baseline force demanded of this bogie is 76 kN, we found that sufficient force can be generated by the proposed magnets. The vehicle is guided by allowing it to rotate in the trough-shaped guideway so separate guidance magnets are not used.

Modeling results for keel effect. Owing to limitations of the program used and the capabilities of the computers available, the forces resulting from the interaction of the propulsion magnets with the finite width guideway could be calculated only at

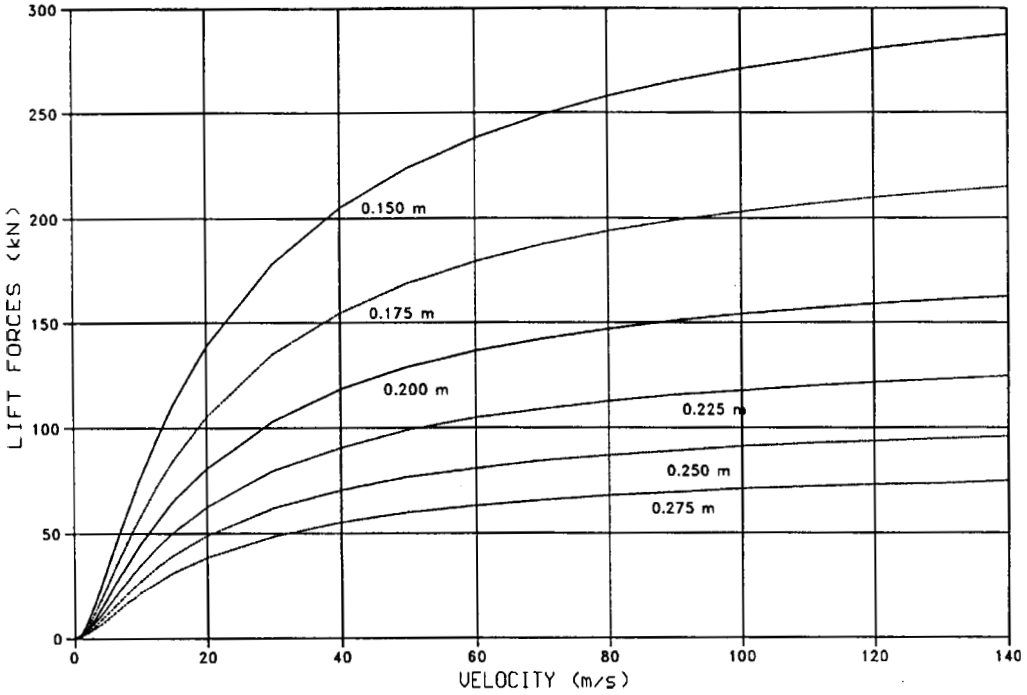

a. Lift forces (2.25 m long, 0.4 m wide, and 0.1 m spacing).

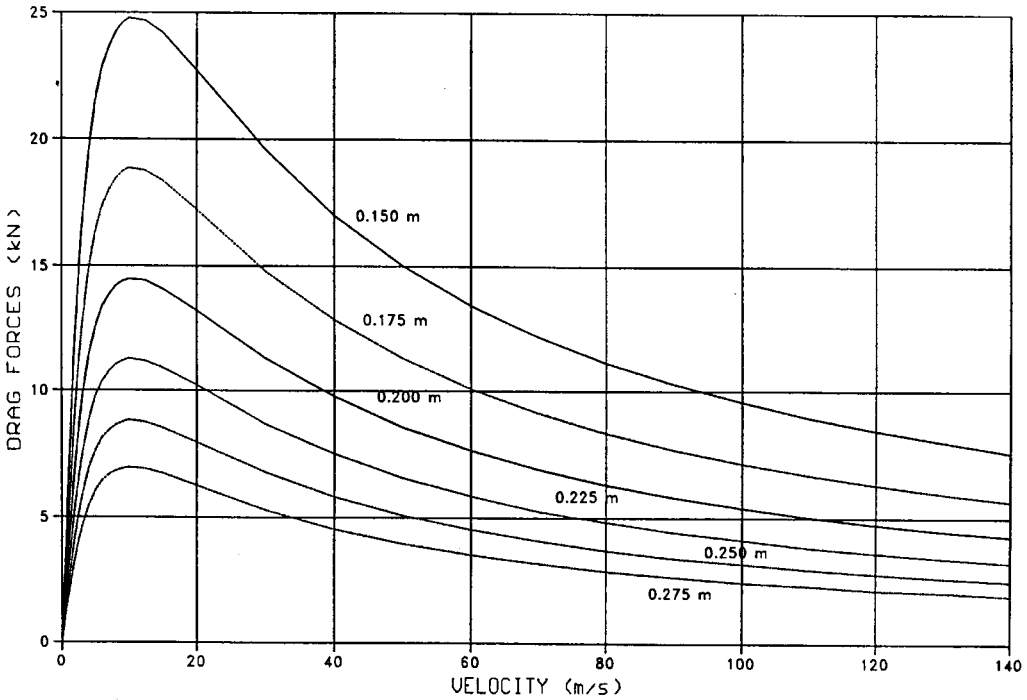

b. Drag forces (2.25 m long, 0.4 m wide, and 0.1 m spacing).

Figure 83. Lift and drag forces for a single bogie of the 45-passenger Magplane (ANL).

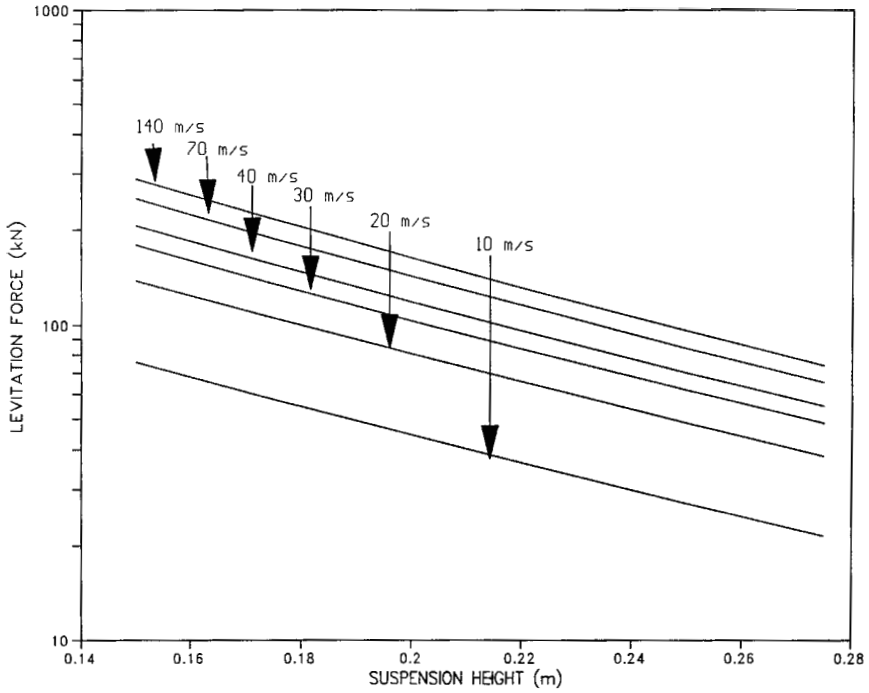

Figure 84. Lift force vs. suspension height for Magplane (ANL).

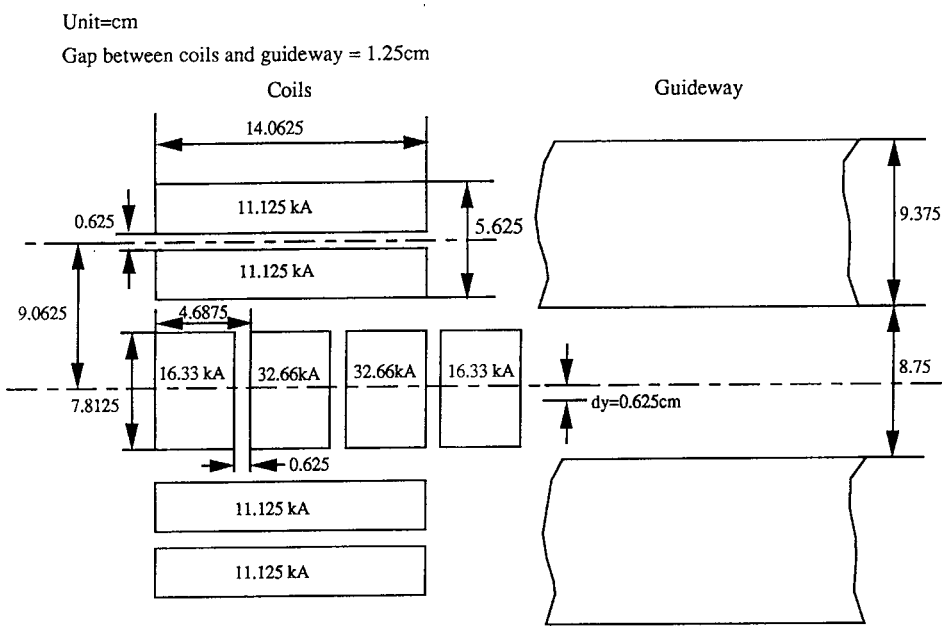

Figure 85. Layout used in Magneplane's analysis for a reduced-size vehicle (ANL).

very low velocities and in greatly reduced sizes. By arbitrarily reducing the size of the vehicle *and the current* by a factor of 16 (see Fig. 85), we obtained the eddy current patterns of Figure 86 at a velocity of 6 m/s. (The Magneplane system uses six propulsion magnets rather than the four modeled here.) In Figure 86a, the eddy current distribution in the guideway induced by the propulsion magnets alone is shown. In Figure 86b, the eddy current induced by the combination of the propulsion and levitation magnets is shown. The forces resulting from these interactions are relied upon to provide roll stabilization of the vehicle. The force tending to restore the vehicle

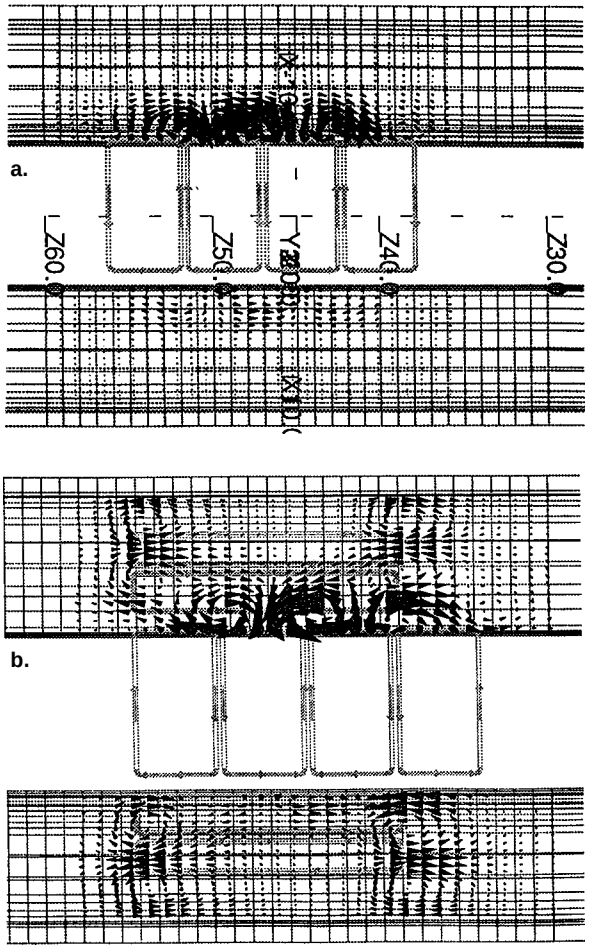

Figure 86. Eddy current patterns from Magneplane's analysis for a reduced-size vehicle (velocity = 6 m/s). The top figure shows the effect of four propulsion magnets alone. The bottom figure shows the eddy currents induced by the four propulsion coils together with the levitation magnets (ANL).

to its neutral position upon displacement laterally by 0.625 cm is shown in Figure 87. We have not attempted to extrapolate this force to a full scale system. That is, although we are able to verify the physical principle of the keel effect, we are unable at present to verify its magnitude.

Modeling results for stray fields. As in the other EDS systems, the most intense stray fields occur when the vehicle is at rest and no currents induced in the guideway oppose the fields generated by the magnets on the vehicle. Our calculated fields along the centerline of the vehicle (Fig. 88a) are comparable to those presented by Magneplane (Fig. 88b). Magneplane proposes to use active normally conducting coils to reduce these fields (Fig. 88c). These cancellation coils were not modeled, but are expected to work as proposed. The computed fields in the cross section A–A′ of Figure 82 (i.e., the centerline of the levitation coils) are shown in Figure 89a, neglecting the effects of the field cancellation coils. The predicted height of the 50-G contour is comparable to that found by Magneplane. Figure 89b shows the fields at this same cross section calculated by Magneplane for the case in which the cancellation coils are active. The active coils substantially reduce field strengths near the vehicle floor. Magneplane did not present a figure for the case where the coils are inactive.

Viability issues. To the extent that the suspension systems have been analyzed in this work, we regard all systems as being capable of generating the forces presented in their respective reports. The analysis of the Magneplane system is more limited than are those for the other systems for the reasons discussed above. No assessment was

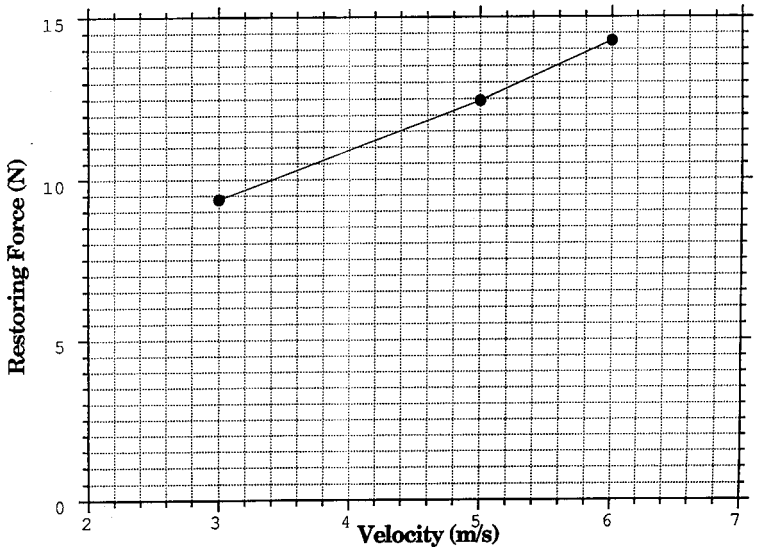

Figure 87. Restoring forces from Magneplane's analysis for a reduced-size vehicle (displacement = 0.625 cm) (ANL).

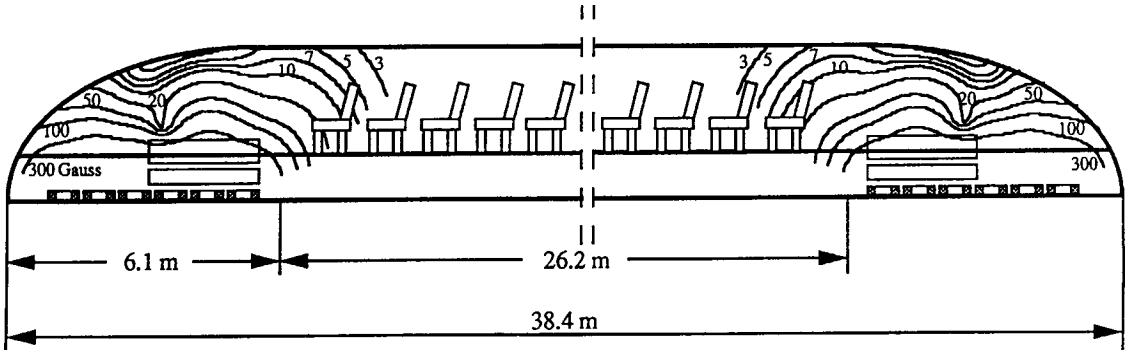

a. Our calculations along the center plane of the vehicle.

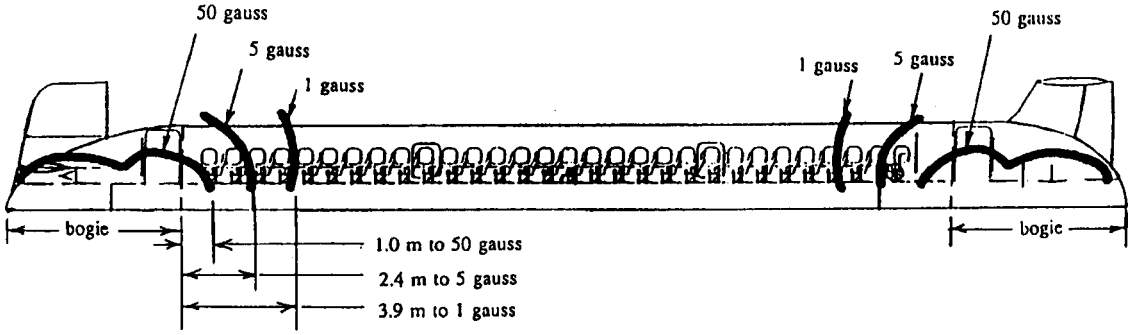

b. Magneplane's calculations in a 140-passenger Magplane with no active shielding coils.

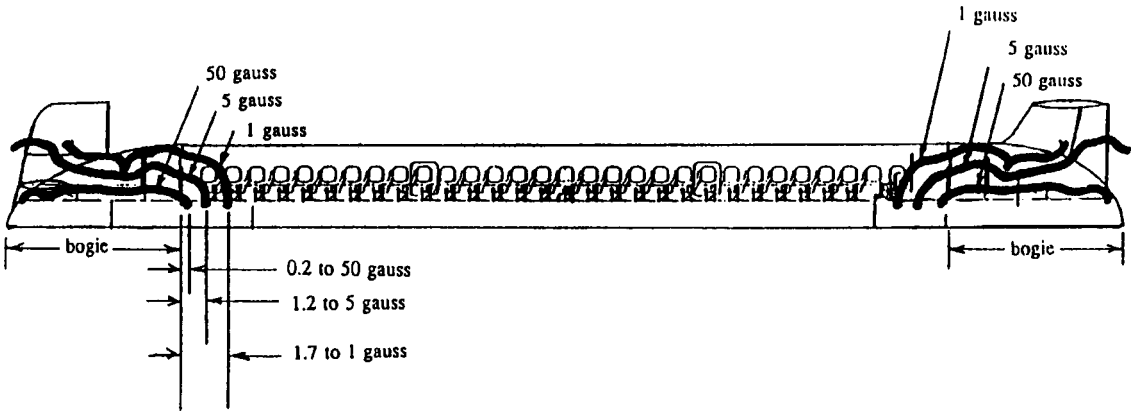

c. Magneplane's calculations in a 140-passenger Magplane with active shielding coils near bogies.

Figure 88. Side view of centerline stray fields in the Magplane.

made of the viability of the superconducting magnets or the cryogenics as they are proposed. A complete assessment will require that these components be evaluated in detail.

In particular, the superconducting magnets and the cryostats containing them will be subjected to eddy current heating caused by the time-varying fields resulting from interaction of the magnets with the guideway. The time variation is caused by the ordinary dynamic motions of the vehicle during operation, by guideway roughness, and by the discontinuous nature of the coils in some of the guideways. Although these interactions were not analyzed, they could require that the magnets be designed with greater margins of safety than proposed by the contractors.

The use of Nb_3Sn magnets in a conduit is an innovative approach. More information and

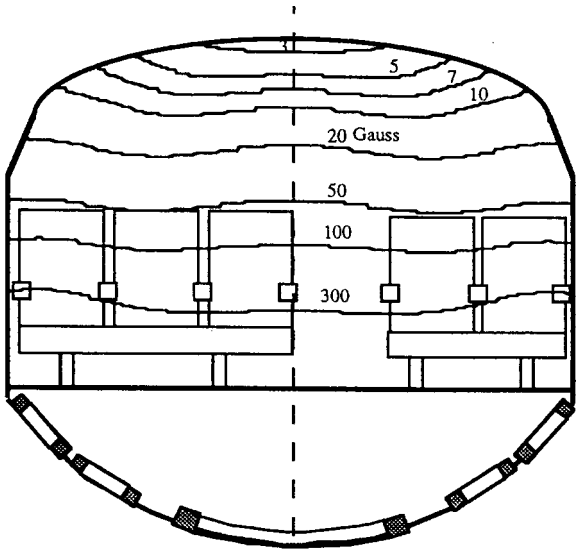

a. Our calculations of those in plane A–A′ of Figure 82.

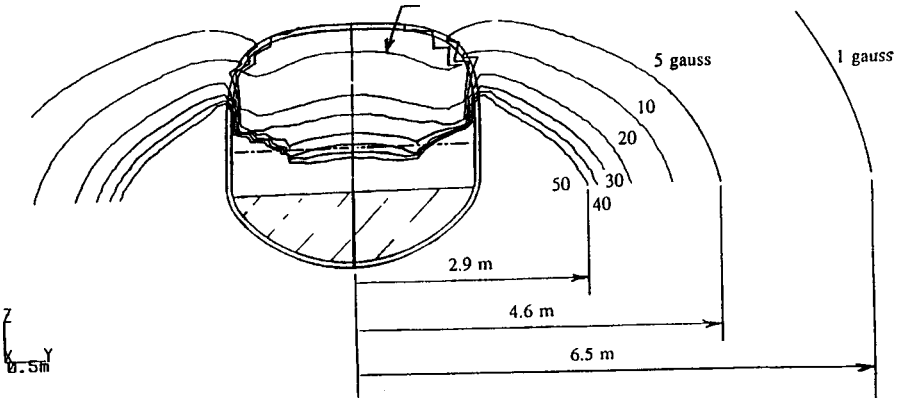

b. Magneplane's calculations of those in plane over a bogie.

Figure 89. Cross-sectional view of stray fields.

experimental data on the performance of these magnets in this application will be required before such systems are deployed. Since adjacent magnets are coupled magnetically, the quench of one magnet will result in a rapid change in current in neighboring magnets and a change in the distribution of the vehicle's load on the guideway. This effect was not evaluated.

The ultimate viability of the various systems is determined by the use of these magnet systems in conjunction with other systems and controls to safely levitate and guide the proposed vehicles. These considerations entail the analysis of the dynamic performance of the vehicle with the guideway, as discussed in the next section.

No attempts were made to optimize the systems proposed by the contractors, and further improvements in the systems proposed might or might not be possible.

3.2.4 Vehicle–guideway interaction*

Objectives

The primary functions of a maglev vehicle suspension are to follow the guideway and to isolate passengers from local guideway variations. These functions translate, respectively, into safety and ride-comfort requirements. The suspension must meet these requirements without imposing excessive forces on the guideway and without needing excessive stroke. These requirements influence selection of guideway stiffness, guideway strength, geometric tolerances, suspension actuators, and controls, and these choices in turn affect guideway and vehicle costs.

* Written by David Tyrell, U.S. Department of Transportation.

This section summarizes the GMSA's assessment of the dynamic vehicle–guideway interactions of TR07 and the four SCD concepts. Our objectives were to determine the advantageous features of each suspension, the features of each that might lead to problems, and the areas warranting further effort. Owing to available time and resources, these analyses focused solely on the vertical dynamics of each concept.

Methodology

The approach used for this effort has been to review each concept, evaluate its performance capability, and do a detailed study of potentially critical performance limitations. The analyses varied for each concept to address specific concerns identified during preliminary assessments. For TR07 the major concern is a magnet striking the guideway because of its small gap. For the Bechtel concept, the major concern is the implementation of its active suspension, consisting of both active aerodynamic surfaces and active elements between the magnet bogies and the vehicle body. For the Foster-Miller concept, the major concern is ride quality owing to its use of discrete bogies and a passive secondary suspension. For the Grumman concept, the major concern is the force–range capability of its levitation control magnets. And for the Magneplane concept, the major concern is the physical implementation of its proposed semi-active suspension.

Traditionally, ground-based vehicles have used a primary suspension with a relatively high natural frequency (5 to 10 Hz) and low damping (0 to 5% of critical damping) to follow the guideway closely, and a secondary suspension with a relatively low natural frequency (0.8 to 1.4 Hz) and relatively high damping (30 to 50% of critical damping) to isolate the passengers. This traditional terminology remains helpful in classifying suspensions, whether they possess passive or active elements or indeed combine the functions of separate primary and secondary suspensions into a single suspension.

Variations in guideway geometry result from its design and construction, the service loads imparted by the vehicle, the environment (soil movement, thermal cycling, snow and ice build-up, etc.), and maintenance. We may describe these geometric variations as the sum of random variations and discrete events. Random variations result from such things as nonuniformity of materials, and discrete events result from design characteristics such as column spacing.

To represent vertical random geometry of a rigid guideway, we used a power spectral density (psd) of the form

$$G(\omega) = \frac{AV}{\omega^2} \tag{1}$$

where $G(\omega)$ = psd of the guideway ($m^2/[rad/s]$)
A = amplitude factor (equal to 6.1×10^{-8} m for high-quality welded rail)
V = speed of vehicle (m/s)
ω = frequency of interest (rad/s).

The discrete perturbations modeled here are those attributable to guideway precamber and flexibility. We modeled the guideway as a simply supported beam, either single span or double span, as shown in Figure 90. We calculated dynamic deflection of the guideway for the flexible-guideway analyses.

We consider the guideway geometry to be the sum total of the random roughness, the precamber, the guideway flexibility, and any irregularities owing to environmental influences. We have not modeled the latter here. How well the vehicle behaves on the rigid and flexible guideways indicates the margin that is allowable for the irregularities owing to environmental influences.

A general difficulty with our modeling is the choice of A (psd amplitude factor) in the absence of measurements for maglev concepts. As a

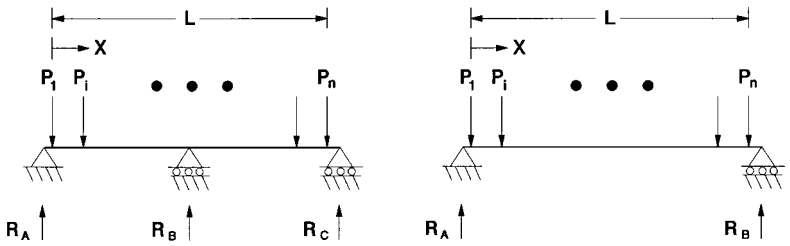

a. Double-span guideway beam. *b. Single-span guideway beam.*

Figure 90. Guideway dynamic model.

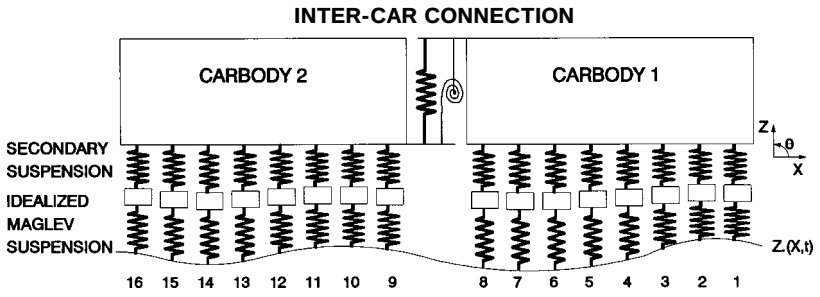

Figure 91. TR07 vertical dynamics model.

baseline, we selected the value measured for U.S. Class 6 railroad track ($A = 6.1\times10^{-8}$ m). This is quite high-quality track suitable for 110-mph (49-m/s) passenger rail operation. Our dynamic analysis of TR07 suggests that it was designed for a random guideway roughness near this value. We also examined the maximum amplitude tolerated by each maglev system, based on ride comfort or safety considerations, and compared this with our baseline value. Such comparisons reveal the construction-tolerance requirements for the maglev systems relative to those of high-speed rail.

Application to TR07

The major concern for TR07 is a magnet striking the guideway, owing to what appears to be a small nominal gap of 8 mm. Gap variations may be caused by the guideway flexibility and by variations in the guideway geometry. The TR07 guideway is generally elevated, and as the vehicle traverses the suspended guideway, the guideway deflects. The suspension of the vehicle responds to this guideway deflection, and to guideway geometry variations such as random roughness, precamber, and misalignment between beams. Either excessive guideway flexibility or geometry may cause poor ride quality and potentially may cause a magnet to strike the guideway.

The vertical dynamics model of TR07 is shown in Figure 91. The model used for the flexible guideway analysis is a two-span guideway. The parameters of the model are listed in Table 36. Although TR07 uses active control of its levitation- and guidance-magnet currents, we may analyze it as a passive primary suspension with fixed natural frequency and damping. We discuss the procedure for determining the equivalent passive suspension for TR07 in the section dealing with Grumman's active suspension.

Figure 92 shows, for speeds of 100, 300, and 500 km/hr (28, 83, and 139 m/s), vehicle response over a rigid guideway corresponding to high quality welded rail construction ($A = 6.1\times10^{-8}$ m).

Plotted in Figure 92 are the RMS accelerations at the front of the lead section of the vehicle. Note that, at 500 km/hr, the 10-Hz, one-third-octave band response is 0.024 g RMS, whereas the ISO 1-hour reduced comfort boundary at 10 Hz is 0.048 g RMS. If the only irregularity was random roughness (i.e., a rigid guideway), a guideway with a roughness coefficient of $A = 12.2\times10^{-8}$ m could be tolerated, based on ride comfort.

Table 36. TR07 model parameters.

Description	*Value*
Vehicle	
Inertia	
Hinge mass	1016 kg
Carbody mass	45,711 kg
Carbody pitch inertia	2.48×10^6 kg m^2
Stiffness	
Primary stiffness	1.45×10^6 N/m
Secondary stiffness	2.26×10^5 N/m
Intercar vertical stiffness	2.26×10^7 N/m
Intercar pitch stiffness	0 N m
Damping	
Primary damping	3.45×10^4 N s/m
Secondary damping	2.15×10^4 N s/m
Intercar vertical damping	0 N s/m
Intercar pitch damping	0 N m s
Geometry	
Distance between magnets	3.125 m
Guideway	
Material	
Modulus of elasticity	21.0×10^9 N/m^2
Density	2.41×10^3 kg/m^3
Geometry	
Cross-section area	1.508 m^2
Area moment of inertia	0.682 m^4
Damping	
First mode	3%
Second mode	3%

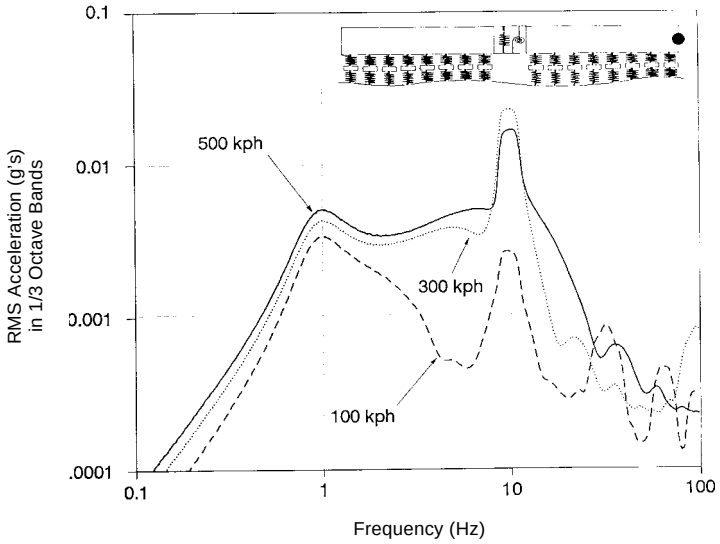

Figure 92. TR07 RMS acceleration vs. frequency (front of vehicle, random roughness).

The corresponding RMS gap variation at 500 km / hr is 1.05 mm. If we assume that 3σ represents the maximum excursion likely, the magnet gap must be at least 3.2 mm. For TR07's 8-mm gap, the maximum permissible roughness coefficient for a rigid guideway would be $A = 15.3\times10^{-8}$ m. This is a less severe requirement than that for ride comfort. Consequently, ride quality dictates the maximum random vertical guideway geometry variations that TR07 can tolerate.

The vehicle response is influenced by guideway flexibility. As the guideway becomes more flexible, gap variations and carbody accelerations tend to increase in magnitude. Figure 93 shows graphs of gap variation and ride quality as functions of guideway flexibility, both for constant and varying beam natural frequencies. The graph has been constructed such that thresholds for both the gap variations and ride quality coincide. Figure 93 indicates that both gap variation and ride quality thresholds are reached for essentially the same guideway flexibility, and that these thresholds are reached for less flexibility if the guideway's natural frequencies are allowed to vary. The graphs also show that, even if a larger magnet gap existed, guideway flexibility would still need to be sufficiently small to provide acceptable ride quality.

For a TR07-type of vehicle, ride quality dictates the flexibility of the guideway. Guideway flexibility in turn dictates the range of the magnet gap variation that must be accommodated. For this type of vehicle, a maglev suspension that could accommodate an increased range of gap variations would *not* allow an increase in guideway flexibility, owing to the requirement of acceptable ride quality. The consequences of poor ride quality may include nausea and fatigue of the occupants; however, these consequences tend to be short-lived. The consequences of one or more magnets exceeding its allowable gap variation and potentially striking the guideway may be long-lived and costly.

TR07 would benefit in two ways from having a larger magnet gap. First, it would increase its safety margin; second, it would allow the vehicle to maintain acceptable ride quality over a rougher guideway. To realize the second benefit, however, TR07 would need either an active secondary suspension or more control authority in its active primary suspension. Such improvements would require substantial redesign of TR07's existing suspension.

Application to SCD concepts

Bechtel. Our major concern for the Bechtel concept is the achievement of an active suspension consisting of both active aerodynamic surfaces and active elements between the magnet bogies and the vehicle body. Active suspension control can potentially allow acceptable ride quality over rougher, more flexible guideways than is possible with passive suspensions. Bechtel's final report did not describe the control strategy for its active suspension or the hardware anticipated for its actuators and controllers. Without such informa-

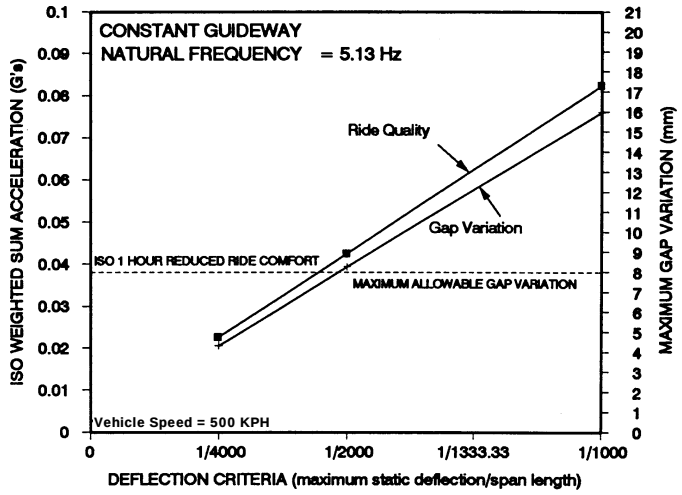

a. Constant guideway.

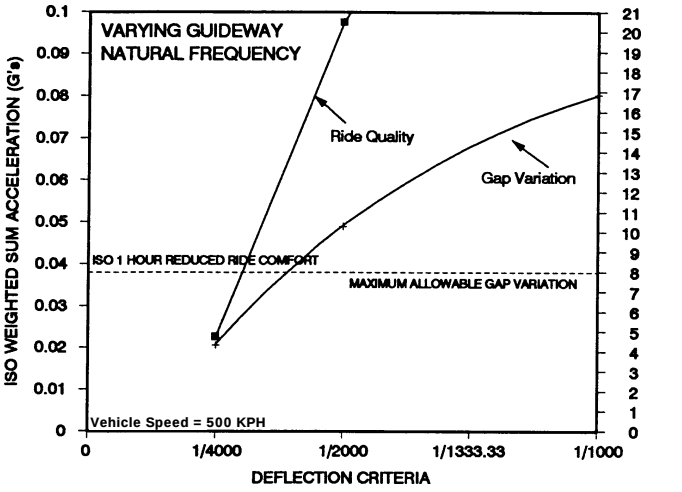

b. Varying guideway.

Figure 93. Influence of guideway flexibility on TR07 gap variations and ride quality.

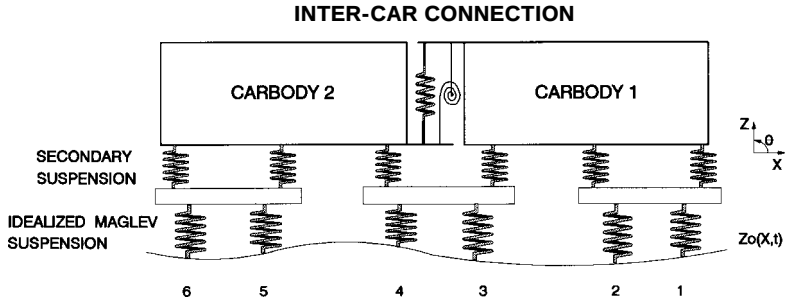

Figure 94. Foster-Miller vehicle model.

tion, the vehicle–guideway interaction of Bechtel's concept cannot be analyzed.

Foster-Miller. Our major concern for the Foster-Miller design is ride quality, and the guideway geometry necessary to provide it. The Foster-Miller vehicle is supported by articulated intermediate bogies between the cars, and by end bogies supporting the ends of the first and last cars. The vehicle model is shown in Figure 94, and the parameters of the model are listed in Table 37. For the flexible guideway analysis, the Foster-Miller guideway is modeled as a double-span beam.

The vertical secondary suspension is lightly damped (about 6%), compared with about 30% for most rail passenger vehicles and about 50% for

most highway passenger vehicles. This light damping, in combination with the vehicle being supported by widely spaced bogies rather than by distributed bogies (like those used on TR07, the Grumman design, and the Bechtel design), tends to make the vehicle response to the flexible guideway sensitive to vehicle speed.

Figure 95 shows the vehicle response to the flexible guideway with a 3-mm precamber. With 6% damping, vertical acceleration at the front of the vehicle exceeds 0.08 g's at 480 km/hr (133 m/s). Increasing the secondary suspension damping to 36% decreases this acceleration to 0.045 g's.

The precamber of the guideway is 3 mm. However, the maximum deflection of the guideway at low speeds is 1 mm and is 1.8 mm at 500 km/hr. Reducing the precamber to approximately one-half the low speed deflection of the guideway would also reduce the maximum carbody accelerations.

Table 37. Foster-Miller model parameters.

Description	*Value*
Vehicle	
Inertia	
Bogie mass	7,380 kg
End bogie mass	6,130 kg
"A" vehicle mass	22,630 kg
Carbody pitch inertia	2.48×10^6 kg m^2
Stiffness	
Primary stiffness	2.651×10^6 N/m
Secondary stiffness	
End bogie	1.2×10^6 N/m
Intermediate bogie	0.6×10^6 N/m
Intercar vertical stiffness	0 N/m
Intercar pitch stiffness	0 N m
Damping	
Primary damping	0 N s/m
Secondary damping	1.0×10^4 N s/m
Intercar vertical damping	0 N s/m
Intercar pitch damping	0 N m s
Geometry	
Distance between magnets	varies (m)
Guideway	
Material	
Modulus of elasticity	30.0×10^9 N/m^2
Density	2.40×10^3 kg/m^3
Geometry	
Cross-section area	3.1 m^2
Area moment of inertia	2.16 m^4
Damping	
First mode	0%
Second mode	8%

The acceleration response at the front of the Foster-Miller vehicle to random guideway surface roughness is shown in Figure 96. This figure also shows the response for increased secondary suspension damping. The guideway roughness characteristic used for this analysis is the same as the characteristic used for the analysis of TR07, the results of which are shown in Figure 92. With increased damping, the response of the Foster-Miller vehicle to the random roughness is similar to the TR07 response, indicating that the Foster-Miller vehicle would require similar tolerances on the guideway geometry as TR07.

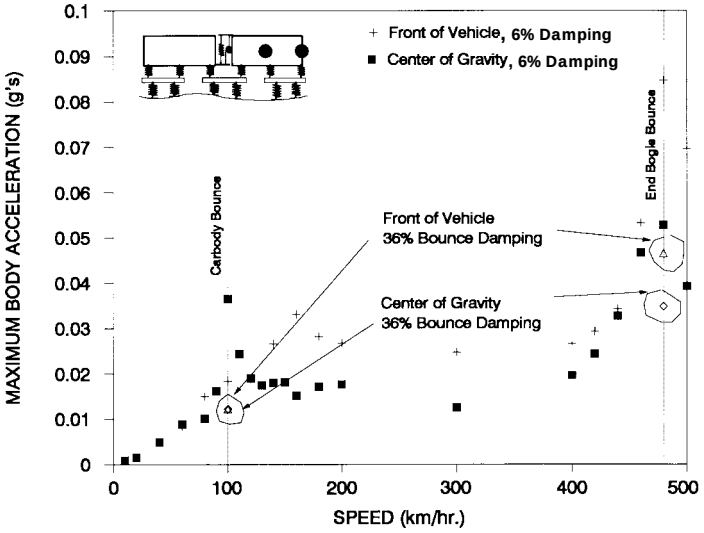

Figure 95. Foster-Miller maximum carbody acceleration vs. speed. Center of gravity and front of vehicle vertical acceleration on a flexible guideway.

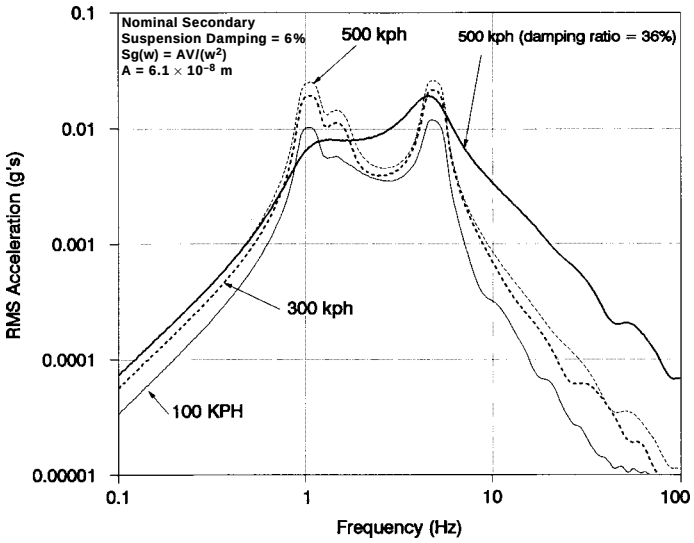

Figure 96. Foster-Miller RMS acceleration vs. frequency (front of vehicle, random roughness, rigid guideway).

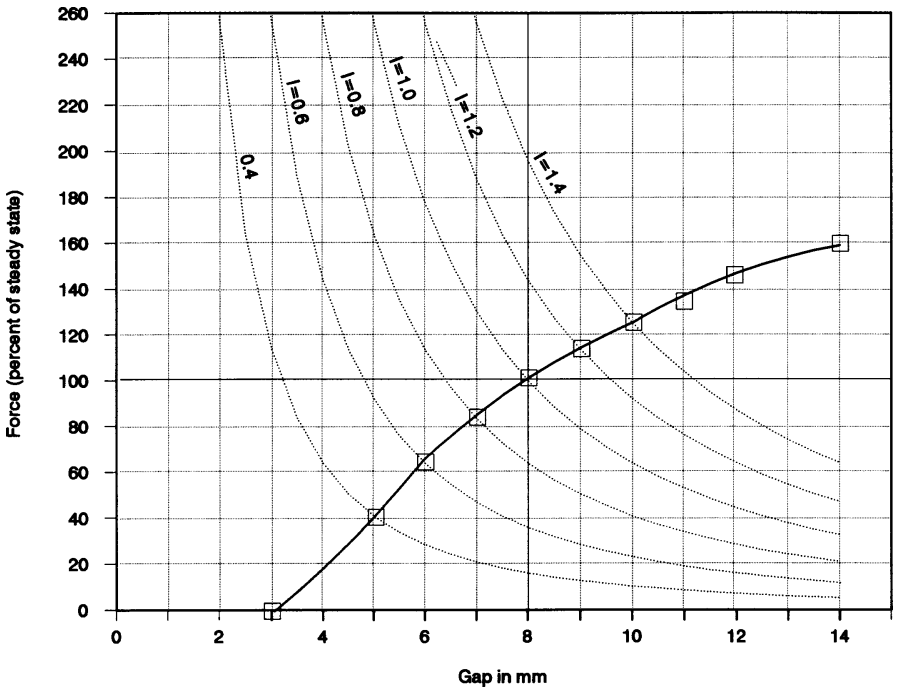

Figure 97. Force–gap characteristics for a typical EMS suspension.

Increasing damping and reducing of guideway precamber are relatively easy to do. We conclude that Foster-Miller's vehicle–guideway interactions would be within allowable ride-comfort and safety limits, provided its random guideway roughness is similar to TR07's. This will require reasonably close tolerances on its null-flux and propulsion coils, but it appears to be achievable.

Grumman. Our major concern with the Grumman vehicle design is the force-range capability of the suspension. The suspension travel must be adequate for the range of guideway perturbations that the vehicle may encounter.

For EMS suspensions, the forces to support the vehicle and to cause it to follow the route alignment are developed by electromagnets interacting with a ferrous reaction rail. This interaction results in a force that attracts the electromagnet to the reaction rail. To maintain the stability of the system, a controller varies the current in the electromagnet's coils as a function of the gap between the electromagnet and the reaction rail and other measurements of the electromagnet's position and velocity. Figure 97 shows the force generated by a typical levitation electromagnet designed to operate at a nominal gap of 8 mm.

The dashed lines in Figure 97 show the force–gap relation that would exist if the current in the electromagnets were kept constant. In this situation, a decrease in gap would result in an increase in the attractive force that would accelerate the electromagnet into the reaction rail, causing an impact. An increase in gap would similarly cause a decrease in the force developed and the force would no longer be large enough to support the weight. Because of this behavior, a permanent magnet or constant current magnet providing levitation by forces of attraction is said to be unstable.

To produce stable levitation forces, the current in the electromagnet is varied as a function of the gap. As the gap becomes smaller, the current is reduced, reducing the attractive force. The electromagnet is then driven away from the reaction rail by the force exerted by the weight of the vehicle. As the gap becomes larger, the current in the electromagnet is increased, resulting in an increase in force produced by the electromagnet, which acts to return it to the nominal gap.

The solid curve in Figure 97 shows the force as a function of gap that would result from a control strategy where the current was changed by 20% of the nominal current for each millimeter of gap change. This force–gap characteristic is believed to represent the electromagnets used in the Transrapid TR06 system and the initial magnets used in the TR07 system.

In Grumman's concept, the force used to support the weight of the vehicle is generated by superconducting coils. These superconducting coils maintain the attraction levitation force with-

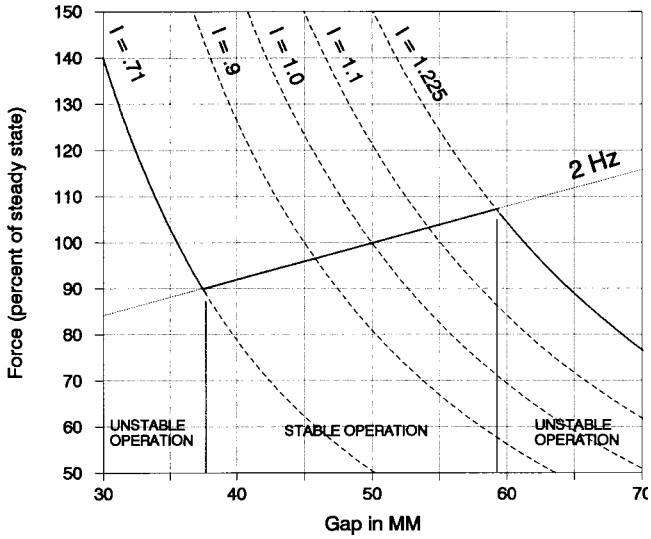

Figure 98. Force–gap characteristics for an electromagnetically trimmed superconducting magnet.

out expending energy in the heating losses associated with an electromagnet. Also, the larger fields generated by the superconducting coils permit the vehicle to maintain a larger equilibrium gap. Stability is established by a set of auxiliary electromagnet coils that adjust the attraction forces by variations in current. The expectation in this approach is that variations in gap and vehicle forces will be small and that a limited electromagnetic field variation will be adequate to maintain control.

Interestingly, the Grumman vehicle does not employ a traditional combination of primary and secondary suspensions. Instead, it uses a single active suspension to follow the guideway closely and to isolate passengers from guideway irregularities.

Figure 98 shows the force–gap characteristic that would be expected for an electromagnetically trimmed superconducting coil magnet that is designed to operate at a gap of 50 mm, with a trim capability to vary the force at the nominal gap 50% either way. The characteristic shown assumes that the control law will maintain an effective stiffness that is equivalent to that of a 2-Hz primary suspension to accommodate dynamic loads. Although Grumman revised their suspension to operate at a gap of 40 mm, the basic conclusions presented here remain valid.

As shown in Figure 98, Grumman's suspension would be stable in a region of gaps between 38 and 59 mm (i.e., a range of 21 mm). This would result in a requirement to keep guideway irregularities at frequencies higher than 2 Hz (or a wavelength of 67 m or less at a speed of 134 m / s) to an amplitude of less than 21 mm peak to peak. Decreasing the system's natural frequency would at most increase the range of stable gaps to 31 mm peak to peak. Increasing the bandwidth of the suspension system has the effect of reducing the range of gap variation that can be tolerated.

Figure 99 shows the block diagram for the force characteristic of a single magnet module of the Grumman maglev vehicle. The guideway's vertical geometry is the vertical position of the guideway at the magnet module, and the vehicle displacement is also at the magnet module. The block diagram shown in the figure is based on the linear-

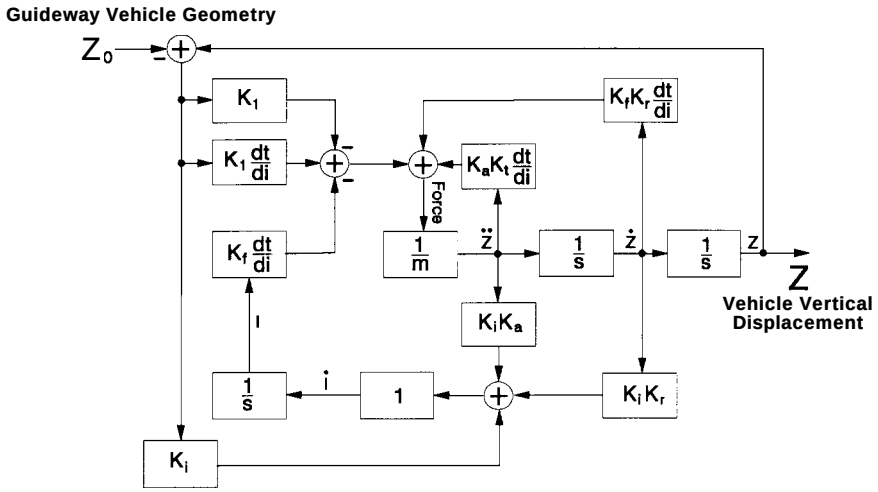

Figure 99. Block diagram of Grumman magnet control system.

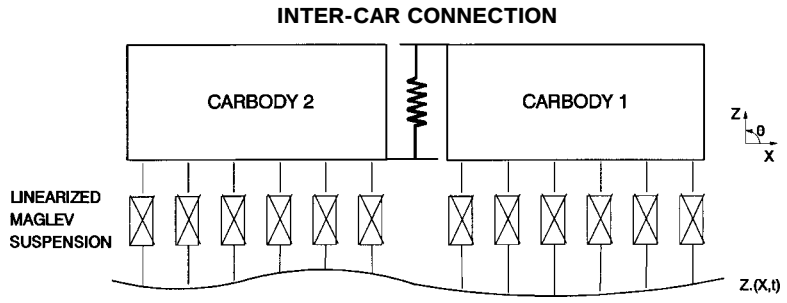

Figure 100. Grumman vehicle model.

ized model developed by Grumman. The model implicitly incorporates the magnet nonlinearities and the magnet module's own servo control.

The force from a magnet acting on the vehicle mass is given by the constant-coefficient differential equation

$$F_n = K_a K_f \frac{\partial f}{\partial i}\ddot{z}_n + K_v K_f \frac{\partial f}{\partial i}\ddot{z}_n + \left(K_f \frac{\partial f}{\partial i} - K_1\right)\left(z_n - zo_n\right) - K_f \frac{\partial f}{\partial i} i_n \qquad (2)$$

where subscript *n* refers to the location of the magnet module. i_n is the current of the particular magnet module, and is given by the constant coefficient differential equation:

$$\dot{i}_n + K_a K_i \ddot{z}_n + K_v K_i \dot{z}_n = K_i\left(z_n - zo_n\right) = 0. \qquad (3)$$

(The force produced by each magnet module is modeled as a point force here, although its behavior is closer to a pressure force. The error from this approximation is small owing to the number of modules supporting each carbody. There are 12 modules with 24 poles supporting each carbody, which were modeled as six forces supporting each carbody.)

The control system diagrammed in Figure 99 and described by eq 2 and 3 is divergently unstable when more than two modules are used to support a single carbody. The carbody motions *Z* and θ are stable, while the magnet module currents i_1, i_2, i_3, i_4, i_5, i_6 are divergently unstable. The following paragraphs discuss the stability of a single carbody supported by six magnet modules controlled using the control loop shown in Figure 99.

Figure 100 shows the model of the baseline Grumman maglev vehicle, which consists of two cars coupled together. Only one carbody of this model is considered in evaluating the stability of a vehicle supported by multiple magnet modules.

There are two equations of motion that describe the behavior of the carbody, and six equations that describe the currents in the magnet modules. These equations are as follows:

$$\left(M + 6K_a K_f \frac{\partial f}{\partial i}\right)\ddot{z} + 6K_v K_f \frac{\partial f}{\partial i}\dot{z} + 6\left(K_f \frac{\partial f}{\partial i} - K_1\right)z - K_f \frac{\partial f}{\partial i}\left(i_1 + i_2 + i_3 + i_4 + i_5 + i_6\right) = \left(K_f \frac{\partial f}{\partial i} - K_1\right)\left(zo_1 + zo_2 + zo_3 + zo_4 + zo_5 + zo_6\right) \qquad (4)$$

$$\left(I + \frac{35}{2}l^2 K_a K_f \frac{\partial f}{\partial i}\right)\ddot{\theta} + \frac{35}{2}l^2 K_v K_f \frac{\partial f}{\partial i}\dot{\theta} + \frac{35}{2}l^2\left(K_f \frac{\partial f}{\partial i} - K_1\right)\theta - lK_f \frac{\partial f}{\partial i}\left(\frac{5}{2}i_1 + \frac{3}{2}i_2 + \frac{1}{2}i_3 - \frac{1}{2}i_4 - \frac{3}{2}i_5 - \frac{5}{2}i_6\right) = l\left(K_f \frac{\partial f}{\partial i} - K_1\right)\left(\frac{5}{2}zo_1 + \frac{3}{2}zo_2 + \frac{1}{2}zo_3 - \frac{1}{2}zo_4 - \frac{3}{2}zo_5 - \frac{5}{2}zo_6\right) \qquad (5)$$

$$\dot{i}_1 + K_a K_i\left(\ddot{z} + \frac{5}{2}l\ddot{\theta}\right) + K_v K_i\left(\dot{z} + \frac{5}{2}l\dot{\theta}\right) + K_i\left(z + \frac{5}{2}l\theta\right) = K_i zo_1 \qquad (6)$$

$$\dot{i}_2 + K_a K_i \left(\ddot{z} + \frac{3}{2} l\ddot{\theta} \right) + K_v K_i \left(\dot{z} + \frac{3}{2} l\dot{\theta} \right) + K_i \left(z + \frac{3}{2} l\theta \right) = K_i zo_2 \quad (7)$$

$$\dot{i}_3 + K_a K_i \left(\ddot{z} + \frac{1}{2} l\ddot{\theta} \right) + K_v K_i \left(\dot{z} + \frac{1}{2} l\dot{\theta} \right) + K_i \left(z + \frac{1}{2} l\theta \right) = K_i zo_3 \quad (8)$$

$$\dot{i}_4 + K_a K_i \left(\ddot{z} - \frac{1}{2} l\ddot{\theta} \right) + K_v K_i \left(\dot{z} - \frac{1}{2} l\dot{\theta} \right) + K_i \left(z - \frac{1}{2} l\theta \right) = K_i zo_4 \quad (9)$$

$$\dot{i}_5 + K_a K_i \left(\ddot{z} - \frac{3}{2} l\ddot{\theta} \right) + K_v K_i \left(\dot{z} - \frac{3}{2} l\dot{\theta} \right) + K_i \left(z - \frac{3}{2} l\theta \right) = K_i zo_5 \quad (10)$$

$$\dot{i}_6 + K_a K_i \left(\ddot{z} - \frac{5}{2} l\ddot{\theta} \right) + K_v K_i \left(\dot{z} - \frac{5}{2} l\dot{\theta} \right) + K_i \left(z - \frac{5}{2} l\theta \right) = K_i zo_6 \quad (11)$$

Table 38 defines and specifies the parameters used in analyses of Grumman's suspension. The displacement, velocity, and current gains depend on the frequency chosen for the magnet module servo control, although this frequency is not directly related to the magnetic force characteristic. We explain below the rationale for examining two equivalent suspension frequencies.

Consider the case when the guideway geometry consists of an even upward displacement of the guideway Z^* and the vehicle and control current have reached steady state, i.e., all their derivatives are 0. Since there is no effective pitch input to the vehicle, the pitch of the vehicle is also 0. These equations then reduce to

$$6\left(K_f \frac{\partial f}{\partial i} - K_1 \right) z - K_f \frac{\partial f}{\partial i} (i_1 + i_2 + i_3 + i_4 + i_5 + i_6) = \left(K_f \frac{\partial f}{\partial i} - K_1 \right) 6Z^* \quad (12)$$

$$lK_f \frac{\partial f}{\partial i} \left(\frac{5}{2} i_1 + \frac{3}{2} i_2 + \frac{1}{2} i_3 - \frac{1}{2} i_4 - \frac{3}{2} i_5 - \frac{5}{2} i_6 \right) = 0 \quad (13)$$

$$K_i z = K_i Z^* . \quad (14)$$

Only two equations contain the six unknown currents, and consequently the currents are divergently unstable. The currents can be made stable in two different ways. One is to add a term in i_n to eq 6–11, which in effect tries to drive the magnet module currents to 0 at all times. This approach involves a substantial revision to the control algorithm. The second approach is to develop a constraint relationship among the currents, such as

Table 38. Grumman vehicle parameters used in analyses.

Description	*Parameter*	*9.1-Hz suspension*	*1-Hz suspension*
Carbody mass	M	30,639 kg	30,639 kg
Carbody pitch inertia	I	8.00×10^5 kg m^2	8.00×10^5 kg m^2
Coupling vertical stiffness	K_{zz}	2.26×10^6 N / m	2.26×10^6 N / m
Distance between magnets	1	2.1 m	2.1 m
Force / gap, open loop	K_1	$4.1\text{x}10^6$ N / m	4.1×10^6 N / m
Force / current	$\partial f / \partial i$	3.33×10^3 N / kAT	$3.33\text{x}10^3$ N / kAT
Current gain	K_i	93 kAT / m s	93 kAT / m s
Magnet servo frequency*	ω_{cl}	60 rad / s	12 rad / s
Acceleration gain	K_a	1.75×10^{-4} s^2	5.75×10^{-4} s^2
Velocity gain	K_v	0.02648 s	0.1517 s
Displacement gain	K_f	1.49×10^4 kAT / m	1.29×10^3 kAT / m

* Affects K_a, K_v, K_f but does not enter directly into analysis.

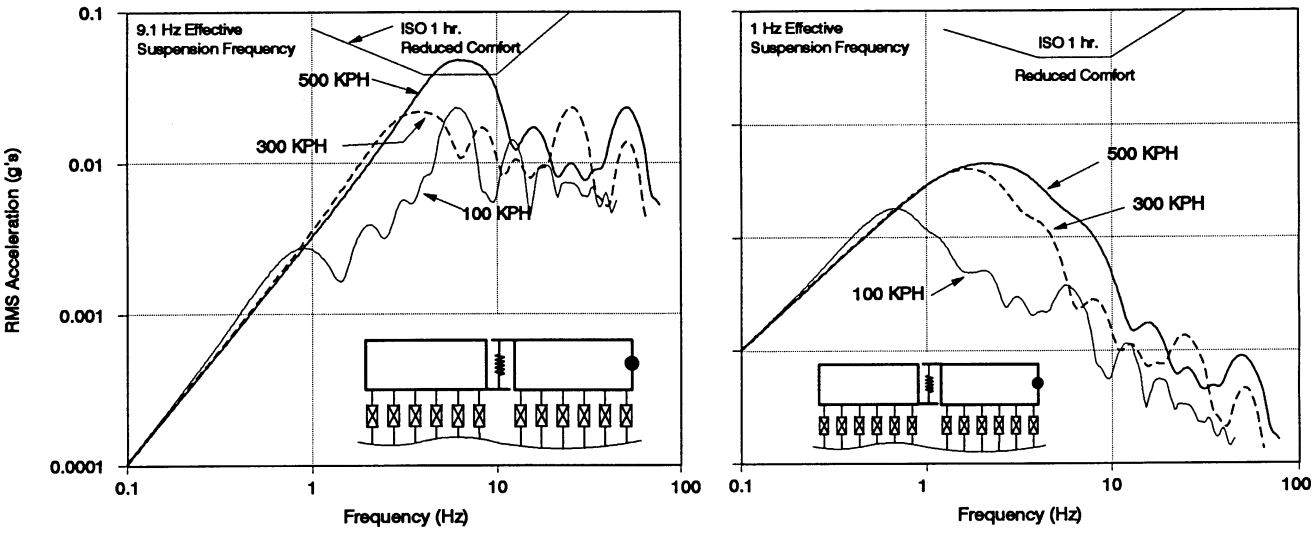

a. 9.1-Hz effective suspension frequency. *b. 1.0-Hz effective suspension frequency.*

Figure 101. Grumman vehicle response to random roughness (rigid guideway).

$i_n = \bar{i} + l_n i'$, where $\bar{i}$ is the average current, l_n is the length from the center of gravity of the car, and i' is the slope required to meet eq 5. This approach does not involve any changes to the control algorithm. However, implementing this approach would involve a substantial change in the philosophy employed in designing the control modules. Grumman's design philosophy requires that the magnet modules be independent of each other as much as possible, while this approach requires the magnet module currents of a carbody to depend upon each other. Nevertheless, we employed this second approach to analyze the Grumman suspension. This makes the force attributable to the currents in the magnet modules behave as analogs to springs. The feasibility of physically implementing this approach has not been evaluated.

The parameter values used by Grumman result in a 9.1-Hz equivalent suspension frequency. Vertically in the steady state, this suspension behaves similarly to a passive suspension with a 9.1-Hz natural frequency and a "skyhook" damping value of 100% (critical damping). Figure 101 shows the response of the model to random roughness in the rigid guideway. As can be seen in the figure, the carbody accelerations exceed the ISO criteria in the front of the vehicle at 500 km / hr.

We wished to determine whether a simple parametric change would allow this suspension to meet the ISO criteria. In the steady state, this suspension can be made to behave similarly to a passive suspension with a 1.0-Hz natural frequency. The carbody accelerations that are calculated for the 1.0-Hz suspension are shown in Figure 101; this suspension easily meets the ISO criteria.

The Grumman guideway is a complex structure. However, the results of the GMSA guideway analysis (section 3.2.1) indicate that the dynamic behavior of the guideway can be approximated as a simply supported beam with a natural frequency of 4.4 Hz and a maximum deflection at the center of the beam of 11 mm when traversed by the baseline vehicle at 500 km / hr. We calculated the response of the vehicle to the flexible guideway. We chose the stiffness such that 11 mm of guideway displacement was calculated at the center of the first guideway beam traversed at 500 km / hr by the vehicle with the 1-Hz suspension, while we chose the mass of the beam such that the first mode frequency of the guideway is 4.4 Hz. The baseline Grumman guideway design has a span length of 27 m and does not call for any precamber of the guideway beams.

Figure 102 shows the maximum carbody accelerations at the center of the vehicle and at the center of gravity of the first car for both the 9.1- and 1-Hz suspensions. The acceleration at the center of the vehicle approaches 1 g for the vehicle with the stiff suspension and reaches 0.12 g for the vehicle with the soft suspension. Although improved by reducing the effective stiffness, the accelerations of the soft suspension are still high relatively high. This is principally ascribable to the

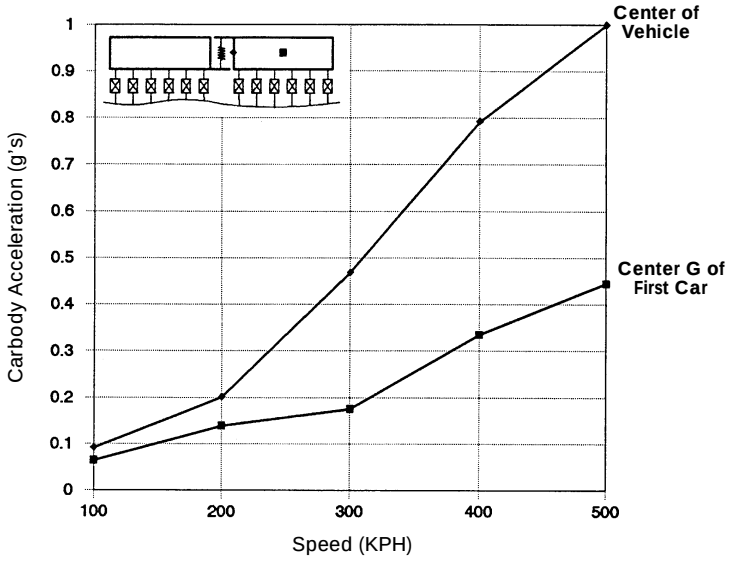

a. 9.1-Hz effective suspension frequency.

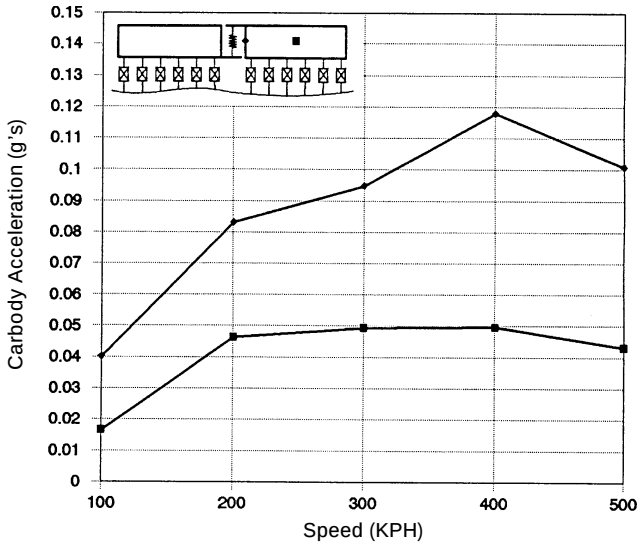

b. 1.0-Hz effective suspension frequency.

Figure 102. Grumman carbody acceleration for vehicle traversing a flexible guideway.

large guideway deflections, in excess of 11 mm. Ride quality could be improved through the introduction of guideway precamber, use of a stiffer guideway, or improved force control characteristics.

Figure 103 shows the maximum gap variations from nominal for the vehicle traversing the flexible guideway with both the 9.1- and 1-Hz suspensions. The stiff suspension follows the guideway more closely. The maximum variation from the nominal gap for the stiff suspension is just over 4 mm, while the maximum variation from nominal is 8 mm for the soft suspension. By following the guideway less closely, the soft suspension is able to provide improved ride quality. Neither suspension uses a large portion of the 50-mm nominal gap.

Figure 104 shows the range of force variations as a function of speed that would be expected for the Grumman vehicle with the 9.1-Hz suspension traveling on the flexible guideway. For the vehicle with the stiff suspension, the analyses tell us that the force between the guideway and the vehicle would become negative, that is, the magnet modules would be required to pull the vehicle down. As the magnet forces cannot become negative, this result says that the magnet modules would become unstable traveling on this guideway. Figure 104 also shows that the force-range capability of the magnet modules would also be exceeded for the 1-Hz suspension, even though the force-range is greatly reduced from the 9.1-Hz suspension. The 50% range of the magnet modules is the *maximum* range at the nominal gap with the vehicle and magnet module control currents at steady state. The actual available force-range may be somewhat less than 50%. If the soft suspension were to be used, it would require a greater force-range capability.

Subsequent to these analyses, Grumman revised its suspension to operate at a nominal 40-mm gap with a steady force variation of ±40% and an intermittent force variation of ±80%. These changes address the concerns noted above. However, time constraints prevented us from analyzing the revised suspension.

Figure 105 shows the forces supporting the vehicle when the vehicle is stationary on a deflected guideway. The vehicle is located over the center of a guideway beam and guideway deflection is approximated as a rectified sine wave with an 11-mm amplitude. Since the vehicle is stationary, the vertical forces between the guideway and vehicle are solely from the effective spring of the force-control characteristic, that is, the force-control characteristic acts as a spring under these conditions. For the stiff suspension, the magnet modules would exceed their force-range capability for the vehicle sitting stationary on such a guideway. In this case, the lead and trail magnet modules carry a load in excess

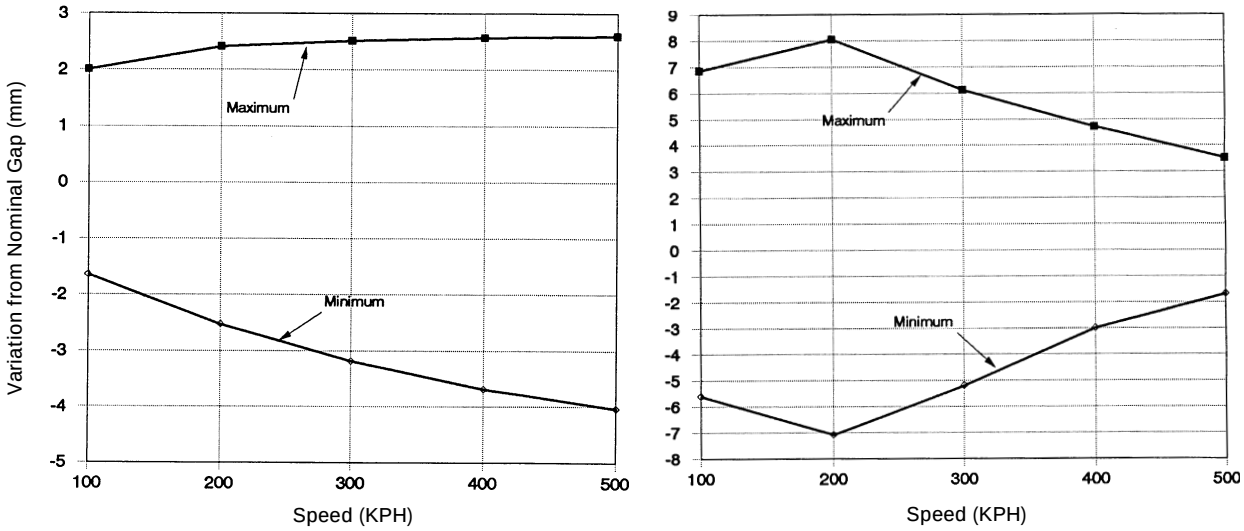

a. 9.1-Hz effective suspension frequency.

b. 1.0-Hz effective suspension frequency.

Figure 103. Grumman gap variation from nominal for vehicle traversing a flexible guideway.

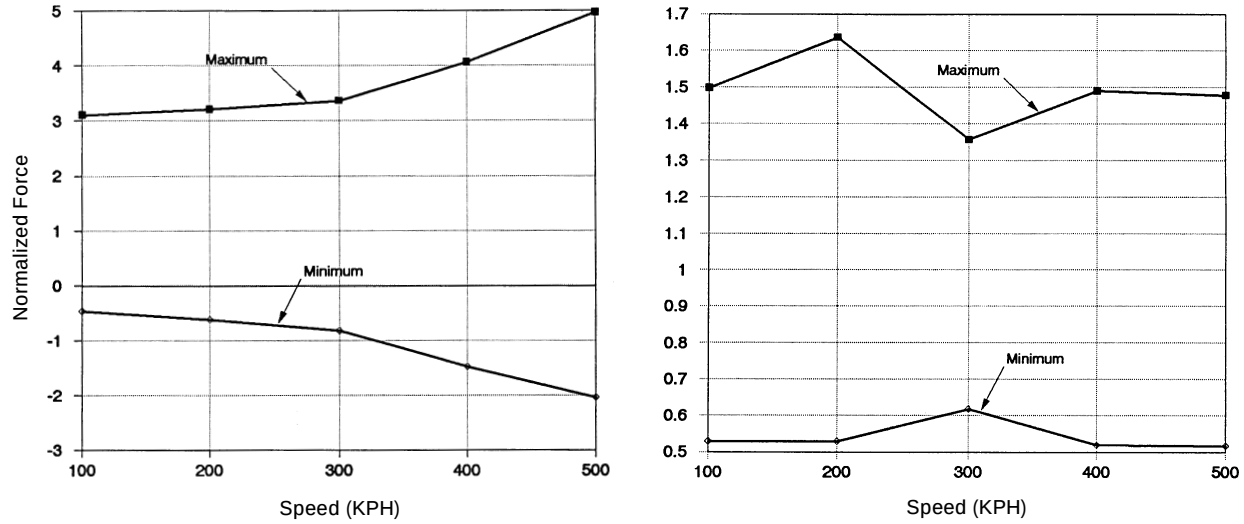

a. 9.1-Hz effective suspension frequency.

b. 1.0-Hz effective suspension frequency.

Figure 104. Guideway force-range acting on the Grumman vehicle.

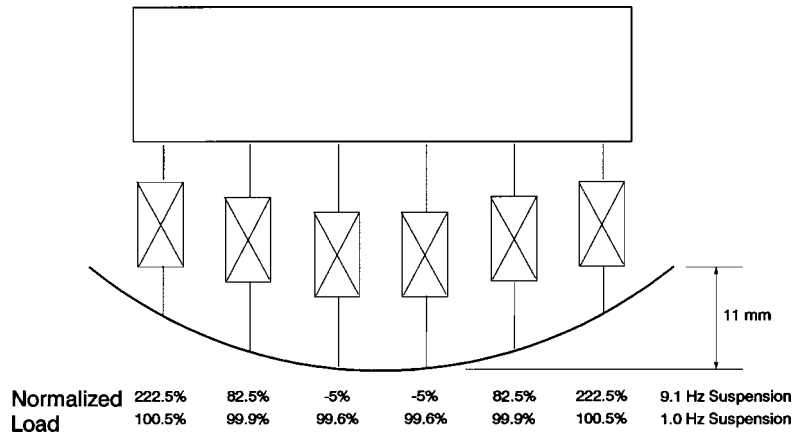

Figure 105. Stationary Grumman vehicle on deflected guideway.

of twice their nominal load, while the two modules closest to the center carry almost no load. For the soft suspension, the variation in force is small, less than 1% from the nominal load. Again, we see that a 1-Hz suspension is superior for the Grumman vehicle. The actual guideway deflection is less than 11 mm when the vehicle is stationary; however, it is greater than 11 mm under some conditions when the vehicle is moving. For the stiff suspension, most of the force variation as the vehicle travels along the guideway is attributable to the effective spring force of the force-control characteristic, in combination with the guideway deflection

The results of the analyses show that the Grumman suspension can be improved, both in terms of the ride quality and in terms of the range of force variations, by reducing its effective natural frequency. However, further improvements in performance may be possible with greater changes in the design of the system. The addition of precamber to the guideway would reduce the effective amplitude of the vertical guideway inputs to the suspension, consequently increasing ride quality and reducing the range of force variations. Revision of the suspension force control characteristic could allow stable independence of the magnet modules and also improve ride quality over poor guideway geometry by taking advantage of the large available gap. It appears that a wide range of force-control characteristics should be possible with the magnet module designed by Grumman, and that it should be capable of a high level of performance (in terms of the ride quality, required guideway geometry and flexibility, and the required force-range capability of the magnet modules). With further work, this innovative suspension would likely achieve its high potential.

Magneplane. Time constraints prevented a thorough analysis of the Magneplane vehicle. We discuss its features only qualitatively here.

The Magneplane suspension is semi-active; that is, only the damping in the suspension is controlled while the effective spring stiffness of the magnetic suspension is not controlled. The optimum strategy for such a suspension is "skyhook" damping. Conceptually, this strategy connects one end of the damper to a (vertically) fixed reference and the other end to the vehicle. (Conventional passive damping, in essence, connects one end of the damper to the guideway and the other end to the vehicle.) The potential advantage of active or semi-active suspensions is a relaxation of the guideway geometry and flexibility requirements for acceptable ride quality.

The Grumman suspension is fully active and its steady-state behavior is similar to a semi-active suspension with a skyhook damping. The Magneplane suspension is semi-active, rather than fully active, and the Magneplane vehicle is suspended only at two locations (essentially a bogie-type vehicle) rather than suspended continuously along its length such as TR07 and Grumman. Because of this, the steady-state behavior of the Magneplane vehicle will be somewhat worse than the steady-state behavior of the Grumman vehicle. That is, the comparable carbody accelerations shown in Figure 101 for the Grumman vehicle will be somewhat greater for the Magneplane vehicle.

Viability issues

Reduced guideway requirements have become a principal issue in developing maglev vehicle suspensions. Guideway construction and maintenance add greatly to the life-cycle cost of a maglev system. Any reduction in these costs could favorably influence the decision to build such a system. This assessment has primarily focused on determining the guideway requirements for proposed maglev systems.

Increased gap sizes have been proposed as a way of allowing reduced guideway requirements. However, the analyses of the dynamic performance of TR07 and the Foster-Miller vehicle, both of which use stiff primary and passive secondary suspensions, indicate that ride quality dictates the minimum level of guideway geometry and stiffness. Consequently, increasing the gap between the vehicle and the guideway will not reduce the guideway's geometry requirements for systems with stiff primary suspensions and passive secondary suspensions.

To relax guideway geometry and stiffness requirements and take advantage of a large gap, significant improvements in vehicle suspensions are required. Specifically, active suspensions are necessary. The Grumman and Magneplane vehicles have unconventional suspensions. They combine the functions of conventional primary and secondary suspensions into one that has actively controlled elements. These suspensions have the potential to capitalize on larger magnet gaps; however, their implementation details will determine how well they achieve this potential. Our analysis showed that the Grumman vehicle, as designed, performs no better than a vehicle

equipped with a well-tuned conventional suspension. Although no detailed analysis was done, it is likely that the Magneplane SCD will not perform as well as the Grumman SCD, primarily because the Magneplane vehicle is a bogie-type vehicle and the Grumman vehicle is a distributed-support-type vehicle.

Clearly, active suspensions warrant further investigation. Such suspensions hold significant potential to maintain adequate levels of safety and ride comfort over relatively rough and flexible (i.e., less expensive) guideways. Properly done, they could be critical to efforts to reduce maglev guideway, and hence system, costs.

Preview control and adaptive control of vehicle suspensions were not explored at all, and feedback control was not explored thoroughly, by the SCD contractors. Research is still needed to make optimal maglev vehicle suspensions.

3.3 SYSTEM-LEVEL VERIFICATION

3.3.1 System performance simulation*

Objectives

Computer simulation of maglev system-level performance transforms technological characteristics (vehicle weight, motor thrust, tilting capability, etc.) into system characteristics that affect ridership (trip time, ride comfort, service frequency, etc.) and costs (fleet size, energy consumption, etc.). Thus, system simulation offers a way to evaluate each concept's ability to serve U.S. markets. It also offers a design tool for developing cost-effective U.S. maglev concepts.

We simulated the performance of TR07 and the four SCDs over two hypothetical routes: 1) a 40-km straight and flat route, and 2) a specially prepared severe segment test (SST). The performance requirement for these simulations was to minimize trip time within the constraints of ride comfort and a 134-m/s maximum speed. The straight and flat route allowed easy comparison of thrust and resistance differences among systems, while the SST highlighted performance differences along route segments broadly representative of common U.S. terrain.

The Government provided the SCD contractors with the SST route specifications at the onset of the contracts. They used this route to estimate system performance and costs. While the SST does not represent the route characteristics of any particular U.S. corridor, average results for real U.S. corridors compare well with those for the SST (using the simulation method described in Martin-Marietta 1992). Thus, we may view the SST results as representative, on average, of U.S. routes. The simulations use as inputs the SST route specifications, ride-comfort constraints, and vehicle and LSM performance data. Outputs include trip time, energy usage, and speed profiles.

A primary objective of these simulations was to compare the performance of the U.S. maglev systems with TR07. Transrapid designed TR07 to be an on-line-station system, connecting closely spaced population centers such as are found in Europe. By comparison, the SCDs focused on systems capable of more frequent service to off-line stations with smaller population densities. Thus, a system-level comparison between TR07 and the SCDs supports a key focus of the NMI program, namely to assess the capability of U.S. industry to improve on available foreign technology. Note that TGV is unable to climb the steep grades included in the SST; we, therefore, did not simulate its performance.

Severe segment test route

The Government developed the SST to permit evaluation of each system's performance along a common route. Figure 106 shows, in graphical form, the 800-km route and its four on-line stations. It consists of three sections. The first 400 km between terminal no. 1 (the origin) and terminal no. 2 is a section of guideway with many closely spaced curves. The vehicles must slow down through most of these curves to meet the ride-comfort criteria. This section is representative of rugged terrain such as may be found along the New York State Thruway. Between terminal no. 2 and terminal no. 3 (at 470 km), the curves are less severe and are separated by greater distances. This is more representative of terrain with rolling hills. The last section (terminal no. 3 to 4) is a straight line section that allows a very high average speed. Compound horizontal and vertical curves occur throughout the SST route. Grades vary over the route from –10% to +10%.

The SST route is described by a horizontal profile and a vertical profile. The horizontal profile specifies the distance along tangents between points of intersection (PI), and specifies the radius of curvature (R_h) and the change in azimuth (I) at

* Written by Dr. James H. Lever, CRREL, Frank L. Raposa, Consulting Engineer, and George Anagnostopoulos, U.S. Department of Transportation.

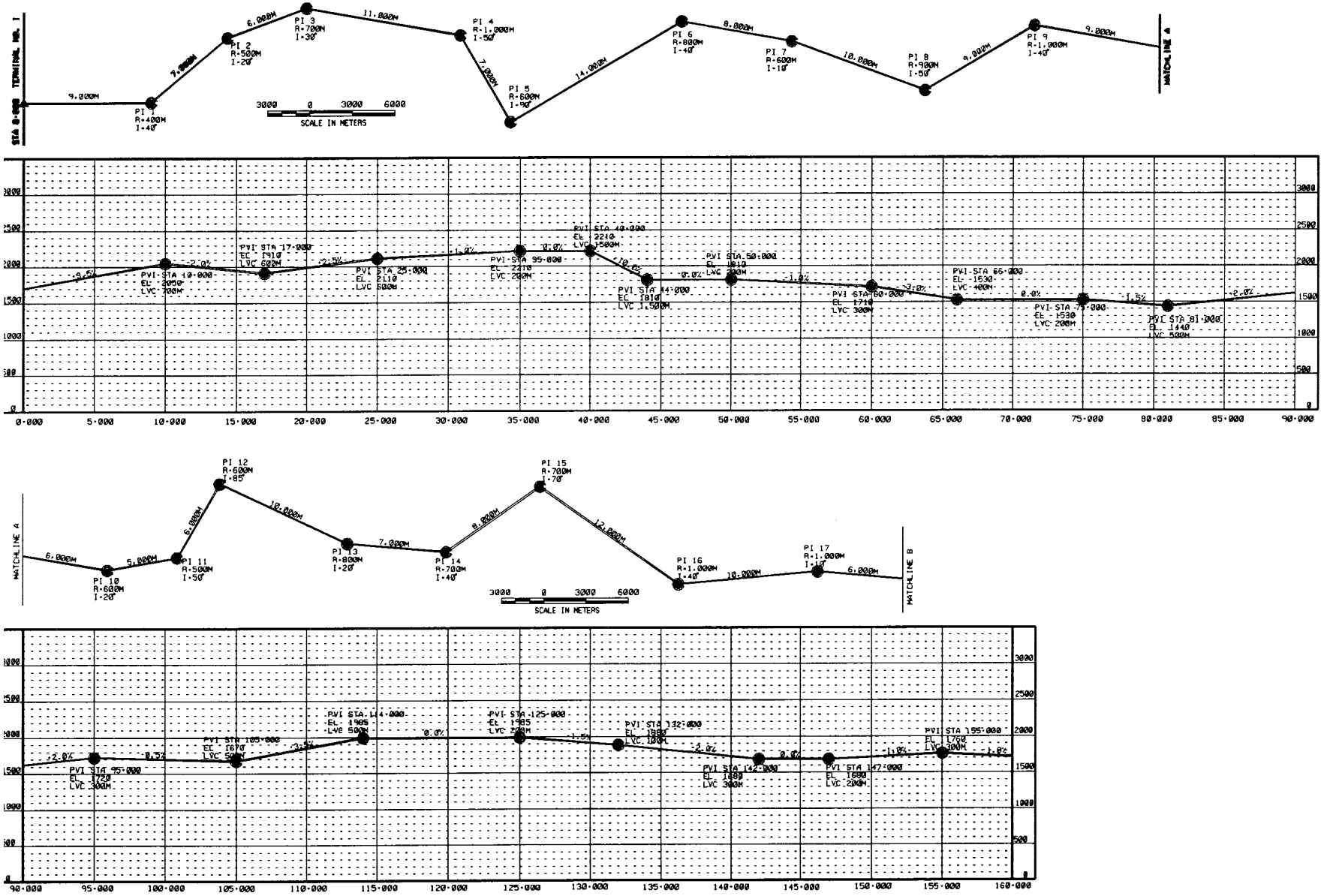

a. 0–160 km.

Figure 106. Severe segment test (SST) route.

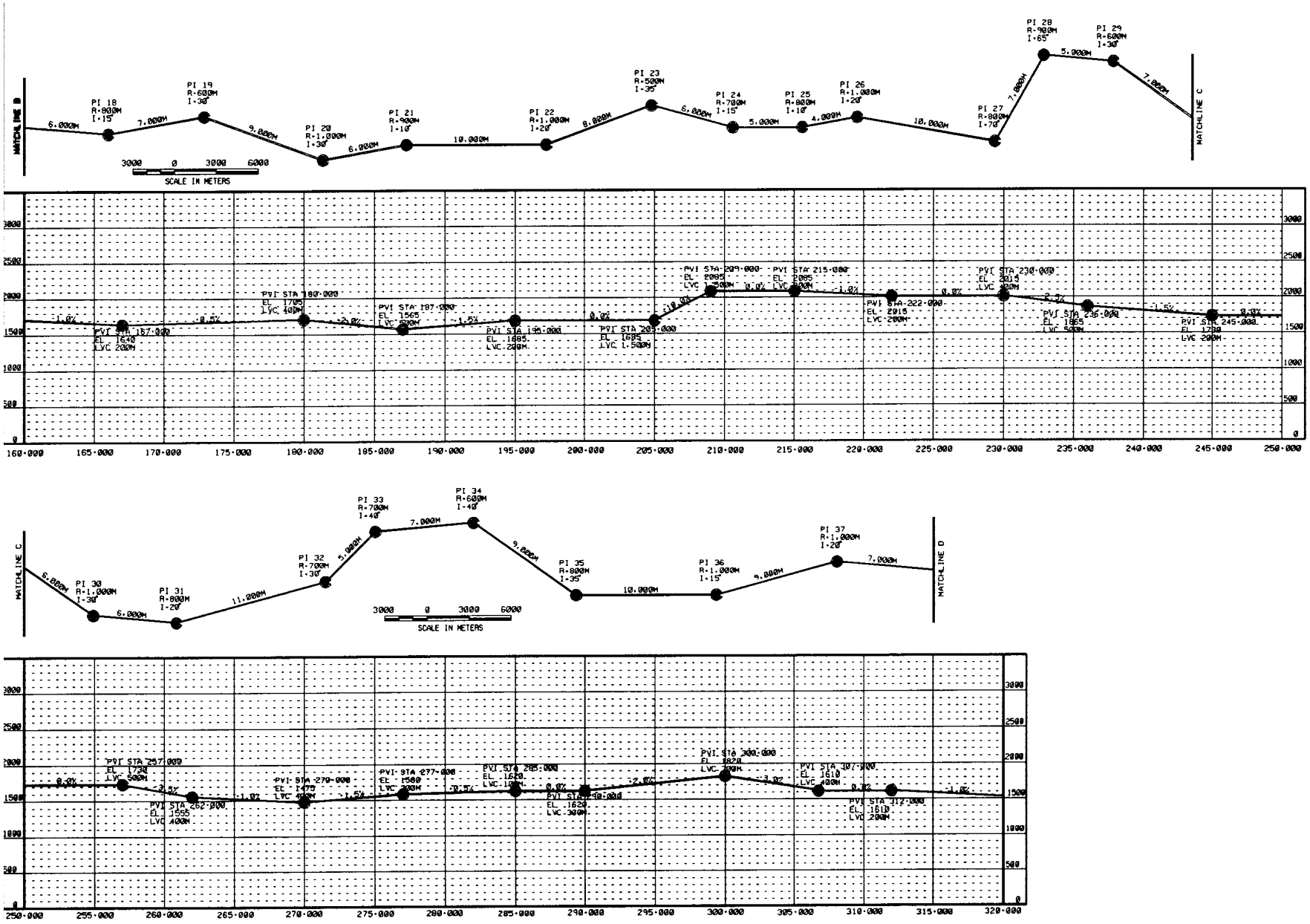

b. 160–320 km.

Figure 106 (cont'd)

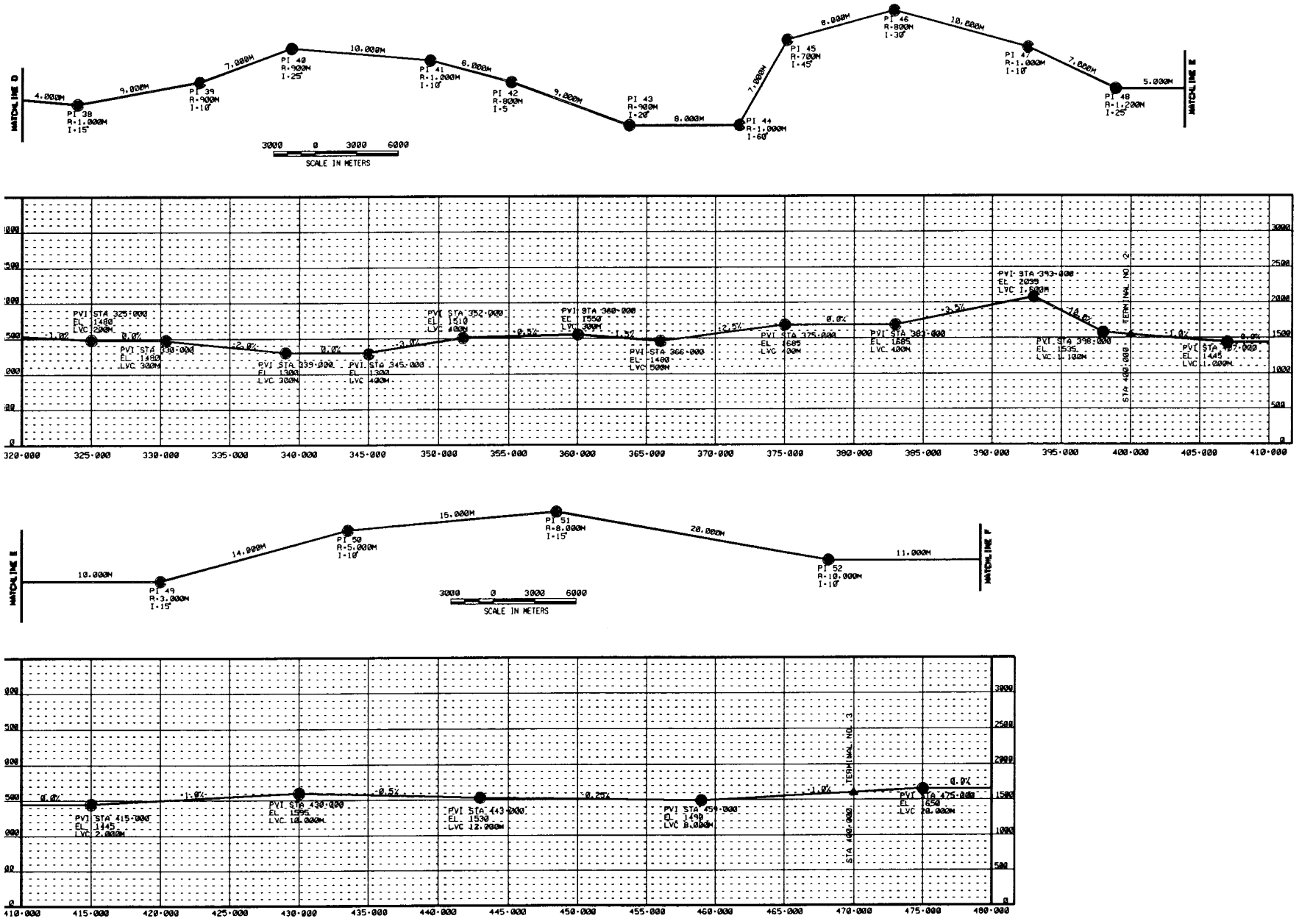

c. 320–480 km.

Figure 106 (cont'd). Severe segment test (SST) route.

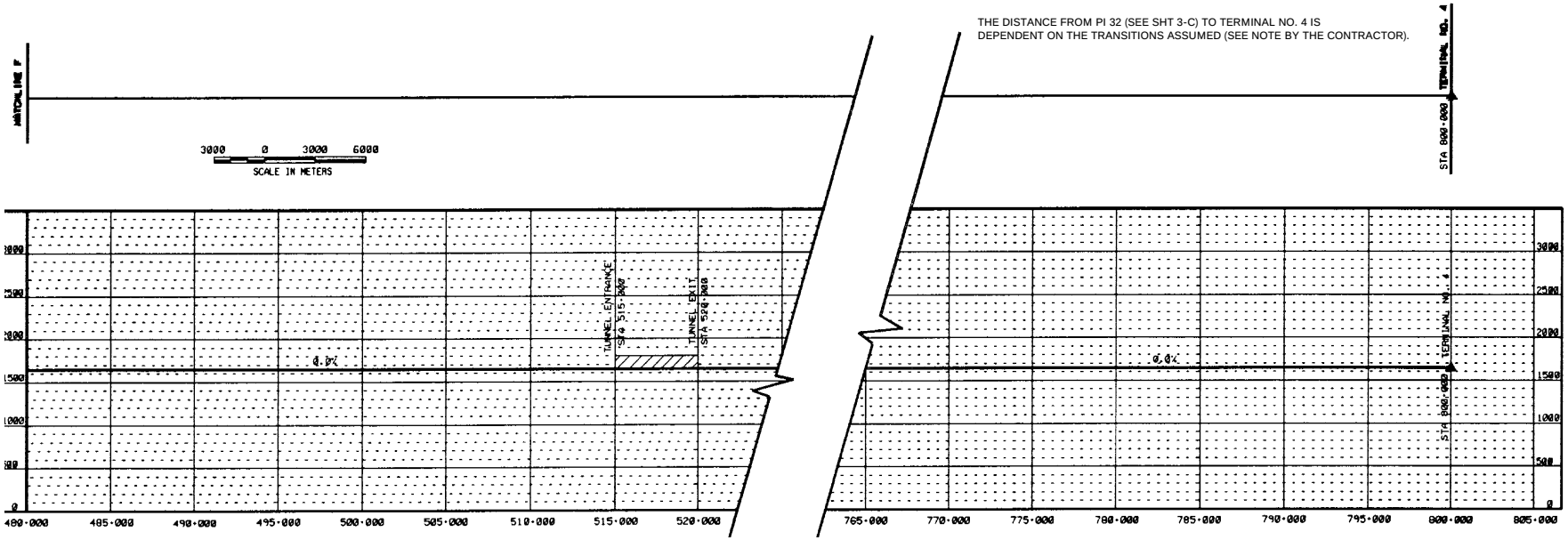

Notes:

1. Numerical data are based on the International System of Units (SI). Stationing, distances, and elevations shown are in meter units.
2. The alignment shown is for guideway centerline.
3. The contractor is restricted to the horizontal and vertical curve data indicated but shall assume transitions as required to complement system performance.
4. The vertical curve data provided are based on equal-distance tangents.
5. The elevations indicated in profile are provided for computation of grades only and are not referenced to a specific vertical datum. The contractor shall assume an atmospheric pressure of one atmosphere at all points along the guideway centerline.
6. Acronyms are defined as follows:

PI = Point of intersection of tangents
R = Radius of curvature
I = Deflection angle between tangents
LVC = Length of vertical curve
PVI = Point of vertical intersection of tangents

d. 480–805 km.

Figure 106 (cont'd)

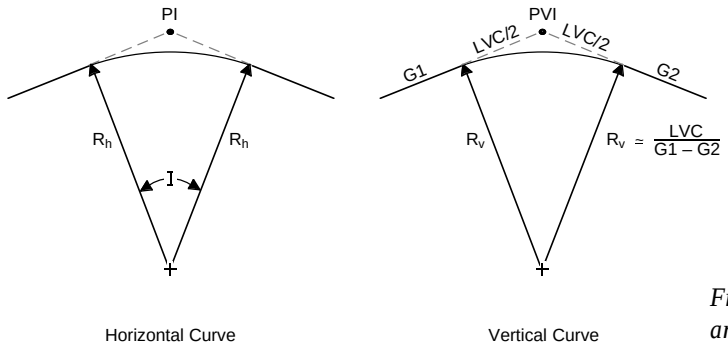

Figure 107. Notation for horizontal and vertical curves for SST route.

each point of intersection. The vertical profile specifies the distance along tangents between points of vertical intersection (PVI), and for each PVI, the elevation, the entering and exiting grades (G1 and G2), and the length of vertical curve (LVC) measured along tangents. Figure 107 shows these curve details. Note that vertical radius of curvature (RV) approximately equals LVC / (G1–G2). The SST consists of 52 PI's and 56 PVI's, of which six are combined horizontal and vertical curves. The SST instructions did not specify the proportion of total turning angle or grade change within the transition sections leading to or away from a curve. However, the vehicle must transit at least a portion of the curve at the given curve radius. Also, the vehicle must stop at each terminal before continuing along the route. We did not simulate the 5-km-long tunnel in segment 3 of the SST because its effects should be small and essentially independent of which system is used.

Table 39. Ride comfort guidelines for curving performance (maximum values for event, i.e., spiral or curve).

	Design goal	*Minimum requirements*	*Seated–belted*
Lateral curves			
Bank angle (deg)	24	30	45
Roll rate (deg / s)	5		10
Lateral (g's)	0.1	0.16	0.2
Roll acceleration (deg / s^2)	15		
Vertical curves			
Vertical (up) (g's)	0.05	0.1	0.1
Vertical (down) (g's)	0.2	0.3	0.4
Acceleration and braking			
Normal (g's)	0.16	0.2	0.6
Vector combinations			
Lateral / longitudinal (g's)	0.2	0.3	0.6
Lateral / vertical (g's)	0.2	0.3	0.4
Total (g's)	0.24	0.36	0.6
Jerk (g's/s filtered at 0.3 Hz) or Jolt (peak to peak g's in 1 s)			
Lateral	0.07	0.25	0.25
Vertical	0.1	0.3	0.3
Longitudinal	0.07	0.25	0.25

Ride comfort guidelines

The motion of a maglev vehicle along a practical route will subject the passengers to a variety of motions arising from acceleration, curving, and braking. Ride comfort guidelines describe the set of maximum rigid-body motions acceptable to passengers under various conditions. On 16 December 1991, a Ride Quality Workshop was held that developed ride comfort guidelines for the SCD contractors to use in their study of the SST. Table 39 summarizes the three sets of guidelines established (see also Appendix A). Design goal (DG) criteria were based on ride comfort values known to be acceptable to passengers when standing and walking in a moving vehicle. Minimum requirement (MR) criteria reflect marginally acceptable conditions for standing and walking passengers. Seated–belted (SB) criteria represent motions acceptable for passengers that are seated and belted. We conducted system simulations only for the DG criteria. These represent the most conservative guidelines in terms of the performance of the vehicle and the comfort of the passengers.

System simulator: SSTSIM

The simulation software, SSTSIM, solves the time-domain equations of motion for a given vehicle at each point along the guideway. It uses two sets of inputs: 1) the SST route characteristics (location of each curve or terminal, entering and exiting grades, curve radius, and maximum allowable speed), and 2) the vehicle–LSM dynamic characteristics (vehicle mass, speed-dependent vehicle

resistance, LSM thrust, and LSM efficiency). Ride comfort criteria restrict the allowable longitudinal acceleration and braking rates and establish the maximum curve speeds.

Local coordinates. The ride comfort criteria refer to the local coordinate system of seated passengers. Local guideway grade, thus, influences allowable longitudinal accelerations. For example, the DG longitudinal acceleration limit is 0.16 g. This means that a vehicle can only accelerate up a 10% grade at 0.06 g to remain within the comfort limit. Conversely, the vehicle can accelerate down a 10% grade at 0.26 g without subjecting the passengers to more than 0.16 g. The influence is reversed for vehicle braking on grades. All vehicles simulated can brake at the local maximum rate dictated by ride comfort. However, net LSM thrust determines the achievable forward acceleration unless this value exceeds the local ride comfort limit.

Ride comfort criteria for lateral and vertical accelerations also refer to the local coordinate system. The SCDs use a combination of guideway superelevation (or cant) and vehicle tilt to increase curving speeds while remaining within these ride comfort limits. Tilt also gives the system the flexibility of stopping in a curve without exceeding acceptable ride-quality constraints.

Figure 108 shows a vector diagram for determining the local lateral and vertical accelerations in a compound horizontal and vertical curve. A force balance yields

$$A_{\text{lat}} = \frac{v^2}{gR_{\text{h}}}\cos\vartheta - \left(1 + \frac{v^2}{gR_{\text{v}}}\right)\sin\vartheta \qquad (15)$$

$$A_{\text{vert}} = \frac{v^2}{gR_{\text{h}}}\sin\vartheta + \left(1 + \frac{v^2}{gR_{\text{v}}}\right)\cos\vartheta \qquad (16)$$

where A_{lat} = local lateral acceleration (g's)
A_{vert} = local vertical acceleration (g's)
v = vehicle speed through curve
g = gravitational acceleration
R_{h} = horizontal radius of curvature
R_{v} = vertical radius of curvature (positive for upward curvature or trough)
ϑ = vehicle bank angle.

Primary ride comfort criteria. Equations 15 and 16 directly establish the maximum speeds allowable at the minimum radius in horizontal, vertical, and combined curves. Vector combinations of

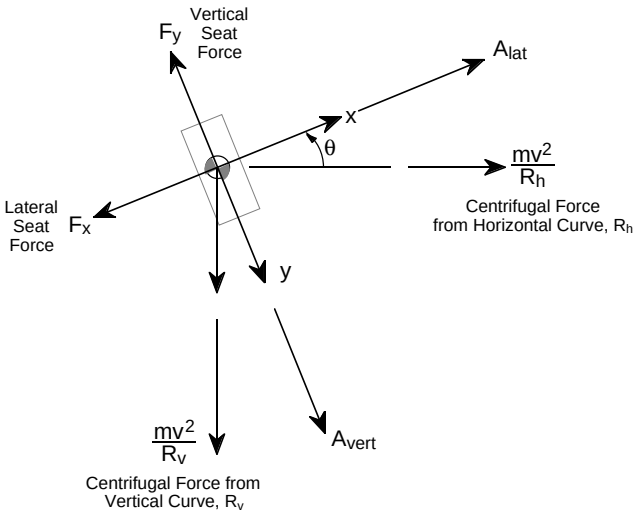

Figure 108. Lateral and vertical acceleration vectors.

accelerations, roll rates, roll accelerations, and jerks (changes in accelerations) can be similarly calculated. To minimize trip time, the vehicle should operate on the mathematical surface bounding the allowable motions. For the DG ride comfort level, a few key criteria actually dictate allowable vehicle motion, namely: lateral acceleration in horizontal or combined curves, vertical acceleration in vertical curves, and longitudinal acceleration–braking and longitudinal jerk during speed changes.

The lateral acceleration criterion establishes a speed limit v_{l} at the minimum radius in a horizontal curve via eq 15. Local vertical acceleration also occurs in a tilting vehicle on a horizontal curve. However, for DG and MR criteria, the speed limit from this cause is higher than v_{l}. Furthermore, transiting the given curve radius at v_{l} ensures that the vehicle satisfies the limits on combined lateral–vertical and total accelerations for DG and MR criteria.

As noted, the SST did not specify the length or shape of curve transition sections (called spirals for horizontal curves). Thus, the design of these sections can accommodate the secondary ride comfort criteria (roll rate, roll acceleration, and lateral and vertical jerks). In addition, it should be possible to vary radius and turning angle along the spiral so that the longitudinal acceleration–braking criterion always dictates the speed profile. A curve offset described by a fourth-degree polynomial appears to meet these requirements. That is, v_{l}, longitudinal acceleration–braking, and longitudinal jerk constitute the DG and MR ride comfort limits for horizontal curves.

The upward or downward vertical-acceleration criterion establishes a speed limit v_v at the minimum radius in a vertical curve via eq 16. Because vehicle tilting yields a negligible performance benefit in a vertical curve, v_v is system independent. For DG ride comfort criteria, v_v is less than 134 m/s for only 23 vertical curves in the SST (excluding combined horizontal–vertical curves) and all of these are cresting cases. The local grades entering and leaving vertical curves cause negligible reductions in the allowable vertical accelerations (applied in local coordinates). The DG and MR criteria for allowable total acceleration are met for all cresting curves by simply meeting the corresponding vertical acceleration limits. Because the vehicles can transit all trough curves at 134 m/s, they experience no additional longitudinal accelerations and thus also meet the total acceleration limits. As with horizontal curves, entry and exit guideway transitions can accommodate vertical jerk criteria. Therefore, v_v, longitudinal acceleration–braking, and longitudinal jerk constitute the DG and MR ride comfort limits for vertical curves.

Equations 15 and 16 can be used to compute the accelerations experienced in the six combined horizontal–vertical curves of the SST route. However, the vertical radii of curvature are all much longer than the horizontal radii, so that acceleration components resulting from the vertical radii can be neglected. If the vehicle transits the curve at speed v_l, computed as if the curve had only a horizontal radius, it easily satisfies the total acceleration criteria. Therefore, v_l, longitudinal acceleration–braking, and longitudinal jerk approximate the DG and MR ride comfort limits for combined curves.

SSTSIM algorithm. Use of the aforementioned set of primary ride comfort criteria simplifies the algorithm required for the simulations of interest here—vehicles traversing the SST route under DG ride comfort criteria. For each system, we computed the speed gates (i.e., the set of maximum vehicle speeds) for the horizontal and combined curves v_{li} from eq 15 using the maximum vehicle bank angle and neglecting the term for vertical curvature. We then combined these with the speed gates for the vertical curves v_{vi}, from eq 16 using zero bank angle, and the required terminal stops, both of which are system independent. Table 40 shows the speed gate file for the SST; cruise speed (134 m/s) is the target speed between speed gates. This speed profile, combined with the longitudinal acceleration–braking limit of 0.16 g (modified by local guideway grade) and the longitudinal jerk limit of 0.07 g/s, establish the kinematic constraints for the SST (maximum speed, acceleration, braking rate, and jerk allowed at each position or time). We set gravitational acceleration g equal to 9.80 m/s^2, a value appropriate for most of the U.S.

Because the performance objective is to minimize trip time, all vehicles accelerate at the system's maximum LSM thrust for that speed, and braking and roll-off and roll-on jerks occur at the ride comfort limits. At each time step, the algorithm computes the distance required to brake from the current speed to the next speed gate. If this distance is less than the distance available, the vehicle follows the local kinematic constraints (acceleration to, or continued motion at, cruise speed); otherwise, the vehicle begins to brake for the speed gate. The algorithm automatically handles acceleration through a speed gate by including a roll-off to zero acceleration, one time step at the gate speed, and roll-on back to maximum acceleration. For a few cases where a low-speed gate closely follows a high-speed gate, the braking path to the low-speed gate establishes the required brake point. In these cases, the vehicle brakes continuously through the high-speed gate at a speed typically well below the gate speed.

Energy consumption during accelerations (including associated roll-on and roll-off jerks) is calculated at maximum-thrust conditions. Energy consumption during cruise periods is calculated for normal-thrust conditions (LSM thrust equal to vehicle resistance); energy consumption is zero during braking. Although regenerative braking is possible with most maglev concepts, we did not include it here. Regenerative braking would lower energy consumption along the SST. SSTSIM calculates energy consumption for each system at the outputs of the converter stations (i.e., the inputs to the LMSs). For subsequent calculations of system energy intensity, based on energy supplied from an electric utility, we manually applied speed-independent converter station efficiencies to the SSTSIM results.

Simulation results (speed profile, trip time, and energy consumption) were not sensitive to time steps between 0.1–0.01 s, and we used 0.1 s for most runs. Overshoots of speed gates were typically less than 0.05 m/s and 10 m, adequate for these simulations. The algorithm reset the vehicle at the gate speed and position to remove any cumulative advantage of overshoots.

SSTSIM does not design guideway curves or

Table 40. Speed gate file for the SST route.

Point of intersection (neg. = PVI)	*Station (m)*	*Speed gate (m/s) (12° bank)*	*Speed gate (m/s) SCDs (24° bank)*	*Length of vertical curve (m)*	*Entering grade, G1*	*Exiting grade, G2*
Terminal 1	0.0	0.0	0.0	0.0	0.000	0.035
1.0000	9,000.0	35.2	46.6	—	0.035	0.035
–1.0000	10,000.0	79.0	79.0	700.0	0.035	–0.020
2.0000	16,000.0	39.3	52.1	—	–0.020	–0.020
–2.0000	17,000.0	161.7	161.7	600.0	–0.020	0.025
3.0000	22,000.0	46.5	61.7	—	0.025	0.025
–3.0000	25,000.0	140.0	140.0	600.0	0.025	0.010
4.0000	33,000.0	55.5	73.7	—	0.010	0.010
–4.0000	35,000.0	99.0	99.0	200.0	0.010	0.000
5.0000	40,000.0	43.0	57.1	1500.0	0.000	–0.100
–6.0000	44,000.0	171.5	171.5	1500.0	–0.100	0.000
–7.0000	50,000.0	99.0	99.0	200.0	0.000	–0.010
6.0000	54,000.0	49.7	65.9	—	–0.010	–0.010
–8.0000	60,000.0	85.7	85.7	300.0	–0.010	–0.030
7.0000	62,000.0	43.0	57.1	—	–0.030	–0.030
–9.0000	66,000.0	161.7	161.7	400.0	–0.030	0.000
8.0000	72,000.0	52.7	69.9	—	0.000	0.000
–10.000	75,000.0	80.8	80.8	200.0	0.000	–0.015
9.0000	81,000.0	55.5	73.7	500.0	–0.015	0.020
–12.000	95,000.0	76.7	76.7	300.0	0.020	–0.005
10.000	96,000.0	43.0	57.1	—	–0.005	–0.005
11.000	101,000.0	39.3	52.1	—	–0.005	–0.005
–13.000	105,000.0	156.5	156.5	500.0	–0.005	0.035
12.000	107,000.0	43.0	57.1	—	0.035	0.035
–14.000	114,000.0	83.7	83.7	500.0	0.035	0.000
13.000	117,000.0	49.7	65.9	—	0.000	0.000
14.000	124,000.0	46.5	61.7	—	0.000	0.000
–15.000	125,000.0	80.8	80.8	200.0	0.000	–0.015
15.000	132,000.0	46.4	61.7	100.0	–0.015	–0.020
–17.000	142,000.0	171.5	171.5	300.0	–0.020	0.000
16.000	144,000.0	55.5	73.7	—	0.000	0.000
–18.000	147,000.0	198.0	198.0	200.0	0.000	0.010
17.000	154,000.0	55.5	73.7	—	0.010	0.010
–19.000	155,000.0	85.7	85.7	300.0	0.010	–0.010
18.000	166,000.0	49.7	65.9	—	–0.010	–0.010
–20.000	167,000.0	161.7	161.7	200.0	–0.010	0.005
19.000	173,000.0	43.0	57.1	—	0.005	0.005
–21.000	180,000.0	88.5	88.5	400.0	0.005	–0.020
20.000	182,000.0	55.5	73.7	—	–0.020	–0.020
–22.000	187,000.0	167.3	167.3	500.0	–0.020	0.015
21.000	188,000.0	52.7	69.9	—	0.015	0.015
–23.000	195,000.0	80.8	80.8	200.0	0.015	0.000
22.000	198,000.0	55.5	73.7	—	0.000	0.000
–24.000	205,000.0	171.5	171.5	1500.0	0.000	0.100
23.000	206,000.0	39.3	52.1	—	0.100	0.100
–25.000	209,000.0	85.7	85.7	1500.0	0.100	0.000
24.000	212,000.0	46.5	61.7	—	0.000	0.000
–26.000	215,000.0	99.0	99.0	200.0	0.000	–0.010
25.000	217,000.0	49.7	65.9	—	–0.010	–0.010
26.000	221,000.0	55.5	73.7	—	–0.010	–0.010
–27.000	222,000.0	198.0	198.0	200.0	–0.010	0.000
–28.000	230,000.0	88.5	88.5	400.0	0.000	–0.025
27.000	231,000.0	49.7	65.9	—	–0.025	–0.025
–29.000	236,000.0	313.0	313.0	500.0	–0.025	–0.015
28.000	238,000.0	52.7	69.9	—	–0.015	–0.015
29.000	243,000.0	43.0	57.1	—	–0.015	–0.015
–30.000	245,000.0	161.7	161.7	200.0	–0.015	0.000
30.000	256,000.0	55.5	73.7	—	0.000	0.000
–31.000	257,000.0	83.7	83.7	500.0	0.000	–0.035
31.000	262,000.0	49.7	65.9	400.0	–0.035	–0.010
–33.000	270,000.0	177.1	177.1	400.0	–0.010	0.015
32.000	273,000.0	46.5	61.7	—	0.015	0.015

Table 40 (cont'd). Speed gate file for the SST route.

Point of intersection (neg. = PVI)	*Station (m)*	*Speed gate (m/s) (12° bank)*	*Speed gate (m/s) SCDs (24° bank)*	*Length of vertical curve (m)*	*Entering grade, G1*	*Exiting grade, G2*
–34.000	277,000.0	99.0	99.0	200.0	0.015	0.005
33.000	278,000.0	46.5	61.7	—	0.005	0.005
34.000	285,000.0	43.0	57.1	100.0	0.005	0.000
–36.000	290,000.0	171.5	171.5	300.0	0.000	0.020
35.000	294,000.0	49.7	65.9	—	0.020	0.020
–37.000	300,000.0	82.8	82.8	700.0	0.020	–0.030
36.000	304,000.0	55.5	73.7	—	–0.030	–0.030
–38.000	307,000.0	161.7	161.7	400.0	–0.030	0.000
–39.000	312,000.0	99.0	99.0	200.0	0.000	–0.010
37.000	313,000.0	55.5	73.7	—	–0.010	–0.010
38.000	324,000.0	55.5	73.7	—	–0.010	–0.010
–40.000	325,000.0	198.0	198.0	200.0	–0.010	0.000
–41.000	330,000.0	85.7	85.7	300.0	0.000	–0.020
39.000	333,000.0	52.7	69.9	—	–0.020	–0.020
–42.000	339,000.0	171.5	171.5	300.0	–0.020	0.000
40.000	340,000.0	52.7	69.9	—	0.000	0.000
–43.000	345,000.0	161.7	161.7	400.0	0.000	0.030
41.000	350,000.0	55.5	73.7	—	0.030	0.030
–44.000	352,000.0	88.5	88.5	400.0	0.030	0.005
42.000	356,000.0	49.7	65.9	—	0.005	0.005
–45.000	360,000.0	85.7	85.7	300.0	0.005	–0.015
43.000	365,000.0	52.7	69.9	—	–0.015	–0.015
–46.000	366,000.0	156.5	156.5	500.0	–0.015	0.025
44.000	373,000.0	55.5	73.7	—	0.025	0.025
–47.000	375,000.0	88.5	88.5	400.0	0.025	0.000
45.000	380,000.0	46.5	61.7	—	0.000	0.000
–48.000	383,000.0	149.7	149.7	400.0	0.000	0.035
46.000	388,000.0	49.7	65.9	—	0.035	0.035
–49.000	393,000.0	76.2	76.2	1600.0	0.035	–0.100
47.000	398,000.0	55.5	73.7	1100.0	–0.100	–0.010
Terminal 2	400,000.0	0.0	0.0	—	–0.010	–0.010
48.000	405,000.0	60.8	80.8	—	–0.010	–0.010
–51.000	407,000.0	442.7	442.7	1000.0	–0.010	0.000
–52.000	415,000.0	626.1	626.1	2000.0	0.000	0.010
49.000	420,000.0	96.2	127.7	—	0.010	0.010
–53.000	430,000.0	571.5	571.5	10,000.0	0.010	–0.005
50.000	434,000.0	124.2	164.9	—	–0.005	–0.005
–54.000	443,000.0	3067.2	3067.2	12,000.0	–0.005	–0.002
51.000	449,000.0	157.1	208.5	—	–0.002	–0.002
–55.000	459,000.0	1120.0	1120.0	8000.0	–0.002	0.010
52.000	469,000.0	175.6	233.1	—	0.010	0.010
Terminal 3	470,000.0	0.0	0.0	—	0.010	0.010
–56.000	475,000.0	989.9	989.9	20,000.0	0.010	0.000
Terminal 4	800,000.0	0.0	0.0	—	0.000	0.000

transition spirals because these relate to secondary ride comfort criteria neglected in our approximations. Consequently, SSTSIM does not calculate guideway offsets (i.e., ROW requirements). However, these are not strongly system dependent. The SST requirement of traversing a portion of the curve at the specified minimum radius is met by establishing the speed gates, as described above.

Thrust, efficiency, and resistance. Section 3.2.2 presents our analysis of the linear synchronous motors used by TR07 and the four SCDs. The tables in that section show LSM thrust and efficiency vs. vehicle speed for the two conditions of interest here: maximum thrust and normal thrust. SSTSIM uses these data in a series of lookup tables to determine the LSM thrust and efficiency at each time step, using linear interpolation between the speeds tabulated. The tables in section 3.2.2 also show calculated vehicle resistance (air and magnetic drag) vs. speed. For completeness, the resistance lookup tables used in SSTSIM also include drag induced by the linear generators used to transfer hotel power (significant only at speeds below about 50 m/s). Table 41 shows the SSTSIM

Table 41. LSM and resistance data used in SSTSIM.

Condition	*Speed (m/s)*	*Thrust (kN)*	*Efficiency*	*Resistance (kN)*
	a. TR07. Vehicle mass is 106,000 kg.			
Cruise	134.00	61.800	0.88000	61.800
Maximum thrust	0.0000	110.20	0.0010000	10.300
	1.0000	110.20	0.030000	10.300
	10.000	110.20	0.23000	10.800
	15.000	110.20	0.31000	11.300
	20.000	110.20	0.38000	11.900
	30.000	110.20	0.48000	13.700
	40.000	110.20	0.55000	15.800
	50.000	110.20	0.60000	16.900
	60.000	110.20	0.64000	19.100
	60.500	109.80	0.65000	19.300
	70.000	101.40	0.70000	22.400
	80.000	94.000	0.74000	26.700
	90.000	87.600	0.77000	31.800
	100.00	82.200	0.80000	37.700
	110.00	77.400	0.83000	44.200
	120.00	73.200	0.85000	51.200
	130.00	69.400	0.86000	58.700
	134.00	68.000	0.87000	61.800
	b. Bechtel. Vehicle mass is 63,300 kg.			
Cruise	134.0	50.9	0.942	50.9
Maximum thrust	0.0	143.0	0.001	10.5
	1.0	143.0	0.030	10.8
	10.0	143.0	0.306	13.2
	15.0	143.0	0.398	14.4
	20.0	143.0	0.468	15.4
	30.0	143.0	0.569	17.3
	40.0	143.0	0.638	18.9
	50.0	143.0	0.688	20.5
	60.0	143.0	0.726	22.2
	70.0	143.0	0.755	24.1
	80.0	143.0	0.779	26.4
	90.0	143.0	0.799	29.1
	100.0	143.0	0.815	32.5
	110.0	143.0	0.829	36.7
	111.8	143.0	0.831	37.6
	120.0	136.6	0.847	41.9
	130.0	129.4	0.863	48.1
	134.0	126.8	0.869	50.9
	c. Foster-Miller. Vehicle mass is 72,700 kg.			
Cruise	134.0	48.0	0.964	48.0
Maximum thrust	0.0	125.8	0.006	7.2
	10.0	125.8	0.920	7.6
	15.0	125.8	0.940	10.3
	20.0	125.8	0.950	13.7
	26.0	125.8	0.955	15.4
	30.0	125.8	0.956	15.7
	40.0	125.8	0.957	17.4
	50.0	125.8	0.955	19.2
	60.0	125.8	0.952	21.3
	70.0	125.8	0.948	23.5
	80.0	125.8	0.944	26.1
	83.5	125.8	0.943	27.1
	90.0	117.0	0.943	29.0
	100.0	105.5	0.944	32.4
	110.0	95.9	0.945	36.3
	120.0	88.2	0.945	40.7
	130.0	81.4	0.946	45.8
	134.0	79.0	0.946	48.0
	d. Grumman. Vehicle mass is 61,200 kg.			
Cruise	134.0	31.0	0.820	31.0
Maximum thrust	0.0	60.0	0.001	4.1
	1.0	60.0	0.015	4.1
	10.0	60.0	0.149	4.3
	15.0	60.0	0.208	4.5
	20.0	60.0	0.260	4.7
	25.0	60.0	0.305	5.1
	30.0	60.0	0.345	5.5
	40.0	60.0	0.412	6.7
	50.0	60.0	0.467	8.1
	60.0	60.0	0.513	9.9
	70.0	60.0	0.551	11.5
	80.0	60.0	0.584	13.5
	90.0	60.0	0.612	16.0
	100.0	60.0	0.637	18.8
	110.0	60.0	0.659	22.0
	120.0	60.0	0.678	25.5
	130.0	60.0	0.695	29.4
	134.0	60.0	0.701	31.0
	e. Magneplane. Vehicle mass is 48,000 kg.			
Cruise	134.0	37.6	0.884	37.6
Maximum thrust	0.0	150.0	0.000	35.1
	1.0	150.0	0.012	35.1
	10.0	150.0	0.124	35.2
	15.0	150.0	0.175	35.3
	20.0	150.0	0.221	35.5
	30.0	150.0	0.299	36.0
	32.0	150.0	0.312	57.3
	35.0	150.0	0.332	54.9
	40.0	150.0	0.362	51.4
	45.0	150.0	0.390	48.3
	50.0	150.0	0.415	47.9
	52.0	144.2	0.434	46.5
	60.0	125.0	0.505	41.9
	70.0	107.1	0.582	38.1
	80.0	93.8	0.645	35.9
	90.0	83.3	0.697	34.8
	100.0	75.0	0.739	34.4
	110.0	68.2	0.774	34.7
	120.0	62.5	0.803	35.6
	130.0	57.7	0.827	36.9
	134.0	56.0	0.836	37.6

lookup tables for all systems, and Figure 109 shows the corresponding plots for maximum thrust conditions.

Analytical validation. We validated SSTSIM by comparing its results with 1) analytical approximations for motion along a straight and flat guideway, and 2) numerical results generated using the program MPS, previously used by the GMSA Team for system simulations.

The one-dimensional momentum and energy equations for motion along a straight, flat guideway are

$$T - R = ma \tag{17}$$

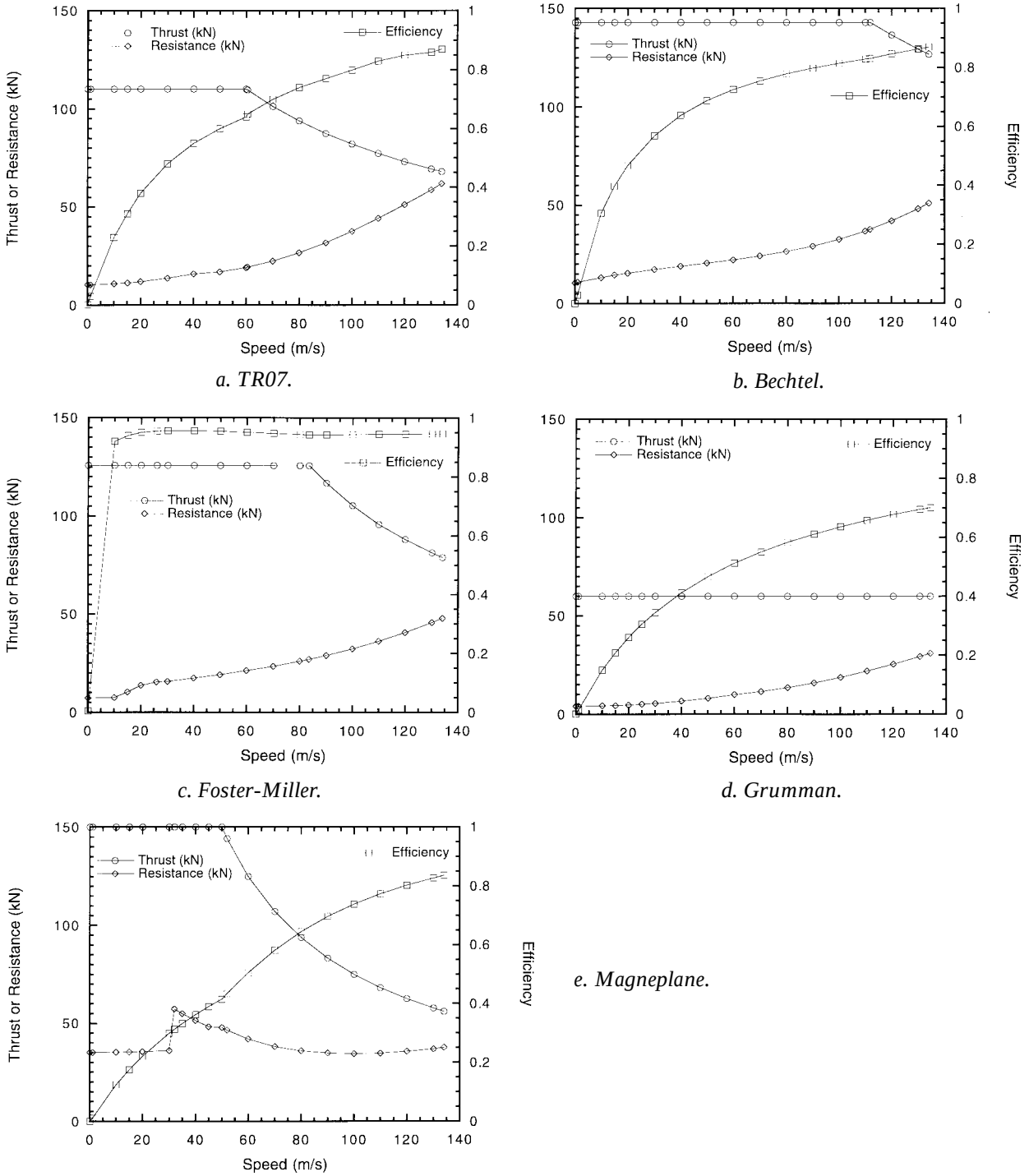

a. TR07.

b. Bechtel.

c. Foster-Miller.

d. Grumman.

e. Magneplane.

Figure 109. LSM and vehicle resistance vs. speed.

Table 42. Electrical energy (kWh) input to each LSM to accelerate the maglev vehicle from zero to 134 m/s. Normalization by the number of standard passengers (SP) corrects for differences in the space allocated per passenger in each vehicle.

E_{0-134}	*TR07*	*Bechtel*	*Foster-Miller*	*Grumman*	*Magneplane*
Equation 21	857	273	293	396	379
SSTSIM	852	278	293	397	382
E_{0-134} / SP	5.4	2.5	2.1	3.3	3.5

$$P = Tv \tag{18}$$

where T = LSM thrust
R = vehicle resistance
m = vehicle mass
a = vehicle acceleration
P = mechanical power provided by LSM
v = vehicle velocity.

Mechanical power provided by the LSM is related to the required electrical power P_e via the LSM efficiency η:

$$P = \eta P_e \ . \tag{19}$$

Combining these three equations and integrating yields the electrical energy required to move the vehicle:

$$E_{1-2} = \int_1^2 \frac{mv}{\eta}\, dv + \int_1^2 \frac{Rv}{\eta}\, dt \ . \tag{20}$$

The first integral is the electrical energy needed to accelerate the vehicle and the second is the electrical energy needed to overcome vehicle resistance (e.g., air and magnetic drag). If the vehicle is accelerating ($a > 0$), the second integral can also be expressed in terms of the change in velocity, $dv = adt$, to yield

$$E_{1-2} = m \int_{v_1}^{v_2} \frac{1}{\eta}\left[1 + \frac{1}{T/R - 1}\right] dv \ . \tag{21}$$

The two terms in the integral retain the same interpretations as in eq 20. For the maglev systems studied here, these terms are functions of velocity only. Note that the resistance contribution to E_{1-2} is small if thrust is much larger than resistance. That is, for a given change in velocity, the LSM will supply less energy to overcome vehicle resistance if the velocity changes quickly. The LSM efficiency as a function of velocity affects both terms in eq 21. To minimize trip time, acceleration occurs at maximum thrust, where efficiency is lowest. Thus, η has a strong influence on E_{1-2}.

Table 42 compares electrical energy required to accelerate each maglev vehicle from zero to 134 m/s calculated from eq 21 and obtained from SSTSIM (for the case of unconstrained acceleration). The deviations are small and attributable to numerical integration errors. Even allowing for differences in standard passengers (SP) carried, TR07 requires about twice the energy to accelerate to cruise speed as the SCD vehicles because its slow acceleration results in more time spent at inefficient, maximum thrust conditions.

We may calculate the trip time and energy consumption for a vehicle traveling along a straight and flat route if the speed profile is known. Figure 110 shows vehicle speed vs. time for straight and flat travel at the ride comfort limits. The Bechtel SCD can approximate this speed profile because it can accelerate at 0.16 g until it reaches about 120 m/s. Although its maximum acceleration drops to 0.12 g at 134 m/s, this adds only about 1 s to the time required to accelerate the vehicle to

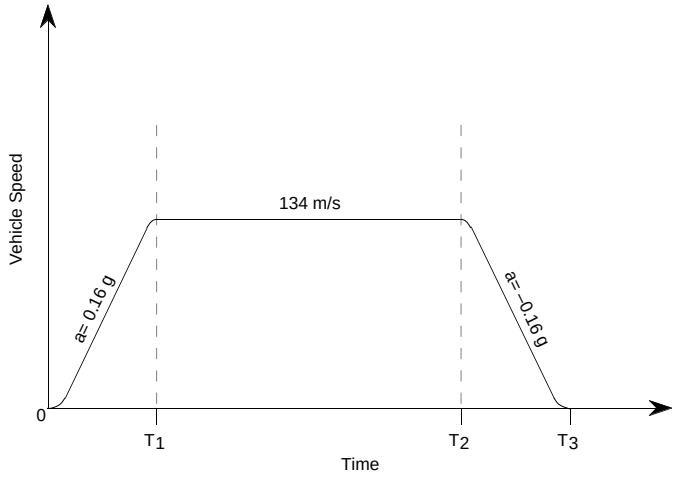

Figure 110. Vehicle speed profile along straight and flat route at ride comfort limits. Jerk limits require acceleration roll-on and roll-off at 0.07 g/s.

Table 43. Incremental time, distance, and energy required for the Bechtel vehicle to traverse a 40-km straight and flat route. Analytical results are for motion at the ride comfort limits.

	Time interval (s)		*Guideway length (m)*		*Energy used (kWh)*	
Phase	*Analytical*	*SSTSIM*	*Analytical*	*SSTSIM*	*Analytical*	*SSTSIM*
Acceleration	87.7	89.0	5,879	6,032	273	278*
Steady cruise	210.8	209.6	28,242	28,100	424	422
Braking	87.7	87.8	5,879	5,872	0	0
Total	386.2	386.4	40,000	40,004	697	700

* SSTSIM energy is for unconstrained acceleration, to compare with analytical value.

cruise speed. Table 43 compares analytical and SSTSIM results for the Bechtel vehicle to cover a 40-km straight and flat route. Allowing for the slightly longer time and distance required for the vehicle to accelerate to cruise speed, the results show excellent agreement. Because SSTSIM computes a braking path that just crosses each speed gate, the vehicle slightly overshoots the terminal stop. Use of a smaller time step reduces this overshoot.

We also compared SSTSIM and analytical results (braking paths, acceleration profiles, energy increments) for travel between nonzero speed gates, including the effects of grade changes. In all cases, SSTSIM results were in excellent agreement with analytical values.

Validation using Maglev Performance Simulator (MPS). The GMSA Team originally used a software package called Maglev Performance Simulator (MPS). Developed by J.E. Anderson Associates, MPS is a suite of eight programs that accepts as inputs the vehicle and LSM technical characteristics, the SST route alignment, and the ride comfort constraints. Like SSTSIM, it attempts to determine the acceleration and speed profiles that allow a vehicle to traverse the SST route in minimum trip time within these constraints. Unlike SSTSIM, however, MPS does not approximate the ride comfort requirements but rather designs each curve (three-dimensional entry and exit spirals) to ensure that the vehicle satisfies all ride comfort constraints.

The comprehensive MPS proved difficult to validate. In particular, the scheme to optimize curve designs did not always result in minimum trip time (e.g., very small increases in trip time could result when a secondary criterion such as lateral jerk was relaxed). That is, the vehicle always satisfied the ride comfort criteria through each curve but it didn't necessarily follow the bounding mathematical envelop defined by the ride comfort criteria. This is a minor shortcoming, and we may compare MPS results with those from SSTSIM to assess the validity of the latter, particularly the validity of approximating the ride comfort constraints.

SST simulations using the final version of MPS were completed only for TR07. The input LSM characteristics were slightly different from those shown in Table 41a, and the total tilt angle (i.e., guideway superelevation in TR07's case) was set at 11.2° rather than the actual value of 12°. Using these modified characteristics, we conducted SST simulations using SSTSIM and compared the results with those from MPS (see Table 44 and Figure 111). Deviations between the MPS and SSTSIM times and energies are typically within 0.5% everywhere along the SST route. Because MPS is entirely independent software, this confirms the validity of SSTSIM.

System comparisons using SSTSIM

We used SSTSIM to simulate the performance of TR07 and the four SCDs along the 40-km

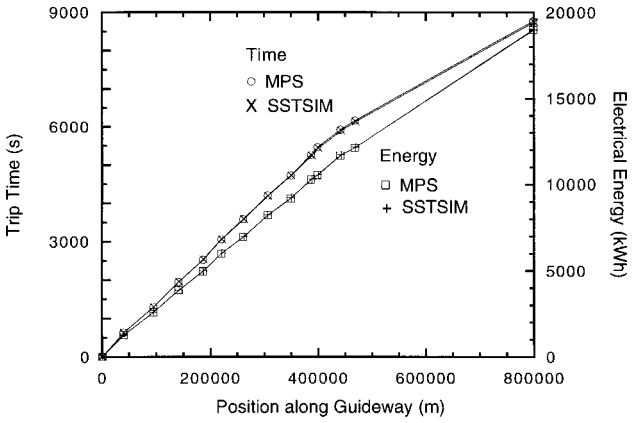

Figure 111. Comparison of SST results for TR07 simulated using SSTSIM and MPS with identical LSM and vehicle characteristics.

Table 44. Comparison of SSTSIM results with MPS results for TR07 using identical LSM and vehicle characteristics.

Location	*Position MPS (m)*	*Position SSTSIM (m)*	*Deviation (%)*	*Time MPS (s)*	*Time SSTSIM (s)*	*Deviation (%)*	*Energy MPS (kWh)*	*Energy SSTSIM (kWh)*	*Deviation (%)*
Terminal 0 (Gate 1)	0	0		0	0		0	0	
Gate 10	39,900	40,004	0.3	637	641	0.6	1,270	1,268	–0.2
Gate 20	94,731	95,007	0.3	1305	1305	0.0	2,583	2,584	0.0
Gate 30	141,179	142,002	0.6	1955	1963	0.4	3,862	3,880	0.5
Gate 40	186,082	187,003	0.5	2534	2538	0.2	4,966	4,989	0.5
Gate 50	220,088	221,005	0.4	3070	3066	–0.1	5,994	6,011	0.3
Gate 60	260,702	262,005	0.5	3595	3596	0.0	6,949	6,982	0.5
Gate 70	306,076	307,002	0.3	4208	4206	0.0	8,207	8,234	0.3
Gate 80	348,547	350,005	0.4	4735	4734	0.0	9,180	9,227	0.5
Gate 90	386,337	388,005	0.4	5274	5253	–0.4	10,290	10,296	0.1
Terminal 2 (Gate 93)	398,334	400,000	0.4	5473	5447	–0.5	10,530	10,547	0.2
Gate 100	441,295	443,008	0.4	5925	5905	–0.3	11,680	11,705	0.2
Terminal 3 (Gate 104)	468,294	470,000	0.4	6169	6144	–0.4	12,130	12,146	0.1
Terminal 4 SST Total	**798,294**	**800,000**	**0.2**	**8779**	**8758**	**–0.2**	**19,000**	**19,019**	**0.1**
Segment 1	398,334	400,000	0.4	5473	5447	–0.5	10,530	10,547	0.2
Segment 2	69,960	70,000	0.1	696	697	0.1	1,600	1,599	–0.1
Segment 3	330,000	330,000	0.0	2610	2614	0.2	6,870	6,873	0.0

straight and flat route and along the SST route. Table 45 summarizes the trip times and LSM energy consumption for these cases.

Figure 112 shows the speed profiles for each system along the 40-km straight and flat route. The SCDs all have much higher thrust/weight ratios than TR07, resulting in shorter distances (and times) to reach cruise speed (see also Table 45).

Figure 113 shows the speed profiles for the TR07 and Bechtel vehicles along the SST route. Results for the other SCDs are similar to the Bechtel results. The SCDs have the largest performance advantage along segment 1 (closely spaced curves) where their higher speed gates and greater acceleration capabilities result in much higher average speeds (see also Table 45). Figure 114 shows in more detail the speed profiles for

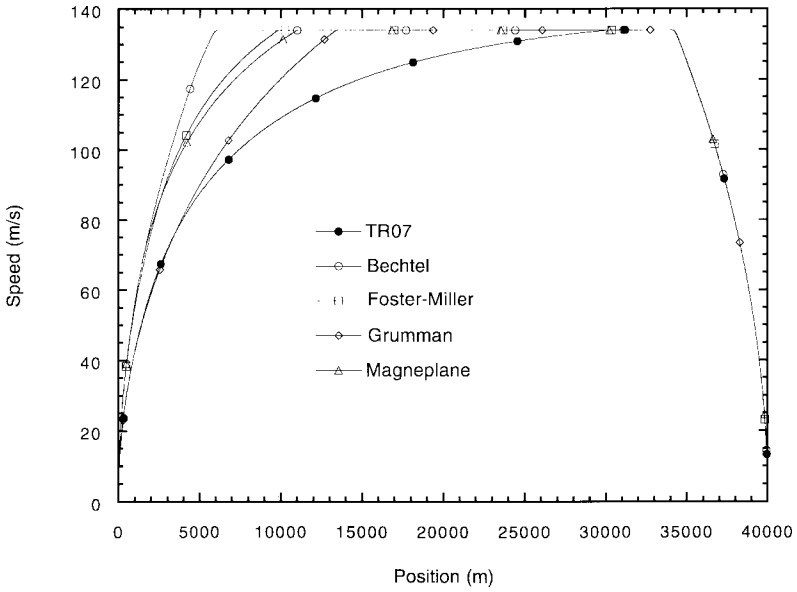

Figure 112. Speed profiles for TR07 and the four SCDs along a 40-km straight and flat route.

TR07 and Bechtel for the first 100 km of the SST. TR07's lower speed gates and lower maximum speeds between curves show more clearly (note that the speed gates for the two systems are equal only for vertical curves). As shown in Figure 115, TR07's longer acceleration periods at peak thrust cause its energy consumption to be higher for the same distance covered, even though its peak power is much lower than Bechtel's.

Table 46 compares the performance of the SCDs against that of TR07 for travel along the 40-km straight and flat and SST routes. Energy intensity (EI) is the electrical energy consumed by a system (i.e., the energy supplied by an electrical utility) to move a standard passenger 1 m along the given route section. Normalization by standard passengers (SP = 0.80 m^2 of vehicle floor area) corrects for differences in vehicle interior space allocated

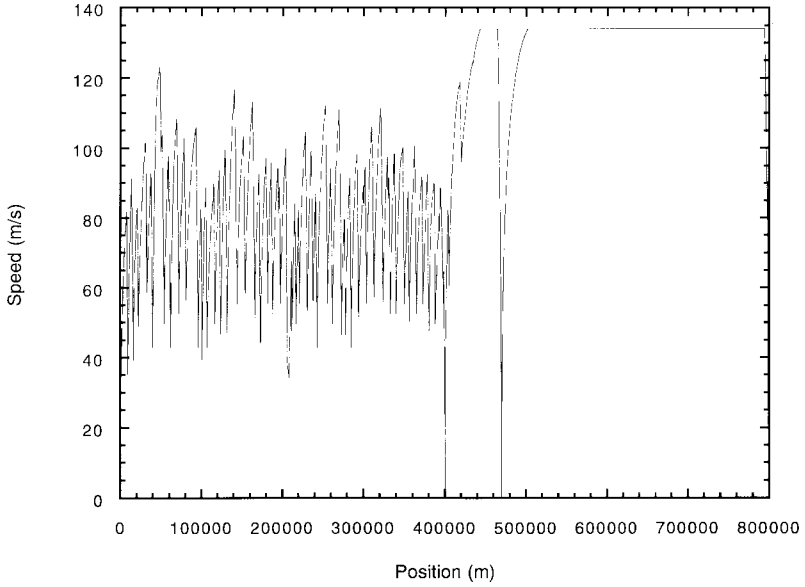

a. TR07.

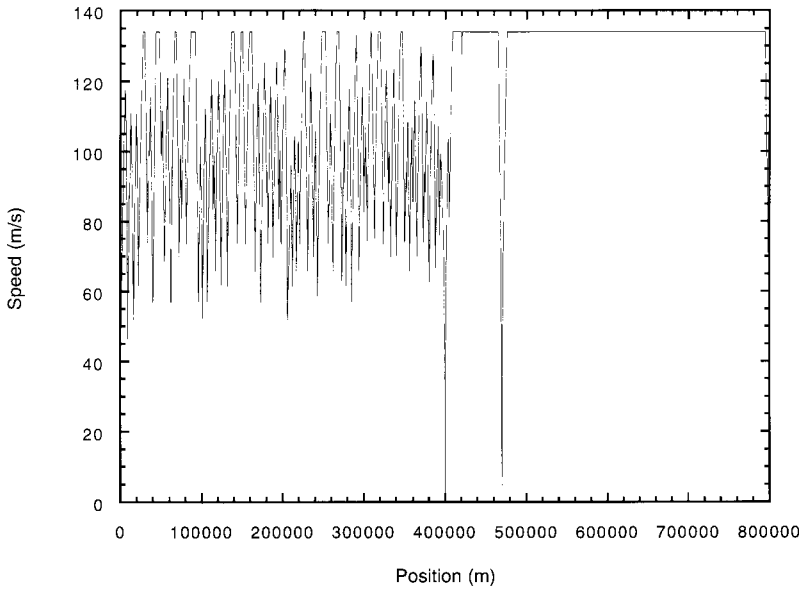

b. Bechtel vehicle.

Figure 113. Speed profiles along SST route.

Table 45. SSTSIM results for TR07 and SCDs along 40-km straight and flat and SST routes. TR07-24° is TR07 with 24° total bank angle (other characteristics unchanged). SST segment 1 is between terminals 1 and 2 (rugged terrain), SST segment 2 is between terminals 2 and 3 (rolling hills), and SST segment 3 is between terminals 3 and 4 (straight and nearly flat).

Item	*TR07*	*Bechtel*	*Foster-Miller*	*Grumman*	*Magneplane*	*TR07-24°*
Time (s)						
0–134 m/s straight and flat	318	89	123	182	133	318
40 km straight and flat	436	386	392	424	393	436
SST segment 1	5,318	4,244	4,359	4,669	4,399	4,762
SST segment 2	755	626	634	654	631	671
SST segment 3	2,607	2,555	2,558	2,596	2,563	2,607
SST total	8,680	7,425	7,551	7,919	7,593	8,040
LSM energy (kWh)						
0–134 m/s straight and flat	852	314	293	397	426	852
40 km straight and flat	930	736	629	614	698	930
SST segment 1	10,159	8,938	7,221	7,304	7908	9,492
SST segment 2	1,546	1,207	1,060	942	1,067	1,527
SST segment 3	6,606	5,095	4,649	3,679	4,138	6,607
SST total	18,311	15,240	12,930	11,925	13,113	17,626

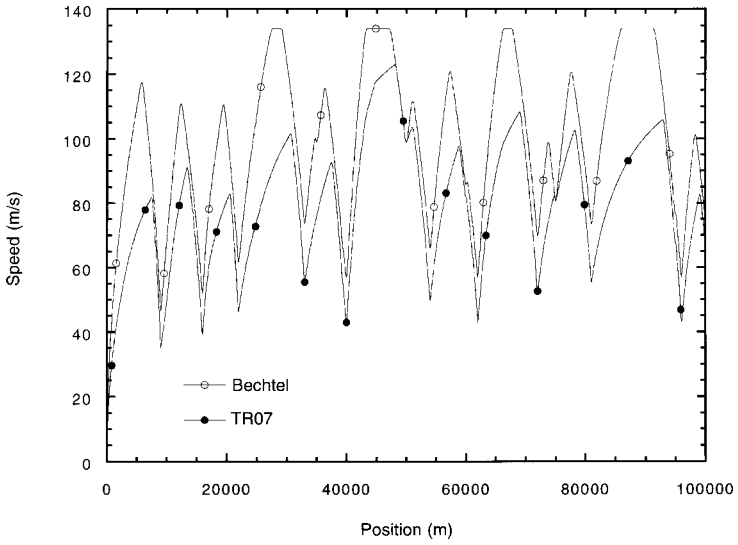

Figure 114. Speed profiles for TR07 and Bechtel vehicle along first 100 km of SST route. Symbols are spaced at 100-s intervals.

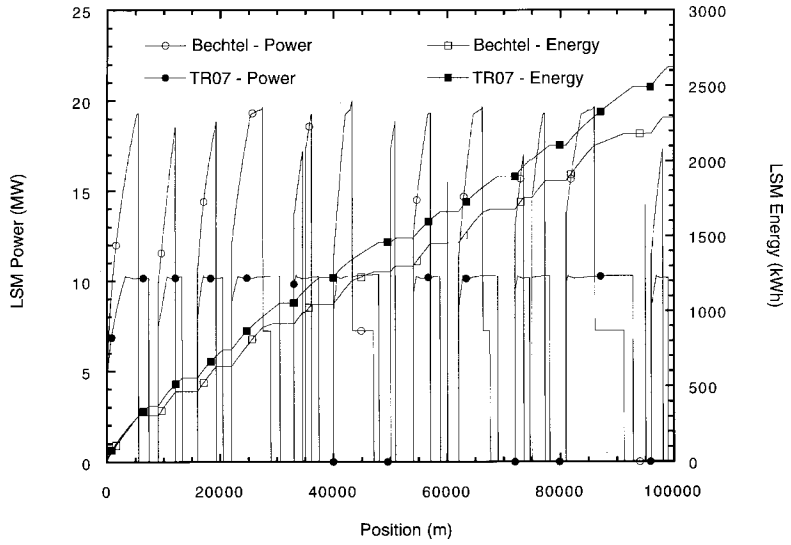

Figure 115. LSM power and energy consumption for TR07 and Bechtel vehicle along first 100 km of SST route. Symbols are spaced at 100-s intervals.

Table 46. Trip times and energy intensities, normalized by results for TR07. Energy intensities include losses through the converter stations.

Item	*TR07*	*Bechtel*	*Foster-Miller*	*Grumman*	*Magneplane*	*TR07-24°*
Standard passengers (SP)	162	106	137	116	108	162
Converter efficiency	0.95	0.90	0.94	0.95	0.95	0.95
Energy intensity (J/SP-m)						
40 km straight and flat	544	694	440	502	612	544
SST segment 1	594	843	505	597	694	555
SST segment 2	517	651	423	440	535	510
SST segment 3	468	583	394	364	440	468
SST total	535	719	452	487	575	515
Time SCD/TR07						
40 km straight and flat	—	0.89	0.90	0.97	0.90	1.00
SST segment 1	—	0.80	0.82	0.88	0.83	0.90
SST segment 2	—	0.83	0.84	0.87	0.84	0.89
SST segment 3	—	0.98	0.98	1.00	0.98	1.00
SST total	—	0.86	0.87	0.91	0.87	0.93
Energy intensity SCD/TR07						
40 km straight and flat	—	1.28	0.81	0.92	1.13	1.00
SST segment 1	—	1.42	0.85	1.00	1.17	0.93
SST segment 2	—	1.26	0.82	0.85	1.04	0.99
SST segment 3	—	1.24	0.84	0.78	0.94	1.00
SST total	—	1.34	0.84	0.91	1.07	0.96

to each passenger. The estimated converter station efficiencies are consistent with those shown in section 3.3.2 and are independent of vehicle speed. They transform the LSM energy consumption calculated by SSTSIM into the energy supplied to the system by an electrical utility.

The SCDs develop the largest trip-time advantages over TR07 along segments 1 and 2 where, as mentioned, they maintain much higher average speeds. To investigate the relative importance of bank angle vs. acceleration capability, we simulated TR07 with an increase in its allowable bank angle to 24°, designated TR07-24°, while keeping its original LSM and vehicle-resistance characteristics. This change brings TR07 close to the performance of the Grumman concept (see Table 46), the SCD with the lowest baseline acceleration capability. For the twisty segment 1, higher bank angles and greater acceleration capabilities of the SCDs contribute roughly equally to their trip time advantages over TR07. Bank angle exerts proportionately more influence on trip time along the gently curved segment 2, while acceleration capability accounts for all of the modest advantage of the SCDs on the straight segment 3. Note that, except for Grumman, the DG ride comfort criterion of 24° used in these simulations limits the maximum bank angles (and hence the gate speeds) of the SCDs. Thus, three of the four concepts would achieve even greater trip-time advantages over TR07 under less conservative ride comfort criteria (e.g., MR, see Table 106). Bechtel and, to a lesser extent, Magneplane would further increase their trip-time advantages with a less restrictive longitudinal acceleration criterion.

The effects of higher average speeds (i.e., reduced trip time) on system energy intensity are more complicated. The major sources of energy loss are aerodynamic drag and LSM inefficiency at maximum thrust. Aerodynamic losses increase by the square of vehicle speed, so they increase with increasing average speed. Conversely, maximum-thrust LSM losses decrease with shorter acceleration times, because of either higher thrust:resistance ratios (see eq 21) or higher gate speeds. The 40-km straight and flat route, because it has no turns, reveals the benefit possible with higher thrust:resistance ratios—two of the SCDs (Foster-Miller and Grumman) have lower energy intensities than TR07 despite having higher average speeds. The SST results for TR07-24° demonstrate the energy benefit of higher gate speeds. Even with the same LSM, reduced acceleration losses from higher gate speeds can more than compensate for increased aerodynamic losses from higher average speed

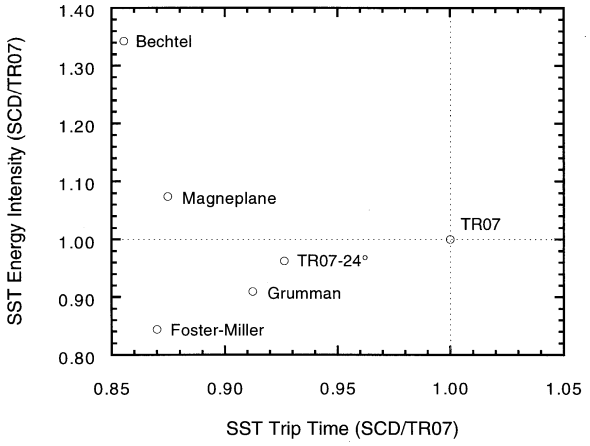

Figure 116. SST total trip time vs. energy intensity for each SCD and TR07-24°, normalized by the corresponding value for TR07.

(see Table 113a). Eventually, however, increasing average speed will lead to increased energy intensity (e.g., Bechtel) because of higher aerodynamic losses. The exact break-even point depends on the vehicle and LSM design, and the characteristics of a particular route.

Figure 116 summarizes the potential real-world performance advantages of the SCDs compared with TR07. Normalized by the values for TR07, the figure shows SST energy intensity vs. trip time for each SCD. Notice that all SCD systems traverse the SST route much faster than TR07. In addition, two of the SCD's (Foster-Miller and Grumman) achieve shorter SST trip times *and* lower energy intensities than TR07. Increasing the total bank angle of TR07 to 24° (which would require a major redesign of the TR07 vehicle and guideway) reduces but does not eliminate the performance advantages of the SCDs. That is, larger bank angles and higher thrust:resistance ratios both contribute to the superior performance of the SCDs, and this combination represents an important design advantage of a U.S. maglev system optimized for typical U.S. routes.

Guideway offset requirements

As noted earlier, SSTSIM does not include features needed to design guideway spiral transitions for horizontal curves. However, MPS has this feature, and we used it to determine the offset of an actual guideway path (with a transition spiral) to that of a circular curve radius without a transition section.

Recall that a segment of circular arc at the specified minimum radius is required for each SST curve. Transition spirals allow for smooth changes between tangent sections (infinite radius) and the required curve radius, and can be designed to satisfy the secondary ride comfort criteria. However, transition spirals offset the guideway towards the center of curvature and away from the PI (Point of Intersection), and these offsets alter ROW geometries. Figure 117 shows a 400-m-radius curve with change in azimuth of 40°. The PI is 9000 m from the last PI. The extent of the 400-m-radius circular arc is indicated by the two radial lines from the center to the points of tangency of the straight tangent sections. The spiral transition displaces the circular arc about 5 m toward the center of curvature; the transition begins 102 m before the circular arc.

Similarly, Figure 118 shows curves of different radii, each with a change in azimuth of 20°. By including spiral transitions, each curve's required circular arc moves inward a distance that depends on the curve's radius. Thus, the guideway offset for a 500-m-radius, 20° curve is approximately 2 m. If the radius were increased to 700 m, the off-

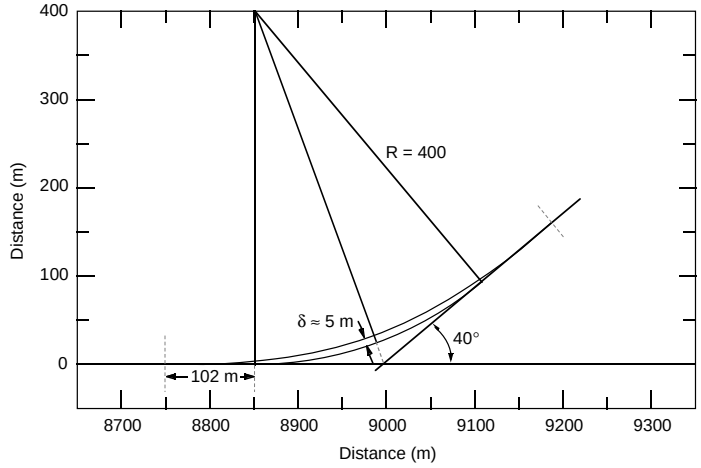

Figure 117. Offset difference between 400-m radius curve and spiral.

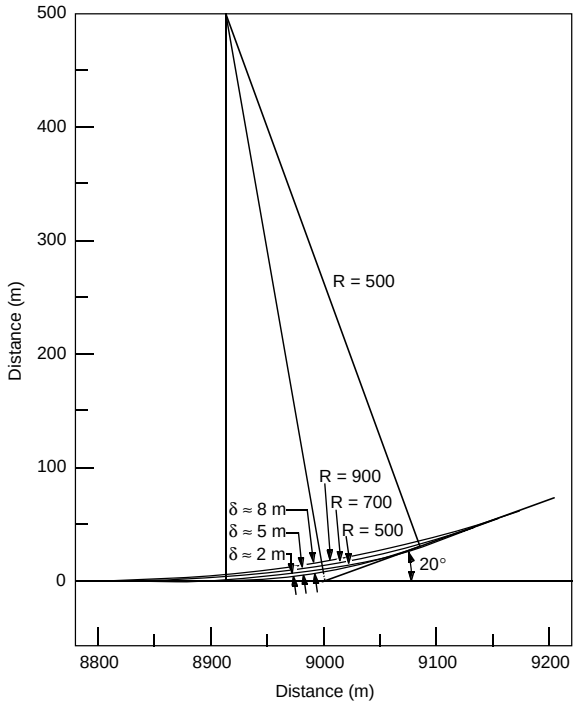

Figure 118. Offset difference for spiral curves, 500–900 m.

set would be 5 m. If it were further increased to 900 m, the offset would increase to 8 m. The associated speed through the curve, assuming 24° of total bank angle, is shown in Table 47. The difference in speed in percent from the 500-m case is shown as the percent difference from cruise speed (134 m/s). Reasonably large speed increases are possible for modest offsets (i.e., modest ROW deviations).

Typically, Interstate Highway ROWs are about 100 m wide and have 11–17 m on either side of the roadway. Although details of route alignment are site specific, there should be sufficient latitude to accommodate the small offsets resulting from spiral transitions. Furthermore, there may be instances where the radius of curvature can be increased, with an associated increase in speed. On the other hand, there may also be instances where planners are so constrained as to require the acquisition of some additional land. These results indicate that land acquisition, if needed, is likely to be on a small scale.

Table 47. Guideway offset and SCD vehicle speed for a 20° turn using spiral transitions. Offset is measured relative to simple circular curve.

R *(m)*	*Offset* *(m)*	V *(m/s)*	$\Delta V/V_{500m}$ *(%)*	V*/134 m/s* *(%)*
500	2	52.1	—	39
700	5	61.7	18	46
900	8	69.9	34	52

Conclusions

We developed software, SSTSIM, to simulate the motion of maglev vehicles along prescribed routes to examine how technological characteristics translate into system characteristics that affect ridership and costs. Inputs to SSTSIM include route specifications, ride comfort criteria, and the system-dependent vehicle and LSM performance data. For the SST route traversed under DG conditions, the primary ride comfort criteria governing vehicle motion are lateral acceleration in horizontal or combined curves, vertical acceleration in vertical curves, and longitudinal acceleration–braking and longitudinal jerk during speed changes. Comparison of the results of SSTSIM with the previous GMSA model, MPS, confirmed the validity of this approach.

We used SSTSIM to compare the performance of TR07 and the four SCDs along a 40-km straight and flat route and along the SST route. These simulations revealed that, compared with TR07, the larger bank angles of the SCDs combined with higher LSM thrust-to-vehicle resistance ratios can yield shorter trip times *and* lower energy intensities. This remarkable result occurs because higher gate speeds (larger bank angle) and more efficient acceleration (higher thrust:resistance ratios) produce energy savings that more than compensate for the increased aerodynamic losses associated with shorter trip times. This combination of shorter trip time and lower energy intensity constitutes an important performance advantage that could result by designing the technological characteristics of a U.S. maglev system to satisfy the requirements of typical U.S. routes.

3.3.2 Guideway cost estimates*

Background

The guideway, with its critical support, propulsion, and control functions, will be the most expensive part of a maglev system. For this reason, the GMSA team developed its own guideway cost estimates for TR07 and the four SCD con-

* Written by Richard Suever and Dr. John Potter, U.S. Army Engineer Division, Huntsville

cepts. We drew heavily on the Corps of Engineers' experience with costing of civil structures and advanced military technologies to develop these estimates.

The guideway cost estimates prepared by the SCD contractors did not allow for easy comparison among them. The estimating approach varied widely by contractor. Variances resulted from different guideway heights, different unit prices for similar commodities, nonuniform allocation of components into subsystems, missing items, and differences in the application of contingencies, overhead, and profit factors.

The inconsistencies in the estimates, particularly in the allocation of design components into subsystems, had a significant effect on the cost model developed by the Volpe National Transportation Systems Center (VNTSC). To obtain the capital cost of a maglev system for a particular corridor, the model takes the length along the alignment and multiplies it by the unit cost for each subsystem. The results obtained from the model are useful in comparing the different concepts in terms of total costs.

A problem arose when the contractors did not uniformly allocate design components to subsystems. For example, the guideway beam subsystem may only consist of the structural elements in one contractor's estimate; it may include magnetic components that are attached to the guideway in another's; and it may include power distribution in a third. Clearly, each subsystem must consist of the same components to compare costs across concepts.

An effort was undertaken by the Government to rework the guideway cost estimates so that the different technologies could be equivalently compared. The specific objectives of the effort were to:

- Compare estimates based on a common set of parameters, such as guideway height.
- Provide an independent assessment of the SCD estimates.
- Develop a standard method of allocating components into subsystems.
- Develop unit costs for each subsystem in each concept for use in VNTSC's cost model.

Note that the total construction cost of a maglev system includes many items that are not dependent on the technology chosen. Such technology-independent items include ROW, site preparation, fencing, stations, central control facility, maintenance facilities, etc. The cost of these items may be estimated reliably using standard practices. Here, we focused on the technology-dependent costs of each guideway concept. The resulting estimates are only about one-third of the total construction cost of each system. Also, we did not estimate vehicle costs for each concept. We did not have the necessary expertise in aerospace construction, and vehicles do not represent a cost related to the length of the guideway. VNTSC's cost model is specifically designed to estimate total maglev system costs, including total construction cost. For its technology-dependent guideway costs, it uses the subsystem unit costs developed here.

Procedure

The guideway cost estimates prepared by the Government were based on the following:

- It is an 11-m-high, dual guideway.
- Consistent unit costs were applied.
- No site work or fencing was included in the costs.
- No high voltage power distribution was included.
- No markups, contingencies, or profits were included.

The unit costs used for each component are an all-inclusive number that takes into account manufacturing, transportation, and installation, unless otherwise noted. The unit costs for the guideway structure and the electrical systems are from standard cost estimating manuals (Walter 1991). These unit costs were adjusted on the basis of Corps of Engineers experience to reflect unusual construction techniques or materials.

The components were allocated to subsystems as follows:

- *Guideway structure*—This subsystem consists only of the structure itself, i.e., the footings, columns, and girders. For Magneplane, the aluminum levitation sheets are included in this item because they are also structural members. In the case of the TR07, the guideway structure includes the steel sliding surface used for emergency braking.
- *Magnetic components*—This subsystem includes the motor windings, coils, stator packs, and guidance rails. In the case of Grumman, we included both the thick and thin laminated rails in this subsystem, even though the thick rail also serves as a structural component.
- *Guideway power distribution*—This subsystem includes the power components between the rectifier, inverter, or converter station, and

the magnetic components on the guideway. This includes primarily the distribution cable and the grounding system. For the Foster-Miller concept, the LCLSM switches are included in this item because they are located on the guideway.

- *Wayside control and communication*—This item is taken directly from the VNTSC model. It includes wayside installations and connections to the central control facility. Although the uniform application of this unit cost to all concepts makes it a technology-independent item, it does represent a significant cost directly related to the guideway.
- *Power stations*—This subsystem includes all of the components in the rectifier, inverter, or converter stations, depending upon the technology. The estimate includes the transformer at the end of the high voltage distribution line. The high voltage distribution line is not included.

The cost estimates reflect the baseline designs as described in the SCD reports. No attempt was made to optimize the designs provided by the SCD contractors. The quantities of materials in the guideway structure have been adjusted for the 11-m height, depending upon the baseline guideway height.

Results

The cost estimates prepared by the Government for each concept are shown in the following tables. Tables 48–51 show the detailed cost breakdown by component for Magneplane, Grumman, Foster-Miller, and Bechtel. Table 52 shows the cost breakdown for TR07. The cost information for the TR07 was taken primarily from the information in the Cal-Nev proposal (City of Las Vegas 1987). The quantities shown in the tables are for a 1-km length of guideway. This information has been summarized at the subsystem level in Table 53a.

In addition, the estimated cost of each concept for an at- or on-grade guideway was prepared so that the SCD concepts and TR07 could be compared to the TGV in the VNTSC model. The Grumman and TR07 concepts require a near- or at-grade guideway because of the wraparound configuration of the vehicle. The guideway for the other concepts can be placed directly on a soil or crushed stone subgrade. The summary of the at- or on-grade guideway cost by subsystem is shown in Table 53b.

The difference in cost between the elevated and at- or on-grade systems is in the guideway structure itself. We assumed that the other subsystem costs were independent of height. The footings, columns, and cross beams were eliminated for the Magneplane, Foster-Miller, and Bechtel designs. Minimum height columns of 0.92 m (3 ft) were used in the Grumman and TR07 concepts. In addition, we decreased the size of the guideway beams and the quantity of reinforcing because an on-grade beam will be uniformly supported by a soil or stone subgrade, providing much of the required stiffness. In the case of Grumman, the spacing of the columns was decreased to 4.6 m (15 ft) as described in the final SCD report.

The TR07 at-grade guideway cost is based on the at-grade section shown in the Cal-Nev proposal. The span length for this section was reduced to 12.34 m (40.50 ft). The higher cost of this at-grade guideway compared with the U.S. concepts reflects the tighter construction tolerances required for the TR07.

U.S. maglev cost estimate

We attempted to estimate the technology-related costs of a U.S. maglev system that might result from further development, despite the difficulty that such an estimate poses. This is useful to efforts by the NMI and others to forecast the market performance of maglev in the U.S.

Clearly, significant concept-related differences exist in the technologies that could be used in a U.S. maglev system. Despite this, relatively little variation exists among subsystem-level costs for the SCD concepts. With a couple of important exceptions (discussed below), it appears that the broadly defined functions of these subsystems generally govern their costs. Thus, by excluding exceptional cases, we may estimate the cost of a U.S. maglev system by averaging the subsystem costs of the SCD concepts. The resulting estimated cost of a "U.S. maglev" is shown in Table 53.

The two exceptional cases are the Foster-Miller and Magneplane concepts. For both elevated and at-grade U.S. maglev systems, we did not average in the cost of the Foster-Miller guideway magnetics, power distribution, and power substation costs. The innovative Foster-Miller LCLSM requires use of components that are very expensive at present (i.e., the inverters). Foster-Miller could use a more conventional approach and bring the cost of these subsystems closer to those of the other concepts; alternatively, the cost reductions Foster-Miller anticipates for mass production of

Table 48. Magneplane system concept cost estimate.
(Elevated guideway)

COMPONENT	UNIT	QUANTITY	UNIT COST	TOTAL	REMARKS
FOOTING/COLUMN/COLUMN CAP					
Concrete (27.58MPa (4000psi))					Adjusted to 11 m height.
Footing	cu. yds.	4,603	$152.00	$699,656	
Column	cu. yds.	1,458	$477.00	$695,466	
Column Cap	cu. yds.	3,239	$530.00	$1,716,670	
Reinforcement (Assumed 60 ksi rebar)	lbs.	1,286,000	$0.75	$964,500	
TROUGH (Span length 9.23m (30 ft.))					
Aluminum Rail (6061 Aluminum)	tons	834	$8,520.00	$7,105,680	Inc. material, fabrication, delivery & erect.
Alignment (Dual Guideway)	km	2	$4,900.00	$9,800	Based on $1.50 per ft. (Magneplane Est.)
SUBTOTAL GUIDEWAY STRUCTURE	km			$11,191,772	
GUIDEWAY MAGNETICS					
LSM WINDING					
Propulson Coil (1000 MCM,15kV, Copper).	ft.	205,920	$10.00	$2,059,200	
Coil Installation (Materials)	lot	1	$205,920	$205,920	10% of Materials Cost (FRP).
Coil Installation (Labor)	ft.	205,920	$2.86	$588,931	
SUBTOTAL GUIDEWAY MAGNETICS	km			$2,265,120	
GUIDEWAY POWER DISTRIBUTION					
LIGHTNING PROTECTION (Inc. Grounding)	lot	1	$15,000.00	$15,000	
GUIDEWAY POWER					
Guideway Cable (1000 MCM,15kV, Aluminum, Shielded, Tri-plex)	ft.	14,000	$27.00	$378,000	
Cable Tray (4" by 18", Aluminum, Covered)	ft.	1,650	$15.76	$26,004	Inc. Installation and Supports.
TOTAL FOR GUIDEWAY POWER	km			$419,004	

Table 48 (cont'). Magneplane system concept cost estimate.
(Elevated guideway)

COMPONENT	UNIT	QUANTITY	UNIT COST	TOTAL	REMARKS
WAYSIDE CONTROL & COMMUNICATION					
SUBTOTAL FOR WAYSIDE CONTROL & COMMO	m			$870	PARSONS BRINKERHOFF MODEL
SUBTOTAL PER KM	km			$869,565	
POWER SUBSTATION AND CONVERTER COST					
34.5 kV SERVICE					
Gang Operated Switch	ea	2	$10,300.00	$20,600	
Conduit (4 in. Galvanized)	lf	200	$30.50	$6,100	
Cable (500 MCM, 34.5 kV, EPR)	lf	600	$10.10	$6,060	
Capacitors - Equipment	mvar	9.6	$3,340.00	$32,064	
Capacitors - Installation	mvar	9.6	$400.00	$3,840	
34.5 kV Switchgear - Equipment	ckt	9	$50,000.00	$450,000	
34.5 kV Switchgear - Installation	ckt	9	$520.00	$4,680	
CONVERTER CIRCUITS					
6 MVA Transformer - Equipment	ea	4	$59,000.00	$236,000	
6 MVA Transformer - Installation	ea	4	$1,040.00	$4,160	
6 MW Converter - Equip. (inc. input transformer)	ea	4	$578,000.00	$2,312,000	
6 MW Converter - Install. (inc. input transformer)	ea	4	$3,000.00	$12,000	
15kV Switchgear - Equipment	ckt	4	$25,000.00	$100,000	
15kV Switchgear - Installation	ckt	4	$520.00	$2,080	
Conduit (4 in. Galvanized)	lf	400	$30.50	$12,200	
Cable (#1/0 AWG, 34.5 kV, EPR)	lf	1500	$5.55	$8,325	
Bus Duct (1200 amp, 5 kV)	lf	100	$2,000.00	$200,000	
Guideway Winding Switch - Equipment	ea	4	$15,000.00	$60,000	
Guideway Winding Switch - Installation	ea	4	$800.00	$3,200	
Cable (3 - 1/0, 500 MCM, 15 kV, Tri-plex)	ft.	30000	$28.00	$840,000	
Cable Tray (24 in. Aluminum Ladder)	ft.	15000	$15.80	$237,000	
Capacitors, Switched - Equipment	mvar	172.8	$3,500.00	$604,800	
Capacitors, Unswitched - Equipment	mvar	172.8	$4,000.00	$691,200	
Capacitors - Installation	mvar	345.6	$400.00	$138,240	
SUBSTATION (480V)	ea	1	$65,000.00	$65,000	Equipment and Installation
MATCHING TRANSFORMER (Special 2500 V, 6 MVA)	each	4	$73,000.00	$292,000	Concept Specific

Table 48 (cont'd).

COMPONENT	UNIT	QUANTITY	UNIT COST	TOTAL	REMARKS
BYPASS BREAKERS	each	4	$31,000.00	$124,000	Concept Specific
BUILDING					Rectifiers and Inverters Inside
Structure (Concrete Block)	sf	5500	$55.00	$302,500	
Equipment Cooling	lot	1	$274,000.00	$274,000	
UPS System (5 KVA)	ea	1	$17,000.00	$17,000	
SECURITY LIGHTING	lot	1	$10,000.00	$10,000	
GROUNDING	lot	1	$10,000.00	$10,000	
SUBTOTAL FOR CONVERTER STATION				$7,079,049	
SUBTOTAL PER KM (SUBTOTAL/8km)	km			$884,881	
COST SUMMARY					**PERCENT**
SUBTOTAL GUIDEWAY STRUCTURE				$11,191,772	71.60
SUBTOTAL GUIDEWAY MAGNETICS				$2,265,120	14.49
SUBTOTAL FOR GUIDEWAY POWER				$419,004	2.68
SUBTOTAL FOR WAYSIDE CONTROL & COMMAND				$869,565	5.56
SUBTOTAL FOR CONVERTER STATION				$884,881	5.66
TOTAL GUIDEWAY (PER KM)				$15,630,342	100.00
TOTAL GUIDEWAY (PER MILE)				$25,169,633	

Table 49. Grumman system concept cost estimate.
(Elevated guideway)

COMPONENT	UNIT	QUANTITY	UNIT COST	TOTAL	REMARKS
GUIDEWAY STRUCTURE					
FOOTING (Cast in Place)					
Concrete (41.37 MPa (6000psi))	cu. yd.	1189	$152.00	$180,728	Adjusted to 11 m. height.
Reinforcement, Conventional (Assumed 60 ksi)	lbs	314635	$0.75	$235,976	
H-Piles, HP-14 (14 X 117)	ft.	10920	$32.04	$349,877	
COLUMN (Cast in Place)					
Concrete (41.37 MPa (6000psi))	cu. yd.	1190	$477.00	$567,630	
Reinforcement, Conventional (Assumed 60 ksi))	lbs	236428	$0.75	$177,321	
BEAM BEARING PAD (4 per span)	ea	148	$750.00	$111,000	
GIRDER SYSTEM (Precast)					
Box Girder (27.5m (90 ft) span)					
Concrete (55.16 MPa (8000 psi))	cu. yd.	4138	$530.00	$2,193,140	
Reinforcement (Assumed 60 ksi steel)					
Conventional	lbs	596895	$0.75	$447,671	
Prestressed	lbs	230447	$2.91	$670,601	
SUBTOTAL GUIDEWAY STRUCTURE	km			$4,933,944	
GUIDEWAY MAGNETICS					
LAMINATED RAIL (2.3m (7.5 ft) span)					
Thick laminations	lbs	1541696	$0.90	$1,387,526	
Thin laminations	lbs	1194540	$0.90	$1,075,086	
BRAKE RAIL	lbs	99672	$0.80	$79,738	
STATOR CABLE (600 MCM, 5 kV, Alumnium)	ft	138000	$6.00	$828,000	
Stator Cable Installation (Material)	lot	1	$41,400.00	$41,400	5% of Material Cost.
Stator Cable Installation (Labor)	ft	138000	$1.60	$220,800	
SUBTOTAL FOR GUIDEWAY MAGNETICS	km			$3,632,550	

Table 49 (cont'd). Grumman system concept cost estimate.
(Elevated guideway)

COMPONENT	UNIT	QUANTITY	UNIT COST	TOTAL	REMARKS
GUIDEWAY POWER					
POWER DISTRIBUTION					
Feeder Cable (1500 MCM, 5 kV, Aluminum, Single Phase)	ft	19600	$10.40	$203,840	
Feeder Cable Installation (Materials)	lot	1	$6,115.20	$6,115	3% of Material Cost.
Cable Tray (6"x24", Aluminum, covered)	ft	3300	$26.85	$88,605	
LIGHTNING PROTECTION (INC GROUNDING)	Lump Sum	1	$15,000.00	$15,000	
SUBTOTAL FOR GUIDEWAY POWER	km			$313,560	
WAYSIDE CONTROL & COMMUNICATION					
SUBTOTAL FOR WAYSIDE CONT. & COMMO	m			$870	Parsons Brinckerhoff Cost Model
SUBTOTAL PER KM	km			$869,565	Parsons Brinckerhoff Cost Model
INVERTER STATION					
EQUIPMENT UNIT					
Transformer (34.5-8.5 kV, 15 MVA)	ea	1	$143,000.00	$143,000	
Circuit breaker (35 kV, 300 amp, 3 phase)	ea	1	$33,000.00	$33,000	
Surge arrestor (34.5 kV, 3 Pole, with isolation switch)	ea	1	$5,000.00	$5,000	
Capacitor (2.4 MVAR, 8.5 kV, 3 phase)	mvar	2.4	$4,000.00	$9,600	
Metal Clad Switch Gear (10 kV)					
Surge arrestor (10 kV, 3 Pole)	ea	2	$5,000.00	$10,000	
Input circuit breaker (1200 amps, 3 pole)	ea	2	$32,000.00	$64,000	
Metal Clad Switch Gear (5 kV)	ea	2	$23,000.00	$46,000	
Input circuit breaker (1200 amps, 3 pole)	ea	2	$32,000.00	$64,000	
Tie breaker (3 pole)	ea	1	$23,000.00	$23,000	
Capacitor (3MVAR, 2100 V, 3 pole)	ea	6	$4,000.00	$24,000	
Capacitor switch (800 amp, 3 pole)	ea	2	$23,000.00	$46,000	
Resister Load Bank (7.5 MVA)	ea	2	$50,000.00	$100,000	
Resister Switch (5 kV, 2000 amp, air, CB)	ea	2	$29,000.00	$58,000	
Output Circuit Breaker (1200 amp, 3 pole)	ea	2	$32,000.00	$64,000	
RECTIFIER/INVERTER (12-pulse,7.5mva plus constant current inverter 2300v output. VVVF)	each	2	$1,610,000.00	$3,220,000	

Table 49 (cont'd). Grumman system concept cost estimate.
(Elevated guideway)

COMPONENT	UNIT	QUANTITY	UNIT COST	TOTAL	REMARKS
STATOR SWITCHES (1200 amps, 5000 V, 3 pole, WP)	each	4	$32,000.00	$128,000	
SUBSTATION (480 V, double-ended)	ea	1	$65,000.00	$65,000	Equipment and Installation
BUILDING					Rectifiers and Inverters Inside.
Structure (Concrete Block)	sf	5500	$55.00	$302,500	
Equipment Cooling	lot	1	$161,000.00	$161,000	
UPS System (5 KVA)	ea	1	$17,000.00	$17,000	Assumed Size - Not in SCD Estimate.
GROUNDING	lot	1	$10,000.00	$10,000	
SECURITY LIGHTING	lot	1	$10,000.00	$10,000	
SUBTOTAL FOR INVERTER STATION				$4,603,100	Per Direction
SUBTOTAL FOR DUAL GUIDEWAY				$9,206,200	
SUBTOTAL PER KM (SUBTOTAL/8km)	km			$1,150,775	
COST SUMMARY					
					PERCENT OF TOTAL:
SUBTOTAL GUIDEWAY STRUCTURE	km			$4,933,944	45.26
SUBTOTAL GUIDEWAY MAGNETICS	km			$3,632,550	33.32
SUBTOTAL FOR GUIDEWAY POWER	km			$313,560	2.88
SUBTOTAL FOR WAYSIDE CONTROL & COMMO	km			$869,565	7.98
SUBTOTAL FOR INVERTER STATION	km			$1,150,775	10.56
TOTAL GUIDEWAY (PER KM)				**$10,900,394**	100.00
TOTAL GUIDEWAY (PER MILE)				**$17,552,970**	

Table 50. Foster-Miller system concept cost estimate.
(Elevated guideway)

COMPONENT	UNIT	QUANTITY	UNIT COST	TOTAL	REMARKS
GUIDEWAY STRUCTURE					
FOOTING/COLUMN/COLUMN CAP					Adjusted to 11 m. height.
Concrete (20.69MPa (3000 psi))					
Footing	cu. yds.	1,100	$152.00	$167,200	
Column	cu. yds.	2,297	$477.00	$1,095,669	
Reinforcement (Assumed 60 ksi rebar)	lbs.	394,283	$0.75	$295,712	
BEAM BEARING PADS (4 per Span)	ea.	74	$760.00	$56,240	Unit Cost per Single Span.
GIRDER (Span length 27m (88 ft.))					
Concrete (55.16MPa (8000 psi))	cu. yds.	6,280	$530.00	$3,328,400	
Reinforcement(Assumed 60ksi)					
prestressed	lbs.	140,240	$2.91	$408,098	
FRP(fiberglass reinforcement)					
Post tensioned	lbs.	48,100	$6.00	$288,600	
SUBTOTAL GUIDEWAY STRUCTURE	km			$5,639,920	
GUIDEWAY MAGNETICS					
PROPULSION					
Propulson Coil	each	4,652	$225.00	$1,046,700	FRP incl. in Cost of Coils.
Coil Installation (Materials)	lot	1	$31,401	$31,401	3% of Material Cost (Incl. bolts, brackets, etc).
Coil Installation (Labor)	each	4,652	$25.00	$116,300	
LEVITATION & GUIDANCE					
Figure 8 Coil (copper, FRP matrix)	each	3,077	$1,140.00	$3,507,780	FRP incl. in Cost of Coils.
Figure 8 Coil Installation (Materials)	lot	1	$105,233	$105,233	3% of Material Cost (Incl. bolts, brackets, etc).
Figure 8 Coil Installation (Labor)	each	4,652	$50.00	$232,600	
CROSS CONNECT. CABLE (1/0, Cu, 5 kV, 40 ft. ea.)	ft.	186,080	$3.32	$617,786	
SUBTOTAL FOR GUIDEWAY MAGNETICS	km			$5,657,800	

Table 50 (cont'd). Foster-Miller system concept cost estimate.
(Elevated guideway)

COMPONENT	UNIT	QUANTITY	UNIT COST	TOTAL	REMARKS
GUIDEWAY POWER DISTRIBUTION					
GUIDEWAY POWER					
DC Bus (Copper, 2.6 in. diam.)	lb.	267,976	$2.25	$602,946	
Cable Tray (6" X 30", Aluminum, Covered)	lf	3,300	$33.36	$110,088	
Disconnect Tap	each	4,652	$30.00	$139,560	
Sectional Sizing Switch (8000 amps, 2pole)	each	1	$33,000.00	$16,500	One per each 2km of track; not commercially available.
LIGHTNING PROTECTION (INC. GROUNDING)	lot	1	$15,000.00	$15,000	
INVERTER (311 kV, 1410 V, 221 amp)	each	2,326	$1,000.00	$2,326,000	
SUBTOTAL FOR GUIDEWAY POWER	km			$3,210,094	
WAYSIDE CONTROL & COMMUNICATION					
SUBTOTAL FOR WAYSIDE CONT. & COMMO	m			$870	Parsons Brinckerhoff Cost Model
SUBTOTAL PER KM	km			$869,565	Parsons Brinckerhoff Cost Model
RECTIFIER STATION					
EQUIPMENT UNIT (Every 8 km)					
Transformer (40 MW,34.5 kV, w/auto tap changers)	each	2	$380,000.00	$760,000	
Oil Circuit Breaker (34.5 kV, 800 amp)	each	2	$40,000.00	$80,000	
Secondary Surge Arrester	each	6	$2,000.00	$12,000	
Circuit breaker (8 kV, 4500 amp)	each	2	$30,000.00	$60,000	Not commercially available in this size.
RECTIFIER (2100 V DC; output 60 MVA (40 MVA nominal))	each	2	$6,840,000.00	$13,680,000	Size and Input Voltage Not Given.
SWITCHGEAR-METAL CLAD (4.2 kV)	each	2	$45,000.00	$90,000	

Table 50 (cont'd)

COMPONENT	UNIT	QUANTITY	UNIT COST	TOTAL	REMARKS
Switch (DC rating, 2900 amp, 2 pole)	each	6	$33,000.00	$198,000	Not available in this size.
Surge Arrester	each	6	$2,000.00	$12,000	
SUBSTATION (480 V, double ended)	lot	1	$65,000.00	$65,000	Equipment and Installation.
BUILDING					
Structure (Concrete Block)	sf	2000	$55.00	$110,000	Rectifiers Only.
Equipment Cooling	lot	1	$627,000.00	$627,000	
UPS System (5KVA)	ea	1	$17,000.00	$17,000	Assumed Size - Not in SCD Estimate.
GROUNDING	lot	1	$10,000.00	$10,000	
SECURITY LIGHTING	lot	1	$10,000.00	$10,000	
SUBTOTAL FOR RECTIFIER STATION				$15,731,000	
SUBTOTAL PER KM (SUBTOTAL/8KM)				$1,966,375	
COST SUMMARY					
					PERCENT OF TOTAL:
SUBTOTAL GUIDEWAY STRUCTURE	km			$5,639,920	32.52
SUBTOTAL GUIDEWAY MAGNETICS	km			$5,657,800	32.62
SUBTOTAL FOR GUIDEWAY POWER	km			$3,210,094	18.51
SUBTOTAL FOR WAYSIDE CONTROL & COMMO	km			$869,565	5.01
SUBTOTAL FOR RECTIFIER STATION	km			$1,966,375	11.34
TOTAL GUIDEWAY (PER KM)				**$17,343,754**	100.00
TOTAL GUIDEWAY (PER MILE)				**$27,928,750**	

Table 51. Bechtel system concept cost estimate.
(Elevated guideway)

COMPONENT	UNIT	QUANTITY	UNIT COST	TOTAL	REMARKS
GUIDEWAY STRUCTURE					
FOOTING/COLUMN/COLUMN CAP					
Concrete (27.58MPa (4000psi))					Adjusted to 11 m. height.
Footing	cu. yds.	2,770	$152.00	$421,040	
Column	cu. yds.	1,080	$477.00	$515,160	
Cross beams	cu. yds.	800	$580.00	$464,000	
Reinforcement (Assumed 60 ksi conventional rebar)	lbs.	1,011,800	$0.75	$758,850	
BEAM BEARING PADS (4 per Span)	ea.	80	$360.00	$28,800	Unit Cost per Single Span.
GIRDER (Span length 25m (82 ft.))					
Concrete (69MPa (10,000 psi))	cu. yds.	3,348	$530.00	$1,774,440	
Reinforcement (Assumed 60ksi)					
Conventional	lbs.	39,690	$0.75	$29,768	
Prestress	lbs.	211,680	$2.91	$615,989	
FRP(fiberglass reinforcement)					
Post tensioned	lbs.	141,120	$6.00	$846,720	
Embedded	lbs.	130,100	$2.00	$260,200	
SUBTOTAL GUIDEWAY STRUCTURE	km			$5,714,966	
GUIDEWAY MAGNETICS					
LSM WINDING					
Propulson Coil (800 MCM,15 kV, Aluminum).	ft.	204,000	$5.36	$1,093,440	Length per Bechtel
Coil Installation (Materials)	lot	1	$109,344.00	$109,344	10% of Material Cost.
Coil Installation (Labor)	ft.	204,000	$1.81	$369,240	
VERTICAL LIFT LADDER, AL. (includes FRP)	Kg.	53,681	$25.50	$1,368,866	
NULL FLUX GUIDANCE COILS	ea.	6,153	$130.00	$799,890	FRP Frame Included.
Coil Installation (Materials)	lot	1	$39,994.50	$39,995	5% of Material Cost.
Coil Installation (Labor)	ea.	6,153	$25.00	$153,825	
SUBTOTAL FOR GUIDEWAY MAGNETICS	km			$3,934,599	

Table 51 (cont'd).

COMPONENT	UNIT	QUANTITY	UNIT COST	TOTAL	REMARKS
GUIDEWAY POWER DISTRIBUTION					
DC DISTRIBUTION (Direct burial, inc. trenching)					
Cable (2000 MCM, 15 kV, Copper, Single Conductor, 2-2000 MCM per pole.)	LF	13,800	$21.33	$294,354	
Cable (1000 MCM, 600 V, Aluminum, Single Conductor)	LF	3,500	$4.15	$14,525	
SPLICE VAULT	each	1	$1,000.00	$1,000	
LIGHTNING PROTECTION (INC. GROUNDING)	lot	1	$15,000.00	$15,000	
SUBTOTAL FOR GUIDEWAY POWER	km			$324,879	
WAYSIDE CONTROL & COMMUNICATION					
SUBTOTAL FOR WAYSIDE CONT. & COMMO	m			$870	Parsons Brinckerhoff Cost Model
SUBTOTAL PER KM	km			$869,565	Parsons Brinckerhoff Cost Model
RECTIFIER STATION					
EQUIPMENT UNIT (per 20 km of guideway)					
Transformer (3 phase, 34.5 kV, 50 MVA)	each	2	$476,000.00	$952,000	May not be in this size with low voltage secondary
69 kV Bus	each	1	$20,000.00	$20,000	
Oil Circuit Breaker (1000 amp, 3 pole)	each	4	$90,000.00	$360,000	
Surge Arrester (69 kV, 3 pole)	each	2	$10,000.00	$20,000	
HV Disconnect Switch (69 kV, 1000 Amps)	each	2	$15,000.00	$30,000	
Circuit Breaker (13.8 kV, 1000 amp, 3 pole)	each	4	$31,000.00	$124,000	Not shown in preliminary design.
Surge Arrester (3.8 kV, 3 pole)	each	2	$5,000.00	$10,000	Not shown in preliminary design.
Switchgear (25 kV, 2000 amp, DC bus)					See the following items.
Circuit Breakers (12 kV, DC, 4000 amp)	each	4	$110,000.00	$440,000	
Circuit Breaker (25 kV, 2000 amp, 3 pole)	each	2	$60,000.00	$120,000	
Circuit Breaker (12 kV, DC,1200 amp)	each	1	$31,000.00	$31,000	For load resister bank.
Lightning Arrestors	each	2	$5,000.00	$10,000	
Switchgear Controls	lot			$20,000	

Table 51 (cont'd). Bechtel system concept cost estimate.
(Elevated guideway)

COMPONENT	UNIT	QUANTITY	UNIT COST	TOTAL	REMARKS
RECTIFIER (12 Pulse, +12 kV, -12 kV)	each	2	$4,000,000.00	$8,000,000	
LOAD BANK (8MW, 30 kV, IDC)	each	1	$100,000.00	$100,000	
SUBSTATION (480 V, Double-Ended)	each	1	$65,000.00	$65,000	
BUILDING					
Structure (Concrete Block)	sf	2700	$55.00	$148,500	Rectifiers and Load Banks Only.
Equipment Cooling	lot	1	$356,000.00	$356,000	
UPS System (5 KVA)	ea	1	$17,000.00	$17,000	Assumed Size - Not in SCD Estimate.
GROUNDING	lot	1	$10,000.00	$5,000	
SECURITY LIGHTING	lot	1	$10,000.00	$10,000	
SUBTOTAL FOR RECTIFIER STATION				$10,838,500	
SUBTOTAL PER KM (SUBTOTAL/20KM)				$541,925	
INVERTER STATION (per 4 KM)					
ISOLATION SWITCH (25 kV (L-L), 60 amp,1 pole)	each	4	$15,000.00	$60,000	
Fuse (25 kV, 800 amp) & holder	each	4	$13,000.00	$52,000	
Surge Arrester (12 kV, 1 pole)	each	4	$1,000.00	$4,000	
Inverter (var. volts & amps, 12 kV in, 12 kV out)	each	2	$2,000,000.00	$4,000,000	
SOLID STATE SWITCH (15 kV, 500 amp, 3 pole)	each	16	$8,000.00	$128,000	
SUBSTATION (480 V., Double-Ended)	each	1	$65,000.00	$65,000	
BUILDING					
Structure (Concrete Block)	sf	1500	$55.00	$82,500	Inverters Only.
Equipment Cooling	lot	1	$227,000.00	$227,000	
UPS System (5 KVA)	ea	1	$17,000.00	$17,000	Assumed Size - Not in SCD Estimate.

Table 51 (cont'd).

COMPONENT	UNIT	QUANTITY	UNIT COST	TOTAL	REMARKS
LIGHTNING PROTECTION	lot	1	$5,000.00	$5,000	
SECURITY LIGHTING	lot	1	$10,000.00	$10,000	
SUBTOTAL FOR INVERTER STATION				$4,650,500	
SUBTOTAL PER KM (SUBTOTAL/4km)	km			$1,162,625	
COST SUMMARY					
					PERCENT TOTAL:
SUBTOTAL FOR GUIDEWAY STRUCTURE	km			$5,714,966	45.54
SUBTOTAL FOR GUIDEWAY MAGNETICS	km			$3,934,599	31.35
SUBTOTAL FOR GUIDEWAY POWER	km			$324,879	2.59
SUBTOTAL FOR WAYSIDE CONTROL & COMMO	km			$869,565	6.93
SUBTOTAL FOR RECTIFIER STATION	km			$541,925	4.32
SUBTOTAL OF INVERTER STATION	km			$1,162,625	9.27
TOTAL GUIDEWAY (PER KM)				$12,548,560	100.00
TOTAL GUIDEWAY (PER MILE)				$20,195,024	

Table 52. TR07 system concept cost estimate.
(Elevated guideway)

COMPONENT	UNIT	QUANTITY	UNIT COST	TOTAL	REMARKS
GUIDEWAY STRUCTURE					
FOOTING/COLUMN/COLUMN CAP					
Concrete (27.58MPa (4000psi))					
Footing	cu. yds.	1,960	$152.00	$297,920	
Column	cu. yds.	2,050	$477.00	$977,850	
Column Cap	cu. yds.	400	$530.00	$212,000	
Reinforcement (Assumed 60 ksi rebar)	lbs.	1,050,000	$0.75	$787,500	
Beam Bearing Pad (4 per span)	each	165	$750.00	$123,750	
GIRDER (Span Length 25m (82 ft))					
Concrete(37.92 MPa (5500 psi))	cu. yds.	3,650	$800.00	$2,920,000	Tight Construction Tolerances.
Reinforcement(steel)					
prestressed	lbs.	267,000	$2.91	$776,970	
conventional	lbs.	490,000	$0.75	$367,500	
SLIDING SURFACE PLATE	lbs.	415,000	$0.41	$170,150	
SUBTOTAL GUIDEWAY STRUCTURE	km			$6,633,640	
GUIDEWAY MAGNETICS					
GUIDANCE STATOR PACK CORE(laminated iron)	lbs.	1,758,500	$0.90	$1,582,650	
GUIDANCE RAIL	lbs.	847,220	$0.41	$347,360	
MOTOR COIL (600 MCM, 6 kV, CU, 1 conductor, 300 mm2)	ft.	88,715	$6.00	$532,290	
Coil Installation (Material)	lot	1	$26,614.50	$26,615	5% of Material
Coil Installation (Labor)	ft.	88,715	$1.70	$150,816	
SUBTOTAL GUIDEWAY MAGNETICS	km			$2,639,730	

Table 52 (cont'd).

COMPONENT	UNIT	QUANTITY	UNIT COST	TOTAL	REMARKS
GUIDEWAY POWER DISTRIBUTION					
FEEDER CABLE (1250 MCM, 6 kV, Aluminum)	ft.	53,000	$8.92	$472,760	
Feeder Cable Installation (Labor)	ft.	53,000	$2.83	$149,990	
CABLE TRAY (4"X12", Solid)	ft.	6,550	$20.90	$136,895	
LIGHTNING PROTECTION	lots			$15,000	
MOTOR VACUUM BKRS., 2000 A (Approx. 10 kV, WP)	each	4	$33,000.00	$132,000	
SUBTOTAL FOR GUIDEWAY POWER	km			$906,645	
WAYSIDE CONTROL & COMMUNICATION	m			$870	Parsons-Brinckerhoff Model
	km			$869,565	
SUBTOTAL FOR WAYSIDE CONTROL & COMMO	km			$869,565	
INVERTER STATION (Every 20KM)					
Disconnect Switch (69 kV)	each	2	$15,000.00	$30,000	
Transformer (50MVA, 60 kV)	each	2	$475,000.00	$950,000	
Transformer (25 MVA, Intermediate volt., 2 winding secondary, y & delta).	each	4	$305,000.00	$1,220,000	Current Split Into Two Directions.
Output Transformer (25 MVA, special).	each	4	$305,000.00	$1,220,000	
Switch (5000 amp, 5 kV, 3 pole)	each	2	$10,000.00	$20,000	
Switch (2500 amp, 5 kV, 3 pole)	each	4	$10,000.00	$40,000	
AC-AC Inverter, (25 MVA, 12 pulse)	each	4	$5,375,000.00	$21,500,000	
Output Circuit Bkr (3000 amp, AC)	each	8	$7,000.00	$56,000	
Misc. Bus (high voltage)	lot			$20,000	
Surge Arrestor (69 kV, 3 pole)	each	2	$10,000.00	$20,000	
HV Feeder Breaker (480 V, 100 amp)	each	2	$20,000.00	$40,000	
5kv Surge Arrestor (5 kV, 3 pole)	each	6	$1,500.00	$9,000	
Switch Gear Controls	lot			$20,000	

Table 52 (cont'd). TR07 system concept cost estimate.
(Elevated guideway)

COMPONENT	UNIT	QUANTITY	UNIT COST	TOTAL	REMARKS
SUBSTATION (480 V)	each	1	$65,000.00	$65,000	
BUILDING					
Structure (Concrete Block)	sf	5500	$55.00	$302,500	
Equipment Cooling	lot	1	$1,025,000.00	$1,025,000	
UPS System (5 KVA)	ea	1	$17,000.00	$17,000	
SECURITY LIGHTING	lot	1	$10,000.00	$10,000	Rectifiers and Inverters Inside.
GROUNDING	lot	1	$10,000.00	$10,000	
SUBTOTAL FOR INVERTER STATION				$26,574,500	
SUBTOTAL PER KM (SUBTOTAL/20)	KM			$1,328,725	
COST SUMMARY					
SUBTOTAL GUIDEWAY STRUCTURE	km			$6,633,640	53.59
SUBTOTAL GUIDEWAY MAGNETICS	km			$2,639,730	21.33
SUBTOTAL FOR GUIDEWAY POWER	km			$906,645	7.32
SUBTOTAL FOR WAYSIDE CONTROL & COMMO	km			$869,565	7.02
SUBTOTAL FOR INVERTER STATION	km			$1,328,725	10.73
TOTAL GUIDEWAY (PER KM)				**$12,378,305**	100.00
TOTAL GUIDEWAY (PER MILE)				**$19,932,859**	

Table 53. Technology cost summary ($1000 per mile).

Subsystem	*Magneplane*	*Grumman*	*Foster-Miller*	*Bechtel*	*TR07*	*U.S. Maglev*
			a. Elevated.			
Guideway structure	18,000	7,900	9,000	9,200	10,700	8,700
Guideway magnetics	3,600	5,800	9,100	6,300	4,200	5,200
Guideway power distribution	700	500	5,200	500	1,500	600
Wayside control and communication	1,400	1,400	1,400	1,400	1,400	1,400
Converter station	1,400	—	—	—	—	—
Inverter station	—	1,900	—	1,900	2,100	2,000
Rectifier station	—	—	3,200	900	—	—
Total	25,100	17,500	27,900	20,200	19,900	17,900
			b. At grade.			
Guideway structure	4,400	1,500	5,600	3,200	8,500	3,700
Guideway magnetics	3,600	5,800	9,100	6,300	4,200	5,200
Guideway power distribution	700	500	5,200	500	1,500	600
Wayside control and communication	1,400	1,400	1,400	1,400	1,400	1,400
Converter station	1,400	—	—	—	—	—
Inverter station	—	1,900	—	1,900	2,100	2,000
Rectifier station	—	—	3,200	900	—	—
Total	11,500	11,100	24,500	14,200	17,700	12,900

these components could bring the LCLSM cost in line with the other concepts.

In the case of Magneplane, the guideway structure is complicated and requires an extremely large amount of aluminum. It is not an efficient structure for large spans, and, thus, it requires close column spacing. This requirement becomes very expensive for the standard 11-m elevation used in this analysis, yet optimizing the beam design for 11-m elevation was beyond our scope. We, therefore, did not include the Magneplane guideway cost in our U.S. maglev estimate.

With these exceptions removed, subsystem costs are quite similar across the U.S. concepts. For example, excluding the Magneplane guideway, the SCD elevated guideway structure costs vary less than 10% from the average value. In general, some cost variability naturally exists because of technological differences. Also, some variability exists because contractors focused their efforts on different subsystems and thus did not optimize all subsystems uniformly. Nevertheless, examination of Table 53 supports the conclusion that the broadly defined function of each subsystem generally governs its cost. Thus, for current efforts to forecast maglev market performance, the derived U.S. Maglev costs should be meaningful despite technological differences among concepts.

It is interesting to compare the subsystem costs for U.S. Maglev with those for TR07. For both elevated and at-grade guideways, essentially the entire cost advantage for U.S. maglev derives from its lower guideway-structure cost. Indeed, TR07's guideway structure is the most expensive of all, except Magneplane's elevated guideway. The difference is particularly striking for at-grade guideways, where TR07's $4,800,000/mile cost disadvantage represents about 40% of the total U.S. Maglev technology costs. Apparently, this cost penalty reflects the need to maintain very tight construction tolerances for the small-gap TR07 system.

Comparison of the Government and SCD cost estimates

The cost estimates prepared by the contractors were compared to the GMSA estimates above. The components in the contractors' estimates were

Table 54. Comparison of cost estimates ($1000).

Subsystem	*Government estimate*	*Contractor estimate*	*Remarks*
		a. Magneplane International.	
Guideway structure	18,000	14,100	Contractor estimate is based on 5.2-m height. Unit costs are different. Reinforcing is not a separate item in contractor estimate.
Guideway magnetics	3,600	4,900	Contractor used higher unit costs.
Guideway power distribution	700	900	Contractor estimate was taken as a percentage (15%) of the total electrification costs.
Wayside control and communication	1,400	500	Government applied a standard unit cost to all SCD concepts.
Converter station	1,400	1,400	
Inverter station	—	—	
Rectifier station	—	—	
Total	25,100	21,800	
		b. Grumman Aerospace.	
Guideway structure	7,900	5,700	Contractor estimate is based on 11.3-m height. Unit costs are different.
Guideway magnetics	5,800	5,300	
Guideway power distribution	500	700	Contractor estimate is per meter of dual guideway. It was not in sufficient detail to determine differences.
Wayside control and communication	1,400	300	Government applied a standard unit cost to all SCD concepts.
Converter station	—	—	
Inverter station	1,900	400	Contractor estimate is per meter of dual guideway. It was not in sufficient detail to determine differences.
Rectifier station	—	—	
Total	17,500	12,400	
		c. Foster-Miller.	
Guideway structure	9,000	7,600	Contractor estimate is based on 7.6-m height. Contractor estimate was not in sufficient detail to determine differences.
Guideway magnetics	9,100	3,300	Unit costs for magnetic components were too low.
Guideway power distribution	5,200	3,500	Unit costs for inverters were too low. Contractor estimate was not in sufficient detail to determine differences.
Wayside control and communication	1,400	500	Government applied a standard unit cost to all SCD concepts.
Converter station	—	—	
Inverter station	—	—	
Rectifier station	3,200	200	Contractor estimate is for one station; two are required for dual guideway.
Total	27,900	15,100	

Table 54 (cont'd).

Subsystem	Government estimate	Contractor estimate	Remarks
			d. Bechtel.
Guideway structure	9,200	12,700	Unit costs are different. Estimated quantities are different.
Guideway magnetics	6,300	6,800	
Guideway power distribution	500	1,100	Contractor estimate was not in sufficient detail to determine differences.
Wayside control and communication	1,400	1,800	Government applied a standard unit cost to all SCD concepts.
Converter station	—	—	
Inverter station	1,900	2,000	
Rectifier station	900	0	Contractor assumed that power utility would provide this station.
Total	20,200	24,400	

reallocated to subsystems in accordance with the procedures used in the Government estimate. The results are shown in Table 54. The reasons for any discrepancy greater than 15% in the two estimates is shown in the remarks column.

The tables show that there are some substantial discrepancies between the two estimates. The primary reasons include differences in unit costs, errors in calculated volumes, and items that were left out of the contractors' estimates. In many cases, the contractors' estimates were not provided in sufficient detail to determine where the differences were.

Except for Bechtel's concept, our estimates are higher than those of the contractors. Based on the information available, the government effort represents a reasonable cost estimate of the technology for each guideway concept.

Conclusions

Much of our cost-estimating effort focused on simple "bookkeeping." We estimated costs based on a common set of guideway parameters and consistent allocation of components into subsystems. More importantly, however, we developed independent guideway cost estimates for all four SCDs and TR07 using common procedures and unit costs. This allows us to draw several general conclusions based on a comparison of these costs and the associated performance characteristics of these systems.

To facilitate this comparison, we may first group systems of similar performance characteristics. Grumman's baseline design meets the SCD system criteria and slightly out-performs TR07 on the SST. Magneplane and Foster-Miller's baseline design have greater banking capability and more powerful motors, and they achieve incrementally better performance along the SST. A U.S. maglev system would also fall into this category. Lastly, Bechtel's baseline design possesses the most powerful motor and the completes the SST is the shortest time. On the basis of this rough grouping, we may draw the following conclusions regarding guideway cost and performance:

- For elevated guideways, the Grumman concept can provide slightly better performance than TR07 at significantly less cost ($17,500,000 / mile vs. $19,900,000 / mile). In addition, the Bechtel concept and U.S. maglev can provide enhanced performance at similar or lower cost ($20,200,000 / mile for Bechtel or $17,900,000 / mile for U.S. maglev vs. $19,900,000 / mile for TR07).
- For at- or on-grade guideways, the Grumman concept is approximately 60% of the cost of the TR07 system ($11,100,000 / mile as compared to $17,700,000 / mile). Also, the Magneplane and Bechtel concepts and U.S. maglev would provide enhanced performance at significantly lower cost ($11,500,000 / mile for Magneplane, $14,200,000 / mile for Bechtel or $12,900,000 / mile for U.S. maglev as compared to $17,700,000 / mile for TR07).
- With two specific exceptions, we found relatively little variability in subsystem costs among U.S. concepts, despite significant dif-

ferences in technology. Apparently, the broadly defined function of each subsystem generally governs its cost. This allowed us to estimate a U.S. maglev cost based on averages of the SCD subsystem costs. This estimate should be meaningful for forecasting market response to maglev in the U.S. and for comparing maglev with existing foreign HSGT systems.

- For both elevated and at-grade guideways, essentially the entire cost advantage for U.S. maglev relative to TR07 derives from its lower guideway-structure cost. The difference is particularly striking for at-grade guideways, where TR07's $4,800,000/mile cost disadvantage represents about 40% of the total U.S. maglev technology costs. Apparently, this cost penalty reflects the need to maintain very tight construction tolerances for the small-gap TR07 system.

Like all cost estimates, the numbers developed here contain a degree of uncertainty. In particular, the U.S. concepts are not fully developed into system designs, and we had limited access to detailed TR07 data. Nevertheless, because we used a common procedure and a common set of unit costs for all systems, these general conclusions are relatively insensitive to this uncertainty.

3.4 OTHER EVALUATION CRITERIA AND ANALYSES

The SCD-RFP system criteria were intended to guide the contractors in the development of their concepts. However, other characteristics of maglev systems may influence their technical viability in the U.S. We, therefore, developed additional evaluation criteria and applied them as cross-checks on each concept in a similar way to the SCD-RFP system criteria (section 3.1). The results of this effort follow.

3.4.1 Mission flexibility*

The market response to maglev in the U.S. is not well known or easy to forecast. If a given concept can serve a variety of transportation missions, it improves its chances of being a commercial success. Suitability to other missions reduces the risk that the originally envisioned mission is not where the greatest market response lies. Also, if a maglev network begins to develop, its ability to serve broader portions of the Nation's travel market will increase ridership and improve economic viability. The adaptability of the technology may also be important for export sales to countries with different transportation needs than those of the U.S.

Table 55. Second numerical rating scheme for each concept.

Rating	*Score*
Highly suited to attribute	2
Capable of attribute	1
Poorly suited to attribute	0
Not capable of attribute	–1

Given the above rationale, we elaborated several mission statements appropriate for maglev; we then listed the primary technological attributes that a concept should possess to serve these missions. Note that the mission defined in the SCD-RFP is essentially that currently performed by short-haul aircraft: short-to-medium distance intercity trunk service. Earlier studies of maglev and the NMI's own market and economic studies view this as the most promising initial market for maglev. By using the SCD system criteria as an evaluation step (section 3.1), we have considered in depth the suitability of each HSGT system to intercity trunk service. Thus, we do not repeat that evaluation here.

Given below is a description of four alternative HSGT missions, their attributes, and the results of our evaluation of each concept against these attributes. We adopted the numerical rating scheme in Table 55 to apply for each technological attribute.

This subsection concludes with Table 60, showing the rating of each concept for each mission, and a rating of each concept's overall mission flexibility. We view mission flexibility as a high-priority criterion for the success of maglev.

Mission 1—Regional airport connector

Objectives.

- To permit multiple airports located within a relatively small region to serve as separate terminals of a distributed "megaport."
- To facilitate transfers between airports and improve network efficiency.

* Written by Christopher J. Boon, Canadian Institute of Guided Ground Transportation, and Dr. James H. Lever, CRREL.

Table 56. Rating concepts as regional airport connectors (mission 1).

Attribute	*TGV*	*TR07*	*Bechtel*	*Foster-Miller*	*Grumman*	*Magneplane*
Efficient at moderate speeds	1	1	1	0*	1	0*
Brisk acceleration / deceleration	0	0	2	2	0	2
High peaking capability	–1	1	1	1	1	2
Transit-style doors, baggage space, and seating	0	1	2	1	1	–1
Tight-radius capability	1	0	0	0	0	0
Electromagnetic compatibility	1	1	1	1	1	1
Total	2	4	7	5	4	4

* High liftoff speed.

Table 57. Rating concepts as a regional commuter trunk (mission 2).

Attribute	*TGV*	*TR07*	*Bechtel*	*Foster-Miller*	*Grumman*	*Magneplane*
Efficient at intermediate speeds	2	2	2	1	2	1
High capacity	2	2	2	2	2	2
Moderate-high accleration	0	1	2	2	1	2
Moderate curving performance	0	1	2	2	2	2
Total	4	6	8	7	7	7

- To improve ground access between population centers and airports.

Examples.
- Dulles–Washington National–BWI–downtown Baltimore.
- LaGuardia–JFK–Newark–Manhattan.
- Midway–downtown Chicago–O'Hare–Milwaukee.

Service characteristics.
- Short distances, moderate speeds (50–60 m / s).
- Frequent service with peaking demands.
- Intermodal passengers and baggage transfers.
- Substantial growth in demand.
- Easy terminal access.
- Constrained ROW.

Table 56 presents the numerical ratings of each concept.

Mission 2—Regional commuter trunk

Objectives.
- To improve regional transportation efficiency.
- To reduce pollution associated with congested commuter highways.
- To reduce or delay investment in highway capacity to cope with peak commuter travel.

Examples.
- Long Island–New Jersey–Connecticut–New York.
- Los Angeles basin.
- Major metropolitan commuter regions (Boston, Chicago, etc.).

Service characteristics.
- 60- to 100-km routes, 8- to 16-km station spacing.
- Intermediate speeds (70–80 m / s).
- Strongly peaked demand.
- Substantial growth in demand.

Table 57 presents the numerical ratings of each concept.

Mission 3—Short to medium distance point-to-point service

Objectives.
- To improve intercity transportation efficiency (similar to SCD mission).
- To improve airport terminal congestion associated with short-haul air.
- To service more diffuse origin–destination pairs than is possible with large airports.

Examples.
- Northeast corridor.
- California corridor.
- Detroit–Chicago–Milwaukee–Minneapolis.

Service characteristics.

- 200- to 1000-km routes, 50- to 200-km station spacing.
- High speed (to 134 m/s).
- Numerous, convenient station locations.
- Smaller vehicles, modest peaking.
- Good interconnection with other public transit.

Table 58 presents the numerical ratings of each concept.

Mission 4—Long-haul trunk service

Objectives.

- To provide surface interconnections among the three major north-south corridors (Boston–Miami, Chicago–Houston, Seattle–San Diego), thereby creating a national HSGT network.
- To supplement long-haul air capacity.
- To reduce pollution generated by aviation and motor vehicles.

Examples.

- New York–Detroit–Chicago–Minneapolis–Salt Lake City–Seattle
- Washington–St. Louis–Denver–San Francisco
- Miami–Atlanta–New Orleans–Dallas–Phoenix–Los Angeles

Service characteristics.

- 2000- to 4000-km routes, 500- to 1000-km station spacing.
- Very high speed (more than 150 m/s).
- High traffic density.
- Long trips, more comfortable cabins, more amenities.
- Larger vehicles (large single or multiple-consist vehicles).
- Interconnections to major airports, maglev hubs.

Table 59 presents the numerical ratings of each concept.

Summary. Table 60 summarizes the ratings for each concept against the four missions. The number of attributes (and hence the maximum rating possible) in each mission generally reflects our priority of each mission in an overall rating of the flexibility of these HSGT concepts to serve missions beyond that identified in the SCD-RFP (intercity trunk service). We applied a final rating to this evaluation using the same rating scheme as in section 3.1 so that we could add the results together. This criterion is a high-priority one (weighting = 3).

This evaluation shows clear separation among the HSGT concepts in overall mission flexibility. TGV is the least flexible. Its fixed-consist, nontilting trains, lower cruise speed, and lower overall acceleration–deceleration render it poorly suited to meet other transportation needs beyond intercity trunk service. TR07 is an improvement over TGV in this regard, but is limited by its nontilting vehicles, modest acceleration, and limited speed potential. By comparison, the SCD maglev concepts show considerable potential to serve additional missions beyond intercity trunk service. Furthermore, they perform that primary

Table 58. Rating concepts for short to medium distance point-to-point service (mission 3).

Attribute	*TGV*	*TR07*	*Bechtel*	*Foster-Miller*	*Grumman*	*Magneplane*
High speed	1	2	2	2	2	2
High acceleration	0	1	2	2	1	2
Good curving performance	0	1	2	2	2	2
Small vehicles	–1	1	2	2	2	2
Short headway, fast switches	1	1	1	2	1	2
Total	1	6	9	10	8	10

Table 59 Rating concepts for long-haul trunk service (mission 4).

Attribute	*TGV*	*TR07*	*Bechtel*	*Foster-Miller*	*Grumman*	*Magneplane*
Very high speed	–1	0	1	1	0	1
Low power at high speed	–1	0	1	1	1	1
Large vehicles, good amenities, and comfort	1	1	1	1	1	0
Total	–1	1	3	3	2	2

Table 60. Summary of ratings for all four missions.

Mission	*TGV*	*TR07*	*Bechtel*	*Foster-Miller*	*Grumman*	*Magneplane*
Regional airport connector	2	4	7	5	4	4
Regional commuter trunk line	4	6	8	7	7	7
Intercity point-to-point service	1	6	9	10	8	10
Long-haul trunk service	–1	1	3	3	2	2
Total (max. 36)	6	17	27	25	22	23
Mission flexibility rating*	–1	1	1.2	1.2	1.2	1.2

*–1 doesn't meet, 1 meets, 1.2 exceeds criterion

Table 61. Assessments of tilting vehicle body.

System	*Evaluation comments*	*Rating*
TGV	None	–1
TR07	None	–1
Bechtel	Internal tilting cabin, 15° banking Aerodynamically clean, low interior noise Weight and complexity penalties—redundant structure, doors, and windows	1
Foster-Miller	Simple cabin construction, circular cradles, 12° banking No feedback correction for tilt—preprogrammed according to route and speed Requires complex fairing between bogies and tilting cabin	1
Grumman	Struts and linkages needed for each bogie, 9° banking Complex bogie–body fairing requirements	1
Magneplane	Passive vehicle banking, magnetic keel (i.e., no mechanical tilting mechanism) 35° banking May be able to pre-roll and correct tilting actively using aerodynamic control, but control not as positive as mechanical means	1

mission, on average, much better than TGV and somewhat better than TR07. This provides some confidence that U.S. maglev concepts will, overall, fulfill a broader spectrum of U.S. transportation needs than either of the two foreign HSGT systems.

3.4.2 Tilting vehicle body

A tilting body allows a broader speed range through curves while maintaining ride comfort. It also provides some flexibility in route alignment and speed profile by permitting pre-roll (i.e., initiating roll in advance of curves). A tilting body also permits a vehicle to return to a near-horizontal position if it is stopped in a curve, thereby easing passenger movement and evacuation. Its disadvantages are basically cost, reliability, maintenance, and weight. Provisions for tilting should maximize the advantages and minimize the disadvantages. This is a medium priority item. We checked the range of tilt and the complexity and weight of the vehicle. Table 61 gives the evaluation comments and ratings for tilting vehicle body.

3.4.3 Energy efficiency*

Energy efficiency is an important performance indicator for HSGT, and we rated it as a high-priority criterion. Here, we summarize energy consumption for all systems and compare the results to that for short-haul air. We show these results normalized per seat-meter, a measure known as energy intensity (EI). Our evaluation used short-haul air as a baseline: –1 for EI higher than air, 1 for comparable EI to air, 1.2 for EI substantially lower than air.

We used two measures of energy consumption—along the SST and at steady cruise. Results for the SST include energy consumed repeatedly accelerating a vehicle, particularly in the first, twisty segment but also for the two intermediate stops. However, the SST simulations did not incorporate energy savings from regenerative braking, the primary braking mode for all maglev concepts. The purpose of regenerative braking is to recover kinetic energy lost during deceleration.

* Written by Dr. James H. Lever, CRREL.

One way to approximate this benefit is to examine energy consumption at steady cruise speed on a level guideway. This value will also approximate vehicle energy consumption on a fairly straight, high-speed guideway.

We obtained cruise energy consumption values for all HSGT concepts by matching vehicle thrust requirements to motor thrust. We then used LSMPOWER and an estimate of converter station efficiency (see section 3.3.2) to obtain electrical energy consumed from a utility. The SST simulator SSTSIM (section 3.3.1) computed energy consumption along the SST route using the motor and resistance data for each concept. We then applied a converter station efficiency to obtain total electrical energy consumed for one trip along the route. These values are "base" energy consumptions—joules of electrical energy consumed at the system connection to an electric utility.

We selected the Boeing 737-300 aircraft to compare the energy efficiencies of HSGT and short-haul air. This aircraft is among the most fuel efficient in the U.S. short-haul fleet, and its energy intensity is about 70–80% that of the fleet, depending on trip length. With about a 30-year replacement cycle for aircraft, the fleet-averaged energy intensity will likely approach that of the 737-300 by the time maglev becomes a significant alternative mode. This is consistent with the estimate by Johnson et al. (1989) that fleet-averaged energy intensity for intercity air travel will drop by about 75% over this period.

Commercial airlines file data on fuel consumption with the USDOT for all flights. We used these data for 737-300 aircraft for the period ending June 1991, and conducted a regression analysis to obtain average fuel consumption per flight as a function of trip length. By converting jet-fuel volume to its energy equivalent (1 U.S. gal = 1.35×10^5 BTU = 1.42×10^8 J Higher Heating Value), we obtained a very good fit of the data to the following equation:

$$EI_{\text{base}}\ (\text{J/seat-m}) = \frac{1.39\times 10^5}{S} + \frac{4.69\times 10^{10}}{S \bullet D} \quad (22)$$

where EI_{base} = base energy intensity in J/seat-m derived from actual fuel consumed
S = the number of seats
D = trip length (m).

As with maglev electrical energy, this estimate derives from energy consumed at the system connection (i.e., at the airport). As reflected in eq 22, idling, taxiing, and takeoff energy requirements cause the energy intensity for short-haul air travel to strongly depend on trip length.

Commonly, energy intensity is calculated on a per-passenger basis. Although experience with foreign HSGT suggests that maglev would operate at higher load factors than short-haul air, we compared energy intensities on a per-seat basis. However, we did correct for differences in cabin space allocated per seat for each system. As discussed in Chapter 2, we defined a standard passenger (SP) as 0.80 m^2 of cabin space (including lavatories and galleys). We then used this definition to determine the number of seats for each system for use in calculating EI.

This is an important correction. The 737-300 allocates 0.54 m^2 of cabin floor area per seat for its 140-seat arrangement. This is slightly less than the Magneplane vehicle, the least spacious of the HSGT systems studied here. Conversion to standard passengers gives this airplane 96 seats.

By using a standard passenger, we acknowledge that seat spacing is a variable easily altered by vehicle designers and operators. Provision for flexibility in seat pitch or changes from spacious five-abreast to compact six-abreast seating is well within the technology of the SCD concepts. Thus, it would be relatively simple for the more spacious concepts to increase their number of seats and hence improve their energy intensities. Although our choice of 0.80 m^2 per SP is somewhat arbitrary, use of a different value simply involves multiplying the EI values here by the appropriate ratio. Comparisons between systems would not change.

Table 62 shows the base energy intensities for each HSGT system at steady cruise, on a level guideway. We show two values for TGV—at its commercial cruise speed of 83 m/s, and projected for 134 m/s based on its parameterized drag. The latter number demonstrates a benefit in EI associated with large consists. Also shown in Table 62 are EI_{base} values for maglev vehicles making 400- and 800-km trips along the SST (TGV cannot complete the SST). The two values shown for the 400-km trip are for the first and second halves of the route, respectively (from terminal 1 to terminal 2, and from terminal 2 to terminal 4, including a stop at terminal 3). The average of these two values equals that of the full 800-km SST. For routes of similar geometric alignment, maglev EI is essentially independent of trip length.

The Foster-Miller concept has the lowest SST

Table 62. Energy intensities for each HSGT system at steady cruise speed, and for 400- and 800-km trips along the SST. These derive from base energy consumed at the utility connection.

System	*Cruise speed (m/s)*	*Standard passengers (SP)*	*Cruise* EI_{base} *(J/SP-m)*	*400-km SST* EI_{base} *(J/SP-m)*	*800-km SST* EI_{base} *(J/SP-m)*
TGV	83	700	130	—	—
	134	—	310	—	—
TR07	134	160	460	590 / 480	540
Bechtel	134	110	560	840 / 600	720
Foster-Miller	134	140	390	510 / 400	450
Grumman	134	120	340	600 / 380	490
Magneplane	134	110	400	690 / 460	580
Average of all SCDs	134	—	420	660 / 460	560
Average of best two SCDs	134	—	370	560 / 390	470

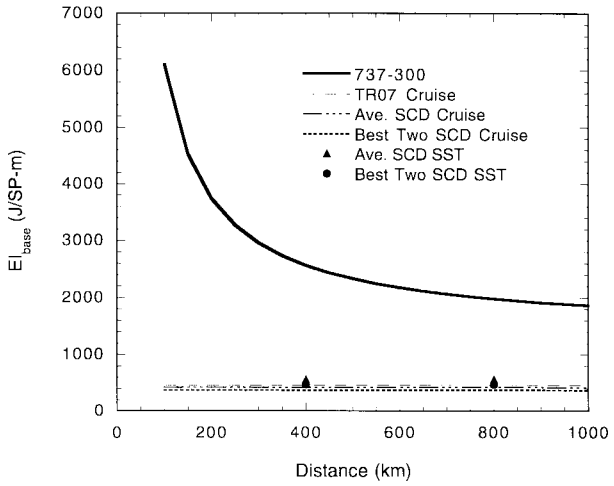

Figure 119. Base energy intensity at system connection (airport or electrical supply).

EI of the maglev concepts studied. It has the most efficient motor (the LCLSM), a fairly small frontal area, and low magnetic drag. Interestingly, Foster-Miller chose relatively conservative aerodynamic drag coefficients (see section 3.4.6), based on existing high-speed trains. TR07, Grumman, and Bechtel have vehicles that wrap around the guideway, resulting in a larger frontal area. All three concepts have low magnetic drag. However, TR07's aerodynamic drag coefficients derive from full-scale tests and thus reflect currently achievable values. Grumman appears to have anticipated drag reductions resulting from thorough study of all vehicle drag sources. Because aerodynamic drag predominates at high speed, Grumman's low cruise EI results primarily from its choice of these lower drag coefficients. Magneplane used aerodynamic drag coefficients similar to Grumman's. However, its magnetic drag at cruise speed is comparable to its aerodynamic drag, and this substantially raises its EI.

Figure 119 compares these base EI values with that of a 737-300 (eq 22) as a function of trip length. To represent U.S. maglev, we use the average of all SCD concepts and the average of the two most efficient ("best") concepts. Based on energy consumed at the system connection (i.e., airport or electrical supply), maglev EI values range from about 13 to 25% of that of a 737-300 for 200- to 1000-km trips. The very large difference for short trips highlights maglev's suitability for serving more closely spaced stations than is practical with aircraft.

Clearly, electricity and jet fuel are different commodities, and their values per joule are different. Energy cost is one way to compare energy consumption for these different fuels, essentially relying on cost to reflect differences in the value of resources used to produce each fuel. The Department of Energy produces annual estimates of fuel prices based on forecasts of supply and demand under different sets of overall economic assumptions. The baseline or "reference case" forecast for the year 2010 (DOE 1993a) predicts a jet fuel price of \$0.89 / gal. and an electricity price for transportation of \$0.065 / kWh in 1991 dollars. That is, on a per-joule basis, electricity is expected to be about three-times more expensive than jet fuel (roughly the same ratio as currently exists). Using these forecast prices, maglev would realize energy-cost savings compared to air travel of 60 to 30% for the 200- to 1000-km trip range.

Another way to reflect the difference in value between jet fuel and electricity is to account for the energy consumed to produce and deliver each fuel. Indeed, this approach has been used in previous comparisons of EI between maglev and air

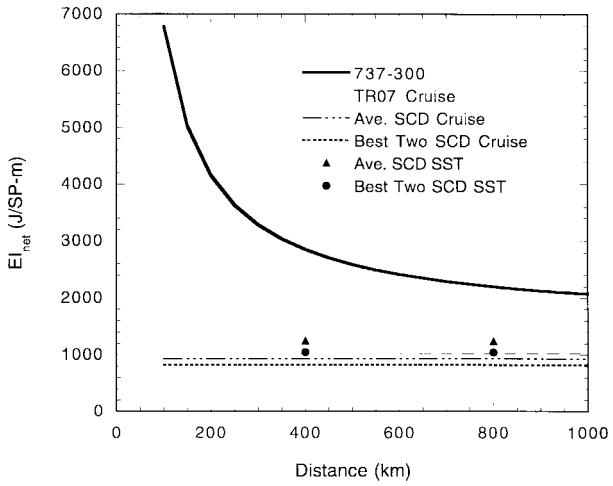

Figure 120. Net energy intensity including energy supply efficiency (90% jet fuel, 45% electricity).

travel (e.g., Johnson et al. 1989). Essentially, this approach identifies possible savings of gross energy by diverting passengers from air travel to maglev. We also did this calculation, but it is not as straightforward as it seems.

The predominant factor in this second approach is the net thermal efficiency of electrical power generation (joules-electrical output/joules-heat input). In effect, applying this factor implies that a unit of jet fuel saved in air travel is burned in a power plant to produce electricity for maglev. It places no direct value on the flexibility of electrical power production. Natural gas, coal, hydro, nuclear, solar, wind, and trash are electrical power sources that simply cannot be used to fuel commercial aircraft. What is the equivalence factor between air travel and maglev using hydro power as the energy source? Furthermore, refined petroleum powers all commercial aircraft and indeed practically all U.S. transportation. Maglev can decouple intercity travel from this dependence on petroleum, and applying simple efficiency factors does not capture this distinction.

Recognizing that it hides this important distinction, we nevertheless applied efficiency factors for energy supplied to aircraft and maglev. For jet fuel, Johnson et al. (1989) applied an efficiency of about 90% to account for transportation, refining, and distribution losses. We adopted this value as the only correction applicable for air travel. For electrical power generation and transmission, Johnson et al. used efficiencies of 35 and 95%, respectively. We also chose a 95% factor for transmission efficiency. However, 35% efficiency for power generation reflects a national average for fossil-fuel plants of varying ages and technologies. Modern natural gas-, oil-, and coal-fired plants are much more efficient than this.

Modern natural gas- and oil-fired combine-cycle plants (gas turbine with steam-turbine bottoming cycle) commonly achieve base-load efficiencies of 47–48%, based on the conservative Higher Heating Value of the fuel (Farmer 1992, Gas Turbine World 1992, DOE 1993a). Modern coal-fired plants are also approaching such efficiencies (Bajura and Webb 1991, DOE 1993b). These power plants have lower capital-cost-per-unit capacity than single-cycle plants, and they produce very low emissions. Indeed, DOE (1993a) forecasts that from 1990 to 2010, combined-cycle generating capability will grow at about 20 times the total growth rate of electrical-generating capability. Furthermore, utilities will add modern, efficient equipment to meet additional demands beyond current forecasts, such as needed to supply a major maglev network. We thus selected an electrical generation efficiency of 47%. Combined with a 95% transmission efficiency, this yields an electrical supply efficiency of 45% for maglev.

Figure 120 shows resulting net EI values for air and maglev as functions of trip length. These are the same data as in Figure 119 with the aforementioned efficiencies applied. Electrical supply efficiencies bring the EIs closer, but the results still overwhelmingly favor maglev. For 200- to 1000-km trips, maglev EI ranges from about 25 to 50% of that of a 737-300. And as noted, this comparison ignores the flexibility of power-plant fuel afforded by maglev's electrical propulsion. In terms of energy consumption and flexibility, maglev is clearly superior to short-haul air travel. TGV also shares these benefits, albeit with at a much lower performance level. Thus, all HSGT concepts studied here earn a rating of 1.2 for energy consumption.

To complete this comparison, we examined maglev trip times achieved along the SST and compared them to those for air travel. The line-haul (station-station) trip times for the SST's two 400-km segments average about 64 minutes for all SCDs. The corresponding value for the full 800-km SST is about 130 minutes. Use of the trip times for the two most energy efficient SCDs does not change these numbers significantly. Airline schedules indicate line-haul (departure–arrival) trip times of about 60 minutes for a 400-km trip and 100 minutes for an 800-km trip. Thus, line-haul trip times are comparable at 400 km, and favor air at 800 km (trip times for trips shorter than 400 km favor maglev). However, access time for maglev

should be much less than for air because maglev facilitates smaller, more conveniently located stations. That is, we would expect maglev and short-haul air to yield comparable total trip times for an 800-km trip; shorter trips should favor maglev.

In summary, maglev can provide intercity travel at much lower energy usage than aircraft, with comparable or shorter trip times, and with flexible choice of power-plant fuel. Average maglev EI would be about 50% of that of short-haul air for an 800-km trip, yet offer a comparable total trip time. As trip length reduces, maglev's energy advantage over air increases dramatically, and it offers an increasingly significant trip-time advantage. For a 200-km trip, maglev would consume about 25% of the energy of a short-haul aircraft and complete the trip in about 25% less time. From the view of energy consumption, fuel flexibility, and trip time, maglev is clearly superior to air for intercity travel.

3.4.4 Use of existing infrastructure

Use of existing highway and railroad ROW improves the likelihood of nationwide implementation of HSGT. This is a high priority item. We checked the following:

- Minimum curve radii.
- Maximum acceleration and grade capability.
- Time to go from 0 to 134 m/s.

Table 63 gives the evaluation comments and ratings for using the existing infrastructure.

3.4.5 Potential for expansion

It may be desirable to expand system capacity beyond 12,000 seats/hour. Here, we rate each concept's ability to expand capacity easily. Note that all the maglev concepts studied are propelled by an LSM. This considerable investment ultimately limits motor thrust and, hence, capacity for all systems. Its replacement with a larger LSM would be very expensive. Fortunately, most concepts can achieve very large capacity using their current LSM, so that this is not generally a serious limit. This has a medium priority. Table 64 provides the evaluation comments and ratings for expansion potential.

3.4.6 Aerodynamics

Aerodynamic drag is the predominant vehicle drag at high speeds for all HSGT systems. It, thus, is the primary source of energy consumption for maglev vehicles along high-speed routes. Both TGV and TR07 have experience with full-scale vehicles to determine drag contributions from various sources. To check the reasonableness of the SCD estimates, we cast all aerodynamic drag estimates into a common format. We also enlisted the help of Dr. D.M. Bushnell, Fluid Mechanics Division, NASA Langley Research Center. He based his comments on existing literature for high-speed trains (Hammit 1974; Railway Technical Research Institute of Japan 1984, 1989; Brockie and Baker 1990) and his broad experience with aerodynamics of aircraft and other vehicles.

Table 63. Assessments of how the concepts can use existing infrastructure.

System	*Evaluation comments*	*Rating*
TGV	Can run directly on existing rail lines, although high-speed service requires dedicated lines Large, 6000-m minimum curve radius at 83 m/s Poor grade capability Not normally elevated (grade crossings, crossing of ROW require elevated structures)	–1
TR07	5800-m minimum curve radius at 134 m/s 0.006-g reserve acceleration (0.6:100) at 134 m/s (present design cannot climb 3.5:100 grade at cruise) 320 s to 134 m/s	1
Bechtel	2600-m minimum curve radius at 134 m/s 0.12-g reserve acceleration at 134 m/s 89 s to 134 m/s	1.2
Foster-Miller	2800-m minimum curve radius at 134 m/s 0.044-g reserve acceleration (4.4:100) at 134 m/s 120 s to 134 m/s	1.2
Grumman	4100-m minimum curve radius at 134 m/s 0.048-g reserve acceleration (4.8:100) at 134 m/s 180 s to 134 m/s	1.2
Magneplane	2200-m minimum curve radius at 134 m/s 0.039-g reserve acceleration (3.9:100) at 134 m/s 130 s to 134 m/s	1.2

Table 64. Assessments of potential for system expansion.

System	*Evaluation comments*	*Rating*
TGV	Very large consists possible Bilevel cars now in production Effort to increase speed to 97 m/s now underway Rail clearance envelope limits vehicle width	1.2
TR07	Wrap-around vehicle permits width increase (although beam width fixed—limits strength) Stator slot width limits conductor current, hence motor thrust Levitation force limited by stator pack size	1
Bechtel	Slots for extra magnets in vehicle to increase payload capacity Wrap-around vehicle permits width increase (although beam width fixed—limits strength) Potential for electromagnetic switch Potential for multi-car consists	1.2
Foster-Miller	LCLSM provides great potential for reduction in headway distance Eight-car trains at 55-s headways possible Passive EM switch is very fast Channel guideway easier to strengthen, but harder to increase vehicle width	1.2
Grumman	Slots for extra magnets in vehicle to increase payload capacity More powerful motor already considered by using copper LSM winding (although slot width eventually limits capacity) Wrap-around vehicle permits width increase (although beam width fixed—limits strength)	1.2
Magneplane	Some flexibility to increase both vehicle and guideway widths Passive EM switch is very fast Very short headways possible (20 s)	1.2

Despite small differences in the methodology used for each system, we may cast each aerodynamic drag estimate in the following form:

$$D_a / q = A_x C_d + P L_n n C_f \qquad (23)$$

where: D_a = aerodynamic drag (kN)
q = dynamic pressure (11 kN/m^2 at 134 m/s)
A_x = vehicle frontal area (m^2)
C_d = drag coefficient for pressure drag (nose, base, protuberances, gaps, etc.)
P = vehicle wetted perimeter (m)
L_n = vehicle wetted length (m)
n = number of cars per consist (we used the baseline number)
C_f = skin friction coefficient.

Table 65 shows the values for these parameters for each HSGT system. Except as noted, we extracted these values directly from TGV and TR07 published literature and reports, and from the SCD final reports. Also shown is the aerodynamic drag per standard passenger (D_a/SP) for

Table 65. Parameters used for estimating aerodynamic drag for each concept.

System	A_x *(m^2)*	C_d	P *(m)*	L_n *(m)*	n	C_f	D_a/SP *(N) at 134 m/s*
TGV-A	11	0.18	13	20	12	0.0039	220
TR07	12	0.18	16	27	2	0.0037	360
Bechtel	15	0.11	18	36	1	0.0040	430
Foster-Miller	9.4	0.21	12	27	2	0.0025	280
Grumman	13	0.11	14	18	2	0.0022	240
Magneplane	7.1	0.10	10	38	1	0.0016	130
Magneplane*	8.0					0.0020	160

*We increased the estimated frontal area for Magneplane based on its revised vehicle shape; we increased Magneplane's skin friction coefficient because 0.0016 appears to be too low for the Reynolds number of the vehicle. We used these revised values to model Magneplane's performance along the SST.

each system at 134 m/s, which is a measure of the aerodynamic efficiency of the vehicle. For comparison, we have calculated D_a/SP for TGV-A at 134 m/s, although its maximum cruise speed is 83 m/s.

Bushnell's literature review suggested that the state-of-the-art for high-speed trains justifies use of $C_d = 0.15$ and $C_f = 0.004$. These values are quite close to those for TVG and TR07; the C_d value is also about midrange for the SCD estimates. However, three of the four SCDs use a much lower skin friction coefficient than that justified by the state-of-the-art. According to Bushnell, careful design and detailed attention to drag sources can yield 25% (perhaps 50%) reductions in both C_d and C_f. It thus appears that some SCD concepts incorporated such anticipated reductions. While this places some concepts at a comparative disadvantage, our aim here is to assess technical viability of U.S. concepts generally. Thus, SCD average drag values appear to be achievable almost immediately, and the lower SCD estimates appear to be achievable with solid technical effort (as would likely be part of U.S. maglev development).

Bushnell also briefly discussed sources of drag and issues affecting drag reduction. Many of these points were also noted in the SCD reports. We list them here for consideration as part of further work in this area.

Drag minimization requires thorough evaluation of all sources, including:

- Three-dimensional nose–base drag, including effects of atmospheric turbulence.
- Frictional drag, including actual surface roughness and guideway channel drag.
- Additional pressure drag components, including:
  - –Protuberances.
  - –Gaps between vehicles or components.
  - –Wake effects attributable to crosswinds or yaw.
  - –Drag ascribable to lift (caused by asymmetrical shapes and boundary conditions).
  - –Magnet bogies.
  - –Compressibility effects from passing vehicles.
  - –Trim drag (of aerodynamic control surfaces).
- Tunnel drag.
- Effects of air flow through open channel guideways and guideway outriggers.

Bushnell suggested that computational fluid dynamics models or wind tunnel tests with a moving ground plane could yield drag estimates for maglev vehicles within 10–20% of their actual values. Naturally, finer details of vehicle geometry would be needed. Present SCD estimates based on analogies with high-speed trains and aerodynamic handbooks are probably within 25–50% of actual values. Given this level of uncertainty and lack of detail, we chose not to rate the systems for aerodynamic performance.

3.4.7 Criteria summary

We may combine with the above other criteria our ratings of each concept against the SCD-RFP criteria (Table 24). This provides an overall evaluation of the ability of each concept to meet transportation needs for the U.S. market. That is, this overall rating assesses the "mission suitability" aspect of each concept's technical viability. Table 66 shows these results.

Interestingly, application of additional evaluation criteria did not change the relative ranking of the concepts. However, the gap between TGV

Table 66. Overall assessment of mission suitablity of HSGT concepts studied.

Parameter	*Weight*	*TGV-A*	*TR07*	*Bechtel*	*Foster-Miller*	*Grumman*	*Magneplane*
RFP system criteria subtotal	53	38	48	46	56	56	56
Other Criteria							
Mission flexibility	3	–1	1	1.2	1.2	1.2	1.2
Tilting	2	–1	–1	1	1	1	1
Energy efficiency	3	1.2	1.2	1.2	1.2	1.2	1.2
Existing infrastructure	3	–1	1	1.2	1.2	1.2	1.2
Expansion	2	1.2	1	1.2	1.2	1.2	1.2
Aerodynamics	0						
Subtotal	13	–2	10	15	15	15	15
Total	66	36	58	61	71	71	71

and the maglev concepts widened substantially. This technology does not meet as extensive a set of U.S. transportation needs as do the maglev technologies. Also, this assessment revealed a somewhat greater capability of the U.S. maglev concepts vs. TR07 to meet U.S. transportation needs. TR07 suffered primarily for its lack of a tilting vehicle and its modest motor capability. Except for Bechtel's selection of a fuel cell for onboard power supply and its incomplete suspension description, all U.S. concepts met or exceeded all criteria and yielded essentially identical scores.

As with the SCD system criteria, evaluation of the concepts against the additional criteria in this section was a helpful step in our technical viability evaluation process. The mission-flexibility criterion forced us to consider transportation needs beyond those served by intercity trunk service. Similarly, our aerodynamic assessment placed the concepts in a common format and improved our understanding of the various procedures used to estimate aerodynamic drag. Perhaps most insightful was our energy-efficiency assessment. This comparison required data from several of our analyses (motor and power, system simulation, aerodynamics) and helped to reveal maglev's role relative to existing short-haul air service. We may now draw upon the insight gained here to discuss the overall technical viability of maglev for the U.S.

CHAPTER 4. OVERALL TECHNICAL VIABILITY OF CONCEPTS

The GMSA effort described in chapters 2 and 3 above concentrated on generating data and examining technical characteristics for each concept. Essentially, this provided the input necessary for evaluating the technical viability of maglev in the U.S. In chapter 4, we use this information to address specific aspects of technical viability (see Tables 1 and 3, which list the general performance features of each concept).

4.1 LONG-TERM POTENTIAL OF MAGLEV COMPARED WITH HSR

High-speed rail possesses impressive performance characteristics and could meet many of the requirements thought to be important for a favorable market response to maglev. Indeed, TGV offers a proven, commercially successful, 83-m/s service, and this service is available for the U.S. with essentially no development risk. In addition, its current performance limits may be governed more by cost–benefit optimization than by physical constraints, and further development will undoubtedly raise these limits. We may then ask whether maglev possesses specific attributes that, in the long term, will provide it a clear performance advantage over HSR. If it does, this provides some rationale for bypassing HSR in favor of developing maglev, despite the latter's significant development cost and risk.

We discussed several technological issues that appear to favor maglev over HSR. In most cases, HSR's shortcomings are not absolute physical constraints and could be mitigated with sufficient development and maintenance efforts. Indeed, HSR's present performance levels have resulted from just such efforts. While laudable, this process has been slow and costly, and future improvements will require proportionately greater investment.

By comparison, maglev is a new technology specifically intended to start with performance capability beyond that of current HSR. While its development costs and risks are substantial, they may be no greater than those required to bring HSR to a similar performance level. More importantly, future incremental improvements should be much easier for maglev than HSR. This difference in incremental effort to achieve incremental performance gains is a basis for identifying long-term advantages of maglev over HSR. Other authors have expressed this same argument for maglev (Gran 1990) and for new technologies generally (Foster 1986).

The following sections (4.1.1 to 4.1.9) contain the technical issues that we feel best reflect the long-term advantages of maglev vs. HSR. Note that commercial service speed (or service speed) denotes a speed that is sustainable in commercial operation with acceptable margins of safety and life-cycle costs. We use TGV-A as our primary HSR example, although we note differing technical characteristics of other HSR systems where appropriate.

4.1.1. Speed

TGV-A offers 83-m/s commercial service, and has demonstrated a sustained speed of 133 m/s and a peak speed of 143 m/s. Thus, steel-wheel-on-rail technology is directionally stable at maglev's design-goal speed of 134 m/s. Nevertheless, such speeds were not the original design target of this technology; high-speed stability has been achieved through incremental improvements in aerodynamics, truck design, and rail-bed stiffness and alignment. For reasons of safety margin or life-cycle costs, TGV does not currently operate at 134 m/s, and it would require further improvements to do so. By their nature, such improvements would entail development, capital, and maintenance costs that are even higher than the significant costs incurred for 83-m/s service.

Power transfer by pantograph–catenary contact may be HSR's most immediate speed limiter. Observers noted that arching between the pantograph and catenary was almost continuous throughout TGV's 143-m/s run. Such arching leads to rapid deterioration of both components. Even with steady contact, pantograph–catenary wear will increase with speed, thereby increasing maintenance costs. TGV must solve both the contact and wear problems to use pantograph–catenary power transfer at service speeds of 134 m/s and higher.

SNCF/Gec Alsthom have begun work to develop an actively controlled pantograph to enable TGV to reach higher speeds. They have allocated $120 million for this and other improvements to TGV to raise its cruise speed to 97 m/s by 1995. Their effort is also supplemented by the general HSR R&D effort worldwide. Such large investments for incremental speed increases are characteristic of mature technologies such as steel wheels on rails. Indeed, both Japan and Germany see 97-m/s service as a goal requiring substantial R&D investment over the next 5–10 years.

By comparison, high-speed potential is essentially an inherent characteristic of maglev. Guid-

ance and propulsion occur without physical contact. Magnetic elements (coil layout, reaction components, field strengths, etc.) are broadly adjustable to achieve the guidance forces necessary for very high speed. Similar flexibility in design exists for guideway structural members. Furthermore, with a long-stator LSM, propulsion power does not need to be transferred to the vehicle. In essence, maglev comes "out-of-the-box" ready for 134-m/s service. Higher-speed service is well within the technology, and its associated higher capital and operating costs become simply part of the system-level trade-off with expected market demand for the service. If run in evacuated tubes, maglev has an extremely high ultimate-speed potential.

In principle, HSR could utilize a long-stator LSM for propulsion to circumvent pantograph–catenary power transfer. However, this would entail high development costs and an enormous infrastructure investment on par with those for a maglev LSM. Essentially, such a system would substitute steel-wheel-on-rail guidance for magnetic guidance and would thus still encounter high incremental development costs for that element.

Speed, through its influence on trip time, strongly influences forecasts of the U.S. market response to HSGT. However, the question of how much speed is enough depends on how much the traveler must pay for it. It seems likely that maglev will achieve service speeds of 134 m/s more easily than will HSR; this should translate into lower costs and hence lower ticket prices for the traveler. While maglev requires development investment just to begin commercial service, HSR will also require substantial R&D to reach 134 m/s (given that 97 m/s is viewed as a significant challenge). Even if the two are comparable in performance and cost at 134 m/s, a desire for future speed increases favors maglev.

4.1.2. Trip time

Trip time strongly influences ridership for transportation systems. In addition to a much higher speed potential, maglev possesses other performance characteristics that combine to deliver shorter trip times than HSR.

TVG's maximum acceleration is 0.04 g from 0–16 m/s, and this falls to 0.03 g at 50 m/s. By comparison, maglev's maximum low-speed acceleration is four times TGV's, constrained basically by ride comfort. Additionally, the U.S. maglev concepts have reserve acceleration in access of 0.04 g at 134 m/s. Superior acceleration capability permits maglev to maintain higher speeds on grades (e.g., 140 m/s on a 3.5% grade for the U.S. concepts compared with 30 m/s for TGV). It also allows for more rapid return to full speed following reduced-speed curves.

TGV's trip times along existing ROW also suffer from lack of vehicle tilting capability. TGV's total bank angle is only 7° compared with an average of about 30° for U.S. maglev concepts. Although tilting HSR systems exist, none are capable of even 83-m/s service.

Longer trip times makes HSR less attractive than air travel, as well as other transportation modes, resulting in lower ridership and revenues. Relative to maglev, such lower revenues can offset HSR's capital cost advantage and yield lower profitability.

4.1.3. Mission flexibility

HSR is best suited to short to intermediate intercity trunk service. TGV's fixed-consist, non-tilting trains, lower cruise speed, and lower overall acceleration–deceleration render it poorly suited to other transportation needs beyond this. This lack of flexibility ultimately limits the market penetration and profitability of HSR.

Besides offering superior intercity trunk service, U.S. maglev concepts show considerable potential to serve additional missions. Such flexibility derives from the much greater performance capability of the technology. Mission flexibility helps to reduce the risk that intercity trunk service is not where the greatest HSGT market lies. Also, by offering other services (regional airport connector, commuter trunk, point-point, long-haul trunk), maglev increases its overall ridership potential in a major transportation network. This provides some confidence that an investment in maglev will fulfill a broad spectrum of U.S. transportation needs.

4.1.4. Maintenance

HSR relies on wheel–rail contact for lift, guidance, acceleration, and braking, and pantograph–catenary contact for power transfer. To achieve low rolling resistance and adequate adhesion, the wheels and rails contact each other over an extremely small area; to avoid arching, the pantograph must firmly press against the catenary. In both cases, the resulting contact stresses are high and thus produce wear. TGV conducts scheduled maintenance to ensure that wheels are smooth and round, rails are correctly profiled and accurately aligned, and pantograph and catenary wear are within allowable limits. This is costly and time consuming. Because wear rates increase with speed, the cost and effort necessary to alleviate them are significant impediments to higher service speeds.

By its nature, maglev requires no physical contact between vehicles and guideways. Lift and guidance forces are distributed over large areas, yielding much lower stresses than wheel–rail contact. Furthermore, an LSM offers contactless propulsion and braking; in long-stator form, it also avoids the need to transfer propulsion power to the vehicle. Through good design, attachments securing magnetic elements to either vehicles or guideways should require little maintenance. Overall, maglev offers a potential for very low maintenance costs.

4.1.5. Adhesion

Wheel–rail adhesion (or contact friction) poses physical limits on HSR's propulsion and braking forces. In normal operation, adhesion limits HSR's grade-climbing ability and maximum acceleration rate. It also limits maximum deceleration during emergency stopping. This results in increased trip times for routes with frequent accelerations and stops. To decouple braking from adhesion limits, Germany's ICE train uses an eddy current brake; it is capable of 0.2–0.25 g of deceleration for speeds over about 10 m/s.

TGV's dependence on adhesion for braking directly affects headway allotments: the maximum no-skid deceleration rate (plus safety margin) limits TGV-A's minimum headway to 4 minutes (expected to be reduced to 3 minutes). Because adhesion depends strongly on the condition of the wheel/rail interface, rain, wet leaves, snow, and ice will tend to worsen HSR performance. TGV-A must reduce speed in heavy rain or snow to maintain its minimum headway.

By comparison, there are no physical limits on maglev's propulsion and braking forces. Its practical limits are subject to design trade-offs involving ride comfort, motor thrust and power, guideway and vehicle structural strength, etc. Because magnetic fields transmit these forces without contact, adverse weather does not alter them. For emergency stopping, maglev may use skids specifically designed for generating high frictional forces rather than being limited to steel-wheel-on-rail friction. These characteristics lead to shorter trip times and substantially reduced headways (less than 1 minute) compared with HSR.

4.1.6. Safety, availability, and cost

HSR in both Europe and Japan have exemplary safety records. However, the technology requires extensive maintenance (inspections and adjustments) to achieve such safety. Maglev possesses characteristics that should permit it to maintain safe, high-speed operations under more extreme conditions and with less maintenance. That is, maglev offers the potential for higher system availability and lower cost at safety levels comparable to HSR.

Several maglev concepts employ vehicles that wrap around their guideways. Others have guideways that partially wrap around their vehicles. Such approaches can provide more than 1 g of "derailment" containment in the event of extreme environmental disturbances or component failures.

Large-gap maglev systems are much more tolerant of ground displacements caused by earthquakes than is HSR. These displacements can be larger for maglev before triggering ride-comfort-, safety-, or wear-related maintenance. Greater tolerance also provides an added margin for bringing high-speed vehicles safely to rest during earthquakes. Such features are extremely important for safety of HSGT in many parts of the U.S.

Maglev's contactless propulsion and braking render it less susceptible to snow, ice, and rain than HSR. Also, maglev concepts with wrap-around guideways offer some protection from crosswinds. These features offer maglev a potential of higher availability in adverse weather for safety comparable to HSR.

Maglev should be capable of achieving HSR's outstanding safety record. Its greater tolerance to both earthquakes and adverse weather may well be decisive advantages in availability and cost in the more demanding U.S. environment.

4.1.7. Noise

Maglev avoids a major source of noise generated by HSR—wheel–rail contact. It also generates no pantograph–catenary noise. These noise sources predominate at low speeds and thus may trigger speed limitations or mitigation measures for HSR sections in urban areas. Maglev at low speeds can be considerably quieter than HSR—it will travel faster through an area with a set noise limit.

Figure 121 shows peak sound-pressure levels (*Lmax*) measured at 25-m distance for several HSGT systems (Hanson et al. 1993). To meet an 80-dBA limit, Shinkansen and Amtrak must stay below about 25 m/s, and ICE must stay below about 40 m/s (data for TGV do not extent to these lower speeds). By comparison, TR07 may proceed as fast as 50 m/s and still meet an 80-dBA noise limit. This is a 25% performance advantage. For noise limits from 85 to 95 dBA, TR07's speed advantage over ICE and TGV is 15–20 m/s. This will yield reduced trip times for routes with noise-limited sections,

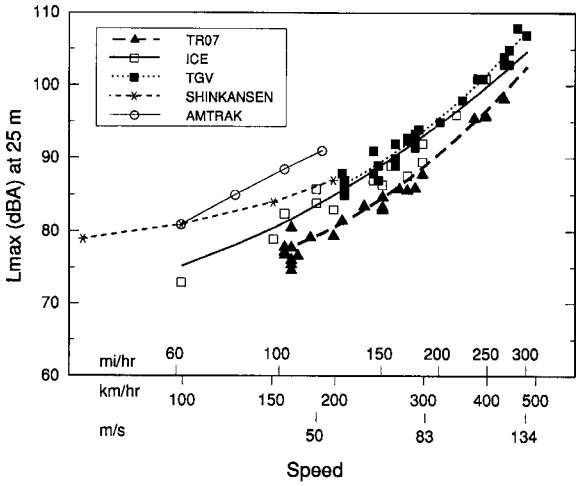

Figure 121. Noise from maglev and high-speed rail systems. (From Hanson et al. 1993.)

such as those along the northeast corridor. Although current high-speed trains cannot achieve cruising speeds of 134 m / s, the data indicate that maglev would be 5–7 dBA quieter at this speed. Such lower noise emissions will be important along high-speed, rural route sections.

4.1.8. Use of existing infrastructure

Despite being able to run at low speed on existing rail lines and use existing railroad stations, HSR has serious shortcomings in its use of existing infrastructure. HSR vehicles are heavier than maglev vehicles (700 kg / SP for TGV-A vs. 530 kg / SP for the SCD concepts). This increases HSR's expense as an elevated system, which may be necessary along existing ROW. HSR also has poorer curving and grade-climbing capability than maglev, and it generates more noise. Collectively, these features place HSR at a serious disadvantage relative to maglev along routes using existing highway and railroad ROW.

4.1.9. Strategic technology

Maglev and HSR represent radically different technologies. HSR represents the end-product of two centuries of incremental development. By comparison, maglev encapsulates many of the best technologies that the late 20th century has to offer. It may well drive the refinement and commercialization of many strategically important spin-off technologies. The country that leads maglev R&D will also be poised to lead this commercialization effort.

The following is a list of the most significant strategic technologies associated with maglev. Note that these technologies have applications in many fields, including military, aerospace, medical, and civil infrastructure:

- Superconductivity
- Cryogenics
- Power electronics
- Composite vehicle structures
- Composite reinforced concrete
- Smart structures (for integrity monitoring)
- Advanced manufacturing and construction techniques
- Active vehicle suspensions
- Automated system controls
- Intrusion / obstacle detection
- Maglev launchers
- EMF shielding
- EMF biological effects
- Market demand modeling (especially verification)
- Ride-comfort modeling
- Public–private joint venturing.

4.2. PERFORMANCE POTENTIAL OF GENERIC U.S. MAGLEV COMPARED WITH TR07

The GMSA team has carefully examined and analyzed the performance of TR07 and four well-defined U.S. maglev concepts. Here, we compare the potential for a U.S. concept to offer superior performance to TR07 in the U.S. market. Because the four SCD concepts differ in detail, some conclusions are valid for specific concepts. However, several performance features are not concept-specific; with care, we may aggregate such characteristics into what may be termed a "generic U.S. maglev" system.

As with our comparison between maglev and TGV, we recognize that TR07 will undoubtedly benefit from further R&D. Nevertheless, the predominant argument in favor of beginning maglev deployment with TR07 is to avoid development costs and risks. This argument assumes that TR07 is basically already in the form needed for rapid commercial acceptance in the U.S. We are, thus, free to compare the possible performance of U.S. maglev concepts against the existing characteristics of TR07. Any significant R&D needed to upgrade TR07 offsets its principal advantage—the perceived lack of development costs and risks.

We may note here that, unlike TGV, TR07 does not offer commercial service anywhere in the world.

Indeed, it has not yet entered production. Apparently, investors have not yet agreed that its performance characteristics justify its costs, particularly its high (guideway-dominated) capital costs. Transrapid may need to conduct additional R&D to rectify this situation. This requirement may place TR07 on a more equal basis with a concerted U.S. maglev development effort.

4.2.1. Performance efficiency

Comparisons of performance and cost of TR07 and U.S. maglev concepts revealed two important findings: 1) U.S. maglev can offer slightly better performance than TR07 at much lower cost (especially for at-grade sections), and 2) U.S. maglev can offer much better performance than TR07 at similar cost.

For example, the Grumman system offers 9% lower SST trip time and 9% lower energy intensity for about 12% lower elevated-guideway cost (or about 37% lower at-grade-guideway cost) compared with TR07. Similarly, the Bechtel concept offers a 14% SST trip-time savings for about 2% higher elevated-guideway cost (or 20% lower at-grade-guideway cost).

While these are specific SCD concepts, they illustrate the potential performance–cost advantages likely to result from a U.S. maglev development effort. Furthermore, the performance advantages of the SCDs increase along twisty routes (e.g., Interstate Highway ROW) and for more aggressive ride-comfort criteria. These results give designers some flexibility in the selection of system characteristics to make performance cost optimal for U.S. market conditions.

4.2.2. Suitability to existing rights-of-way

The SCD concepts indicate that a generic U.S. maglev system will be much better suited than TR07 to deployment along existing ROW. A U.S. system will require about half the curve radius of TR07 at 134 m/s (about 3 vs. 6 km). It will climb much steeper grades at full speed (more than 4% grade vs. less than 1%). From a stop, it will reach 134 m/s in less than half the time (about 130 vs. 320 s). These characteristics mean that a U.S. maglev system will achieve much shorter trip times along existing, lower-speed ROW (e.g., Interstate Highways, conventional rail). For example, 18 minutes of Bechtel's 21-minute SST trip-time savings take place in the first, twisty segment that represents an Interstate ROW. Essentially, greater curving and acceleration capability allows U.S. maglev to have an average trip speed closer to its peak speed than TR07.

In principle, Transrapid could upgrade TR07 with a tilting vehicle body to improve curving performance and a larger LSM to increase grade climbing ability and peak acceleration. However, the former would involve a major redesign of the vehicle, an increase in roll stiffness of the magnetic suspension, and strengthened curved guideway beams. Upgrading the LSM may prove more difficult because the slots in the stator pack limit the diameter (and hence the current capacity) of the stator windings. While these improvements are possible, they would not occur without significant R&D time, costs, and risks.

4.2.3. Gap size

By using normal electromagnets, TR07 must operate with a small, 8-mm suspension gap. It must, therefore, maintain very tight guideway tolerances to avoid magnet contact and ensure adequate ride comfort. It achieves these tolerances by precision machining of steel guideway beams and using very conservative foundation designs. These measures come with significant cost penalties, including the inability to use conventional concrete beam construction. Tight tolerances also imply that even small earthquake deformations may require a costly system shut-down and realignment of beams. This could render TR07 impractical along several important U.S. corridors.

By comparison, all U.S. concepts operate with much larger suspension gaps (40–150 mm) by using powerful, superconducting magnets. Such large gaps provide greater design freedom—larger construction tolerances are permissible, as are more flexible guideways (provided active suspensions are used). Both effects can substantially reduce the cost of guideway structures (10–40%). Larger gaps also provide much more leeway in foundation design and much greater operational and safety margins in earthquake-prone regions. Indeed, earthquake considerations are thought to be among the reasons that workers in Japan elected to develop a large-gap EDS.

Typically, maglev vehicles may safely transit step irregularities about half as high as their gap clearance. For the U.S. systems, with their much larger gap, this implies greater tolerance of debris, snow, and ice, and guideway misalignment from earthquakes. Also, large-gap systems are less susceptible to thermal disturbances. As with HSR, U.S. maglev should be capable of higher availability than TR07 at similar safety levels. To ensure adequate ride comfort over very rough or flexible guideways, vehicles may require active suspensions (three of the four SCD concepts incorporate

active suspensions). However, improvements in availability and reductions in guideway costs more than compensate for this added complexity.

4.2.4. Energy efficiency

Energy consumption can be the largest variable cost for high-speed ground transportation systems. Energy usage in transportation is also a national strategic concern. Systems with high energy efficiency are therefore more desirable, other factors being equal, than those of lower energy efficiency.

We have used energy intensity, EI (joules / standard-passenger-meter), as a measure for the HSGT systems studied here. Compared with TR07, the average energy intensity of the two most efficient U.S. concepts is 18% lower at steady cruise and 12% lower for the SST. Interestingly, these same two concepts complete the SST in about 11% less time than TR07. It appears that U.S. maglev may offer superior performance for less energy, an impressive combination.

Several factors account for U.S. maglev's superior trip times and energy efficiency. The most important is the provision of vehicle tilting. Tilting allows a vehicle to maintain good ride comfort at higher speeds through turns. This reduces trip time directly and reduces energy needed to accelerate the vehicle back to cruise speed following the turn. The effect is most pronounced along twisty routes (e.g., typical interstate ROW). U.S. maglev concepts are also lighter than TR07, which further helps to reduce both trip times and energy consumption.

Another important factor affecting trip time and energy consumption is the aerodynamic drag acting on the vehicle. TR07's aerodynamic drag coefficients are well established and are comparable to those of high-speed trains. Some SCD contractors, however, selected lower drag coefficients that anticipate drag-reduction efforts expected in a U.S. maglev development program. Nevertheless, one of the two most energy-efficient concepts (Foster-Miller) has similar drag coefficients as TR07. Its aerodynamic drag is lower because of its lower frontal area. Foster-Miller's higher energy efficiency also in part comes from its more efficient motor. Improvements in aerodynamic drag and motor efficiency are reasonable to expect under a comprehensive U.S. maglev development program. Such improvements, combined with lighter, tilting vehicles, would indeed provide U.S. maglev with superior energy efficiency and lower trip times compared with TR07.

4.2.5. Vehicle efficiency

All SCD vehicles will be built with modern aerospace construction techniques, and two of the four use advanced composite construction. Superconducting magnets also have greater lift per magnet-weight than TR07's normal electromagnets and do not require heavy backup batteries to ensure safe hover. Thus, despite including the vehicle tilting capability, U.S. maglev vehicles are lighter than TR07. On average, the SCD vehicles are 18% lighter per standard passenger than TR07, and the composite vehicles average 24% less mass per standard passenger. Composites also better resist fatigue and corrosion than does aluminum construction.

Lower vehicle mass improves energy efficiency and lowers guideway costs by reducing vehicle loads. Although composite construction currently carries a cost premium, system life-cycle costs may favor its use. Also, further developments in the aerospace industry should improve the cost effectiveness of composite vehicles. The U.S. aerospace industry leads the world in composite aircraft construction; it is thus reasonable to expect that U.S. maglev vehicles will benefit from this expertise.

4.2.6. Switching

TR07's switch is a steel guideway section that is bent elastically in the turnout direction. This high-precision mechanical switch moves relatively slowly and may be susceptible to adverse weather effects (ice, blown sand, thermal expansion, etc.). These factors also suggest that TR07's switches will require frequent maintenance (inspections and adjustments).

Two of the SCD concepts (Foster-Miller and Magneplane) have electromagnetic switches that require no moving structural elements. They switch null-flux coils to guide their vehicles though turnouts. A third SCD (Bechtel) explored an electromagnetic switch as an alternative to their bendable-beam switch. Such electromagnetic switching can be very fast, leading to shorter possible headways. Without moving parts, these switches should also be less susceptible to adverse weather. They should thus require less frequent maintenance compared to mechanical switches. That is, U.S. maglev offers a potential for higher-performance, more-reliable guideway switches than TR07.

4.2.7. Higher speed potential

GMSA motor and suspension analyses showed that TR07 is near its speed limit at 134 m / s. To meet levitation requirements, TR07's LSM has a shorter pole pitch than the SCD concepts. It thus operates at a higher frequency (255 Hz compared with less than 100 Hz for the SCD concepts), increasing performance demands on converter-station power elec-

tronics. As noted, stator slot width also limits the LSM current and hence its peak thrust. Altering these parameters would entail a major redesign of TR07's motor and levitation systems.

Despite very tight guideway tolerances, TR07's suspension appears to be near its ride-comfort and safety limits at 134 m / s. Power transfer to the vehicle, saturation of the levitation magnets, and the use of a passive secondary suspension provide a second set of limits to the speed potential of TR07.

The U.S. concepts, by comparison, are much farther from their ultimate speed limits at 134 m / s than is TR07. They use lower frequency LSMs and have greater freedom in stator conductor sizing. They also require much less onboard power. Furthermore, several concepts have adopted active suspensions to maintain adequate safety and ride comfort over rougher, more flexible guideways than TR07's; if these concepts had guideways built to TR07's tolerances, their suspensions could handle much higher speeds.

4.3 ADVANTAGES AND DISADVANTAGES OF U.S. MAGLEV CONCEPTS

As noted in Chapter 1, the goals of the GMSA were to assess the technical feasibility of maglev concepts, to assess their abilities to meet U.S. transportation needs, and to compare their performance potential with foreign HSGT alternatives. Neither the GMSA nor the National Maglev Initiative sought to pick a "winning" U.S. maglev concept. As reflected in sections 4.1 and 4.2, our interest was primarily in determining the range of technical capability represented by the SCD concepts.

Nevertheless, every technical approach to HSGT carries with it advantages and disadvantages. Through our modeling efforts and comparative assessments, these features became apparent. Sections 4.1 and 4.2 discussed the merits of the U.S. concepts compared with TGV and TR07. Here, we discuss the advantages and disadvantages of each SCD concept. We have made no attempt to rate these systems relative to each other. Again, this was not our goal, and it would not be meaningful at this concept-definition stage.

4.3.1 Bechtel

Advantages

- Octapole magnet configuration:
  - Fields fall rapidly with distance (reduces passenger shielding requirements).
  - Transferable to other concepts.
- Powerful LSM:
  - High acceleration throughout speed range reduces trip times (0.16-g acceleration maintained to 118 m / s).
  - Can climb 10% grade at 140 m / s.
- High magnetic lift / drag (magnetic $L/D > 100$ at 134 m / s):
  - High payload:weight ratio possible.
  - Low-speed liftoff out of stations does not require auxiliary support (assisted by vertical motor thrust to about 10 m / s).
- No landing wheels (air bearings used): this provides weight, reliability, and cost advantages.
- Fault-tolerant headway, suspension, and propulsion control:
  - Greater safety, reliability, and availability.
  - Six-phase LSM offers significant degraded-mode capability.
- Cable-in-conduit superconducting magnets:
  - Potential for greater stability, lower weight, and lower thermal losses.
  - No external leads needed.
- Sidewall null-flux levitation provides more than 3-g vertical derailment protection.
- Some flexibility in vehicle outer dimensions.
- Tilting inner cabin allows aerodynamically clean exterior.
- Door sizes and spacing, and interior dimensions, permit rapid loading and unloading.

Disadvantages

- Large aerodynamic loads (especially side loads) from wrap-around vehicle:
  - Low crosswinds limit for ride comfort and safety (lower weather-related availability).
  - Large aerodynamic drag per standard passenger (high energy intensity).
- Aerodynamic control surfaces:
  - Increased control complexity.
  - Susceptible to atmospheric turbulence.
  - Increased aerodynamic drag.
- Bending-beam switch:
  - Must be made of FRP (expensive, unproven durability).
  - Long cycle times.
  - Moving load-bearing parts (lower reliability, higher cost).
- May require FRP reinforcing rods:
  - Expensive compared with conventional steel rods.
  - Unproven durability of rods and anchorages.
- Tilting inner cabin increases weight and complexity.

4.3.2 Foster-Miller

Advantages

- Locally commutated linear synchronous motor (LCLMS):
  - High efficiency (short energized length).
  - Power transfer possible with same guideway coils and switches.
  - Very short headways possible, and it is easy to vary headways operationally.
  - Can use motor to bring emergency vehicle to a stationary vehicle.
  - Transferable to other concepts.
  - Individually controlled coils offer significant degraded-mode capability.
- U-shaped guideway:
  - Partially protects vehicle from crosswinds (improves safety and ride comfort).
  - Together with null-flux levitation, provides more than 3-g vertical derailment protection.
  - Yields low cross-sectional area, hence low aerodynamic drag.
- High-speed electromagnetic switch:
  - Load-bearing parts are stationary (low maintenance, high reliability).
  - Very fast cycle times possible.
- Magnets in bogies at ends of vehicles:
  - Reduces suspension weight.
  - Reduces frontal area and hence aerodynamic drag.
  - Separation from passengers reduces shielding requirements.
  - Permits simple pivot arrangement for tilting.
- Most well developed EDS levitation and guidance configuration, provides low development risk.
- High magnetic lift / drag (magnetic $L/D > 140$ at 134 m / s):
  - High payload:weight ratio possible.
  - Low magnetic losses.
  - Low-speed liftoff out of stations possible using vertical motor thrust (although not proposed by contractor).
- Series coupled propulsion coils for guidance:
  - High lateral stiffness.
  - Less complex than independent guidance configurations.
- High guideway roll stiffness.

Disadvantages

- High risk with LCLSM:
  - Critically dependent on high-volume cost reductions (factor of 10) for IGBT-based inverters rated for the required voltages and currents.
  - Unproven concept for vehicle control (requires real-time computer control of individual H-bridges).
- May require FRP post-tensioning rods:
  - Expensive compared with conventional steel rods.
  - Unproven durability of rods and anchorages.
- Bogie design increases dynamic amplification factor so that a stiffer guideway is needed to meet ride comfort criteria.
- Complex vehicle and bogie fairing needed to permit tilting.
- High liftoff speed proposed (50-m / s takeoff, 20-m / s landing). This requires low-speed equipment for normal operation, with associated weight, reliability, and cost penalties.
- Highest magnetic fields to mitigate (although the design achieved 1 G at a modest weight penalty).
- Vehicle width fixed by U-shaped guideway.
- At-grade U-shaped guideway susceptible to snow drifting.

4.3.3 Grumman

Advantages

- Large-gap electromagnetic suspension:
  - Active primary suspension offers potential to meet safety and ride-comfort constraints over rougher, more flexible (hence cheaper) guideways.
  - No secondary suspension needed (saves weight, cost, maintenance).
  - Integrated lift–guidance–propulsion saves weight, space, and cost (vehicle and guideway).
  - Active control of magnetic suspension avoids need for aerodynamic control surfaces (saves weight, complexity, and cost, and there is less influence of turbulence).
- Innovative spine-girder dual guideway:
  - Structurally very efficient, yields low cost for dual guideway.
  - At-grade guideway costs also low because inexpensive Y-shaped beams can be supported directly on piers.
- Conventional guideway materials and construction techniques:
  - No FRP needed.
  - Close tolerances needed only at Y-shaped beams (lowers cost for spine-girder and outriggers).

- Distributed magnets lower guideway stresses and dynamic amplification factors, giving a smoother ride for a given guideway roughness than bogies.
- Zero-speed levitation eliminates routine need for low-speed support (wheels, etc.).
- Low stray magnetic fields, so little or no shielding needed to meet 1-G level, which saves weight, and cost.
- Simple, conservative superconducting magnet design, having a good quench margin.
- Recompression of helium vapor avoids liquefying refrigerator, giving improved reliability and energy consumption.
- Small onboard power storage requirements since main levitation force derives from superconducting magnets

Disadvantages

- High-risk active primary suspension:
  – Demanding active control of electromagnets superimposed on superconducting magnets.
  – All control modes coupled.
- Wrap-around vehicle requires bending-beam switch:
  – Longer cycle times.
  – Mechanically complex, and susceptible to adverse weather.
- Large frontal area from wrap-around vehicle increases aerodynamic drag.
- Complex outrigger, slab girder (Y-shaped beam) and LSM attachments:
  – Some tensile stresses in concrete outriggers.
  – Tight packaging of LSM.
- Demanding packaging of superconducting and normal magnets:
  – Space limits iron-core size (Vanadium-Permendur near saturation).
  – Limited liquid helium reservoir.

4.3.4 Magneplane

Advantages

- Self-banking vehicle, so no tilting mechanism needed (saves weight, complexity, cost).
- Very smooth lift and guidance forces from sheet guideway.
- Trough guideway:
  – Provides some crosswind protection.
  – Permits small vehicle cross-section (low aerodynamic drag).
- High-speed electromagnetic switch:
  – Load-bearing parts are stationary (low maintenance, high reliability).
  – Very fast cycle times possible.
- Active suspension and very large gap:
  – Permits use of rough, flexible (hence less costly) guideway.
  – Gap of 150-mm provides significant tolerance to settlement and earthquake displacements before triggering safety- or ride-comfort-driven maintenance.
  – No secondary suspension needed (lower weight, complexity and cost).
- Simple guideway magnetics (sheet guideway):
  – Fewer attachments and adjustments needed.
  – Potentially low maintenance.
- Very short headway possible:
  – Electromagnet switch permits fast cycle times, high turnout speed.
  – High braking rate possible.

Disadvantages

- Expensive guideway:
  – Nationally significant aluminum content.
  – Most sensitive to energy prices.
- Aerodynamic control surfaces:
  – Increased control complexity.
  – Susceptible to atmospheric turbulence.
  – Increased aerodynamic drag.
- High magnetic drag:
  – High, nearly constant thrust requirements even at low speeds.
  – High liftoff (50 m/s) and landing (30 m/s) speeds increases performance demands on low-speed supports.
- Single LSM, no redundancy in phases, which increases the risk of single-point failure.
- Unproven low-speed air bearings, which is a substantially higher speed application of this technology than current state-of-the-art (about 5 m/s).
- Fewer suspension magnets, which means increased consequences of magnet failure.

4.4 KEY INNOVATIONS: RISKS AND BENEFITS

The SCD concepts contain numerous innovations in maglev technology. Many of these offer the potential for significant performance or cost advantage over existing German and Japanese technology. Naturally, these same innovations carry some development risk. Here, we summarize the key innovations revealed by the SCDs, describe their potential benefits, and indicate the level of risk associated with each. The order below is random.

4.4.1 LCLSM

Foster-Miller's locally commutated linear synchronous motor (LCLSM) energizes discrete guideway coils through individual inverters to propel a maglev vehicle. A computer controls the current and synthesizes a three-phase wave form through each set of coils using pulse-width modulation of a DC supply voltage. Foster-Miller proposes to use fast IGBTs as the necessary switches for these inverters. The LCLSM could become a very significant innovation in vehicle propulsion.

This motor achieves very high efficiency (99%) because it energizes only that section of the guideway opposite vehicle magnets. By activating individual coils on a 0.86-m spacing, it provides very flexible thrust and regenerative-braking control of the vehicles.

Another significant advantage is the ability of the LCLSM system to operate in a degraded mode in the presence of disabled LSM coils. All coils are electrically connected in parallel with respect to the power source and disabled coils can be disconnected without adversely affecting the operation of the remaining LSM coils. This is in contrast to the more conventional blocklength LSM, where a failure of the LSM could disable the entire block (a few hundred to a few thousand meters in length) and either stop the system or severely curtail its operation until repaired.

The LCLSM also acts as the power-transfer mechanism, where the guideway coils form the primary of an inductively coupled system. The computer switches the guideway coils located between vehicle bogies from propulsion mode to power-transfer mode. Power is then inductively transferred to auxiliary power coils located between bogies on the vehicle.

Its principal risk is that the IGBT-based inverters are at present much too expensive for the LCLSM to be economical. Foster-Miller has argued that the large number of inverters needed (about 2400 / km of dual guideway) will enable mass production to reduce their cost by a factor of 10. This will be difficult to prove until there actually is mass production. However, any serious commitment to maglev development could become one of the device's major development drivers in much the same way that electrification in transit and railroads has driven the development of the GTO power electronics device. The historical trend in the costs of electronics, including power devices, has been downward, and there is no reason to think that this trend will reverse in foreseeable future.

Vehicle control with an LCLSM is also unproven. Issues include the LCLSM's ability to control acceleration and speed, and to maintain adequate lateral stability. Lateral stability may become a concern because the LCLSM, as currently configured, also provides the lateral guidance forces. Real-time computer control of the individual coils is also a demanding technical requirement. However, reduced-scale testing can address these issues sufficiently to establish the technical feasibility of the LCLSM in a reasonably short period.

4.4.2 Fiber-reinforced plastics

Two of the four SCD concepts (Bechtel and Foster-Miller) have sufficiently high magnetic fields in portions of their concrete guideway beams that they may not be able to use conventional steel post-tensioning rods. Thus, they have both proposed using FRP rods. Bechtel has also proposed a bending-beam switch constructed entirely of FRP.

Although well established as an aerospace structural material, FRPs have not significantly penetrated civil construction. However, they possess many potential advantages over steel reinforcing, including high strength to weight, high corrosion resistance, and high failure stress. Many researchers expect that FRPs will eventually be commonplace in civil structures. Maglev may well prove to be the first broad construction use of these materials.

Despite their higher cost, FRPs do not pose a significant overall capital cost penalty on guideways employing them. Because they are new, however, FRPs have unknown durability for long-life civil structures (typically 50 years). The effects of long-term, cyclic loading on the attachments for post-tensioning rods are particularly difficult to predict. This durability risk is critical for concepts that must employ FRP. Indeed, FRP rods become enabling technology for such concepts.

4.4.3 Active vehicle suspensions

Three of the four SCDs use some form of active vehicle suspension (actuators driven by control signals to minimize vehicle response to disturbances). With sufficient control authority and the proper control algorithm, an actively controlled vehicle can maintain a smooth ride over very flexible and rough guideways. This allows use of, respectively, less structural material and less stringent construction tolerances than would be the case for passively suspended vehicles. Both of these benefits significantly reduce guideway costs.

Modern control technology appears sufficient to ensure that active vehicle suspensions are technically feasible. Maglev's large magnetic forces make active control of the primary suspension an attractive option; Grumman selected this approach. Active control of aerodynamic surfaces is also an option, although unsteady air flow may complicate its implementation. For example, Bechtel's proposed side-mounted ailerons may not see clean air flow during crosswinds. However, overhead ailerons, similar to those proposed by Magneplane, may alleviate such concerns.

The main risks with active suspensions are their added weight, cost, and reliability penalties compared with passive suspensions. A reasonable R&D effort should minimize these risks. Small-scale testing of active magnetic suspensions should quickly demonstrate their feasibility. Similarly, wind-tunnel testing and computational fluid-dynamics may be used to establish the feasibility of active aerodynamic control.

4.4.4 Large-gap EMS

A major concern about TR07's suitability for the U.S. environment is its small, 8-mm suspension gap. To achieve adequate ride comfort and safety margin, TR07's guideway must be very stiff and well aligned. These requirements increase the guideway's cost and its susceptibility to foundation settlement, earthquake movement, thermal expansion, and ice accretion.

Grumman uses iron-core superconducting magnets to increase the suspension gap of its EDS concept to 40 mm. It actively controls this gap with normal electromagnets (for high-frequency disturbances such as guideway irregularities) and by varying currents in the superconducting magnets (for low-frequency disturbances such as payload changes and curves). With this suspension, the vehicle maintains good ride comfort and a safety margin over irregularities that are an order of magnitude larger than TR07's limits. This suspension also uses the same magnets and reaction rails to provide all necessary lift and guidance forces. These improvements offer the potential to simplify guideway design and construction, and increase allowable guideway tolerances to permit use of standard concrete beam construction. This system also incorporates desirable active control in the primary suspension, eliminating completely the need for a secondary suspension.

The main risks with this approach are with the details of the suspension itself. The control coils must deliver adequate control forces to ensure stability and safety under all possible conditions. The high currents needed must not induce excess losses in the superconducting magnets. Furthermore, the control algorithm must take advantage of the hardware's capabilities. These issues may be addressed quickly through laboratory testing of a complete magnet–control system. Also, an EMS suspension with integrated lift and guidance magnets is an unproven concept. Its verification may require complete vehicle tests at either full or reduced scale.

4.4.5 Power transfer

Both the Magneplane and Grumman concepts use the LSM stator winding as an inductive linear generator to transfer auxiliary power from the wayside to the vehicle. Their vehicles have power pickup coils directly opposite the LSM stator windings.

The Grumman concept uses high-frequency (600-Hz) single-phase power in conjunction with a linear generator. The single-phase power is injected into the LSM feeder cables, which also supply three-phase propulsion power. This single-phase current is a control that provides the dominant power transfer at low vehicle speeds. At high speeds, the linear generator, which uses the harmonics of the three-phase propulsion current, provides the dominant power transfer.

The Magneplane concept uses three-phase auxiliary current in the LSM winding that is connected 180° out of phase from the main propulsion current. This connection produces auxiliary-current traveling waves in the opposite direction to those of the propulsion currents. The opposite-direction traveling waves produce a slip frequency that transfers power from the from the LSM windings to the pickup coil.

Both concepts have potentially adverse effects on LSM performance, but they reduce onboard battery requirements and hence save weight. These concepts warrant reduced-scale investigation to demonstrate their feasibility and to establish cost to weight trade-offs.

4.4.6 High efficiency EDS

At cruise speed, Bechtel's ladder EDS concept achieves a magnetic lift:drag ratio greater than 100, and Foster-Miller's coil EDS approach has a magnetic lift:drag ratio that is over 170. These are very efficient EDSs. Their benefits include lower energy consumption, higher payload to weight ratio, and lower liftoff and landing speeds. Indeed, Bechtel's

10-m/s liftoff speed allowed it to propose to use vertical motor thrust to support its vehicle into and out of stations (it would use air bearings only for emergencies). Essentially, high-efficiency EDSs offer low-speed support capability and low energy consumption, similar to EMS concepts.

4.4.7 Cable-in-conduit superconducting magnets

Superconducting magnets used to date for levitating test or prototype maglev vehicles are made with niobium-titanium (NbTi) superconductors immersed in liquid helium near its boiling point of 4.2 K. Since the refrigeration efficiency increases as the temperature of the refrigerant increases, it is desirable to operate the magnets at the highest temperature possible. In addition, it may be desirable to avoid the use of liquid helium in transportation—sloshing of the liquid can result in "flashing" or evaporation of the liquid as it comes into contact with surfaces at temperatures only marginally higher than it is.

The cable-in-conduit magnets proposed in some of the concepts offer the opportunity of operating at higher temperatures without liquid helium by using niobium-tin (Nb_3Sn) superconductors with supercritical helium as the coolant. This approach is not practical with NbTi, since the transition temperature of this material is too close to the temperature of the coolant (about 8 K). In this approach, many wires of Nb_3Sn conductor (a cable) are contained in a tube that is then wound to form the magnet. Supercritical helium is circulated through the tube to cool the superconductor.

From a refrigeration viewpoint, this approach could be much superior to the method of using NbTi cooled in a helium bath. However, vibratory levitation, guidance, and propulsion forces acting on the superconductors are a concern. Most NbTi magnets are completely potted in epoxies to avoid motion of the conductor, so forces are transmitted to the entire body of the magnet through the epoxy. This will not be possible in a cable-in-conduit magnet, since coolant must circulate through the windings contained in the tube, and epoxy would block its flow.

Furthermore, Nb_3Sn is a brittle intermetallic compound that is much more subject to fracture than NbTi. To mitigate this problem, hundreds or thousands of filaments of Nb_3Sn are often contained in a copper matrix, so that the overall conductor is much more flexible than a single Nb_3Sn conductor of the same diameter. Also, the SCD designs propose swaging the conductors inside the conduit. Still, the conductors appear to be susceptible to flexing, and any resulting filament breakage would reduce the critical current of the conductor.

The adequacy of the safety and reliability of cable-in-conduit conductors used with superconducting magnets has not been demonstrated, but the benefits appear sufficient to warrant detailed analytical and experimental evaluations.

4.4.8 Electromagnetic switches

Foster-Miller and Magneplane proposed electromagnetic (EM) switches as their high-speed switches, and Betchel investigated an EM switch as an alternate concept. Relative to TR07's bending-beam switch, EM switches offer much shorter cycle times, no moving structural members, less maintenance, and lower susceptibility to snow, ice, and dust. Additionally, Foster-Miller's and Magneplane's vehicles both retain their tilt capability in the turnout direction. This permits higher exit speeds than is possible for TR07 for a given switch length.

4.4.9 Spine-girder dual guideway

Grumman has proposed an innovative dual guideway concept called a spine girder. A central structural "spine" girder carries a narrow Y-shaped EMS guideway along either side on outriggers. Government cost estimates confirm that this is a very efficient structure in terms of performance and cost. Indeed, it is responsible for Grumman's 20% cost advantage over TR07's guideway (also an EMS concept).

Its risks appear to be limited. Detailed stress analysis and design optimization are needed to ensure that tensile stresses in the concrete outriggers are within allowable limits for durability. Also, adequate alignment of the Y-shaped guideways on the outriggers must be achievable and maintainable, although Grumman's large-gap EMS permits fairly loose alignment tolerances. Lastly, high-speed air flow past the outriggers may induce unacceptably large vehicle drag; mitigating this effect will require detailed aerodynamic modeling (and may lead to fairing of the outriggers).

4.4.10 Air bearings

Two of the three EDS concepts (Bechtel and Magneplane) proposed using air bearings for low-speed support rather than wheels. Such bearings, which have been used for very low speed (less than 5 m/s) support of freight pallets, use a thin air film trapped between the vehicle and the guideway.

Relatively low flow rates are needed so equipment and power requirements are very modest. They offer a potential for lower weight, cost, and stresses relative to conventional wheels.

Their main risk is that the application here requires support at speeds that are 2–10 times higher than common for existing air bearings. That is, they will require further work to be applied to maglev vehicles. Also, the mating guideway surface must be fairly smooth and well aligned to minimize air flow requirements and ensure adequate support pressure. Such issues should be resolvable with laboratory and reduced scale tests.

4.4.11 Cryosystems

To date, EDS maglev vehicles have used niobium-titanium (NbTi) superconductors immersed in liquid helium, with cryogenic refrigerators reliquefying the helium vapor. Such refrigerators consume significant power and are considered the least reliable component in the maglev suspension. All four SCD concepts have avoided using this approach.

The two concepts using liquid-helium baths (Foster-Miller and Grumman) recompress the helium vapor and store it, rather than reliquefy it. They replenish the liquid helium as a daily maintenance operation. This avoids the need for a reliquefying onboard refrigerator that uses much energy and is unreliable; stationary reliquefaction is more efficient and reliable.

The other two SCD concepts, Bechtel and Magneplane, use cable-in-conduit superconductors. These Nb_3Sn superconductors operate at 6–8 K, with supercritical helium as the coolant. Bechtel proposes to use an isochoric (constant volume) system. The vehicle is charged daily with liquid helium, which resides in a sealed reservoir–magnet loop. As the coolant warms up, it pressurizes the loop but retains sufficient heat capacity for the day's cooling needs. Magneplane uses a cryorefrigerator to keep the supercritical helium in the working temperature range. However, the energy required to do so is much less than that needed to reliquify the helium, and the refrigerator needed is much more reliable.

Provided that they allow adequate liquid helium storage and minimize sloshing, the Foster-Miller and Grumman approaches carry little risk. Magnets of this type may be tested as an assembly in a laboratory. The two cable-in-conduit magnet concepts carry an additional risk associated with the brittleness of Nb_3Sn superconductors. This material will not tolerate high cyclic stresses, so that load variations caused by moving vehicles must be examined. Such testing can also be conducted in a laboratory but would likely require validation at reduced or full scale.

4.5 SPECIFIC TECHNICAL ISSUES

In conducting its work, the GMSA team has gathered and analyzed technical data pertaining to high-speed rail (TGV), a commercially ready maglev system (TR07), and four well-defined U.S. maglev concepts. Here, we apply this knowledge to address a number of technical issues frequently raised concerning the viability of maglev for the U.S. market. Where appropriate, we may again judiciously aggregate the performance characteristics of the four SCD concepts and consider some issues as they pertain to a generic U.S. maglev concept.

4.5.1 What is the feasibility of routing HSGT along existing transportation and utility rights-of-way?

The routing of maglev along existing ROW was contemplated early in the NMI program. Indeed, the SCD-RFP reflected this possibility by containing system criteria appropriate to such routing. Thus, we find that all SCD concepts can negotiate very tight curves, possess very good performance in curves at high speed, climb steep grades, and accelerate very quickly to full speed. Without question, generic U.S. maglev is significantly better suited to routing along existing ROW than either TGV or TR07 in their present forms.

TGV is unlikely ever to be well suited to this mission. Traction limits its maximum acceleration and grade-climbing ability; its modest 7° superelevation and nontilting body limit maximum speeds in curves. These limitations would require very significant R&D investment to overcome. Although other HSR systems incorporate tilting vehicles, none achieve even TGV's 83-m/s service. Safety may limit HSR cornering speeds—the higher guidance forces needed for high-speed cornering may be beyond the capability of standard-gauge rail.

TR07 could be more easily adapted to this mission. LSM and power system capacity limit its maximum acceleration and grade-climbing ability. These are subject to design trade-offs, although ultimately the size of the stator slots limits stator current and, hence, maximum thrust. As with U.S. maglev, wheel–rail contact does not limit TR07's

cornering speeds. However, significant R&D investment (for both vehicle and guideway) would be needed to incorporate vehicle tilting to increase TR07's curving performance. Increased roll stiffness of the magnetic suspension would be needed, as would stronger, curved guideway beams.

As noted earlier, U.S. maglev vehicles are about 20% lighter than TR07 vehicles, despite having tilting capability. If straight maglev routes become the norm so that tilting vehicles become unnecessary, U.S. maglev vehicles could be made even lighter. This would reduce both vehicle and guideway costs (lighter vehicles deliver smaller loads to the guideway).

The superiority of generic U.S. maglev here is an example of good engineering practice—define the problem you wish to solve, specify the characteristics that the solution must possess to be acceptable, then develop the product that possesses these characteristics. This process invariably leads to better results than attempting to use existing products to solve problems that they were not specifically designed to solve.

4.5.2 Can HSGT be constructed along existing rights-of-way?

HSR's cost advantage over maglev is for at-grade construction. But this poses problems along existing ROW where numerous grade separations will be necessary. The structures needed for grade separation of HSR (viaducts and tunnels) are expensive and hence erode HSR's cost advantage.

Maglev vehicles are lighter and more easily elevated than trains. Only support columns need intrude on an existing ROW. Also, maglev construction can be highly automated and modular. Essentially, only footings must be constructed at the site. Piers may be prefabricated and guideway beams certainly will be. This type of modular construction offers the potential for minimal disruption of collocated services. In particular, overhead construction permits much lower impact on ROW entry–exit points and existing bridges than does at-grade construction.

4.5.3 What design features or construction methods will reduce maglev guideway costs?

Maglev guideways will benefit from several basic cost-saving measures. All guideways are highly modular, making them naturals for high-volume, automated production. Most concepts use concrete beams. Over time, such beams will drop in cost or increase in performance because of general improvements in high-strength–low-weight concrete and the fabrication methods being pursued throughout the construction industry.

Both TR07's steel beams and Magneplane's aluminum ones also lend themselves to automated production and should drop in price with time. Unfortunately, steel and especially aluminum are much more sensitive to energy prices than is concrete.

Because maglev is a new technology, guideway designs incorporate conservatism owing to unknown loads. As these loads become better established, guideways will become more efficient and hence less costly.

Lastly, near-grade guideways, where applicable, offer the potential for significant cost reductions. Maglev offers the potential for normally elevated guideways where they are necessary but will benefit from lower costs where they are not.

4.5.4 What advanced construction materials and techniques are likely to improve guideway performance and reduce costs in the long term?

Several emerging technologies appear likely to improve guideway performance and reduce costs in the long term. By its conservative nature, the construction industry has been slow to develop and adopt these technologies. However, maglev's guideways are its most expensive component; any improvements will pay large dividends. Thus, maglev will be a significant driver for innovation in the entire construction industry. Other sectors of the industry will benefit as a result.

- All SCD-EDS concepts avoid the use of steel reinforcing in the vicinity of their powerful superconducting magnets. The resulting demand for FRP rods to post-tension concrete will be by far the most significant construction use of this material. The performance and cost of the various FRP rods will undoubtedly improve with time.
- In essence, maglev represents a high-tech, high-volume application of the most basic of construction materials: concrete. It will thus accelerate the development of high-strength–low-weight concrete, including fiber-reinforced concrete.
- At present, composite materials have found commercial use primarily in the aerospace industry. Although they are currently much more expensive than concrete and steel as structural materials, this could change with further development. Maglev vehicles will likely use advanced composite structures, and

guideway switches may also. Maglev's high-volume demand will spur development of more efficient, cheaper fabrication methods. Because they possess tremendous performance advantages, composite materials could eventually become the preferred choice for maglev guideways.
- New, so-called "smart materials" have recently emerged. These materials fall into categories according to their properties. Some provide self-diagnostics for structural integrity; others self-heal small fractures or surface damage; still others vary their mechanical properties such as stiffness and damping in response to applied signals. Again, maglev will represent a high-volume application for these materials.
- To avoid disruption along an existing ROW, maglev will likely use cantilever (bridge) construction off the end of the guideway. This construction method will become more efficient and less costly with wide-scale application.

4.5.5 What methods exist to minimize maglev's stray magnetic fields?

Stray magnetic fields represent perhaps the greatest uncertainty in eventual public acceptance of maglev. However, several design options exist to minimize these fields:

- *Maglev approach*—EMS concepts use iron-core magnets that intrinsically concentrate magnetic fields near the magnets. They thus generate much smaller stray fields both inside and outside of vehicles than do EDS concepts. However, EMS iron-core magnets carry a weight penalty relative to EDS air-core magnets.
- *Magnet grouping*—Grouping magnets so that their poles alternate causes stray fields to drop very rapidly with distance. This reduces field strengths both inside and outside of vehicles. All three SCD-EDS concepts take this approach, and they require no shielding to achieve less than 50-G static fields in passenger seating areas.
- *Distance*—Stray fields drop rapidly with distance. Thus, two of the three SCD-EDS concepts contain magnets in bogies located at the ends of vehicles, as far as possible from passenger seating areas. The other SCD-EDS concept makes the vertical separation of passengers above distributed magnets as large as possible.
- *Diamagnetic shielding*—Good conductors such as copper resist the penetration of AC magnetic fields by establishing eddy currents that generate opposing fields. A superconductor will in fact resist all magnetic field penetration (DC and AC) provided the incident fields are sufficiently small. High-temperature superconductors might soon be available for the task of passenger-compartment shielding.
- *Bucking coils*—Energized copper coils may be placed over magnet bogies or at bulkheads to generate opposing DC magnetic fields. Such coils provide very effective shielding with modest weight, cost, and power penalties. Coils of high-temperature superconductors may soon be available that will fully shield 10-G fields at bulkheads. Such coils would incur very little penalty by using inexpensive liquid nitrogen for cooling.
- *Ferromagnetic shielding*—Ferromagnetic materials such as iron and steel may be incorporated into a vehicle's structure to reduce stray fields in passenger seating areas. Indeed, Foster-Miller incorporated a ferromagnetic box shield to meet the 1-G limit with a modest weight penalty (2000 kg or 3% of baseline consist mass). Despite this, their vehicle is 20% lighter per standard passenger than TR07. Ferromagnetic materials may also be incorporated into station platforms to shield passengers entering and exiting vehicles. Here, the weight penalty is not an important issue, although the magnetic forces attracting the vehicle to the shield will be significant and must be accommodated.
- *Exposure limits*—Prudent operation of a maglev system may include limits on the duration of exposure to very high fields. For passengers, these would occur during entry and exit and will require careful station design. Consideration of exposure limits for crew and maintenance personnel will also be necessary. Design considerations might include extra shielding around galleys, placement of inspection and service hatches away from magnets, etc.

4.5.6 What are the advantages and disadvantages of various maglev propulsion options?

Several options exist to propel maglev vehicles along guideways. Here, we discuss only electric motors using the vehicle and the guideway as the two halves of a motor (an active primary and an

active or passive secondary). Other propulsion options, such as jets, turbofans, or electrically driven fans, generally are less efficient, more noisy, and require greater maintenance to overcome mechanical wear. Also, use of electric power permits flexibility in selection of the generating source (fossil, nuclear, hydro, etc.) and control of pollution from that source.

As with the construction industry, the electric power industry is very conservative. Maglev will be a significant driver for the development of low-cost, high-power electronics. This will bring down the cost of power conditioning over time, which should in turn improve the performance and reduce both the capital and operating costs of maglev motors.

Long-stator linear synchronous motor (LSM)

This motor has its primary or stator windings imbedded in the guideway; energized magnets on the vehicle are the secondary. These magnets may be ones also used for generating lift or may be separate propulsion magnets. The wayside power supply energizes long sections of the stator windings (typically a few kilometers) and generates a traveling magnetic wave that pulls the vehicle along. The vehicle remains synchronous with this traveling wave. TR07 and all four SCD concepts employ a long-stator LSM.

Advantages.

- Avoids the critical need to transfer high power for propulsion to vehicles traveling at 134 m/s.
- Vehicles are lighter and less costly because power conditioning equipment is along the wayside.

Disadvantages.

- Guideway capital costs are high because of frequently spaced power supplies.
- Wayside power supplies occupy significant land areas.
- Peak capacity of the system is constrained by stator current density and, ultimately, stator slot width; increasing it would require a change-out of the entire stator pack.

Short-stator linear induction motor (LIM)

The LIM has its active primary on the vehicle (a short length of stator windings) and uses a passive secondary on the guideway (typically iron structures). The vehicle must pick up propulsion power from the guideway and condition it on board. Such motors are well proven for low speeds, and several people-movers use LIMs for both propulsion and levitation.

Advantages.

- Less expensive guideways (assuming costs for power transfer equipment and motor secondaries are less than long stator windings and additional wayside power supplies).
- Simpler, cheaper wayside power distribution because all frequency conversion occurs on vehicles.
- May increase peak capacity by allowing additional vehicles without the need to change-out guideway power equipment (although this has not yet been proven for very high system capacities).

Disadvantages.

- High power transfer to vehicles at high speeds is an enabling technology. Extensive R&D would be necessary to develop reliable and cost-effective multi-megawatt power transfer at 134 m/s. It is unlikely that pantograph–catenary power transfer will work satisfactorily at such high speeds.
- Vehicles are more expensive and heavier because of onboard stator and power conditioning equipment.

Other LSMs

Several experimental linear motors exist that use passive secondaries. The secondaries are typically made of iron and would mount on the vehicle to avoid the limitations of high-power transfer technology. These motors include the homopolar LSM and the transverse flux LSM (in the European literature sometimes called the magnetic river). Each of these concepts have been shown experimentally to provide thrust, levitation, and lateral control capabilities. Attractive because of their simplicity over conventional iron- and air-core LSMs, these machines warrant R&D to determine their costs and performance compared with conventional LSMs.

LITERATURE CITED

ACI (1989) *Building Code Requirements for Reinforced Concrete*. Detroit, Michigan: American Concrete Institute, ACI 318-89.

ADINA R&D, Inc. (1987) A finite element program for automatic dynamic incremental nonlinear analysis, Vol. 1. Watertown, Massachusetts, Report ARD 87-1.

ASCE (1990) Wind loads. In *Minimum Design Loads for Buildings and Other Structures*, Section 6. ASCE 7-88. New York: American Society of Civil Engineers.

Bajura, R.A., and H.A. Webb (1991) The marriage of gas turbines and coal. In *Mechanical Engineering*. American Society of Mechanical Engineers, New York, pp. 58–63.

Barbee, T.W., et al. (1968) The hypervelocity rocket sled—A design analysis. SRI Project PMU 7014.

Bauingenieur (1983) Bauausfuhrung des Betonfahrweges der Transrapid Versuchsanlage Emsland—TVE, Spring (in German).

Bechtel (1992a) Maglev system concept definition. Final report. Prepared for U.S. Department of Transportation, Federal Railroad Administration under contract DTFR 53-92-C-00003.

Bechtel (1992b) Maglev system concept definition. Hypothetical route report. Prepared for U.S. Department of Transportation, Federal Railroad Administration under contract DTFR 53-92-C-00003.

Bohn, G., and G. Steinmets (1985) The electromagnetic suspension system of the magnetic train Transrapid. In *Proceedings of the International Conference on Maglev Transport '85*, pp. 107–114.

Brockie, N.J.W. and C.J. Baker (1990) The aerodynamic drag of high-speed trains. *Journal of Wind Engineering and Industrial Aerodynamics*, **34**: 273–290.

Brown, D., and E. Hamilton (1984) *Electromechanical Energy Conversion*. New York: MacMillan.

Chilton, F., and H.T. Coffey (1971) Magnetic levitation: Tomorrow's transportation. Washington, DC: The Helium Society, p. 288.

City of Las Vegas (1987) Super-speed ground transportation project—Las Vegas / Southern California corridor. Submitted to the Federal Railroad Administration, June.

Coffey, H.T., F. Chilton and W.T. Barbee (1969) Suspension and guidance of vehicles by superconducting magnets. *Journal of Applied Physics*, **40**(5): 2161.

Coffey, H.T., F. Chilton, and L.O. Hoppie (1972) The feasibility of magnetically levitating high speed ground vehicles, February, 1972. National Technical Information Center, Alexandria, Virginia, PB 210505.

Coffey, H.T., J.D. Colton, and K.D. Mahrer (1973) Study of a magnetically levitated vehicle, February, 1973. National Technical Information Center, Alexandria, Virginia, PB 221696.

Davenport, A.G. (1961) The spectrum of horizontal gustiness near the ground in high winds. *Quarterly Journal of the Royal Meteorological Society*, **87**: 194–211.

Davis, L.C., and J.R. Reitz (1972) Eddy currents in finite conducting sheets. *Journal of Applied Physics*, **42**: 4119–4127.

Department of Energy (1993a) Annual energy outlook, 1993, with projections to 2010. Report no. DOE / EIA-0383(93).

Dietrich, F.M., and W.E. Feero (1992) Safety of high speed magnetic levitation transportation systems: Magnetic field testing of the TR07 maglev vehcile and system. U.S. Department of Transportation, Federal Railroad Administration, Office of Research and Development, Washington, D.C. DOT / FRA / ORD-92 / 09.1, 2.

Dietrich, F.M., W.E. Feero, and W.L. Jacobs (1993) Safety of high speed guided ground transportation systems: Comparison of magnetic and electric fields of conventional and advanced electrified transportation systems. U.S. Department of Transportation, Federal Railroad Administration, Office of Research and Development, Washington, D.C. DOT / FRA / ORD-93 / 07.

Department of Energy (1993b) Assumptions for the annual energy outlook. Report No. DOE / EIA-0527(93).

Dukowicz, J.K., L.O. Hoppie, and T.C. Wang (1973) DC magnetic propulsion and levitation system for high speed vehicles. U.S. Patent 3,815,511, filed 26 April 1973.

Electric Research and Management, Inc . (no date) Measurement and analysis of magnetic and electric fields for existing and advanced rail transportation systems. Contract DTFR 53-91-C-00047.

Farmer, R. (1992) Combined cycle power: Delivering new levels of net plant efficiency. *Gas Turbine World*, Sept.–Oct., pp. 20–34.

Fishbein, J., and H. Abramowitz (1992) Hybrid power packaging for automotive applications. *IEEE Power Electronics in Transportation Workshop, 22–23 October, Deerborn, Michigan*, Publication No. 92TH0451-5, pp. 88.

Fitzgerald, A., C. Kingsley, and A. Kusko (1971) *Electric Machinery*. Third Edition. New York: McGraw Hill.

Foster, R.N. (1986) *Innovation—The Attacker's Advantage*. New York: Simon & Schuster.

Foster-Miller, Inc. (1992a) Maglev system concept definition report. U.S. Department of Transporta-

tion, Federal Railroad Administration, Office of Research and Development, Washington, D.C. Report DOT/FRA/ORD-92/01, October.

Foster-Miller, Inc. (1992b) Maglev severe segment test report. U.S. Department of Transportation, Federal Railroad Administration, Office of Research and Development, Washington, D.C. Report DOT/FRA/ORD-92/01, November.

Freidrich, R., K. Dreinmann, R. Leistikow, E. Bohm, and A. Weller (1985) Propulsion and power supply system of the Transrapid 06 Vehicle: Design and test results. Part 1: Propulsion. In *Proceedings of the International Conference on Maglev Transport '85*, pp. 75–82.

Friedrich, R., V. Dreimann, and R. Leistikow (1986) The power supply and the propulsion system of the Transrapid 06 vehicle, results of trials. In *Proceedings of the International Conference on Maglev and Linear Drives, 14–16 May*, pp. 243–249.

Gas Turbine World (1992) *The 1992–93 Handbook*. Fairfield, Connecticut: Pequot Publishing.

Government Maglev System Assessment Team (1992) Transrapid TR-07 baseline report. April.

Gran, R.J. (1990) Benefits of magnetically levitated high speed transportation for the United States. In *Magnetic Levitation Technology and Transportation Strategies*. Warrendale, Pennsylvania, SAE Publication SP-834, pp. 1–9.

Grumman Aerospace Corp. (1989a) Benefits of magnetically levitated high-speed transportation for the United States. Vol. 1, Executive report. June.

Grumman Aerospace Corp. (1989b) Benefits of magnetically levitated high-speed transportation for the United States. Vol. 2, Technical report. June.

Grumman Aerospace Corp. (1992a) System concept definition of a superconducting maglev electromagnetic system. Final report. Prepared for National Maglev Initiative, U.S. Army Corps of Engineer, Huntsville, under contract DTFR 53-92-C-0004.

Grumman Aerospace Corp. (1992b) System concept definition of a superconducting maglev electromagnetic system. SST route report. Prepared for National Maglev Initiative, U.S. Army Corps of Engineer, Huntsville, under contract DTFR 53-92-C-0004.

Guderjahn, C.A., et al. (1969) Magnetic suspension and guidance for high-speed rockets by superconducting magnets. *Journal of Applied Physics*, **40**(5): 2133–2140.

Hammit, A.G. (1974) The aerodynamics of high speed ground transportation. *High Speed Ground Transportation Journal*, **8**(2): 93–100.

Hanson, C., P. Abbot and I. Dyer (1993) Noise from high speed maglev systems. U.S. Department of Transportation, Washington DC, Report DOT/FRA/NMI-92/18,

He, J.L., D.M. Rote, and H.T. Coffey (1991) Computation of magnetic suspension of maglev systems using dynamic circuit theory. Argonne National Laboratory, Argonne, Illinois, Report ANL/CP-72983, August.

Heinrich, K., and R. Kretzschmar (Ed.) (1989) *Transrapid Maglev System*. Darmstadt: Hestra-verlag.

HKS Inc. (1988) ABAQUS users manual. Version 4.9. Hibbitt, Karlasson and Sorensen, Inc., Pawtucket, Rhode Island.

Institute of Electrical and Electronics Engineers (1992) Electric vehicles. Special Report, *IEEE Spectrum*, November.

International Conference of Building Officials (1992) Uniform building code. Whittier, California

Johnson, L.R., D.M. Rote, J.R. Hull, H.T. Coffee, J.G. Daly and R.F. Giese (1989) Maglev vehicles and superconductor technology: Integration of high-speed ground transportation into the air travel system. Argonne National Laboratory, Energy and Environmental Systems Division, Argonne, Illinois, Report ANL/CNSV-67.

Johnson, L.R., D.M. Rote, J.R. Hull, H.T. Coffey, J.G. Daley, and R.F. Giese (1989) Maglev vehicles and superconductor technology: Integration of high-speed ground transportation into the air travel system. Argonne National Laboratory, Argonne, Illinois, Report ANL/CNSV-67.

Kassakian, J., M. Schlecht, and G. Verghese (1991) *Principles of Power Electronics*. Addison Wesley.

Kolm, H.H., and R.D. Thornton (1972) Magneplane: Guided electromagnetic flight. In *Proceedings of the Applied Superconductivity Conference*, IEEE Publication No. 72CH0682-5-TABSC.

L'Industria Italiana del Cemento (1989) Experimental magnetic levitation railway line (transrapid) at Emsland in Western Germany, March, pp. 170–181.

Lee Shung-Wu and R.C. Menendez (1974) Force on current coils moving over a conducting sheet with application to magnetic levitation. In the *Proceedings of the IEEE*, **62**: 567–577.

Maglev Transit, Inc. (1989) Magnetic levitation demonstration project. Vol. 1 and 2. Application to Florida Department of Transportation and Florida High Speed Rail Committee.

Magneplane International, Inc. (1992a) System concept definition report for the National Maglev Initiative. Prepared for National Maglev Initiative, U.S. Army Corps of Engineers, Huntsville, under contract DTFR 53-92-C-0006.

Magneplane International, Inc. (1992b) Hypothetical route report for the National Maglev Initiative. Prepared for National Maglev Initiative, U.S. Army Corps of Engineers, Huntsville, under contract DTFR 53-92-C-0006.

Martin Marietta Corp. (1992a) Maglev guideway and route integrity requirements. Comprehensive report. U.S. Department of Transportation, Federal Railroad Administration, Washington, D.C. Report DOT/FRA/NMI-92/04; FRA-31-92-0008.

Martin Marietta Corp. (1992b) Maglev guideway route alignment and right-of-way requirements. U.S. Department of Transportation, Federal Railroad Administration, Washington, D.C. Report DOT/FRA/NMI-92/10; FRA-24-92-0014.

Meins, J., L. Miller, and W.J. Mayer (1988) The high-speed MAGLEV transportation system TRANSRAPID. *IEEE Transactions on Magnetics*, **24**(2).

Miller, L. (1987) Transrapid 06II, performance and characteristics. In *Proceedings of the International Conference on Maglev and Linear Drives, 19–24 May*, pp. 155–162.

Mulcahy, T.M., J.L. He, D.M. Rote, and T.D. Rossing (1993) Forces on a magnet moving past figure-eight coils. Paper presented at the *International Magnetics '93 Conference, 13–16 April, Stockholm, Sweden*.

Nasar, S., and I. Boldea (1987). *Linear Electric Motors*. Englewood Cliffs, N.J.: Prentice Hall.

Nerem, A., et al. (1992) Advanced power conditioning for maglev systems. U.S. Department of Transportation, Washington, DC, DOT/FRA/NMI-92/14, Final Report, August.

Nilson, A.H. (1978) *Design of Prestressed Concrete*. New York: John Wiley & Sons.

Pepler, R.D., et al. (1978) Development of techniques and data for evaluating ride quality, Vol. II. U.S. Department of Transportation, Washington, D.C., Report DOT-TSC-RSPD-77-1, II, February.

Powell, J.R. (1963) The magnetic railroad: A new form of transport. In *Proceedings of the ASME Railroad Conference, 23–25 April*, Paper 63-RR4.

Powell, J.R., and G.R. Danby (1966) High-speed transport by magnetically suspended trains. ASME Paper 66-WA/RR-5.

Powell, J.R., and G.R. Danby (1967) A 300-mph magnetically suspended train. *Mechanical Engineering*, **89**: 30–35.

Railway Technical Research Institute of Japan (1984) Japanese studies of Shinkansen trains. *Quarterly Report*, **25**(4): 140–143.

Railway Technical Research Institute of Japan (1989) Japanese studies of Shinkansen trains. *Quarterly Report*, **30**(1): 48–56.

Rajashekara, K. (1992) Evaluation of power devices for electric propulsion systems. *IEEE Power Electronics in Transportation Workshop, 22–23 October, Deerborn, Michigan*, Publication No. 92TH0451-5, pp. 46.

Reitz, J.R. (1970) Forces on moving magnets due to eddy currents. *Journal of Applied Physics*, **41**(5): 2067–2071.

Reitz, J.R. (1970) Forces on moving magnets due to eddy currents. *Journal of Applied Physics*, **41**: 2067–2071.

Simiu, E., and R. H. Scanlan (1978) *Wind Effects on Structures: An Introduction to Wind Engineering*. New York: Wiley.

Terman, F. (1943) *Radio Engineer's Handbook*. First Edition. New York: McGraw Hill.

The Indian Concrete Journal (1991) Experimental railway line for high-speed maglev train, West Germany, May, pp. 205–208.

U.S. Army Corps of Engineers (1990) Preliminary implementation plan. National Maglev Initiative, June.

U.S. Department of Transportation, Federal Railroad Administration (1991) Competitive request for proposal number DTFR 53-91-R-00021. Maglev system concept definition. Office of Procurement, Federal Railroad Administration, Washington, D.C.

U.S. Department of Transportation, Federal Railroad Administration (1993) Final report on the National Maglev Initiative (NMI). Washington, D.C. Report DOT/FRA/NMI-93/03.

Walter, P.R., Sr. (Ed.) (1991) *Means Building Construction Cost Data*. 50th Edition. Kingston, Massachusetts: R.S. Means Co., Inc., Construction Publishers and Consultants.

Wyczalek, F.A. (1990) A national vision for maglev transit in America. In *Magnetic Levitation and Transportation Strategies*: *Collection of papers presented at the SAE Future Transportation Technology Conference and Display, San Diego, California, 13–16 August 1990*. SAE Publication SP-834, Paper 901482.

Youngwood, P.E. (1991) *IGBT Module Application and Technical Data Book*. Powerex Inc, pp. 1–17.

APPENDIX A: RIDE COMFORT GUIDELINES

This appendix gives the new ride comfort guidelines sent to the contractors after the SCD-RFP was issued.

A1. Ride vibration regime 1.0–25 Hz

Pepler equation

- 4-Minute moving window for root mean square calculation.
- Measurements at center of percussion.
- Pepler equation is the "composite" method described in *Development of Techniques and Data for Evaluating Ride Quality* (Pepler et al. 1978).
- Calculated only for reference

ISO (International Standard 2631/1, 1985, Fig. A1).

- 50-Second moving window for RMS in 1/3 octave band analysis.
- Measurements at worst case seat in local coordinates.
- Design goal—1-hour reduced comfort.
- Minimum requirement—15-minutes reduced comfort.

A2. Motion sickness regime 0.1–1.0 Hz

- ISO extended (Fig. A2).
- 4-Minute moving window for RMS in 1/3 octave band analysis.
- Measurements at worst case seat in local coordinates.
- Design goal—1-hour reduced comfort.
- Minimum requirement—15 minutes reduced comfort.

A3. Curving performance

Table A1. Average values for event (i.e., spiral or curve).

	Design	*Min. Req.*	*Seat/Belt*
a. Lateral curves			
Bank angle	24°	30°	45°
Roll rate	5°/s		10°/s
Lateral	0.1 g's	0.16	0.2
Roll accel.	15°/s^2		
b. Vertical curves (g)			
Vertical (up)	0.05	0.1	0.1
Vertical (down)	0.2	0.3	0.4
c. Acceleration and braking (g)			
Normal	0.16	0.2	0.6
d. Vector combinations (g)			
Lat./long.	0.2	0.3	0.6
Lat./vert.	0.2	0.3	0.4
Total	0.24	0.36	0.6

Table A2. Jerk (g/s filtered at 0.3 Hz) or jolt (peak to peak g's in 1 second).

	Design	*Min. Req.*	*Seat/Belt*
Lateral	0.07	0.25	0.25
Vertical	0.1	0.3	0.3
Longitudinal	0.07	0.25	0.25

A4. Other factors

- Temperature: 18–23°C
- Noise: 70–75 dBA

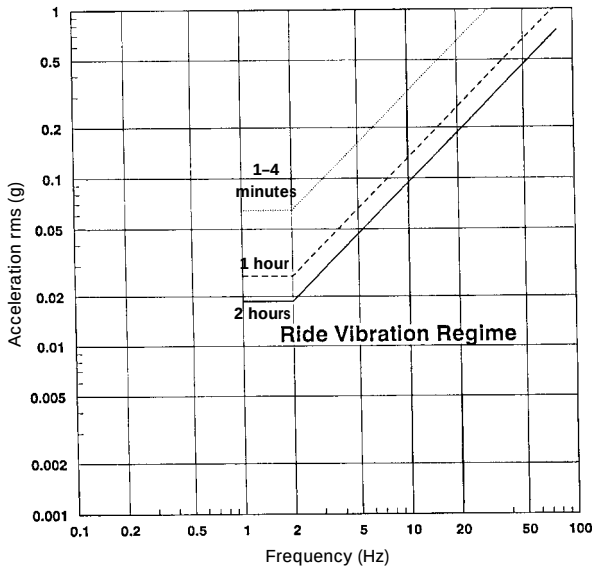

Figure A1. ISO vibration exposure limits for lateral acceleration.

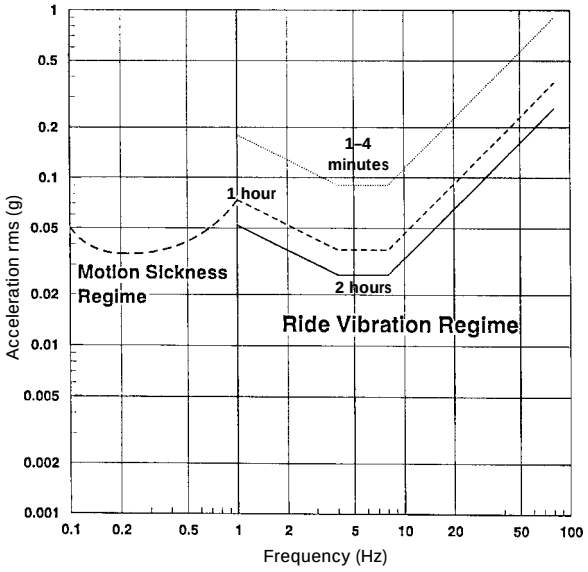

Figure A2. ISO vibration exposure limits for vertical acceleration.

APPENDIX B: WIND SPECIFICATIONS FOR MAGLEV SYSTEM CONCEPT DEFINITIONS

To ensure that maglev systems possess superior adverse weather performance to alternative modes, SCD contractors shall treat wind thresholds I and II (defined below) as minimum requirements.

B.1 Threshold I—operational wind threshold

During wind conditions that are less severe than this threshold, a maglev system will operate at 100% capability. That is, the system will maintain its maximum potential throughput and acceptable levels of safety and ride comfort during wind conditions below threshold I. Threshold I wind conditions are as follows:

- A 1-hour average wind speed of 13.4 m/s (30 mph) any direction.
- A peak gust of 21 m/s (47 mph) any direction.

Gust velocity spectrum is defined below.

These conditions occur, on average, six times per year at Boston, Massachusetts, and 13.4 m/s represents roughly twice the crosswind speed that disrupts landings of light commercial aircraft. Also, the 1-hour average and 1-second gust specifications are compatible with the referenced spectrum.

B.2 Threshold II—structural wind threshold

For wind conditions that are less severe than this threshold, a maglev system will experience no structural failure. That is, the support structure (guideway, piers, footings, and all attachments including motor elements), any vehicles on it, and all power, communications, command, and control equipment will be fully operational following a wind condition below threshold II.

Contractors shall use the methodology defined below for determining wind loads at threshold II (ASCE 1990):

$$F = q_z G_h C_f A_f$$

where F = wind load (N)
q_z = velocity pressure ($0.613 K_z [I V]^2$, N/m^2)
K_z = exposure coefficient
I = importance factor
V = basic wind speed (m/s)
G_h = gust response factor
C_f = force coefficient
A_f = projected area normal to wind (m^2).

Default values are as follows:

K_z = 1.0
I = 1.10
V = 38 m/s (85 mph)
G_h = 1.25
C_f = 2.0.

These default values represent wind conditions over flat, open terrain at a height of 10 m. A basic wind speed of 38 m/s or less represents a 50-year mean recurrence speed over about 90% of the continental U.S. An importance factor of 1.10 is suitable for regions within 160 km of a hurricane coastline (e.g., Northeast corridor).

Contractors shall include appropriate analyses to demonstrate that their concepts meet wind thresholds I and II. If they deviate from the values or methodology described above, they shall include appropriate technical justification.

In addition, contractors shall include supporting analyses and documentation that establish wind conditions representing thresholds III and IV for their concepts (as defined below).

B.3 Threshold III—vehicle safety wind threshold

During wind conditions that are less severe than this threshold, maglev vehicles may be present on the guideway. That is, vehicles may safely operate at reduced speed or may be safely stationary during wind conditions below threshold III. This threshold will be between thresholds I and II. Contractors must consider safety issues such as vehicle–guideway contact and vehicle derailment when determining this threshold.

B.4 Threshold IV—ride comfort wind threshold

During wind conditions that are less severe than this threshold, a maglev system will maintain acceptable levels of ride comfort but may reduce throughput to achieve it. This threshold will be between thresholds I and III.

Contractors shall specify thresholds III and IV as a 1-hour average wind speed and direction. To analyze dynamic effects, contractors shall use the gust velocity spectrum described in section B.5 or provide technical justification for using an alternative.

Contractors should examine relevant wind engineering literature to determine how wind

may affect their concepts and to guide their analyses. The material presented in Simiu and Scanlan (1978) constitutes a general survey of this field.

B.5 Wind gust velocity spectrum

This is from Davenport (1961):

$$nS(n) / u_t^2 = 4.0\ x^2 / \left(1 + x^2\right)^{4/3}$$

where $S(n)$ = gust velocity spectrum ($[\mathrm{m/s}]^2/\mathrm{Hz}$)

n = gust frequency (Hz)
u_t = friction velocity (m/s)
x = $1200\ n / U_{10}$
U_{10} = 1-hour average wind speed at a 10-m height.

Also, the standard deviation u' is assumed to be

$$u' = 2.5\ u_t = U_{10} / 5.7.$$

APPENDIX C : ASSESSMENT OF THE POWER ELECTRONICS FOR THE LOCALLY COMMUTATED LINEAR SYNCHRONOUS MOTOR (LCLSM)*

C.1 LCLSM CONCEPT SUMMARY

The Foster-Miller, Inc., maglev concept takes an innovative approach to the linear synchronous motor (LSM) that is called the locally commutated linear synchronous motor (LCLSM). The LCLSM, a superconducting motor, has individually connected guideway coils that are connected in parallel to the power source. It requires variable frequency inverters at every LSM coil position on the guideway. The guideway coils that are opposite to each other are connected in parallel. Each pair of coils is then connected to and controlled by one H-bridge inverter. The concept requires LCLSMs to be located at approximately 1-m spacings along the guideway. This is in contrast to conventional blocklength LSMs (BLSM), which typically require the variable frequency inverters along the guideway to be located with separations of every 2 to 10 km.

The Foster-Miller concept makes use of a DC distribution system along the guideway. The voltage magnitude is 2 kV and has rectifier substations located at approximately 8-km intervals. Feeder cables connect the rectifier output to the LCLSMs. The feeder cables are sized to limit the voltage drop from the rectifier to the farthest LCLSM to 5% or less. The output of the rectifier substations is not intended to be regulated or controlled in normal operation.

The inverter power level required for each of the individual LCLSM inverters is significantly different from the inverter power level for the BLSM. The inverter power level for the LCLSM is in the range of 0.5 to 1.0 MVA per inverter, whereas the BLSM inverter power level is in the range of 10 to 20 MVA per inverter. The power ratings are further made different from each other by the on-time portion of each inverter's duty cycle (this is the time when the inverter is energized and supplying power to its LSM). The LCLSM's on-time per passing consist is on the order of 0.5 to 1.5 seconds; the corresponding BLSM's on-time is of the order of 4 to 10 seconds per passing consist.

The power electronics circuit technology selected by Foster-Miller for control of the LCLSM is a pulse-width-modulated voltage source inverter, operating at a switch modulation frequency of approximately 10 kHz. Foster-Miller chose this frequency to reduce the potentially adverse effects of harmonics contained in the LSM current, and to control the magnitude of the H-bridge current during low speed operation, since the 2-kV DC input voltage bus to the H-bridge is not a controlled parameter. The back EMF of the LSM is proportional to vehicle speed and, at low speed operation, the voltage difference between the back EMF and the DC input voltage is large. For low speed operation (this would also include acceleration), each conduction pulse time of the H-bridge at the 10-kHz rate must be made as small as possible to limit the peak current that the H-bridge devices must switch.

C.2 APPLICATION OF POWER ELECTRONICS DEVICES

C.2.1 Review of power electronics device technology

Power electronics devices can be grouped into two categories, depending upon the basic junction structure of the device: the thyristor and the transistor. Thyristors are generally high-voltage and high-current devices, with ratings that can achieve several thousand amperes at several thousand volts. The commercially available devices in the thyristor family include the SCR (silicon controlled rectifier), the GTO (the gate turn-off thyristor), and the MCT ([metal oxide semiconductor] MOS-controlled thyristor). The SCR has been in commercial use for more than 25 years and the GTO for about 10 years. The MCT is about to be introduced in limited quantities and ratings.

Transistors are generally medium voltage and current devices with current ratings that can achieve a few hundred amperes at voltage ratings of several hundred volts in the higher current ratings, and with voltage ratings of about 1000 to 1500 V in the lower current ratings. The commercially available devices in the transistor family include the BJT (bipolar transistor), the power MOSFET (metal oxide field effect transistor), and the IGBT (insulated gate bipolar transistor). The BJT has been available for more than 30 years and the power MOSFET for less than 10 years. The IGBT has become commercially available only in the last year or so.

* Written by Frank L. Raposa, Consulting Engineer.

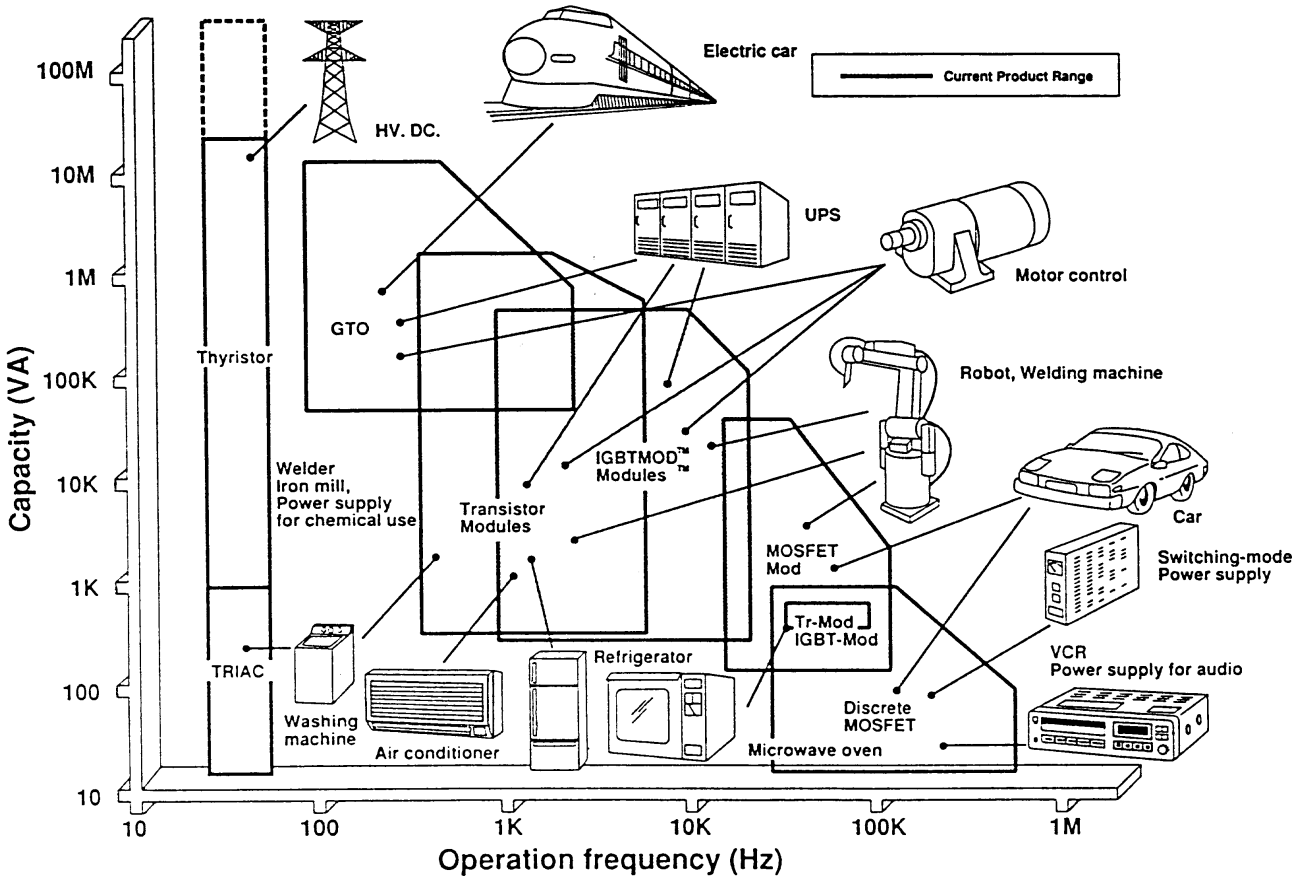

Figure C1. Typical applications for power electronics devices. (Line art courtesy of Powerex, Inc., and Mitsubishi Electric Company.)

The power module package was introduced some time ago to achieve higher ratings with transistor assemblies than are possible with discrete devices. With the power module package, several transistors at the semiconductor die level of fabrication are connected in parallel on a substrate to achieve current ratings of several hundred amperes. The mounting substrate, which is typically a copper-clad ceramic, has two major requirements. It must have good heat transfer capability and it must have high dielectric strength.

The assembly process for dual IGBT device modules uses each side of the substrate for mounting them. The current material used for the semiconductor die mounting substrate limits the voltage withstanding capability of the completed assembly to only about 3 kV DC. Consequently, this dielectric strength constraint limits the maximum voltage rating for a dual device power module to a maximum of about 3 kV. The high voltage IGBT dual device power modules that are currently available have rating capabilities that are slightly less than 3 kV for the two devices connected in series. Devices with these voltage ratings are available for only lower currents. Typical dual device ratings for higher current units are about 2.4 kV where they are connected in series. Research has been going on for some time to improve the substrate capability of power modules in both its thermal capacity and dielectric strength (Fishbein and Abramowitz 1992).

Figure C1, published by Powerex Inc. (Youngwood 1991) in their IGBT documentation, provides a comprehensive summary of power electronics device and module applications as a function of the device capacity in volt-amperes and the operating frequency that the devices switch in a power electronics circuit. One of the principal applications of GTOs is traction drives for rail systems; this includes equipment installed either in substations or vehicles. Other applications for GTOs include medium voltage (13.8-kV) motor drives used in utility systems. One of the major uses of both BJT and IGBT modules is for the control of motors that have the moderate voltage and current requirements that are compatible with the

available ratings of these devices. The power MOSFET is principally used for nontraction applications in automobiles and to a lesser extent for high-frequency, low-power motor drives. The IGBT is likely to become a serious candidate for traction control in the emerging electric automobile market.

Power electronics devices were recently summarized at the IEEE Power Electronics in Transportation Workshop held in Deerborn, Michigan. Table C1 compares the BJT, MOSFET, IGBT, and MCT for several performance areas, including switching speed, current density, and voltage rating. The data provided for the MCT in this summary are conjectural, as this device is just coming out of its development cycle and is about to be introduced in only limited quantities and with limited ratings. A 600-V, 75-A device is about to be introduced by Harris Semiconductor, who are also evaluating devices with voltage ratings of 2 to 3 kV.

The recently completed BAA study on power conditioning for maglev concluded that GTOs are the best likely candidates for conventional LSM systems (Nerem et al. 1992). It also concluded that the IGBT is an attractive choice for the lower power level requirements of vehicle auxiliary power systems.

C.2.2 Application of power electronics for motor drive inverters (after Kassakian et al. 1991)

There are three major considerations in the choice and application of a solid-state device in power electronics circuits: the required current and voltage ratings of the device and its switching characteristics. The current imposed by the LSM on the device must be within its thermal ratings, since the internal junction temperature of the device must be kept within a specified limit. This junction temperature is usually set by design to be 125°C or less; this value is somewhat less than the maximum allowable semiconductor temperature of 150°C and leaves a slight design margin. Further, the thermal time constant of a power semiconductor is quite small and almost all design approaches operate on the assumption that the junction is always at steady-state temperature.

Table C1. Qualitative characteristics of solid-state switches (after Kajashekara 1992).

Field effect transistor (FET)	*Bipolar transistor*	*Insulated gate bipolar transistor (IGBT)*
O Optimally applied 50 to 200 V	O Optimally applied 500 to 1400 V	+ Optimally applied 400 to 1200 V
+ Fast turn-on and turn-off	+ Medium turn-on and turn-off speed	+ Fast turn-on, medium turn-off speed
O Reverse conducting (equal to forward current rating)	O Reverse blocking, but only at low voltage	O Reverse blocking, but to a low voltage
+ Wide safe operating area, no second breakdown; rugged	☐ Safe operating area has second breakdown	+ Wide safe operating area, no second breakdown
O Positive temperature coefficient of resistance (parallel sharing)	☐ Negative temperature coefficient of resistance makes sharing difficult	+ Positive temperature coefficient of resistance (parallel sharing)
+ Active device, conductivity modulated via gate	O Active device, conductivity modulated via base	+ Active device, conductivity modulated via base
+ Little temperature effect on switching parameters	☐ Temperature affects switching parameters	O 1-V threshold and then less than a linear voltage rise with current
☐ High on-state resistance at high voltage ratings	☐ High on-state voltage drop at high current	+ Little temperature effect on switching parameters
	☐ Conduction requires base drive of 10% of forward current	☐ High on-state voltage drop at high voltage

Silicon controlled rectifier	*Gate turn-off thyristor (GTO)*	*MOS controlled thyristor (MCT)*
O Optimally applied 50 to 6500 V	+ Optimally applied 800 to 8000 V	+ Excellent promise for high voltage, low-loss turn-off switch
+ Highest power device; lowest cost per watt switched	+ Turns off with a gate counter-pulse—15% of forward current	☐ Not commercially available
☐ Only turns off at zero current	+ Reverse blocking types available	☐ Negative temperature coefficient of resistance makes sharing difficult
☐ Negative temperature coefficient of resistance makes sharing difficult	☐ Negative temperature coefficient of resistance makes sharing difficult	O Loses turn-off capability above rating, but device will survive if turn-off is attempted
☐ Requires recovery time for voltage hold-off after zero current	O Moderate turn-on time, but low dI/dt	
+ Reverse blocking to full forward voltage	+ Highest power self-commutated turn-off switch available	
+ Moderate turn-on time and dI/dt*	+ Moderate on-state voltage drop	
+ Low on-state voltage drop	☐ Device destruction if turn-off attempted above rating, if dI/dt rating is exceeded, if gate pulse is inadequate, or if retriggered too soon	
☐ Device destruction if dI/dt rating is exceeded, but otherwise very rugged		

+ Advantage
O Typical characteristic
☐ Disadvantage
* dI/dt = rate of current change

This is virtually a universally accepted assumption and is considered valid, unless a particular design requirement has the inverter operating at duty cycles that are significantly less than the microsecond-duration thermal time constant of the device. Heat removal techniques to assure safe junction temperature are a choice for the power electronics designer and there are many options that can be considered.

The voltage rating of the device is one of its most critical, as a solid-state power electronics device cannot withstand an over-voltage condition. An inadvertent device turn-on because of an over-voltage almost invariably leads to catastrophic failure either of the device itself or the inverter. Because it is very difficult to accurately specify all voltage conditions that may exist in a system (i.e., over-voltage surges resulting from transients coupling into the power system), it is common practice in designing power electronics circuits to significantly derate the device with respect to its voltage rating. In cases where a failure could very significantly affect system availability, it is not unusual to see deratings of 2.5 to 3 or more applied to the voltage rating of a device. For example, in a system where the nominal DC voltage is 2 kV, one might see the specification voltage rating on the solid-state device to be 5 kV or more.

The switching characteristics are related to the power electronics device's current and voltage ratings, but must also consider the nature of the load that the inverter drives and the desired switching speed of the device. For example, an LSM is a highly inductive load and imposes on the inverter conditions of simultaneous high voltage and high current during the interval when the device is switching from its *on* state to its *off* state. This is sometimes referred to as the turn-off switching transient state. Transistor manufacturers usually provide safe operating area (SOA) data as part of a device's specifications. The SOA describes the voltage-current area where a device can safely operate during the switching condition. For low voltage devices, where the voltage does not exceed a few hundred volts, the SOA is usually a rectangular area with its corners set at the device's ratings or at multiples of the device's ratings. For almost all transistor devices with voltage ratings approaching 1 kV or more, the SOA is not a rectangle. It has an area that is rectangular only in the low-current–low-voltage region, but the high-voltage–high-current region is triangular. An example of the SOA for a high voltage IGBT is shown in Figure C2. For many inverter applications, the SOA requirement becomes the principal application constraint.

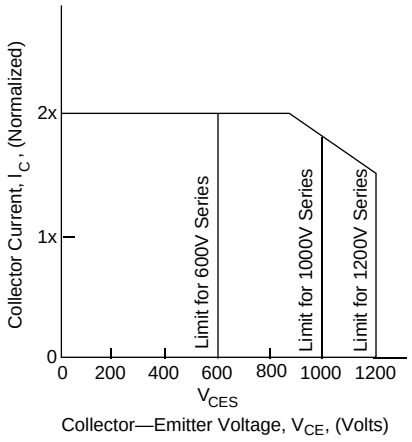

Figure C2. Typical turn-off switching SOA for IGBT devices.

C.2.3 Comments on the Foster-Miller concept for the LCLSM

The concept for the LCLSM is described in the Foster-Miller final report to the FRA (Foster-Miller 1992a). Figure C3 is the electrical schematic for the drive module for one propulsion coil pair. The module consists of a single-phase H-bridge with two IGBT devices connected in series per bridge leg and with regenerative diodes connected across each IGBTB. The regenerative diodes serve a dual function. For operation in the propulsion mode, the diodes provide a path for the phase shift current flow caused by the reactive load of the LSM winding. In the braking mode, the diodes form the path for current to be returned to the DC bus. Comments on the Foster-Miller concept for several key areas follow.

C.2.4 Power electronic device selection for the LCLSM

Foster-Miller rejected the use of the GTO because of its switching speed limitations

The GTO device, as far as its voltage and current ratings are concerned, is more than adequate for its use in the LCLSM. Its use would enable the DC bus voltage to operate at a much higher voltage level than the 2 kV, which is currently envisioned by Foster-Miller. However, the GTO switching speed capability limits its use to an inverter that operates at switching speeds of only a few kilohertz. This device was dropped from consideration by Foster-Miller because of the switching

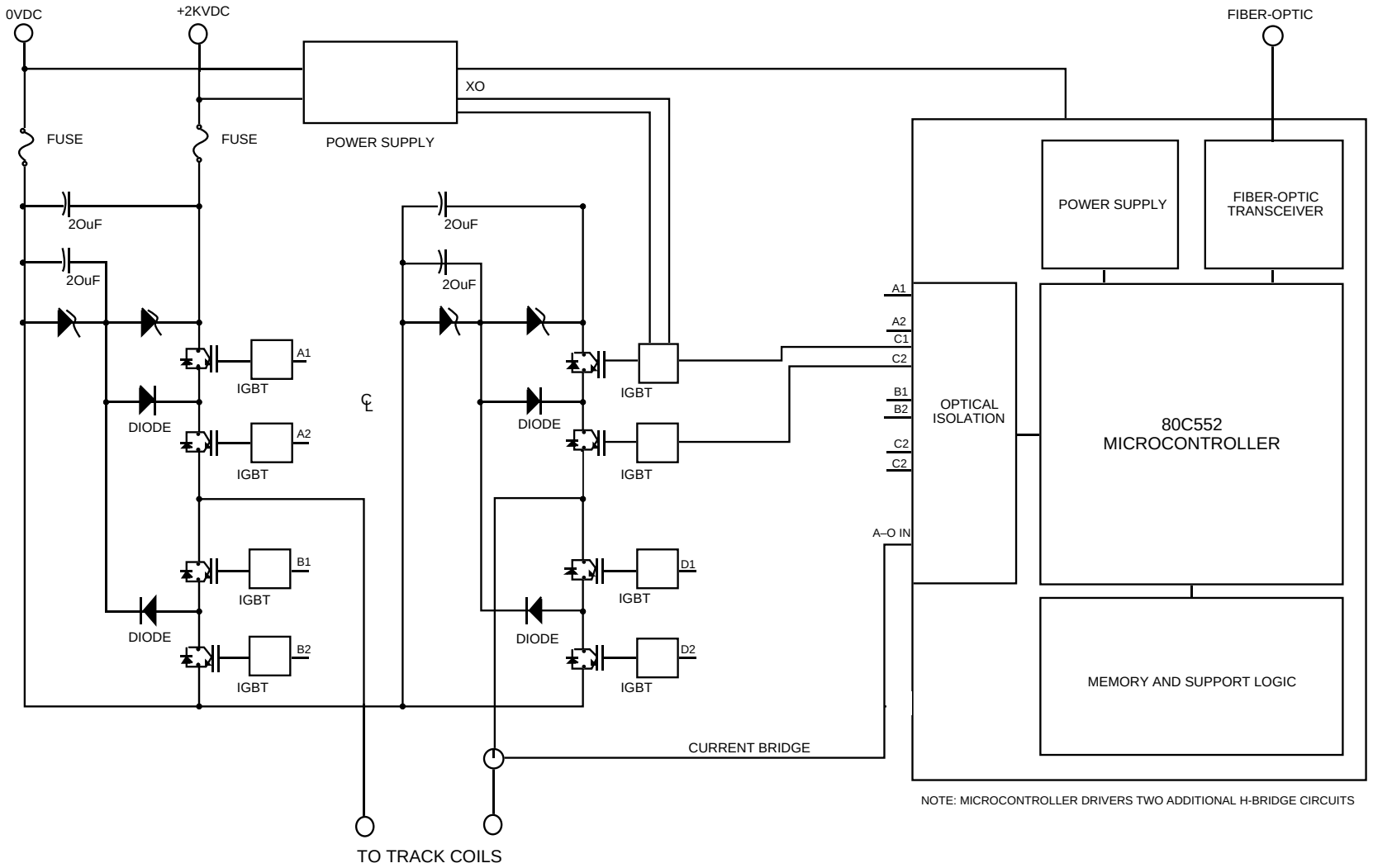

Figure C3. Electronic schematic of Foster-Miller's IGBT module.

speed limitation and the need envisioned by them for operating the H-bridge inverter at a frequency on the order of 10 kHz.

Foster-Miller selected the IGBT as the switching device of choice

The IGBT is the only available transistor device capable of approaching the LCLSM requirements. Since its relatively recent introduction, both its voltage and current capability continue to increase. However, present single devices do not have adequate current and voltage capacity, and series and parallel strings of devices must be considered. The availability of future devices with sufficient current capacity to eliminate the need for parallel devices is likely. Having sufficient voltage ratings to eliminate or reduce the number of series devices is less certain.

A key question is, can we maintain acceptable system operation with failed bridges? An overvoltage condition that causes a bridge to fail will also likely cause several bridges to fail in the immediate area of the surge, unless sufficient voltage derating is provided.

Foster-Miller has stated that the MCT device may become the future device of choice for the LCLSM

The MCT is just reaching commercial availability and the initial devices that are now being introduced will have ratings of about 75 A at 600 V. It is unclear at this time what direction the MCT will take with respect to current–voltage capability, although operating these devices at several kilovolts is now being investigated. If a widespread market with needs similar to the current, voltage, and switching speed requirements of the LCLSM materializes, the MCT could conceivably meet the LCLSM need.

C.2.5 DC voltage distribution system

Foster-Miller selected 2 kV DC as the distribution voltage to the H-bridge inverters. The selection of the distribution voltage is somewhat interdependent with the device technology used in the H-bridge inverters. However, the magnitude of the power called for is quite large for a 2-kV supply. For example, Foster-Miller's eight-car consist is sized at 30 MW for acceleration performance; this results in the requirement for large feeder cables and relatively close substation spacings. The DC distribution voltage level on a power rating basis alone should be much higher than the 2 kV initially selected and perhaps should be as high as 5 to 6 kV. Operation at voltages as high as 6 kV is still within the capability of commercial DC switchgear.

C.2.6 Estimated costs for the IGBT H-bridge inverter

Foster-Miller estimated the 1994 cost for the inverter at $5181 and the breakdown is given in Table C2, which is taken from Table 9–18 of the Foster-Miller (1992a) concept definition report. The cost of the components listed in the table represent reasonable 1994 cost estimates. However, the estimate of $5181 could be understated by as much as $2300 per inverter. The understated costs result from either missing components, or in the case of the IGBT, the listing of the incorrect number of components required. Missing from the list are the components that are required to complete the protection and sensing functions for the inverter and its control circuits.

C.2.7 IGBT device selection

The need for having sufficient DC voltage ratings in conjunction with the estimated 800-A requirement for the IGBTs would most likely

Table C2. Present-day costs for IGBT discrete component (after Foster-Miller 1992a).

Item	*Quantity*	*Description*	*Manufacturer*	*Part no.*	*Cost each ($)*	*Total cost ($)*
1	4	IGBT module	Powerex	CM200DY-24E	199.93	800
2	1	Module heat sink	EG&G	510-12-M	58.75	59
3	4	Clamp diodes	IR	IRKEL132-14s20	46.15	185
4	4	Gate drive modules	Custom	N/A	295.00	1180
5	8	Capacitors	LCC	2M1FPG66X0105J	50.00	400
6	1	Controller	Custom	N/A	300.00	300
7	1	Misc. hardware	Custom	N/A	250.00	250
8	1	Enclosure	Custom	N/A	453.30	453
				Material at 70% of labor		3626
				Labor at 30% of total		1554
				Total		5181

require doubling the number of IGBTs per bridge. The Foster-Miller concept is based on a series-connected dual-device power module component per bridge leg as shown in Figure C3. However, achieving an adequate voltage margin in conjunction with the needed current rating is most likely going to require high-current single-device modules connected in series.

Using a single-device module seems to be more consistent with current developments in the IGBT than the extension of the dual device component considered by Foster-Miller. For example, both Powerex and Fuji have recently introduced 600-A, 1400-V single device power modules, and achieving devices with 800-A capabilities is quite likely in the near future. The higher current ratings are obtained by paralleling more of the lower current devices at the die level of fabrication.

As previously described, a dual-device module is typically made by having the parallel IGBTs mounted on each side of the substrate. Until mounting substrates with higher dielectric strengths become commercially available, the voltage ratings of the module will continue to be limited.

The cost of the IGBT module should be increased from the $800 value cited by Foster-Miller to $1600 to account for doubling the number of devices required.

C.2.8 Missing components for protection and control

Not included in the Foster-Miller cost estimate are the components necessary for current and voltage sensing needed for control and protection, current limiting reactances in the DC link-to-limit fault currents, and EMI filters for control of electromagnetic noise emissions. These components are estimated to cost an additional $1500 per inverter.

C.2.9 Estimated costs for the IGBT integrated module costs

The cost estimated by Foster-Miller for the integrated module is $529 and is summarized in Table C3, which is from Table 9-19 of the Foster-Miller (1992a) concept definition report. Correcting this table for some of the missing components would probably add an additional $400 to the estimated cost, making it approximately $930. Foster-Miller's rationale for their estimate was to use the analogy to the cost savings of consumer electronics resulting from very large scale production. The example used by Foster-Miller was the television set, where they estimated production quantities of 5 million sets per year. For an LCLSM maglev application, FMI estimated a requirement for about 1.1 million inverters for a dual guideway of 480 km (300 miles) as the rationale for the production scale similarity.

Table C3. Estimated costs for IGBT integrated module (after Foster-Miller 1992a).

Item	*Description*	*Factor (%)*	*Cost ($)*
1	IGBT module	10	80
2	Module heat sink	50	29
3	Clamp diodes	25	46
4	Gate drive modules	3	35
5	Capacitors	30	120
6	Controller	5	15
7	Misc. hardware	10	25
8	Enclosure	5	23
	Labor	10	155
		Total	529

Historically, semiconductor equipment has been experiencing about a 15% cost reduction per year. This has been based on both market growth as well as improvements in manufacturing processes. Beyond this historical basis, it is very speculative to attempt with any confidence to estimate or attempt to verify the anticipated cost reductions that have been put forth by Foster-Miller for the H-Bridge inverter in the quantity scale anticipated. However, having stated that, we can make the following comments about these anticipated cost reductions.

Construction time for a 480-km guideway is likely to be 4 years or more. The 1.1 million inverters estimated by Foster-Miller gives a requirement of nearly 275,000 inverters per year. This is about 5% of the annual production of TV sets. Further, the majority of electronics used in TV sets are also used in other consumer electronics, as well as for automotive electronics, thus resulting in comparative production scales that are greatly beyond that estimated for the LCLSM.

The consumer electronics and the automotive electronics industries are very large and highly competitive businesses. This allows production scales that enable major companies to control and, in many instances, own sources of materiel, manufacturing plants, and integrated manufacturing facilities, and to use other factors that enable lowest cost production. It is unclear the extent to which that situation can be translated to the more limited mass transportation industry.

The principal components of the IGBT inverter—IGBTs, diodes, capacitors, and inductors—are high voltage or high current units, or both, and are not the type of devices that are commonly found in consumer electronics. Traction applications similar to maglev, for example, mass transit and railroads, appear to be the only analogy to the LCLSM inverter. This is true even with the emerging electric vehicle market, where the expected operating voltages will only be a few hundred volts (IEEE 1992). Any projections on cost savings should be addressing potential growth in the high power traction market. In fact, maglev could be one of the major drivers for the technology for that market.

Current world-wide production of transistor power modules is estimated to be about 600,000 modules per month.* This includes both BJT and IGBT modules and includes devices with current ratings that vary from 8 to 800 A. The bulk of the present demand is for devices of the lower current ratings rather than those for the higher current ratings. Of this quantity, only about 20%, or about 120,000 modules per month, are currently IGBTs; the rest are conventional BJTs. The IGBT portion is expected to grow as time goes on. On the basis of Foster-Miller's quantity estimate above, and the 4-year production period for the 480-km dual guideway, the requirement for LCLSM modules would be in excess of 180,000 IGBT modules per month. This not only exceeds current IGBT production, but is also a significant portion of the total monthly production of transistor modules.

Several semiconductor manufacturers have said that the capital cost investment needed to satisfy the LCLSM inverter requirement alone is of the order of 500 to 800 million dollars. This includes the device fabrication, processing, and assembly facilities needed to produce just the power semiconductors for the inverter. Some portion of this investment would probably have to be carried as a cost by a major maglev construction project, absent the need for any other major use of the facilities.

To arrive at some of idea of the potential impact, assume that 50% of the investment would have to be carried by a major maglev construction project and that, further, it is the first 480-km project that bears this cost. This assumption leads to an inverter cost increment of about $300 for each, which has to be added to the other cost elements of the inverter. Foster-Miller's estimate for the IGBT Integrated Module of $530, corrected to $930 to account for the missing components, would then have to be increased to $1330 per module to allow for the amortization of the incremental capital cost requirements.

Similar capital cost arguments could be made for the other major components of the module. Some of these components, such as inductors and EMI filters, may have to be uniquely configured to the IGBT module and, as a consequence, also require significant one-time costs that would also have to be amortized.

The above assumptions only illustrate some of the factors that would influence cost. A more detailed study would be necessary to more accurately determine the cost scaling reductions and the impact of significant capital cost requirements to meet production capacity requirements.

A likely price for the LCLSM power electronics is in the range of $1000 to $1200 per inverter. This is for very high production quantities with a significantly sustained production schedule. This assumes that the economies of scale postulated by Foster-Miller are realized and that the capital costs of increasing production capacity for the solid-state devices does not have to be carried by the maglev project.

C.2.10 Estimated number of power semiconductors required for LSM blocklength systems

GTOs have been identified as the principal power semiconductor by the other SCD studies that make use of conventional blocklength LSMs. The following is a preliminary assessment of the availability of GTOs to satisfy a major maglev construction requirement. It is intended as a point of comparison to the IGBT situation for the LCLSM.

As stated above, the major present use of GTOs includes traction applications and utility medium voltage level (13.8-kV) motor drives. Present production of GTOs is about 7000 per month and includes GTOs in the 4500-V, 2000 to 3000-A ratings that would be typical of a maglev requirement. A representative from Toshiba, a major supplier of traction type GTOs, stated that current production rates are well below available manufacturing capacity. *

* Personal communication with J. Mathis of Collmer Semiconductor, Inc., U.S. representative for Fuji Electric Co.

* Personal communication with G. Ward, Toshiba Electric Co.

Let's use the same 480-km route, 48-month construction example as described above for the IGBT assessment. Typical inverter station spacings would be about every 4 km, thus requiring about 120 inverter stations for the route. Depending upon the particular SCD LSM blocklength concept, an inverter station would require from 24 to 48 GTOs per station. Using the 48 GTOs per station as the example requirement results in a requirement of 120 GTOs per month. This requirement is slightly less than 2% of the present monthly production of GTOs. In the next few years, the traction market in Europe and in third world countries is expected to significantly grow, thus increasing the production output of GTOs. Therefore, a maglev requirement for GTOs for the blocklength concept does not appear to materially affect the availability of GTO devices.

C.3 CONCLUSIONS AND RECOMMENDATIONS

C.3.1 Technical viability

The LCLSM could become a significantly innovative propulsion system. Some of its principal potential advantages over the more conventional blocklength LSM are the improved efficiency and power factor resulting from only the LSM propulsion coils of a maglev consist length being energized at any given time. Guideway to vehicle power transfer using those LSM coils between vehicle bogies as part of an air-core transformer enhances the potential for this concept. Perhaps the most significant possible advantage for the LCLSM concept is its potential for providing propulsion when it is degraded, with some of the LSM windings inoperative. The degree of degradation would of course depend on the number of LSM windings that are disabled. This is in contrast to the blocklength LSM, where a failed LSM winding could disable the entire block and either stop the system or severely curtail operation until it is repaired.

There are many questions that must be addressed to establish the technical viability of the LCLSM. These include questions of the ability to control acceleration, velocity, and lateral stability. Lateral stability may be of concern, as the currently configured LCLSM also provides the lateral guidance forces.

The LCLSM concept operates with all of the LSM coils electrically connected in parallel and the question of the degree of equal current sharing in the bridge inverters is an important issue. In addition, there is a possible stability question. For example, if the degree of current sharing in the inverters is such that the most forward bogies are not conducting as much current as the rearmost bogies, how will this influence lateral stability?

The LSM coils are individually controlled by inverters controlling single coil pairs and will operate in a way that is similar to a single-phase motor or perhaps analogously to a DC stepper motor. This raises the question of potential thrust variations (sometimes referred to as cogging) and how this might adversely affect ride comfort.

Another area of concern is the overall effectiveness of the power transfer concept. Its effectiveness depends critically on obtaining a high degree of coupling between the guideway primary coils and the vehicle secondary coils. A choice of lower modulation frequencies for the inverter is compatible with the LCLSM operating in the propulsion mode, as the LSM frequency is quite low. To what extent would power transfer capability be compromised with the lower switching frequency?

The choice of the 2-kV DC system for power distribution is recognized to be intrinsically connected to the inverter device technology selected. However, for the power levels envisioned for operating multiple car consists, such as the eight-car consist, the tentative selection of 2-kV DC may be a too low a voltage to use. Its choice requires the relatively close DC rectifier station spacings that are similar to those of transit systems and further requires large feeder cables to minimize voltage drop and energy losses. It is not apparent that any trade study was ever conducted on the selection of the DC voltage level.

C.3.2 Economic viability

The relative economics of the LCLSM depend very heavily on the progress of ongoing developments in power electronics devices and the development of the LCLSM probably won't directly influence device costs. However, a serious commitment to maglev development could be one of the major drivers in the development of power electronics devices in much the same way that electric traction requirements for both transit and railroads have pushed the development of GTOs.

The historical trend in the costs of electronics, including power electronics devices, has been downward and there is no reason to think that this trend will reverse in the foreseeable future. The eventual success of the LCLSM will depend quite heavily on this trend continuing and eventually

pushing inverter costs into the commodity cost category.

C.3.3 Recommendations

We recommend that an experimental development program be started on the LCLSM, with the emphasis on the power electronics part of the system and controllability issues. A small-scale model development and evaluation study could address almost all of the issues discussed here. It could also address some of the more subtle issues of switching frequencies, waveform synthesis, and polyphase vs. single-phase performance, to name a few. Answers to these questions could provide some direction in the development that might lead to an easing of some of the known economic constraints.

We also recommend that further analysis be done on the selection of the best DC voltage distribution system for the LCLSM. For example, what would be the potential cost savings for a 4-kV or a 6-kV DC system or possibly an even higher distribution voltage? What would the development requirements be, if any, to achieve these expected savings? To what extent, if any, would this affect the selection and configuration of the power electronics and the LSM propulsion coils?

GLOSSARY

AT	Ampere turns.
ANL	Argonne National Laboratory.
BAA	Broad Agency Announcement. A notice from the Government that requests scientific or research proposals from private firms concerning certain areas of interest to the Government. The proposals submitted by private firms may lead to contracts.
BJT	Bipolar transistor.
bogie	Railroad car or locomotive undercarriage.
commutate	Reverse the direction of an alternating current each half cycle to yield a unidirectional current.
consist	Composition (number and specific identity) of individual units of a train.
CGS	Continuous sheet guideway.
cryogenics	Science of low temperature phenomena.
cryostat	Device for maintaining constant low temperature.
DG	Design goals.
DOE	U.S. Department of Energy.
DLF	Dynamic load factor.
USDOT	U.S. Department of Transportation.
EDS	Electrodynamic suspension.
EMS	Electromagnetic suspension.
Emsland	Test site of the TR07 in Germany.
EI	Energy intensity.
EM	Electromagnetic.
FHWA	U.S. Federal Highway Administration.
FRP	Fiber reinforced plastic—polymer-based alternative to ferrous reinforcement of concrete and other materials.
FRA	U.S. Federal Railroad Administration.
GMSA	Government Maglev System Assessment.
guideway	Riding surface (including support structure) that physically guides vehicles specially designed to travel on it.
GTO	Gate turnoff thyristors.
H-bridge	Four-arm, alternating current bridge, the balance of which varies with electrical frequency.
headway	Interval between the passing of the front ends of successive vehicles moving in the same direction along the same lane, track, or other guideway.
HSGT	High speed ground transportation.

HSR	High speed rail.
HSST	High speed surface transportation.
ICE	Intercity Express (German high-speed train).
IGBT	Insulated gate bipolar transistors.
invertor	Electrical circuit device that reverses an input to an opposite output in terms of some electrical characteristics, such as polarity, voltage, or frequency.
JNR	Japanese National Railway.
LCLSM	Locally commutated linear synchronous motor.
levitation	Rise or cause to rise into air and float in apparent defiance of gravity.
levitation, magnetic	Support technology that keeps a vehicle separated from its guideway by riding a surface of magnetic force.
life cycle	Useful or total productive life of an asset or system.
life cycle cost	Present value total cost for acquisition and operation over the useful life of an asset or system.
IEEE	Institute of Electrical and Electronics Engineers.
long-stator	Propulsion using an electrically powered linear motor winding in the guideway.
LSM	Linear synchronous motor.
maglev	Magnetic levitation.
MOSFET	Metal oxide field effect transistor.
magnetic levitation	Support technology that keeps a vehicle separated from its guideway by riding a surface of magnetic force.
MLU	Japanese maglev system employing a U-shaped guideway.
MCT	MOS controlled thyristor.
MR	Minimum requirements.
NMI	National Maglev Initiative.
OCS	Overhead catenary system.
pantograph	Device for collecting current from an overhead conductor, characterized by a hinged vertical arm operating by springs or compressed air and a wide, horizontal contact surface that glides along the wire.
PI	Point of intersection.
PSE	Paris-Sud-EST or Paris-Lyon Route on which the TGV has been in service since 1981 in France.
ROW	Right-of-way—A general term denoting land, property, or interest therein, usually in a strip, acquired for or devoted to transportation.
R&D	Research and development.

SB	Seated and belted criteria.
SCD-FRP	System concept definition, request for proposal
SOA	Safe operating area (electronics).
SST	Severe segment test route.
SRI	Stanford Research Institute.
stator	Nonrotating part of the magnetic structure in an induction motor.
superconductivity	Abrupt and total disappearance of resistance to direct current that occurs in some materials at temperatures near to or somewhat above absolute zero (such as 90 K for some high temperature superconductors).
superelevated curves	Banked curves.
TGV	Train à Grande Vitesse.
Transrapid (TR07)	German high speed maglev system. This system is nearest to commercial readiness.
TSC	Transportation Services Center.
USACE	United States Army Corps of Engineers.
VNTSC	Volpe National Transportation Systems Center.
SP	Standard passenger.
SSTSIM	Severe segment test route simulator.
SCR	Silicon controlled rectifier.
SNCF	French National Railways.

REPORT DOCUMENTATION PAGE

Form Approved
OMB No. 0704-0188

1. AGENCY USE ONLY (Leave blank)	2. REPORT DATE	3. REPORT TYPE AND DATES COVERED
	October 1998	

4. TITLE AND SUBTITLE
Technical Assessment of Maglev System Concepts
Final Report by the Government Maglev System Assessment Team

5. FUNDING NUMBERS

6. AUTHORS
James H. Lever, Editor

7. PERFORMING ORGANIZATION NAME(S) AND ADDRESS(ES)

U.S. Army Cold Regions Research and Engineering Laboratory
72 Lyme Road
Hanover, New Hampshire 03755-1290

8. PERFORMING ORGANIZATION REPORT NUMBER

Special Report 98-12

9. SPONSORING/MONITORING AGENCY NAME(S) AND ADDRESS(ES)

National Maglev Initiative, U.S. Department of Transportation, U.S. Army Corps of Engineers, U.S. Department of Energy, and Argonne National Laboratory

10. SPONSORING/MONITORING AGENCY REPORT NUMBER

11. SUPPLEMENTARY NOTES
For conversion of SI units to non-SI units of measurement, consult ASTM Standard E380-93, *Standard Practice for Use of the International System of Units*, published by the American Society for Testing and Materials, 100 Barr Harbor Drive., West Conshohocken, Pennsylvania 19428-2959.

12a. DISTRIBUTION/AVAILABILITY STATEMENT

Approved for public release; distribution is unlimited.

Available from NTIS, Springfield, Virginia 22161

12b. DISTRIBUTION CODE

13. ABSTRACT (*Maximum 200 words*)

The Government Maglev System Assessment Team operated from 1991 to 1993 as part of the National Maglev Initiative. They assessed the technical viability of four U.S. maglev system concepts, using the French TGV high-speed train and the German TR07 maglev system as assessment baselines. Maglev in general offers advantages that include high speed potential, excellent system control, high capacity, low energy consumption, low maintenance, modest land requirements, low operating costs, and ability to meet a variety of transportation missions. Further, the U.S. maglev concepts could provide superior performance to TR07 for similar cost or similar performance for less cost. They also could achieve both lower trip times and lower energy consumption along typical U.S. routes. These advantages result generally from the use of large-gap magnetic suspensions, more powerful linear synchronous motors and tilting vehicles. Innovative concepts for motors, guideways, suspension, and superconducting magnets all contribute to a potential for superior long-term performance of U.S. maglev systems compared with TGV and TR07.

14. SUBJECT TERMS

High-speed ground transportation
High-speed trains
Maglev
Magnetic levitation

15. NUMBER OF PAGES
241

16. PRICE CODE

17. SECURITY CLASSIFICATION OF REPORT	18. SECURITY CLASSIFICATION OF THIS PAGE	19. SECURITY CLASSIFICATION OF ABSTRACT	20. LIMITATION OF ABSTRACT
UNCLASSIFIED	UNCLASSIFIED	UNCLASSIFIED	UL